

VOLUME 76 NOVEMBER 23, 1972 NUMBER 24

JPCA X

---

THE JOURNAL OF  
PHYSICAL  
CHEMISTRY

---

PUBLISHED BIWEEKLY BY THE AMERICAN CHEMICAL SOCIETY



*American Chemical Society*

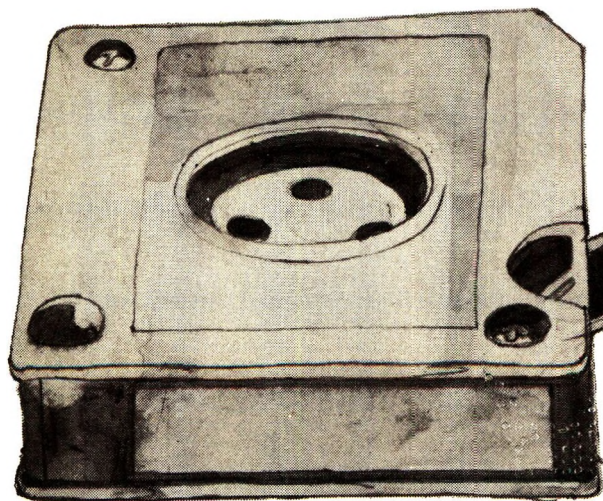
# "Primary Publications on Microfilm"

*Your Key to—*

■ Dramatic savings in archival space and dollars . . . over 1,000,000 pages of chemical literature contained in a carousel measuring only 17" x 17" x 39".

■ Faster access to needed data. Slash costly search and retrieval time required of your scientists and librarians.

■ Unlimited distribution of copyrighted scientific data. "ACS Primary Publications on Microfilm" are available under a unique licensing agreement permitting you to make as many enlarged photocopies per page as desired . . . for distribution throughout your company.



*American Chemical Society Primary Publications included in this microfilm program:*

JOURNAL OF THE AMERICAN CHEMICAL SOCIETY  
INDUSTRIAL & ENGINEERING CHEMISTRY  
CHEMICAL TECHNOLOGY  
CHEMICAL & ENGINEERING NEWS  
CHEMICAL & ENGINEERING NEWS ANNUAL INDEXES  
ANALYTICAL CHEMISTRY  
JOURNAL OF PHYSICAL CHEMISTRY  
JOURNAL OF AGRICULTURAL AND FOOD CHEMISTRY  
JOURNAL OF ORGANIC CHEMISTRY  
JOURNAL OF CHEMICAL AND ENGINEERING DATA  
CHEMICAL REVIEWS  
JOURNAL OF CHEMICAL DOCUMENTATION  
I&EC FUNDAMENTALS  
I&EC PROCESS DESIGN AND DEVELOPMENT  
I&EC PRODUCT RESEARCH AND DEVELOPMENT  
BIOCHEMISTRY  
INORGANIC CHEMISTRY  
JOURNAL OF MEDICINAL CHEMISTRY  
CHEMISTRY  
ENVIRONMENTAL SCIENCE & TECHNOLOGY  
ACCOUNTS OF CHEMICAL RESEARCH  
MACROMOLECULES

*For information on "ACS Primary Publications on Microfilm", write or call:*

**Special Issues Sales  
American Chemical Society  
1155 16th Street, N.W.  
Washington, D. C. 20036  
(202-872-4364)**

# THE JOURNAL OF PHYSICAL CHEMISTRY

---

**BRYCE CRAWFORD, Jr.,** *Editor*

STEPHEN PRAGER, *Associate Editor*

ROBERT W. CARR, Jr., FREDERIC A. VAN-CATLEDGE, *Assistant Editors*

**EDITORIAL BOARD:** A. O. ALLEN (1970-1974), J. R. BOLTON (1971-1975),  
F. S. DAINTON (1972-1976), M. FIXMAN (1970-1974),  
H. S. FRANK (1970-1974), R. R. HENTZ (1972-1976), J. R. HUIZENGA (1969-1973),  
W. J. KAUZMANN (1969-1973), R. L. KAY (1972-1976), W. R. KRIGBAUM (1969-1973),  
R. A. MARCUS (1968-1972), W. J. MOORE (1969-1973), J. A. POPLE (1971-1975),  
B. S. RABINOVITCH (1971-1975), H. REISS (1970-1974), S. A. RICE (1969-1975),  
F. S. ROWLAND (1968-1972), R. L. SCOTT (1968-1972),  
R. SEIFERT (1968-1972), W. A. ZISMAN (1972-1976)

---

CHARLES R. BERTSCH, *Manager, Editorial Production*

---

AMERICAN CHEMICAL SOCIETY, 1155 Sixteenth St., N.W., Washington, D. C. 20036

#### Books and Journals Division

JOHN K CRUM, *Director*

JOSEPH H. KUNEY, *Head, Business Operations Department*

RUTH REYNARD, *Assistant to the Director*

©Copyright, 1972, by the American Chemical Society. Published biweekly by the American Chemical Society at 20th and Northampton Sts., Easton, Pa. 18042. Second-class postage paid at Washington, D. C., and at additional mailing offices.

All manuscripts should be sent to *The Journal of Physical Chemistry*, Department of Chemistry, University of Minnesota, Minneapolis, Minn. 55455.

*Additions and Corrections* are published once yearly in the final issue. See Volume 75, Number 26 for the proper form.

*Extensive or unusual alterations in an article after it has been set in type are made at the author's expense*, and it is understood that by requesting such alterations the author agrees to defray the cost thereof.

The American Chemical Society and the Editor of *The Journal of Physical Chemistry* assume no responsibility for the statements and opinions advanced by contributors.

Correspondence regarding accepted copy, proofs, and reprints should be directed to Editorial Production Office, American Chemical Society, 20th and Northampton Sts., Easton, Pa. 18042. Manager: CHARLES R. BERTSCH. Assistant Editor: EDWARD A. BORGER. Editorial Assistant: JOSEPH E. YURVATI.

Advertising Office: Centcom, Ltd. (formerly Century Communications Corporation), 142 East Avenue, Norwalk, Conn. 06851.

#### Business and Subscription Information

Remittances and orders for subscriptions and for single copies,

notices of changes of address and new professional connections, and claims for missing numbers should be sent to the Subscription Service Department, American Chemical Society, 1155 Sixteenth St., N.W., Washington, D. C. 20036. Allow 4 weeks for changes of address. Please include an old address label with the notification.

Claims for missing numbers will not be allowed (1) if received more than sixty days from date of issue, (2) if loss was due to failure of notice of change of address to be received before the date specified in the preceding paragraph, or (3) if the reason for the claim is "missing from files."

Subscription rates (1972): members of the American Chemical Society, \$20.00 for 1 year; to nonmembers, \$60.00 for 1 year. Those interested in becoming members should write to the Admissions Department, American Chemical Society, 1155 Sixteenth St., N.W., Washington, D. C. 20036. Postage to Canada and countries in the Pan-American Union, \$5.00; all other countries, \$6.00. Single copies for current year: \$3.00. Rates for back issues from Volume 56 to date are available from the Special Issues Sales Department, 1155 Sixteenth St., N.W., Washington, D. C. 20036.

This publication and the other ACS periodical publications are now available on microfilm. For information write to: MICROFILM, Special Issues Sales Department, 1155 Sixteenth St., N.W., Washington, D. C. 20036.



From The American Chemical Society

# Famous Scientists

**Tape cassettes** from the unique ACS radio program **Men & Molecules**

## NOBEL PRIZE WINNERS

- Dr. Linus Pauling**  
The Committed Scientist  
**Dr. Jacob Bronowski**  
Science and Man
- Dr. Glenn Seaborg** The Atomic World of Glenn Seaborg  
**Dr. George Wald** Vision, Night Blindness, & Professor Wald
- Dr. Melvin Calvin** The Search for Significance—Parts I & II

## BIO-MEDICAL

- Engineering Enzymes**  
Dr. Victor Edwards  
**On Drugs, Plasticizers, & Mass Spec**  
Dr. G. W. A. Milne
- Body Metal** Dr. Thomas Clarkson  
**Judging Technology** Dr. E. G. Mesthene
- Prospects for the Living Filter**  
Dr. Richard Parizek  
**Coral Designs** Dr. Eugene White
- Bones, Teeth, & Ceramics**  
Thomas Driskell  
**PCBs: The Accidental Pollutants**  
Dr. Henry Enos
- Birth Control: Problems & Prospects**  
Dr. Carl Djerassi  
**Hormones, Terpenes, & the German Air Force** Dr. A. J. Birch
- Prospects for Implants**  
Dr. Donald Lyman  
**New Dimensions for Polymers**  
Dr. Alan Michaels
- Fabricating Life** An Essay Report  
**New Ways to Better Food**  
Dr. R. W. F. Hardy
- Chemistry of the Mind: Schizophrenia**  
Dr. Larry Stein  
**Chemistry of the Mind: Depression**  
Dr. Joel Elkes
- The Molecules of Memory**  
Dr. W. L. Byrne & Dr. A. M. Golub  
**The Matter with Memory**  
Dr. J. McGaugh
- Dissonant Harmony**  
Dr. Denham Harman  
**Why We Grow Old** Dr. Howard Curtis

- New Materials for Spare Parts**  
Dr. V. Gott & Dr. A. Rubin  
**Against Individuality**  
Dr. R. Reisfeld & Dr. B. Kahan
- A Richness of Lipids**  
Dr. Roscoe O. Brady  
**Life: Origins to Quality**  
Dr. Stanley Miller
- The Nitrogen Fixer**  
Dr. Eugene van Tamelen  
**Prostaglandins: A Potent Future**  
Dr. E. J. Corey & Dr. S. Bergstrom
- A Glass Revolution** Dr. S. D. Stookey  
**A View of Genes** Dr. Norman Davidson
- Chemical Evolution**  
Dr. Russell Deolittle  
**An Evolving Engine** Dr. R. E. Dickerson

## CANCER RESEARCH

- Cancer Research I—Perspective & Progress** Dr. Frank Rauscher  
**Cancer Research II—Viruses**  
Dr. R. Gallo & Dr. G. Todaro
- Cancer Research III—Chemotherapy**  
Dr. C. Gordon Zubrod  
**Cancer Research IV—Immunology**  
Dr. Paul Levine
- Cancer Research V—Environmental Agents** Dr. Umberto Saffiotti  
**Cancer Research VI—NCI Roundtable**

## ENERGY

- Energy: A Critique**  
Dr. Dean Abrahamson  
**Puzzles of Air Pollution** Arthur Levy
- Fusion: Prospects & Pitfalls—I**  
Dr. H. Furth & Dr. H. Forsen  
**Fusion: Prospects & Pitfalls—II**  
Dr. H. Furth & Dr. H. Forsen
- Antidote to the Energy Crisis**  
George Long  
**Chemicals in the Environment**  
Dr. Samuel Epstein
- Fusion and Fission: An Appraisal**  
Dr. James L. Tuck  
**The Prospects for Energy**  
Dr. M. King Hubert

## ENVIRONMENT

- The Struggle for Clean Water—I**  
**The Struggle for Clean Water—II**
- The Oil Mystery** Harold Bernard  
**The Language of Odors**  
Dr. Stanley Freeman
- The Muskogean County Experiment**  
Dr. W. Bauer & Dr. J. Sheaffer  
**The Sophisticated Dowser**  
Dr. Richard Parizek
- The Lonely Atom** Dr. Philip Skell  
**How Green the Revolution**  
Lester Brown
- Mercury: Another Look, Part I**  
Dr. John Wood  
**Mercury: Another Look, Part II**  
Dr. John Wood & D. G. Langley
- The Troubles with Water**  
Dr. Daniel Okun  
**Pure Oxygen for Polluted Water**  
Dr. Jack McWhirter
- Bubble Machines & Pollution Finders**  
Dr. K. Patel & Dr. L. Kreuzer  
**The Steam Engine: A Modern Approach** Dr. W. Doerner & Dr. M. Bechtold
- Insects: The Elements of Change—Parts I & II** Dr. Carroll M. Williams
- New Weapons Against Insects**  
Dr. G. Staal & Dr. J. Siddall  
**Moths, Drugs, & Pheromones**  
Dr. Wendell Roelofs
- The Lead Issue**  
H. Mayrhoen & M. H. Hyman  
**Smog: An Environmental Dilemma**  
Dr. James Pitts
- The Fusion Torch**  
Dr. B. Eastlund & Dr. W. Gough  
**The Impermanent Plastic**  
Dr. James Guillet

- Nitrosamines: A Reappraisal**  
Dr. Phillip Issenberg  
**The Emperor of Ice Cream**  
Dr. Wendell Arbuckle
- Ethics and Genetics**  
Dr. Robert F. Murray  
**The American Diet: A Critique**  
Dr. Arnold Schaefer
- Probing Creation** Dr. Myron A. Coler  
**New Directions in U.S. Science**  
Dr. William McElroy
- Aspirins, Enzymes, & Fragrant Redheads** An Essay Report  
**Vitamin D: A New Dimension**  
Dr. Hector Deluca
- Pica** Dr. J. Julian Chisolm, Jr.  
**Technology in the Nursery**  
Dr. William J. Dorson
- Engineering Microbes**  
Dr. Elmer Gaden  
**Liquid Crystals: A Bright Promise**  
Dr. George Heilmeyer
- Hot Brines in the Red Sea**  
Dr. David Ross  
**Complete Corn** Dr. Edwin T. Mertz
- Lively Xenon** Dr. Neil Bartlett  
**The Repressor Hunt**  
Dr. Mark Ptashne
- The New Prospectors**  
Dr. William Prinz  
**A Sober Look at Alcoholism**  
Dr. Jack Mendelsohn
- Probing the Active Site**  
Dr. David Pressman  
**The Puzzle of Diversity**  
Dr. Oliver Smithies
- Help for the Have Nots**  
Dr. Harrison Brown  
**The Closing Circle** Dr. Preston Cloud

## OUTER SPACE

- Molecules in Space**  
Dr. D. Buhl & Dr. L. Snyder  
**Chemistry Among the Stars**  
Dr. Bertram Donn
- Molecules Meeting Molecules**  
Dr. John Richards  
**The Neutrinos of the Sun**  
Dr. Raymond Davis

## SCIENCE

- Science, Scientists, & the Public Interest—I**  
**Science, Scientists, & the Public Interest—II**

	ACS Members	Nonmembers
Single Cassette	\$4.49	\$5.49
Any Six Cassettes	\$3.95/cassette	\$4.95/cassette
Any 18 or more cassettes to one Address \$3.75/cassette		

Large Volume Orders Negotiable  
For orders outside U.S.A. add 75 cents handling charge  
5% Discount if payment accompanies order  
Order From: American Chemical Society, 1155 16th Street,  
N.W., Washington, D.C. 20036, ATTN: A. Poulos



THE JOURNAL OF  
PHYSICAL CHEMISTRY

---

Volume 76, Number 24 November 23, 1972

JPCAx 76(24) 3509-3676 (1972)

Reactions of Fluorine-18 Atoms with Ethylene . . . . .	Ronald L. Williams and F. S. Rowland*	3509
Absolute Rate Constants for the Reaction $H + O_2 + M \rightarrow HO_2 + M$ over the Temperature Range 203-404 K . . . . .	Michael J. Kurylo	3518
Pressure Dependence and Mechanism of the Reaction of Atomic Oxygen and Carbon Monoxide . . . . .	W. B. DeMore	3527
Reactions of Borane (BH <sub>3</sub> ). VII. Reaction with Ketene . . . . .	T. P. Fehlner	3532
The Chemical Kinetics of the Pyrolysis of Hydrogen Deuteride . . . . .	T. Niki and Gilbert J. Mains*	3538
Detection of Species Resulting from Condensed Phase Decomposition of Ammonium Perchlorate . . . . .	E. Ellsworth Hackman, III, Henry H. Hesser, and Harold C. Beachell*	3545
Structure Effect on the Fading Rate of Photochromic 3-Substituted Benzothiazolinic Spiropyrans . . . . .	A. Samat, J. Metzger,* F. Mentiènnè, F. Garnier, J. E. Dubois, and R. Guglielmetti	3554
Excited State Dissociation Rate Constants in Naphthols . . . . .	Jerome L. Rosenberg and Ira Brinn*	3558
Fluorescence Quenching by Benzoic Acid . . . . .	Nelson H. C. Cooke and Barton S. Solomon*	3563
A Study of Alkylbenzene Luminescence . . . . .	Peter M. Froehlich and Harry A. Morrison*	3566
Electron Spin Resonance of Triplet Nitrenes from Aryl Isocyanates . . . . .	V. J. Kuck,* E. Wasserman, and W. A. Yager	3570
An Electron Spin Resonance Study of Several DNA Base Cation Radicals Produced by Photoionization . . . . .	M. D. Sevilla,* C. Van Paemel, and C. Nichols	3571
Reactions of the Cation and Anion Radicals of Several DNA Bases . . . . .	M. D. Sevilla,* C. Van Paemel, and G. Zorman	3577
Studies of the Ester Bond. II. Nuclear Magnetic Resonance Studies of <i>tert</i> -Butyl Formate . . . . .	Torbjörn Drakenberg* and Sture Forsén	3582
Chemiluminescence Excited by Atomic Fluorine . . . . .	G. Schatz and M. Kaufman*	3586
Vibrational Analyses and Barrier to Internal Rotation of 1,1-Dichloroethane and 1,1-Dichloroethane- <i>d</i> <sub>4</sub> . . . . .	J. R. Durig,* A. E. Sloan, and J. D. Witt	3591
The Crystal Structure of 2,4,6-Trinitroaniline . . . . .	James R. Holden,* Charles Dickinson, and Charles M. Bock	3597
Non-Poisson Distributions Observed during Counting of Certain Carbon-14-Labeled Organic (Sub)Monolayers . . . . .	John Lynde Anderson	3603
Model Calculations of Secondary $\alpha$ -Deuterium Isotope Effects in Addition Reactions to Olefinic Double Bonds . . . . .	I. Safarik and O. P. Strausz*	3613
Theoretical Models for Acid-Base Equilibrium Data in Nonaqueous Solvents . . . . .	Neal G. Sellers, Peter M. P. Eller, and Joseph A. Caruso*	3618
Kinetics of Adsorption of Mineral Acids on Alumina . . . . .	Lj. Jaćimović, J. Stevović, and S. Veljković	3625
Brønsted Acid Sites on Porous Glass from Membrane Potentials . . . . .	L. S. Hersh* and M. P. Teter	3633



Here is the ideal way  
to obtain the  
most reliable reference data  
available today! All you need  
is a subscription to the new  
**JOURNAL OF PHYSICAL AND  
CHEMICAL REFERENCE DATA**  
published by the American Chemical  
Society and the American Institute of  
Physics for the National Bureau of  
Standards.

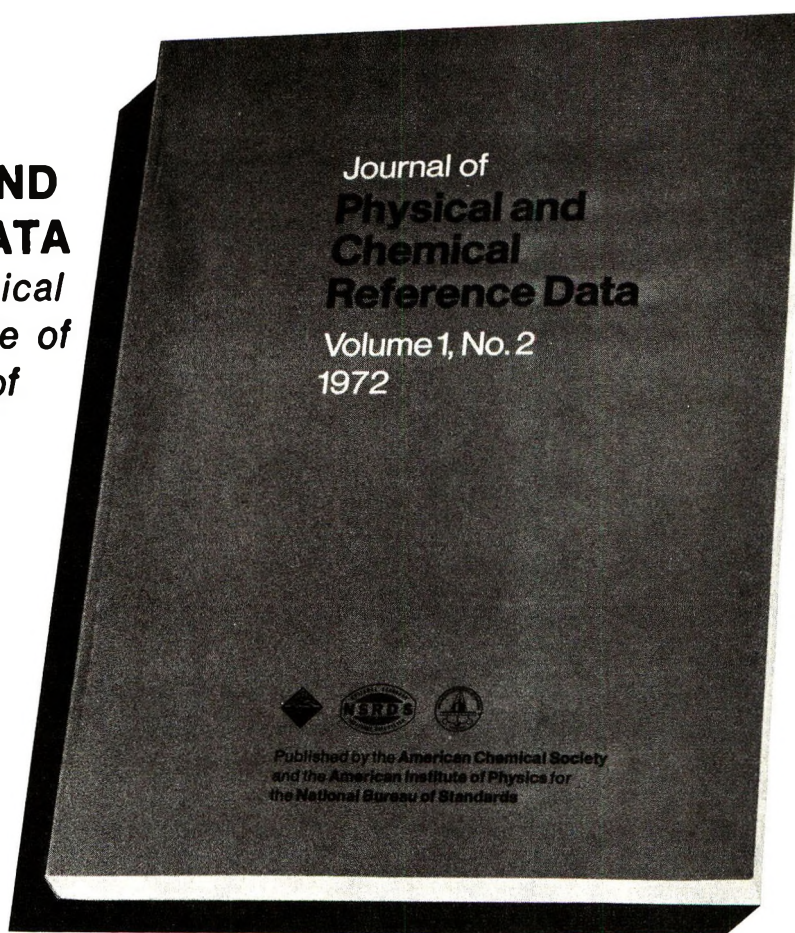
The *Journal of Physical and Chemical Reference Data* fills an important gap in the literature of the physical sciences. Its subject matter is the quantitative numerical data of physics and chemistry. As the new publication vehicle of the National Standard Reference Data System, the *Journal* will contain carefully evaluated data, with recommended values and uncertainty limits chosen by experts in each field. Critical commentary on methods of measurement and sources of error, as well as full references to the original literature, will be an integral part of each compilation.

Examples of some of the critical compilations scheduled for publication in the four issues of Volume 1 (1972) include:

- Tables of Molecular Vibrational Frequencies, Part 5, T. Shimanouchi
- Gaseous Diffusion Coefficients, by T. R. Marrero and E. A. Mason
- The Spectrum of Molecular Oxygen, by P. Krupenie
- Thermal Conductivity of the Elements, by C. Y. Ho, R. W. Powell and P. E. Liley
- Selected Values of Critical Supersaturation for Nucleation of Liquids from the Vapor, by G. M. Pound
- Gas Phase Reaction Kinetics of the Hydroxyl Radical, by W. E. Wilson, Jr.
- Selected Values of Heats of Combustion and Heats of Formation of Organic Compounds Containing the Elements CHNOPS, by E. S. Domalski
- Microwave Spectra of Molecules of Astrophysical Interest: Formaldehyde, Formamide, Thio-Formaldehyde, by D. R. Johnson, F. J. Lovas and W. H. Kirchhoff

Future compilations are expected to cover areas such as the following:

Band gaps in semiconductors  
Nuclear moments  
Atomic energy levels and transition probabilities  
Diffusion in metals  
Electron swarm data  
Elastic constants of metals  
Surface tension of liquids  
Properties of molten salts  
Activity coefficients of electrolytes  
Equation of state of atmospheric gases  
Ionization and appearance potentials



The *Journal of Physical and Chemical Reference Data* is intended to be a definitive source of reliable data on physical and chemical properties. Just fill in the order form at the bottom of this page to receive this invaluable reference source.

**JOURNAL OF PHYSICAL AND CHEMICAL REFERENCE DATA  
AMERICAN CHEMICAL SOCIETY  
1155 Sixteenth Street, N.W.  
Washington, D.C. 20036**

Yes, I would like to receive the JOURNAL OF PHYSICAL AND CHEMICAL REFERENCE DATA at the one-year rate checked below:

	U.S.	Canada	PUAS	Other Countries
AIP and ACS members	\$20.00	\$20.00	\$23.00	\$23.00
Nonmembers	\$60.00	\$60.00	\$63.00	\$63.00

Bill me  Bill company  Payment enclosed

Name \_\_\_\_\_

Street \_\_\_\_\_ Home   
Business

City \_\_\_\_\_ State \_\_\_\_\_ Zip \_\_\_\_\_

JP 72



Hyperfiltration in Charged Membranes. Prediction of Salt Rejection from Equilibrium Measurements	E. Hoffer* and O. Kedem	3638
Oxidation Kinetics of 2-Dimethylaminoethanethiol Hydrochloride by Ferricyanide Ion in Acid Medium	R. K. Chohan, B. P. Sinha, and R. C. Kapoor*	3641
Kinetics of Oxygen Reduction on Graphite Cobalt-Iron Oxide Electrodes with Coupled Heterogeneous Chemical Decomposition of H <sub>2</sub> O <sub>2</sub>	J. R. Goldstein and A. C. C. Tseung*	3646
Dissolution of Copper in Weakly Acidic Solutions	A. J. Read	3656
Sodium and Magnesium Sulfate Ion Pairing: Evidence from Raman Spectroscopy	Francis P. Daly, Chris W. Brown,* and Dana R. Kester	3664
Quenching of the Excited States of Benzene and Substituted Benzenes by Olefins	G. Das Gupta and D. Phillips*	3668

#### COMMUNICATIONS TO THE EDITOR

Ultraviolet Absorption Spectra of Polyphosphate Solutions	M. Bennoson and D. J. Williams*	3673
On the Alleged Resolution of an Infrared Band of HDO	Paul A. Giguère	3675
Concerning the Direct Effect in the Radiolysis of 0.4 M Sulfuric Acid	B. Lesigne,* C. Ferradini, and J. Pucheault	3676



## AUTHOR INDEX

- |  |  |  |   |  |
|--|--|--|---|--|
| Anderson, J. L., 3603<br>Beachell, H. C., 3545<br>Bennozon, M., 3673<br>Bock, C. M., 3597<br>Brinn, I., 3558<br>Brown, C. W., 3664<br><br>Caruso, J. A., 3618<br>Chohan, R. K., 3641<br>Cooke, N. H. C., 3563<br><br>Daly, F. P., 3664<br>Das Gupta, G., 3668<br>DeMore, W. B., 3527<br>Dickinson, C., 3597<br>Drakenberg, T., 3582<br>Dubois, J. E., 3554 | Durig, J. R., 3591<br>Eller, P. M. P., 3618<br>Fehlner, T. P., 3532<br>Ferradini, C., 3676<br>Forsén, S., 3582<br>Froehlich, P. M., 3566<br><br>Garnier, F., 3554<br>Giguère, P. A., 3675<br>Goldstein, J. R., 3646<br>Guglielmetti, R., 3554<br><br>Hackman, E. E., III,<br>3545<br>Hersh, L. S., 3633<br>Hesser, H. H., 3545<br>Hoffer, E., 3638 | Holden, J. R., 3597<br>Jaćimović, L., 3625<br>Kapoor, R. C., 3641<br>Kaufman, M., 3586<br>Kedem, O., 3638<br>Kester, D. R., 3664<br>Kuck, V. J., 3570<br>Kurylo, M. J., 3518<br><br>Lesigne, B., 3676<br><br>Mains, G. J., 3538<br>Mientienne, F., 3554<br>Metzger, J., 3554<br>Morrison, H. A., 3566<br><br>Nichols, C., 3571 | Niki, T., 3538<br><br>Phillips, D., 3668<br>Pucheault, J., 3676<br><br>Read, A. J., 3656<br>Rosenberg, J. L., 3558<br>Rowland, F. S., 3509<br><br>Safarik, I., 3613<br>Samat, A., 3554<br>Schatz, G., 3586<br>Sellers, N. G., 3618<br>Sevilla, M. D., 3571,<br>3577<br>Sinha, B. P., 3641<br>Sloan, A. E., 3591<br>Solomon, B. S., 3563<br>Stevović, J., 3625 | Strausz, O. P., 3613<br><br>Teter, M. P., 3633<br>Tseung, A. C. C., 3646<br><br>Van Paemel, C., 3571,<br>3577<br>Veljković, S., 3625<br><br>Wasserman, E., 3570<br>Williams, D. J., 3673<br>Williams, R. L., 3509<br>Witt, J. D., 3591<br><br>Yager, W. A., 3570<br><br>Zorman, G., 3577 |
|--|--|--|---|--|

In papers with more than one author the name of the author to whom inquiries about the paper should be addressed is marked with an asterisk in the by-line.



# NOTICE TO AUTHORS

---

## I. General Considerations

*The Journal of Physical Chemistry* is devoted to reporting both experimental and theoretical research dealing with fundamental aspects of physical chemistry. Space limitations necessitate giving preference to research articles dealing with previously unanswered basic questions in physical chemistry. Acceptable topics are those of general interest to physical chemists, especially work involving new concepts, techniques, and interpretations. Research that may lead to reexaminations of generally accepted views is, of course, welcome.

Authors reporting data should include an interpretation of the data and its relevance to the theories of the properties of matter. However, the discussion should be concise and to the point and excessive speculation is to be discouraged. Papers reporting redeterminations of existing data will be acceptable only if there is reasonable justification for repetition: for example, if the more recent or more accurate data lead to new questions or to a reexamination of well known theories. Manuscripts that are essentially applications of chemical data or reviews of the literature are, in general, not suitable for publication in *The Journal of Physical Chemistry*. Detailed comparisons of methods of data analysis will be considered only if the paper also contains original data, or if such comparison leads to a genesis of new ideas.

Authors should include an introductory statement outlining the scientific rationale for the research. The statement should clearly specify the questions for which answers are sought and the connection of the present work with previous work in the field. All manuscripts are subject to critical review. It is to be understood that the final decision relating to a manuscript's suitability rests solely with the editors.

Symposium papers are sometimes published as a group, but only after special arrangement with the editor.

Authors' attention is called to the "Handbook for Authors," available from the Special Issues Sales Department, American Chemical Society, 1155 Sixteenth St., N.W., Washington, D. C. 20036, in which pertinent material is to be found.

## II. Types of Manuscripts

*The Journal of Physical Chemistry* publishes two types of manuscripts: *Articles* and *Communications*.

A. *Articles* should cover their subjects with thoroughness, clarity, and completeness. However, authors should also strive to make their *Articles* as concise as possible, avoiding unnecessary historical background. Abstracts to *Articles* should be brief—300 words is a maximum—and should serve to summarize the significant data and conclusions. The abstract should convey the essence of the *Article* to the reader.

B. *Communications* are of two types, *Letters* and *Comments*. Both types are restricted to three-quarters of a page (750 words or the equivalent) including tables, figures, and text, and both types of *Communications* are

subject to critical review, but special efforts will be made to expedite publication.

*Letters* should report preliminary results whose immediate availability to the scientific community is deemed important, and whose topic is timely enough to justify the double publication that usually results from the publication of a *Letter*.

*Comments* include significant remarks on the work of others. The editors will generally permit the authors of the work being discussed to reply.

The category of *Notes* has been discontinued since the handling of such manuscripts was precisely the same as that of *Articles* save for the requirement of an Abstract, and since even a short *Article* will need an Abstract ultimately, it seems as well to ask the author to provide this. Short *Articles* will of course continue to be welcome contributions.

## III. Introduction

All manuscripts submitted should contain brief introductory remarks describing the purpose of the work and giving sufficient background material to allow the reader to appreciate the state-of-knowledge at the time when the work was done. The introductory remarks in an *Article* should constitute the first section of the paper and should be labeled accordingly. In *Communications*, the introductory material should not be in such a separate section. To judge the appropriateness of the manuscript for *The Journal of Physical Chemistry*, the editors will place considerable weight on the author's intentions as stated in the Introduction.

## IV. Functions of Reviewers

The editors request the scientific advice of reviewers who are active in the area of research covered by the manuscript. The reviewers act only in an advisory capacity and the final decision concerning a manuscript is the responsibility of the editors. The reviewers are asked to comment not only on the scientific content, but also on the manuscript's suitability for *The Journal of Physical Chemistry*. With respect to *Communications*, the reviewers are asked to comment specifically on the urgency of publication. Authors are encouraged to suggest, when submitting a manuscript, names of scientists who could give a disinterested and informed and helpful evaluation of the work. All reviews are anonymous and the reviewing process is most effective if reviewers do not reveal their identities to the authors. An exception arises in connection with a manuscript submitted for publication in the form of a comment on the work of another author. Under such circumstances the first author will, in general, be allowed to review the communication and to write a rebuttal, if he so chooses. The rebuttal and the original communication may be published together in the same issue of the journal. Revised manuscripts are generally sent back to the original reviewers, who are asked to comment on the revisions. If only minor revisions are involved, the editors examine the revised manuscript in light of



the recommendations of the reviewers without seeking further opinions. For the convenience of reviewers, authors are advised to indicate clearly, either in the manuscript or in a covering letter, the specific revisions that have been made.

## V. Submission of Manuscripts

All manuscripts must be submitted in triplicate to expedite handling. Manuscripts must be typewritten, double-spaced copy, on  $8\frac{1}{2} \times 11$  in. paper. Legal sized paper is not acceptable. Authors should be certain that copies of the manuscript are clearly reproduced and readable. Authors submitting figures must include the original drawings or photographs thereof, plus three xerographic copies for review purposes. These reproductions of the figures should be on  $8\frac{1}{2} \times 11$  in. paper. Graphs must be in black ink on white or blue paper. Lettering at the sides of graphs may be penciled in and will be typeset. Figures and tables should be held to a minimum consistent with adequate presentation of information. All original data which the author deems pertinent must be submitted along with the manuscript. For example, a paper reporting a crystal structure should include structure factor tables for use by the reviewers.

Footnotes and references to the literature should be numbered consecutively within the paper; the number should also be placed in parentheses in the left margin opposite the line in which the reference first appears. A complete list of references should appear at the end of the paper. Initials of the authors referred to in the citations should be included in the complete reference at the back of the paper. Nomenclature should conform to that used in *Chemical Abstracts* and mathematical characters should be underlined for italics, Greek letters should be annotated, and subscripts and superscripts clearly marked.

Papers should not depend for their usefulness on unpublished material, and excessive reference to material in press is discouraged. References not readily available (*e.g.*, private technical reports, preprints, or articles in press) that are necessary for a complete review of the paper must be included with the manuscript for use by the reviewers.

## VI. Revised Manuscripts

A manuscript sent back to an author for revision should be returned to the editor within 6 months; otherwise it will be considered withdrawn and treated as a new manuscript when and if it is returned. Revised manuscripts returned to the editor must be submitted in triplicate and all changes should be made by typewriter. Unless the changes are very minor, all pages affected by revision must be retyped. If revisions are so extensive that a new typescript of the manuscript is necessary, it is requested that a copy of the original manuscript be submitted along with the revised one.

## VII. Supplementary Material

From time to time manuscripts involve extensive tables, graphs, spectra, mathematical material, or other "supplementary material" which, though of value to the specialized reader who needs all the data or all the detail, does not help and often hinders the effective presentation of the work being reported. The Ameri-

can Chemical Society has instituted a policy of including such supplementary material in the *microfilm* editions of its journals, which are available in many scholarly libraries; in addition, interested readers will be able to obtain the microfilm material directly at nominal cost. Authors are encouraged to make use of this resource, in the interests of shorter articles (which mean more rapid publication) and clearer, more readable presentation.

Supplementary material for inclusion in the microfilm edition should accompany a manuscript at the time of its original submission to an editor. It should be clipped together and attached at the end of the manuscript, along with a slip of paper clearly indicating that the material is "supplementary material for the microfilm edition." A footnote should appear in the paper indicating the nature of the supplementary material and the means by which the interested reader might be able to obtain copies of the data without use of the microfilm edition itself. The following is an example:

(3) Listings of structure factors, coordinates, and anisotropic temperature factors will appear following these pages in the microfilm edition of this volume of the journal. Single copies may be obtained from the Business Operations Office, Books and Journals Division, American Chemical Society, 1155 Sixteenth St., N.W., Washington, D. C. 20036. Remit check or money order for \$0.00 for photocopy or \$2.00 for microfiche, referring to code number JPC-00-0000.

The amount of money to be indicated in the blanks will be filled in by the Editorial Office at Easton, Pa., after the acceptance of an article.

## VIII. Proofs and Reprints

Galley proofs, original manuscript, cut copy, and reprint order form are sent by the printer directly to the author who submitted the manuscript. The attention of the authors is directed to the instructions which accompany the proof, especially the requirement that all corrections, revisions, and additions be entered on the proof and not on the manuscript. Proofs should be checked against the manuscript (in particular all tables, equations, and formulas, since this is not done by the editor) and returned as soon as possible. No paper is released for printing until the author's proof has been received. Alterations in an article after it has been set in type are made at the author's expense, and it is understood that by entering such alterations on proofs the author agrees to defray the cost thereof. The filled-out reprint form must be returned with the proof, and if a price quotation is required by the author's organization a request for it should accompany the proof. Since reprinting is generally done from the journal press forms, all orders must be filed before press time. None can be accepted later, unless a previous request has been made to hold the type. Reprint shipments are made a month or more after publication, and bills are issued by the printer subsequent to shipment. Neither the editors nor the Washington office keeps any supply of reprints. Therefore, only the authors can be expected to meet requests for single copies of papers.

A page charge is assessed to cover in part the cost of publication. Although payment is expected, it is not a condition for publication. Articles are accepted or rejected only on the basis of merit, and the editor's decision to publish the paper is made before the charge is assessed. The charge per journal page is \$50.



# THE JOURNAL OF PHYSICAL CHEMISTRY

Registered in U. S. Patent Office © Copyright, 1972, by the American Chemical Society

VOLUME 76, NUMBER 24 NOVEMBER 23, 1972

## Reactions of Fluorine-18 Atoms with Ethylene<sup>1</sup>

by Ronald L. Williams and F. S. Rowland\*

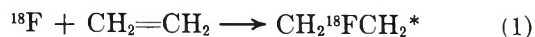
Department of Chemistry, University of California, Irvine, California 92664 (Received June 26, 1972)

Publication costs assisted by Division of Research, U. S. Atomic Energy Commission

Energetic <sup>18</sup>F atoms formed by the <sup>19</sup>F(n,2n)<sup>18</sup>F nuclear reaction can undergo both hot and thermal addition reactions with ethylene to form excited CH<sub>2</sub><sup>18</sup>FCH<sub>2</sub>\* radicals. The hot reactions of <sup>18</sup>F can be almost entirely suppressed by moderation with SF<sub>6</sub> or CF<sub>4</sub>, and the excited CH<sub>2</sub><sup>18</sup>FCH<sub>2</sub>\* radicals exhibit normal stabilization-decomposition (to CH<sup>18</sup>F=CH<sub>2</sub> + H) behavior *vs.* pressure for monoenergetically excited radicals. The stabilized radicals are observed as CH<sub>3</sub>CH<sub>2</sub><sup>18</sup>F after reaction with scavenger HI. The half-stabilization pressures for SF<sub>6</sub> and CF<sub>4</sub> are 80 and 135 Torr, respectively, and are essentially unchanged for moderator fractions >0.75. The difference in half-stabilization pressures indicates that SF<sub>6</sub> is more efficient, per molecule, in removing the excitation energy of CH<sub>2</sub><sup>18</sup>FCH<sub>2</sub>\* radicals. In less-moderated systems, hot reactions are also observed: (a) the formation of CH<sup>18</sup>F=CH<sub>2</sub> by a more energetic route; (b) the formation of CH<sup>18</sup>F from secondary decomposition of CH<sup>18</sup>F=CH<sub>2</sub>; and (c) the formation of CH<sub>2</sub><sup>18</sup>F by decomposition of CH<sub>2</sub><sup>18</sup>FCH<sub>2</sub>\*. The rupture of the C-C bond in CH<sub>2</sub><sup>18</sup>FCH<sub>2</sub>\* probably occurs predominantly after capture of <sup>18</sup>F at high-impact parameters with consequent high-angular momentum in the excited radical. Similarly, substitution of <sup>18</sup>F/H at high-impact parameters is postulated to lead to the C=C bond rupture in CH<sup>18</sup>F=CH<sub>2</sub>\*.

### Introduction

Study of the reactions of atomic fluorine with various olefins has not progressed very rapidly, largely because of the experimental difficulties involved with the handling of F<sub>2</sub>, HF, and other highly reactive fluorinated reactants and products. Valuable information concerning the elementary processes involved in the reactions of atomic fluorine with ethylene has been obtained as a by-product to the use of C<sub>2</sub>H<sub>4</sub> as a scavenger for <sup>18</sup>F atoms formed by the <sup>19</sup>F(γ,n)<sup>18</sup>F reaction in CF<sub>4</sub>.<sup>2,3</sup> In this work, the <sup>18</sup>F atoms which failed to react with CF<sub>4</sub> were effectively removed by addition to ethylene, as in (1).



The subsequent fate of these excited CH<sub>2</sub><sup>18</sup>FCH<sub>2</sub>\* radicals was then determined by a pressure-dependent competition between collisional stabilization (eq 2) and decomposition by hydrogen atom loss (eq 3).



The stabilized CH<sub>2</sub><sup>18</sup>FCH<sub>2</sub> radical was then detected after reaction with scavenger molecular I<sub>2</sub> as CH<sub>2</sub><sup>18</sup>FCH<sub>2</sub>I, as in (4).



The pressure dependence of the CH<sup>18</sup>F=CH<sub>2</sub>/CH<sub>2</sub><sup>18</sup>FCH<sub>2</sub>I ratio in excess CF<sub>4</sub> further showed that the excited CH<sub>2</sub><sup>18</sup>FCH<sub>2</sub>\* radicals were almost uniformly monoenergetic, indicating that the radicals were excited chiefly by the exothermicity of the <sup>18</sup>F atom addition with small or negligible additional contribution from extra translational energy of the <sup>18</sup>F atom. A similar F atom addition-plus-decomposition mechanism has been invoked in explanation of C<sub>2</sub>H<sub>3</sub>F as a product from the photolysis of ONF in the presence of C<sub>2</sub>H<sub>4</sub>.<sup>4</sup> Very

(1) This research was supported by A.E.C. Contract No. AT-(04-3)-34, Agreement No. 126.

(2) N. Colebourne, J. F. J. Todd, and R. Wolfgang, "Chemical Effects of Nuclear Transformations," Vol. 1, International Atomic Energy Agency, Vienna, 1965, p 149.

(3) J. F. J. Todd, N. Colebourne, and R. Wolfgang, *J. Phys. Chem.*, **71**, 2875 (1967).

(4) A. L. Flores and B. deB. Darwent, *ibid.*, **73**, 2203 (1969).

recent studies with crossed beams of F atoms (from thermal dissociation of F<sub>2</sub>) and C<sub>2</sub>H<sub>4</sub> or C<sub>2</sub>D<sub>4</sub> have convincingly shown that the substitution of F for H (or D) proceeds through a long-lived intermediate, C<sub>2</sub>H<sub>4</sub>F (or C<sub>2</sub>D<sub>4</sub>F).<sup>5</sup> The relative kinetic energy of F atoms and ethylene molecules averaged only 1.98 and 1.94 kcal/mol, respectively, with C<sub>2</sub>H<sub>4</sub> and C<sub>2</sub>D<sub>4</sub> in these experiments. We have recently reported the results of some experiments on fluorine atom additions to olefins and acetylene, using <sup>18</sup>F atoms generated at tracer levels by the nuclear reaction <sup>19</sup>F(n,2n)<sup>18</sup>F,<sup>6-8</sup> and obtained some information on reactions with ethylene in the process. We have now carried out a more extensive study of the reactions of <sup>18</sup>F atoms with ethylene with careful attention to the effects of several parameters.

First, we have utilized HI as the scavenger molecule instead of I<sub>2</sub>, because of the much greater ease of radio gas chromatographic determination of its scavenged radical product, CH<sub>3</sub>CH<sub>2</sub><sup>18</sup>F, than of the iodo compound formed in (4). In general, our measurements of the



yields for <sup>18</sup>F reaction with ethylene in HI-scavenged excess CF<sub>4</sub> are in excellent agreement with the earlier I<sub>2</sub>-scavenged experiments.

Secondly, subsequent investigations of the chemistry of energetic <sup>18</sup>F atom reactions with CF<sub>4</sub> have shown the presence of appreciable amounts of CF<sup>18</sup>F indicative of (a) extensive decomposition of excited CF<sub>3</sub><sup>18</sup>F\* molecules,<sup>9,10</sup> and as a corollary (b) that CF<sub>4</sub> is not quite as inert a reactant as originally believed. Accordingly, most of our experiments have been carried out with SF<sub>6</sub> as the nearly inert source of <sup>18</sup>F atoms. Approximately 1% of the <sup>18</sup>F atoms formed in SF<sub>6</sub> react while translationally "hot" to form SF<sub>5</sub><sup>18</sup>F, and the remainder are available for reaction at much lower energies with minor components mixed with the SF<sub>6</sub> moderator.<sup>6-8</sup>

Finally, we have been concerned with CH<sub>2</sub>=CH<sub>2</sub> as the primary substrate, and have made measurements in excess C<sub>2</sub>H<sub>4</sub>, thereby permitting observation of both thermal and hot reactions with the substrate molecule.

### Experimental Section

A detailed discussion of most of the experimental aspects of <sup>18</sup>F recoil chemistry as conducted in this laboratory has recently been presented.<sup>6-8</sup> Our present experiments have been carried out with gas samples in quite similar manner, and only a brief summary is given here. As in earlier systems, the sample irradiation temperature could only be 10° because of the present design characteristics of the target area of the fast neutron generator.

The <sup>18</sup>F atoms were formed by the <sup>19</sup>F(n,2n)<sup>18</sup>F nuclear reaction on the fluorinated gaseous substrates SF<sub>6</sub> or CF<sub>4</sub> during the irradiation of 15-ml glass ampoules with fast neutrons produced by a Kaman A711

neutron generator. The total absolute <sup>18</sup>F production from SF<sub>6</sub> or CF<sub>4</sub> was evaluated with an accuracy of ±10% using the external Teflon-sleeve monitor system. Loss of <sup>18</sup>F from the gas phase by recoil into the walls of the glass bulbs is unimportant (<10%) at approximately 1000 Torr and progressively less important at higher pressures.

Research grade chemicals were used in these experiments: ethylene, Phillips; methane, sulfur hexafluoride, hydrogen iodide, and tetrafluoromethane, all Matheson. These gases were not further purified except by the removal of polymerization inhibitors when present by distillation from -78° baths, and by rigorous degassing *in vacuo*. Samples were prepared by standard vacuum line procedures using a grease-free system. Hydrogen iodide pressures and low-pressure hydrocarbon components were measured in a mercury-free portion of the vacuum system using a spiral-gauge manometer.

The maximum pressure in the ampoules was effectively limited to about 3500 Torr by the characteristics of the glass vacuum line and the ampoules themselves. With the ampoule diameter limited to 2 cm by the irradiation geometry requirements of the neutron generator, the lower pressure limit for experimentation was determined by increasing recoil loss into the walls at lower pressures. The decrease in statistical accuracy at lower pressures is also significant for products with low percentage yields since the total <sup>18</sup>F production is linearly proportional to the pressure of the fluorinated substrate in the system.

The <sup>18</sup>F-labeled products were analyzed by radio gas chromatography with an external flow proportional counter detector.<sup>6,11</sup> Chromatographic separation of the products observed in these systems is routinely carried out with dimethylsulfolane or di-*n*-butyl phthalate columns 50 or 100 ft in length, and with silicone oil columns 25 or 50 ft in length.

A typical separation of the radioactive products observed from <sup>18</sup>F reaction with HI-scavenged C<sub>2</sub>H<sub>4</sub> in excess SF<sub>6</sub> is shown in the upper half of Figure 1. The corresponding radio gas chromatogram without scavenger present (lower half of Figure 1) shows essentially unchanged yields of SF<sub>5</sub><sup>18</sup>F and CH<sup>18</sup>F=CH<sub>2</sub>, while CH<sub>3</sub><sup>18</sup>F and C<sub>2</sub>H<sub>5</sub><sup>18</sup>F are not formed at all without HI as an H atom donor. In the absence of HI, an additional minor radioactivity peak from c-C<sub>3</sub>H<sub>5</sub><sup>18</sup>F is found in

(5) J. M. Parson and Y. T. Lee, *J. Chem. Phys.*, **56**, 4658 (1972).

(6) T. Smail, G. Miller, and F. S. Rowland, *J. Phys. Chem.*, **74**, 3464 (1970).

(7) T. Smail, R. S. Iyer, and F. S. Rowland, *J. Amer. Chem. Soc.*, **94**, 1041 (1972).

(8) R. L. Williams and F. S. Rowland, *ibid.*, **94**, 1047 (1972).

(9) Y.-N. Tang, T. Smail, and F. S. Rowland, *ibid.*, **91**, 2130 (1969).

(10) C. F. McKnight and J. W. Root, *J. Phys. Chem.*, **73**, 4430 (1969).

(11) T. Smail and F. S. Rowland, *ibid.*, **74**, 1866 (1970).



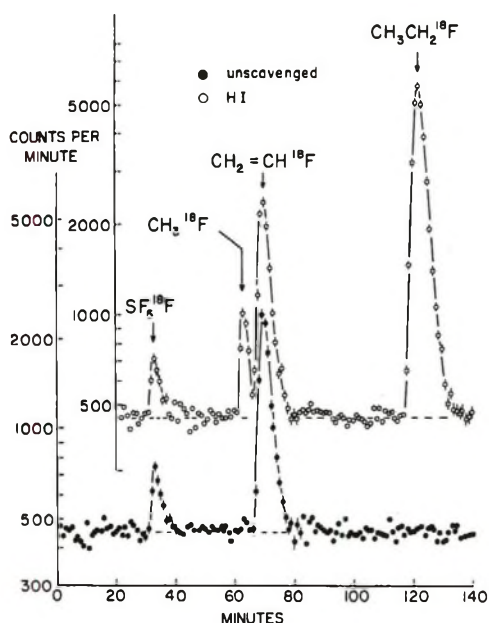


Figure 1. Radio gas chromatographic separation of  $^{18}\text{F}$ -labeled products formed by  $^{18}\text{F}$  reactions with  $\text{C}_2\text{H}_4$  in mixture with  $\text{SF}_6$  (analysis on 100-ft DMS column), mixture composition (in Torr): (●)  $\text{SF}_6$  730,  $\text{C}_2\text{H}_4$  730, HI 0; (○)  $\text{SF}_6$  740,  $\text{C}_2\text{H}_4$  730, HI 40.

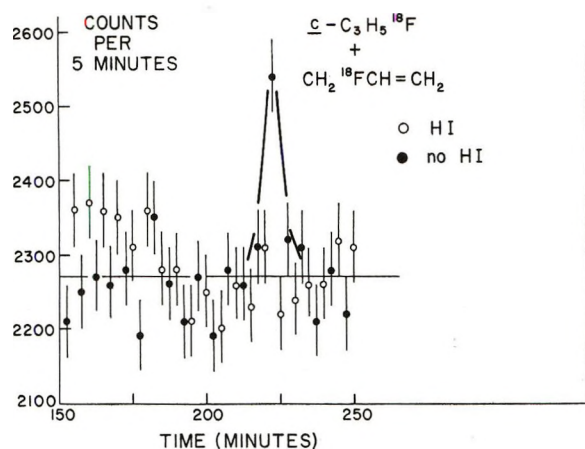


Figure 2. Radio gas chromatographic separation of  $c\text{-C}_3\text{H}_5^{18}\text{F}$  formed by  $^{18}\text{F}$  reactions with  $\text{C}_2\text{H}_4$  in absence of HI scavenger. (Analysis with two 50-ft DMS columns in series, with peaks through  $\text{C}_2\text{H}_5^{18}\text{F}$  passing through all 100 ft, see Figure 1. After  $\text{C}_2\text{H}_5^{18}\text{F}$ , the second 50-ft column was by-passed, and the peaks still in the first 50-ft column were allowed to emerge directly from it into the counter.) Mixture compositions and symbols as in Figure 1.

$\text{C}_2\text{H}_4/\text{SF}_6$  mixtures, as illustrated in Figure 2. The  $c\text{-C}_3\text{H}_5^{18}\text{F}$  radioactivity is not separated from  $\text{CH}_2^{18}\text{F}\text{-CH}=\text{CH}_2$  on the dimethylsulfolane column used in Figure 2. Separate measurements with the butyl phthalate column confirm that  $c\text{-C}_3\text{H}_5^{18}\text{F}$  is the major component of this minor peak; the yield of  $\text{CH}_2^{18}\text{F}\text{-CH}=\text{CH}_2$ , if present, is so low that it is not statistically significant.

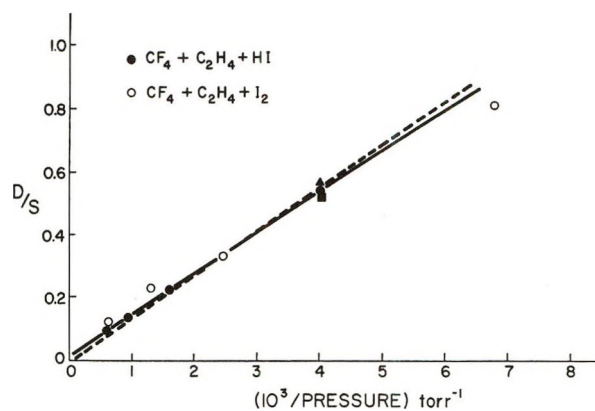


Figure 3. Ratio of decomposition/stabilization vs.  $(\text{pressure})^{-1}$  for  $^{18}\text{F}$ -labeled products from  $^{18}\text{F}$  reactions with  $\text{C}_2\text{H}_4$  in excess  $\text{CF}_4$  (all samples contained  $\text{CF}_4/\text{C}_2\text{H}_4$  in the approximate ratio 18/1): ○,  $\text{C}_2\text{H}_3^{18}\text{F}/\text{CH}_2\text{ICH}_2^{18}\text{F}$  with  $\text{I}_2$  as scavenger at  $25^\circ$ ; data of Wolfgang *et al.*, ref 2 and 13; solid points,  $\text{C}_2\text{H}_3^{18}\text{F}/\text{CH}_3\text{CH}_2^{18}\text{F}$  with HI as scavenger at  $10^\circ$  (this work); ratios, HI/ $\text{C}_2\text{H}_4$  (●), 0.2; (▲) 0.5; (■) 1.0.

An additional difficulty was observed at very low pressures ( $<100$  Torr) when nominal HI concentrations of about 1 Torr were tried. Occasionally, no  $\text{CH}_3\text{-CH}_2^{18}\text{F}$  was observed, and in other cases, the amount was variable for apparently duplicate samples. In these experiments, the yields of  $\text{CH}^{18}\text{F}=\text{CH}_2$  showed no obvious abnormalities. It may be that wall absorption problems, variable from sample to sample, can sometimes deplete the HI when its total concentration is low.

Most of the remaining  $^{18}\text{F}$  can be found on the wall in  $\text{SF}_6\text{-C}_2\text{H}_4$  mixtures as expected for  $\text{H}^{18}\text{F}$ , and has been determined in a few experiments. In most instances here, however, no separate determination was made of the  $\text{H}^{18}\text{F}$  yield since quantitative yield comparisons are less accurate than those involving the chromatographically separable components.

All of the pressure measurements quoted in these experiments were those performed in filling the bulbs at room temperature (about  $23^\circ$ ) and have not been corrected for the lower actual temperature (about  $10^\circ$ ) and, therefore, pressure during the irradiation itself. The pressures for stabilization of one-half of the  $\text{CH}_2^{18}\text{F}\text{-CH}_2$  radicals can be converted to moles/liter of  $\text{SF}_6$  or  $\text{CF}_4$  on the basis that 760 Torr pressure is equivalent to molar volumes of about 24.3 M.

## Results and Discussion

**$\text{CF}_4\text{-C}_2\text{H}_4$  Mixtures.** A set of experiments has been performed with 18/1  $\text{CF}_4/\text{C}_2\text{H}_4$  mixtures, using HI as the radical scavenger. The moderator ratio was chosen to match that used in the earlier experiments of Colebourne, Todd, and Wolfgang. The yields of the observed volatile products from our experiments are shown in Table I and Figure 3 for some typical experiments. The labeled  $\text{CF}_3^{18}\text{F}$  is made by direct  $^{18}\text{F}/\text{F}$  substitution in  $\text{CF}_4$ , while  $\text{CHF}_2^{18}\text{F}$  arises from  $\text{CF}_3^{18}\text{F}$  decomposition by C-F bond break followed by HI

Table I: Volatile Radioactive Products from  $^{18}\text{F}$  Atom Reactions in Typical Mixtures of  $\text{C}_2\text{H}_4$  with  $\text{CF}_4$  or  $\text{SF}_6$ 

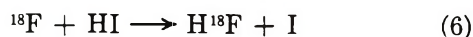
	Pressure, Torr						
	1480	570	232	3840	1570	287	94
$\text{CF}_4$							
$\text{SF}_6$							
$\text{C}_2\text{H}_4$	83	31	13	209	87	16	5
HI	17	6	2	42	17	3	1
	Product Yields, % Absolute $^{18}\text{F}$						
$\text{CF}_3^{18}\text{F}$	$2.24 \pm 0.09$	$1.90 \pm 0.17$	$2.33 \pm 0.21$				
$\text{CHF}_2^{18}\text{F}$		$0.21 \pm 0.07$	$0.22 \pm 0.17$				
$\text{CH}_3^{18}\text{F}$	$0.58 \pm 0.09$	$0.32 \pm 0.07$	$0.52 \pm 0.20$	$0.21 \pm 0.02$	$0.20 \pm 0.03$	$0.35 \pm 0.18$	
$\text{CH}^{18}\text{F}=\text{CH}_2$	$5.61 \pm 0.08$	$10.6 \pm 0.2$	$17.9 \pm 0.4$	$1.67 \pm 0.03$	$3.0 \pm 0.1$	$11.2 \pm 0.3$	$16.9 \pm 0.6$
$\text{CH}_3\text{CH}_2^{18}\text{F}$	$58.7 \pm 0.3$	$47.9 \pm 0.4$	$32.9 \pm 0.7$	$53.2 \pm 0.2$	$59.0 \pm 0.2$	$45.2 \pm 0.6$	$23.0 \pm 0.9$
$\text{SF}_5^{18}\text{F}$				$1.29 \pm 0.02$	$1.06 \pm 0.03$	$1.09 \pm 0.13$	$0.3 \pm 0.3$

Table II: Volatile Radioactive Products from  $^{18}\text{F}$  Atom Reactions in Mixtures of  $\text{CF}_4$ ,  $\text{C}_2\text{H}_4$ , and HI at 1000 Torr Total Pressure

	Pressure, Torr				
	945	919	946	951	956
$\text{CF}_4$					
$\text{C}_2\text{H}_4$	52	61	45	23	12
HI	11	30	45	23	12
	Product Yields, % Absolute $^{18}\text{F}$ Production				
$\text{CF}_3^{18}\text{F}$	$2.08 \pm 0.07$	$1.82 \pm 0.07$	$1.94 \pm 0.07$	$1.83 \pm 0.07$	$1.70 \pm 0.06$
$\text{CHF}_2^{18}\text{F}$	$0.12 \pm 0.04$				
$\text{CH}_3^{18}\text{F}$	$0.44 \pm 0.06$	$0.82 \pm 0.08$	$1.01 \pm 0.06$	$0.68 \pm 0.08$	$0.52 \pm 0.07$
$\text{CH}^{18}\text{F}=\text{CH}_2$	$7.45 \pm 0.12$	$6.54 \pm 0.13$	$5.48 \pm 0.12$	$5.45 \pm 0.12$	$4.80 \pm 0.12$
$\text{CH}_3\text{CH}_2^{18}\text{F}$	$53.2 \pm 0.3$	$49.8 \pm 0.4$	$42.1 \pm 0.3$	$40.4 \pm 0.3$	$36.4 \pm 0.3$
$D/S, (\text{CH}^{18}\text{F}=\text{CH}_2)/$ $(\text{CH}_3\text{CH}_2^{18}\text{F})$	$0.140 \pm 0.003$	$0.131 \pm 0.003$	$0.130 \pm 0.003$	$0.135 \pm 0.003$	$0.132 \pm 0.004$

scavenging of  $\text{CF}_2^{18}\text{F}$ . The  $\text{CH}^{18}\text{F}=\text{CH}_2$  and  $\text{CH}_3\text{-CH}_2^{18}\text{F}$  are the decomposition and stabilization products, respectively, from reactions 2, 3, and 5. The  $\text{CH}_3^{18}\text{F}$  is a hot product, discussed in detail later.

The general lack of dependence of the measured  $D/S$  ratio upon  $\text{C}_2\text{H}_4$  and HI concentrations is shown by the set of data in Table II, gathered at about 1000 Torr total pressure. These data are completely consistent with the assumption that almost all of the  $\text{CH}_2^{18}\text{FCH}_2^*$  radicals were formed by addition to ethylene of essentially thermal  $^{18}\text{F}$  atoms. At any HI/ $\text{C}_2\text{H}_4$  ratio  $\geq 0.1$ , sufficient HI is present to capture all of the stabilized  $\text{CH}_2^{18}\text{FCH}_2$  radicals. As the ratio of HI/ $\text{C}_2\text{H}_4$  is increased, however, a smaller percentage of  $^{18}\text{F}$  atoms are captured by  $\text{C}_2\text{H}_4$  because of competition with reaction 1 by reaction 6.<sup>12</sup>



The data of Table I can be plotted in the usual manner for chemically activated species, *i.e.*, decomposition/stabilization ( $D/S$ ) *vs.* reciprocal pressure, giving a good straight line for the  $\text{CH}^{18}\text{F}=\text{CH}_2/\text{CH}_3\text{CH}_2^{18}\text{F}$  ratio as expected when the sources for both are  $\text{CH}_2^{18}\text{FCH}_2^*$  radicals with reasonably monoenergetic excitation. Our HI-scavenger data are in good agreement with the

$\text{CH}^{18}\text{F}=\text{CH}_2/\text{CH}_2^{18}\text{FCH}_2\text{I}$  ratios measured earlier in the presence of  $\text{I}_2$  scavenger by Colebourne, Todd, and Wolfgang,<sup>13</sup> as shown in Figure 3. Our best straight-line fit does not pass through zero, indicating that about 2% of the  $(\text{CH}^{18}\text{F}=\text{CH}_2 + \text{CH}_3\text{CH}_2^{18}\text{F})$  sum is actually  $\text{CH}^{18}\text{F}=\text{CH}_2$  produced by some hot process, and not by decomposition of a  $\text{CH}_2^{18}\text{FCH}_2^*$  radical activated by the addition of a *thermal*  $^{18}\text{F}$  atom to  $\text{C}_2\text{H}_4$ . Two hypothetically possible sources for this small increment of "hot"  $\text{CH}^{18}\text{F}=\text{CH}_2$  are (a) decomposition of much more highly excited  $\text{CH}_2^{18}\text{FCH}_2^*$  radicals formed by the addition of *hot*  $^{18}\text{F}$  atoms to  $\text{C}_2\text{H}_4$  and (b) direct  $^{18}\text{F}/\text{H}$  substitution without the intervention of a true radical intermediate.

The pressure for half-stabilization of these  $\text{CH}_2^{18}\text{FCH}_2^*$  radicals is  $135 \pm 10$  Torr, corresponding to an average lifetime of about  $10^{-9}$  sec. The linearity of the best fit indicates an absence of appreciable spread in the excitation energies of the decomposing radicals. However, such fits are not very sensitive to the pres-

(12) R. L. Williams and F. S. Rowland, *J. Phys. Chem.*, **75**, 2709 (1971).

(13) The data were given only in graphical form of a different kind in ref 2. The original data were kindly furnished to us by the late Professor Wolfgang and have been replotted here to facilitate direct comparison on a  $D/S$  *vs.*  $1/P$  graph.



ence of 10–30% of the radicals with energies 5–15 kcal/mol greater than the remainder, and data of our accuracy could be accommodated either with a distribution corresponding to the normal spread from thermal fluorine atoms plus thermal ethylene, or from a thermal distribution plus a minor component of moderately larger energies.

The reasonably monoenergetic nature of the excitation implies that the major source of this excitation energy is the exothermicity of the  $^{18}\text{F}$  atom addition to the olefin, with any extra translational energy of the  $^{18}\text{F}$  atom minor in comparison. The excitation energy of  $\text{CH}_2^{18}\text{FCH}_2^*$  radicals formed by addition of thermal fluorine atoms is approximately 44 kcal/mol.<sup>14–16</sup>

*Comparison of Systems Using HI and I<sub>2</sub> as Scavengers.* The comparative results of I<sub>2</sub>-scavenged and HI-scavenged  $\text{CF}_4$ - $\text{C}_2\text{H}_4$  mixtures illustrated in Figure 3 indicate reasonable quantitative agreement for two systems involving two different nuclear reactions as the  $^{18}\text{F}$  source:  $^{19}\text{F}(\gamma, n)^{18}\text{F}$  for the I<sub>2</sub> system and  $^{19}\text{F}(n, 2n)^{18}\text{F}$  for the HI system. The best straight line fit to the I<sub>2</sub> data of Figure 3 has a lesser slope (and a greater intercept) than for the HI data on the same graph. Evaluation of the graphical data of ref 2 indicates about 150 Torr as the pressure for half-stabilization in the I<sub>2</sub> system.<sup>17</sup>

Both sets of data in Figure 3 are graphed *vs.* filling pressures in the samples, *i.e.*, room temperature in each case, and hence can be directly compared even though the samples were irradiated at 25° for I<sub>2</sub>-scavenged and 10° for HI-scavenged experiments. However, the  $\text{C}_2\text{H}_4$  bath molecules have slightly less thermal energy at 10° (about 0.12 kcal/mol) than at 25°, and the  $\text{CH}_2^{18}\text{FCH}_2$  radicals should be correspondingly less energetic and have therefore a higher density for half-stabilization at the lower temperature. The actual slopes of 135 and 150 Torr in Figure 3 vary in the opposite direction; so far, we have not been able to vary our sample temperature to make direct measurements of the actual magnitude of the temperature effect on  $\text{CH}_2^{18}\text{FCH}_2$  decomposition.

*Absolute Yields in the  $\text{CF}_4$ - $\text{C}_2\text{H}_4$  System.* The emphasis in the present paper is on the reactions of  $^{18}\text{F}$  atoms with  $\text{C}_2\text{H}_4$  and not with  $\text{CF}_4$ . Nevertheless, certain discrepancies with the earlier  $\text{CF}_4$  experiments should be noted. Absolute yields of  $2.9 \pm 3$  and  $2.3 \pm 0.3\%$  were reported in  $\text{C}_2\text{H}_4/\text{I}_2$  scavenged  $\text{CF}_4$  for  $\text{CF}_3^{18}\text{F}$  and  $\text{CF}_2^{18}\text{F}$  (determined as  $\text{CF}_2^{18}\text{FI}$ ).<sup>2</sup> The data on  $\text{CF}_3^{18}\text{F}$  yield in Tables I and II indicate a yield of only about 2.0%, rather than 2.9%. The prime source of this discrepancy resides in the question of volatile yields *not* determined by radio gas chromatographic analysis.<sup>6</sup> Our summed yields of  $\text{CH}^{18}\text{F}=\text{CH}_2$  plus  $\text{C}_2\text{H}_3^{18}\text{F}$  amount to only about 65% of the total  $^{18}\text{F}$  formed, and we attribute ~30% to formation of  $\text{H}^{18}\text{F}$  by reaction with  $\text{C}_2\text{H}_4$ .

In our own experiments with  $\text{C}_2\text{H}_2$ , we have shown that substantially more organically bound  $^{18}\text{F}$  can be recovered (about 83%) than is found with  $\text{C}_2\text{H}_4$ , consistent with a much lower yield of  $\text{H}^{18}\text{F}$  from  $\text{C}_2\text{H}_2$  than from  $\text{C}_2\text{H}_4$ . We believe that the absolute yield of  $\text{CF}_3^{18}\text{F}$  from the I<sub>2</sub>-scavenged experiments would be reduced to within statistical error of our value of about 2.0%, if correction is made for  $\text{H}^{18}\text{F}$  yields equivalent to that found in our system. The apparently much greater discrepancy between the  $2.3 \pm 0.3\%$   $\text{CF}_2^{18}\text{F}$  yield as  $\text{CF}_2^{18}\text{FI}$  and the values a factor of 10 lower in Tables I and II is the result of preferential  $\text{CF}_2^{18}\text{F}$  reaction with  $\text{C}_2\text{H}_4$  rather than HI. In the absence of  $\text{C}_2\text{H}_4$ , the yield of  $\text{CHF}_2^{18}\text{F}$  from  $\text{CF}_4$  is about 1.4%, reflecting the same generally lower estimate of absolute yields in our experiments.

*SF<sub>6</sub>-C<sub>2</sub>H<sub>4</sub> Mixtures.* Experiments with a variety of mixtures have demonstrated that hot  $^{18}\text{F}$  atom reactions occur with lower yield in  $\text{SF}_6$  than in  $\text{CF}_4$ , and hence that the former has some advantages as an “inert” fluorine atom source for reactions with other substrates. The yields of observed products from typical high- and low-pressure  $\text{SF}_6$  samples are also listed in Table I and illustrated in Figures 1 and 2, while a graph of the ratio of  $\text{CH}^{18}\text{F}=\text{CH}_2/\text{CH}_3\text{CH}_2^{18}\text{F}$  yields *vs.*  $1/P$  is shown in Figure 4 for HI-scavenged 18/1  $\text{SF}_6/\text{C}_2\text{H}_4$  mixtures. The data fall onto a good straight line fit which extrapolates to an infinite pressure limit of about 1%  $\text{CH}^{18}\text{F}=\text{CH}_2$  from hot sources. The band illustrated in Figure 4 shows the limits for a pressure for half-stabilization of  $80 \pm 5$  Torr and an intercept of 0.006. Clearly, the error in the intercept could be as much as 0.005, but the slope for any intercept must correspond to a pressure for half-stabilization of about 80 Torr. Flores and Darwent also measured the stabilization of  $\text{C}_2\text{H}_4\text{F}^*$  by  $\text{SF}_6$  and found that pressures of about 100 Torr were required.<sup>4</sup> In their system, however, the  $\text{SF}_6$  may have been quenching an

(14) Since the  $\Delta H_f$  values for  $\text{CH}_2$  and most of the partially fluorinated molecules have uncertainties of  $\pm 1$ –3 kcal/mol, the  $\Delta H$  values for reactions involving them are only approximate with possible errors as large as  $\pm 3$ –5 kcal/mol. Heats of formation in kcal/mol, as given in ref 7 and 15, are

F	+18.9	$\text{CH}_2\text{F}$	-7	$\text{C}_2\text{H}_2$	+54.2
HF	-64.8	CHF	+25	$\text{C}_2\text{H}_4$	+12.5
H	+52.1	$\text{CH}_2$	+93 <sup>16</sup>	$\text{CH}_2=\text{CHF}$	-28

$\Delta H_f$  for  $\text{CH}_3\text{F}$  is -55.9 kcal/mol. Assuming that the substitution of  $\text{CH}_3$  for H has the same effect on  $\text{CH}_3\text{F}$  as on  $\text{CH}_4$ ,  $\Delta H_f(\text{C}_2\text{H}_3\text{F}) = -58$  kcal/mol. If the bond dissociation energy for  $\text{CH}_2\text{FCH}_2\text{-H}$  is 98 kcal/mol as in  $\text{C}_2\text{H}_3\text{-H}$ , then  $\Delta H_f(\text{CH}_2\text{FCH}_2)$  is -12 kcal/mol, and the addition of thermal F to  $\text{C}_2\text{H}_4$  is about 44 kcal/mol exothermic.

(15) “Selected Values of Chemical Thermodynamic Properties,” Circular 500, National Bureau of Standards, 1952.

(16) We use a value of +93 kcal/mol as our weighted average of these values: 93.9, V. H. Dibeler, *et al.*, *J. Chem. Phys.*, **42**, 3701 (1965); 94.6, W. A. Chupka and C. Lifschitz, *ibid.*, **48**, 1109 (1968); 91.9, W. A. Chupka, *ibid.*, **48**, 2337 (1968); 95.5, W. A. Chupka, J. Berkowitz, and K. M. A. Refaey, *ibid.*, **50**, 1938 (1969).

(17) This value was read from the graph of  $S/D$  *vs.*  $P$  in Figure 9 of ref 2. A  $p_{1/2}$  of 150 Torr corresponds to approximately 4.7 l./mol at 25°, and not the value of 10.7 l./mol listed in ref 2.

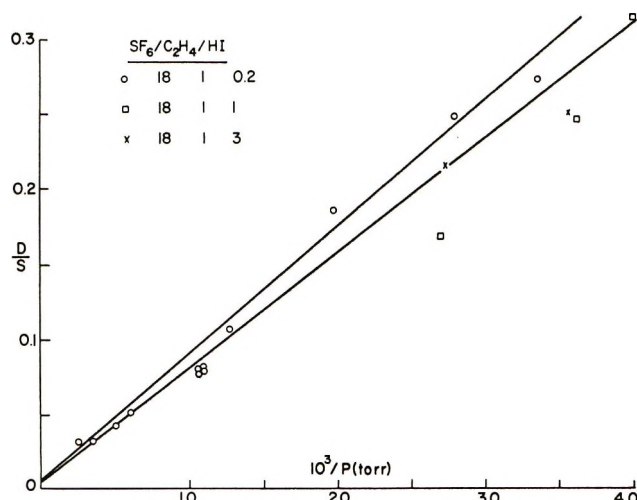


Figure 4. Ratio of decomposition/stabilization *vs.* (pressure)<sup>-1</sup> for <sup>18</sup>F-labeled products from <sup>18</sup>F reactions with C<sub>2</sub>H<sub>4</sub> in excess SF<sub>6</sub> (all samples contained SF<sub>6</sub>/C<sub>2</sub>H<sub>4</sub> in the approximate ratio 18/1):  $D/S = C_2H_3^{18}F/C_2H_5^{18}F$ ; HI/C<sub>2</sub>H<sub>4</sub> ratios: (○) 0.2, (□) 1.0, (×) 3.0. The slopes illustrated cover the range of pressures for half-stabilization between 75 and 85 Torr.

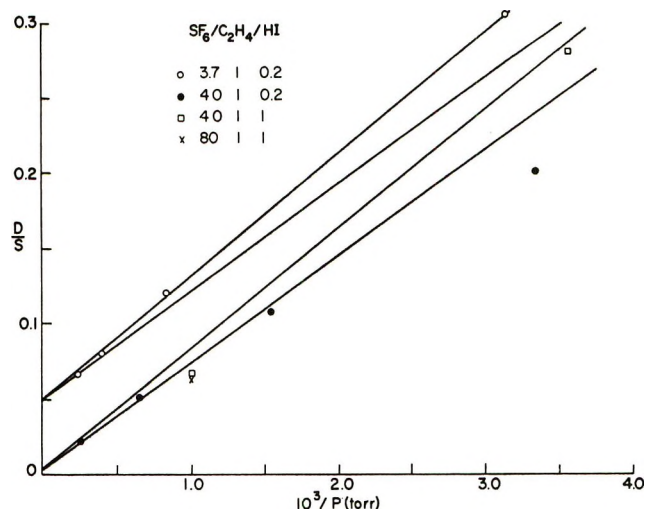


Figure 5. Ratio of decomposition/stabilization *vs.* (pressure)<sup>-1</sup> for <sup>18</sup>F-labeled products from <sup>18</sup>F reactions with C<sub>2</sub>H<sub>4</sub> for varying ratios of C<sub>2</sub>H<sub>4</sub>/SF<sub>6</sub>:  $D/S = C_2H_3^{18}F/C_2H_5^{18}F$ ; ratios, SF<sub>6</sub>/C<sub>2</sub>H<sub>4</sub>/HI (○) 3.7/1/0.2, (●) 4.0/1/0.2, (□) 4.0/1/1, (×) 8.0/1/1. The slopes illustrated cover the range of pressures for half-stabilization between 75 and 85 Torr.

electronically excited ONF\* precursor to the F atoms, as well as stabilizing C<sub>2</sub>H<sub>4</sub>F\* itself. The observed pressure effects could not be separated into these individual processes.

Additional experiments have also been run at other ratios, chiefly 3.7/1 and 40/1, with the results shown in Figure 5. The linear plots of  $D/S$  *vs.*  $1/P$  with non-zero intercepts at  $P = \infty$  can be treated as mixtures of radicals with two different half-pressures for stabilization: (i) the radicals formed by thermal <sup>18</sup>F atom addition and (ii) some very hot radicals with stabilization pressures very much higher than the experimental range. The contribution from the latter should be crudely proportional to the fraction of hot collisions which occur with the substrate, C<sub>2</sub>H<sub>4</sub>, and not with the moderator, SF<sub>6</sub>. The intercepts of Figures 4 and 5 are roughly proportional to the C<sub>2</sub>H<sub>4</sub>/SF<sub>6</sub> ratios of the mixtures, consistent with an increased hot contribution of CH<sup>18</sup>F=CH<sub>2</sub> for increased C<sub>2</sub>H<sub>4</sub> mole fraction.

The slopes of these  $D/S$  lines, after the small correction required for the presence of the hot reactions shown by the nonzero intercept, are all reasonably consistent with the same  $80 \pm 5$  Torr pressure for half-stabilization. The points at low pressures and/or low HI concentrations are the least accurate because of statistical problems associated with low <sup>18</sup>F total production at low pressures and the scavenging problems associated with very low HI concentrations. The slopes of these curves are very sensitive to any change in average rate of decomposition of C<sub>2</sub>H<sub>4</sub><sup>18</sup>F\*—a factor of 2 in slope corresponds to a factor of 2 in the rate, which in turn represents only 1 or 2 kcal/mol excitation

energy. Therefore, the nearly equivalent slopes for all three mole fractions indicate that very little additional excitation energy is being removed by the progressive increase in the fraction of collisions of <sup>18</sup>F with the moderator SF<sub>6</sub>. In turn, this implies that most of the <sup>18</sup>F atoms react while essentially thermal even in 3.7/1 mixtures, and certainly in 18/1 or 40/1 mixtures.

The half-pressure of 80 Torr is substantially less than the  $135 \pm 10$  Torr found in CF<sub>4</sub> mixtures. Although SF<sub>6</sub> is somewhat larger than CF<sub>4</sub>, we have estimated that the normal cross sections for CH<sub>2</sub><sup>18</sup>FCH<sub>2</sub> collisions with SF<sub>6</sub> are only about 20% larger than with CF<sub>4</sub>.<sup>18</sup> Since the excitation energy of the radical is presumably determined almost entirely by the exothermicity of the <sup>18</sup>F atom addition reaction and is therefore independent of the source for these thermalized <sup>18</sup>F atoms, this change in half-stabilization pressures implies that SF<sub>6</sub> is considerably more efficient per collision than CF<sub>4</sub> in stabilizing excited CH<sub>2</sub><sup>18</sup>FCH<sub>2</sub>\* radicals. This in turn implies that a "strong," single collision assumption for the stabilization of CH<sub>2</sub><sup>18</sup>FCH<sub>2</sub>\* radicals is not entirely adequate, at least for collisions with CF<sub>4</sub>. Less than unit stabilization efficiency, *i.e.*, energy loss per collision insufficient for total stabilization in one collision at any pressure, also leads to curvature in  $D/S$  *vs.*  $1/P$  plots, but such curvature is negligibly small until the experimental  $D/S$  ratios are well in excess of 1.0. Experiments in the  $\ll 100$  Torr range would be required in order to determine whether

(18) Approximate collision diameters, from J. O. Hirschfelder, C. F. Curtiss and R. B. Bird, "Molecular Theory of Gases and Liquids," Wiley, New York, N. Y., 1954. SF<sub>6</sub>, 5.51 Å; CF<sub>4</sub>, 4.70 Å; CH<sub>2</sub>FCH<sub>2</sub>, estimated as  $\cong$  C<sub>2</sub>H<sub>6</sub>, 3.95 Å.



**Table III:** Pressures for Stabilization of One-Half of the Excited Fluorinated Ethyl Radicals Formed by Addition of Near-Thermal  $^{18}\text{F}$  Atoms to Olefins

Reaction source	Excited source	Decomposition route	Half-pressure, Torr	Ref
$^{18}\text{F} + \text{CH}_2=\text{CH}_2$	$\text{CH}_2^{18}\text{FCH}_2^*$	$\text{CH}^{18}\text{F}=\text{CH}_2 + \text{H}$	$80 \pm 5$	This work
$^{18}\text{F} + \text{CHF}=\text{CF}_2$	$\text{CHF}^{18}\text{FCF}_2^*$	$\text{CHF}^{18}\text{F} + \text{CF}_2$	$45 \pm 5$	7
$^{18}\text{F} + \text{CF}_2=\text{CF}_2$	$\text{CF}_2^{18}\text{FCF}_2^*$	$\text{CF}_2^{18}\text{F} + \text{CF}_2$	$218 \pm 15$	6

**Table IV:** Absolute Yields of Volatile  $^{18}\text{F}$  Products from  $^{18}\text{F}$  Reactions in HI-Scavenged Gaseous  $\text{SF}_6\text{-C}_2\text{H}_4$  Mixtures

Total pressure, Torr	1510	1510	1720	1430	1530
HI pressure, Torr	43	43	44	46	7.5
Mole fraction $\text{C}_2\text{H}_4$	0.74	0.43	0.17	0.16	0.024
Absolute Yield, % Total $^{18}\text{F}$ Product					
$\text{SF}_5^{18}\text{F}$	$0.6 \pm 0.1$	$0.55 \pm 0.1$	$1.16 \pm 0.03$	$0.96 \pm 0.03$	$1.08 \pm 0.04$
$\text{CH}_3^{18}\text{F}$	$3.5 \pm 0.2$	$2.0 \pm 0.1$	$0.38 \pm 0.02$	$0.33 \pm 0.02$	$0.08 \pm 0.03$
$\text{CH}^{18}\text{F}=\text{CH}_2$	$9.0 \pm 0.3$	$7.3 \pm 0.1$	$4.76 \pm 0.05$	$5.14 \pm 0.06$	$3.03 \pm 0.18$
$\text{CH}_3\text{CH}_2^{18}\text{F}$	$25.1 \pm 0.4$	$34.0 \pm 0.3$	$53.6 \pm 0.2$	$55.8 \pm 0.2$	$59.8 \pm 0.2$

such curvature exists in this system. At such low pressures, our total  $^{18}\text{F}$  production becomes statistically marginal, and the recoil losses to the walls rapidly rise toward 100%.

The collision efficiencies of both  $\text{SF}_6$  and  $\text{CF}_4$  for the stabilization of excited alkyl radicals have earlier been determined by Rabinovitch and coworkers,<sup>19-22</sup> although apparently never in directly comparable experiments with the same excited radicals. While both perfluoro molecules are relatively efficient in removing excitation energy, some measurements with  $\text{CF}_4$  suggest an average energy loss per collision as low as  $\langle E \rangle = 4.5$  kcal/mol (with excited 2-pentyl radicals).<sup>21,22</sup> Our observation that  $\text{SF}_6$  is apparently more effective than  $\text{CF}_4$  in stabilizing excited  $\text{CH}_2\text{-}^{18}\text{FCH}_2^*$  radicals thus shows no inconsistency with the scattered prior observations of the stabilizing ability of these two molecules for a variety of alkyl radicals. Some of the earlier experiments with  $\text{CF}_4\text{-C}_2\text{H}_4\text{-I}_2$  mixtures were carried out in the presence of neon as a moderator gas. At a constant total pressure of 1 atm, the amount of decomposition product ( $\text{C}_2\text{H}_3^{18}\text{F}$ ) rose steadily with increasing neon mole fraction until it even exceeded the stabilization product ( $\text{CH}_2^{18}\text{FCH}_2\text{I}$ ) yield.<sup>2</sup> Per molecule,  $\text{CF}_4$  was calculated to be 7.5 times more efficient than Ne in removal of the excitation energy of  $\text{CH}_2^{18}\text{FCH}_2^*$  radicals. The lesser efficiency of neon than polyatomic molecules is consistent with all of the observations on noble gas stabilization of excited molecules.

The pressure for half-stabilization in  $\text{SF}_6$  of the excited radicals formed by the  $^{18}\text{F}$  addition to ethylene is listed in Table III with the corresponding half-pres-

ures found for other fluorinated ethyl radicals in similar experiments.<sup>6,7</sup> The difference in decomposition mechanisms (C-H *vs.* C-C bond rupture) makes direct comparison of the numerical values for half-pressure relatively meaningless. The mechanism change itself is related to the unusually high stability of  $\text{CF}_2$  fragments (C-F bonds with  $\sim 125$  kcal/mol bond strength).

*Hot  $^{18}\text{F}$  Reactions with  $\text{CH}_2=\text{CH}_2$ .* The probability that  $^{18}\text{F}$  atoms can react with  $\text{C}_2\text{H}_4$  while still carrying appreciable extra kinetic energy is greatly increased by increasing the mole fraction of the target  $\text{C}_2\text{H}_4$  in the mixture. The yields of  $^{18}\text{F}$  products found in  $\text{SF}_6\text{-C}_2\text{H}_4$  mixtures scavenged with HI are summarized in Table IV and Figure 6 for a wide range in mole fractions of  $\text{SF}_6$ . At any given energy, the probability that the *next* collision will be with  $\text{C}_2\text{H}_4$  rather than with  $\text{SF}_6$  is about 60 times greater in 25%  $\text{SF}_6$  mixtures than in 95%  $\text{SF}_6$ , and the likelihood of hot reactions is greatly enhanced for the former.

The yields of two products,  $\text{CH}_3^{18}\text{F}$  and  $\text{CH}^{18}\text{F}=\text{CH}_2$ , increase with decreasing mole fraction of  $\text{SF}_6$ , as expected for products whose formation is initiated by the reaction of a hot  $^{18}\text{F}$  atom. The approximate linearity of these decreases in hot product yields suggests, similar to the observations in  $\text{SF}_6\text{-C}_2\text{H}_2$  mixtures,<sup>8</sup> that the inelastic nonreactive scattering processes are

(19) G. H. Kohlmaier and B. S. Rabinovitch, *J. Chem. Phys.*, **38**, 1709 (1963).

(20) D. C. Tardy and B. S. Rabinovitch, *ibid.*, **48**, 5194 (1968).

(21) C. W. Larson and B. S. Rabinovitch, *ibid.*, **51**, 2293 (1969).

(22) J. H. Georgakakos, B. S. Rabinovitch, and E. J. McAlduff, *ibid.*, **52**, 2143 (1970).



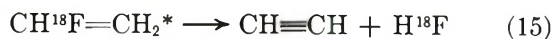


**Table V:** Absolute Yields of Volatile  $^{18}\text{F}$  Products from  $^{18}\text{F}$  Reactions in  $\text{SF}_6\text{-C}_2\text{H}_4$  Mixtures

Pressure, Torr	$\text{SF}_6$ $\text{C}_2\text{H}_4$	842 842
Absolute Yields, % $^{18}\text{F}$		
$\text{SF}_6^{18}\text{F}$		$0.64 \pm 0.03$
$\text{CH}^{18}\text{F}=\text{CH}_2$		$6.9 \pm 0.1$
<i>c</i> - $\text{C}_3\text{H}_6^{18}\text{F}$		$0.62 \pm 0.17$
$\text{CH}_2^{18}\text{FCH}=\text{CH}_2$		$0.20 \pm 0.08$

requires about 55 kcal/mol more excitation energy than is available from the exothermic addition of thermal  $^{18}\text{F}$  to  $\text{C}_2\text{H}_4$ . On the other hand, addition and subsequent loss of  $^{18}\text{F}$  is thermoneutral, while the replacement of H by  $^{18}\text{F}$  is 7 kcal/mol exothermic.<sup>14</sup> The observed minimum energy pathway for  $\text{CH}_2\text{-}^{18}\text{FCH}_2^*$  decomposition is that of H atom loss, as shown by the data of Table I and Figure 6.

Although the decomposition of  $\text{CH}^{18}\text{F}=\text{CH}_2$  by C=C bond break is approximately 146 kcal/mol endothermic, the positive identification through *c*- $\text{C}_3\text{H}_5^{18}\text{F}$  of the presence of  $\text{CH}^{18}\text{F}$  is good evidence that this reaction can readily occur for energetic  $^{18}\text{F}$  atoms. One alternative decomposition path for  $\text{CH}^{18}\text{F}=\text{CH}_2$  (the loss of H, endothermic by about 109 kcal/mol) should lead to no observed volatile activity unless HI is present and should reform the parent  $\text{CH}^{18}\text{F}=\text{CH}_2$  when HI is present. The incremental yield with and without HI as scavenger is quite small (about 7.3 in Table IV *vs.* 6.9 in Table V), indicating that very little H loss occurs from excited  $\text{CH}^{18}\text{F}=\text{CH}_2^*$ . Another alternative path for decomposition (the 1, 2 elimination of  $\text{H}^{18}\text{F}$ ) seems likely by analogy with other systems,<sup>25,26</sup> but has not been measured in these experiments, since the only radioactive trace would be  $\text{H}^{18}\text{F}$ . This reaction is only 17 kcal/mol endothermic and has been observed from tritium-labeled excited vinyl fluoride, in which  $\text{CH}=\text{CT}$  is left as an observable product.<sup>27</sup>



Decomposition by C=C bond break is not a completely new observation for  $^{18}\text{F}$  atom addition experiments: it is readily observed with  $\text{CF}^{18}\text{F}=\text{CF}_2^*$ , for which rupture into  $\text{CF}^{18}\text{F} + \text{CF}_2$  requires only 76 kcal/mol. Moreover, the average energy for  $^{18}\text{F}/\text{H}$  replacement in  $\text{CH}_3\text{CF}_3$  has been estimated as  $6.3 \pm$

1.0 eV ( $\sim 145$  kcal/mol)<sup>25</sup> so that postulated excitation energies in the 150 kcal/mol range are consistent with other experimental observations for hot  $^{18}\text{F}$  atom reactions. A concurrent question can be raised, however: why should very highly excited  $\text{CH}^{18}\text{F}=\text{CF}_2^*$  molecules decompose by the highly endothermic pathway of C=C bond rupture when several much less endothermic routes (loss of H; loss of  $^{18}\text{F}$ ; elimination of  $\text{H}^{18}\text{F}$ ) are available? Qualitatively, the answer may well lie in the rotational angular momentum imparted to the resulting radical if  $^{18}\text{F}$  is captured by ethylene at high-impact parameters. Such rotational angular momentum is available for stressing the C=C bond, and is not readily transmitted into the loss of H or elimination of  $\text{H}^{18}\text{F}$ ; the immediate loss of  $^{18}\text{F}$  in such a hot addition reaction corresponds quite closely to simple inelastic scattering of  $^{18}\text{F}$  and may not be easily detected.

As indicated above, an entirely comparable question can be phrased for the decomposition of excited  $\text{CH}_2^{18}\text{F-CH}_2^*$  radicals: why is C-C bond break ever remotely competitive with the less endothermic routes of loss of  $^{18}\text{F}$  or H atoms? A very similar answer presumably holds here as well, the capture of  $^{18}\text{F}$  at high impact parameters imparts to the excited radical an amount of rotational angular momentum which is not readily effective for the loss of an H atom, but which is quite available for bending and rupturing the C-C bond. The loss of  $^{18}\text{F}$ , again almost indistinguishable from inelastic scattering even in concept, is quite possible, but would be difficult to detect. The loss of  $^{18}\text{F}$  from  $\text{CH}_2^{18}\text{FCH}_2^*$  as formed by near-thermal addition to ethylene has been shown to be unimportant,<sup>12</sup> but then rotational angular momentum is much less important for slow  $^{18}\text{F}$  atoms. In both instances, our suggestion of the possible importance of rotational angular momentum in these reactions has been stimulated by similar postulates by Bunker<sup>28</sup> for the isomerization of  $\text{CH}_2\text{TNC}$  excited by tritium recoil and for the decomposition of excited  $\text{CH}_2^{18}\text{FCF}_3^*$  formed by  $^{18}\text{F}/\text{H}$  substitution in  $\text{CH}_3\text{CF}_3$ .

(25) K. A. Krohn, J. J. Parks, and J. W. Root, *J. Chem. Phys.*, **55**, 2690 (1971); **55**, 5771 (1971); **55**, 5785 (1971).

(26) E. Tschuikow-Roux and W. J. Quiring, *J. Phys. Chem.*, **75**, 295 (1971).

(27) W. S. Smith and Y.-N. Tang, presented at the 161st National Meeting of the American Chemical Society, Los Angeles, Calif., March 1971.

(28) D. Bunker, *J. Chem. Phys.*, **57**, 332 (1972).

# Absolute Rate Constants for the Reaction $\text{H} + \text{O}_2 + \text{M} \rightarrow \text{HO}_2 + \text{M}$ over the Temperature Range 203–404 K<sup>1a</sup>

by Michael J. Kurylo<sup>1b</sup>

National Bureau of Standards, Washington, D. C. 20234 (Received July 28, 1972)

Publication costs assisted by Climatic Impact Assessment Program, Office of the Secretary, Department of Transportation

Absolute rate constants for the reaction  $\text{H} + \text{O}_2 + \text{M} \rightarrow \text{HO}_2 + \text{M}$  have been measured by the flash photolysis-resonance fluorescence technique. For  $\text{M} = \text{He}$ , rate measurements over the temperature range 203–404 K and pressure range 10–400 Torr gave the Arrhenius expression  $k_1^{\text{He}} = [6.66 (+1.2, -1)] \times 10^{-33} \exp[(473 \pm 92) \text{cal mol}^{-1}/1.987T] \text{cm}^6 \text{molecule}^{-2} \text{sec}^{-1}$ . Comparisons of third-order rate constants at 298 K gave relative deactivation efficiencies of  $\text{CH}_4/\text{N}_2/\text{He}/\text{Ar} = 15.7:3.4:1.0:1.0$ . The efficiency ratio of  $\text{N}_2$  to  $\text{He}$  was 4.5 at 226 K.

The combination reaction of atomic hydrogen with molecular oxygen is the dominant loss mechanism for H atoms in both the troposphere and stratosphere, thereby serving as a source for the hydroperoxyl ( $\text{HO}_2$ ) radical. The reaction also serves as the chain termination step at the second explosion limit of the hydrogen-oxygen system. To date, kinetic studies of the  $\text{H} + \text{O}_2 + \text{M}$  reaction consist of numerous high-temperature shock tube and flame data<sup>2–5</sup> and scattered experiments near 300 K by both direct<sup>6–13</sup> and indirect<sup>14</sup> techniques. Until recently few data were available below 300 K, and Arrhenius parameters were subject to rather large uncertainties.

To assess the role of this reaction in the chemistry of the stratosphere, accurate values of the rate parameters for various inert gases (M) over a temperature range extending to 200 K must be known. Determinations from high-temperature data (near 1000 K) are inadequate due to the errors involved in long extrapolations. Data at lower temperature have been obtained predominantly from discharge flow systems where the H-atom concentrations were followed by a calorimetric probe,<sup>7</sup> HNO emission,<sup>6</sup> mass spectroscopy,<sup>8</sup> and electron spin resonance spectroscopy.<sup>10,12</sup> These flow data are complicated by wall reactions and often require large corrections for longitudinal diffusion of H atoms and loss of H atoms by reaction with  $\text{HO}_2$ . More recent studies with static systems have employed kinetic absorption spectroscopy using pulse radiolysis<sup>9</sup> and mercury photosensitization<sup>11</sup> for atom production.

Because of the overall uncertainties in the rate constant conditions applicable to atmospheric modeling, we have undertaken a flash photolysis-resonance fluorescence study of the chemical system over a range of temperature and inert gas pressure comparable to atmospheric conditions. Experimental conditions were chosen such that stoichiometric corrections due to secondary reactions were not needed.

## Experimental Section

The apparatus and technique have been described in detail previously.<sup>15,16</sup> In the present experiments, mixtures of an H-atom source compound ( $\text{CH}_4$  or

- (1) (a) Contribution of the National Bureau of Standards, Washington, D. C. (b) Supported in part by the Climatic Impact Assessment Program, Office of the Secretary, Department of Transportation.
- (2) (a) R. R. Baldwin, L. Mayor, and P. Doran, *Trans. Faraday Soc.*, **56**, 92 (1960); (b) R. R. Baldwin and P. Doran, *ibid.*, **57**, 1578 (1961); (c) R. R. Baldwin, P. Doran, and L. Mayor, *Symp. (Int.) Combust.*, [Proc.] *8th*, 103 (1962); (d) R. R. Baldwin, *Symp. (Int.) Combust.*, [Proc.] *9th*, 218 (1963); (e) R. R. Baldwin, R. B. Moyes, B. N. Rossiter, and R. W. Walker, *Combust. Flame*, **14**, 181 (1970).
- (3) (a) R. W. Getzinger and G. L. Schott, *J. Chem. Phys.*, **43**, 3237 (1965); (b) R. W. Getzinger and L. S. Blair, *Combust. Flame*, **13**, 271 (1969); (c) L. S. Blair and R. W. Getzinger, *ibid.*, **14**, 5 (1970).
- (4) (a) D. Gutman, E. A. Hardwidge, F. A. Dougherty, and R. W. Lutz, *J. Chem. Phys.*, **47**, 4400 (1967); (b) G. Dixon-Lewis and A. Williams, *Symp. (Int.) Combust.*, [Proc.] *11th*, 951 (1967).
- (5) W. G. Browne, D. R. White, and G. R. Smookler, *Symp. (Int.) Combust.*, [Proc.] *12th*, 557 (1968).
- (6) (a) M. A. A. Clyne, *Symp. (Int.) Combust.*, [Proc.] *9th*, 211 (1963); (b) M. A. A. Clyne and B. A. Thrush, *Proc. Roy. Soc., Ser. A*, **275**, 559 (1963).
- (7) F. S. Larkin and B. A. Thrush, *Discuss. Faraday Soc.*, **No. 37**, 112 (1964).
- (8) A. F. Dodonov, G. K. Lavrovakaya, and V. L. Talrose, *Kinet. Katal.*, **10**, 701 (1969).
- (9) (a) W. P. Biship and L. M. Dorfman, *J. Chem. Phys.*, **52**, 3210 (1970); (b) T. Hikida, J. A. Eyre, and L. M. Dorfman, *ibid.*, **54**, 3422 (1971).
- (10) A. A. Westenberg and N. de Haas, *J. Phys. Chem.*, **76**, 1586 (1972).
- (11) J. Michael, private communication.
- (12) G. K. Moortgat and E. R. Allen, presented at 163rd National Meeting of the American Chemical Society, Boston, 1972.
- (13) W. Wong and D. D. Davis, private communication.
- (14) Several references are cited in D. L. Baulch, D. D. Drysdale, D. G. Horne, and A. C. Lloyd, "Evaluated Kinetic Data for High Temperature Reactions," Vol. 1, Butterworth & Co., London, 1972.
- (15) W. Braun and M. Lenzi, *Discuss. Faraday Soc.*, **44**, 252 (1967).
- (16) (a) M. J. Kurylo, N. C. Peterson, and W. Braun, *J. Chem. Phys.*, **53**, 2776 (1970); **54**, 943 (1971); **54**, 4662 (1971); (b) D. D. Davis, R. E. Huie, J. T. Herron, M. J. Kurylo, and W. Braun, *ibid.*, **56**, 4668 (1972); (c) M. J. Kurylo, *Chem. Phys. Lett.*, **14**, 117 (1972).



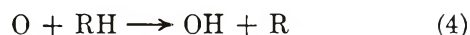
$\text{C}_3\text{H}_8$ ),  $\text{O}_2$ , and an inert diluent (He, Ar, or  $\text{N}_2$ ) were flash photolyzed at wavelengths above 105 nm producing on the order of 0.1 to 0.01 mTorr of atomic hydrogen. A Lyman  $\alpha$ -resonance lamp<sup>16a,17</sup> operated continuously was used to excite a small fraction of the atoms, and the atom decay in the mixture was monitored by following the Lyman  $\alpha$ -resonance fluorescence with a magnetic electron multiplier placed at right angles to both the flash and resonance lamps. Emissions from the resonance lamp at wavelengths other than 121.6 nm were filtered out by using a molecular oxygen filter between the resonance lamp and the reaction cell. In this way no interference due to resonance fluorescence from O atoms, also produced by the flash, was obtained. This was checked by flashing mixtures containing only inert gas and  $\text{O}_2$ . Fluorescence signals were accumulated on a multichannel analyzer and treated by nonlinear least-squares analysis. Since as many as 200 flashes were sometimes used to generate one kinetic curve (Figure 1), the reaction mixture was changed several times to avoid depletion of atom source or  $\text{O}_2$  and accumulation of any reactive product species. Atom concentrations were varied by changing either the hydrocarbon pressure or the flash energy. This made it possible to assess the importance of H-atom depletion by reaction with  $\text{HO}_2$  according to the scheme



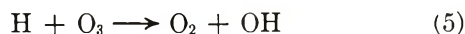
Similar intensity studies coupled with variation in the H atom to O atom ratio served to analyze for the possible production of H atoms by the fast reaction



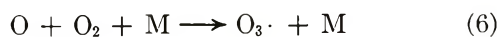
Calculations were performed to estimate the importance of OH production by



followed immediately by reaction 3. Such secondary H-atom generation was found to be more important when propane rather than methane was used as an H-atom source and only then at the higher O-atom concentrations ( $[\text{O}_2] > 500$  mTorr). These results were verified experimentally, and consequently only experiments with  $\text{CH}_4$  as the H-atom source and  $[\text{O}_2] < 500$  mTorr were used in the final analysis. Under these conditions, calculations showed that H-atom loss by



where  $\text{O}_3$  originated from



was insignificant during the time scale of our measurements (usually several milliseconds). All experiments were consequently performed under conditions not re-

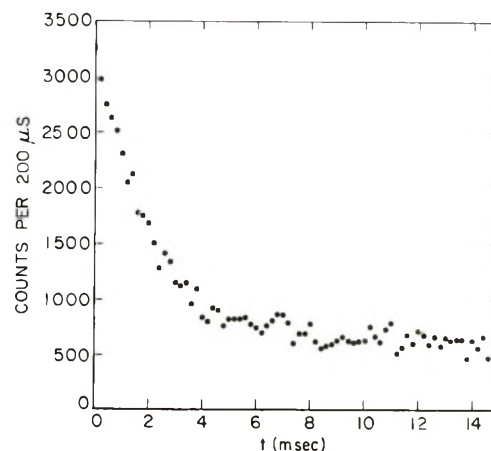


Figure 1. Typical H-atom decay curve: 200 mTorr of  $\text{CH}_4$ , 100 mTorr of  $\text{O}_2$ , 200 mTorr of He, 45-J flash energy, 298 K.

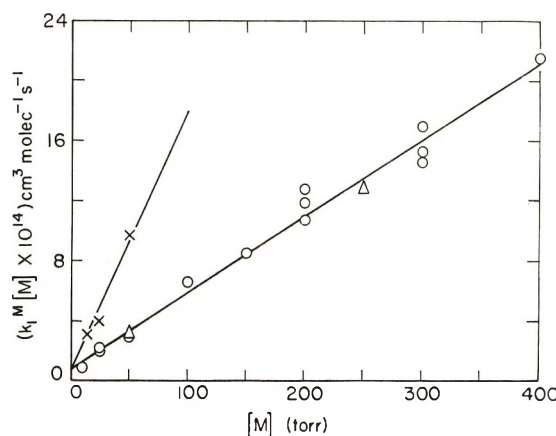


Figure 2. Plots of  $k_1^M[M]$  vs.  $[M]$  for He (O), Ar ( $\Delta$ ), and  $\text{N}_2$  (X) at 298 K.

quiring stoichiometric corrections and not controlled or complicated by O-atom chemistry.

Thus, in the presence of inert gas M, the loss of H atoms can be represented as

$$-\frac{d[\text{H}]}{dt} = [\text{H}][\text{O}_2]\{k_1^M[\text{M}] + k_1^{\text{CH}_4}[\text{CH}_4] + k_1^{\text{O}_2}[\text{O}_2]\} + [\text{H}]\{D + k_9[\text{CH}_4] + k_{\text{imp}}[\text{M}]\}$$

where  $k_1^M$ ,  $k_1^{\text{CH}_4}$ , and  $k_1^{\text{O}_2}$  are third-order rate constants for H- $\text{O}_2$  combination employing the indicated third bodies;  $D$  is the rate constant for diffusional loss of H atoms out of the viewing zone;  $k_9$  is a bimolecular rate constant for H atom reaction with  $\text{CH}_4$ ; and  $k_{\text{imp}}$  takes into account reaction with any impurity present in the inert gas. We have not included a term accounting for impurities in the oxygen since two different sources of oxygen were used without noticeable change in the atom decay rates.

(17) D. D. Davis and W. Braun, *Appl. Opt.*, **7**, 2071 (1968).

Applying the foregoing analysis, the first-order H-atom decay rates at a fixed total pressure were plotted vs. the O<sub>2</sub> pressure to give slopes of  $k_1^M[M] + k_1^{CH_4}[CH_4]$  and intercepts expressing the rate of H-atom loss by second-order reactions and diffusion at pressure [M]. Here we have ignored the term accounting for O<sub>2</sub> as a third body. Studies of the O + O<sub>2</sub> + M system have shown O<sub>2</sub> to be approximately 1.6<sup>18</sup> times more efficient than He or Ar. The assumption of a similar efficiency ratio in the present study would make corrections negligible. The effect of CH<sub>4</sub> as a third body was determined from runs in which the CH<sub>4</sub> concentration was varied while keeping O<sub>2</sub> and He fixed. By subtracting the effect of CH<sub>4</sub> we were thus able to obtain values for  $k_1^M[M]$  the "second-order rate constant at pressure M." These second-order rate constants were then plotted against the inert gas pressure, and the slopes of these plots constitute the values of  $k_1^M$  reported here. Plots for He, Ar, and N<sub>2</sub> at 298 K are shown in Figure 2. This procedure was repeated at several temperatures between 200 and 400 K. The temperature study was done primarily with He as the deactivator. Although N<sub>2</sub> represents the most interesting M species for atmospheric applications, it serves as a very efficient quencher of Lyman  $\alpha$  fluorescence<sup>19</sup> thereby greatly reducing our signal levels. Because of the difficulty in obtaining the N<sub>2</sub> data, values of  $k_1^{N_2}$  were determined only at 298 and 226 K, the latter temperature being descriptive of the stratosphere. A value of  $k_1^{Ar}$  was determined only at 298 K.

Ultrahigh-purity gases (O<sub>2</sub>, He, Ar, and N<sub>2</sub>) were used without further purification. Research grade methane was degassed briefly at liquid N<sub>2</sub> temperature and then distilled from liquid O<sub>2</sub>. Pressures were measured on a two-turn Bourdon gauge (20–700 Torr), a one-turn 0–20 Torr Bourdon gauge (1–20 Torr), and a capacitance manometer (<1 Torr). The calibrations of the latter two were checked frequently against a dibutyl phthalate manometer. Reaction mixtures were usually made up and stored in 2-l. glass bulbs. In experiments employing mixtures made up in the reaction cell, identical rate constants were obtained.

## Results and Discussion

The experimental results of this study are presented in Tables I–IV. The precision associated with the exponential fit of the first-order decay curves was generally 3%. From these first-order rates, the second-order rate constants could be determined within an uncertainty of 5–10%. Consequently, the error associated with the final third-order rate coefficients presented in the tables is realistically assessed at 15%. Since these errors are associated with the linear fits of the data, the uncertainty could presumably be reduced by improving the statistics (*i.e.*, by increasing the number of experiments).

**Table I:** Rate Measurements for the Reaction  
H + O<sub>2</sub> + CH<sub>4</sub> → HO<sub>2</sub> + CH<sub>4</sub> at 298 K

He, Torr <sup>a</sup>	O <sub>2</sub> , mTorr	CH <sub>4</sub> , mTorr	Flash energy, J <sup>b</sup>	First- order rate, sec <sup>-1</sup>
10	0	100	45	60.7
10	0	100	45	63.6
10	0	350	45	64.6
10	0	350	45	67.1
10	0	600	45	64.6
10	0	600	45	64.6
9.65	250	100	45	142
9.65	250	100	45	142
9.65	250	100	45	140
9.4	250	350	45	157
9.4	250	350	45	160
9.15	250	600	45	167
9.15	250	600	45	171
9.15	250	600	45	177

$$k_1^{CH_4} = (24.6 \pm 7.4) \times 10^{-32} \text{ cm}^6 \text{ molecule}^{-2} \text{ sec}^{-1}$$

<sup>a</sup> 1 Torr = 133.32 N m<sup>-2</sup> = (9.66/T(K)) × 10<sup>18</sup> molecules cm<sup>-3</sup>. <sup>b</sup> A flash energy of 80 J corresponds to an incident light intensity at the reaction cell of approximately 1 × 10<sup>13</sup> quanta/flash.

**Table II:** Rate Measurements for the Reaction  
H + O<sub>2</sub> + Ar → HO<sub>2</sub> + Ar at 298 K

Ar, Torr <sup>a</sup>	O <sub>2</sub> , mTorr	CH <sub>4</sub> , mTorr	Flash energy, J <sup>b</sup>	First- order rate, sec <sup>-1</sup>	$k_1^{Ar}[Ar]$ × 10 <sup>14</sup> , cm <sup>3</sup> mole- cule <sup>-1</sup> sec <sup>-1</sup> <sup>c</sup>
50	26	200	45	109	3.14
	50.5			125	
	100			180	
	151			243	
	200			307	
	250			333	
250	25	200	45	204	12.84
	25			189	
	50			438	
	50			410	
	100			588	
	100			647	
	150			762	
	200			943	
	225			1127	

<sup>a</sup> 1 Torr = 133.32 N m<sup>-2</sup> = (9.66/T(K)) × 10<sup>18</sup> molecules cm<sup>-3</sup>. <sup>b</sup> A flash energy of 80 J corresponds to an incident light intensity at the reaction cell of approximately 1 × 10<sup>13</sup> quanta/flash. <sup>c</sup> Corrected for  $k_1^{CH_4}[CH_4]$ .

The rate constant for H + O<sub>2</sub> + CH<sub>4</sub> → HO<sub>2</sub> + CH<sub>4</sub> was determined at 298 K in the presence of 10 Torr of He (Table I). The value of  $k_1^{CH_4}$  under the conditions

(18) F. Kaufman and J. R. Kelso, *J. Chem. Phys.*, **46**, 4541 (1967).

(19) W. Braun, C. Carlone, T. Carrington, G. Van Volkenburgh, and R. A. Young, *ibid.*, **53**, 4244 (1970).



**Table III:** Rate Measurements for the Reaction  $\text{H} + \text{O}_2 + \text{N}_2 \rightarrow \text{HO}_2 + \text{N}_2$ 

$T, \text{K}$	$\text{N}_2, \text{Torr}^a$	$\text{O}_2, \text{mTorr}$	$\text{CH}_4, \text{mTorr}$	Flash energy, $\text{J}^b$	First-order rate, $\text{sec}^{-1}$	$k_1^{\text{N}_2}[\text{N}_2] \times 10^{14}, \text{cm}^3 \text{molecule}^{-1} \text{sec}^{-1}{}^c$	$k_1^{\text{N}_2} \times 10^{21}, \text{cm}^6 \text{molecule}^{-2} \text{sec}^{-1}$
226	5	50	300	80	70		
	5	100	300	80	131		
	5	200	300	80	213	1.80	
	30	52.5	300	80	306		
	30	105	300	80	564	11.10	8.70
298	15	15.8	180	80	112		
	15	30.6	180	80	132		
	15	61.5	180	80	172		
	15	90.6	180	80	207		
	15	120.6	180	80	213		
	15	150.6	180	80	264	3.13	
	25	26.3	300	80	131		
	25	51	300	80	174		
	25	102.5	300	80	285		
	25	151	300	80	321		
	25	201	300	80	364		
	25	251	300	80	456	3.98	
	50	25	200	80	163		
	50	50	200	80	222		
	50	102	200	80	438		
	50	150.5	200	80	569		
	50	202	200	80	722	9.80	5.33

<sup>a</sup> 1 Torr =  $133.32 \text{ N m}^{-2} = (9.66/T(\text{K})) \times 10^{18} \text{ molecules cm}^{-3}$ . <sup>b</sup> A flash energy of 80 J corresponds to an incident light intensity at the reaction cell of approximately  $1 \times 10^{13} \text{ quanta/flash}$ . <sup>c</sup> Corrected for  $k_1^{\text{CH}_4}[\text{CH}_4]$ .

shown was found to be  $24.6 \times 10^{-32} \text{ cm}^6 \text{ molecule}^{-2} \text{ sec}^{-1}$  and was used to correct the Ar, He, and  $\text{N}_2$  data as mentioned earlier. Even with 5% precision in the first-order rates, the absolute uncertainty in  $k_1^{\text{CH}_4}$  is closer to 30% due to the obvious problems in measuring small differences in large numbers.

The rate constant data for  $\text{H} + \text{O}_2 + \text{Ar} \rightarrow \text{HO}_2 + \text{Ar}$  at 298 K are presented in Table II. Since the values of  $k_1^{\text{Ar}}[\text{Ar}]$  fell within the scatter of the similar

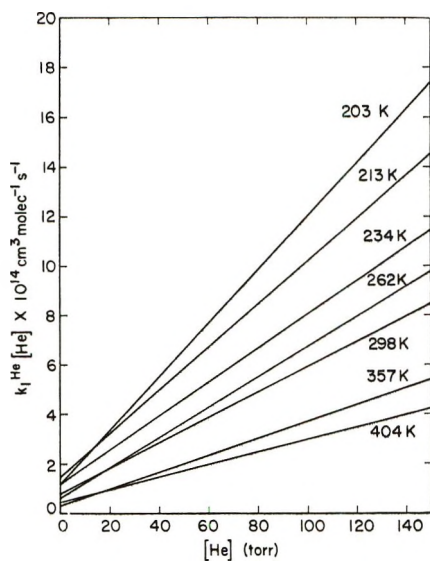


Figure 3. Plots of  $k_1^{\text{He}}[\text{He}]$  vs.  $[\text{He}]$  at various temperatures.

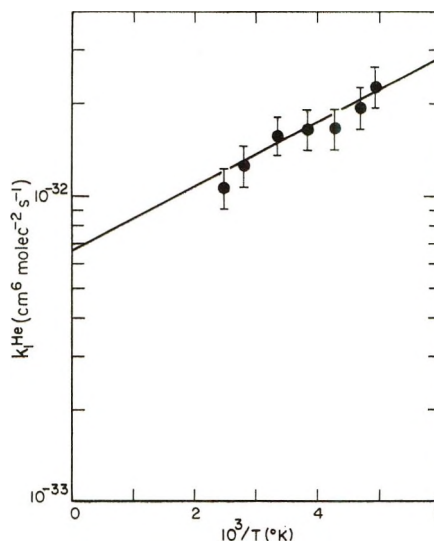


Figure 4. Arrhenius plot of the third-order rate constant for the reaction  $\text{H} + \text{O}_2 + \text{He} \rightarrow \text{HO}_2 + \text{He}$ .

He data presented in Figure 2, both the Ar and He points were analyzed together to determine  $k_1^{\text{Ar,He}}$ . The two Ar points by themselves predict a slightly lower value for  $k_1^{\text{Ar}}$  than does the analysis used. Both approaches agree within the quoted error limits.

The data from the  $\text{N}_2$  studies at both 298 and 226 K are shown in Table III. The analysis gives values of  $k_1^{\text{N}_2}$  of  $5.33 \times 10^{-32}$  and  $8.70 \times 10^{-32} \text{ cm}^6 \text{ molecule}^{-2} \text{ sec}^{-1}$  at 298 and 226 K, respectively.

Table IV: Rate Measurements for the Reaction  $\text{H} + \text{O}_2 + \text{He} \rightarrow \text{HO}_2 + \text{He}$ 

$T$ , K	He, Torr <sup>a</sup>	O <sub>2</sub> , mTorr	CH <sub>4</sub> , mTorr	Flash energy, J <sup>b</sup>	First-order rate, sec <sup>-1</sup>	$k_1^{\text{He}}[\text{He}] \times 10^{14}$ , cm <sup>3</sup> molecule <sup>-1</sup> sec <sup>-1</sup> <sup>c</sup>	$k_1^{\text{He}} \times 10^{12}$ , cm <sup>3</sup> molecule <sup>-2</sup> sec <sup>-1</sup>	
203	40	24	133	55	145			
	40	48	133	55	232			
	40	80	133	55	310			
	40	120	133	55	460			
	40	160	133	55	513	5.58		
	80	48	266	55	426			
	80	96	266	55	757			
	80	160	266	55	870	9.74		
	120	72	400	55	658			
	120	144	400	55	1331			
	120	240	400	55	1688	14.24	2.27	
	213	30	25	127	55	126		
30		50	127	55	185			
30		75	127	55	240			
30		150	127	55	332			
30		200	127	55	494	4.04		
60		50	253	55	246			
60		100.7	253	55	360			
60		200	253	55	638			
60		300.7	253	55	931			
60		400	253	55	1393	6.67	1.93	
234		30	50	127	55	153		
		30	75	127	55	194		
	30	100	127	55	244			
	30	150	127	55	298			
	30	200	127	55	371	3.25		
	60	50	253	55	205			
	60	100.7	253	55	329			
	60	150.7	253	55	422			
	60	200	253	55	518			
	60	300.7	253	55	783			
	60	400	253	55	1018	5.30		
	100	50	253	55	270			
100	100	253	55	438				
100	150	253	55	615				
100	200	253	55	842				
100	300	253	55	1070				
100	400	253	55	1499	8.03	1.65		
262	75	25	125	55	143			
	75	50	125	55	180			
	75	75	125	55	227			
	75	100	125	55	310			
	75	150	125	55	403			
	75	200	125	55	468	5.18		
	150	50	250	55	304			
	150	100	250	55	506			
	150	200	250	55	818			
	150	300	250	55	1243	9.75	1.65	
	298	10	100	100	45	140 <sup>e</sup>		
		10	200	100	45	176 <sup>e</sup>		
10		300	100	45	210 <sup>e</sup>			
10		300	100	45	188 <sup>e</sup>			
10		300 <sup>d</sup>	100	45	197 <sup>e</sup>			
10		300	100	20	204 <sup>e</sup>			
10		300	100	80	202 <sup>e</sup>			
10		400	100	45	244 <sup>e</sup>	0.87		
25		10	110	45	170			
25		25	110	45	176			
25		50	110	45	186			
25		100	110	45	251			
25	150	110	45	262				
25	200	110	45	313				



$T, \text{K}$	He, Torr <sup>a</sup>	O <sub>2</sub> , mTorr	CH <sub>4</sub> , mTorr	Flash energy, J <sup>b</sup>	First-order rate, sec <sup>-1</sup>	$k_1^{\text{He}}[\text{He}] \times 10^{14}$ , cm <sup>3</sup> molecule <sup>-1</sup> sec <sup>-1</sup> <sup>c</sup>	$k_1^{\text{He}} \times 10^{12}$ , cm <sup>6</sup> molecule <sup>-2</sup> sec <sup>-1</sup>	
298	25	300	110	45	372	2.09		
	25	0	100	45	91			
	25	0	100	45	113			
	25	25	100	45	131			
	25	25	100	45	123			
	25	50	100	45	139			
	25	50	100	45	139			
	25	100	100	45	192			
	25	100	100	45	188			
	25	200	100	45	245			
	25	200	100	45	251			
	25	300	100	45	308			
	25	300	100	45	304			
	25	400	100	45	402		2.05	
	50	25	220	72	215			
	50	50	220	72	271			
	50	100	220	72	294			
	50	130	220	72	379			
	50	200	220	72	398			
	50	300	220	72	517	3.04		
	100	25	105	72	210			
	100	50	105	72	271			
	100	100	105	72	357			
	100	150	105	72	482			
	100	200	105	72	556			
	100	250	105	72	717		6.58	
	150	50	100	45	214			
	150	50	100	45	225			
	150	100	100	45	359			
	150	150	100	45	510			
	150	150	100	45	473			
	150	200	100	45	649			
	150	300	100	45	819			
	150	400	100	45	1215	8.55		
	200	50	160	45	430			
	200	50	160	45	437			
	200	100	160	45	675			
	200	150	160	45	833			
	200	200	160	45	1020	11.91		
	200	100	105	72	590			
	200	200	105	72	966			
	200	300	105	72	1429			
	200	400	105	72	1826		12.78	
200	0	200	45	102				
200	0	200	45	77				
200	100	200	45	458				
200	100	200	45	408				
200	100	200	45	490				
200	200	200	45	792				
200	200	200	45	839				
200	300	200	45	1143				
200	300	200	45	1131	10.67			
300	100	40	45	651				
300	100	40	45	705				
300	200	40	45	1097				
300	300	40	45	1585				
300	400	40	45	2200		15.32		
300	37.5	150	45	281				
300	75	150	45	468				
300	75	150	45	495				
300	112.5	150	45	811				
300	150	150	45	939				
300	150	150	45	951				

Table IV (Continued)

<i>T</i> , K	He, Torr <sup>a</sup>	O <sub>2</sub> , mTorr	CH <sub>4</sub> , mTorr	Flash energy, J <sup>b</sup>	First-order rate, sec <sup>-1</sup>	<i>k</i> <sub>1</sub> <sup>He</sup> [He] × 10 <sup>14</sup> , cm <sup>3</sup> molecule <sup>-1</sup> sec <sup>-1</sup> <sup>c</sup>	<i>k</i> <sub>1</sub> <sup>He</sup> × 10 <sup>11</sup> , cm <sup>3</sup> molecule <sup>-2</sup> sec <sup>-1</sup>
298	300	225	150	45	1283		
	300	225	150	72	1246		
	300	225	150	187	1264		
	300	300	150	45	1499	14.61	
	300	50	240	45	738		
	300	100	240	45	997		
	300	200	240	45	1572	17.04	
	400	25	200	45	270		
	400	50	200	45	496		
	400	50	200	45	467		
	400	75	200	45	695		
	400	100	200	45	794		
	400	100	200	45	806		
	400	150	200	45	1144		
	400	200	200	45	1545	21.55	1.57
357	35	28.3	140	55	169		
	35	56.8	140	55	178		
	35	84.0	140	55	206		
	35	112.6	140	55	217		
	35	168.3	140	55	227	1.54	
	75	60.6	300	55	193		
	75	60.6	300	55	165		
	75	121.8	300	55	225		
	75	180	300	55	279		
	75	241.2	300	55	329		
	75	360	300	55	420	2.84	
	150	121.2	600	55	308		
	150	243.6	600	55	489		
	150	360.0	600	55	727		
	150	482.4	600	55	796		
150	721.2	600	55	1258	5.41	1.25	
434	50	30	167	55	211		
	50	60	167	55	232		
	50	100	167	55	234		
	50	200	167	55	295		
	50	300	167	55	327	1.75	
	150	90	500	55	219		
	150	180	500	55	317		
	150	300	500	55	444		
	150	450	500	55	595		
	150	600	500	55	772	4.28	1.06

<sup>a</sup> 1 Torr = 133.32 N m<sup>-2</sup> = (9.66/*T*(K)) × 10<sup>18</sup> molecules cm<sup>-3</sup>. <sup>b</sup> A flash energy of 80 J corresponds to an incident light intensity at the reaction cell of approximately 1 × 10<sup>13</sup> quanta/flash. <sup>c</sup> Corrected for *k*<sub>1</sub><sup>CH<sub>4</sub></sup>[CH<sub>4</sub>]. <sup>d</sup> Ultrahigh-purity O<sub>2</sub> from a Pyrex storage bulb. <sup>e</sup> Corrected for third-body effect of O<sub>2</sub> assuming *k*<sub>1</sub><sup>O<sub>2</sub></sup> = 1.6*k*<sub>1</sub><sup>He</sup>.

As mentioned earlier, the most extensive data were taken on the H + O<sub>2</sub> + He system (Table IV). These data were analyzed as for other M species with the exception that the 10-Torr He data were corrected for the third-body effect of O<sub>2</sub>. We have taken the efficiencies of O<sub>2</sub> and He as deactivators to be in the same ratio as measured for the O + O<sub>2</sub> + M reaction.<sup>18</sup> The positive intercepts appearing in plots of *k*<sub>1</sub><sup>M</sup>[M] vs. [M] (Figure 2) are not predicted by the data analysis outlined earlier. Such intercepts could be attributed to either a radiative combination not requiring a third body or a wall component of the measured reaction. The room temperature intercept of 8 × 10<sup>-15</sup> cm<sup>3</sup>

molecule<sup>-1</sup>sec<sup>-1</sup> is some two orders of magnitude higher than expected for radiative combination, and we thus prefer the latter explanation. Although our observation zone is defined by the intersection of three columnated beams (flash lamp, resonance lamp, and photomultiplier) in the center of the cell, the cell used in these experiments was very small and a small fraction of the H atoms could have been observed at the walls. This explanation is consistent with the observation in Figure 3 that the intercept tends to become more positive with decreasing temperature. Measurements were therefore taken over extended pressure ranges thereby minimizing the significance of the intercept. The slope of



**Table V:** A Summary of Rate Data on the Reaction  $\text{H} + \text{O}_2 + \text{M} \rightarrow \text{HO}_2 + \text{M}$ 

<i>T</i> , K	M	<i>k</i> , cm <sup>6</sup> molecule <sup>-2</sup> sec <sup>-1</sup>	Method	Reference
298	CH <sub>4</sub>	24.6 × 10 <sup>-32</sup>	Flash photolysis-resonance fluorescence	This work
298	Ar	1.57 × 10 <sup>-32</sup>		
298	He	1.57 × 10 <sup>-32</sup>		
203-404	He	6.66 × 10 <sup>-33</sup> × exp(473 cal mol <sup>-1</sup> /1.987 <i>T</i> )		
298	N <sub>2</sub>	5.33 × 10 <sup>-32</sup>		
226	N <sub>2</sub>	8.70 × 10 <sup>-32</sup>		
298	Ar	1.6 × 10 <sup>-32</sup>	Pulsed absorption spectro- photometry	Dorfman, <i>et al.</i>
298	H <sub>2</sub>	4.7 × 10 <sup>-32</sup>		
297	Ar	1.54 × 10 <sup>-32</sup>	Discharge flow (esr)	Moortgat and Allen
297	He	1.49 × 10 <sup>-32</sup>		
297	H <sub>2</sub>	6.34 × 10 <sup>-32</sup>		
298	Ar	1.87 × 10 <sup>-32</sup>	Discharge flow (esr)	Westenberg and de Haas
298	He	1.87 × 10 <sup>-32</sup>		
298	Ar	0.61 × 10 <sup>-32</sup>	Pulsed absorption spectro- photometry (mercury photosensitized)	Michael
298	He	3.75 × 10 <sup>-32</sup>		
298	H <sub>2</sub>	1.22 × 10 <sup>-32</sup>		
298	Ne	3.16 × 10 <sup>-32</sup>		
298	Kr	1.1 × 10 <sup>-32</sup>		
298	Ar	1.95 × 10 <sup>-32</sup>	Flash photolysis-resonance fluorescence	Wong and Davis
298	He	1.88 × 10 <sup>-32</sup>		
298	N <sub>2</sub>	5.3 × 10 <sup>-32</sup>		
298	CH <sub>4</sub>	41.5 × 10 <sup>-32</sup>		
220-360	Ar	6.75 × 10 <sup>-33</sup> × exp(685 cal mol <sup>-1</sup> /1.987 <i>T</i> )		
220	N <sub>2</sub>	8.35 × 10 <sup>-32</sup>		
293	Ar	3.3 × 10 <sup>-32</sup>	Discharge flow (HNO emission)	Clyne
293	Ar	2.2 × 10 <sup>-32</sup>		
244	Ar	4.0 × 10 <sup>-32</sup>	Discharge flow (HNO emission)	Clyne and Thrush
225	Ar	3.5 × 10 <sup>-32</sup>		
293	He	2.1 × 10 <sup>-32</sup>		
293	H <sub>2</sub> O	52.1 × 10 <sup>-32</sup>		
293	Ar	3.7 × 10 <sup>-32</sup>	Discharge flow calorimetric probe	Larkin and Thrush
293	He	6 × 10 <sup>-32</sup>		
293	He	6 × 10 <sup>-32</sup>	Mass spectrometric probe of diffusional cloud	Dodonov, <i>et al.</i>

the helium and argon plot in Figure 2 gives a value for  $k_1^{\text{He}} = k_1^{\text{Ar}} = 1.57 \times 10^{-32} \text{ cm}^6 \text{ molecule}^{-2} \text{ sec}^{-1}$ . The slopes from similar plots at other temperatures (Figure 3) are presented in Arrhenius fashion in Figure 4. The Arrhenius expression, determined from a weighted least-squares treatment of the data, was found to be

$$k_1^{\text{He}} = [6.66 (+1.2, -1)] \times 10^{-33} \exp\left[\frac{(473 \pm 92) \text{ cal mol}^{-1}}{1.987T}\right]$$

in units of  $\text{cm}^6 \text{ molecule}^{-2} \text{ sec}^{-1}$ . The weights for the points were chosen according to the quantity and quality of the data. The error limits given are standard deviations from the least-squares fit. An unweighted least-squares analysis of the Arrhenius data gives

$$k_1^{\text{He}} = [5.89 (+0.80, -0.70)] \times 10^{-33} \exp\left[\frac{(522 \pm 66) \text{ cal mol}^{-1}}{1.987T}\right]$$

By making use of the full 15% error bars shown in Figure 4, the preexponential factor ranges from 4.2 to  $7.6 \times 10^{-33} \text{ cm}^6 \text{ molecule}^{-2} \text{ sec}^{-1}$  and the exponential term from 380 to 700 cal/mol.

At 298 K the ratios of third-body efficiencies for stabilizing the HO<sub>2</sub> adduct are CH<sub>4</sub>/N<sub>2</sub>/He/Ar = 15.7:3.4:1.0:1.0. The ratio of efficiencies of N<sub>2</sub> to He is 4.5:1 at 226 K. These trends in efficiencies are in good agreement with those recently observed for the O + O<sub>2</sub> + M reaction system.<sup>20</sup>

In Table V the results of the present work are summarized along with recent measurements of other workers. Excluded from the table are the numerous high-temperature flame and shock tube data as well as any other studies dealing with inert gases and temperatures outside the scope of the present work. At 298 K excellent agreement is obtained with Dorfman, *et al.*,<sup>9</sup> Moortgat and Allen,<sup>12</sup> Westenberg and deHaas,<sup>10</sup> and

(20) R. E. Huie, J. T. Herron, and D. D. Davis, *J. Phys. Chem.*, **76**, 2653 (1972).

Wong and Davis<sup>13</sup> for  $M = \text{He, Ar, and N}_2$ . The difference between the  $k_1^{\text{CH}_4}$  values of this work and that of Wong and Davis is within the expanded error limits which must be assigned to both values (as described earlier). The Arrhenius parameters show somewhat different temperature dependences with nearly equal  $A$  factors although both are within the quoted uncertainties. Since identical techniques were used, however, it would have been more gratifying were there better overlap in the temperature dependence. This difference in temperature dependence for He or Ar coupled with the identical  $\text{N}_2$  results solely accounts for the discrepancy in the relative deactivation efficiency ratios at low temperature. The data of Michael<sup>11</sup> give rate constants much lower than those of most present studies. Whereas no definite explanation for the low values can be given at this time, it is possible that production of H atoms in the mercury hydride system could account for slower measured decay rates. We cannot say whether this would affect the measured relative deactivation efficiencies.

The uncertainties in the flow data of Clyne,<sup>6a</sup> Clyne and Thrush,<sup>6b</sup> and Larkin and Thrush<sup>7</sup> can be ascertained from the variation in rate constants between successive studies and temperatures. These studies required corrections for longitudinal diffusion, reaction with product species, wall reactions, and efficiencies of other inert gases present. They are not as precise or accurate as the more recent flow studies of Moortgat and Allen or Westenberg and de Haas, who were able to use information from the earlier studies in making these corrections. Nevertheless, the agreement with our present work is probably within the error limits of these earlier studies.

The high value for  $k_1^{\text{He}}$  obtained by Dodonov, *et al.*,<sup>8</sup> was determined by mass spectrometric probing in a diffusional cloud. The extreme uncertainties in defining the chemistry and physical boundary of the reacting system tend to question the reliability of the results.

Since our temperature coverage did not exceed 404 K, any comparisons with the previous high-temperature

flame and shock tube work must rely on the validity of extrapolating our Arrhenius fit outside of our measurement range. If we assume no gross disparity from the fit in going to high temperatures, the present study predicts a change in rate constant from  $7.6 \times 10^{-33}$  to  $8.4 \times 10^{-33} \text{ cm}^6 \text{ molecule}^{-2} \text{ sec}^{-1}$  over the temperature interval 1600–1000 K. This is to be compared with measured values of  $8.3 \times 10^{-33}$  (1435–1650 K),<sup>3c</sup>  $9.1 \times 10^{-33}$  (1100 K),<sup>4a</sup> and  $3.9 \times 10^{-33}$  (1500 K).<sup>3a</sup> Many of the similar high-temperature studies suffer from the inability to specify the M species and the necessary assignment of a complicated mechanism. All have reported uncertainties neighboring 50%.

Several reviews<sup>14</sup> have appeared dealing with reaction 1. The recommended Arrhenius parameters are, as explained earlier, subject to large uncertainties due to the large scatter in the high-temperature data and the lower precision and accuracy of the earlier low-temperature work. The recent review of Baulch, *et al.*,<sup>14</sup> assigns (in units of  $\text{cm}^6 \text{ molecule}^{-2} \text{ sec}^{-1}$ )

$$k_1^{\text{Ar,He}} = [4.1 \pm 1.0] \times 10^{-33} \exp \left[ \frac{(1000 \pm 500) \text{ cal mol}^{-1}}{1.987T} \right]$$

The present work has established the rate constant for the combination reaction of atomic hydrogen with molecular oxygen as a function of temperature for a number of collision partners. Measurements were made in a static system free from the possible large uncertainties due to secondary and wall reactions. Conditions were chosen to match those needed for atmospheric modeling. The results indicate a smaller temperature dependence of  $k_1^{\text{M}}$  than previously assumed as well as lower absolute values than reported in the early discharge flow work. The very recent measurements of other workers fully support these observations.

*Acknowledgment.* The author would like to thank the numerous workers<sup>10–13</sup> who made their results available prior to publication.



# Pressure Dependence and Mechanism of the Reaction of Atomic Oxygen and Carbon Monoxide

by W. B. DeMore

*Jet Propulsion Laboratory, California Institute of Technology, Pasadena, California 91103 (Received July 20, 1972)*

*Publication costs assisted by the Jet Propulsion Laboratory*

The rate of the O + CO reaction has been measured at room temperature from 0.74 to 41.9 atm with CO<sub>2</sub> or N<sub>2</sub> as the major third body. The method was based on relative rate measurements, with the O + O<sub>2</sub> reaction as reference. The pressure dependence is more complex than that normally observed for simple atom association reactions. Below 1 atm the reaction appears to be intermediate between second and third order, in agreement with the earlier results of Simonaitis and Hecklen. However, at higher pressures a further increase in rate constant is observed. This latter effect is attributed to a reaction path which is negligible at low pressures but which becomes dominant at higher pressures. Detailed mechanisms are suggested.

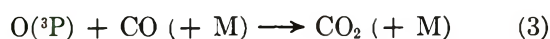
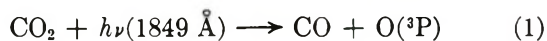
## Introduction

The mechanism of the O + CO reaction is not known with certainty. The CO<sub>2</sub> potential energy diagram is complex, and several paths from reactants to product are available. It is quite possible, in fact, that different mechanisms predominate under different conditions of temperature and pressure. The experimental situation is complicated by the fact that CO is subject to spurious oxidation in the presence of hydrogenous impurities and by other mechanisms which are not understood.<sup>1</sup>

This paper deals with the pressure dependence of the O + CO reaction, which can provide insight into the mechanism. Hecklen and Simonaitis<sup>2</sup> have recently reported that the reaction enters the second-order limit at pressures of about 0.5 atm of N<sub>2</sub>O. They consider that this result is not due to impurity effects which may have led to earlier reports<sup>3,4</sup> that the reaction is second order at low pressures. In the present work the rate constant has been measured at pressures from 0.74 to 41.9 atm of CO<sub>2</sub> at room temperature. A few experiments were also carried out with N<sub>2</sub> as the major third body. The results agree well with those of Simonaitis and Hecklen at low pressures, but at higher pressures the rates increase more rapidly than a linear extrapolation of the low pressure data would predict.

## Experimental Section

The O + CO rate was measured relative to the reaction O + O<sub>2</sub> + M → O<sub>3</sub> + M. Atomic oxygen was produced by photolysis of CO<sub>2</sub> at 1849 Å



The rate constant ratio was then determined from the expression

$$(R_0/R)_P = 1 + \frac{k_{\text{CO}}[\text{CO}]}{k_{\text{O}_2}[\text{O}_2]} \quad (4)$$

where  $(R_0/R)_P$  is the ratio by which the rate of O<sub>3</sub> production was suppressed at any given pressure by the O + CO reaction. In most of the experiments the CO<sub>2</sub> concentration was so high that the significant properties of the mixtures (rate of light absorption and effective third-body concentration) were independent of the presence or absence of the CO. Nevertheless, in the mixtures used to determine  $R_0$  the CO was replaced by an equal pressure of N<sub>2</sub> to compensate for any possible effects. The CO pressures ranged from about 50 to 1000 Torr with sufficient O<sub>2</sub> being added to give CO/O<sub>2</sub> ratios in the range 100–800.

The quantities  $k_{\text{CO}}$  and  $k_{\text{O}_2}$  are the effective second-order rate constants for the respective reactions. Values of  $k_{\text{O}_2}$  as a function of pressure were calculated from the results of Sauer<sup>5</sup> and also Hippler and Troe.<sup>6</sup> Since N<sub>2</sub> was the third body in the experiments of Hippler and Troe, their results were recalculated for CO<sub>2</sub> as third body by assuming a ratio of 2.7 for the efficiency of CO<sub>2</sub> relative to N<sub>2</sub>. The rate expressions are

$$k_{\text{O}_2} (M^{-1} \text{ sec}^{-1}) = \frac{1.1 \times 10^9}{1 + 64/P_{\text{CO}_2} (\text{atm})} \quad (\text{Sauer}) \quad (5)$$

(1) L. M. Arin and P. Warneck, *J. Phys. Chem.*, **76**, 1514 (1972).

(2) R. Simonaitis and J. Hecklen, *J. Chem. Phys.*, **56**, 2004 (1972).

(3) B. H. Mahan and R. B. Solo, *ibid.*, **37**, 2669 (1962).

(4) L. I. Avramenko and R. V. Kolesnikova, *Bull. Acad. Sci. USSR*, **9**, 1506 (1959).

(5) M. C. Sauer, Jr., *J. Phys. Chem.*, **71**, 3311 (1967).

(6) H. Hippler and J. Troe, *Ber. Bunsenges. Phys. Chem.*, **75**, 27 (1971).

$$k_{O_2} (M^{-1} \text{ sec}^{-1}) = \frac{1 \times 10^9}{1 + 31.5/P_{CO_2} (\text{atm})} \quad (\text{Hippler and Troe}) \quad (6)$$

In the low pressure limit, these expressions correspond to  $k_{O_2}' = 4.2 \times 10^8$  and  $7.8 \times 10^8 M^{-2} \text{ sec}^{-1}$ , respectively. These numbers bracket recent measurements of the  $O + O_2$  rate constant in the presence of  $CO_2$ ,<sup>7,8</sup> with the former being perhaps closer to presently accepted values. Virtually all of the recent measurements, which are summarized in ref 8, fall in the range  $5 \pm 2 \times 10^8 M^{-2} \text{ sec}^{-1}$ . In the high pressure limit, both expressions approach a limiting  $k_{O_2}$ , which is in good agreement with the rate constant for isotopic exchange of atomic oxygen with  $O_2$  (multiplied by a factor of 2), which is  $k_{ex} = 1.2 \times 10^9 M^{-1} \text{ sec}^{-1}$ .<sup>9</sup> At intermediate pressures, the above expressions predict somewhat different behavior, and since it is not clear which is more nearly correct, the  $O + CO$  results were calculated according to both equations.

At high pressures, nonideality of  $CO_2$  was corrected for in a first-order fashion by dividing the measured pressure by the compressibility factor.<sup>10</sup>

An important feature of the experimental method was an  $O_2$ - $O_3$  filter used to remove 2537-Å light. This was necessary to avoid complications arising from  $O_3$  photolysis, such as production of  $O(^1D)$ . The filter consisted of a cylindrical quartz cell (2-in. diameter by 1-cm path length) which was filled with 2 atm of Matheson ultrahigh-purity  $O_2$  and which was water-jacketed so that it could be cooled to  $0^\circ$  by means of a circulating water system. Under these conditions, the  $O_3$  optical density at 2537 Å rapidly reached values greater than 3.5 and remained constant as long as the lamp was left on. Since  $O_3$  absorbs relatively weakly at 1849 Å, the transmission at that wavelength was constant and practically independent of small changes in the  $O_3$  concentration.

Several types of cells were used, differing in geometry, surface to volume ratio, and construction materials. Some of these are illustrated in Figure 1. The stainless steel cell (Figure 1a) was used in the initial experiments at high pressure. At lower pressures this cell proved unsuitable because, with a lower rate of  $O_3$  production resulting from the reduced  $CO_2$  absorption, surface decomposition was no longer negligible. Thus, at low pressures an all-quartz cell was used in which the rate of  $O_3$  decomposition was much reduced compared to the metal cell. Finally, to bridge the gap between these two pressure regimes and to assure independence of the results on cell type, counterpressurized quartz cells (Figures 1b and c) were constructed. Two cell diameters were used to test for effects of wall proximity to the photochemical region.

The  $O_3$  concentrations were measured on a Cary Model 15 spectrophotometer.

Impurity effects are the most serious potential source

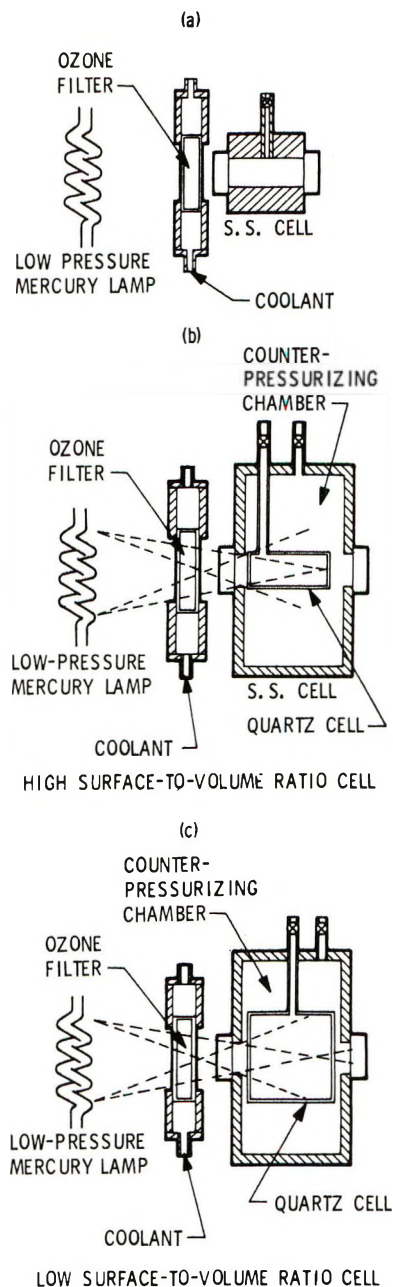


Figure 1. Schematic diagrams of apparatus, showing low pressure mercury lamp,  $O_3$  filter to remove 2537-Å light, and different types of high pressure cells which were used.

of error in these experiments, and therefore strenuous efforts were taken to assess the influence of these effects, including deliberate addition of  $H_2$  and  $H_2O$  to the mixtures. The results were found to be quite independent of the presence of these impurities, even at concentrations exceeding that of the  $O_2$ . In most of the experiments the  $CO_2$  was Matheson "Aqua-rater" grade, but

(7) F. Kaufman, *Ann. Rev. Phys. Chem.*, **20**, 45 (1967).

(8) R. E. Huie, J. T. Herron, and D. D. Davis, *J. Phys. Chem.*, **76**, 2653 (1972).

(9) S. Jaffe and F. S. Klein, *Trans. Faraday Soc.*, **62**, 3135 (1966).

(10) J. Hilsenrath, *et al.*, "Tables of Thermal Properties of Gases," *Nat. Bur. Stand. (U. S.) Circ.*, 564 (1955).



Table I: Summary of Experimental Results

$P$ , atm		$P_{\text{eff.}}^a$ atm	Cell <sup>b</sup>	Ratio $k_{\text{CO}}/k_{\text{O}_2} \times 10^4$	$\log k_{\text{CO}}$ , $M^{-1} \text{sec}^{-1}$	
CO <sub>2</sub>	N <sub>2</sub>				c	d
0.74		0.74	Q	4.17	4.99	4.72
0.91		0.91	Q	3.80	5.04	4.77
1.01		1.01	Q	3.40	5.03	4.76
1.27		1.27	Q	2.88	5.05	4.79
1.93		1.93	Q	2.32	5.13	4.86
2.6		2.6	SCPQ	1.64	5.09	4.84
2.6		2.6	Q	1.60	5.08	4.83
3.2		3.3	LCPQ	1.40	5.11	4.88
3.2		3.3	SCPQ	1.50	5.14	4.91
3.2		3.3	SS	1.80	5.21	4.98
4.9		5.0	SCPQ	1.46	5.30	5.06
6.6		6.8	SCPQ	1.28	5.36	5.13
3.2	10.2	7.1	SCPQ	1.24	5.36	5.13
7.8		8.2	SS	1.50	5.50	5.28
3.2	24.9	12.5	LCPQ	0.73	5.32	5.11
3.2	24.9	12.5	SCPQ	0.88	5.40	5.19
14.6		16.0	SS	1.00	5.53	5.34
3.2	38.4	17.5	SS	1.08	5.58	5.40
21.4		24.0	SS	0.81	5.55	5.39
3.2	66	27.8	SS	0.77	5.56	5.41
28.2		34.0	SS	0.63	5.51	5.38
3.2	100	40.3	SS	0.78	5.64	5.52
41.9		56.0	SS	0.54	5.54	5.44

<sup>a</sup> $P_{\text{eff.}} = P(\text{CO}_2)/K + P(\text{N}_2)/2.7$ , where  $K$  = compressibility factor. <sup>b</sup> Q = all-quartz cell; SCPQ = small counterpressurized quartz cell (Figure 1b); LCPQ = large counterpressurized quartz cell (Figure 1c); SS = stainless steel walled cell (Figure 1a). <sup>c</sup>  $k_{\text{CO}}$  calculated from data of Hippler and Troe, ref 6. <sup>d</sup>  $k_{\text{O}_2}$  calculated from data of Sauer, ref 5.

in general the results were not sensitive to the grade of CO<sub>2</sub> used. This independence of hydrogenous impurities probably stems largely from the absence of O(<sup>1</sup>D), since O(<sup>3</sup>P) does not react rapidly with most of these substances. It was found necessary, however, to purify the CO carefully by passage through packed spirals at liquid N<sub>2</sub> or liquid Ar temperature. Without this treatment little or no O<sub>3</sub> could be produced in the CO mixtures, even though research grade CO was used. It was occasionally noted that the initial O<sub>3</sub> production rates were low, but later increased to a constant value with continuing radiation. This behavior may have been due to impurity consumption, a process which has previously been found in O<sub>3</sub>-CO mixtures.<sup>1</sup>

With adequate purification of the CO and with clean, conditioned cells, the rates of O<sub>3</sub> production in both reference and CO-containing mixtures were linear with time, usually to within 5% or better. To avoid buildup of excessive O<sub>3</sub> concentrations and the resultant possibility of secondary reactions, the O<sub>3</sub> was frequently decomposed by exposure to 2537-Å light between radiation intervals. The maximum O<sub>3</sub> concentrations were not permitted to exceed about 0.1 Torr.

## Results

Figure 2 shows the results of a series of experiments to test the linear dependence of  $R_0/R$  on the CO/O<sub>2</sub> ratio, as predicted by eq 4. The ratios  $R_0/R$  were found to be independent of the absolute amounts of

CO and O<sub>2</sub> present, when these quantities were varied by a factor of 4.

Table I summarizes the results of all experiments at different pressures and in the various cell types. Included also are experiments in which a constant pressure of CO<sub>2</sub> was added to serve as a source of O(<sup>3</sup>P), and varying additional pressures of N<sub>2</sub> were added. The purpose of these experiments was to test for possible effects due to impurities or nonideality of the CO<sub>2</sub>. In calculating the "effective" pressure of N<sub>2</sub> (*i.e.*, the equivalent pressure of CO<sub>2</sub>), it was assumed that N<sub>2</sub> is 2.7 times less efficient as a third body compared to CO<sub>2</sub>. This is undoubtedly valid for the O + O<sub>2</sub> reaction but is only an approximation for the O + CO reaction. Nevertheless, the resulting O + CO rate constants calculated in this way are consistent with those obtained in CO<sub>2</sub>. This is a strong indication that the increase of  $k_{\text{CO}}$  at high pressures reflects a true pressure dependence and is not an artifact arising from impurities in the CO<sub>2</sub>.

The rate data at pressures near 1 atm, if arbitrarily calculated as third-order rate constants, give good agreement with results obtained by others at lower pressures by different methods. For example, at 0.74 atm  $k_{\text{CO}} = 5.3 \times 10^4$  or  $9.8 \times 10^4 M^{-1} \text{sec}^{-1}$ , depending on whether eq 5 or 6 is used to calculate  $k_{\text{O}_2}$ . Taking the average of these two values, the corresponding third-order rate constant  $k_{\text{CO}}' = 2.5 \times 10^6 M^{-2} \text{sec}^{-1}$ .

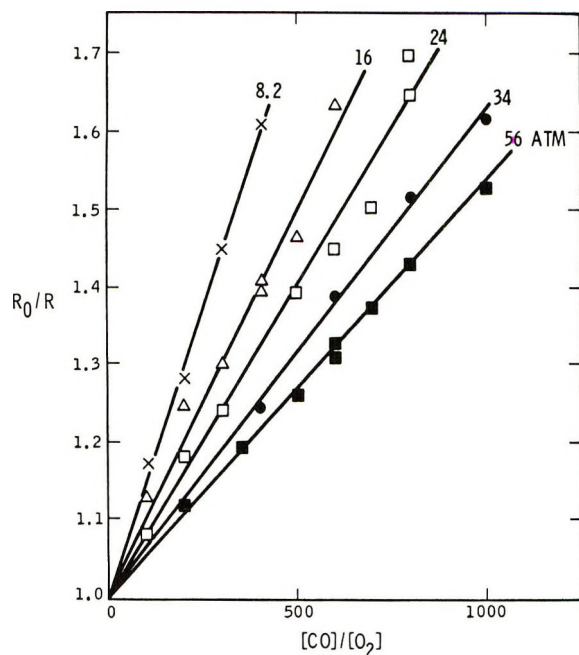


Figure 2. Plots of data according to eq 4 for different pressures of  $\text{CO}_2$ . The pressures listed are "effective pressures," *i.e.*, the measured pressure divided by the compressibility factor.

This value is in good agreement with the result of Slanger, Wood, and Black,<sup>11</sup> who obtained  $k_{\text{CO}}' = 2.2 \times 10^6 M^{-1} \text{sec}^{-1}$  with  $\text{CO}_2$  as third body. The important conclusion, therefore, is that the present measurements show no evidence of impurity effects, which would give an apparent high rate constant.

Inspection of Table I reveals, however, that the increase of  $k_{\text{CO}}$  is not proportional to pressure, so that the reaction cannot be in the third-order region. This behavior (below 2 atm) agrees with that observed by Simonaitis and Heicklen,<sup>2</sup> as can be seen in Figure 3.

Figure 3 shows that, below about 2 atm, the  $\text{O} + \text{CO}$  reaction behaves as if it were entering the high pressure (second-order) limit, with a transition pressure  $P_{1/2}$  equal to 0.5 (Figure 3a) or 0.3 atm (Figure 3b). However, at higher pressures  $k_{\text{CO}}$  continues to increase, rather than approaching the limit obtained by extrapolation of the low pressure data. This behavior cannot be ascribed to uncertainty in the  $\text{O} + \text{O}_2$  pressure dependence.

### Discussion

A suitable mechanism must account for the fact that fall-off behavior is observed at pressures much lower than normally expected for simple atom association reactions involving a triatomic product. The  $\text{O} + \text{O}_2$  reaction, which may be cited as an example, remains third order at pressures about 100-fold higher. To explain the low pressure fall-off, Simonaitis and Heicklen invoked the mechanism originally suggested by Clyne and Thrush<sup>12,13</sup> in connection with the chemi-

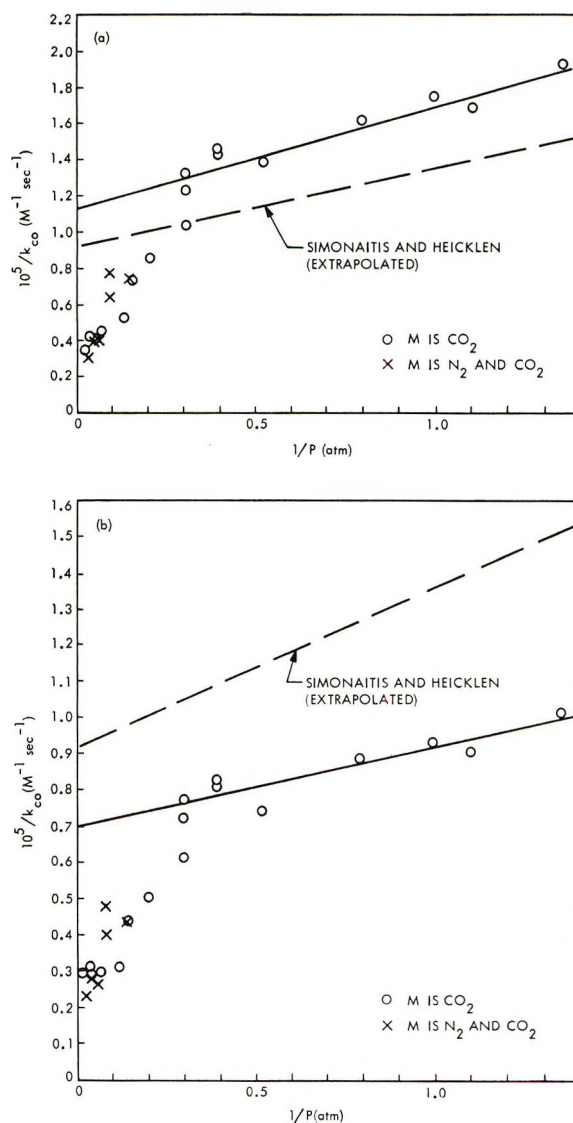
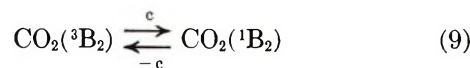
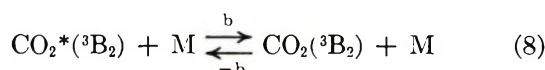
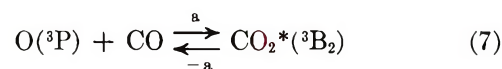


Figure 3. Plots of  $1/k_{\text{CO}}$  vs.  $1/P$ : a,  $k_{\text{CO}}$  calculated from the data of Sauer<sup>6</sup> for  $k_{\text{O}_2}$ ; b,  $k_{\text{CO}}$  calculated from the data of Hippler and Troe<sup>6</sup> for  $k_{\text{O}_2}$ .

luminescent combination of  $\text{O}$  and  $\text{CO}$ . This mechanism (mechanism I) is shown below in eq 7–10, with the modification that the initial step of formation of  $\text{CO}_2(^3\text{B}_2)$  is not constrained to be in the low pressure limit, as was done in the earlier work.



(11) T. G. Slanger, B. J. Wood, and G. Black, *J. Chem. Phys.*, **57**, 233 (1972).

(12) M. A. A. Clyne and B. A. Thrush, *Proc. Roy. Soc., Ser. A*, **269** 404 (1962).

(13) M. A. A. Clyne and B. A. Thrush, *Symp. (Int.) Combust., [Proc.] 9th*, 177 (1963).





Figure 4 shows the relevant potential energy diagram, as proposed by Clyne and Thrush.

The properties of mechanism I are

$$\frac{d[\text{CO}_2]}{dt} = \frac{k_a k_b k_c k_d [\text{O}][\text{CO}][\text{M}]}{k_{-a}(k_{-c}k_{-b} + k_d k_c) + k_d [\text{M}](k_{-a}k_{-b} + k_c k_b)} = k_{\text{CO}}[\text{O}][\text{CO}] \quad (11)$$

$$[\text{M}] \rightarrow \infty; \quad k_{\text{CO}} \rightarrow k_\infty = \frac{k_a k_b k_c}{k_{-a}k_{-b} + k_c k_b} \leq k_a \quad (12)$$

$$[\text{M}] \rightarrow \text{O}; \quad k_{\text{CO}} \rightarrow k_0 = \frac{k_c k_d}{k_{-c}k_{-b} + k_c k_d} \times \frac{k_a k_b [\text{M}]}{k_{-a}} \leq \frac{k_a k_b [\text{M}]}{k_{-a}} \quad (13)$$

The characteristic fall-off pressure (at which  $k_{\text{CO}} = 0.5k_0$ ) occurs at

$$[\text{M}]_{1/2} = \frac{k_{-a}(k_{-c}k_{-b} + k_c k_d)}{k_d(k_{-a}k_{-b} + k_c k_b)} \quad (14)$$

From eq 12, it is seen that the limiting high pressure rate constant,  $k_\infty$ , approaches a value less than  $k_a$  if  $k_{-a}k_{-b} \geq k_c k_b$ . An independent estimate of the quantity  $k_a$  can be obtained from the experiments of Jaffe and Klein<sup>9</sup> on the exchange of isotopically labeled O with CO. Taking  $k_a$  as twice the rate constant for isotopic exchange at room temperature, the result is  $k_a = 1.2 \times 10^6 \text{ M}^{-1} \text{ sec}^{-1}$ . This value is an order of magnitude higher than  $k_\infty$  obtained from Figure 3a or b by extrapolation of the low pressure data, including that of Simonaitis and Heicklen. Further, eq 14 shows that the low pressure fall-off behavior cannot be accounted for unless  $k_{-a}k_{-b} > k_c k_b$ , because otherwise it is necessary to postulate an abnormally long lifetime of  $\text{CO}_2^*(^3\text{B}_2)$ . However, if the condition  $k_{-a}k_{-b} > k_b k_c$  is met, then eq 14 takes the form

$$[\text{M}]_{1/2} \simeq \frac{k_{-c}}{k_d} + \frac{k_c}{k_{-b}} \quad (15)$$

The quantities  $k_d$  and  $k_{-b}$  are rate constants for collisional processes and are unlikely to be greater than  $10^{11} \text{ M}^{-1} \text{ sec}^{-1}$  and may be considerably less. Thus, to account for the observed fall-off at  $P_{1/2} \sim 0.5 \text{ atm}$  ( $M_{1/2} \sim 0.02 \text{ M}$ ), it is necessary that

$$k_{-c} + k_c < 10^9 \text{ sec}^{-1} \quad (16)$$

It is important to note that the  $\text{CO}_2(^3\text{B}_2)$  produced in eq 8 is probably not in low vibrational levels of the  $^3\text{B}_2$  state. In fact, the temperature dependence of the high pressure rate constant observed by Simonaitis and

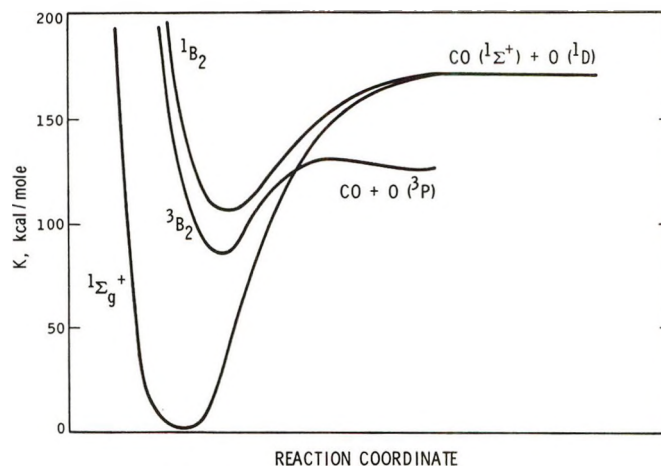
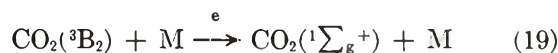
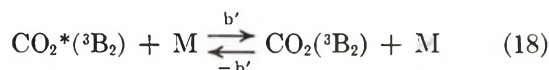
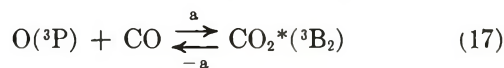


Figure 4.  $\text{CO}_2$  potential energy diagram similar to that of Clyne and Thrush.<sup>12</sup>

Heicklen was consistent with an activation energy for  $k_{-b}$  of about 1 kcal/mol. (In the context of their experiments, high pressure refers to the region of about 1 atm.) It appears, therefore, that crossing to the  $^1\text{B}_2$  state occurs predominantly from vibrational levels near the dissociation limit of the  $^3\text{B}_2$  state. Population of lower vibrational levels of the  $^3\text{B}_2$  state undoubtedly occurs, but would not affect the rate behavior except when direct collisional quenching to the ground state competes at a significant rate. If this latter process occurs, the mechanism is (mechanism II, eq 17-19)



The primed notation in eq 18 is intended to denote the fact that different (possibly lower) vibrational levels of the  $^3\text{B}_2$  state are involved. The properties of mechanism II are

$$\frac{d[\text{CO}_2]}{dt} = \frac{k_a k_b k_e [\text{O}][\text{CO}][\text{M}]}{k_{-a}k_{-b}' + k_{-a}k_e + k_b k_e [\text{M}]} = k_{\text{CO}}[\text{O}][\text{CO}] \quad (20)$$

$$[\text{M}] \rightarrow \infty; \quad k_{\text{CO}} \rightarrow k_\infty = k_a \quad (21)$$

$$[\text{M}] \rightarrow \text{O}; \quad k_{\text{CO}} \rightarrow k_0 = \frac{k_c}{k_{-b}' + k_e} \times \frac{k_a k_b' [\text{M}]}{k_{-a}} \leq \frac{k_a k_b' [\text{M}]}{k_{-a}} \quad (22)$$

$$[\text{M}]_{1/2} = \frac{k_{-a}}{k_b'} \left( \frac{k_{-b}' + k_e}{k_e} \right) \geq \frac{k_{-a}}{k_b'} \quad (23)$$

As seen by eq 21, this mechanism predicts a limiting

high pressure rate constant equal to the rate constant of the initial step,  $k_a$ . The value of  $k_a$  obtained by extrapolation of the high pressure rate constants ( $0.5$  to  $1.0 \times 10^6 M^{-1} \text{sec}^{-1}$ ) is in good agreement with the estimate of  $k_a$  based on the exchange experiments of Jaffe and Klein, as previously discussed. This can explain why mechanism II is dominant in the high pressure region.

At low pressures, the relative unimportance of mechanism II can be accounted for most simply by the condition that  $k_d \gg k_e$ . This reflects the not unexpected fact that  $\text{CO}_2(^3\text{B}_2)$  is more resistant to collisional quenching than  $\text{CO}_2(^1\text{B}_2)$ .

The predicted fall-off behavior of mechanism II is similar to that of a "normal" association reaction, in which the reactants correlate with the ground state of the product and the mechanism is of the energy transfer type. Under these circumstances  $[M]_{1/2}$  is given by the ratio of the reciprocal lifetime of the collision complex and the rate constant for collisional deactivation of the complex. In the present case an even stronger pressure dependence is possible, depending on the relative magnitudes of  $k_{-b}$ , and  $k_e$ .

A referee has suggested that the pressure dependence

in Figure 3 may be related to the curvature which is frequently observed in plots of  $1/k$  vs.  $1/P$ . Such curvature arises from a spread in the energy of the initial reaction complex, so that the overall pressure dependence is actually a composite of a range of different pressure dependences. However, this interpretation is equivalent to attributing the low pressure fall-off behavior of the  $\text{O} + \text{CO}$  reaction to a long lifetime of the  $\text{CO}_2^*(^3\text{B}_2)$  intermediate. Otherwise, the onset of curvature could not occur at relatively low pressures. The  $\text{O} + \text{O}_2$  reaction, using the data of Hippler and Troe, shows no curvature in the same pressure range when plotted in this fashion. To the present author, it seems preferable to explain the low pressure fall-off in terms of a low  $k_e$  rather than a low  $k_{-a}$ , and to account for the curvature by the onset of mechanism II.

*Acknowledgments.* The author is grateful to Dr. Ara Chutjian for helpful conversations concerning the  $\text{CO}_2$  potential energy surfaces. This paper presents the results of one phase of research carried out at the Jet Propulsion Laboratory, California Institute of Technology, under Contract No. NAS7-100 sponsored by the National Aeronautics and Space Administration.

## Reactions of Borane ( $\text{BH}_3$ ). VII.<sup>1</sup> Reaction with Ketene

by T. P. Fehlner

Department of Chemistry, University of Notre Dame, Notre Dame, Indiana 46556 (Received June 27, 1972)

Publication costs assisted by the National Science Foundation

The reaction of borane with ketene to produce a single addition product having the composition  $\text{BC}_2\text{H}_5\text{O}$  has been shown to occur. At  $460^\circ\text{K}$ , 4.5 Torr total pressure of helium, and low partial pressures of reactants, the bimolecular rate constant for this reaction is  $4 \times 10^9 M^{-1} \text{sec}$ . All available evidence indicates that  $\text{BC}_2\text{H}_5\text{O}$  is a donor-acceptor adduct involving  $\text{BH}_3$  and the carbon-carbon  $\pi$  bond. The significance of these results with regard to the reactivity of borane is discussed.

One of the objectives of studying the elementary reactions of borane is to obtain a better understanding of the relationship between the electronic structure of this species and its chemical reactivity. One approach to such an understanding is to compare and contrast the nature and the rates of the reactions of  $\text{BH}_3$  with those of other reactive species. Singlet methylene, a reactive species isoelectronic with  $\text{BH}_3$ , readily undergoes reaction 1.<sup>2,3</sup>



As  $\text{BH}_3$  undergoes the isoelectronic reaction<sup>4</sup>



the reaction of  $\text{BH}_3$  with ketene has been examined.

(1) Part VI: T. P. Fehlner, *Inorg. Chem.*, **12**, 98 (1973).

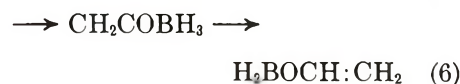
(2) R. A. Cox and K. F. Preston, *Can. J. Chem.*, **47**, 3345 (1969).

(3) W. Braun, A. M. Bass, and M. Pilling, *J. Chem. Phys.*, **52**, 5131 (1970).

(4) M. E. Garabedian and S. W. Benson, *J. Amer. Chem. Soc.*, **86**, 176 (1964).



A number of modes of reaction of  $\text{BH}_3$  with  $\text{CH}_2\text{CO}$  are possible.



All except reaction 7 which is highly endothermic may be fast reactions.<sup>5</sup> Reaction 3 is analogous to (1); (4) and (5) are so-called hydroborations;<sup>6</sup> and (6) corresponds to a reduction of the carbonyl group which is now known to proceed through the two discrete steps indicated.<sup>1,7</sup>

Because of the multitude of possible reaction paths, the reaction of  $\text{BH}_3$  with ketene and other difunctional molecules has another interesting aspect. Borane reacts readily with ethylene and somewhat less readily with acetone. When a molecule has both the carbon-carbon  $\pi$  bond and the carbonyl functional groups, the interesting question arises as to which feature of the molecular electronic structure, if either, will control the initial reactivity of the molecule. The answer to this question is directly related to how the electronic structures of chemical species interact in the course of a reaction. If, as has been suggested,<sup>8</sup> the highest occupied molecular orbital of one species and the lowest unoccupied molecular orbital of the other species determine the reaction character, then one should be able to predict the initial products of the reaction with  $\text{BH}_3$  as the lowest unoccupied orbital is always on  $\text{BH}_3$ . On the other hand, if these fast exothermic reactions with little or no activation energy proceed either through loose collision complexes with no specific bonding interaction or through donor-acceptor adducts with finite lifetimes, then other factors may well control the products observed. The study reported below was also carried out to test some of these ideas.

### Experimental Section

The apparatus utilized in this work, which has been described in detail previously,<sup>9-11</sup> consists of a fast-flow, gas-phase, tubular reactor directly coupled with modulated molecular beam sampling to a mass spectrometric analysis system. This system provides for variation in reactant partial pressures and reaction time. Total pressure and temperature were not easily changed and were held constant. Product identification was carried out by both conventional analysis of the mass spectra and by analysis of the relative phases of selected ions.<sup>11-14</sup>

The conditions of the present experiments were as follows.  $\text{BH}_3$  was prepared by the thermal decomposi-

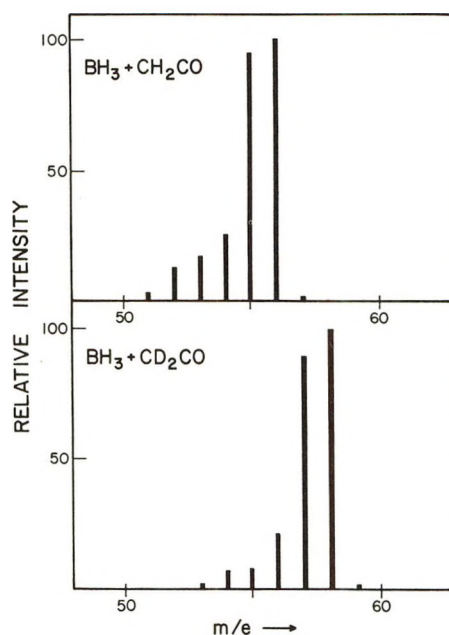


Figure 1. Mass spectra of the parent ion regions of the product of the reaction of  $\text{BH}_3$  and  $\text{CH}_2\text{CO}$  (top) and the reaction of  $\text{BH}_3$  and  $\text{CD}_2\text{CO}$  (bottom).

tion of  $\text{F}_3\text{PBH}_3$  in a hot zone similar to that shown at the top of Figure 1 in ref 10. Rate constant measurements were carried out by changing the position of the gas probe only.<sup>15</sup> The movement of this probe defines a reaction zone consisting of the last 2 cm of the reactor. The temperature of this zone was  $460 \pm 10^\circ\text{K}$ . The total pressure in the reactor was 4.5 Torr, and the flow velocity was *ca.*  $10^4$  cm/sec. Calibrations of stable materials were carried out as described previously.<sup>10</sup>

Trifluorophosphine borane and diborane were prepared and purified as described previously.<sup>15</sup> Ketene was prepared by the pyrolysis of acetic anhydride (J. T. Baker, Reagent).<sup>16</sup> Ketene- $d_2$  was prepared by the pyrolysis of acetic anhydride- $d_6$  (Merck Sharp and Dohme). Purification was by trap-to-trap fractiona-

(5) The techniques used here only allow the observation of reactions of  $\text{BH}_3$  with rate constants  $> 10^6 \text{ M}^{-1} \text{ sec}$ .

(6) H. C. Brown, "Hydroboration," W. A. Benjamin, New York, N. Y., 1962; *Chem. Brit.*, 7, 458 (1971).

(7) T. P. Fehlner, *Inorg. Chem.*, 11, 252 (1972).

(8) K. Fukui, H. Fujimoto, and S. Yamabe, *J. Phys. Chem.*, 76, 232 (1972), and references cited therein.

(9) G. W. Mappes and T. P. Fehlner, *J. Amer. Chem. Soc.*, 92, 1562 (1970).

(10) G. W. Mappes, S. A. Fridmann, and T. P. Fehlner, *J. Phys. Chem.*, 74, 3307 (1970).

(11) T. P. Fehlner, *J. Amer. Chem. Soc.*, 90, 4817 (1968).

(12) S. N. Foner, *Advan. At. Mol. Phys.*, 2, 385 (1966).

(13) R. M. Yealland, R. L. LeRoy, and J. M. Deckers, *Can. J. Chem.*, 45, 2651 (1967).

(14) M. H. Boyer, E. Murad, H. Inami, and D. L. Hildenbrand, *Rev. Sci. Instrum.*, 39, 26 (1968).

(15) S. A. Fridmann and T. P. Fehlner, *J. Phys. Chem.*, 75, 2711 (1971).

(16) R. L. NuHall, A. H. Laufer, and M. V. Kilday, *J. Chem. Thermodyn.*, 3, 167 (1971).

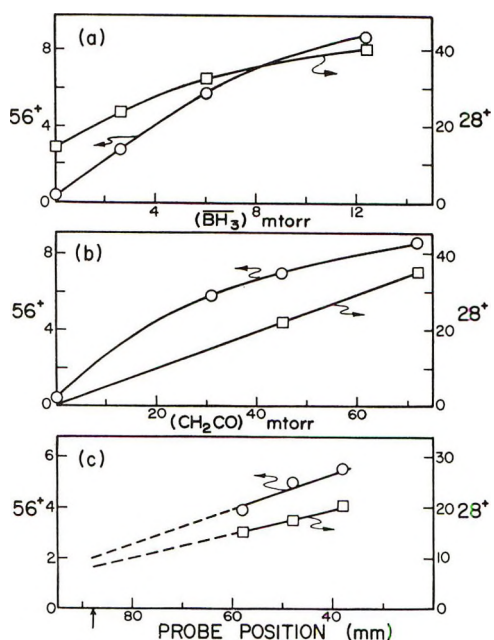


Figure 2. Variation in the intensities of the  $m/e$  56 and 28 ions (a) with mean borane partial pressure,  $(\text{BH}_3)_8$  at a constant ketene partial pressure of 72 mTorr and a probe position of 38.0; (b) with ketene partial pressure at a constant mean borane partial pressure of 12 mTorr and a probe position of 38.0; (c) with probe position (reaction time) at a mean borane partial pressure of 6 mTorr and a ketene partial pressure of 72 mTorr. In (c) the arrow indicates the relative position of the sampling orifice. In these experiments the mean temperature was  $460^\circ\text{K}$ , the total pressure was 4.5 Torr, and the flow velocity was  $1.2 \times 10^4$  cm/sec.

tion and the purified material was stored at  $-196^\circ$  in a black-painted bulb. Ketene was metered into the flow system from a bulb held at  $-78^\circ$ . Purities were checked mass spectrometrically.

### Product Identification

**Mass Spectra.** The mass spectrum was searched at  $m/e$  values that were not obscured by major fragment ions of molecules known to be present, *i.e.*,  $\text{F}_3\text{PBH}_3$ ,  $\text{PF}_3$ ,  $\text{BH}_3$ ,  $\text{B}_2\text{H}_6$ , and  $\text{CH}_2\text{CO}$ . With  $\text{CH}_2\text{CO}$  being injected immediately downstream of the  $\text{BH}_3$  preparation zone at a partial pressure of *ca.* 50 mTorr such that the total reaction time was *ca.* 0.5 msec, the most obvious change in the mass spectrum was the appearance of ions with  $m/e$  values corresponding to those expected for an addition product of  $\text{BH}_3$  and ketene. The relative intensities of these ions are shown in Figure 1. The presence of these ions depended on both  $\text{BH}_3$  and  $\text{CH}_2\text{CO}$  partial pressures and on reaction time as illustrated in Figure 2. These ions were easily observable, being only *ca.*  $10\times$  less intense than those from ketene. This is a qualitative indication of a large rate constant.

Changes in the intensity of  $m/e$  28 were also observed on the addition of  $\text{BH}_3$ . As illustrated in Figure 2,  $m/e$  28 increased with increasing  $\text{BH}_3$  at constant

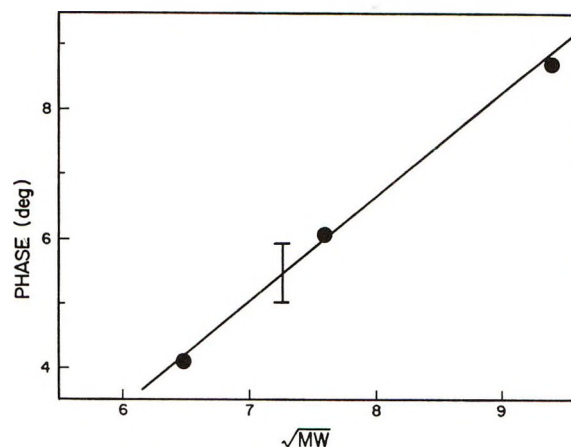


Figure 3. Plot of relative phase vs. the square root of the molecular weight of the neutral progenitor of the ion. Calibration points are  $m/e$  42 from  $\text{CH}_2\text{CO}$ ,  $m/e$  42 from *n*-butane, and  $m/e$  69 from  $\text{PF}_3$ . All calibrations were carried out under operating conditions of temperature, pressure, and flow. The relative phase of  $m/e$  56 from the borane-ketene addition product and the uncertainty in the measurement is shown by the hash mark. The calculated apparent molecular weight is  $53 \pm 4$ .

$\text{CH}_2\text{CO}$ , increased with increasing  $\text{CH}_2\text{CO}$  at constant  $\text{BH}_3$ , and increased with increasing reaction time. These observations are consistent with either  $m/e$  28 resulting from ionization of another product or  $m/e$  28 resulting from fragmentation of the molecular ion of the ketene-borane addition product. Clearly, these changes in  $m/e$  28 cannot be due to  $\text{CO}^+$  from  $\text{CH}_2\text{CO}$  as ions known to arise from ketene decrease with increasing  $\text{BH}_3$ . Because the intensity change of  $m/e$  28 is comparable in magnitude to the intensities in the  $m/e$  51-56 region, the former explanation is appealing. If correct, this would imply that changes in  $m/e$  28 are due to  $\text{CO}$  and/or  $\text{CH}_3\text{BH}_2$  production and the ions at  $m/e$  51-56 are due to  $(\text{CH}_3\text{BH}_2)_2$ . However, as is shown below, this explanation is not correct.

Ions were sought at  $m/e$  values greater than 56. Although very small, nonreproducible ion intensities were observed at a few  $m/e$  values, no ions that could be attributed to products were observed. No high-mass products with an ion intensity greater than 1% of  $m/e$  56 from the ketene-borane addition product were observed.

The reaction of  $\text{B}_2\text{H}_6$  with ketene was also examined as  $\text{B}_2\text{H}_6$  is always present from the association of  $\text{BH}_3$ . The reaction was examined with a total reaction time of 0.8 msec, at temperatures of 440 and  $570^\circ\text{K}$ , and for partial pressures of  $\text{B}_2\text{H}_6$  and ketene up to 50 and 30 mTorr, respectively. No ion intensities corresponding to those reported above were found. In addition no evidence was found for the rapid addition of  $\text{B}_2\text{H}_6$  and ketene.

**Phase Spectra.** Additional information concerning the identity of the reaction products was obtained by measuring the relative phase angle of selected ion sig-



nals. This phase angle is directly related to the molecular weight of the neutral progenitor of a given ion signal.<sup>11-14</sup> The relative phase angles of ions of both known and unknown molecular sources were obtained from plots of the ion signal at phase angle  $\phi$  minus the signal at phase angle  $\phi + 180^\circ$  vs. the phase angle  $\phi$ .<sup>17</sup> The results for  $m/e$  56 are shown in Figure 3, and it is clear that this ion results from a species having an apparent molecular weight of  $53 \pm 4$ . In contrast to the situation with the reaction of  $C_2H_4$  and alcohols<sup>1</sup> with  $BH_3$ , there is no suggestion at all that this ion is produced in part from fragmentation of higher mass products. This observation, along with the mass spectrometric results above, strongly suggests that there is no further reaction of the ketene-borane addition product either by dimerization or by addition of another molecule of ketene.

The relative phase of the  $m/e$  28 ion signal was also examined. This was somewhat difficult because of the noisy character of this mass number. However, although the results are qualitative, they are conclusive. The detector was nulled on  $m/e$  28 in the absence of  $BH_3$  when  $m/e$  28 is due only to  $CO^+$  from  $CH_2CO$ . In the presence of  $BH_3$  the sign of the detector response is characteristic of a neutral progenitor having a molecular weight greater than ketene. This behavior was checked using other known gases. Therefore, the  $m/e$  28 ion signal that is produced by the reaction of  $BH_3$  and  $CH_2CO$  is a fragment ion from the ketene-borane addition product.

**Isotopic Substitution.** To obtain final verification of the stoichiometric identification of the reaction products, the reaction of  $BH_3$  with  $CD_2CO$  was examined. The resulting mass spectrum in the  $m/e$  51-58 region is shown in Figure 1. The net effect of deuteration of ketene is a shift of the entire spectrum two mass units higher. This fact, plus the strong parent ion intensity, eliminates  $(CH_3BH_2)_2$  as a possible product as any 1,1-dimethyldiborane produced by the dimerization of methyl borane should contain four D atoms. In turn, the absence of  $(CH_3BH_2)_2$  implies the absence of  $CH_3BH_2$  as monoalkylboranes dimerize very readily.<sup>17</sup> Therefore the composition of the ketene-borane addition product produced from  $CD_2CO$  is  $BC_2H_3D_2O$ .

The ion production observed at  $m/e$  28 for  $CH_2CO$  shifted up to  $m/e$  30 for  $CD_2CO$ . The relative phase angle of the  $m/e$  30 ion indicated that it was derived from a species of molecular weight greater than 44. Therefore the composition of the  $m/e$  30 ion is  $BCH_3D_2$ . All the evidence shows that this ion is a fragment ion of the addition product  $BC_2H_3D_2O$ .

### Rate Measurements

**Sensitivities.** The most precise way to obtain a rate constant for the reaction of  $BH_3$  with ketene in this system is to measure the formation of the addition product as a function of time. In order to do so it is necessary

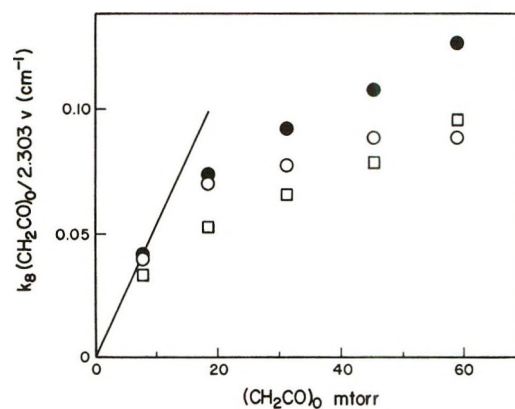
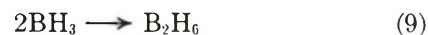


Figure 4. Plot of  $k_8(CH_2CO)_0/2.303v$  vs.  $(CH_2CO)_0$  at  $460^\circ K$  a total pressure of 4.5 Torr. The open circles refer to data taken at a mean  $(BH_3) = 2.4$  mTorr, the closed circles to data taken at a mean  $(BH_3) = 2.9$  mTorr, and the squares to data taken at mean  $(BH_3) = 5.6$  mTorr. The linear flow velocity,  $v$ , was  $1.3 \times 10^4$  cm/sec. The straight line corresponds to a bimolecular rate constant of  $4.3 \times 10^9 M^{-1} sec$ .

to determine a sensitivity for  $BC_2H_5O$ . From past experience the strong product signals indicated that reaction 8 would effectively swamp out reaction 9 at



high  $CH_2CO$  levels. Therefore  $CH_2CO$  was used to titrate the  $BH_3$  in the flow stream in the same manner as has been done previously.<sup>17</sup> The ion intensity of  $m/e$  56 at  $1/(CH_2CO) = 0$  is taken to represent a partial pressure of  $BC_2H_5O$  equal to the partial pressure of  $BH_3$  at the injection probe position in the absence of ketene. The partial pressure of  $BH_3$  is known<sup>9,10</sup> and was checked in this work. It was found that the sensitivity of  $m/e$  56 from  $BC_2H_5O$  is 1.7 times the sensitivity of  $m/e$  13 from  $BH_3$  and 0.3 times the sensitivity of  $m/e$  42 from  $CH_2CO$ . From the rate constant calculated below it is clear that reaction 8 is more than 20 times faster than (9) when  $(CH_2CO) > 10(BH_3)$  which is the case for these titrations.

**Rate Constant.** Using the  $m/e$  56 ion intensity as a monitor of the addition product, the amount formed as a function of probe position (time) at various fixed ketene partial pressures and various initial  $BH_3$  partial pressures was measured. An example of the data is shown in Figure 2. A rate constant for reaction 8 was obtained by ignoring reaction 9 and by assuming that the ketene partial pressure is independent of the extent of reaction. Both assumptions are valid for  $(CH_2CO) > 10(BH_3)$ . With these assumptions the integrated kinetic equation that is applicable is

$$\log [1 - (BC_2H_5O)/(BH_3)_0] = -k_8(CH_2CO)_0l/2.303v$$

where  $(BH_3)_0$  is the partial pressure of  $BH_3$  at the par-

(17) T. P. Fehlner, *J. Amer. Chem. Soc.*, **93**, 6366 (1971).

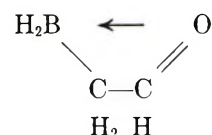
ticular probe position in the absence of ketene,  $(BC_2H_5O)$  is the partial pressure of the ketene-borane addition product,  $k_8$  is the bimolecular rate constant,  $(CH_2CO)_0$  is the initial ketene partial pressure,  $l$  is the probe position, and  $v$  is the linear flow velocity. These data were treated in the manner described previously,<sup>15</sup> and slopes of plots of  $\log [1 - (BC_2H_5O)/(BH_3)_0]$  vs.  $l$  are plotted against  $(CH_2CO)_0$  in Figure 4 for various mean values of  $BH_3$ . These plots should be straight lines with slopes equal to  $k_8/2.303v$ . The initial slope indicated by the straight line in Figure 4 corresponds to a  $k_8 = 4.3 \times 10^9 M^{-1} \text{ sec}$ . This is the largest rate constant that we have measured for a reaction of  $BH_3$  thus far. The fall-off in the apparent rate constant with increasing  $(CH_2CO)_0$  and at higher mean  $BH_3$  partial pressures is due mainly to the very rapid reaction rate.<sup>18</sup> In this system the error due to excessively fast reaction will tend to lower the apparent rate constant. As the error increases with increasing extent of reaction one expects the pseudo-first-order rate constant to fall off with increasing ketene partial pressure. For this reason the data reported here are only semi-quantitative and  $k_8$  may well vary by a factor of 4 to 5. It is, however, more likely to be low than high. An analysis of the various errors in our procedures has been given previously.<sup>10, 15</sup>

## Discussion

*Nature of the Elementary Reaction.* Products corresponding to reaction 3 are not observed and, because it is endothermic, reaction 7 would not be observed under these conditions. The composition of the product corresponds to  $BC_2H_5O$  and thus reactions 4-6 are possible. In addition one must consider the possibility that  $BC_2H_5O$  is a donor-acceptor adduct of  $BH_3$  as, for example, the intermediate product in reaction 6. Any more conclusive identification of the nature of the reaction of  $BH_3$  with ketene requires information on the structure of the product,  $BC_2H_5O$ . No direct structural evidence has been produced in this study but circumstantial evidence concerning the structure of  $BC_2H_5O$  exists and is presented below.

Previous observations indicate that tricoordinate boron compounds, *i.e.*, substituted boranes, behave quite differently from tetracoordinate boron compounds, *i.e.*, donor-acceptor adducts, in our system. Monosubstituted boranes tend to readily dimerize or form disubstituted boranes, both of which are easily identified by their high mass spectra, dependence on reagent partial pressures, and by phase measurements.<sup>1, 17</sup> Donor-acceptor adducts appear quite inert toward further reaction under our conditions.<sup>7, 15</sup> In the reaction of  $BH_3$  with ketene there is no evidence for the formation of higher mass products; thus, no evidence for further reaction. In contrast, allene, which is isoelectronic with ketene, produces easily visible high-mass products.<sup>19</sup> These facts indicate that  $BC_2-$

$H_5O$  contains tetracoordinate boron. However, this evidence does not distinguish between a ketene-borane donor-acceptor adduct and a tricoordinate borane with an internal donor-acceptor interaction, *e.g.*



The second clue concerning the structure of the addition product is the magnitude of the rate constant. The rate constant for the reaction of  $BH_3$  with carbonyl oxygen is *ca.* 10 times smaller than the rate constant for the reaction of  $BH_3$  with the double bond of ethylene.<sup>7, 17</sup> As calculated above, the rate constant for the reaction of  $BH_3$  with ketene is larger than that for the reaction with ethylene. Assuming that the collision probabilities for the reaction of  $BH_3$  with the carbon-carbon  $\pi$  bond and carbonyl oxygen are the same in ketene as in the separate molecules, one would expect reaction with the carbon-carbon  $\pi$  bond to occur with a rate constant of  $2 \times 10^9 M^{-1} \text{ sec}$ . If this naive argument is correct, one would also expect to see a product corresponding to the bis adduct of  $BH_3$  with ketene at roughly  $1/10$  the level of the mono adduct. The fact that one does not observe any ions that would correspond to the bis adduct can be explained by the conjugation between the carbon-carbon  $\pi$  bond and the nonbonding electrons on oxygen.<sup>20</sup> Such conjugation would tend to reduce the reactivity of the oxygen site after addition of  $BH_3$  to the carbon-carbon  $\pi$  bond. However, the existence of this conjugation makes the argument based on separate reactive sites somewhat tenuous. The other possible explanation for the non-observation of the bis adduct was mentioned above. Namely, the borane is formed and the lone pair on the carbonyl oxygen reacts intramolecularly with the tricoordinate boron.

The final structural evidence results from the unique ion fragmentation behavior of the addition product. One striking characteristic of the mass spectrum of this species is the very large relative abundance of the parent ion. No other addition product of  $BH_3$  exhibits a parent ion that is the base peak of the parent envelope. This discounts the possibility that  $BC_2H_5O$  is some generalized adduct of ketene and  $BH_3$  and requires  $BH_3$  to be associated with a specific donor site on ketene. The two most likely sites are the carbon-carbon  $\pi$  bond or a lone pair on oxygen. Interaction with either would leave the type of ionization site that could explain the large parent ion intensity. As the first addition product of  $BH_3$  with allene does not have a strong

(18) R. E. Walker, *Phys. Fluids*, **4**, 1211 (1961).

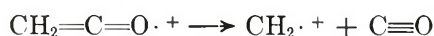
(19) S. A. Fridmann and T. P. Fehlner, unpublished observation.

(20) R. N. Dixon and G. H. Kirby, *Trans. Faraday Soc.*, **62**, 1406 (1966).



parent ion,<sup>19</sup> it seems likely that  $\text{BH}_3$  interacts with the carbon-carbon  $\pi$  bond of ketene thereby leaving the nonbonding electrons on oxygen for ionization. This observation also tends to eliminate the tricoordinate borane with an internal donor-acceptor interaction as the structure of  $\text{BC}_2\text{H}_5\text{O}$ . None of the known acid-base adducts of  $\text{BH}_3$  have parent ions as base peaks.

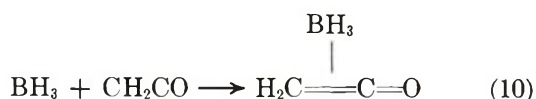
Perhaps the strongest piece of evidence results from the identification (see above) of a strong  $\text{BCH}_5^+$  fragment ion from the addition product. Roughly 30% of the total ionization of  $\text{BC}_2\text{H}_5\text{O}$  is due to the odd electron ion  $\text{BCH}_5^+$ . The predominant fragment ion in the spectrum of ketene itself is the odd electron ion  $\text{CH}_2^+$  which accounts for ca. 36% of the total ionization.<sup>21</sup> As abundant odd electron ions are almost always formed by elimination of a molecule from the molecular ion,<sup>22</sup> the latter process is represented as



Therefore, a strong  $\text{BCH}_5^+$  ion from  $\text{BC}_2\text{H}_5\text{O}$  is likely only if  $\text{BH}_3$  is associated with the  $\text{CH}_2$  end of ketene. About 60% of the total ionization of  $\text{BC}_2\text{H}_5\text{O}$  is due to ions of composition  $\text{BCH}_z$  whereas for ketene  $\text{CH}_z$  accounts for 45% of the total ionization. The increased fragmentation for  $\text{BC}_2\text{H}_5\text{O}$  vs.  $\text{CH}_2\text{CO}$  suggests that  $\text{BH}_3$  interacts with the carbon-carbon  $\pi$  bond thereby weakening it. Finally, it is difficult to envision a process for the formation of an abundant  $\text{BCH}_5^+$  ion from the products of reactions 4, 5, or 6.

The hydrogen fragmentation of  $\text{BC}_2\text{H}_5\text{O}$  can also be analyzed from the results presented in Figure 1. Considering the parent ion envelope alone ( $m/e$  51-56), 52% of the total ion intensity is parent ion, 34% involves the loss of one or more hydrogens originally on  $\text{BH}_3$ , and 14% involves the loss of one or more hydrogens originally on  $\text{CH}_2\text{CO}$ . This is the same behavior exhibited by a known donor-acceptor adduct.<sup>1</sup> Although this does not eliminate tricoordinate borons, they do appear to exhibit more hydrogen fragmentation.<sup>17</sup>

All the evidence may be summarized by rewriting reaction 8 as



This expresses our conclusions that  $\text{BC}_2\text{H}_5\text{O}$  is a 1:1 adduct of  $\text{BH}_3$  and  $\text{CH}_2\text{CO}$ , that the boron atom is most likely tetracoordinate, and that  $\text{BH}_3$  is most likely associated with the  $\text{CH}_2$  end of ketene.

**Reactivity of  $\text{BH}_3$ .** The results of this investigation continue to refine our picture of the detailed mechanism of the reactive interaction of  $\text{BH}_3$  with molecules. All existing data can be explained by, or require, the following mechanism



where M is any species that reacts with  $\text{BH}_3$ ,  $\text{H}_3\text{BM}$  is the donor-acceptor adduct, and c represents further reaction of the adduct to produce a substituted borane, *i.e.*, rearrangement or molecular elimination. The product observed in any given reaction of  $\text{BH}_3$  is governed by the stability of  $\text{H}_3\text{BM}$ . Thus, depending on the magnitudes of  $k_a$ ,  $k_b$ , and  $k_c$ , the product distribution may be  $\text{H}_3\text{BM}$ ,  $\text{H}_3\text{BM}$  and the substituted borane, the substituted borane, or no product at all. In the reaction of  $\text{BH}_3$  with ketene only  $\text{H}_3\text{BM}$  is observed. Thus, these results continue to support the view that the initial rapid reactions of  $\text{BH}_3$  consist solely of forming donor-acceptor adducts.<sup>1</sup> The nature of reaction 11c is then determined by the modification of the electronic structures of both species in the donor-acceptor interaction.

The results of this work gain added significance when compared to the results of previous investigations. In the reaction of  $\text{BH}_3$  with  $\text{C}_2\text{H}_4$ ,<sup>17</sup>  $\text{H}_2\text{BC}_2\text{H}_5$  clearly is formed but the presence of  $\text{H}_3\text{BC}_2\text{H}_4$  is not excluded. In lieu of positive evidence for  $\text{H}_3\text{BC}_2\text{H}_4$ , the reaction of  $\text{BH}_3$  with  $\text{C}_2\text{H}_4$  was considered to be a direct reaction to produce  $\text{H}_2\text{BC}_2\text{H}_5$ . In light of the data presented here it appears that (11) more properly describes the process, and the donor-acceptor adduct,  $\text{H}_3\text{BC}_2\text{H}_4$ , is a real intermediate rather than an activated complex.<sup>17</sup> Picturesquely, the replacement of 2H in ethylene by an oxygen atom serves to trap the addition product in the donor-acceptor form.

If the detailed mechanism 11 is correct for the reaction of  $\text{BH}_3$  with ketene, then these results do not answer the question as to what the product of reaction 11c for ketene will be. Presumably, paths leading to the products of reactions 4-6 exist and the one that may predominate depends upon the nature of the donor-acceptor adduct. Indeed, reaction 3 is still possible. These results do suggest that reaction 1 might be better viewed as an addition reaction followed by elimination of CO rather than a simple displacement reaction.

Recent theoretical calculations conclude that the highest occupied orbital in ketene is a  $\pi$  type which is principally a bonding orbital between the carbon atoms.<sup>23</sup> As the results of this work suggest an initial interaction of  $\text{BH}_3$  with the carbon-carbon  $\pi$  bond leading to the donor-acceptor adduct of reaction 10, the views of Fukui and others<sup>8</sup> would seem to be supported. Unfortunately, the first band in the photoelectron spectrum of ketene is tentatively assigned to

(21) A. Cornu and R. Massot, "Compilation of Mass Spectral Data," Heyden, London, 1966.

(22) F. W. McLafferty, "Interpretation of Mass Spectra," W. A. Benjamin, New York, N. Y., 1966.

(23) J. E. DelBene, *J. Amer. Chem. Soc.*, **94**, 3713 (1972).

electron loss from an oxygen nonbonding orbital.<sup>24</sup> Thus, the answer to the important question concerning the relationship between the orbital characters of the reactants and the nature of the products is not clearly answered by this work. The approach is promising, however, and deserves further study.

*Acknowledgment.* The support of the National Science Foundation under Grant No. GP 28320 is gratefully acknowledged.

(24) D. W. Turner, C. Baker, A. D. Baker, and C. R. Brundle, "Molecular Photoelectron Spectroscopy," Interscience, New York, N. Y., 1970, p 139.

## The Chemical Kinetics of the Pyrolysis of Hydrogen Deuteride<sup>1</sup>

by T. Niki and Gilbert J. Mains<sup>2</sup>

Department of Chemistry, University of Detroit, Detroit, Michigan 48221 (Received February 8, 1972)

The chemical kinetics of the pyrolysis of hydrogen deuteride into hydrogen and deuterium was studied mass spectrometrically over the temperature range 833–1018°K and in the pressure range 4–36 Torr using a double-walled 2-l. quartz reaction vessel. The data fitted a pseudo-first-order reaction equation similar to that found for the reverse combination after an induction period. The induction period was attributed to a rapid heterogeneous reaction which was dominated by the commonly accepted atomic chain mechanism at long times or at higher temperatures. The order of the reaction in the region following the induction period was found to be approximately  $3/2$  and the overall activation energy was  $55.8 \pm 2.4$  kcal/mol. Rate constants for the chain propagating steps,  $k_3$ ,  $k_4$ ,  $k_5$ , and  $k_6$  were computed at 1000°K and shown to be consistent with earlier studies using other methods, but computations of  $k_3$  and  $k_5$  were lower than those reported by earlier experimentalists and theoretical predictions. Activation energies were shown to be dependent upon the nature of chain initiation and termination steps and data are reported for  $E_3$ ,  $E_4$ ,  $E_5$ , and  $E_6$  for two extreme assumptions. The surface to volume ratio was varied by a factor of 2 and 4 and found to have negligible effect in the homogeneous reaction region. Earlier studies of the  $H_2 + D_2$  reaction had found an effect attributed to oxygen diffusing through the walls of the reaction vessel but this was not confirmed for the reverse pyrolysis of HD. An *ad hoc* assumption made by investigators of the  $H_2 + D_2$  pyrolysis reaction was shown to be experimentally valid.

### Introduction

One of the most curious enigmas in the field of chemical kinetics is represented by the elementary reaction between one of the isotopes of the hydrogen atom and molecular hydrogen, isotopically substituted and/or one of its nuclear spin isomers. This  $H + H_2$  reaction has challenged theoreticians for many years representing, as it does, a three-electron problem. The variety of empirical, semiempirical, and *ab initio* approaches to the computation of the  $H_3$  surface has been the subject of an excellent review by Karplus<sup>3</sup> and contributions are still being published.<sup>4</sup> The accuracy to which the potential energy barrier is known,  $9.0 \pm 1.5$  kcal/mol, is still unsatisfactory.<sup>3</sup> From an experimental viewpoint, the challenge has been equally long,<sup>5</sup> ranging from careful studies of the pyrolysis of the  $H_2 + D_2$  system<sup>6</sup> to systems where the H atom was generated by microwave discharge, nuclear recoil, or photolysis. These studies have been well summarized by Rowland.<sup>7</sup> Experimental activation energies are in the 7–9 kcal/mol range, in fair agreement with the po-

tential barrier computations in view of the problems involved in interpretation of the data.

The research reported here was undertaken in 1966, prior to the classic study of Westenberg<sup>8</sup> using the esr technique, with the hope that interpretation of the kinetic data obtained from a careful study of the pyrolysis of HD would be simpler and involve fewer *ad hoc* assumptions, providing more reliable rate constants than

(1) Based on the Ph.D. Thesis of T. Niki, University of Detroit, Detroit, Mich., 1971.

(2) Department of Chemistry, Oklahoma State University, Stillwater, Okla. 78074.

(3) M. Karplus in "Molecular Beams and Reaction Kinetics," C. Schlier, Ed., Academic Press, New York, N. Y., 1970, p 339.

(4) C. A. Parr and D. G. Truhar, *J. Phys. Chem.*, **75**, 1844 (1971).

(5) A. Farkas and L. Farkas, *Proc. Roy. Soc., Ser. A*, **152**, 124 (1935).

(6) A. Cimino, E. Molinari, and G. G. Volpi, *J. Chem. Phys.*, **33**, 616 (1960); G. Boato, G. Careri, A. Cimino, E. Molinari, and G. G. Volpi, *ibid.*, **24**, 783 (1956).

(7) F. S. Rowland in ref 3, p 293.

(8) A. A. Westenberg and N. de Haas, *J. Chem. Phys.*, **47**, 1933 (1967).



obtainable from the studies of the pyrolysis of  $H_2$ - $D_2$  mixtures. Furthermore, one of the *ad hoc* assumptions necessary to deduce rate constants from the earlier  $H_2$ - $D_2$  pyrolysis studies, *i.e.*, that the ratio  $(H)/(D)$  was independent of the extent of reaction, could be experimentally verified by a careful study of the chemical kinetics of the pyrolysis of HD. As will be seen later, the first hope was not realized, and while reliable rate data were obtained in this study, they suggest that pyrolysis kinetic studies are *not* the optimum experimental route to accurate experimental rate constants. Future research should probably approach the reaction through nonequilibrium such as Westenberg's<sup>8</sup> or LeRoy's<sup>9</sup> flow systems or *via* a molecular beam<sup>10</sup> approach. The second objective of the research, verification of the *ad hoc*  $(H)/(D)$  assumption, was successfully achieved.

### Experimental Section

*A. Apparatus and Procedure.* A double-walled fused quartz reaction vessel, similar in configuration to that used by BCCMV<sup>6</sup> but of larger dimensions, was used. The volume of the internal vessel was 2.17 l., calibrated by expansion of a gas from a known volume. Because the vessel was quite close to cylindrical, the calculated surface to volume ratio,  $0.417\text{ cm}^{-1}$  is fairly accurate. Inlets to the vessel and its outer jacket emerged from the bottom of the vessel as it was located in the high-temperature oven (Blue M Electric Co., Model 8006C-1) and connected to a conventional high-vacuum gas handling system. In experiments in which the surface to volume was increased, pieces of quartz tubing were packed into the inner chamber of the reaction vessel.

A pinhole sampling probe, fabricated by a Tesla coil discharge through a thin quartz wall at the end of the tubular probe, extended downward axially so as to sample the gas in the geometric center of the cylinder. The leak rates for  $H_2$  were determined mass spectrometrically to be  $1.75 \times 10^{13}$  molecules/sec at 1.31 Torr and  $6.95 \times 10^{13}$  molecules/sec at 5.02 Torr, respectively, corresponding to a calculated ideal pinhole size of 1.1  $\mu$ . This leak rate was sufficiently low to permit accurate measurements of the peak heights in the mass spectrometer (C.E.C. Model 21-103C) to which the probe was attached and yet not diminish the equilibrium  $H_2$ , HD, and  $D_2$  pressures in the reaction vessel discernibly over a 10-hr observation period.

The high-temperature oven was equipped with a Honeywell indicating potentiometer to control the temperature to  $\pm 1^\circ$  over the temperature range 300–1280°K. The temperature was monitored by a chromel–alumel thermocouple (Omega Engineering) which was calibrated against a platinum–platinum–10% rhodium thermocouple (Omega Engineering) calibrated by the U. S. National Bureau of Standards. The thermocouple was located against the outer wall of the reaction vessel midway down the cylinder. The

temperature thus monitored agreed with temperatures measured by sliding the thermocouple up the gas inlet to the probe tip, leading us to believe that the radial temperature gradient measured from the cylinder axis was negligible. The vertical temperature gradient so measured from below was  $12^\circ$  at 730°K and  $7^\circ$  at 950°K. The heat leak was expected to be large at the bottom of the reaction vessel where the two inlets emerged and, while it was not measured, it must have been much smaller at the top of the reaction vessel where the small outlet from the probe to the mass spectrometer was situated. Thus, the temperature gradients measured were probably the largest in the entire reaction vessel in any direction.

The reaction vessel, even after thorough outgassing at 1100°, showed retention of small amounts of hydrogen. (This was demonstrated by monitoring the formation of HD upon introducing pure  $D_2$  into the vessel following pretreatment with  $H_2$  and high-temperature outgassing.) The reaction vessel was evacuated for at least 1 hr before each experiment. The best reproducibility was obtained by leaving an equilibrium mixture of  $H_2$ -HD- $D_2$  in the vessel between experiments. Because BCCMV<sup>6</sup> reported effects of oxygen diffusing through the walls of the reaction vessel, some experiments were performed in which either air or  $O_2$  was admitted to the *outer* chamber.

In a typical experiment HD (or an  $H_2$ - $D_2$  mixture) was Toepler pumped into the thermally equilibrated reaction chamber and the mass spectrum of the mixture, ranging from  $m/e = 1$  to  $m/e = 4$ , was determined every 5 min. Periodically during an experiment, the mass spectrum was determined in the region  $m/e = 12$  to  $m/e = 44$  as a check for atmospheric contamination. None was ever found.

*B. Materials.* Hydrogen deuteride was obtained from two sources, Merck Sharp and Dohme, Ltd., Canada, and Volk Radiochemical Co. The first source of HD provided a sample containing 0.43%  $H_2$  and 0.22%  $D_2$  and this was used for all of the kinetic studies in which additional  $H_2$  was not added to the system. The latter source sample contained 10.1%  $H_2$  and 2.5%  $D_2$  and was used in the kinetic studies of the  $H_2$ -HD mixtures. The samples as provided by the manufacturers were further treated to remove trace atmospheric contaminants by absorption and desorption on Pittsburgh activated charcoal (Type BPL) at liquid nitrogen temperature.<sup>11</sup> After treatment the hydrogen samples contained no detectable nitrogen or oxygen by mass spectrometry, *i.e.*, less than 0.001%.  $H_2$  and  $D_2$  gases were obtained from Matheson Co. and purified by passing them separately through a pal-

(9) W. R. Schulz and D. J. LeRoy, *Can. J. Chem.*, **42**, 2480 (1965).

(10) W. L. Fite and R. J. Brackman in "Atomic Collision Processes," M. McDowell, Ed., Elsevier Press, Amsterdam, 1964.

(11) D. Lewis and S. H. Bauer, *J. Amer. Chem. Soc.*, **90**, 5390 (1968).

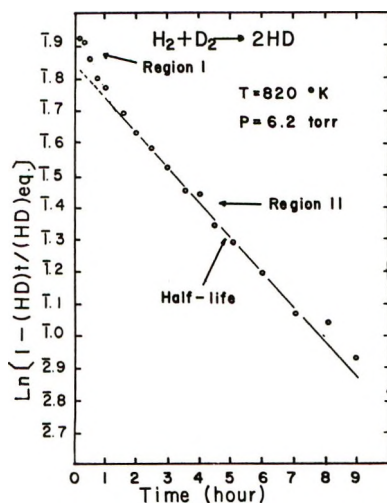


Figure 1. Pseudo-first-order plot for the  $H_2 + D_2 = 2HD$  reaction at  $820^\circ K$ .

ladium thimble at about  $500^\circ$ . After treatment a small amount of hydrogen deuteride, less than 0.08%, was the only impurity detectable by mass spectrometry.

### Results

*A. The Forward Reaction:  $H_2 + D_2 = 2HD$ .* The forward reaction was studied at  $820^\circ K$  and at a pressure of 6.2 Torr, equimolar  $H_2$ - $D_2$  mixture, to test the validity of the experimental setup. The peaks at  $m/e = 2$  and  $m/e = 4$  decreased smoothly to equilibrium values and the peak at  $m/e = 3$  rose from its initial impurity to an equilibrium value in a little over 11 hr, as expected, and was unchanged some 34 hr later. The pseudo-first order behavior observed by others<sup>5,6</sup> was obtained and is presented in Figure 1. The observed half-life, 4.9 hr is in good agreement with the value of 4.7 hr observed at  $855^\circ K$  and 10 Torr by Farkas and Farkas.<sup>5</sup> It should be noted that the observed rate in Region 1, at the very early stages of the reaction, was faster than that in Region II where agreement with earlier workers was quite good. This was also observed in the HD kinetic studies and will be discussed in more detail later. Having established the ability to reproduce earlier measurements on the  $H_2$ - $D_2$  system, attention was then focused on the previously unstudied HD system.

*B. The Reverse Reaction:  $2HD = H_2 + D_2$ .* Typical experimental results for the reverse reaction are presented in Figure 2, where the data have been fitted to the anticipated pseudo-first-order equation,  $\ln [1 - (D_2)/(D_2)_{eq}] = k_r t$ , having been obtained at  $833^\circ K$  and 36 Torr of initial HD pressure. Of course, an identical plot is obtained when the concentrations of  $H_2$  are substituted for  $D_2$  and the observed variation of  $H_2$  plotted. This establishes the gross stoichiometry and merits no further comment. Observe in Figure 2 that the transition from Region I to Region II was near 40

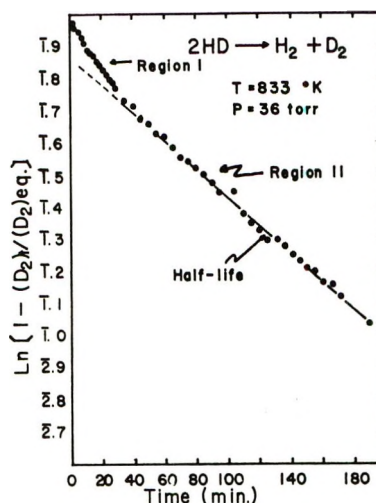


Figure 2. Pseudo-first-order plot for the  $2HD = H_2 + D_2$  reaction at  $833^\circ K$ .

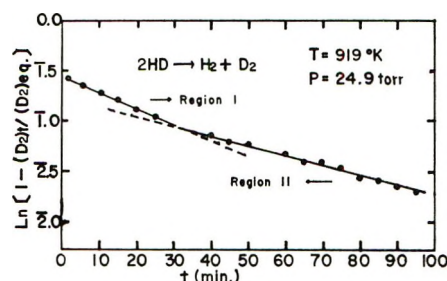


Figure 3. Pseudo-first-order plot for the  $2HD = H_2 + D_2$  reaction at  $919^\circ K$ .

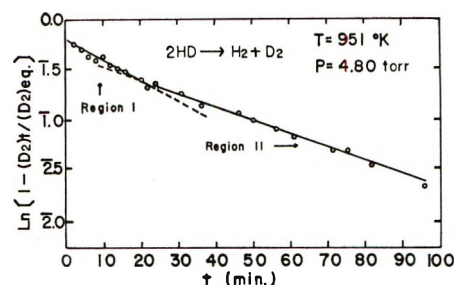


Figure 4. Pseudo-first-order plot for the  $2HD = H_2 + D_2$  reaction at  $951^\circ K$ .

min whereas in the forward reaction at  $820^\circ K$  the transition required approximately 90 min. Additional data obtained at  $919^\circ K$  and initial HD pressure of 24.9 Torr,  $951^\circ K$  and initial HD pressure of 4.8 Torr, and  $1018^\circ K$  and initial HD pressure of 5.40 Torr are presented in Figures 3, 4, and 5, where lines have been drawn through Region I in an attempt to define the transition time more reliably. A comparison of Figures 2-5 suggests that the transition between Region I and Region II is strongly temperature dependent and shows a steady progression of the intercept toward zero (more precisely, toward the value predicted from the 0.22% initial impurity level of  $D_2$ ). It need be mentioned



that over one hundred kinetic experiments were performed in the temperature range 833–1049°K and initial HD pressures of 4–36 Torr. The data presented in Figures 2–5 are representative of the totality of many experiments and are typical.

Experimental rate constants,  $k_r$ , were deduced from the slopes of graphing the data as in Figures 2–5, were normalized to a "standard" pressure of 29.00 Torr by multiplying by the ratio of the square roots of the experimental and "standard" pressure of 29.00 (to be justified later), and are presented in the form of an Arrhenius plot in Figure 6. (The data are summarized in Table I.) The best straight line was obtained by

Table I: Experimental Results

Remarks	T, °K	P, Torr	Ln $k_r$ ( $P =$ 29.0 Torr) (region II)
a, b	833.1	36.03	-9.636
a, b	869.3	27.24	-9.383
b	918.9	24.98	-8.602
b	942.4	20.78	-7.877
b	948.7	30.25	-7.511
b	951.3	4.80	-7.490
b	953.1	17.75	-7.276
b	953.7	8.80	-7.561
b	956.2	16.56	-7.079
b	958.2	12.37	-7.156
b	958.6	21.79	-6.862
b	960.8	9.08	-7.253
c, d	982.3	3.96	-6.164
d	983.8	9.11	-6.336
b	987.8	31.93	-6.696
b	988.4	7.98	-5.975
b	989.6	6.72	-6.214
e, d	993.0	9.40	-6.078
c, d	994.7	18.20	-6.151
f, d	997.6	6.36	-5.929
d	998.6	26.91	-6.001
g, d	1000.5	13.96	-5.819
d	1001.2	8.92	-6.015
d	1002.1	23.79	-5.839
b	1003.1	15.75	-6.016
d	1018.1	5.40	-5.425
c, d	1020.4	7.75	-5.608
d	1046.1	4.86	-4.932
h, d	947.5	3.55	-7.168
h, b	948.5	6.52	-7.674
h, b	957.7	7.24	-7.181
h, d	996.3	7.97	-5.994
h, d	997.5	7.88	-5.858
h, d	1007.8	8.39	-5.580
i, d	945.3	5.12	-7.009
i, d	930.6	9.16	-7.723
i, d	1022.3	5.50	-5.091

<sup>a</sup> Deviate from the Arrhenius linear plot. <sup>b</sup> Regions I and II observed. <sup>c</sup> 0.5 atm of the air in outer jacket. <sup>d</sup> Region I not observed. <sup>e</sup> 0.5 atm of the oxygen in outer jacket. <sup>f</sup> 1 atm of the oxygen in outer jacket. <sup>g</sup> 1 atm of the air in outer jacket. <sup>h</sup>  $S/V$  increased by twofold. <sup>i</sup>  $S/V$  increased by fourfold.

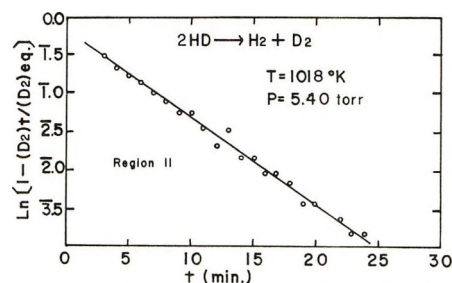


Figure 5. Pseudo-first-order plot for the  $2\text{HD} = \text{H}_2 + \text{D}_2$  reaction at 1018°K.

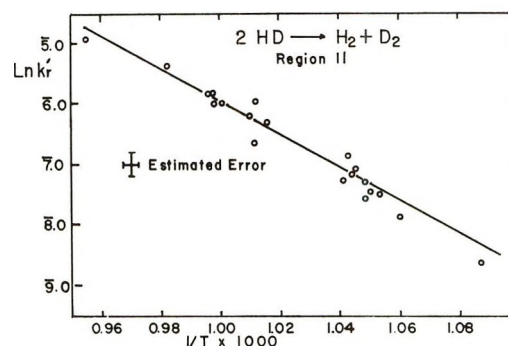


Figure 6. Arrhenius plot of  $\ln k_r'$  vs.  $1000/T$  for the  $2\text{HD} = \text{H}_2 + \text{D}_2$  reaction.

the least-square method and corresponded to the equation:  $\ln k_r' = [22.1 \pm 1.2] - [55.8 \pm 2.4]/RT$  where  $k_r'$  is the pressure-normalized rate constant,  $R$  is the gas constant in kcal/mol deg, and  $T$  is the absolute temperature.

The overall order of the reaction in Region II was determined at 954 and 1001°K. These data are presented in Figure 7. A least-square fit of the data gave slopes of  $0.58 \pm 0.15$  at 954°K and  $0.58 \pm 0.11$  at 1001°K suggesting a  $3/2$ -order reaction and the relationship  $k_r' = k_r/P^{1/2}$ , which was mentioned earlier as the basis of normalizing the observed  $k_r$  values in Figure 6.

Because of the previously observed effect on the rate of oxygen permeating through the walls of the reaction chamber,<sup>6</sup> a number of experiments were performed in the temperature range 1020–982°K with 1 atm of air in the outer jacket,  $1/2$  atm of  $\text{O}_2$  in the outer jacket, and 1 atm of  $\text{O}_2$  in the outer jacket (See Table I). The kinetic data were indistinguishable from those presented in Figures 2–5 and the normalized  $k_r'$  fell on the line presented in Figure 6 within the statistical uncertainty. Therefore, we are unable to confirm for the back reaction the effect of oxygen cited by BCCMV<sup>6</sup> for the forward reaction.

Since there is some question regarding the role of the surface in experiments involving small atoms and molecules, especially H and  $\text{H}_2$  and its isotopes, the reaction vessel was packed with short pieces of quartz tubing to increase the surface to volume ratio by factors of 2 and 4. The results of kinetic studies in Region II across

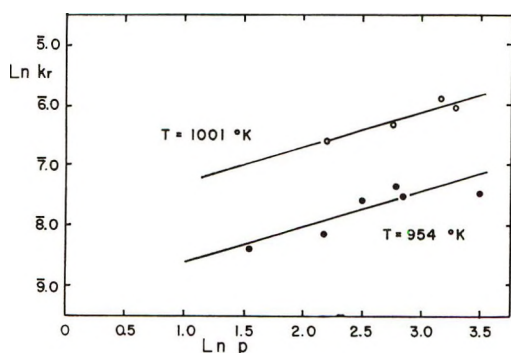


Figure 7. Determination of the order of the reaction at 954 and 1001°K by plotting  $k_r$  vs. initial pressure of HD.

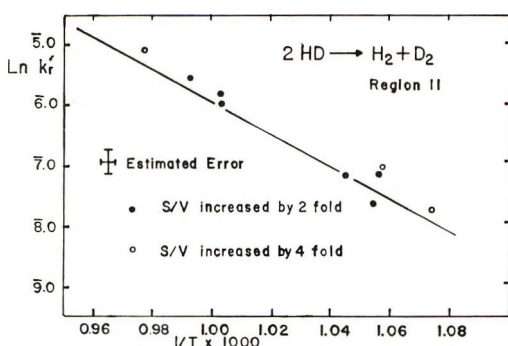


Figure 8. Effect of surface to volume on the Arrhenius plot of  $\ln k_r'$  vs.  $1000/T$ , straight line computed from Figure 6.

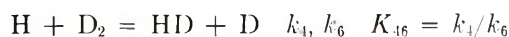
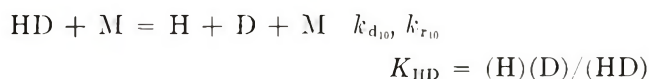
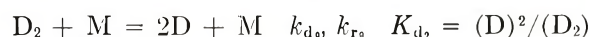
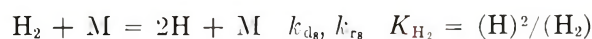
the temperature range of these experiments are presented in Figure 8 along with the line computed from the data of Figure 6. If there is a  $S/V$  effect in Region II, it is small and is within statistical precision of the measurements.

## Discussion

The rate data obtained initially, designated as Region I in Figures 2–5, have been a source of puzzlement from the outset. Tentative explanations for the faster initial reaction have ranged from traces of  $O_2$  catalyzing a chain reaction in the lower temperature region and becoming less important as the temperature is raised and the  $O_2$  is consumed, through instrumental artifacts, to a heterogeneous component to the reaction which became less important than the homogeneous component at high temperature and longer times. Various aspects of these are considered in detail in Niki's thesis.<sup>1</sup> A variety of reasons, beginning with the necessity of conditioning the walls of the reaction vessel to obtain reproducible results (in Region I, not Region II, depicted *exclusively* in Figures 6, 7, and 8), and extending to experimental observations of small increases in total pressure ( $H_2 + HD + D_2$ ) in Region I, which were temperature dependent, and disappeared in Region II, causes us to favor a *heterogeneous* reaction at the early stages, Region I, which becomes less and less important as the atomic chain homogeneous reac-

tion becomes more important at later times and at the higher temperatures. Thus, we would attribute the observation of a Region I to the more rapid reaction,  $2HD(\text{absorbed}) = H_2(\text{absorbed}) + D_2(\text{absorbed})$ , predominating until the concentration of (H) and (D) atoms in the system build up to their equilibrium values and the homogeneous chain process dominates, Region II. The time required for the transition from Region I to Region II is then a complex measure of the time required to establish equilibrium H and D atom concentrations and the magnitude of their reaction rates at the temperature being considered. This is consistent with the observations provided in Figures 1–5, respectively. A "pseudo order" calculated from  $k_r$  values in Region I as a function of initial HD pressure was found to be  $1.7 \pm 0.8$ , supporting the heterogeneous hypothesis for Region I. The data are too imprecise to warrant a lengthy discussion of Region I and further understanding of this kinetic region is left to future studies.

Because of the fundamental implications of accurate rate data, already noted in the Introduction, the observations in Region II are of much more general interest. Figure 7 reasonably establishes this as the atomic reaction region and Figure 8 suggests that the heterogeneous contribution is negligible. Therefore, it seems reasonable to consider the mechanism in Region II to be the atomic chain process similar to that used by Farkas and Farkas<sup>5</sup> and BCCMV.<sup>6</sup> To avoid confusion in data comparison, the system of numbering reactions used by BCCMV<sup>6</sup> will be used throughout. The mechanism postulated to occur in the atomic chain homogeneous region is as follows.



The first three equations and their reverse represent the possible chain initiation or termination steps, depending upon the initial concentrations of  $H_2$ ,  $D_2$ , and  $HD$ , and similarly the last two equations are the propagation steps. BCCMV<sup>6</sup> have advanced arguments that the reactions which lead to chain initiation, the decomposition reactions designated with rate constants  $k_8$ ,  $k_9$ ,  $k_{10}$  above, are not homogeneous but occur at the walls of the reaction vessel. Our observations of Region I certainly do not conflict with this interpretation and, if anything, add additional credence to this interpretation. However, whether M is actually the walls of the chamber or not, the atom concentrations are almost certainly the equilibrium values and this will be assumed henceforth.



Since the system contains five identifiable chemical species presumably in thermal equilibrium with their surroundings, *i.e.*, (H<sub>2</sub>), (D<sub>2</sub>), (HD), (H), and (D), five differential equations may be written to describe the kinetics. However, only four are different and they are summarized below

$$d(\text{H}_2)/dt = -k_3(\text{H}_2)(\text{D}) + k_5(\text{HD})(\text{H}) \quad (\text{a})$$

$$\text{D}_2 + \text{M} = 2\text{D} + \text{M} \quad k_{d_2}, k_{r_2}, K_{\text{D}_2} = (\text{D})^2/(\text{d}_2)$$

$$d(\text{D}_2)/dt = -k_4(\text{D}_2)(\text{H}) + k_6(\text{HD})(\text{D}) \quad (\text{b})$$

$$d(\text{HD})/dt = k_3(\text{H}_2)(\text{D}) - k_5(\text{HD})(\text{H}) + k_4(\text{D}_2)(\text{H}) - k_6(\text{HD})(\text{D}) \quad (\text{c})$$

$$d(\text{H})/dt = -d(\text{D})/dt \quad (\text{d})$$

$$d(\text{H})/dt = k_3(\text{H}_2)(\text{D}) - k_5(\text{HD})(\text{H}) - k_4(\text{D}_2)(\text{H}) + k_6(\text{HD})(\text{D}) \quad (\text{e})$$

where the initiation and termination steps have been neglected. In addition, we have imposed the following stoichiometric restrictions

$$(\text{H}_2)_0 - (\text{H}_2) = (\text{D}_2)_0 - (\text{D}_2) = (\text{HD})/2 - (\text{HD})_0/2 \quad (\text{f})$$

as the atom concentrations may be neglected under these conditions. Finally, we have the condition of Microscopic Reversibility at equilibrium, *viz.*

$$K_{\text{eq}} = (\text{HD})_{\text{eq}}^2/(\text{H}_2)_{\text{eq}}(\text{D}_2)_{\text{eq}} = k_3k_4/k_5k_6 \quad (\text{g})$$

Application of the stationary-state condition to differential equations d and e leads to the equations

$$(\text{H}) + (\text{D}) = \text{constant} = [K_{\text{H}_2}(\text{H}_2)_0]^{1/2} + [K_{\text{D}_2}(\text{D})_0]^{1/2} \quad (\text{h})$$

$$(\text{H})/(\text{D}) = [k_3(\text{H}_2) + k_6(\text{HD})]/[k_4(\text{D}_2) + k_5(\text{HD})] \quad (\text{i})$$

which are insufficient to permit the integration of any of the differential equations a, b, or c which constitute the macroscopic observables in the pyrolysis experiments. Hence, an additional *ad hoc* assumption was made directly by Farkas and Farkas<sup>5</sup> and indirectly by BCCMV<sup>6</sup> that for the initial concentration conditions (H<sub>2</sub>)<sub>0</sub> = (D<sub>2</sub>)<sub>0</sub>, the left-hand side of eq i is constant throughout the course of the reaction. This leads directly to the conclusion

$$(\text{H})/(\text{D}) = k_3/k_4 - k_6/k_5 = [K_{\text{H}_2}/K_{\text{D}_2}]^{1/2} \quad (\text{j})$$

which permits eq c to be cast into the form d(HD)/dt = A - B(HD) and leads to the integrated pseudo-first-order equation given earlier, graphed in Figure 1, and subjected to the experimental tests of the earlier studies of the H<sub>2</sub> + D<sub>2</sub> reaction.

If attention is focused now on the HD pyrolysis reaction, it is possible to recast eq b in the following form, assuming as a first approximation that (D<sub>2</sub>)<sub>0</sub> = 0

$$d(\text{D}_2)/dt = k_6(\text{HD})_0(\text{D}) - [2k_6(\text{D}) + k_4(\text{H})](\text{D}_2) \quad (\text{k})$$

Now, only if (D) [and (H)] is constant, can we reduce eq k to the pseudo-first-order differential equation form, d(D<sub>2</sub>)/dt = C - E(D<sub>2</sub>), and integrate it into the form tested in Figures 2-5, and given earlier. We need to note that k<sub>r</sub> = E = k<sub>6</sub>(HD)<sub>0</sub>(D) and (D<sub>2</sub>)<sub>eq</sub> = C/E, where E = 2k<sub>6</sub>(D) + k<sub>4</sub>(H). Thus, since C is indeed a constant in the regions where the pseudo-first-order rate constant describes the kinetic behavior, we conclude that (D), and from eq h, also (H) is constant and independent of the extent of reaction, experimentally verifying the *ad hoc* assumption of earlier workers that the left-hand side of eq i is constant. It is worth emphasizing that the applicability of the pseudo-first-order plot of the integrated form of d(HD)/dt = A - B(HD) did not provide such a test because the "constants," A and B, each contained terms in (H) and (D) which could compensate for any variation during the course of the reaction. Thus the applicability of the pseudo-first-order integrated rate equation did not test the *ad hoc* assumption in the studies of the H<sub>2</sub> + D<sub>2</sub> pyrolysis studies, but did directly test the assumption in the HD pyrolysis studies reported here. Furthermore, it is possible to deduce from the experimentally measured k<sub>r</sub> by application of eq g, j, and E = 2k<sub>6</sub>(D) + k<sub>4</sub>(H), experimental values for each rate constant in the propagation steps (k<sub>3</sub>, k<sub>4</sub>, k<sub>5</sub>, and k<sub>6</sub>). The rate constants so obtained, normalized to 1000°K for comparison purposes, are presented in Table II, where it can be seen that reasonable agreement between the experimental numbers obtained in this study and those obtained from other experimental studies was obtained for k<sub>6</sub> and k<sub>4</sub>, which also agree best with theoretical predictions. The values obtained for k<sub>3</sub> and k<sub>5</sub> are almost a factor of 2 lower than theoretical predictions and the experimental measurements of others, suggesting a computational error. However, none has been found and we have no explanation for these discrepancies which appear outside our experimental error. Since the equilibrium constants used by BCCMV were taken from Brickwedde, *et al.*,<sup>12</sup> this source of discrepancy can be ruled out. Therefore, while our data reinforce the experimental deductions of values for k<sub>6</sub> and k<sub>4</sub>, they regrettably only add to the confusion regarding k<sub>3</sub> and k<sub>5</sub>.

From the temperature coefficient of k<sub>r</sub>', and the temperature coefficients of the equilibrium processes,<sup>12</sup> it is possible to compute activation energies for each of the chain-propagating steps. Unfortunately, it is not possible to be quite so cavalier in dismissing the nature of the initiation and termination reactions in making these computations. For example, it can be shown that E<sub>3</sub> = E<sub>r</sub> - [ΔH<sub>D<sub>2</sub></sub><sup>°</sup> - ΔH<sub>rx</sub><sup>°</sup>]/2, where ΔH<sub>D<sub>2</sub></sub><sup>°</sup> is the standard enthalpy change for the dissociation of D<sub>2</sub> into

(12) H. W. Wooley, R. B. Scott, and F. G. Brickwedde, *J. Res. Nat. Bur. Stand.*, **41**, 379 (1948).

**Table II:** Comparison of Rate Constants (cm<sup>3</sup>/molecule sec × 10<sup>11</sup>) at 1000°K

Reaction	Theory <sup>a</sup>	Experimental	
		Others	This work
D + H <sub>2</sub> $\xrightarrow{k_3}$ HD + H	11.72	9.79 <sup>b</sup> 12.9 <sup>c</sup> 9.8 <sup>e</sup>	6.1 ± 0.6
H + D <sub>2</sub> $\xrightarrow{k_4}$ HD + D	5.01	4.55 <sup>b</sup> 1.11 <sup>d</sup> 6.1 <sup>e</sup>	4.6 ± 0.5
H + HD $\xrightarrow{k_5}$ H <sub>2</sub> + D	4.42	3.7 <sup>e</sup>	2.3 ± 0.2
D + HD $\xrightarrow{k_6}$ D <sub>2</sub> + H	3.41	4.0 <sup>e</sup>	3.1 ± 0.3

<sup>a</sup> I. Shavitt, *J. Chem. Phys.*, **49**, 4048 (1968). <sup>b</sup> A. A. Westenberg and N. deHaas, *ibid.*, **47**, 1393 (1967). <sup>c</sup> B. A. Ridley, W. R. Schulz, and D. J. LeRoy, *ibid.*, **44**, 3344 (1966). <sup>d</sup> W. R. Schulz and D. J. LeRoy, *Can. J. Chem.*, **42**, 2480 (1964). <sup>e</sup> G. Boato, *et al.*, *J. Chem. Phys.*, **24**, 783 (1956).

two D atoms and  $\Delta H_{rx}^\circ$  is the standard enthalpy change for the overall exchange reaction  $H_2 + D_2 = 2HD$ . Therefore, whether or not the primary mechanism by which D atoms are formed is homogeneous or heterogeneous determines which value of  $\Delta H_{D_2}^\circ$  is used to compute  $E_3$ . Furthermore, while the gas phase value of  $\Delta H_{D_2}^\circ$  can be accurately calculated from spectrographic data<sup>12</sup> the heterogeneous value for  $\Delta H_{D_2}^\circ$  for D<sub>2</sub> adsorbed can only be estimated semiempirically.<sup>13</sup> Therefore, it was decided to carry out the computation two different ways, one in which  $E_r$  was arbitrarily set at 60.00 kcal/mol and accurate gas-phase values for the  $\Delta H^\circ$ 's used, and the other in which  $E_r$  was chosen to be 55.8 kcal/mol from Figure 6 and the estimated value for  $\Delta H_{D_2}^\circ$  for D<sub>2</sub> adsorbed on silica, 95.0 kcal/mol, used. The computed activation energies are presented in Table III. These are the first experimental estimates of  $E_5$  and  $E_6$ . It is clear that the two methods of computation yield results which span previously reported values and could allow the authors the luxury of indecision. However, the data obtained assuming the initiation and termination steps are primarily heterogeneous as suggested by BCCMV are in better agreement with other experimental determinations and are preferred. At the risk of repetition, the authors wish to point out that heterogeneous initiation and termination steps are not inconsistent with the data of Figure 8 so long as the atomic chain length is long.

**Table III:** Comparison of Activation Energies

Reaction	Activation energies, kcal/mol			
	Experimental	Theory	This work	
D + H <sub>2</sub> $\xrightarrow{E_3}$ HD + H	7.61 <sup>a</sup> 9.40 <sup>b</sup>	7.42 <sup>d</sup>	6.1 <sup>h</sup>	8.4 <sup>i</sup>
H + D <sub>2</sub> $\xrightarrow{E_4}$ HD + D	9.39 <sup>a</sup> 7.30 <sup>c</sup>	11.0 <sup>e</sup> 7.7 <sup>f</sup>	6.9	9.2
H + HD $\xrightarrow{E_5}$ H <sub>2</sub> + D		9.8 <sup>g</sup>	6.9	9.1
D + DH $\xrightarrow{E_6}$ D <sub>2</sub> + H			6.0	8.3

<sup>a</sup> A. A. Westenberg and N. deHaas, *J. Chem. Phys.*, **47**, 1393 (1967). <sup>b</sup> B. A. Ridley, N. R. Schulz, and D. J. LeRoy, *ibid.*, **44**, 3344 (1966). <sup>c</sup> W. R. Schulz and D. J. LeRoy, *Can. J. Chem.*, **42**, 2480 (1964). <sup>d</sup> L. Pedersen and R. N. Porter, *J. Chem. Phys.*, **47**, 4751 (1967). <sup>e</sup> I. Shavitt, R. M. Stevens, F. L. Minn, and M. Karplus, *ibid.*, **48**, 2700 (1968). <sup>f</sup> H. Conroy and B. L. Bruner, *ibid.*, **42**, 4047 (1965); **47**, 921 (1967). <sup>g</sup> I. Shavitt, *ibid.*, **49**, 4048 (1968). <sup>h</sup> These values were obtained assuming  $E_r = 60.0$  kcal/mol. <sup>i</sup> These values were obtained assuming  $1/2\Delta H_{D_2}^\circ = 47.5$  kcal/mol.

Finally, it is pertinent to return to the comments made in the Introduction of this paper regarding the goals of this research and the pyrolysis method of approaching the computation of these fundamental rate constants. We feel that in spite of great care, we were only partially successful in providing more reliable rate constants and we warn the reader contemplating further pyrolysis studies in the H<sub>2</sub>-HD-D<sub>2</sub> system that this road to more accurate rate constants will require significant advances in temperature control, temperature uniformity, and wall reproducibility before success is achieved. It is our opinion that approaches which produce H or D atoms out of equilibrium with their precursors but still in thermal equilibrium with their surroundings stand a much better chance of success in the immediate future.

*Acknowledgments.* We are grateful to the National Science Foundation for support of this research for 3 years, to the University of Detroit for support of T. N. for 1 year, and finally to Oklahoma State University for allowing G. M. time from his duties to revise this manuscript *in toto*.

(13) J. H. deBoer and J. van Steenis, *Koninkl. Ned. Akad. Wetenschap. Proc.*, **B55**, 578 (1952).



# Detection of Species Resulting from Condensed Phase Decomposition of Ammonium Perchlorate<sup>1</sup>

by E. Ellsworth Hackman, III,

*Thiokol Chemical Corporation, Elkton Division, Elkton, Maryland 21921*

Henry H. Hesser, and Harold C. Beachell\*

*Department of Chemistry, University of Delaware, Newark, Delaware 19711 (Received March 23, 1972)*

*Publication costs assisted by the Air Force Office of Scientific Research*

The thermal decomposition of current or potential propellant ingredients has been studied from a number of aspects. A variety of mechanisms have been proposed. Further theory development and acceptance, however, is being restrained by the fact that some of the key species used in the theories have not been detected by chemical analysis. Ammonium perchlorate (AP) has been a favorite candidate for study because it seems to be a ubiquitous oxidizer in current solid propellants. Detection of initial and transitory decomposition species is nearly impossible by wet methods, chromatography, and slower analytical techniques. Time-of-flight and, for the first time, higher resolution methods of mass spectrometry of ultrahigh purity AP and of its deuterated derivative were used in this study. Of particular importance to several proposed decomposition mechanisms is the sure detection of nitroxyl (HNO), the hydrides of nitrogen, and the oxides of chlorine. The detection method must not cause confusion by adding species of its own, such as by cracking due to electron bombardment in the mass spectrometer. Furthermore, it is important to find what species might be present in the condensed phase—as opposed to the gas phase—that would indicate strong exothermic reactions. Since it is ultimately desirable to relate the species found by mass spectrometry to what might be presented during combustion under higher pressures, the pertinence of the one to the other is discussed. The species of most concern, HNO (mass 31), was found as a minor constituent by both high and low resolution measurement at temperatures above 80°. It was confirmed by the strong reduction of mass 31 when deuterated AP was decomposed. DNO occurs at mass 32. It is considered highly improbable that HNO could have occurred by reactions other than surface thermal reactions. High resolution spectra were used to separate the atomic oxygen (or doubly charged  $\text{O}_2$ ) and  $\text{NH}_2$  peaks at mass 16, thereby confirming the presence of a key hydride of nitrogen. The other hydrides of nitrogen were also found:  $\text{NH}_4$ ,  $\text{NH}_3$ , and  $\text{NH}$ . No condensed phase decomposition species were found at 80° or below. Perchloric acid, atomic chlorine, and all the simple chlorine oxides were found, but  $\text{Cl}_2$ ,  $\text{HClO}$ ,  $\text{HClO}_2$ ,  $\text{HClO}_3$ , and  $\text{ClO}_4$  were not detected. Also not detected in the condensed phase were nitrogen,  $\text{N}_2\text{O}$ , and  $\text{NO}_2$ . The mass range monitored was from  $m/e$  12 to 200. No parent  $\text{NH}_4\text{ClO}_4^+$  ion was detected in any experiments. Evidence of enough strong exothermic reactions in the condensed phase was found. It supports theories stating that this is a major source of energy to help balance the endothermic requirements for vaporization to sustain combustion.

## I. Introduction

For several decades there has been interest in clearly defining the important energy absorption, generation, and transfer steps during solid propellant combustion.<sup>2,3</sup> Better understanding should lead to better control. Early simplified theories stated that ignition took place on a surface when a critical temperature was reached. The flame zone that was then established above the surface provided the sustaining energy by conduction and radiation for steady-state surface regression. For solid propellants there are many strongly exothermic reactions that can be proposed to take place in the flame zone to support such theories. Oxidation of hydrocarbons to  $\text{CO}_2$  and  $\text{H}_2\text{O}$  and of aluminum to  $\text{Al}_2\text{O}_3$  are good examples.

The experimental difficulties associated with detecting and measuring initial and midcourse reaction products, gas, and solid zone dimensions and temperature gradients for a burning solid propellant are nu-

merous. In the late 1950's the final reaction products for simple systems were readily calculated by computer. By the mid-1960's reliable final product distributions were being calculated for complex propellant mixtures and were being confirmed as well as possible by chemical and spectral analyses.

The great experimental difficulty lies in capturing and identifying the proper quantity of a species before a loss of temperature or pressure, or before reactions with other species or with surfaces cause a change in mole fraction. Gas temperatures range from 2000 to 3500°K; the zones being observed range from  $10^0$  to  $10^3$   $\mu\text{m}$ . The surface being observed regresses linearly

(1) This research was sponsored by a grant from the Air Force Office of Scientific Research to the University of Delaware.

(2) (a) A. D. Crow and W. E. Grimshaw, *Phil. Trans. Roy. Soc. London, Ser. A*, **230**, 389 (1931); (b) O. K. Rice and R. Ginnel, *J. Phys. Chem.*, **54**, 885 (1950).

(3) R. G. Parr and B. L. Crawford, Jr., *ibid.*, **54**, 929 (1950).

at rates in centimeters per second and the ambient pressure is usually between 20 and 200 atm.

The high temperatures severely restrict the range of materials and processes usable for sampling and analysis. The minute dimensions being observed and the rapid movement of the reference vastly complicate the study of a given plane in the reacting system, while the customary high pressures reduce the dimensions and materials usable for viewing and spectrometry.

**Condensed Phase Reactions.** To circumvent some of these difficulties, spectral analyses of individual decomposition zones have been made at much lower temperatures and pressures; most of the effort has been concentrated on one material: ammonium perchlorate. This report deals with primary reactions occurring largely at the decomposing surface. Microcinematography of burning ammonium perchlorate surfaces and scanning electron microscopy of quenched surfaces have shown the qualitative features of the reacting surface in good detail.<sup>4</sup>

Those photographs have shown almost conclusively that important reactions other than sublimation are taking place at, and somewhat below, the surface. Figure 1 is an artist's conception, based on a number of photographs, showing what the structure of the condensed phase looks like under certain conditions of high pressure combustion. We are most interested in Z4, the porous or noncrystalline zone, that even shows evidence of a liquidlike phase. This evidence of some condensed phase reactions supports some radiation heat transfer calculations. They showed that the flame zone could not have the requisite temperature and emissivity to transfer enough heat to the surface and thus satisfy the endothermic requirements of solids gasification or sublimation. This meant that conduction and heat generation in other zones must be important processes. Since there is strong convection or mass transport away from the surface, there would appear to be only limited molecular back-diffusion from hot gas to surface. This means that important exothermic reactions must be occurring in the condensed phase to at least partially satisfy the endothermic requirements for steady-state gasification.

Further interest in the condensed phase springs from the conviction that if overall combustion rates are to be tailored or altered, the condensed phase reactions are the slowest and are also probably rate limiting, and therefore the best point for study and attack. Chemical analyses have been made of quenched propellant surfaces. They have not been too rewarding since they indicate largely undecomposed products, as well as other products that could have been condensed from the gas phase during quenching. But, of course, during quenching, severe changes of state are taking place.

Another reason for great interest in surface reactions is the desire to get at the very earliest stages of decom-

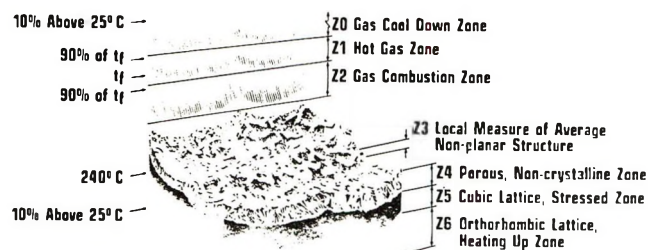


Figure 1. Crystalline oxidizer, single crystal combustion model.

position. Key transient or intermediate species might be present and detectable in the condensed phase, but may rapidly disappear and be lost to detection in the gas phase.

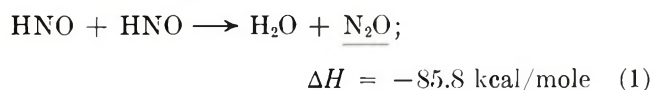
## II. Theory

### *Postulated Existence and Importance of HNO and NH<sub>2</sub>.*

A detailed theoretical analysis of AP decomposition by Jacobs and Pearson<sup>5</sup> calls for the formation of nitroxyl, HNO, as



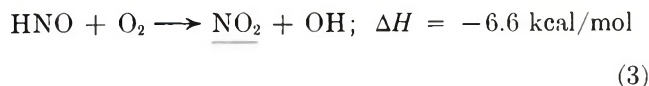
but NH<sub>2</sub> has not been detected as a decomposition product. They point out that the method of production of the oxides of nitrogen in AP decomposition was first theorized<sup>6</sup> on the basis of HNO reactions as



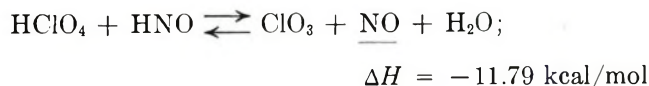
unimolecular to give nitric oxide



and oxidation to give nitrogen dioxide



Guirao and Williams<sup>7</sup> proposed an additional reaction for HNO leading to nitric oxide



They state that the above reaction is essential to their gas phase kinetic scheme, in the sense that the overall reaction rate would be much lower without the

(4) T. L. Boggs, K. H. Kraeutle, and D. E. Zurn, *AIAA J.*, 10, 15 (1972).

(5) P. W. M. Jacobs and G. S. Pearson, *Combust. Flame*, 13, 419 (1969).

(6) J. V. Davies, P. W. M. Jacobs, and A. Russell-Jones, *Trans. Faraday Soc.*, 63, 1737 (1967).

(7) C. Guirao and F. A. Williams, *AIAA J.*, 9, 1345 (1971).



postulated step. They point out, however, that HNO has never been observed in AP decomposition or combustion experiments.

Wilde<sup>8</sup> has also pointed out the importance of HNO in the gaseous  $\text{H}_2\text{-NO}$  reaction.

*Selection of Experimental Method.* The method we feel holds the greatest promise at this time for further definition of overall reaction mechanisms and of surface decomposition products is mass spectrometry. Small samples can be heated to temperatures near the surface temperatures obtained during combustion. Such temperatures can be supplied to a small sample near the inlet to a mass spectrometer by resistance heating of the sample container or by radiant heating of the surface. Under the ambient high vacuum conditions, any surface decomposition should be rapidly followed by vaporization. Unfortunately, in the case of ammonium perchlorate, rapid sublimation will also be taking place. Once in the gas phase, under high vacuum, the species have little chance of collision reactions. They are ionized in the electron stream and carried to the detector. Hopefully, this occurs with a minimum of fragmentation or cracking. Pai Verneker and Maycock<sup>9,10</sup> and others have warned that electron bombardment of the sublimate can also produce many species. However, the ionizing voltage can be varied over a wide range to see if drastic changes in species take place for different electron energies. Species requiring bimolecular reactions should not occur due to bombardment. Also, as a check on the mass spectrometer operation, analyses can be run under test conditions in which other quantitative methods can be used. Check methods have revealed good correlation. However, the mass spectrometer also identifies a number of highly reactive species that could not exist long enough to be detected by the slower methods.

At any rate, time-of-flight and high resolution mass spectrometry hold the promise of providing data on primary species that have long been postulated to occur, but have not been proved. Time-of-flight analyses have been used in the past and have detected some of the primary species.<sup>9-12</sup>

Pellett<sup>12</sup> has shown that much the same kinds of products occur whether decomposition is caused by laser flash heating or by conduction heating of the sample in the spectrometer heater.

To simplify the species identification problem, we have used neat, high purity ammonium perchlorate (AP) and its deuterated derivative as the candidate propellants. AP has been found to burn as a monopropellant under a variety of physical conditions and thus makes an ideal test case.<sup>13</sup> It is also a major component of most solid propellants.

We and others have postulated the following primary products capable of being formed in the condensed phase:  $\text{NH}_4$ ,  $\text{NH}_3$ ,  $\text{ClO}_4$ ,  $\text{HClO}_4$ , and the other hydrides and oxides of nitrogen and oxides of chlorine.

None of these occur as final products of combustion, either by chemical analyses or by thermochemical calculation. As stated above, Jacobs and Pearson and Guirao and Williams have postulated detailed mechanisms for the combustion process depending on the existence of HNO in addition.

Time-of-flight spectrometry was chosen to scan all mass/charge values, while higher resolution methods were used to study regions of interest. Prior work reported has not used high resolution spectra. In the future, further isotopic tagging is to be used to assure separation of species with similar mass/charge values. Future work will also be devoted to anionic and cationic changes to the candidate propellant material. Mack and Guillory<sup>14-16</sup> have initiated some of this work, which will allow study of the reactivity of a variety of species to help strengthen the validity of the models proposed.

*Postulated Relationship of Lower Temperature, Vacuum Conditions to Combustion Environments.* The usual combustion testing environment for ammonium perchlorate as a single crystal monopropellant has been about 65 atm in a bomb pressurized with nitrogen at about 25°. Under these conditions, the linear burning rate is about 1 cm/sec. The calculated equilibrium gas temperature is 1130°, the most prominent gas species being  $\text{H}_2\text{O}$ ,  $\text{O}_2$ ,  $\text{HCl}$ , and  $\text{N}_2$ . Dode<sup>17</sup> and Levy<sup>18</sup> have partially confirmed the products by chemical analyses. Attempts at measurement have indicated that this temperature might be as low as 1000°, probably due to nonequilibrium conditions and mixing with surrounding cooler gases.

The surface temperature is known from photographs to be well beyond the orthorhombic-to-cubic phase transition temperature of 240° and is probably close to the fast decomposition temperature recorded by differential thermal analysis of 300 to about 450°, depending strongly on the purity of the AP. Apparently, at temperatures greater than about 300°, the steady-state, self-sustaining decomposition reaction we call combustion can take over. Below that temperature, only about 30% of the AP decomposes, and then reaction stops. Maycock<sup>9</sup> has proposed a theory for this be-

- (8) K. A. Wilde, *Combust. Flame*, **13**, 173 (1969).
- (9) J. N. Maycock, V. R. Pai Verneker, and P. W. M. Jacobs, *J. Chem. Phys.*, **46**, 2857 (1967).
- (10) V. R. Pai Verneker and J. N. Maycock, *ibid.*, **47**, 3618 (1967).
- (11) G. A. Heath and J. R. Majer, *Trans. Faraday Soc.*, **60**, 1783 (1964).
- (12) G. L. Pellett and A. R. Saunders, "Mass Spectrometer Pyrolysis of Ammonium Perchlorate at Low Pressure," CPIA Publ. No. 138, Vol. 1, John Hopkins Press, Baltimore, Md., 1967, pp 29-38.
- (13) E. E. Hackman, III, and H. C. Beachell, *AIAA J.*, **6**, 561 (1968).
- (14) J. L. Mack and G. B. Wilmot, *J. Phys. Chem.*, **71**, 2155 (1967).
- (15) W. A. Guillory and M. King, *ibid.*, **73**, 4367 (1969).
- (16) W. A. Guillory, J. L. Mack, and M. King, *ibid.*, **73**, 4370 (1969).
- (17) M. Dode, *Bull. Soc. Chim. Fr.*, **5**, 170 (1938).
- (18) J. B. Levy, *J. Phys. Chem.*, **66**, 1092 (1962).



havior. Our assumption in working at temperatures of 100 to 300° which is about the only practical range for examination by mass spectrometers, unless a flash heating method is used, is that the majority of the non-electronic reactions will be the same, at least initially, while the 30% decomposition is taking place. The higher combustion temperatures simply remove surface decomposition products fast enough by vaporization to allow steady-state and complete decomposition to take place.

The pressure effect on combustion rates is very strong. In fact, single AP crystals of millimeter dimensions will not burn at all below about 10 atm. Reasons for this were analyzed by Olfe and Penner.<sup>19</sup> Even though some of the bases they used for calculations have been later found to be somewhat in error, their fundamental conclusions seem valid. In addition to the first effect one would predict—that of increasing reaction rates with increasing pressure due to greater reacting mass concentrations—the greatest effect is on the emissivity of the hot gases. Pressure would be expected to have little effect on the hot surface emissivity, but its value would be much larger than that of the gas cloud for small dimensions and low pressures. Olfe and Penner showed that radiation from the gas cloud to the surface for millimeter size dimensions increases tenfold when pressure is increased from 25 to 300 atm. Even more striking is the effect of increasing the simple geometric (not necessarily the physical size with all its irregularities) size of the burning surface from a square of 20 mm on a side to one of 20 cm on a side. This increases the radiant energy flux from gas to surface by about 30,000 times because the larger gas cloud above the larger surface has a larger beam length, which increases the gas cloud's emissivity greatly.

Thus, it can be seen that where a surface temperature of greater than 300° is required, the hottest source available is the hot gas, and its effectiveness can be increased several hundred thousandfold by nonchemical changes; factors like pressure and geometry are merely acting as a hotter source to stimulate and sustain surface reaction.

Therefore, we make the assumption that, in mass spectrometry, although the pressures we use are very many times lower than those used in combustion, we are compensating for the lost thermal input from the gas phase by providing a direct input to the sample by the mass spectrometer heater.

It is realized that dissociative sublimation will be very strong under the mass spectrometer conditions. Here we hope that the high sensitivity of the devices being used will enable us to detect the surface decomposition products amid an anticipated flood of ammonia and perchloric acid, the first products of decomposition.

It is interesting that most ammonium perchlorate containing propellants burn quite well, although very

slowly, at 1 atm. We believe this indicates that, in comparison with pure AP, condensed phase exothermic reactions are stronger and more controlling for the propellant (as opposed to gas phase radiant heating). The likely candidates are the oxidations  $C \rightarrow CO_2$  and  $Al \rightarrow Al_2O_3$ .

### III. Equipment and Experimental Procedures

The three experimental features of the study were the mass spectrometers used, the special sample probe designed to get surface decomposition products to the detector with minimum delay, and the high purity of the sample materials.

*Mass Spectrometers. Time-of-Flight (TOF).* For screening studies of wide temperature ranges, probe experimental work, and the like, two time-of-flight mass spectrometers were used. This gave an opportunity to compare background traces and to determine the presence of any equipment artifacts in the scans. The instruments were Bendix Model 12-101 spectrometers operating with ionizing currents of 70 eV. This level of electron energy gave good reproducible spectra. We realize that this energy level may be causing some cracking of the gas species in addition to causing ionization sufficient for detection. Room temperature is associated with only about 0.025 eV. Expected surface temperatures of burning AP (400–900°) might be considered to have an energy level of approximately 0.10 eV. The energy associated with the highest gas combustion temperatures would be less than 0.33 eV, so the electron beam energies used in any spectrometer have a far higher potential for causing decomposition than the thermal stress applied. The critical difference between the electron beam and thermal energy is that there is usually only one electron impact with a species, but thermal radiation impinges on the species for a finite time.

Other investigators have already recorded the chlorine oxides spectra produced by hot  $HClO_4$ . Guillery and King refer to the spectra as a cracking pattern quite similar to the species we find from AP. Other investigators have used very low electron beam energies in the region of 20 eV. This is further discussed in section V.

The time-of-flight instruments had a capture sensitivity of  $10^{-8}$  A. A Bendix Model 843 hot filament sample controller was used to control sample temperatures. A sample of approximately 10 mg was used. When the desired test temperature was reached and stabilized, a number of spectra were run until they were reproducible.

*Time-of-Flight (TOF) Sample Probe.* Sample orien-

(19) D. Olfe and S. S. Penner, "Radiant Energy Emission from the Equilibrated Reaction Products of a Pure Ammonium Perchlorate Pellet," Air Force Office of Scientific Research Technical Note No. 59-1094 (Contract No. AF 49 (638)-412), Lockheed Missiles and Space Division, Sunnyvale, Calif., Sept 1959.



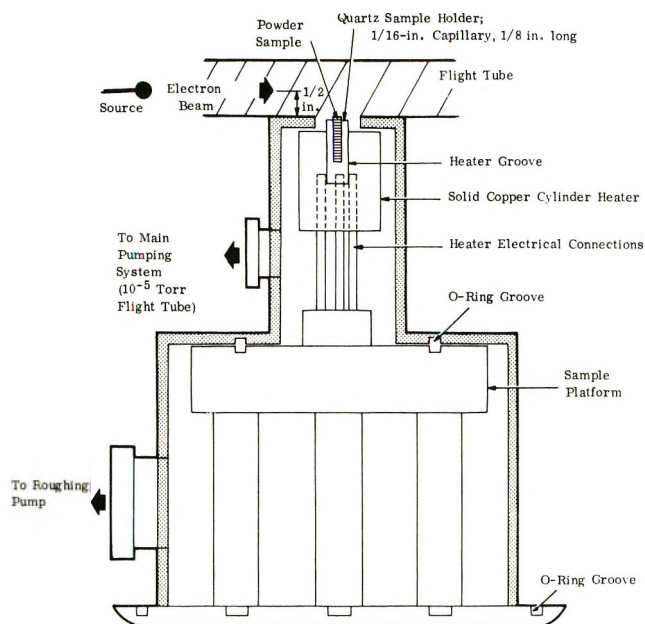


Figure 2. Top mass spectrometer probe sketch.

tation and thermal conditioning within the spectrometer are critical to reproducibility. The probe we used is shown in Figure 2. In our studies we endeavored to assure that the sample was heated uniformly and placed as near as possible to the electron beam. The limitation on nearness was to restrict the beam from being able to impinge directly on the solid sample. Our goal was to know the temperature of the solid phase, to operate at temperatures that would cause measurable decomposition of the condensed phase and production of gaseous species, and then to identify those species before any further decomposition or collisions could take place. The short period of time ( $10^{-6}$  sec) and high vacuum ( $10^{-5}$  Torr) during the period from vaporization to detection would tend to preserve the species from collision reactions. On the other hand, the high vacuum and the electron impact will tend to cause decomposition that is an artifact of the analytical method. Our hope is that the artifact will be quantitative, rather than qualitative. That is, we are tacitly assuming at this stage that the degree of decomposition we are measuring for a given temperature is really that for a somewhat higher temperature—if higher pressures and no electron beam were the ambient conditions. Thus, we are putting emphasis on detecting condensed phase decomposition rather than gas phase reactions.

**High Resolution Spectrometry.** A CEC DuPont 211-110B instrument was used for these studies. A molecular leak of perfluorokerosene was used in the background as a reference. With high resolution spectroscopy a number of runs are required to give assurance that peak heights at a given mass/charge are meaningful, particularly with solid samples. A burst of decomposition occurring when the detector was measuring a given mass/charge would make that peak unrealisti-

cally large. The vacuum in the sample region was  $10^{-5}$  Torr and at the detector it was  $10^{-8}$  Torr.

**High Resolution Sample Probe.** As Figure 3 shows, the solid sample of AP to be tested is placed as near as possible to the electron stream. As the sample is depleted during the test, it recedes somewhat from the ionization area, but in no case is it farther than about 20 mm. As shown, a Knudsen effusion cell is available, although it was not used during these tests.

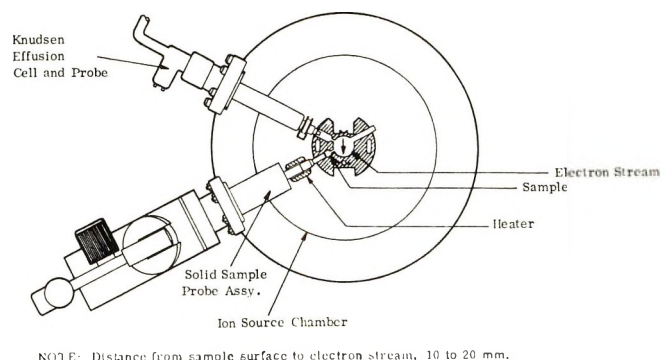
**Materials.** The ammonium perchlorate used was ultra high-purity grade prepared by American Potash Corp. This material had previously been used to prepare very pure single crystals. The deuterated version was prepared by triple recrystallization from  $\text{D}_2\text{O}$ . After vacuum drying, it gave no detectable proton signal on nmr analysis.

#### IV. Results

With the mass spectrometers used, resolution could be varied from differentiating between unit masses (TOF) to differentiating between masses differing only at the fourth decimal place.

Background traces were a necessary adjunct to the understanding of sample species and their amounts. Although care is taken to clean sample and ionization chambers and stabilize the trace recording network, there is always the possibility of a peak being misinterpreted if sufficient background traces and repetitive traces are not available.

The background trace in Figure 4 is typical for time-of-flight (TOF) measurements. Air impurities are readily seen. Doubly charged nitrogen and oxygen are seen at  $m/c$  14 and 16. Hydroxyl and water are seen at 17 and 18. The mass 29 peak is probably  $\text{C}_2\text{H}_5^+$  from a previous hydrocarbon sample. The peak at mass 40 is  $\text{Ar}^+$  as a minor impurity in air, as is the  $\text{CO}_2^+$  at mass 44. Although attempts were made to keep AP samples pure and dry, there is the possibility that some water and  $\text{CO}_2$  were absorbed and were introduced into the results. This tends to confuse the understanding of how much water is due to AP decomposition and how much is due to absorbed water. When only



NOTE: Distance from sample surface to electron stream, 10 to 20 mm.

Figure 3. Sample and probe orientation, high resolution spectrometer.

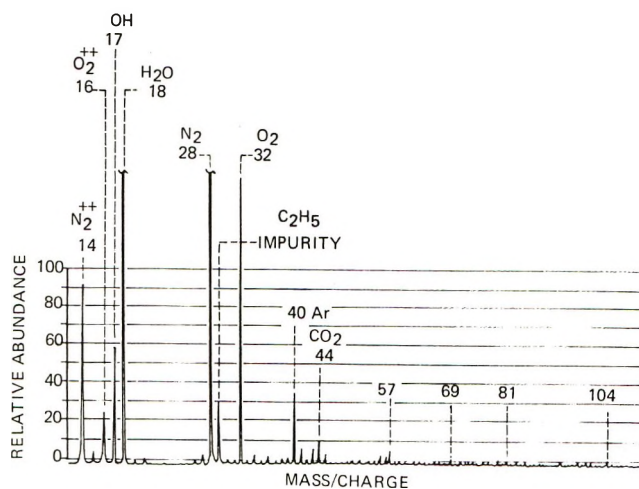


Figure 4. Time-of-flight mass spectrometer scan; background at 100°.

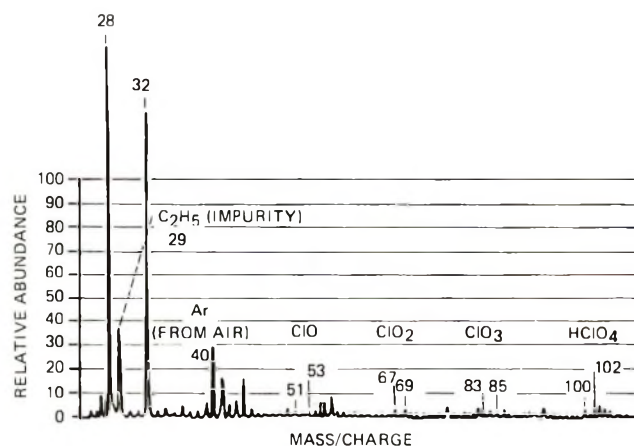


Figure 5. Time-of-flight mass spectrometer scan;  $\text{NH}_4\text{ClO}_4$  at 80°.

unit mass discrimination is possible, such as with TOF, the  $\text{CO}_2$  peak also covers the region at mass 44 where  $\text{N}_2\text{O}$  might be detected. We are very much interested, however, in the complete absence of any peak at mass 31, where  $\text{HNO}$  is being sought in the sample.

In our time-of-flight screening studies, 80° was found to be the highest temperature at which there was no detectable decomposition of AP (see Figure 5). Scans made at 10 to 20° intervals from room temperature to 80° detected nothing but background. The strong peaks at 28 and 32 are due to a background of air. It can be seen that nothing is detectable at masses: 51 or 53 ( $^{35}\text{ClO}$  and  $^{37}\text{ClO}$ ); 67 or 69 ( $^{35}\text{ClO}_2$  and  $^{37}\text{ClO}_2$ ); 83 or 85 ( $^{35}\text{ClO}_3$  and  $^{37}\text{ClO}_3$ ); or at 100 or 102 ( $\text{H}^{35}\text{ClO}_4$  and  $\text{H}^{37}\text{ClO}_4$ ), any of which would indicate perchlorate decomposition.

Referring to Figure 6, it can be seen that at 95° the appearance of the chlorine oxide species has begun. There is also evidence for  $\text{NO}$  at 30,  $\text{HNO}$  at 31, and atomic chlorine at 35 and 37.  $\text{HCl}$  at masses 36 and

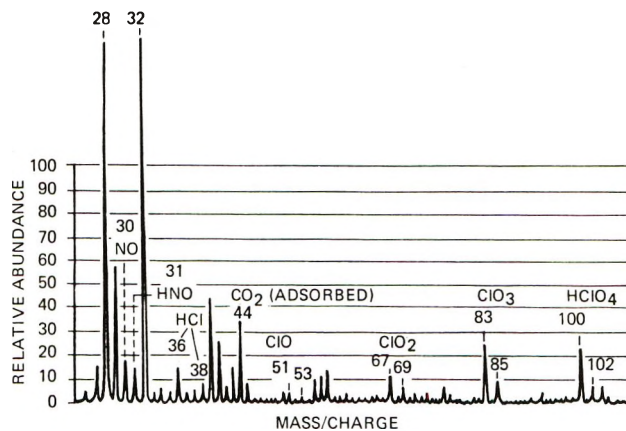


Figure 6. Time-of-flight mass spectrometer scan;  $\text{NH}_4\text{ClO}_4$  at 95°.

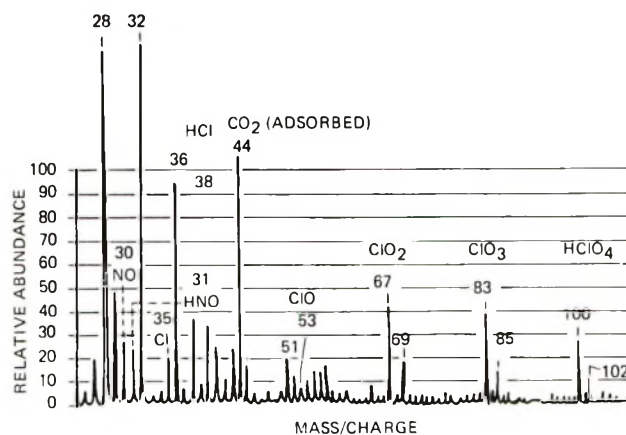


Figure 7. Time-of-flight mass spectrometer scan;  $\text{NH}_4\text{ClO}_4$  at 115°.

38 has not yet appeared, and molecular chlorine at 70 is definitely absent.

At 115°, Figure 7,  $\text{HCl}$  at 36 and 38 suddenly becomes prominent. High resolution scans show that the strong increase in mass 44 is due to further  $\text{CO}_2$  being desorbed from the sample.  $\text{N}_2\text{O}$  was detected.  $\text{HNO}$  as mass 31 and  $\text{NO}$  at mass 30 and  $\text{Cl}$  at 35 and 37 have all reached a maximum, the examination for hydrides of nitrogen at lower  $m/c$  is discussed later.

At 135° (Figure 8)  $\text{HNO}$ ,  $\text{ClO}$ , and  $\text{ClO}_2$  are seen to be no more abundant than at 115°.  $\text{ClO}_3$  (83 and 85) and  $\text{HClO}_4$  (100 and 102) now appear at a maximum.  $\text{HCl}$  at mass 36 is now about as prominent as  $\text{ClO}_3$  at 85. It can be easily seen that there is no  $\text{ClO}_4$  in any of these or in the following traces at masses 99 and 101.

In Figure 9, at 165°,  $\text{HCl}$  and  $\text{ClO}_3$  still vie for position as the most abundant species. There is still absolutely no indication of molecular chlorine. No  $\text{NO}_2$  at mass 46 was detected in any of the scans; nor was  $\text{HOCl}$  at masses 46 and 48.

Figure 10 is the decomposition pattern for deuterated AP at 140°.  $\text{DClO}_4$  is now prominent at masses 101



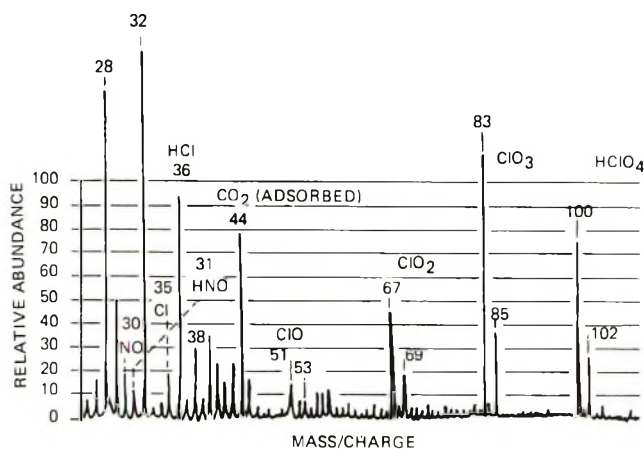


Figure 8. Time-of-flight mass spectrometer scan;  $\text{NH}_4\text{ClO}_4$  at  $135^\circ$ .

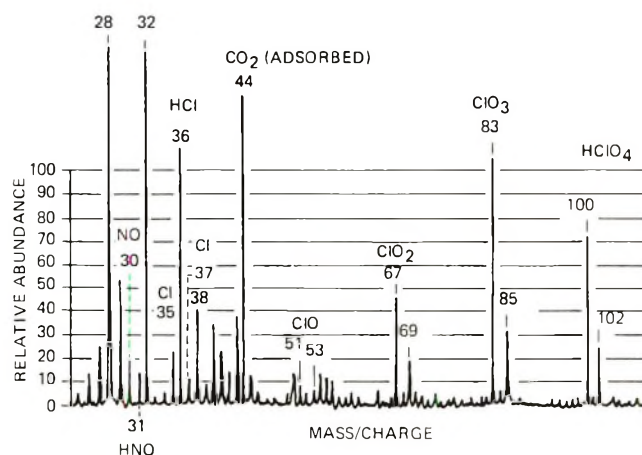


Figure 9. Time-of-flight mass spectrometer scan;  $\text{NH}_4\text{ClO}_4$  at  $165^\circ$ .

and 103. The extent of proton impurity can be readily detected by the  $\text{HClO}_4$  peaks at 100 and 102 amounting to about 10% of the total. This seems to indicate that delays in analysis of deuterated AP, while subject to ambient air from time to time, can lead to absorption of water and significant reversion to  $\text{NH}_4\text{ClO}_4$ . The freshly prepared deuterated AP, after drying, gave no minimum signal on nmr analysis, indicating less than a few hundredths of 1% proton content.

Most significant in this figure is the absence of mass 31, evidently due to DNO now occurring at mass 32 (along with  $\text{O}_2$ ). A puzzling part of this trace is the nearly 50% content of HCl in the overall HCl-DCl signal. There is no indication of  $\text{ND}_4$  at mass 22 in this lower sensitivity run, but ND is present at mass 16 and  $\text{D}_2\text{O}$  is strong at mass 20.

A typical higher resolution (complete peak separation between OH and  $\text{NH}_3$ ) scan of the lower mass numbers is shown in Figure 11. The major peak at mass 14 is doubly charged  $\text{N}_2$ , but it is entirely due to the background. The major peak at mass 15 is NH. The smaller in size, but higher mass number peaks, at

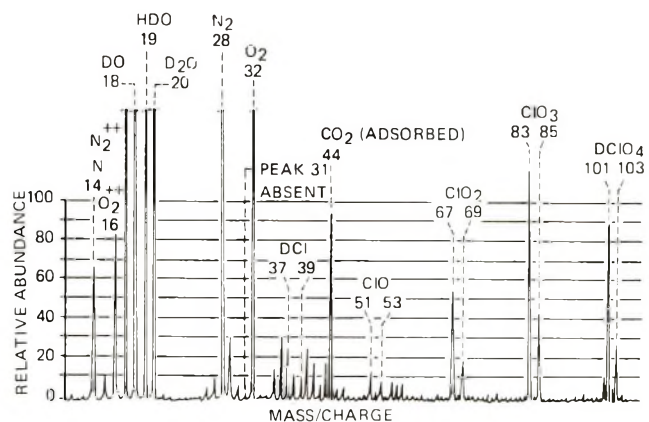


Figure 10. Time-of-flight mass spectrometer scan;  $\text{ND}_4\text{ClO}_4$  at  $140^\circ$ .

16, 17, and 18, respectively, are  $\text{NH}_2$ ,  $\text{NH}_3$ , and  $\text{NH}_4$ .  $\text{NH}_4$  is quite small and easily lost on lower sensitivity and low resolution traces. The presence of some  $\text{NH}_4^+$  was confirmed by detection even when the electron beam of the mass spectrometer was turned off. The  $\text{NH}_2$  peak at mass 16 is roughly 50% of the overall mass 16 signal due to the combination of doubly charged oxygen and  $\text{NH}_2$ . The oxygen, unlike nitrogen, is mostly due to AP decomposition. The strong OH signal is almost all due to the sample; we assume part is due to AP decomposition. The strong water signal is almost all due to the sample, and we assume some part of it is AP decomposition and the remainder is water and or an impurity in the sample. Although not shown here, the higher mass scans showed  $\text{CO}_2$  to be present due to the AP, but no  $\text{N}_2\text{O}$  was present at mass 44.

## V. Data Evaluation

In our studies, as compared with those conducted at atmospheric or higher pressures, we should be producing larger quantities of  $\text{NH}_3$  and  $\text{HClO}_4$  due to dissociative sublimation. If we did not detect these two as initial and major species as temperature was raised, we would suspect that the low pressure in the mass spectrometer and the electron beam energy were cracking the ammonia and perchloric acid known to be formed and were producing the decomposition species. A review of the figures showing uncorrected relative species abundance from 80 to  $165^\circ$  shows that  $\text{NH}_3$  and  $\text{HClO}_4$  are among the first species formed, and they remain as major species at all temperatures tested.

Maycock and Pai Verneker<sup>10</sup> have proposed a point defect mechanism to explain the fact that at atmospheric pressure only 30% of ammonium perchlorate decomposes below  $300^\circ$ . At temperatures above  $350^\circ$ , decomposition is complete. The species we have found and the mechanisms to account for them are in accord with their mechanism, which calls for production of species such as  $\text{NH}_3$ ,  $\text{NH}_3$ ,  $\text{H}_2\text{O}$ ,  $\text{HClO}_4$ , and  $\text{ClO}_5$  in the condensed phase.

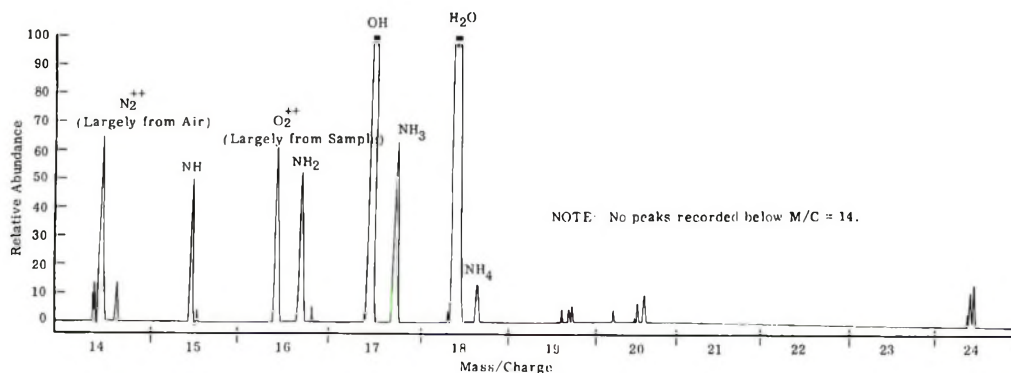


Figure 11. High resolution mass spectra; ammonium perchlorate at 165°,  $m/c$  14–24.

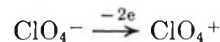
In this set of experiments we did not find a temperature at which  $\text{NH}_3$  and  $\text{HClO}_4$  were the only products. In the first appearance of  $\text{HClO}_4$  at 95°,  $\text{ClO}_3$ , the first decomposition product of  $\text{HClO}_4$ , is already equally abundant and  $\text{ClO}_2$  is possibly one-third as abundant. A more detailed study of the temperature range 80–95° should be made. Our spectra seemed to correlate quite closely with the figures and descriptions given by Guillory and King.<sup>15</sup> This includes the chlorine oxide species “reversal effect” they referred to. Guillory and King also gave the spectrum for perchloric acid itself. However, they state that  $\text{HClO}_4$  produced as an evaporated product remains relatively stable up to 320°. Therefore, they attribute chlorine oxide species in the 200° region and below to  $\text{HClO}_4$  cracking by the electron beam. This may well be, but Levy<sup>18</sup> reports heterogeneous  $\text{HClO}_4$  reactions below 300°, the rate depending on the nature of the surface with which it is in contact. It might be expected that the surface of decomposing AP, containing  $\text{NH}_1$  and  $\text{NH}_3$  species, and probably  $\text{NH}_2$  and  $\text{NH}$  species, could provide an environment favoring  $\text{HClO}_4$  decomposition. The abstraction of OH at the weaker Cl–OH bond would start the formation of the three chlorine oxides.

Apparently, we cannot yet say for certain what portion of the  $\text{HClO}_4$  decomposition species (and by analogy the hydrides of nitrogen species) is due to thermal decomposition and what portion is due to electron beam cracking. We do know that the intensities of the species grow in a striking fashion as the temperature is increased from 95 to 165°. Also Pellett and Saunders<sup>12</sup> have reported not much difference in the relative abundance of the species when reducing electron beam energy from 70 down to 20 eV. They also state that cracking products and solid decomposition products can be differentiated. It must be realized, however, that 20-eV electrons are approximately several hundred times more powerful than the thermal environment for initiating uncatalyzed decomposition.

The factor that adds credence to thermal decomposition as the source of many species—as opposed to cracking—is the presence of species such as  $\text{HCl}$ ,  $\text{HNO}$ ,

and  $\text{NO}$ . Perchloric acid has not been shown to produce  $\text{HCl}$  as a decomposition product.  $\text{HNO}$  and  $\text{NO}$  almost certainly require a number of decomposition steps by  $\text{NH}_3$  and  $\text{HClO}_4$ , followed by oxidation of nitrogen hydrides. Such reasoning leads us to believe that many of the species detected actually were formed on the surface of the thermally decomposing  $\text{NH}_4\text{ClO}_4$ . Once such species are formed on the surface, it requires only that they be vaporized, usually as a radical, struck with an electron which strips off one electron and forms the positive ion. Then, with almost no chance of any further reaction, the ion is accelerated to the identification sector of the mass spectrometer. Thus, surface reactions should be the last reactions occurring.

Table I gives a series of reactions we believe could occur on the surface of thermally decomposing ammonium perchlorate at temperatures as low as about 100° when under high vacuum. Although direct spectral evidence for mobile  $\text{ClO}_4^-$  has not been found, the detection of small quantities of  $\text{NH}_4^+$  both with and without the electron beam turned on indicate that the perchlorate ion might have been present. Reaction 1c indicates pathways by which both  $\text{NH}_4$  and  $\text{NH}_4^+$  might have been formed. To make the perchlorate ion a positive ion so that it can be detected requires stripping off an electron pair



This is much less likely to occur than



and the radical would not be detected. On the other hand, any  $\text{NH}_4^+$  leaving the surface in the high resolution apparatus would be immediately accelerated to the detector. Such was found with the electron beam turned off. Further work will be required to determine the proportions of  $\text{NH}_4$  and  $\text{NH}_4^+$  being formed.

The presence of  $\text{NH}_4$  and absence of  $\text{ClO}_4$  might seem to militate against the interpretation that radicals left the surface because, in that case, one might assume a nearly equal probability of detecting either ammonium





condensed phase products providing support for two theories of decomposition mechanisms.

3. Small quantities of  $\text{NH}_4$  were found, but no  $\text{ClO}_4$ .  $\text{NH}_4^+$  leaving the condensed phase was detected with the electron beam turned off.  $\text{ClO}_4^-$ , on the other hand, could only have been detected by the loss of two electrons.  $\text{ClO}_4$  could have been formed, but unimolecularly decomposed so rapidly as not to be detected.

4. No evidence for  $\text{Cl}_2$  was found. Atomic chlorine was formed among all decomposition species. This is probably due to the low pressure studied. This checks

with the results of Guillory and King, but is at variance with the results of a number of other investigators.

5. Nitrogen,  $\text{N}_2\text{O}$ ,  $\text{NO}_2$ , and  $\text{HOCl}$  were not detectable as condensed phase decomposition products.

6. There is evidence that the majority of all proposed reactions of AP decomposition take place in the condensed phase at least to some extent. Thus, sufficient exothermic reactions can be made available under proper pressure conditions to feed energy to the prime condensed phase endothermic reactions and to sustain combustion once the reaction chain is established.

## Structure Effect on the Fading Rate of Photochromic 3-Substituted Benzothiazolinic Spiroprans

by A. Samat, J. Metzger,\*

*Laboratoire de chimie organique A associé au C.N.R.S. (LA126), Université de Provence, 13-Marseille (13<sup>e</sup>), France*

F. Mientienne, F. Garnier, J. E. Dubois,

*Laboratoire de chimie organique physique associé au C.N.R.S. (LA34), Université de Paris VII, 75-Paris (5<sup>e</sup>), France*

and R. Guglielmetti

*Laboratoire de synthèse organique, Université de Bretagne Occidentale, 29283 Brest-Cedex, France  
(Received March 30, 1972)*

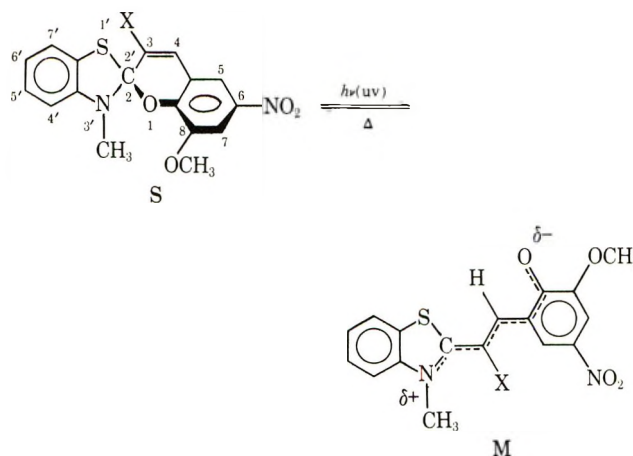
*Publication costs assisted by the Université de Bretagne Occidentale*

Reversible transformations of spiroprans into merocyanines are studied in a series of seventeen photochromic 3-substituted benzothiazolinic spiroprans. The absorption spectra of the colored photomerocyanines and their first-order thermal fading kinetics are followed using a rapid scanning spectrometer coupled to a flash photolysis apparatus. Activation energies and entropies are calculated in toluene. The rate processes are shown to be very sensitive to H bonding of the solvent and to the nature and position of substituents; a rate enhancement of  $10^5$  is observed between the substituents  $\text{X} = \text{OCH}_3$  and  $\text{X} = i\text{-C}_3\text{H}_7$ . The data indicate that steric hindrance of substituents in the 3 position of a planar photomerocyanine has major importance in the rate of conversion of the colored form back to the spiropran.

### Introduction


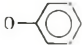
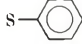
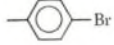
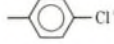
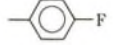
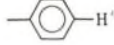
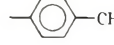
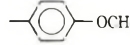

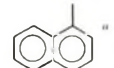
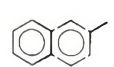
Spiroprans are known to behave as photochromic compounds giving merocyanine dyes when uv irradiated.

The stability of the photomerocyanine is related to the high degree of conjugation allowed by a nearly planar conformation. A great deal of data collected on the spiroprans has led to the structure and properties of this colorless form S. On the other hand, thermodynamic and spectroscopic properties of the colored form and the effect of substituent X in the 3 position are not very well known. In the work reported here, we analyze the problem, often mentioned in the literature but rarely discussed, of the conformation and stability





**Table I:** Kinetic, Thermodynamic, and Spectral Data of 3-Substituted Benzothiazolinic Spiroprans

Compound	Substituent X	Toluene				Ethanol		
		$k$ , sec <sup>-1</sup> , at 25°	$E_a$ , kcal mol <sup>-1</sup>	$\Delta H^\ddagger$ , kcal mol <sup>-1</sup>	$\Delta S^\ddagger$ , eu	$\lambda_{max}$ , nm (visible)	$k$ , sec <sup>-1</sup> , at 25°	$\lambda_{max}$ , nm (visible)
BT1	CH <sub>3</sub> <sup>a</sup>	2.5	21.7 ± 0.3	21.1 ± 0.3	17.1 ± 0.2	600, (545), 420	7.7 × 10 <sup>-4</sup>	490, 420
BT2	C <sub>6</sub> H <sub>5</sub> <sup>a</sup>	23.2	21.8 ± 0.4	21.2 ± 0.4	18.8 ± 0.3	635, 410	15.5 × 10 <sup>-4</sup>	412.5
BT3	CH(CH <sub>3</sub> ) <sub>2</sub> <sup>a</sup>	680 <sup>b</sup>	20.1 ± 0.5	19.5 ± 0.5	19.5 ± 0.5	610, 420-410	5.7 × 10 <sup>-3</sup>	430
BT4		612	18.9 ± 0.2	18.3 ± 0.2	18.8 ± 0.2	620, 610-590, 400	4.65 × 10 <sup>-3</sup>	430
BT5	OCH <sub>3</sub>	9.5 × 10 <sup>-3</sup>	25.6 ± 0.5	25.0 ± 0.5	16.3 ± 0.2	640, 420	(7 × 10 <sup>-6</sup> ) <sup>c</sup>	532 (415)
BT6		16.2 × 10 <sup>-3</sup>	24.1 ± 0.2	23.5 ± 0.2	12.3 ± 0.2	625, 415		542
BT7	SCH <sub>3</sub>	76	19.3 ± 0.7	18.7 ± 0.7	12.8 ± 0.5	635, 415	5.85 × 10 <sup>-2</sup>	596 (402)
BT8		163	17.4 ± 0.2	16.8 ± 0.2	7.4 ± 0.1	605, 425, 400	1.68 × 10 <sup>-1</sup>	529 (407)
BT9		17.5	19.3 ± 0.7	18.7 ± 0.7	10.3 ± 0.7	605	2.07 × 10 <sup>-4</sup>	532 (404)
BT10		18	18.9 ± 0.3	18.3 ± 0.3	8.7 ± 0.2	605, 405	21.8 × 10 <sup>-4</sup>	532 (402)
BT11		9.9	20.1 ± 0.3	19.5 ± 0.3	11.7 ± 0.2	610, 400	8.8 × 10 <sup>-4</sup>	530 (408)
BT12		6.44	21.2 ± 0.2	20.6 ± 0.2	14.8 ± 0.2	635, 395	12.5 × 10 <sup>-4</sup>	530 (408)
BT13		5.25	20.0 ± 0.3	18.4 ± 0.3	10.1 ± 0.2	620, 405	3.86 × 10 <sup>-4</sup>	520 (398)
BT14		4.74	19.5 ± 0.2	18.9 ± 0.2	8.1 ± 0.2	620, 405	2.34 × 10 <sup>-4</sup>	525 (402)
BT15		3.13	21.9 ± 0.5	21.3 ± 0.5	15.2 ± 0.4	605, 395	6.25 × 10 <sup>-4</sup>	530 (408)
BT16		3.04	19.4 ± 0.2	18.8 ± 0.2	7.3 ± 0.2	620		527
BT17		10.8	19.8 ± 0.2	19.2 ± 0.1	11.2 ± 0.1	650, 440, 425	10.05 × 10 <sup>-4</sup>	520

<sup>a</sup> Synthetized and studied by R. Guglielmetti<sup>16</sup> (for comparison). <sup>b</sup>  $k$ , sec<sup>-1</sup>, at 25.4°. <sup>c</sup> Approximate value.

of a photomerocyanine in relation to substituents in the 3 position.<sup>1-6</sup> We have determined in two solvents and at different temperatures the rate constants of the thermal decoloration reaction and the absorption spectra of a series of photochromic<sup>7-9</sup> 3-substituted benzothiazolinic spiropyran synthesized in the Department of Organic Chemistry in the University of Provence.<sup>10,11</sup>

### Experimental Section

A flash photolysis apparatus available in the Physical Organic Chemistry Laboratory at Paris was used to induce the opening of the C<sub>2</sub>-O<sub>1</sub> bond of the colorless form and to produce the colored photomerocyanine derivative. The visible absorption spectrum of this open form was recorded on a scanning Warner-Swasey spectrometer which was coupled with the flash photolysis apparatus and was operated at high speed (1 spectrum per millisecond). The spectrometer was

programmed to allow the recording of several successive spectra. From these spectra we measured the kinetics

- (1) M. W. Windsor, R. S. Moore, and J. R. Novack, *Spectrochim. Acta*, **18**, 1364 (1962).
- (2) J. Ch. Metras, M. Mosse, and C. Wippler, *J. Chim. Phys.*, **62**, 659 (1965).
- (3) T. Bercovici, R. Heiligman-Rim, and E. Fischer, *Mol. Photochem.*, **1**, 23 (1969).
- (4) R. Heiligman-Rim, Y. Hirshberg, and E. Fischer, *J. Phys. Chem.*, **66**, 2465, 2470 (1962).
- (5) Y. Hirshberg and E. Fischer, *J. Chem. Soc.*, 3129 (1954).
- (6) J. Arnaud, M. Niclause, and C. Wippler, *J. Chim. Phys.*, **65**, 2150 (1968).
- (7) R. Guglielmetti and J. Metzger, *Bull. Soc. Chim. Fr.*, 2824 (1967).
- (8) R. Guglielmetti, E. Davin, and J. Metzger, *ibid.*, 556 (1971).
- (9) J. Rondon, R. Guglielmetti, and J. Metzger, *ibid.*, 3029 (1971).
- (10) R. Guglielmetti and J. Metzger, *ibid.*, 3029 (1969).
- (11) A. Samat, Organic Chemistry Speciality Thesis, Marseilles, 1972.

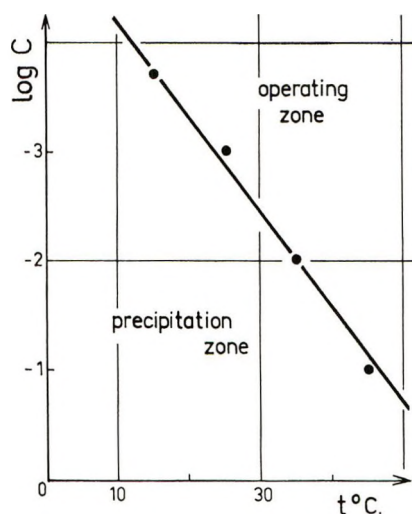


Figure 1. Effect of spiropyran BT5 concentration on the precipitation of the colored open form at different temperatures in toluene.

of disappearance of the colored form M and calculated the kinetic constants of ring closure ( $k\Delta$ ). Cells of path 10 cm were used. For kinetic measurements the temperature of cells was controlled ( $\pm 0.1^\circ$ ) by the circulation of water from an external thermostat. Two flash lamps produced a discharge with an energy of about 500 J in a few microseconds.

The compounds investigated are represented by the main formula S with X = CH<sub>3</sub>, C<sub>2</sub>H<sub>5</sub>, *i*-C<sub>3</sub>H<sub>7</sub>, cyclohexyl, OCH<sub>3</sub>, OC<sub>6</sub>H<sub>5</sub>, SCH<sub>3</sub>, SC<sub>6</sub>H<sub>5</sub>, C<sub>6</sub>H<sub>4</sub>Br, C<sub>6</sub>H<sub>4</sub>Cl, C<sub>6</sub>H<sub>4</sub>F, C<sub>6</sub>H<sub>5</sub>, C<sub>6</sub>H<sub>4</sub>CH<sub>3</sub>, C<sub>6</sub>H<sub>4</sub>OCH<sub>3</sub>, C<sub>6</sub>H<sub>4</sub>OH,  $\alpha$ -naphthyl,  $\beta$ -naphthyl.

The absorption spectra and fading rates were determined in ethanol (H<sub>2</sub>O = 200 ppm) at 25° and in toluene (H<sub>2</sub>O = 20 ppm) at 15, 25, 35, 45, and 55°. These results were used to calculate the activation enthalpies and entropies in the last solvent (Table I). The concentration ranges were about 10<sup>-5</sup> to 10<sup>-6</sup> mol/l. owing to complex phenomena which appeared at high concentrations (10<sup>-2</sup> to 10<sup>-3</sup> mol/l.) with some compounds (X = OCH<sub>3</sub>, OC<sub>6</sub>H<sub>5</sub>, SCH<sub>3</sub>, SC<sub>6</sub>H<sub>5</sub>). Thus with the compound X = OCH<sub>3</sub>, the open form precipitates in toluene at a concentration level which is a function of temperature as shown in Figure 1.

The synthesis of the spiropyran with a phenoxy group in the 3 position leads to a colored product containing a great proportion of the photomerocyanine derivative. We thermally faded the solution in order to obtain the spiropyranic form of the compound. The 3-substituted spiropyranes with chloro and hydroxy functional groups are obtained partly as open form but they degrade when flashed.

## Results and Discussion

Two important features appear in Table I. The first is a high sensitivity of the ring closure rate to the solvent, and the second is an important structure

effect on this rate; a rate enhancement of  $\sim 10^5$  is observed between the substituents X = OCH<sub>3</sub> and X = *i*-C<sub>3</sub>H<sub>7</sub>.

The large decrease of the rate observed in the passage from a nonpolar and aprotic solvent like toluene to a polar and protic solvent like ethanol is consistent with earlier studies on benzothiazolinic and indolinic spiropyranes.<sup>12-14</sup> This decrease is related to a polar structure of the open form of these compounds stabilized in ethanol by H bonding and by the high polarity of the solvent.

These solvent-photomerocyanine interactions must be very large if we consider the difference of a factor of about 1000 observed on the decoloration kinetics in those two solvents. We will discuss now the structure effects on the decoloration rates in terms of charge and its delocalization.

Alkyl substituents induce both a polar and a steric effect. Three types of substituents have been used: alkyl or alicyclic, para-substituted aryl, and functional groups. First we consider the polar effect of the substituent. By using the  $\sigma^*$  parameters as defined by Taft, we observe that the stability of these compounds is sensitive to polar effects. The fading rate varies by a factor of 10 between CH<sub>3</sub> ( $\sigma^* = 0.00$ ) and C<sub>2</sub>H<sub>5</sub> ( $\sigma^* = -0.10$ ) substituents; with an isopropyl group ( $\sigma^* = -0.19$ ) the rate increases by a factor 30. This important variation of the kinetic rate is due to the intervention of the steric effect ( $E_s = -0.47$  for *i*-C<sub>3</sub>H<sub>7</sub> whereas  $E_s$  parameter values are comparable for CH<sub>3</sub> and C<sub>2</sub>H<sub>5</sub>, respectively, +0.00 and -0.07).

This steric effect sensitivity appears much more clearly with the cyclohexyl substituent ( $E_s = -0.79$ ) which has a kinetic rate near that of isopropyl but its  $\sigma^*$  coefficient (-0.13) lies between  $\sigma^*$  of *i*-Pr and ethyl substituents.

These results show that steric effects are determinant in the ring closure kinetic rates of the photomerocyanine form; the rate increases as the groups in the 3 position become more bulky.

To evaluate this steric interaction and to determine the most stable configuration for the photomerocyanine form, theoretical computations have been made with the Symon's program taking account of van der Waals nonbonding interactions.<sup>15</sup> These computations have shown that among the various possible *cis* and *trans* configurations for these compounds, two *trans* structures A and B are favored.

A theoretical conformational investigation using the Extended Hückel method has been developed on the

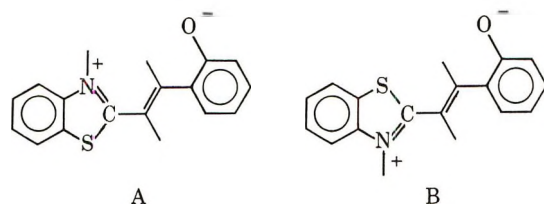
(12) R. Guglielmetti, M. Mosse, J. Ch. Metras, and J. Metzger, *J. Chim. Phys.*, **65**, 454 (1968).

(13) O. Chaudé, *Cah. Phys.*, **51**, 22 (1954).

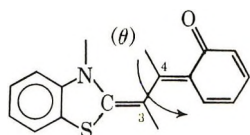
(14) J. B. Flannery, *J. Amer. Chem. Soc.*, **90**, 5660 (1968).

(15) A. Samat, R. Guglielmetti, Y. Ferre, H. Pommier, and J. Metzger, *J. Chim. Phys.*, **69**, 1202 (1972).



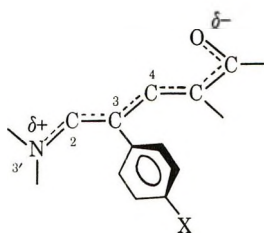


quinonic structure of the more stable A configuration for determining the rotation angle  $\theta$  which corresponds to the minimum energy.



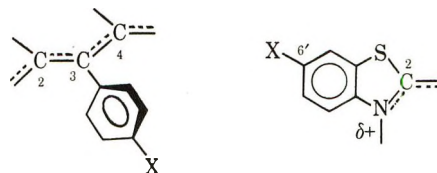
The rotation angle  $\theta$  increases with volume of the substituent ( $50^\circ$  for H,  $70^\circ$  for  $\text{CH}_3$ ,  $75^\circ$  for  $i\text{-C}_3\text{H}_7$ ). These results are compatible with the experimental observations on the destabilization of the open form with increasing of hindrance of the 3-position substituent.

To determine the electronic contribution to the whole substituent effect it is necessary to keep constant the large steric interaction. For this investigation, we have selected para-substituted aryl groups  $\text{C}_6\text{H}_4\text{X}$  with  $\text{X} = \text{H}, \text{CH}_3, \text{OCH}_3, \text{OH}, \text{Cl}, \text{Br},$  and  $\text{F}$  for which steric effects may be considered as invariant. In this series of substituents the variation of reactivity has to be related to the sensitivity to electronic effects. It appears that the stability of the photomerocyanine is governed by inductive and resonance effects of the para X substituents which transmitted to the carbon atom in the  $\alpha$  position of the aryl group. Using the  $\sigma$  para constants defined by Hammett, we have obtained a linear relationship (coefficient correlation  $R = 0.973$ ) between reactivity and substituent effect (Figure 2). The slope (+1.21) of this relation indicates that a positive charge density is located on the atom 3.



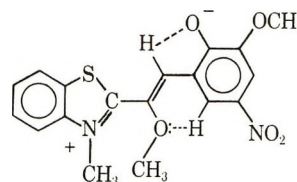
The existence for a  $\sigma_p$  relationship for 3-position substituents has to be compared to a  $\sigma_p^+$  relationship for 6' substitution.<sup>12,16</sup> In the latter case, the strained planarity of the molecule involves a maximal resonance interaction between substituents and reaction center. In the former case, however, the steric hindrance leads to rotation of a 3-substituted para-aryl group out of the plane defined by the charge atoms  $\text{C}_2, \text{C}_3,$  and  $\text{C}_4$ .

This very weak degree of conjugation for 3-position substituents can be estimated by a Yukawa-Tsuno



relation<sup>17</sup>  $\log k/k_0 = \rho(\sigma + r\Delta\sigma)$ , where  $\rho$  is the reaction parameter,  $\sigma$  is the inductive constant of the substituent,  $\Delta\sigma = \sigma^+ - \sigma$  is the resonance contribution of the substituent effect as defined in the reference reaction of Brown and Okamoto,<sup>18</sup> and  $r$  is the degree of resonance interaction between the substituent and the reactive center in the studied reaction. The computation of this relation with a multiple regression program gives  $\log k/k_0 = 1.50(\sigma + 0.27\Delta\sigma)$  with a correlation coefficient  $R = 0.997$ . The value obtained for  $r(0.27)$  confirms the very weak degree of the resonance interaction of the para substituent, which is related to the large rotation of aryl groups with respect to the plane of electronic delocalization.

The colored form of methoxy and phenoxy derivatives is largely stabilized when compared to their methylthio and phenylthio homologs. In addition to the electronic and steric effects, a supplementary factor of stabilization may be proposed for oxygen comparatively with sulfur: an intramolecular chelation by H bonding.



In this series of compounds, the study of the  $\text{X} = \text{H}$  derivative would be of major interest, but this compound exists only in its open merocyanine form. This infinite stability must be related to the absence of steric effect and hence to a maximal conjugation.<sup>15</sup>

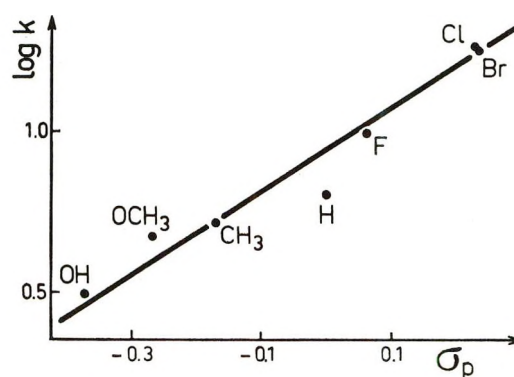


Figure 2.  $\log k = f(\sigma_p)$  toluene,  $25^\circ$ .

(16) R. Guglielmetti, Sciences Thesis, Marseilles, 1967.

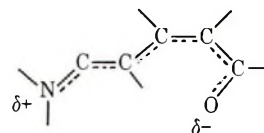
(17) Y. Yukawa and Y. Tsuno, *Bull. Chem. Soc. Jap.*, **32**, 965 (1959); **32**, 971 (1959).

(18) H. C. Brown and Y. Okamoto, *J. Amer. Chem. Soc.*, **80**, 4979 (1958); **79**, 1913 (1957).

Moreover the comparison between  $X = H$  and  $X = SCH_3$  substituents argues for the determining influence of steric effects on stability of photomerocyanine when compared to electronic effects. Although the  $\sigma$  polar constants are the same for these two substituents ( $\sigma_H = \sigma_{SCH_3} = 0$ ), an important rate of fading is observed for the  $SCH_3$  derivative ( $k_{25^\circ} = 76 \text{ sec}^{-1}$  in toluene).

### Conclusion

The investigation of the thermal fading kinetics for these 17 3-substituted benzothiazolinic spiropyrans in ethanol and toluene solvents shows the important electronic delocalization developed in the colored photomerocyanine structure of



This electronic delocalization is responsible for the influence of the polarity of the solvent on the fading rate of the photomerocyanine. In agreement with theoretical calculations the steric effect in the 3 position is of major importance in the nonplanarity of the molecule and in the destabilization of the colored photomerocyanine form.

*Acknowledgment.* We are grateful for support of this work by the D.R.M.E, Optical Division 75996, Paris Armées.

## Excited State Dissociation Rate Constants in Naphthols

by Jerome L. Rosenberg and Ira Brinn\*<sup>1</sup>

Department of Chemistry, University of Pittsburgh, Pittsburgh, Pennsylvania 15213 (Received February 1, 1972)

Publication costs assisted by the University of Pittsburgh

Experimentally determined proton dissociation (and reassociation) rate constants for substituted naphthols in the first excited singlet state are reported. The results are rationalized on the basis of a charge-transfer explanation supported by CNDO/2 and PPP molecular orbital calculations.

### I. Introduction

It has long been known that the dissociation constant of an organic acid is dependent on the electronic state of the molecule. Two possible explanations for this phenomenon have been advanced: (1) the acidity is related to some gross orbital feature of the state reflected in the symmetry of its wave function;<sup>2</sup> and (2) a more subtle aspect of electronic rearrangement is involved such as a small change in charge-transfer character.<sup>3</sup> The first explanation has been shown to be an oversimplification by the work of Vander Donckt and Porter,<sup>4</sup> who showed that the excited singlet and triplet states of anthrols, where both states are derived from anthracene states of the same symmetry, still have appreciably different acidities.

Proton dissociation and reassociation rate constants have previously been reported<sup>5</sup> for 2-naphthol. In this paper we report experimentally determined proton dissociation and reassociation rate constants for 1-naphthol, 2-naphthol, and various substituted naphthols in the first excited singlet state. The results are rationalized on the basis of a charge-transfer explana-

tion supported by CNDO/2 and PPP molecular orbital calculations.

### II. Experimental Section

*A. Materials.* The water used was filtered through both a Barnstead mixed bed ion-exchange column and a Barnstead organic removal column. The following naphthols were used: 1-naphthol and 2-naphthol (Eastman reagent), 2-chloro-1-naphthol, 4-chloro-1-naphthol, 1-bromo-2-naphthol, 6-bromo-2-naphthol, and 1-chloro-2-naphthol (K & K Laboratories 95-

(1) Correspondence should be addressed to Departamento de Bioquímica, Instituto de Biociências, Universidade Federal de Pernambuco, Recife, Pernambuco, Brasil. This article is based in part on a dissertation submitted by I. B. in partial fulfillment of the requirements for the Ph.D. at the University of Pittsburgh in 1968.

(2) T. Förster, "Reactivity of the Photoexcited Organic Molecule," Interscience, New York, N. Y., 1965, p 111.

(3) J. N. Murrell, "The Theory of the Electronic Spectra of Organic Molecules," Methuen and Co., Ltd., London, 1963.

(4) E. Vander Donckt and G. Porter, *Trans. Faraday Soc.*, **64**, 3218 (1968).

(5) (a) L. Stryer, *J. Amer. Chem. Soc.*, **88**, 5708 (1966); (b) N. M. Trieff and B. R. Sundheim, *J. Phys. Chem.*, **69**, 2044 (1965); (c) A. Weller, *Z. Phys. Chem. (Frankfurt am Main)*, **3**, 238 (1955).



99%), 6-methyl-2-naphthol and 7-methyl-2-naphthol (Columbia Chemical Co. >95%). The unsubstituted naphthols were purified by vacuum sublimation while the substituted naphthols were purified by recrystallization from ethanol. None of the naphthols gave fluorescence peaks at longer wavelengths than published values.

Buffers were prepared from the following reagents or certified grade chemicals at total concentrations not exceeding 0.001 M (except at pH <3 or >11): HCl, H<sub>2</sub>SO<sub>4</sub>, CH<sub>3</sub>CO<sub>2</sub>H, CH<sub>3</sub>CO<sub>2</sub>Na, H<sub>3</sub>BO<sub>3</sub>, and KOH.

*B. Equipment.* Absorption spectra were measured on either a Cary 14 or a Bausch and Lomb Spectronic 505. The fluorescence spectra (uncorrected) were measured at room temperature (22°) on an Aminco-Bowman spectrophotofluorimeter with a 1P21 (S-4 response) photomultiplier. These spectra were recorded on a Hewlett-Packard Mosely 7035A X-Y recorder. The uncertainty in wavelength of the absorption and fluorescence peaks was assumed to be ±1 nm. The uncertainty in the peak heights varied but was generally about 2%.

Lifetime measurements were performed on a single photon counting apparatus which has been described in detail elsewhere.<sup>6</sup> In this apparatus only a small fraction (approximately 4%) of periodic excitations (usually 5000/sec) cause a photon to reach a photomultiplier of negligible dark current. These single photon responses are then stored in a multichannel analyzer according to the time between the flash and the reception of the photon. The data are taken out of the multichannel analyzer onto data cards, fed into the IBM 360 at the Columbia University Computer Center, and a best lifetime is fitted. The uncertainties given for the lifetimes are chosen from the results of the curve fitting program such that two standard deviations from the best value of the lifetime are contained within the error limits.

The pH measurements were made with a Beckman Research pH meter with a calomel reference electrode, standardized with a Fisher phosphate buffer (pH 6.85).

*C. Förster Cycle.* The Förster cycle<sup>7</sup> (eq 1)

$$pK_{gd} - pK_{exc} = h(\nu_{HA} - \nu_{A^-})/2.3kT \quad (1)$$

has been used to calculate the difference in pK between the ground and the first excited singlet state. In accordance with Weller's suggestion<sup>8</sup> each frequency was taken as the average of the absorption and fluorescence maxima for the lowest excited singlet.

Förster cycle calculations were performed on two unsubstituted and on seven substituted naphthols. The results are shown in Table I.<sup>9,10</sup> pK<sub>gd</sub> was determined experimentally by plotting absorbance vs. pH, following the method of Davis and Geissman.<sup>11</sup>

*D. Intensity vs. pH.* In this method the relative fluorescence intensity (arbitrary units) of the naphtholate ion is plotted against pH.<sup>8</sup> Experimentally,

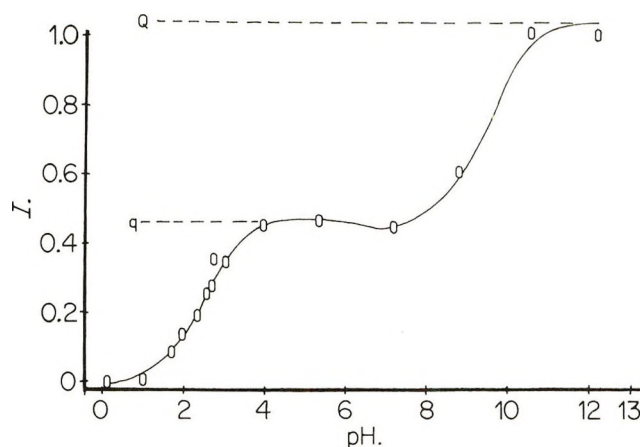


Figure 1. Fluorescence intensity vs. pH for 1-naphthol. Concentration of 1-naphthol,  $5.6 \times 10^{-6}$  M; exciting wavelength, 309 nm;  $I$  is relative emission intensity at 467 nm.

equimolar (in acid plus conjugate base) solutions were prepared in different buffers, the fluorescence was excited at an isosbestic point, and the emission intensity,  $I$ , was recorded at a wavelength where the conjugate acid fluorescence makes a negligible contribution. An example of such a plot for 1-naphthol is shown in Figure 1.

From such results the rate constants for dissociation ( $k_t$ ) and association ( $k_b$ ) in the excited state were calculated using the following equations, first derived<sup>8</sup> by Weller

$$k_t = \frac{q}{(Q - q)t} \quad (2)$$

$$\frac{Q}{I} = \frac{1}{k_t t} + 1 + \frac{k_b t'}{k_t t} [H_3O^+] \quad (3)$$

where  $Q$  is the relative fluorescence intensity of  $A^-$  on direct excitation of  $A^-$ ,  $q$  is the relative fluorescence intensity of  $A^-$  on direct excitation of  $HA$  where the pH is high enough to render the reassociation negligible (*i.e.*, the first plateau region in Figure 1),  $t$  and  $t'$  are the actual lifetimes of the first excited singlet states of the acidic and basic forms, respectively, at very low and very high pH.

Equation 2 yields  $k_t$ , assuming one knows  $t$ , as a function of the ratios of the heights of the two plateaus (see Figure 1). Equation 3 is merely the  $[H_3O^+]$  dependence of the fluorescence intensity of the basic form. Thus a plot of  $Q/I$  vs.  $[H_3O^+]$  should yield a straight

(6) T. Tao, *Biopolymers*, **8**, 609 (1969).

(7) T. Förster, *Z. Elektrochem.*, **54**, 42 (1950).

(8) A. Weller, *ibid.*, **56**, 662 (1952).

(9) A. Weller, *Z. Phys. Chem. (Frankfurt am Main)*, **17**, 224 (1958).

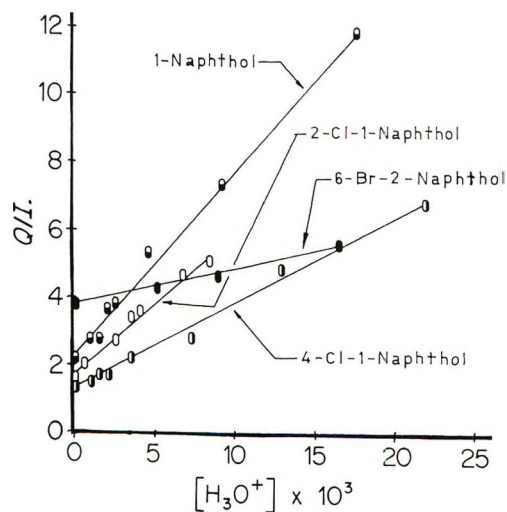
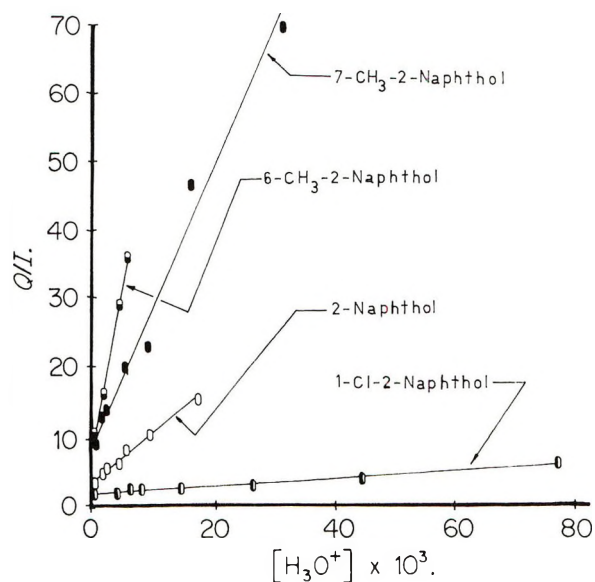
(10) G. Jackson and G. Porter, *Proc. Roy. Soc., Ser. A*, **260**, 13 (1961).

(11) C. T. Davis and T. A. Geissman, *J. Amer. Chem. Soc.*, **76**, 3507 (1954).

Table I: Acidity Constants and Lifetimes of Substituted Naphthols

	Frequency $\times 10^{-4}$ , $\text{cm}^{-1}$		Fluorescence ( $\pm 0.01$ )		$t$	Lifetimes, nsec	$k_f \times 10^{-7}$ , $\text{sec}^{-1}$	$k_b \times 10^{-10}$ , $M^{-1} \text{sec}^{-1}$	$pK_{\text{exc}}$	
	HA	A <sup>-</sup>	HA	A <sup>-</sup>					Förster	$I_{\text{bs}}$ , pH
1-Naphthol	3.11	3.00	2.71	2.13	$\leq 1$	8.2 $\pm$ 0.1	$\geq 85$	5.9 $\pm$ 0.2	2.1 $\pm$ 0.4	$\leq 1.84$
2-Chloro-1-naphthol	3.08	2.99	2.75	2.17	13 <sup>a</sup>	8.4 <sup>a</sup>	$\geq 160$	7.3 $\pm$ 0.5	0.7 $\pm$ 0.4	$\leq 1.66$
4-Chloro-1-naphthol	3.06	2.94	2.54	2.10	$\leq 1$	10.2 $\pm$ 0.3	$\geq 380$	10 $\pm$ 2	2.9 $\pm$ 0.4	$\leq 1.43$
2-Naphthol	3.06	2.91	2.90	2.43	8.9 $\pm$ 0.7	8.8 $\pm$ 0.4	5.6 $\pm$ 0.5	4.0 $\pm$ 0.3	3.0 $\pm$ 0.5	2.85 $\pm$ 0.05
1-Bromo-2-naphthol	3.03	2.84	2.79	2.36	7.6 <sup>a</sup>	8.0 <sup>a</sup>	5.3 <sup>b</sup>	5.5 <sup>b</sup>	3.1 <sup>c</sup>	3.02 <sup>b</sup>
6-Bromo-2-naphthol	2.98	2.82	2.78	2.35	0.48 $\pm$ 0.04 <sup>d</sup>	0.72 $\pm$ 0.04 <sup>d</sup>	57 $\pm$ 9	6 $\pm$ 1	1.4 $\pm$ 0.4	
6-Methyl-2-naphthol	2.99	2.87	2.76	2.39	0.52 $\pm$ 0.05 <sup>d</sup>	0.61 $\pm$ 0.04 <sup>d</sup>	70 $\pm$ 10	4.0 $\pm$ 0.6	3.1 $\pm$ 0.3	1.9 $\pm$ 0.1
7-Methyl-2-naphthol	3.06	2.89	2.82	2.42	8.1 $\pm$ 0.3	11.4 $\pm$ 0.2	1.3 $\pm$ 0.2	2.8 $\pm$ 0.2	4.4 $\pm$ 0.4	3.49 $\pm$ 0.09
1-Chloro-2-naphthol	3.02	2.84	2.77	2.36	8.1 $\pm$ 0.3	9.9 $\pm$ 0.4	1.6 $\pm$ 0.1	1.1 $\pm$ 0.1	3.7 $\pm$ 0.3	3.24 $\pm$ 0.05
					4.2 $\pm$ 0.3	9.5 $\pm$ 0.3	49 $\pm$ 5		1.7 $\pm$ 0.4	1.35 $\pm$ 0.05

<sup>a</sup> Reference 9. <sup>b</sup> Reference 5a. <sup>c</sup> Reference 10. <sup>d</sup> Obtained by comparison of fluorescence intensities to acidic and basic forms of 2-naphthol.

Figure 2.  $Q/I$  vs.  $[H_3O^+]$ .Figure 3.  $Q/I$  vs.  $[H_3O^+]$ .

line of slope  $k_b t' / k_f t$  and intercept  $1 + 1/k_f t$ . In practice the  $y$  intercept of a  $Q/I$  vs.  $[H_3O^+]$  plot can be quite close to 1.0 (see Figures 2 and 3), leading to a great deal of uncertainty in  $k_f$  values determined in this manner. Therefore, eq 2 was used to determine  $k_f$  in all cases.  $k_b$  values were then determined from the slopes.

As mentioned previously, the lifetime measurements were done on a single photon counting apparatus and the results are shown in Table I. The naphthols were measured at pH 1, and the naphtholates at pH 13. However, seven of the lifetimes were not accessible on the single photon device because they were in the order of 1 nsec, or less, and could not be resolved from the lamp lifetime. Of these seven, four lifetimes were obtained by comparison with reference compounds (acidic and basic forms of 2-naphthol) whose lifetimes could be determined.



**Table II:** Determination of Lifetimes Oscillator Strengths and Relative Fluorescent Quantum Yields

	$f \times 10^2$		$\phi/\phi_0$	
	Base	Acid	Base	Acid
2-Naphthol	$8.0 \pm 0.1$	$3.31 \pm 0.07$	1.00	1.00
1-Bromo-2-naphthol	$6.8 \pm 0.1$	$3.26 \pm 0.06$	$0.064 \pm 0.004$	$0.049 \pm 0.003$
6-Bromo-2-naphthol	$5.8 \pm 0.2$	$4.1 \pm 0.2$	$0.048 \pm 0.004$	$0.064 \pm 0.006$

**Table III:** Summary of CNDO/2 and PPP Results

	1-Naphthol			2-Naphthol		
	Set A	Set B	Exptl	Set A	Set B	Exptl
$E_{exc}$ , eV	3.84	8.25	3.61	3.81	8.32	3.70
$\mu_{gd}$ , D		0.99	1.44 <sup>a</sup>		1.40	1.49 <sup>a</sup>
$\mu_{exc}$ , D		6.40	$5.8 \pm 0.9^b$		7.27	$3.5 \pm 0.7^b$
Oxygen $\rho_e$ -(gd)	1.9585 <sup>c</sup>	6.2014		1.9599 <sup>c</sup>	6.2208	
Oxygen $\rho_e$ -(exc)	1.9530 <sup>c</sup>	6.1332		1.9481 <sup>c</sup>	6.1486	

<sup>a</sup> Reference 17. <sup>b</sup> Reference 18. <sup>c</sup>  $\pi$  densities only.

By comparing the compound of interest to a reference compound one obtains

$$t = \frac{f_0 \omega_0^2 \phi}{f \omega^2 \phi_0} t_0 \quad (4)$$

where  $\omega$  is the frequency of the fluorescence peak,  $f$  is the oscillator strength,  $\phi$  is the fluorescence quantum yield, and the zero subscripts refer to the corresponding values for the reference compound.  $\phi/\phi_0$  is approximated by the ratio of the fluorescence peak heights. The lifetimes obtained from eq 4 are also shown in Table I, with the oscillator strengths and relative fluorescence quantum yields appearing in Table II.

The dissociation and association rate constants are shown in Table I along with the  $pK$ 's calculated by the intensity *vs.* pH method.

### III. Molecular Orbital Calculations

*A. General Description.* Two sets of molecular orbital calculations for 1-naphthol and 2-naphthol were carried out on the IBM 7090 at the University of Pittsburgh Computer Center. Set A was a PPP<sup>12,13</sup> approach which considered only the  $\pi$  system. Set B was based on a CNDO/2 treatment<sup>14</sup> which considers all valence orbitals. The excited states were obtained by considering some 25 singly excited configurations for set B (all 30 singly excited configurations were considered in set A) as the basis set and applying configuration interaction (CI).

*B. Set A.* The results of two of the PPP calculations are given in Table III. Several sets of parameters were taken directly from Forster.<sup>15</sup>

*C. Set B.* Our set B deviated from Pople's procedure in that we used Nesbet's convergence formula<sup>16</sup> to speed convergence and we neglected overlap among other than adjacent atoms.

The excited singlet states were calculated from the ground state molecular orbitals by taking only singly excited configurations. Because of the large number of these present in the naphthols (675), only a few of the lowest energy singly excited configurations were considered (in general, 25). However, preliminary calculations on phenol produced the result that the calculated lowest excited singlet state was a  $\pi$ - $n^*$ ,  $n$ - $\pi^*$ . Experimentally, the lowest excited singlet is a  $\pi$ - $\pi^*$ . Thus it was concluded that the calculated energies are not reliable and for information on the wavefunctions only  $\pi$ - $\pi^*$  and  $\sigma$ - $\sigma^*$  configurations were included in the naphthol calculations.

In set B the molecules were assumed to be composed of regular hexagons with bond lengths: C-C, 1.40 Å; C-O, 1.36 Å; C-H, 1.08 Å; and O-H, 0.96 Å. The H-O-C angle was assumed to be 109°, with the H atom in the plane of the ring and oriented away from the C<sub>9</sub>-C<sub>10</sub> axis. Calculated values of the energies and the ground and excited state dipole moments are given in Table III.<sup>17</sup>

### IV. Discussion

*A. Förster Cycle.* A comparison of the  $pK$ 's determined by the Förster cycle method with those determined by the intensity *vs.* pH method (Table I) shows the former to be higher in all cases, save one. This can

(12) R. Pariser and R. G. Parr, *J. Chem. Phys.*, **21**, 466, 767 (1953).

(13) J. Pople, *Trans. Faraday Soc.*, **49**, 1375 (1953).

(14) J. Pople and G. Segal, *J. Chem. Phys.*, **44**, 3289 (1966).

(15) L. Forster and K. Nishimoto, *J. Amer. Chem. Soc.*, **87**, 1459 (1965).

(16) R. K. Nesbet, *Rev. Mod. Phys.*, **35**, 552 (1963).

(17) K. Higasi and S. Ogata, *Oyo Denki Kenkyusho Hokoku*, **19**, 28 (1967).

be rationalized by considering that the Förster equation (eq 1) should really be written

$$2.3RT(\text{p}K_{\text{gd}} - \text{p}K_{\text{exc}}) = \ln N(\nu_{\text{HA}} - \nu_{\text{A}^-}) - T(\Delta S_{\text{HA}} - \Delta S_{\text{A}^-}) + P(\Delta V_{\text{HA}} - \Delta V_{\text{A}^-}) \quad (5)$$

where  $N$  is Avogadro's number and the  $\Delta X_y$  represent the change in variable  $X$  of species  $y$  upon excitation.

The Förster assumption that  $\Delta V_{\text{HA}} = \Delta V_{\text{A}^-}$  is probably quite valid in condensed systems. However the assumption that  $\Delta S_{\text{HA}} = \Delta S_{\text{A}^-}$  is not.

If we first consider the undissociated form, the dipole moment increases upon excitation.<sup>18</sup> The increased dipole moment probably encourages more clustering of solvent molecules about the excited state than the ground state; therefore  $\Delta S_{\text{HA}}$  is negative. In the case of the dissociated form the clustering is probably considerable in the ground state and in all probability decreases slightly upon excitation as the charge is most likely delocalized. Thus  $\Delta S_{\text{A}^-}$  is probably positive and almost certainly has a smaller absolute value than  $\Delta S_{\text{HA}}$ . This would account for  $(\text{p}K_{\text{gd}} - \text{p}K_{\text{exc}})$  being greater than that value calculated from eq 1.

*B. Lifetimes.* The measured lifetimes (Table I) of the substituted naphthols are not at all surprising in comparison with the corresponding unsubstituted naphthols. The bromo compounds would be expected to have shortened lifetimes owing to increased intersystem crossing (considerably more likely in the presence of heavy atoms). The other substituents seem to have no great effect on lifetimes. The un-ionized 1-naphthols studied here all have short lifetimes, in contradiction of the lifetime given by Weller<sup>9</sup> for 1-naphthol of 13 nsec.

*C. Rate Constants.* The measured rate constants for acid dissociation and reassociation in the lowest excited singlet state (Table I) can be rationalized in terms of valence bond theory. If we consider ionization of the naphthols to be a process in which a proton dissociates from an electron cloud which is somewhat localized on the adjoining oxygen atom, we would expect that dissociation would be retarded ( $k_t$  decreased) by an increase of electron density on the oxygen atom. Methyl is an electron donor by both induction and resonance (hyperconjugation), thus the small  $k_t$  values. Bromo and chloro substituents are electron withdrawers by means of the inductive effect; thus they would be expected to have large  $k_t$ 's. This is strikingly shown. However, bromo and chloro are electron donors by means of the resonance effect which would tend to decrease  $k_t$ . From the fact that none of the halonaphthols shows a decrease in  $k_t$  one can generalize that the inductive effect is more important, as is usually found for the halogens.

It is quite common to predict trends in equilibrium

constants of simple dissociation reactions by considering only the undissociated species. The implicit assumption of such a comparison is that  $k_b$  will remain constant. Upon scanning the  $k_b$  values in Table I we see that although they approach the diffusion limiting magnitude for a bimolecular process, there are some differences. A full discussion of substituent effects on  $k_b$  is probably not justified because the measurements leading to  $k_b$  for many of the compounds (having  $\text{p}K_{\text{exc}} \leq 2$ ) had to be done in solutions of high acidity where the neglect of activity coefficient corrections is no longer justified.

*D. Charge-Transfer Explanation of Acidities.* A major reason for this research was to explain why there are differences in  $\text{p}K_a$  values between the ground and lowest excited singlet states. Let us consider differences in the ease of heterolytic dissociation of the O-H bond to be due to purely electrostatic attractions between the hydrogen nucleus (proton) and an electron cloud localized on the adjacent oxygen atom. From this simplified model it is obvious that as the electron density on the oxygen decreases the O-H bond weakens, giving rise to a lower  $\text{p}K_a$ .

The PPP calculations do support, at least qualitatively, the validity of the charge-transfer explanation of differential acidities. Though only two of the 11 parameter sets done are shown in Table III, all 11 indicated the higher oxygen electron density to be in the ground state, thus predicting a higher  $\text{p}K_a$  for the ground state, as is observed. The arbitrarily picked sets shown in Table III correspond to the parameters  $\gamma_{\text{CC}} = 9.50$ ,  $\gamma_{\text{OO}} = 16.50$ ,  $W_{\text{C}} = 11.42$ ,  $W_{\text{O}} = 33.00$ ,  $\beta_{\text{CC}} = 2.24$ , and  $\beta_{\text{CO}} = 2.12$ .

The results of set B are also shown in Table III. If we consider the predicted excitation energies, they compare very poorly with experiment. However the ground and excited state dipole moments give an additional criterion of the accuracy of the wave functions obtained. In general, the results are moderately satisfactory. The set B wave functions also satisfactorily predict a higher electron density on the oxygen in the ground state. The parameters were those of Pople and Segal.<sup>14</sup>

*Acknowledgments.* The authors would like to express their thanks to Professor Richard Bersohn for the use of his laboratory, especially the single photon counting instrument, to Dr. Terence Tao for having written the program which calculates the fluorescence lifetimes, to the staffs at the University of Pittsburgh and Columbia University Computer Centers, and to the National Science Foundation for support through Grant GP-7932.

(18) Ira Brinn, Doctoral Dissertation, University of Pittsburgh, 1968.



# Fluorescence Quenching by Benzoic Acid<sup>1</sup>

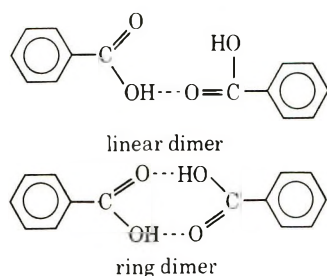
by Nelson H. C. Cooke and Barton S. Solomon\*

*Department of Chemistry, Merrimack College, North Andover, Massachusetts 01845 (Received June 2, 1972)*

Fluorescence quenching of various naphthalene derivatives by benzoic acid has been investigated in an attempt to elucidate the mechanism of the quenching reaction. In contrast to the results of Miwa and Koizumi, we have found that benzoic acid can quench by two different interactions. Our results indicate that the quenching of the fluorescence of molecules, capable of forming a hydrogen bond with benzoic acid, involves the formation of an exciplex where the primary interaction contributing to binding is hydrogen bonding. On the other hand, if the excited molecule is incapable of forming a hydrogen bond, the binding interaction is due to electron transfer. These conclusions follow from the correlation of the quenching reactivity of benzoic acid with the oxidation potentials of a series of naphthalene derivatives. The effect of added *p*-dioxane on the fluorescence quenching has been studied in both types of systems and the results support the above conclusions.

## Introduction

Fluorescence quenching by benzoic acid was first reported by Miwa and Koizumi<sup>2,3</sup> who studied the quenching of the fluorescence of 2-naphthol, 2-naphthylamine, 2-methoxynaphthalene, and 2(*N,N*-dimethyl)naphthylamine. Their results, along with the fact that benzoic acid is largely dimerized in solution, led them to suggest that benzoic acid quenches the fluorescence of the above compounds by an electron transfer mechanism. They proposed that benzoic acid dimer acts as an electron acceptor and the excited naphthalene derivative as the electron donor. Although benzoic acid is largely dimerized in solution, a simple equilibrium calculation shows that there is a significant monomer concentration. In the systems studied here we estimate that about 10% of the benzoic acid is in the form of the monomer. Further, there are two possible dimers of benzoic acid, a ring dimer and a linear dimer.



Two of the forms of benzoic acid (monomer and linear dimer) can hydrogen bond with all of the fluorescent compounds used by Miwa and Koizumi. Therefore, we do not feel that the results and arguments presented by them rule out the possibility of quenching involving a hydrogen bonding interaction. We have undertaken a complete study of fluorescence quenching in these systems and have reported some of our preliminary results elsewhere.<sup>4</sup>

## Experimental Section

Fluorescence spectra were obtained on a Farrand Optical Co. Mark I spectrophotofluorometer. The solutions were thoroughly degassed by several freeze-pump-thaw cycles on a high-vacuum line.

The solvent (cyclohexane) used was spectrophotometric grade and was checked for fluorescence before use. The fluorescent materials were the purest commercially available grades and were further purified by recrystallization and vacuum sublimation. Scintillation grade *p*-dioxane was distilled and then passed through a column of alumina immediately before use. We have previously found this technique useful for removing quenching impurities.<sup>5</sup> Benzoic acid was purified by multiple recrystallization from benzene followed by vacuum sublimation.

Fluorescer concentrations used were generally between  $10^{-6}$  and  $10^{-5}$  *M* and, in order to minimize inner filter effects, were adjusted so that less than 5% of the incident light was absorbed. Benzoic acid concentrations were varied up to 0.08 *M*.

## Results and Discussion

Fluorescence quenching by an electron transfer mechanism has received considerable theoretical and experimental consideration. Weller and coworkers<sup>6-9</sup>

(1) A preliminary report on this work was presented at the Third Northeast Regional Meeting of the American Chemical Society, Buffalo, N. Y., Oct 1971.

(2) (a) T. Miwa and M. Koizumi, *Bull. Chem. Soc. Jap.*, **36**, 1619 (1963); (b) *ibid.*, **38**, 529 (1965).

(3) T. Miwa and M. Koizumi, *ibid.*, **39**, 6651 (1966).

(4) D. W. Ellis, R. G. Hamel, and B. S. Solomon, *Chem. Commun.*, 1697 (1970).

(5) B. S. Solomon, T. F. Thomas, and C. Steel, *J. Amer. Chem. Soc.*, **90**, 2249 (1968).

(6) B. S. Solomon, C. Steel, and A. Weller, *Chem. Commun.*, 927 (1969).

(7) H. Beens and A. Weller, *Acta Phys. Pol.*, **34**, 593 (1968).

(8) D. Rehm and A. Weller, *Ber. Bunsenges. Phys. Chem.*, **73**, 834 (1969).

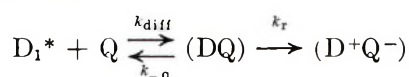
Table I

Compound	$\tau,^a$ nsec	${}^1\Delta E_D,^b$ eV	$E(D_s^+/D_s),^c$ eV	${}^1\Delta E_D - E(D_s^+/D_s),$ eV	$k_q\tau,$ $M^{-1}$	$k_q \times 10^{-4},$ $M^{-1} \text{ sec}^{-1}$
Naphthalene	96	3.95	1.72	2.23	11	1.1
2-Methylnaphthalene	59	3.87	1.55	2.32	14	2.4
1-Methylnaphthalene	67	3.91	1.52	2.38	67	10
Fluorene	10	4.12	1.65	2.47	31	31
Acenaphthene	46	3.87	1.36	2.51	190	41
2-Methoxynaphthalene	13	3.76	1.52	2.24	34	21
1-Methoxynaphthalene	49	3.82	1.38	2.44	340	69

<sup>a</sup> Obtained from I. B. Berlman, "Hand Book of Fluorescence Spectra of Aromatic Molecules," 2nd ed, Academic Press, New York, N. Y., 1971, or determined by the oxygen quenching technique, *ibid.*, p 58. <sup>b</sup> Estimated from the absorption and fluorescence spectra. <sup>c</sup> From N. L. Weinberg and H. R. Weinberg, *Chem. Rev.*, **68**, 449 (1968).

have shown that for a series of experiments with the same quencher, the same solvent, and various fluorescers, a correlation between the Stern-Volmer quenching constant ( $k_q$ ) and  ${}^1\Delta E_D - E(D_s^+/D_s)$  would be expected. The singlet excitation energy of the fluorescer (electron donor) is given by  ${}^1\Delta E_D$  and  $E(D_s^+/D_s)$  represents the polarographic oxidation potential of the fluorescer. As a first test of the postulated electron transfer quenching mechanism of benzoic acid, the quenching constants were measured for a series of fluorescers including some which could and some which could not form a hydrogen bond with benzoic acid monomer and linear dimer. The results of this study are shown in Table I. For the first five fluorescers listed in Table I, for which there is no possibility of hydrogen bonding with benzoic acid, there appears to be a nonlinear correlation between  ${}^1\Delta E_D - E(D_s^+/D_s)$  and  $k_q$ .

For diffusion-controlled reactions North<sup>10</sup> has presented a scheme



where  $k_{diff}$  is the rate constant for diffusion of  $D_1^*$  (electron donor excited singlet) and  $Q$  (quencher) to form the proximity pair  $(DQ)$ ,  $k_{-q}$  is the rate constant for diffusive separation of  $D_1^*$  and  $Q$ , and  $k_r$  is the rate constant of the electron transfer reaction. This scheme illustrates the quenching mechanism for full charge transfer. Other interactions, such as weak charge resonance and hydrogen bonding, can also contribute to exciplex binding and fluorescence quenching. For the electron transfer case, with a constant quencher, a constant solvent, and a series of fluorescers, a linear correlation between

$$\ln \frac{k_q}{k_{diff} - k_q}$$

and

$${}^1\Delta E_D - E(D_s^+/D_s)$$

is expected<sup>10-14</sup> where

$$\frac{k_r}{k_{-q}} = \frac{k_q}{k_{diff} - k_q}$$

The data of Table I are plotted in Figure 1 and indeed a linear relationship does emerge between

$$\log \frac{k_q}{k_{diff} - k_q}$$

and

$${}^1\Delta E_D - E(D_s^+/D_s)$$

On the other hand, the data for 1-methoxynaphthalene and 2-methoxynaphthalene do not fit this relationship. We therefore propose that benzoic acid can interact in two different ways with excited molecules to form an exciplex. In the series of aromatic hydrocarbons, incapable of forming hydrogen bonds, the quenching occurs by a charge-transfer interaction to form the exciplex. On the other hand, we propose that the fluorescence quenching of 1-methoxynaphthalene and 2-methoxynaphthalene by benzoic acid involves a hydrogen bonding interaction leading to binding in the exciplex.

We have also investigated the effect of adding *p*-dioxane on the quenching in two model systems: 2-methoxynaphthalene and 2,3-dimethylnaphthalene, both of which are quenched by benzoic acid. Figure 2 is a plot of  $I_0/I$  vs. *p*-dioxane concentration, where  $I_0$  is the 2-methoxynaphthalene fluorescence intensity in the absence of benzoic acid and  $I$  is the fluorescence intensity in the presence of 0.02 *M* benzoic acid. Notice that as the *p*-dioxane concentration increases

(9) D. Rehm and A. Weller, *Isr. J. Chem.*, **8**, 259 (1970).

(10) A. M. North, *Quart. Rev., Chem. Soc.*, **20**, 421 (1966).

(11) T. R. Evans, *J. Amer. Chem. Soc.*, **93**, 2081 (1971).

(12) H. Knibbe, D. Rehn, and A. Weller, *Ber. Bunsenges Phys. Chem.*, **72**, 257 (1968).

(13) A. Weller, *Progr. React. Kinet.*, **1**, 192 (1961).

(14) A. Weller, *Proc. Nobel Sym.*, **5th**, 413 (1967).



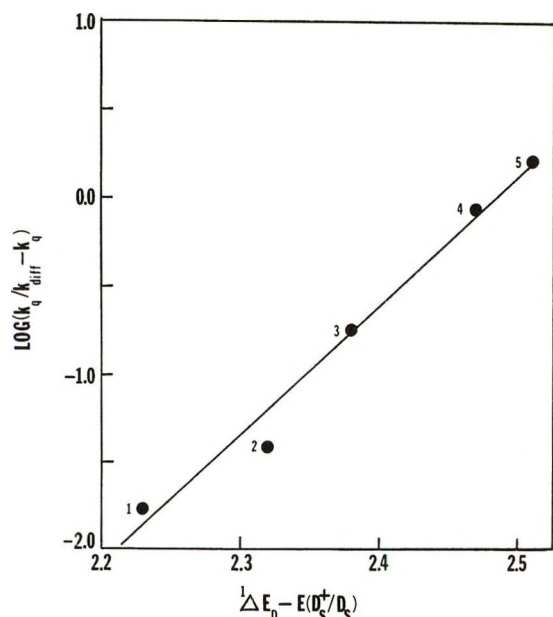


Figure 1. Correlation between rate constants of fluorescence quenching by benzoic acid and the oxidation potentials of the excited molecules: (1) naphthalene, (2) 2-methylnaphthalene, (3) 1-methylnaphthalene, (4) fluorene, (5) acenaphthene, with  $k_{diff}$  (cyclohexane) =  $6.6 \times 10^9 M^{-1} \text{sec}^{-1}$ .

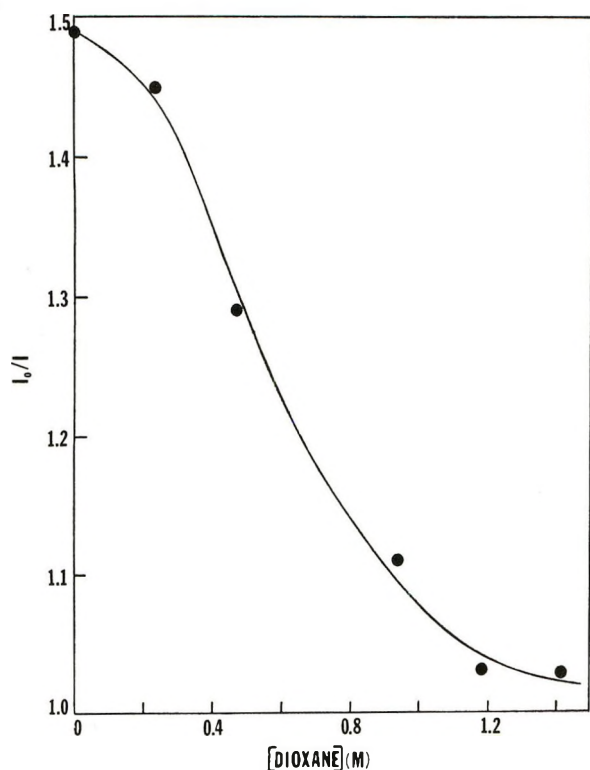
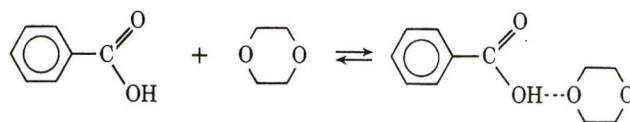


Figure 2: Effect of adding *p*-dioxane on the quenching of the fluorescence of 2-methoxynaphthalene ( $10^{-6} M$ ) by benzoic acid ( $0.02 M$ ).

the quenching decreases, *i.e.*,  $I_0/I$  approaches unity. This can be rationalized in terms of the proposed quenching mechanism and the following equilibrium between benzoic acid and *p*-dioxane.



Since the proposed quenching mechanism in this system involves a hydrogen bonding interaction, it is apparent that added *p*-dioxane hydrogen bonds with the benzoic acid thus decreasing the  $I_0/I$  value. At high *p*-dioxane concentrations most of the benzoic acid is hydrogen bonded and little if any quenching *via* hydrogen bonding interaction can occur. Since the excited state oxidation potential  ${}^1\Delta E_D - E(D_s^+/D_s)$  of 2-methoxynaphthalene is small and the benzoic acid concentration is low, we would expect to see very little quenching due to electron transfer interaction. Thus the  $I_0/I$  value approaches unity at high *p*-dioxane concentrations.

Figure 3 is a plot of  $I_0/I$  vs. *p*-dioxane concentration, where  $I_0$  is the 2,3-dimethylnaphthalene fluorescence

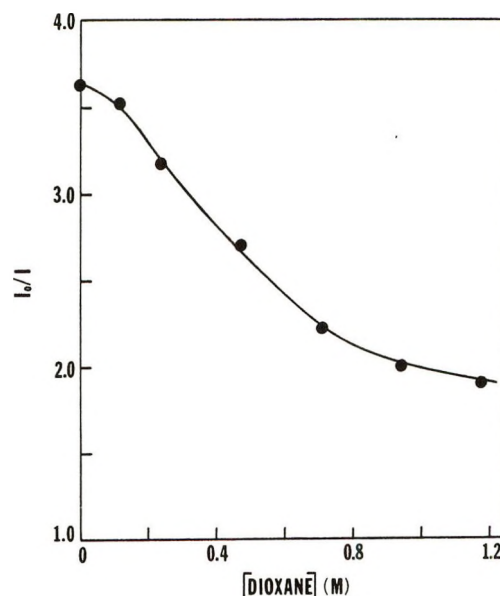


Figure 3. Effect of adding *p*-dioxane on the quenching of the fluorescence of 2,3-dimethylnaphthalene ( $10^{-6} M$ ) by benzoic acid ( $0.02 M$ ).

intensity in the absence of benzoic acid and  $I$  is the fluorescence intensity in the presence of  $0.02 M$  benzoic acid. Notice in this case that  $I_0/I$  does decrease as the *p*-dioxane concentration increases but the  $I_0/I$  value levels off at a value above unity. This indicates that the hydrogen bonded, benzoic acid-*p*-dioxane complex can quench by an electron transfer interaction although less effectively than benzoic acid. Since in the electron transfer quenching the benzoic acid acts as an electron acceptor, one would expect the complex to be less effective than benzoic acid.

We conclude from the above results that there are two different interactions that can lead to exciplex

binding between benzoic acid and an excited molecule. In cases where there is no possibility of hydrogen bonding, an electron transfer interaction occurs, but if the molecules have the ability to hydrogen bond then this interaction leads to the fluorescence quenching. The results also lead to the conclusion that in the electron transfer cases all three species of benzoic acid (monomer, ring dimer, and linear dimer) may act as

quenchers. In the hydrogen bonding case only the monomer and linear dimer can quench.

*Acknowledgment.* The authors are grateful to the Research Corporation for their financial support of these investigations. We would also like to acknowledge the assistance of the Nuclear Engineering Department of Lowell Technological Institute.

## A Study of Alkylbenzene Luminescence<sup>1,2</sup>

by Peter M. Froehlich and Harry A. Morrison\*

Department of Chemistry, Purdue University, Lafayette, Indiana 47907 (Received March 17, 1972)

The relative (to toluene) fluorescence (at room temperature and 77°K) and phosphorescence (77°K) intensities as well as excited singlet lifetimes of a number of alkylbenzenes are tabulated. Empirical correlations of the data include the previously observed "xylene effect" (whereby ortho and para substituents enhance  $\phi_f$ ) and a new " $\alpha$ -substitution effect" (whereby alkyl substituents on a carbon  $\alpha$  to the ring reduce  $\phi_f$ ). In the latter case, it can be shown that for monosubstituted alkylbenzenes, relative fluorescence intensity decreases as a linear function of the number of  $\beta$ -hydrogens. The "xylene" effect is shown to be a consequence of increased  $k_t$  whereas the " $\alpha$ -substitution" effect is a result of decreased  $k_t$  plus increased  $k_d$  (two  $\alpha$ -hydrogens) or a particularly large increase in  $k_d$  (one or zero  $\alpha$ -hydrogens) ( $k_d$  represents internal conversion and intersystem crossing). Though the "xylene effect" is insensitive to temperature, those compounds with enhanced non-radiative decay show dramatic enhancements in fluorescence relative to toluene at 77°K.

### Introduction

In the course of a study of the quenching of alkylbenzene luminescence by dienes,<sup>3</sup> it was necessary to examine the fluorescence and phosphorescence emission of a number of alkylbenzenes, including many for which such spectral data have not yet been reported. The resulting quantum efficiency and lifetime data prove useful, not only in their own right, but also in that they permit valid empirical correlations to be discerned. Such an approach has been quite successfully demonstrated for benzenoid aromatics in the compendia by Beriman,<sup>4</sup> and further references to these works will be made throughout this paper.

### Experimental Section

*Chemicals.* Aromatic hydrocarbons were obtained from commercial sources and were tested for purity by vpc using either an Aerograph Autoprep A-700 or a Varian-Aerograph 90-P instrument equipped with a 20 ft  $\times$  0.25 in. 15% Carbowax on Chromosorb W DMCS-treated column or a 20 ft  $\times$  0.25 in. 30% Carbowax on Chromosorb P column. If the reagent contained impurities, it was purified by preparative vpc with one of the above columns. All aromatic compounds were molecularly distilled and rechecked for

purity by vpc with a 5 ft  $\times$  0.125 in. 3% SE-30 column before use. Burdick and Jackson "distilled in glass" hexane was used as received. The uv spectrum of each lot (in a 1-cm cell vs. air) was recorded to ensure that there was no absorption above 230 nm. Phillips "instrument grade" isopentane (99.5 mol %) was passed through two chromatography columns containing either Merck alumina or Matheson Coleman and Bell silica gel. The uv spectrum of each lot (in a 1-cm cell vs. air) was recorded to ensure that there was no absorption above 230 nm.

*Spectroscopy.* Ultraviolet spectra were recorded using 1-cm quartz cells with a Cary 14 spectrophotometer. Absorbance measurements were obtained with the Cary instrument or a Gilford photometer (Model 222A) coupled to a Beckman DU monochromator.

(1) Organic Photochemistry, Part XX; Part XIX: P. Froehlich and H. Morrison, *Chem. Commun.*, 184 (1972).

(2) Abstracted from the doctoral dissertation of P. Froehlich, Purdue University, Aug 1971. Presented, in part, at the 162nd National Meeting of the American Chemical Society, Washington, D. C., Sept 1971.

(3) P. Froehlich and H. Morrison, to be published.

(4) (a) I. B. Beriman, "Handbook of Fluorescence Spectra of Aromatic Hydrocarbons," Academic Press, New York, N. Y., 1965; (b) I. B. Beriman, *ibid.*, 2nd ed, 1971.



Table I: Relative Fluorescence Intensities of Alkylbenzenes

Alkylbenzene	Room temperature			77°K rel fluorescence <sup>d</sup>
	Rel fluorescence <sup>a</sup>	$\phi_f^b$	$\phi_f(\text{lit.})^c$	
Benzene	0.26	0.036	0.058, <sup>e</sup> 0.07 <sup>f</sup>	
Toluene	(1.00)	(0.14)	0.14, <sup>e</sup> 0.23 <sup>f</sup>	(1.00)
Ethyl-	0.77	0.11	0.15 <sup>e</sup>	0.86
<i>n</i> -Propyl-	0.82	0.11	0.12 <sup>e</sup>	1.01
Isopropyl-	0.52	0.076	0.10 <sup>e</sup>	0.82
<i>n</i> -Butyl-	0.82	0.11		0.85
Isobutyl-	0.86	0.12		1.02
<i>sec</i> -Butyl-	0.62	0.088	0.12 <sup>e</sup>	0.72
<i>tert</i> -Butyl-	0.23	0.032		0.58
<i>n</i> -Hexyl-	0.88	0.12		0.91
Cyclohexyl-	0.64	0.089	0.13 <sup>e</sup>	
<i>n</i> -Decyl-	0.85	0.12		
<i>n</i> -Nonadecyl-	0.82	0.11		
1,2-Dimethyl-	1.21	0.17	0.16, <sup>e</sup> 0.20 <sup>f</sup>	1.25
1,3-Dimethyl-	0.94	0.13	0.14, <sup>e</sup> 0.18 <sup>f</sup>	0.95
1,4-Dimethyl-	1.60	0.22	0.33, <sup>e</sup> 0.24 <sup>f</sup>	1.55
1,4-Di- <i>tert</i> -butyl-	0.44	0.061		1.48
1,3,5-Trimethyl-	0.63	0.088	0.14, <sup>e</sup> 0.14 <sup>f</sup>	0.61
1,2,3-Trimethyl-	0.58	0.081	0.08 <sup>f</sup>	
1,2,4-Trimethyl-	2.03	0.28	0.34, <sup>e</sup> 0.31	
1,3,5-Tri- <i>tert</i> -butyl-	~0.07	~0.01		0.64
1,2,3,4-Tetramethyl-	0.81	0.11		
1,2,3,5-Tetramethyl-	0.84	0.13		
1,2,4,5-Tetramethyl-	2.12	0.30	0.32 <sup>f</sup>	
Pentamethyl-	0.54	0.075		
Hexamethyl-	~0.01	<0.01	0.02 <sup>e</sup>	0.54
Hexaethyl-	~0.01	<0.01		0.74

<sup>a</sup> Relative to toluene; all solutions 1–3 mM in *n*-hexane with data corrected for relative light absorption at 254 nm; error estimated at  $\pm 5\%$ . <sup>b</sup> Based on a value of 0.14 for toluene (see text). <sup>c</sup> Data from Berlman and Krongauz corrected as discussed in the text. <sup>d</sup> Relative to toluene; all samples 1–3 mM in an isopentane glass; error estimated at  $\pm 10\%$ . <sup>e</sup> Reference 4. <sup>f</sup> Reference 8. <sup>g</sup> Reference 9.

Emission spectra were recorded on a "homemade" spectrophotofluorometer<sup>5</sup> using a 253.7-nm mercury pen lamp source. Fluorescence spectra at room temperature (*ca.* 22°) in hexane were obtained using 1-cm square quartz cells, while spectra at 77°K in isopentane were obtained using 3-mm i.d. Suprasil optical quartz tubes.

*Sample Preparation.* Solutions of the various aromatic hydrocarbons ( $\sim 1.3 \times 10^{-3}$  M) in hexane were deoxygenated by bubbling argon through the cells for 15 min and then sealed with a stopcock. Solutions in isopentane were deaerated by eight freeze-pump-thaw cycles at less than 1  $\mu$  using a high-vacuum rotary oil and oil diffusion pump (Sargent Welch, Co., Model S-71780) and were also sealed by a Kel-F stopcock. The pressure was measured by a pirani gauge (Consolidated Vacuum Co., Type GP-110). Relative fluorescence intensities at room temperature of the aromatic hydrocarbons studied, using toluene as reference, were obtained from their fluorescence spectra. The area of each spectrum and the solvent blank were obtained by use of a computer program developed by R. B. Brainard and R. W. Peiffer of these laboratories.<sup>6</sup> The area

under the emission spectrum for toluene was corrected to reflect the difference in absorption between the solution containing hydrocarbon under study and the toluene solution. Relative fluorescence intensities at 77°K were obtained from total emission spectra in the same manner as at room temperature (except for sample preparation). Examination of the total emission spectra showed that the overlap between fluorescence and phosphorescence spectra was negligible. Relative phosphorescence intensities were obtained in the same manner as fluorescence intensities. Singlet lifetimes were measured with a TRW nanosecond fluorometer (Model 31A) using a deuterium lamp. The photomultiplier output was fed into a dual-beam oscilloscope (Tecktronix Corp., Type 555) and the decay curve displayed on an X-Y recorder (Hewlett-Packard, 7035B). Data were analyzed 15 nsec after the flash, and linear log *I* vs. time plots were obtained in all cases.

(5) R. B. Brainard and H. Morrison, *J. Amer. Chem. Soc.*, **93**, 2685 (1971).

(6) R. B. Brainard, Ph.D. Thesis, Purdue University, Aug 1970.

## Results

Fluorescence intensities (relative to toluene) for various alkylbenzenes in dilute hexane solution at room temperature are listed in Table I, together with quantum efficiencies ( $\phi_f$ ) calculated using  $\phi_f$  for toluene as 0.14. This value is that reported by Berlman,<sup>4</sup> as corrected by Birks;<sup>7</sup> the correction derives from the use of a  $\phi_f$  for the primary fluorescence standard (9,10-diphenylanthracene) of 0.83, as opposed to Berlman's use of 1.0. Thus, all values taken from Berlman have been reduced by 17%. Several citations from Berenfel'd and Krongauz<sup>8</sup> are included in Table I<sup>9</sup> but are corrected so as to bring these workers' toluene value (0.23) in line with the base number used in the table. Relative fluorescence intensities at 77°K in an isopentane glass are also included in Table I.

Phosphorescence intensities for a number of these alkylbenzenes were measured relative to toluene at 77°K in isopentane; the data are listed in Table II. Also presented in this table are phosphorescence lifetimes ( $\tau_p$ ) as measured for several of the samples.<sup>10,11</sup>

**Table II:** Relative Phosphorescence Intensities of Alkylbenzenes<sup>a</sup>

Alkylbenzene	Rel phosphorescence	$\tau_p$ , sec
Toluene	(1.00)	3.50 ± 0.07
Ethyl-	0.85	
<i>n</i> -Propyl-	0.91	3.72 ± 0.03
Isopropyl-	0.25	2.17 ± 0.03
<i>n</i> -Butyl-	0.90	
Isobutyl-	1.02	
<i>sec</i> -Butyl-	0.20	
<i>tert</i> -Butyl-	None obsd	
<i>n</i> -Hexyl-	0.76	
Cyclohexyl-	0.26	
1,2-Dimethyl-	1.16	
1,3-Dimethyl-	0.95	
1,4-Dimethyl-	1.89	4.60 ± 0.06
1,4-Di- <i>tert</i> -butyl-	1.22	3.94 ± 0.03
1,3,5-Trimethyl-	1.14	4.09 ± 0.05
1,3,5-Tri- <i>tert</i> -butyl-	0.06	
Hexamethyl-	None obsd	
Hexaethyl-	None obsd	

<sup>a</sup> Samples 1–3 mM in isopentane at 77°K; data presented relative to toluene.

Singlet lifetimes ( $\tau_f$ ) were measured at room temperature using a TRW nanosecond decay time fluorometer (Model 31A). Data are presented in Table III.<sup>12</sup> Also included in Table III are values for  $k_f$  (from  $k_f = \phi_f/\tau_f$ ) and  $k_d$  (from  $\phi_d = 1 - \phi_f$  and  $k_d = \phi_d/\tau_d$ ). Note that  $k_d$ , as here defined, includes internal conversion and intersystem crossing (*i.e.*,  $k_{ic}$  and  $k_{isc}$ ).

## Discussion

Several comments can be made concerning the data in Table I. First, as has been commented on else-

**Table III:** Singlet Lifetimes for Alkylbenzenes at Room Temperature<sup>a</sup>

Alkylbenzene	$\tau_f$ , nsec	Lit. <sup>b</sup>	$k_f \times 10^9$ , sec <sup>-1</sup>	$k_d \times 10^9$ , sec <sup>-1</sup> <sup>c</sup>
Benzene	33.6	(29.0)	1.1	29
Toluene	35.2	(34.0)	4.0	24
Ethyl-	35.1	(31.0)	3.1	25
<i>n</i> -Propyl-	36.0	(32.4)	3.1	25
Isopropyl-	24.5	(22.0)	3.1	38
<i>n</i> -Butyl-	35.1		3.1	25
Isobutyl-	33.3		3.6	26
<i>sec</i> -Butyl-	29.2	(25.0)	3.0	31
<i>tert</i> -Butyl-	10.0		3.2	97
<i>n</i> -Hexyl-	35.3		3.4	25
Cyclohexyl-	29.2	(26.4)	3.0	31
<i>n</i> -Nonadecyl-	34.2		3.2	26
1,2-Dimethyl-	38.2	(32.2)	4.5	22
1,3-Dimethyl-	32.7	(30.8)	4.0	27
1,4-Dimethyl-	33.3	(30.0)	6.6	23
1,3-Di- <i>tert</i> -butyl-	14.5		4.2	65
1,3,5-Trimethyl-	38.3	(36.5)	2.3	24
1,2,4-Trimethyl-			10.3 <sup>d</sup>	26 <sup>d</sup>
1,3,5-Tri- <i>tert</i> -butyl-	15.1		0.66	66
1,2,3,4-Tetramethyl-	33.8		3.3	26
1,2,3,5-Tetramethyl-	27.9		4.7	31
1,2,4,5-Tetramethyl-	28.6		10.5	24
Pentamethyl-	15.7		4.8	59
Hexamethyl-	<1.6, 0.6 <sup>e</sup>		2 <sup>o</sup>	1600 <sup>o</sup>
	(6 <sup>f</sup> )			

<sup>a</sup> Samples 1–3 mM in *n*-hexane and prepared as for the fluorescence intensity measurements. <sup>b</sup> Reference 4b. <sup>c</sup>  $k_{ic} + k_{isc}$ . <sup>d</sup> Calculated using  $\tau$  from ref 4b. <sup>e</sup> Obtained by oxygen quenching, *cf.* ref 4a. <sup>f</sup> Reference 12. <sup>o</sup> Using 0.6 nsec.

where,<sup>4b</sup> extension of a linear alkyl chain beyond two carbons seems not to have appreciable effect on  $\phi_f$ ; compare, for example, *n*-propylbenzene ( $\phi_f = 0.11$ ) and *n*-hexylbenzene ( $\phi_f = 0.12$ ). A similar insensitivity to chain length has been noted in ultraviolet absorption spectra.<sup>4b</sup> Second, ortho and para substitution of the benzene ring enhances  $\phi_f$ , whereas meta substituents have, if anything, a negative effect; compare 1,2-dimethylbenzene ( $\phi_f = 0.17$ ), 1,3-dimethylbenzene ( $\phi_f = 0.13$ ) and 1,4-dimethylbenzene ( $\phi_f = 0.22$ ) or 1,2,4-trimethylbenzene ( $\phi_f = 0.28$ ) and 1,3,5-trimethylbenzene ( $\phi_f = 0.09$ ). This "xylene effect" was first noted by Berenfel'd and Krongauz<sup>8</sup> and a large effect of

(7) J. B. Birks, "Photophysics of Aromatic Molecules," Wiley-Interscience, New York, N. Y., 1970.

(8) V. M. Berenfel'd and V. A. Krongauz, *Theor. Exp. Chem. USSR*, 3, 63 (1967).

(9) M. D. Lumb and D. A. Wehl, *J. Mol. Spectrosc.*, 23, 365 (1962).

(10) Such data are markedly dependent on degassing techniques and solvent purity and are presented here only for the purpose of reference. A complete study of phosphorescence lifetimes may be found in ref 11.

(11) J. W. Rabalais, H. J. Maria, and S. P. McGlynn, *J. Chem. Phys.*, 51, 2259 (1969).

(12) T. V. Ivanova, P. I. Kudryashov, and B. Ya. Sveshnikov, *Sov. Phys. Dokl.*, 6, 407 (1961).



1,4 disubstitution on absorption has been known for some time.<sup>4b</sup> To this phenomenon can now be added an "α-substitution effect," whereby alkyl substituents on the α-carbon attached to a benzene ring bring about a reduction in  $\phi_f$ ; compare toluene ( $\phi_f = 0.14$ ), ethylbenzene ( $\phi_f = 0.11$ ), isopropylbenzene ( $\phi_f = 0.07$ ) *tert*-butylbenzene ( $\phi_f = 0.03$ ).

The effect of a change in temperature on these phenomena is of interest. Whereas the "xylene effect" is essentially unchanged from room temperature to 77°K, the effect of α substitution is considerably diminished at low temperature. Thus, *tert*-butylbenzene changes from 23 (relative to toluene) to 58% at 77°K. More dramatically, 1,4-di-*tert*-butylbenzene goes from 44 (room temp) to 148% (77°K) and 1,3,5-tri-*tert*-butylbenzene from 7 to 64%. There is, in fact, a general enhancement of fluorescence intensity relative to toluene, with those compounds having the smallest values at room temperature showing the greatest increase. For example, hexamethylbenzene and hexaethylbenzene have barely measurable fluorescence at room temperature but relative intensities of 54 and 74%, respectively, at 77°K. (Of course, these changes in relative intensity are, in turn, superimposed on an increase in the absolute values for  $\phi_f$  at lower temperature.<sup>13</sup>)

Finally, it should be noted that the relative phosphorescence intensities at 77°K (Table II) show the same trends discussed above for fluorescence at room temperature, *i.e.*, independence of chain length, a "xylene effect" and an "α-substitution effect."

Any explanatory discussion of these trends requires that the relative radiative and nonradiative rate constants, rather than emission intensities, be considered. The fluorescence efficiency is the ratio  $k_f/k_f + k_d$  (where  $k_d$  represents all unimolecular<sup>14</sup> nonradiative decay modes)<sup>15</sup> and is obviously subject to effects on the radiative and/or nonradiative rates. We have therefore collected, in Table III, values for  $k_f$  and  $k_d$ .

An examination of Table III now reveals that the "xylene" and "α-substitution" effects have their origin in different decay modes. Thus, as has been noted elsewhere,<sup>4b,8,16</sup> the enhancement of fluorescence in *p*-xylene is primarily due to an increase in  $k_f$ , with  $k_d$  almost identical with that for toluene.<sup>17</sup> This shows up even more dramatically with 1,2,4,5-tetramethylbenzene. The increase in  $k_f$  parallels a rise in the molar extinction coefficient for absorption and is generally attributed to the distortion of the benzene symmetry and a concomitant diminution in the forbiddenness of the 0-0 transition.<sup>4b,18</sup>

By contrast, changes in both  $k_d$  and  $k_f$  are responsible for the "α-substitution effect." When the alkylbenzene contains no α-hydrogens (ethylbenzene, *n*-propylbenzene, *n*-butylbenzene, isobutylbenzene, *n*-hexylbenzene), a decrease in  $k_f$  is primarily responsible for lower fluorescence efficiency. Derivatives containing one or zero α-hydrogens (isopropylbenzene,

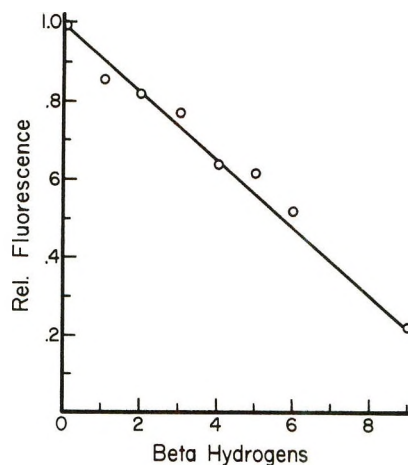


Figure 1. Plot of the monoalkylbenzene fluorescence intensity (relative to toluene) vs. the number of β-hydrogens.

*sec*-butylbenzene, cyclohexylbenzene, *tert*-butylbenzene) are also associated with sizable increases in  $k_d$ , the change being most dramatic with the *tert*-butyl derivatives. This enhancement of  $k_d$  is likely related to a conclusion drawn from studies of triplet alkylbenzene radiative and nonradiative decay, namely "C-H stretching vibrations of alkyl group appended to a benzene ring are efficient in modulating nonradiative transitions. This quenching ability extends as far as carbon centers which are twice removed from the ring and not much further."<sup>11</sup> A striking correlation between relative fluorescence intensity and the number of β-hydrogens is shown in Figure 1.

Finally, as regards the effect of temperature on the relative fluorescence intensities, it is now clear that those compounds which show the greatest increase at low temperature<sup>19</sup> are exactly those which have unusually large  $k_d$  values. Again, one would like these data in terms of  $k_{ic}$  and  $k_{isc}$ ; however,  $k_d$  has been

(13) See, for example, E. J. Bowen and S. Sahu, *J. Phys. Chem.*, **63**, 4 (1959); J. N. Eastman, *J. Chem. Phys.*, **49**, 4617 (1968), and ref 4b, p 458, for complete list of leading references on temperature effects.

(14) The possibility that steric hindrance to self-quenching is a factor in comparative alkylbenzene emission intensity has been suggested,<sup>4b</sup> but we are presuming that self-quenching, at the concentrations used in this study (*ca.*  $10^{-3}$  M), can be neglected.

(15) A further dissection of  $k_d$  into  $k_{ic}$  (internal conversion) and  $k_{isc}$  (intersystem crossing) would be still more desirable, but this requires intersystem crossing efficiencies, values for which are noticeably lacking for all but a few of the compounds in these tables. Experiments in this direction are in progress.

(16) V. M. Berenfel'd and V. A. Krongauz, *Bull. Acad. Sci. USSR, Phys. Ser.*, **32**, 1463 (1968).

(17) There is some evidence that the increase in  $\phi_f$  in *p*-xylene occurs at the expense of internal conversion rather than intersystem crossing, *cf.* K. Sandros, *Acta Chem. Scand.*, **23**, 2815 (1969).

(18) It has been suggested<sup>16</sup> that the increase in  $k_f$  is due to the inductive effect of the methyl groups.

(19) The studies at low temperature did, of course, involve a large increase in viscosity as well; we have here assumed (see also ref 21) that low temperature alone is responsible for the enhanced  $\phi_f$ , but future studies of relative emission vs. viscosity are clearly called for.

shown to be made up of temperature-dependent and temperature-independent components with the temperature-dependent component in benzene and its derivatives attributed to "thermally activated  $S_1-S_0$  internal conversion *via* an isomeric state."<sup>20</sup> If this view is valid, increasing  $\alpha$  substitution may then be facilitating such isomerism, and in this light, it is interesting that the sterically crowded pentamethyl- and hexamethylbenzenes also have characteristically high  $k_d$  values and temperature dependencies for  $\phi_f$ .<sup>21</sup>

*Acknowledgments.* We are grateful to Professor Fred Lytle for his generous assistance throughout this program and to the National Science Foundation for support of this research.

(20) Reference 7, p 146.

(21) Upon completion of this work and manuscript, a Communication appeared containing fluorescence data for several polymethylbenzenes. Particularly interesting is the reported observation (from unpublished data) of a large temperature effect on the fluorescence intensity of hexamethylbenzene; *cf.* A. Reiser and L. J. Leyshon, *J. Chem. Phys.*, **56**, 1011 (1972).

## Electron Spin Resonance of Triplet Nitrenes from Aryl Isocyanates<sup>1</sup>

by V. J. Kuck,\* E. Wasserman, and W. A. Yager

*Bell Laboratories, Murray Hill, New Jersey 07974 (Received July 10, 1972)*

*Publication costs assisted by Bell Laboratories*

The photolysis of benzoyl azide at 77°K with 2537-Å light in a methylcyclohexane-isopentane glass was studied by means of uv and esr. The rearrangement to form phenyl isocyanate was observed in the uv. No triplet signal in the esr corresponding to benzoylnitrene was obtained. However, upon further irradiation a signal was found whose zero-field parameters,  $D$  and  $E$ , were identical with those of phenylnitrene which had been independently produced from the photodecomposition of phenyl azide. Phenyl isocyanate, *o*-tolyl isocyanate, and naphthyl-1 isocyanate were irradiated at 77°K in a rigid matrix with 2537-Å light, and the zero-field parameters of the nitrenes that were produced were found to be the same as the parameters of nitrenes made from the corresponding azides. No nitrene signals were detected by means of esr upon irradiation at 77 and 4°K of alkyl isocyanates with and without sensitizers.

We have observed the electron spin resonance (esr) spectra of aromatic nitrenes obtained from the photolytic decomposition of aromatic isocyanates. It had been previously postulated that isocyanates yielded nitrenes upon photolysis<sup>2,3</sup> although no direct evidence had been obtained supporting this conclusion. While this work was in progress, Porter and Ward<sup>4</sup> reported the observation of the ultraviolet spectrum of phenylnitrene during the flash photolysis of phenyl isocyanate.

Initially we sought to clarify the existence of triplet benzoylnitrene as an intermediate in the photolytic decomposition of benzoyl azide. A 1% solution of benzoyl azide in 95% methylcyclohexane-5% isopentane was prepared and then irradiated at 77°K with 2537-Å light. A Varian V-4502 100-Hz field modulation esr spectrometer was used to detect resonance absorptions. An esr spectrum was obtained which was identical with one observed when phenyl azide was photolytically decomposed to form phenylnitrene.<sup>5</sup> No lines other than those corresponding to phenylnitrene were detected. Thus, there was no direct evidence for triplet benzoylnitrene as an intermediate in the photolytic decomposition of benzoyl azide.

In another experiment, the photolytic decomposition of benzoyl azide in the same matrix and under the same conditions was observed by ultraviolet spectroscopy. Absorption lines at 269 and 277 nm, corresponding to the formation of phenyl isocyanate, appeared upon irradiation. The decomposition of the phenyl isocyanate was then thought to be the source of phenylnitrene. A 1% solution of phenyl isocyanate in methylcyclohexane-isopentane was irradiated at 77°K and the decomposition was followed by means of esr. The observed spectrum was identical with that recorded when phenylnitrene had been generated from phenyl azide. These results might be explained by the following equation.

(1) Given in part at the Middle Atlantic Regional Meeting, Feb 1968, held in Philadelphia, Pa., by V. J. Kuck.

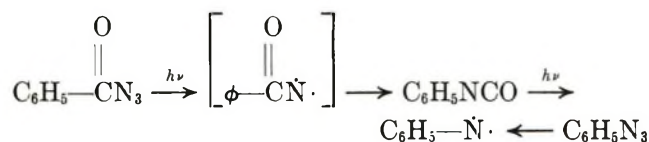
(2) (a) D. A. Bamford and C. H. Bamford, *J. Chem. Soc.*, **30** (1941); (b) J. H. Boyer, W. E. Krueger, and G. J. Micol, *J. Amer. Chem. Soc.*, **89**, 5504 (1967).

(3) J. S. Swenton, *Tetrahedron Lett.*, 2855 (1967).

(4) G. Porter and B. Ward, *Proc. Roy. Soc., Sec. A*, **303**, 139 (1968).

(5) G. Smolinsky, E. Wasserman, and W. A. Yager, *J. Amer. Chem. Soc.*, **84**, 3220 (1962).





Other 1% solutions of aromatic isocyanates in methylocyclohexane-isopentane were irradiated at 77°K and the esr spectra of the resulting nitrenes were recorded. From the spectra the zero-field parameters  $D$  and  $E^s$  were determined, where  $D$  is a measure of the magnitude of the spin-spin interaction of the unpaired electrons and  $E$  its deviation from cylindrical symmetry. Assuming  $g = 2.0023$  the following values were obtained: phenylnitrene  $|D| = 1.003 \text{ cm}^{-1}$ , *o*-tolyl nitrene  $|D| = 0.957$  and naphthyl-1-nitrene  $|D| = 0.798$ ;  $|E| < 0.003$  in each case. These results agreed with those previously obtained when the corresponding azide was decomposed.<sup>7</sup>

Previously, by use of esr, it has been established that alkyl nitrenes are generated in the photolytic decomposition of alkyl azides.<sup>8</sup> If the decomposition was carried out in the presence of sensitizers, nitrene formation could be observed by means of esr at 77°K. When direct irradiation of alkyl azides was employed there

was much less efficient generation of stabilized nitrenes and a signal could be detected only at 4°K. In hope of observing alkyl nitrenes generated from the photolytic decomposition of alkyl isocyanates, 1% solutions of cyclohexyl, *tert*-butyl, and *n*-propyl isocyanates were irradiated with an Osram HBO 200-W mercury lamp both at 77 and 4°K. No esr absorptions corresponding to nitrene formation were detected. These results could be explained by the fact that alkyl isocyanates absorb between 2100 and 2400 Å,<sup>2a</sup> a region where our lamp output is very low. Sensitizers such as acetone, benzene, and acetophenone were used and again no signals corresponding to nitrene formation were observed. The failure of sensitized decomposition might be due to inefficient energy transfer to the excited triplet states of the alkyl isocyanate. Since population of the excited singlet states occurs far into the uv, the nearby triplet states may well be of high energy.

(6) E. Wasserman, L. C. Snyder, and W. A. Yager, *J. Chem. Phys.*, **41**, 1763 (1964).

(7) E. Wasserman, *Progr. Phys. Org. Chem.*, **8**, 319 (1971).

(8) E. Wasserman, G. Smolinsky, and W. A. Yager, *J. Amer. Chem. Soc.*, **86**, 3166 (1964).

## An Electron Spin Resonance Study of Several DNA Base Cation Radicals Produced by Photoionization

by M. D. Sevilla,\* C. Van Paemel, and C. Nichols

Department of Chemistry, Oakland University, Rochester, Michigan 48063 (Received May 15, 1972)

Publication costs assisted by Oakland University

$\pi$ -Cation radicals of a number of DNA bases have been produced in aqueous glasses (8 *N* NaOD, 5 *M* K<sub>2</sub>CO<sub>3</sub>-D<sub>2</sub>O, 5.7 *M* D<sub>3</sub>PO<sub>4</sub>) at low temperature by uv photolysis. Well-resolved esr spectra of  $\pi$ -cations of 5-methylcytosine (NaOD, K<sub>2</sub>CO<sub>3</sub>, D<sub>3</sub>PO<sub>4</sub>), thymine (K<sub>2</sub>CO<sub>3</sub>), and thymidine (NaOD) are found and reduced to hyperfine coupling constants. The methyl proton splittings for  $\pi$ -cations of 5-methylcytosine show a great dependence on pH. The methyl proton splitting is 20 G in 5 *M* K<sub>2</sub>CO<sub>3</sub> and 5.7 *M* D<sub>3</sub>PO<sub>4</sub>, whereas in 8 *N* NaOD it is 14 G. This lowered splitting is explained by a comparison of the experimental results with theoretical splittings based on McLachlan MO computations. This comparison suggests that at high pH the amino nitrogen loses one proton and fully conjugates with the ring  $\pi$ -electron system. Results found for thymine in 5 *M* K<sub>2</sub>CO<sub>3</sub> are nearly identical with previous results in NaOD and D<sub>3</sub>PO<sub>4</sub>. The thymidine  $\pi$ -cation is found to have similar splittings to the thymine  $\pi$ -cation, however, anomalously low  $g$  values are found for this radical.

### Introduction

Positive and negative ions of the DNA bases are likely primary intermediates in the radiolysis of crystalline pyrimidines and purines as well as in the radiolysis of DNA itself. Recent esr investigations by several

authors have implicated ions as the primary intermediates toward radical production in the radiolysis of pyrimidine single crystals.<sup>1-4</sup> Several workers have

(1) J. Hüttermann, J. F. Ward, and L. S. Myers, *Int. J. Radiat. Phys. Chem.*, **3**, 117 (1971).

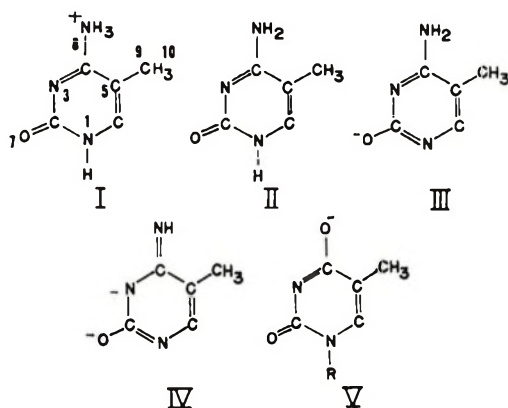


Figure 1. Structures of 5-methylcytosine (I-IV) and thymidine (V).

suggested the role of ion radicals in the radiolysis of DNA.<sup>5-6</sup> In recent work Gräslund, *et al.*, have assigned esr spectra of irradiated DNA found at low temperatures to positive and negative ions on the DNA bases.<sup>7</sup> In addition, several esr studies of DNA base ions in aqueous glasses have also appeared.<sup>5,8-11</sup> These studies are of significance in that they can aid in the identification of ions formed in crystalline DNA bases and in composite spectra found in DNA.

This study continues our investigations of the ion radicals of the DNA bases.<sup>8,9,12</sup> In previous work it was shown that the positive ion of thymine was produced by photoionization of thymine in alkaline and acid aqueous glasses.<sup>8</sup> Results indicated this was a biphotonic process involving ionization from a metastable triplet state. In the present work we report an esr study of radical " $\pi$ -cations" of 5-methylcytosine and several other DNA bases (Figure 1). " $\pi$ -Cations"<sup>13</sup> are produced *via* uv photolysis, and results are found which show the effects of protonation on the spin density distribution in pyrimidine cations. In addition, decomposition reactions of the  $\pi$ -cations were observed and are reported in a subsequent article in this journal.<sup>14</sup>

### Experimental Section

The details of the esr spectrometer used have been described previously.<sup>8</sup> The glasses were produced by cooling solutions of 8 *N* NaOD (92% D), 8 *N* NaOH, 5.7 *M* D<sub>3</sub>PO<sub>4</sub> (97% D), 5.7 *M* H<sub>3</sub>PO<sub>4</sub>, or 5 *M* K<sub>2</sub>CO<sub>3</sub> and the solute (0.25 mg/ml) in a 4 mm o.d. Spectrosil tube to 77°K. The use and properties of these glasses have been discussed by other workers in detail.<sup>15-17</sup> Deuterated glasses were usually employed to increase resolution. The uv photolysis was performed at 77°K outside the esr cavity employing a helical low-pressure mercury lamp. Solutions were prepared in doubly distilled D<sub>2</sub>O with blank runs made to assure the absence of background signal due to the glass. All samples were deoxygenated prior to irradiation by bubbling with nitrogen. Potassium ferricyanide (2

$\times 10^{-3}$  *M*) was used as an electron scavenger to obtain spectra uncomplicated by an overlap spectra of the anion. Since this compound was noted to react with several DNA bases (as evidenced by a loss of the color of the ferricyanide ion), solutions containing K<sub>3</sub>Fe(CN)<sub>6</sub> and the solute were made separately, cooled to -50°, and then mixed quickly while cold.

DNA bases were obtained from Calbiochem (grade A) except for thymidine which was from Schwarz. All *g* values and hyperfine splittings were measured *vs.* peroxyamine disulfonate with *a<sub>N</sub>* taken as 13.0 G and *g* taken as 2.0056.

### Results and Interpretation of Spectra

**5-Methylcytosine Cation and Anion.** To obtain information about the effect of pH and differing matrices on the esr spectra of radicals formed, 5-methylcytosine was photolyzed in three deuterated aqueous glasses: 8 *N* NaOD, 5 *M* K<sub>2</sub>CO<sub>3</sub>, and 5.7 *M* D<sub>3</sub>PO<sub>4</sub>. Photolysis at 77°K for 1 min in each case resulted in strong visible phosphorescence from the sample which persisted for several seconds after photolysis ceased. The phosphorescence indicated an appreciable steady-state triplet population which is considered essential to the photoionization process.<sup>18,19</sup>

Uv photolysis of 5-methylcytosine in 5 *M* K<sub>2</sub>CO<sub>3</sub> imparted a purple color in the glass characteristic of the trapped electron. The esr spectrum at 110°K taken immediately after photolysis is shown in Figure

- (2) A. Dulcic and J. N. Herak, *Radiat. Res.*, **47**, 573 (1971).
- (3) J. N. Herak and V. Galogaza, *J. Chem. Phys.*, **50**, 3101 (1969).
- (4) S. Carpy and H. Dertinger, *Int. J. Radiat. Biol.*, **18**, 359 (1970).
- (5) R. A. Holroyd and J. W. Glass, *ibid.*, **14**, 445 (1968).
- (6) M. G. Ormerod, *ibid.*, **9**, 291 (1965).
- (7) A. Gräslund, A. Ehrenberg, A. Rupprecht, and G. Ström, *Biochim. Biophys. Acta*, **254**, 172 (1971).
- (8) M. D. Sevilla, *J. Phys. Chem.*, **75**, 626 (1971).
- (9) M. D. Sevilla and C. Van Paemel, *Photochem. Photobiol.*, **15**, 407 (1972).
- (10) V. T. Srinivasan, B. B. Singh, and A. R. Gopal Ayengar, *Int. J. Radiat. Biol.*, **17**, 577 (1970).
- (11) N. B. Nazhat and J. J. Weiss, *Trans. Faraday Soc.*, **66**, 1302 (1970).
- (12) M. D. Sevilla, *J. Phys. Chem.*, **74**, 805 (1970).
- (13) It should be noted that the radicals produced by loss of one electron from structures I, III, IV, and V do not have a unit formal positive charge. This is due to differences in protonation. The term " $\pi$ -cation" is used here to mean a radical produced by loss of an electron from the  $\pi$ -electron system and does not refer to the total charge on the molecule.
- (14) M. D. Sevilla, C. Van Paemel, and G. Zorman, *J. Phys. Chem.*, **76**, 3577 (1972).
- (15) (a) L. Kevan in "Radiation Chemistry of Aqueous Systems," G. Stein, Ed., Wiley-Interscience, New York, N. Y., 1968, pp 21-72; (b) L. Kevan in "Progress in Solid-State Chemistry," Vol. 2, H. Reiss, Ed., Pergamon Press, Elmsford, N. Y., 1965, pp 304-329.
- (16) B. G. Ershov and A. K. Pkaev, *Radiat. Res. Rev.*, **1**, 2 (1969).
- (17) D. M. Brown and F. S. Dainton, *ibid.*, **1**, 241 (1968).
- (18) C. Helene, R. Santus, and P. Douzou, *Photochem. Photobiol.*, **5**, 127 (1966).
- (19) R. G. Shulman and R. O. Rahn, *J. Chem. Phys.*, **45**, 2940 (1966).



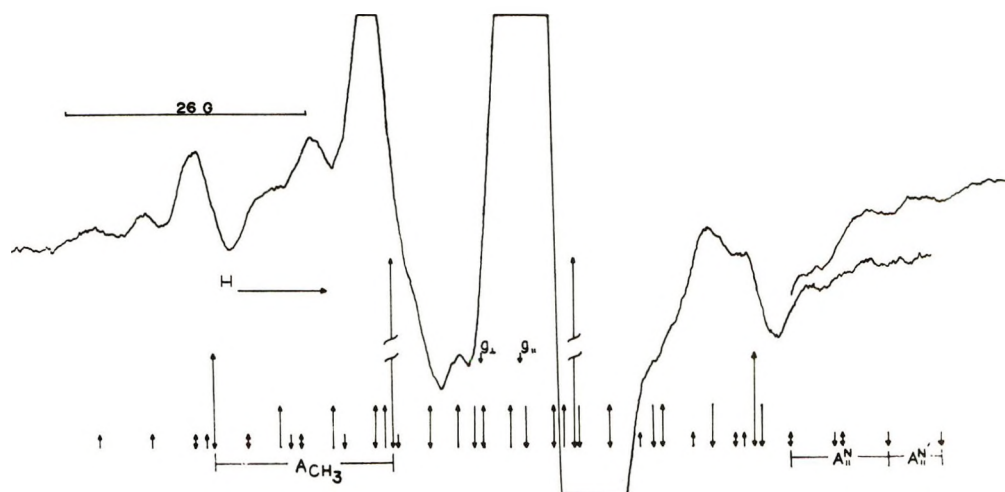


Figure 2. ESR spectrum of the  $\pi$ -cation radical of 5-methylcytosine (structure III) in 5 M  $\text{K}_2\text{CO}_3\text{-D}_2\text{O}$  at 110°K produced by photoionization. The large central component is due to the electron. The overlay at the high-field end shows the end components more clearly. The stick reconstruction is based on theoretical parameters described in the text.

Table I: ESR Spectral Parameters for  $\pi$ -Cation Radicals of DNA Bases

Parent molecule	Matrix	Hyperfine splittings, G			$g$ values	
		$a_{\text{CH}_3}^{\text{H}}$	$A_{  }^{\text{N}}$	$A_{\perp}^{\text{N}}$	$g_{  }$	$g_{\perp}$
5-Methylcytosine	5 M $\text{K}_2\text{CO}_3$	$19.7 \pm 0.2^a$	$5.9 \pm 0.3$	$\leq 2.5$	$2.0025 \pm 0.003$	$2.0049 \pm 0.0006$
	8 N NaOD	$13.8 \pm 0.2$	$10.9 \pm 0.3$	$\leq 2.5$	$2.0025 \pm 0.0003$	$2.0046 \pm 0.0006$
	6 M $\text{D}_3\text{PO}_4$	$20.0 \pm 0.2$	...	...	$2.0030 \pm 0.0005^b$	
Thymine	5 M $\text{K}_2\text{CO}_3$	$20.3 \pm 0.3$	$11.9 \pm 0.3$	$\leq 2.0$	$2.0024 \pm 0.0002$	$2.0043 \pm 0.0006$
	8 N NaOD <sup>c</sup>	$20.5 \pm 0.2$	$12.0 \pm 0.3$	$\leq 2.0$	$2.0023 \pm 0.0002$	$2.0042 \pm 0.0006$
	6 M $\text{D}_3\text{PO}_4^c$	$20.4 \pm 0.2$	$11.8 \pm 0.2$	$\leq 2.0$	$2.0026 \pm 0.0002$	$2.0046 \pm 0.0006$
Thymidine	8 N NaOD	$21.4 \pm 0.3$	$14.0 \pm 0.5$	$\leq 3.0$	$1.9986 \pm 0.006^d$	$2.0010 \pm 0.0006^d$

<sup>a</sup> The error limits represent the reproducibility in these values. <sup>b</sup> Because of poor resolution the values of  $g_{||}$  and  $g_{\perp}$  could not be determined. This value is that found at the center of the spectrum and should be considered an estimate of the isotropic  $g$  value. <sup>c</sup> M. D. Sevilla, *J. Phys. Chem.*, **75**, 626 (1971). <sup>d</sup> See text for a discussion of these  $g$  values.

2. The strong central absorption at  $g = 2.001$  is also characteristic of the electron.<sup>20</sup> The remaining components are attributed to the 5-methylcytosine  $\pi$ -cation radical. These hyperfine components show a large 1:3:3:1 methyl proton splitting of 19.7 G. In addition, there are several smaller splittings which have components with line shapes characteristic of anisotropic nitrogen hyperfine splittings with approximately axial symmetry,  $A_{||} \gg A_{\perp}$  and  $g_{\perp} > g_{||}$ .

The spectrum gives evidence for two such anisotropic nitrogen hyperfine splittings. The spin Hamiltonian has been solved for molecules containing a single anisotropic nitrogen hyperfine splitting.<sup>8,21</sup> Extending the solution to two nitrogens results in expressions 1 and 2 for the positions in magnetic field of various extrema in the spectrum. In the interpretation of

$$H = H_{||}^{\circ} - g_e/g_{||}(A_{||}^1 M_N + A_{||}^2 M_N + a_{\text{CH}_3} M_H) \quad (1)$$

$$H = H_{\perp}^{\circ} - g_e/g_{\perp}(A_{\perp}^1 M_N + A_{\perp}^2 M_N + a_{\text{CH}_3} M_H) \quad (2)$$

the spectrum it must be remembered that each ex-

pression generates a spectrum independent of the other.<sup>22</sup> In the case of expression 2 we find that the experimental values of  $A_{\perp}$  are small and simply contribute to the line width; thus components generated by (2) are due to the methyl proton splitting only. Components generated by expression 1 will arise from two nitrogen  $A_{||}$  splittings as well as by the methyl group splitting. These peaks should therefore be much less intense than those interpreted as arising from expression 1. This is found to be the case in Figure 2. The analysis of this spectrum in terms of the parameters in expressions 1 and 2 gives the values

(20) M. J. Blandemer, L. Shields, and M. C. R. Symons, *Nature (London)*, **199**, 902 (1963).

(21) F. J. Adrian, *J. Chem. Phys.*, **36**, 1692 (1962).

(22) In fact the spectrum consists of an overlap of spectra at every possible orientation to the external magnetic field; however, at magnetic fields corresponding to the parallel and perpendicular directions changes in first derivative spectra occur which can easily be identified in terms of the parameters in expressions 1 and 2 (P. W. Atkins and M. C. R. Symons, "The Structure of Inorganic Radicals," Elsevier, Amsterdam, 1967, pp 268-271).

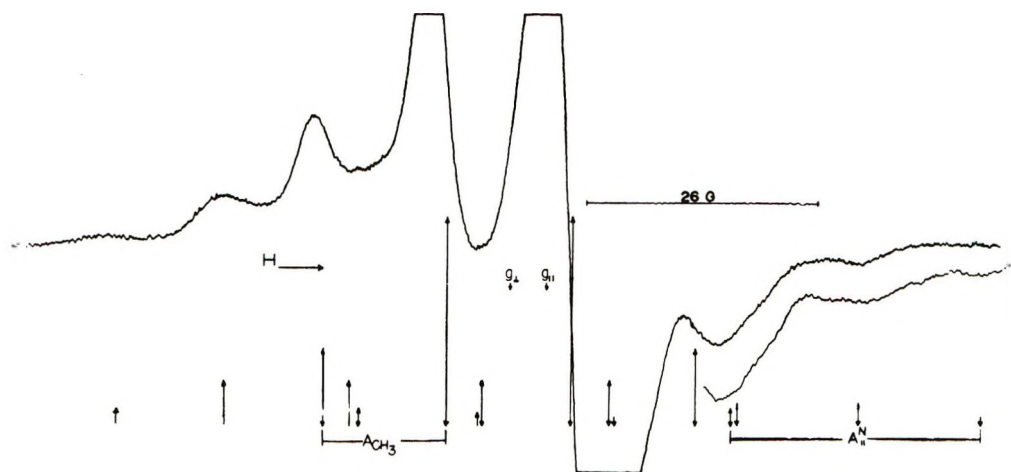


Figure 3. ESR spectrum of the 5-methylcytosine  $\pi$ -cation radical (structure IV) in 8 *N* NaOD at 110°K. The large central component is due to the electron. The stick reconstruction is in excellent agreement with experiment and is described in the text.

tabulated in Table I. A stick reconstruction based on these parameters is shown in Figure 2. Agreement between theory and experiment is considered excellent.

The esr spectrum found in Figure 3 was obtained after photolysis of 5-methylcytosine in 8 *N* NaOD at 77°K. A deep blue color associated with trapped electrons was observed in the sample. This spectrum also shows the strong absorption due to the electron at  $g = 2.001$ . We again associate the remaining spectral components to the 5-methylcytosine  $\pi$ -cation radical. A comparison of Figures 2 and 3 shows a great change in the hyperfine structure with the change in solvent pH. The spectrum in Figure 3 shows a significantly reduced methyl proton splitting. In addition, the remaining hyperfine structure including line shape and intensities can be accounted for by one large anisotropic nitrogen splitting. Analysis of the spectrum on this basis yields the splittings and  $g$  values reported in Table I. A stick reconstruction based on these parameters is shown in Figure 3. The agreement between the theoretical reconstruction and experiment is again considered excellent. Only those components overlapped by much more intense components are not resolved in the spectrum.

Photobleaching the sample containing the 5-methylcytosine  $\pi$ -cation and electron in 8 *N* NaOD produces a mixed spectrum of the anion and cation. The anion has been produced in the absence of cation by photooxidation of the ferrocyanide ion in the alkaline glass to produce trapped electrons followed by photobleaching to produce the anion by electron attachment. This gives an esr spectrum which has a doublet splitting of 15 G and a line width of 12 G. These results are similar to those found for the thymine anion and the anions of other pyrimidines in our previous work.<sup>8</sup>

Upon photoionization of 5-methylcytosine in  $D_3PO_4$  spectra indicative of products of electron attachment and deuterium atom attack are found in addition to

the spectrum of the cation radical. This is attributed to the fact that the electron is not trapped significantly at 77°K in this glass. To prevent such attack, samples were prepared containing  $2 \times 10^{-3}$  *M* ferricyanide ion which acts as an electron scavenger. The photoionization of 5-methylcytosine in glasses containing the ferricyanide ion resulted in spectra such as shown in Figure 4. The spectrum consists of a quartet of *ca.* 1:3:3:1 with 20.0 G separating the individual components. This large splitting is attributed to the methyl group. The large line width found (*ca.* 9 G) suggests relatively large unresolved hyperfine splittings.

**Thymine  $\pi$ -Cation Radical.** Photolysis of thymine in 5 *M*  $K_2CO_3$  ( $D_2O$ ) at 77°K produced a purple color in the originally clear glass. During and after photolysis the sample phosphoresced strongly. The esr spectra show the thymine  $\pi$ -cation radical and the electron. The spectra are virtually identical with those previously found for the thymine  $\pi$ -cation in alkaline and acid glasses except for slightly improved resolution.<sup>8</sup> Parameters found from the analysis of these spectra are reported in Table I along with those found in our previous work in the other glasses.<sup>8</sup>

**Thymidine and 5-Methyldeoxycytidine  $\pi$ -Cation Radicals.** Upon photolysis at 77°K in NaOD or  $K_2CO_3$  glasses thymidine and 5-methyldeoxycytidine both emitted strong phosphorescence. In addition, the presence of the electron in the samples was indicated by the deep blue or purple color and by the esr spectra. The spectra of the  $\pi$ -cation radicals are poorly resolved and in most cases uninterpretable. Only in the case of thymidine in the NaOD glass was resolution sufficient for interpretation. This spectrum is displayed in Figure 5A. As expected, the hyperfine structure is similar to that found for the thymine  $\pi$ -cation radical in the same matrix. Warming to 195°K in the presence of the ferricyanide ion greatly improved resolution



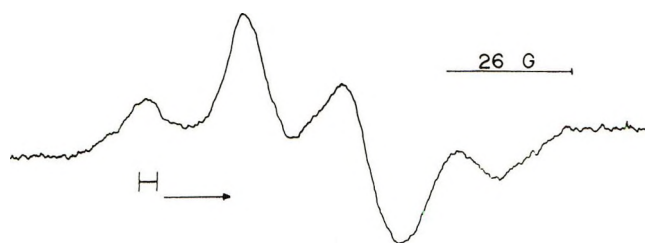


Figure 4. ESR spectrum of the 5-methylcytosine  $\pi$ -cation radical (structure I or II) in 5.7 M  $D_3PO_4$  at 110°K. Electrons produced during photolysis have been scavenged with ferricyanide ion.

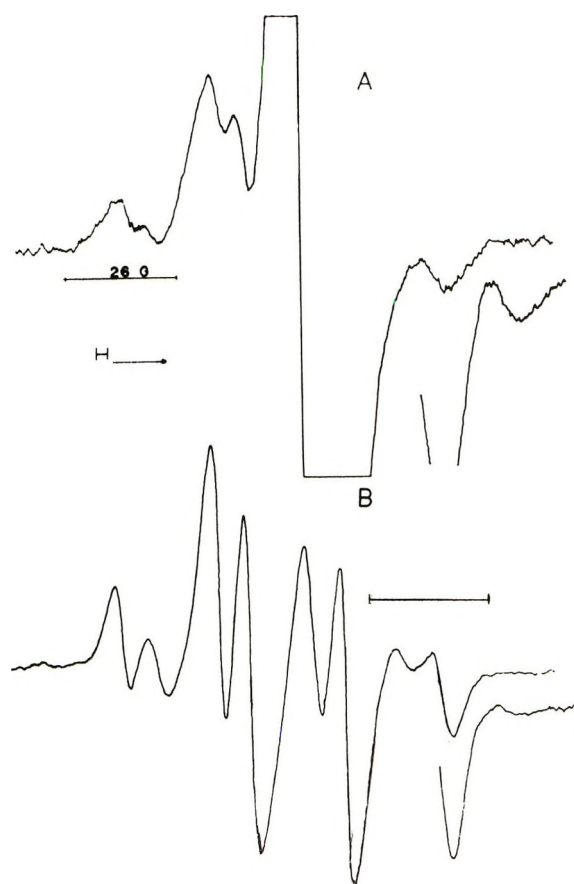


Figure 5. ESR spectra of thymidine  $\pi$ -cation radical (structure V) in 8 N NaOD: A, immediately after photolysis at 110°K; B, after warming to 195°K in the presence of ferricyanide ion. The overlay shows the high-field end portion more clearly.

and removed the electron signal (see Figure 5B). This change in resolution was not reversible. However, measurement of the spectral parameters at both temperatures demonstrated the hyperfine splittings and  $g$  values do not change significantly with temperature. These parameters are reported in Table I. The  $g$  values are *strikingly low* for a radical of this type. This was thought to indicate complex ion formation with a transition metal; however, the fact that (1) the  $g$  values did not change with the addition of the ferricyanide, (2) chemical doping with  $CN^-$  had no effect on the

spectra, and (3) the hyperfine splittings for the thymidine  $\pi$ -cation are so similar to those for thymine  $\pi$ -cation argues against this.

### Discussion

The hyperfine splittings for the 5-methylcytosine  $\pi$ -cation radicals differ significantly from glass to glass. We attribute these differences to changes in protonation of the amino group and ring nitrogen at position 1. Possible structures for 5-methylcytosine at different pH's are shown in Figure 1. The  $pK$ 's for the nitrogens are 4.6 for the amino nitrogen and 12.4 for the ring nitrogen.<sup>23</sup> Structure I would then be expected in the  $D_3PO_4$  glass for the parent compound; however, structure II is possible for the  $\pi$ -cation since protonation would be less favored for a positively charged species. In the  $K_2CO_3$  glass (pH *ca.* 12.5) structure III is likely for the  $\pi$ -cation for the same reason. In the strongly alkaline 8 N NaOH glass structure III or IV would be expected. In the case of thymidine  $\pi$  cation structure V is most likely in the NaOH glass. McLachlan MO spin density calculations have been performed for each of the possible structures. These spin densities are reported in Table II. Parameters used for these calculations were those found to give reasonable agreement with experiment in our previous work on the thymine  $\pi$ -cation and the pyrimidine anions.<sup>8,12</sup> Other parameters are given in the table. For comparison to the experimental results theoretical hyperfine splittings were calculated from the spin densities and are listed in Table II. Values of  $Q$  employed are  $Q_{N^N} = +27$ ,  $Q_{CH_3^H} = +40$ , and  $Q_{CH^H} = -30$ .<sup>8</sup>

It has been noted that  $A_{||}$  is approximately 2.3 times the isotropic nitrogen splitting for a number of nitrogen containing free radicals.<sup>7</sup> We find a factor of 2.5 places values of  $a^N$  (iso) clearly within the limits specified by the values of  $A_{||}$  and  $A_{\perp}$ . We have used this factor to approximate the experimental isotropic nitrogen splittings given in Table II.

The results in Table II show that either calculation based on structure I or II accounts for the large methyl group splitting in the experimental results for the  $\pi$ -cation in the acid glass. The lack of further resolution in the spectrum may also be explained by the calculations. Resolution is found for the  $\pi$ -cation in  $K_2CO_3$  and NaOD where the 6H hyperfine splitting is predicted to be small; however, in the acid glass the 6H splitting is predicted to be moderately large. Since  $\alpha$ -proton splittings cause greater line broadening than an equivalent nitrogen splitting the large line width in the acid medium may be expected.<sup>24</sup>

(23) D. O. Jordan, "The Chemistry of Nucleic Acids," Butterworths, Washington, D. C., 1960, pp 134-139.

(24) However it should be noted that theoretical calculations for thymine also predict such a difference in the 6-position hyperfine splitting. The experimental results however show only a slight increase in the line width.

**Table II:** Theoretical Spin Densities and Hyperfine Splittings for 5-Methylcytosine and Thymidine  $\pi$ -Cations

Position	Structure				
	I <sup>a</sup>	II	III	IV <sup>b</sup>	V
	McLachlan spin densities				
1	0.105	0.110	0.121	0.148	0.228
2	-0.020	-0.018	0.072	0.001	-0.016
3	0.171	0.145	-0.012	0.011	0.109
4	-0.035	-0.032	0.062	-0.038	-0.014
5	0.396	0.406	0.458	0.379	0.410
6	0.152	0.158	0.046	0.004	0.047
7	0.153	0.141	0.053	0.008	0.156
8	-0.001	0.008	0.106	0.424	0.008
9	0.005	0.005	0.007	0.000	0.002
10	0.075	0.076	0.087	0.062	0.072

Position	Structure								
	I	Exptl <sup>c</sup> (D <sub>2</sub> PO <sub>4</sub> )	II	III	Exptl <sup>c</sup> (K <sub>2</sub> CO <sub>3</sub> )	IV	Exptl <sup>c</sup> (NaOD)	V	Exptl <sup>c</sup> (NaOD)
	Theoretical splittings, G								
1(N)	2.8	≤4	3.0	3.3	4.4	4.0	≤2	6.2	5.6
3(N)	4.6	≤4	3.9	0.3	≤2	0.3	≤2	2.9	≤2
5(CH <sub>3</sub> )	15.9	20.0	16.2	18.4	19.7	15.2	13.8	16.4	21.4
6(H)	4.6	≤9	4.7	1.4	≤5	0.1	≤5	1.4	≤5
8(N)	0.0	≤9	0.2	2.9	2.4	11.5	11.4	...	...

<sup>a</sup> Nitrogen parameters used for the protonated amino group are  $h_N = 2$  and  $k_{C-N} = 0.8$ . <sup>b</sup> A great number of resonance hybrids are conceivable for structure IV. We find that assuming an equal double bonded character for all three nitrogens ( $h_N = 0.8$ ,  $k_{C-N} = 1.08$ ) gives the best agreement with experiment. <sup>c</sup> The experimental line width sets an upper limit to the magnitude of the unresolved hyperfine splittings. A hydrogen splitting less than the line width would not be expected to be resolved; however, an isotropic nitrogen splitting of  $>1/2.5$  times the line width would give rise to resolvable  $A_{||}$  splittings.

The results found for the 5-methylcytosine  $\pi$ -cation in the K<sub>2</sub>CO<sub>3</sub> matrix are in good agreement with the calculations based on either structures II or III. Improved agreement is found for III where the magnitude of the methyl group splitting concurs more favorably with experiment. Since structure III is also expected to predominate in this alkaline matrix, we tentatively assign the experimental splittings to positions according to the calculation based on this structure.

The experimental hyperfine splittings for the 5-methylcytosine  $\pi$ -cation in the NaOD glass are in agreement only with the values based on structure IV. The large experimental nitrogen splitting and the reduced magnitude of the methyl proton splitting are predicted by this calculation. One point of disagreement is that the nitrogen splitting at position 1 is predicted to be relatively large and would be expected to be observed in the experimental spectrum. There would be some experimental difficulty in determining a second nitrogen splitting if its magnitude were one-half the larger splitting. In this event, the spectrum found would be nearly identical with that found in the absence of such a splitting except that new low intensity components should be found at the ends of the spectrum. We searched for these components but did not find them. The overall agreement between theory and experiment is such that structure IV is strongly indicated as that of the  $\pi$ -cation in the NaOD glass.

This of course results in the assignment of the nitrogen splitting to the amino nitrogen.

The calculated results for the thymidine  $\pi$ -cation radical (V) are in reasonable agreement with experiment. However, the smaller nitrogen splitting predicted by theory is not found experimentally. A comparison with the calculated results for thymine in our previous work shows that the increase in the experimental value of the nitrogen splitting is correctly predicted; however, a decreased value of the methyl group splitting is incorrectly predicted.

Several anion and cation radicals have been found in irradiated single crystals of pyrimidines<sup>1-4</sup> or in pulse radiolytic studies.<sup>25,26</sup> Herak and Galogaza<sup>3</sup> find the cytosine cation and suggest a spin density distribution similar to that found for 5-methylcytosine  $\pi$ -cation (III) in this work. Hüttermann, *et al.*, report the 5-methylcytosine anion radical is stabilized at low temperatures.<sup>1</sup> The anion is reported to have a doublet splitting of 17 G which compares favorably with the 15 G found in this work in the NaOD glass even though different structures due to protonation are expected in the different matrices. Hartig and

(25) P. Neta, *Radiat. Res.*, **49**, 1 (1972).

(26) G. Nucifora, B. Smaller, R. Remko, and E. C. Avery, *ibid.*, **49**, 96 (1972).

(27) G. Hartig and H. Dertinger, *Int. J. Radiat. Biol.*, **20**, 577 (1971).



Dertinger report the thymidine positive ion in powdered thymine crystals.<sup>27</sup> The resolution is sufficient to resolve only the large methyl proton splitting of 19 G.

This value is in good agreement with that found in our previous work<sup>8</sup> considering the differences in molecular environment.

## Reactions of the Cation and Anion Radicals of Several DNA Bases<sup>1</sup>

by M. D. Sevilla,\* C. Van Paemel, and G. Zorman

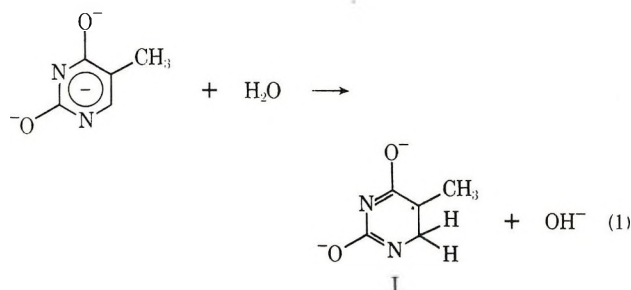
Department of Chemistry, Oakland University, Rochester, Michigan 48063 (Received May 15, 1972)

Publication costs assisted by Oakland University

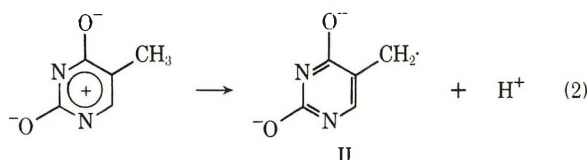
The reactions of the  $\pi$ -cation and anion radicals of several DNA bases are investigated in a number of aqueous glasses. For thymine and 5-methylcytosine the  $\pi$ -cations initially formed at 77°K react upon warming in 8 *N* NaOH or 5 *M* K<sub>2</sub>CO<sub>3</sub> by deprotonation of the methyl group to produce a RCH<sub>2</sub>· radical. This is verified by the production of the RCH<sub>2</sub>· radical by an independent method in the case of thymine. Results are found which indicate possible cation radical decomposition in the cases of thymidine and 5-methyldeoxycytidine. Computer simulations of the glassy spectra expected for the thymine RCH<sub>2</sub>· radical where the nitrogens are either protonated or unprotonated suggest splittings near 17 G for the CH<sub>2</sub> group and 6 G for the 6-position proton in the unprotonated case. The anion of thymine in 12 *M* LiCl which is stable at low temperatures is found to protonate upon warming to form the 5,6-dihydro-5-thymyl radical. Identical results are found for thymidine. The results found for the reactions of cation and anion radicals are discussed in terms of results found in crystalline DNA bases and recent pulse radiolysis results. A mechanism of radiation damage to DNA is discussed.

### Introduction

The study of the reactions of ion radicals of biological molecules is of importance to the understanding of the effect of radiation on these structures. Holroyd and Glass were the first to show that the thymine  $\pi$ -anion in an alkaline matrix reacts by protonation to form the 5,6-dihydro-5-thymyl or "thymyl" radical (reaction 1).<sup>2</sup> Since the esr spectra of irradiated DNA



clearly show the thymyl radical, this reaction has been suggested to be significant in the radiolysis of DNA.<sup>2</sup> In a preliminary report Sevilla indicated that the thymine  $\pi$ -cation radical in an alkaline matrix decomposed by deprotonation of the methyl group to form radical II by reaction 2.<sup>3</sup> A number of other investigations



have also found evidence for the role of positive ion radicals toward the production of more stable radical species.<sup>4-6</sup>

In our preceding work we reported an esr study of the  $\pi$ -cation radicals of several DNA bases.<sup>3,7</sup> In this work we report an esr investigation of the reactions of these ion radicals. Experimental evidence is given which confirms that the thymine  $\pi$ -cation undergoes the deprotonation reaction (reaction 1). In addition, the results suggest the  $\pi$ -cation radicals of 5-methyl-substituted DNA bases react by this deprotonation

(1) This research was supported in part by the Division of Biology and Medicine of the U. S. Atomic Energy Commission.

(2) (a) R. A. Holroyd and J. W. Glass, *Int. J. Radiat. Biol.*, **14**, 445 (1968); (b) M. G. Ormerod, *ibid.*, **9**, 291 (1965).

(3) M. D. Sevilla, *J. Phys. Chem.*, **75**, 626 (1971).

(4) J. Hüttermann, J. F. Ward, and L. S. Myers, *Int. J. Radiat. Phys. Chem.*, **3**, 117 (1971).

(5) G. Hartig and H. Dertinger, *Int. J. Radiat. Biol.*, **20**, 577 (1971).

(6) A. Gräslund, A. Ehrenberg, A. Rupprecht, and G. Ström, *Biochim. Biophys. Acta*, **254**, 172 (1971).

reaction. Work is also reported which shows the protonation of the anions of thymine and thymidine to form the thymyl radical is not pH dependent.

### Experimental Section

The details of the experimental procedure can be found in our previous publication.<sup>7</sup> In this work a new aqueous glass is employed. It is found that 12 *M* LiCl is compatible with the photooxidation of ferrocyanide technique for generating electrons. The electron is stable in this glass at 77°K. Although we know of no previous report of the use of this glass with the ferrocyanide method, there are investigations of the radiolysis of the glass in which its characteristics are described.<sup>8</sup>

The  $\gamma$  irradiations were performed using a <sup>60</sup>Co source.

### Results

*Reactions of Cation Radicals. Thymine.* In previous work it was shown that photolysis of thymine (0.25 mg/ml) in 8 *N* NaOH glass at 77°K produces the well-resolved esr spectrum of the  $\pi$ -cation radical and the electron.<sup>3</sup> Photobleaching the trapped electron produces the  $\pi$ -anion and  $\pi$ -cation radicals in about equal concentrations.<sup>3</sup> We find that warming the glass containing the cation and anion to about 140°K results in the loss of the  $\pi$ -cation radical esr spectrum. Further warming to 190°K results in loss of the  $\pi$ -anion spectrum and production of the spectrum shown in Figure 1A. This spectrum is considered to be the overlapped spectrum of the thymyl radical and the radical produced by the decomposition of the  $\pi$ -cation. The eight-line spectrum of the "thymyl" radical is clearly present. The reaction of the anion to form this species has been reported by other workers and shown to be a reaction of the anion with water in the aqueous solvent.<sup>2a</sup> The dotted curve in the spectrum shown in Figure 1A is the thymyl radical in an 8 *N* NaOH glass in the absence of the  $\pi$ -cation decomposition product. This species is produced in a separate experiment by electron attachment to thymine and subsequent protonation of the  $\pi$ -anion by warming to 190°K. The electrons are generated by the photooxidation of ferrocyanide ion. Subtraction of the thymyl radical spectrum from the overlapped spectrum results in the spectrum shown in Figure 1B. This spectrum is considered to be the  $\pi$ -cation decomposition product. The spectrum extends 53 G, consists of eight components, is anisotropic in nature, and cannot be interpreted directly. However, the spectrum appears as an overall triplet which is further split. This radical species is believed to be radical II since it has been observed in irradiated crystalline thymine.

To verify that radical II is the decomposition product of the  $\pi$ -cation radical, the same radical was produced by an independent means. It is known that at

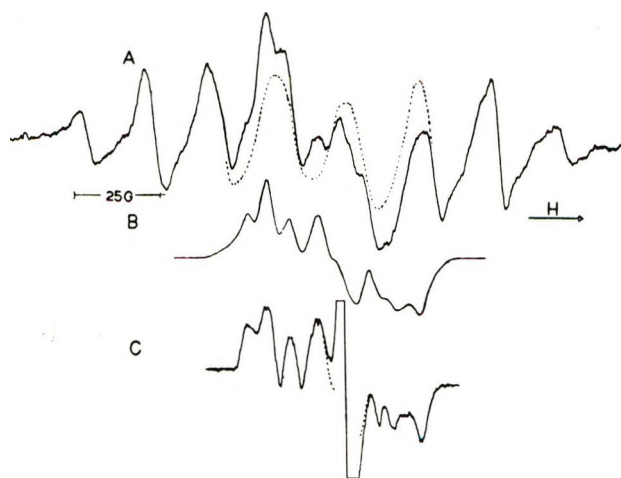


Figure 1. (A) ESR spectrum of the 5,6-dihydro-5-thymyl radical and the thymine  $\pi$ -cation decomposition product at 190°K in an 8 *N* NaOH-H<sub>2</sub>O glass. The dotted curve is the "thymyl" radical alone. (B) Spectrum of the  $\pi$ -cation decomposition product resulting from a subtraction of the two curves in A. (C) Spectrum of radical II at 190°K produced by  $\cdot\text{O}^-$  attack on thymine in 8 *N* NaOD-D<sub>2</sub>O. The central peak is a background signal. The nearly identical spectra in B and C confirm the identity of the  $\pi$ -cation decomposition product.

high pH hydroxyl radicals ( $\cdot\text{O}^-$ ) attack the methyl group of thymine to produce radical II.<sup>9,10</sup> To produce this species only, an alkaline D<sub>2</sub>O glass containing 1 *mM* thymine and saturated with N<sub>2</sub>O at low temperature was irradiated with <sup>60</sup>Co  $\gamma$  rays (dose  $2.4 \times 10^{18}$  eV/g) at 77°K. This produces  $\cdot\text{O}^-$  and electrons which are both stabilized at this temperature. Upon warming to 180°K the electrons react with N<sub>2</sub>O to produce  $\cdot\text{O}^-$  and N<sub>2</sub>. The predominant attacking species is then  $\cdot\text{O}^-$ . Figure 1C shows the spectrum of the irradiated sample at 190°K after  $\cdot\text{O}^-$  attack. The large central peak is background signal resulting from the irradiated quartz sample tube. Except for increased resolution of the hyperfine components and the background signal in Figure 1C the spectra in Figures 1B and 1C are identical. The increased resolution is due to the fact that the irradiated sample was prepared in D<sub>2</sub>O while that which yielded spectrum 1B was prepared in H<sub>2</sub>O.

A second method was used to separate the  $\pi$ -cation decomposition spectrum from the thymyl radical. Samples of thymine (1 *mM*) in 8 *N* NaOD containing 1 *mM* ferricyanide ion were photoionized with uv light. The ferricyanide ion acts as an electron scavenger. Photobleaching the electron in these samples results

(7) M. D. Sevilla, C. Van Paemel, and C. Nichols, *J. Phys. Chem.*, **76**, 3571 (1972).

(8) L. Kevan in "The Chemical and Biological Action of Radiations," M. Haissinsky, Ed., Masson, Paris, 1969.

(9) L. S. Myers, J. F. Ward, W. T. Tsukamoto, D. E. Holmes, and J. R. Julca, *Science*, **148**, 1234 (1965).

(10) N. Nazhat and J. Weiss, *Trans. Faraday Soc.*, **66**, 1302 (1970).



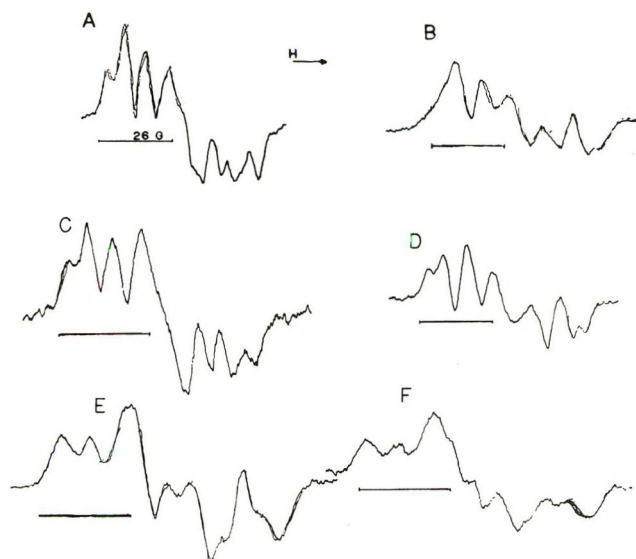
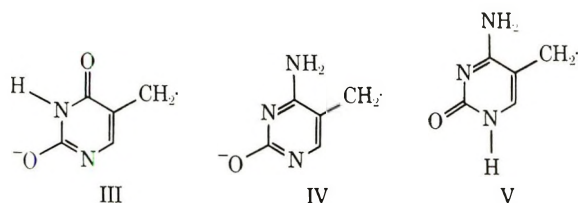


Figure 2. ESR spectra of radicals produced by warming the  $\pi$ -cation radicals of several DNA bases to 190°K in 8 N NaOD-D<sub>2</sub>O or 170°K in 5 M K<sub>2</sub>CO<sub>3</sub>-D<sub>2</sub>O in the presence of an electron scavenger (1 mM ferricyanide ion): A, thymine in 8 N NaOD; B, thymine in 5 M K<sub>2</sub>CO<sub>3</sub>; C, cytosine in 8 N NaOD; D, cytosine in 5 M K<sub>2</sub>CO<sub>3</sub>; E, thymidine in 5 M K<sub>2</sub>CO<sub>3</sub>; F, 5-methyldeoxycytidine in 5 M K<sub>2</sub>CO<sub>3</sub>.

in an esr spectrum of the cation and a small signal due to the anion radical. The electron is thus effectively scavenged. Warming this sample to 190°K results in the spectrum shown in Figure 2A. This spectrum is virtually identical with Figure 1C and is more resolved than Figure 1B as would be expected due to the deuterated matrix. From these results we conclude that the ferricyanide ion is an effective electron scavenger which does not take part in the reaction. From the overall results in this section we can conclude that the thymine  $\pi$ -cation radical deprotonates to form radical II.

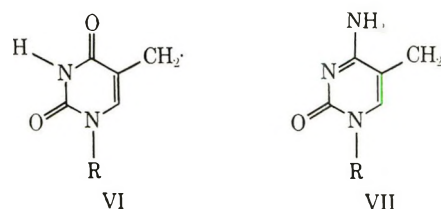
Since the decomposition mechanism could be matrix dependent, it was of interest to perform experiments at a lower OH<sup>-</sup> concentration. Photolysis of thymine (1 mM) in 5 M K<sub>2</sub>CO<sub>3</sub>/D<sub>2</sub>O with 1 mM ferricyanide ion produced the esr spectrum of the  $\pi$ -cation and electron. Photobleaching and warming to 170°K resulted in the spectrum shown in Figure 2B. This spectrum is 56 G in width and is similar to that found in the NaOH glass. We associate this spectrum with radical III. These results are good evidence that the mechanism is the same in NaOD and K<sub>2</sub>CO<sub>3</sub> matrices.



**5-Methylcytosine.** Samples of 5-methylcytosine (1 mM) in 8 N NaOH containing 1 mM ferricyanide

were photoionized with uv light. Warming the sample containing the  $\pi$ -cation to 190°K results in the esr spectrum found in Figure 2C. In 5 M K<sub>2</sub>CO<sub>3</sub>-D<sub>2</sub>O a similar procedure produced the spectrum shown in Figure 2D. These spectra are virtually identical with those found for thymine and suggest an identical mechanism of decomposition to form radical IV in NaOH<sup>11</sup> and V in K<sub>2</sub>CO<sub>3</sub>.<sup>12</sup>

**Thymidine and 5-Methyldeoxycytidine.** Neither the thymidine or 5-methyldeoxycytidine  $\pi$ -cations gave evidence for decomposition in 8 N NaOH. In fact, thymidine  $\pi$ -cation was observed at temperatures as warm as 195°K. However, warming the  $\pi$ -cations of these nucleotides in 5 M K<sub>2</sub>CO<sub>3</sub> to 190°K produced esr spectra shown in Figures 2E and 2F. These spectra differ from the virtually unresolved spectra originally found for the  $\pi$ -cations. This change in spectra was found to be irreversible and may suggest a further reaction. The total width of both of these spectra is approximately 60 G and is somewhat larger than the 56-G width found for the thymine and 5-methylcytosine  $\pi$ -cation decomposition radicals. In addition, line components for the nucleosides are not in agreement with those found for the pyrimidines. Results of spin density calculations and spectrum simulations (discussed later) suggest that such differences in spectra may be expected for a radical of the same form as radical II when substitution occurs at the nitrogen. However, owing to the fact that the positive ions were stable in 8 N NaOH and that the  $\pi$ -cation spectra would appear as similar quartets, we can only tentatively associate the radicals which give rise to the spectra in Figures 2E and F to radicals VI and VII.



**Reactions of Thymine and Thymidine Anion Radicals.** Photolysis of 10 mM ferrocyanide ion in 12 M LiCl-H<sub>2</sub>O glasses containing ca. 1 mM thymine or thymidine produces the anion radicals (see Figure 3A). The results found for thymine and thymidine are virtually identical. The spectra of these anions which consist of 14-G doublets are similar to those found in our previous work in 8 N NaOH glasses.<sup>3,13</sup> Both anion spectra show the presence of a small amount of the thymyl radical which is probably explained by the

(11) In view of our results for the 5-methylcytosine  $\pi$ -cation in 8 N NaOH (ref 7) a structure with one amino proton is also possible.

(12) This structure is considered most likely in 5 M K<sub>2</sub>CO<sub>3</sub> glasses since production of this radical in concentrated D<sub>3</sub>PO<sub>4</sub> by ·OD attack produces an identical spectrum.

(13) M. D. Sevilla and C. Van Paemel, *Photochem. Photobiol.*, 15, 407 (1972).

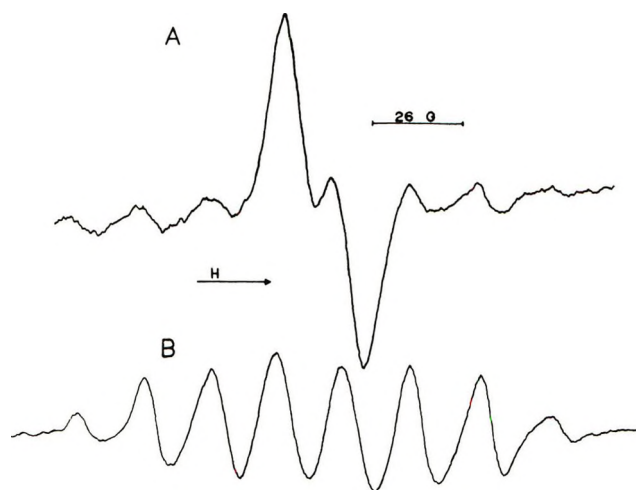
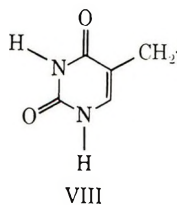


Figure 3. (A) ESR spectrum of the thymine anion produced by electron attachment at 110°K in 12 M LiCl. (B) ESR spectrum of the 5,6-dihydro-5-thymyl radical produced by warming the anion in A to 170°K.

fact that reaction 1 can be induced by uv light.<sup>14</sup> Upon warming the samples to 170°K a loss of the anion signal occurs with a concurrent buildup in the characteristic eight-line spectrum of the thymyl radical. Figure 3B shows the spectrum for thymine after the reaction has gone to completion. Analysis of the final spectrum for thymine yields  $a_{\text{CH}_2} = 20.3$  G and  $a_{\text{CH}_2(\text{av})} = 39.6$  G at 110°K. For thymidine we find  $a_{\text{CH}_2} = 20.2$  G and  $a_{\text{CH}_2(\text{av})} = 37.6$  G at 110°K. These results are similar to those found by Holroyd and Glass in NaOH glasses.<sup>2a</sup> Through computer simulations these workers estimated the difference between the two methylene proton splittings to be 9 G for the thymidine case.

**Spectrum Analysis by Computer Simulations.** Simulations of the polycrystalline spectrum of  $\pi$ -cation decomposition radical (radical II) are possible from previous work on thymine single crystals. Hüttermann reports the hyperfine and  $g$  tensors and their direction cosines for radical VIII.<sup>15</sup> This radical



differs from radical II only by the protonation of the nitrogens. The reported isotropic components are 15 G for the  $\text{CH}_2$  protons and 11.3 G for the 6-position proton. Transforming the hyperfine tensors into the  $g$  tensor axis system and utilizing a computer program which simulates the polycrystalline spectrum to first order<sup>16</sup> results in the spectrum in Figure 4A. In the simulation the line components were assumed to be gaussian and the line width was 3.5 G for each com-

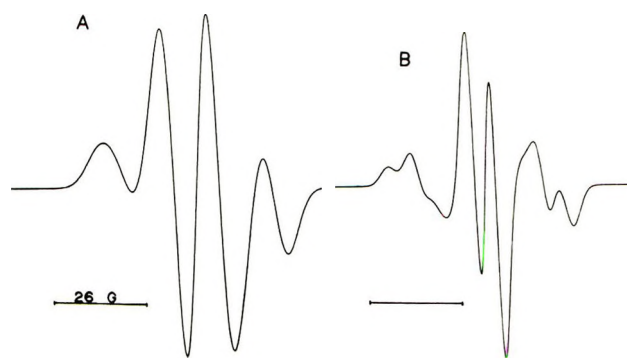


Figure 4. (A) Computer simulation of the glassy spectrum of radical VIII based on parameters from single crystal work. (B) Computer simulation of the glassy spectrum of radical II based on parameters described in text.

ponent. The resultant spectrum consists of a quartet of unequal spacing. Although this spectrum is similar to that found in polycrystalline thymine by Hartig and Dertinger<sup>5</sup> which they assigned to radical VIII, it is unlike that found here for radical II. This suggests a relatively large effect due to the differences in protonation between radicals II and VI. Neta has produced the monoprotonated radical by  $\text{O}^-$  attack at high pH in a steady-state radiolytic technique.<sup>17</sup> This radical is found to have isotropic hyperfine splittings of approximately 16 G for the  $\text{CH}_2$  protons and 8 G for the 6-position proton. Thus a small increase in the  $\text{CH}_2$  splitting and a significant reduction in the 6-position splitting is induced by the deprotonation of position 1. A greater change in hyperfine splittings may be expected in 8 N NaOH where both nitrogens at position 1 and 3 are deprotonated. McLachlan MO calculations of the spin density distribution employing usual parameters<sup>7</sup> for radical II indicate an increase in the spin density at the  $\text{CH}_2$  group and a decrease at position 6 over that calculated for radical VIII. We have simulated the ESR spectrum of radical II by employing the same  $g$  and hyperfine tensor elements found by Hüttermann for radical VIII but have altered the tensor elements proportionately so that the isotropic components correspond to the theoretically indicated values of 17 G for  $\text{CH}_2$  and 6 G for the 6-position proton splitting (see Figure 3B). Gaussian lines with 1.5-G line width are assumed. The resolution of individual components and peak heights in Figure 3B is not in good agreement with experiment; however, the line positions are in relatively good agreement, *i.e.*, the average of the magnitudes of the deviations of theoretical positions from experiment is 1 G.

(14) Y. Lion and A. Van de Vorst, *Int. J. Radiat. Phys. Chem.*, **3**, 513 (1971).

(15) J. Hüttermann, *Int. J. Radiat. Biol.*, **17**, 249 (1970).

(16) M. Si Swin Wei, Ph.D. Thesis, The University of Michigan, 1970.

(17) P. Neta, *Radiat. Res.*, **49**, 1 (1972).



The line positions are even in better agreement (0.8-G average deviation) with those found for the 5-methylcytosine radical in Figure 2C. These results indicate that the isotropic splittings of 17 and 6 G used in the reconstruction are near the true isotropic splittings of radicals II and IV.

The results found for thymidine and perhaps 5-methyldeoxycytidine may now be explainable in terms of the effects of ribose substitution at position 1. The expected effect of this substitution would be to increase the 6-position splitting so as to produce a spectrum which appeared as a quartet. This is what is found experimentally in Figure 2E.

### Discussion

The results found here suggest that the mechanism of decomposition of the  $\pi$ -cation radicals of 5-methyl-substituted DNA bases in aqueous glasses is deprotonation of the methyl group. These results are in good agreement with recent results obtained on irradiated crystalline DNA bases. Hüttermann, *et al.*, in work with irradiated 5-methylcytosine single crystals suggest that the positive and negative ions first produced react to form more stable secondary radicals by mechanisms analogous to reaction 1 and 2.<sup>4</sup> Hartig and Dertinger report results for irradiated dry powders of thymine, thymidine, and DNA.<sup>5</sup> For thymine they find that the positive ion initially formed deprotonated to form radical VIII. For thymidine and even DNA, radicals of the form of radical VIII are observed in the esr spectra. They suggest that deprotonation is the mechanism of formation of these radicals as well.

In recent results on irradiated single crystals of 6-azathymine Herak and Schoffa suggest a radical analogous to radical VIII is formed by hydrogen atom abstraction.<sup>18</sup> Results found here would suggest the deprotonation of the positive ion as an alternative explanation.

Our results for the reactions of the thymine and thymidine anions have a bearing on a point of disagreement between esr and pulse radiolytic experiments. Esr investigations show that thymine anion undergoes irreversible protonation in alkaline matrices to produce the 5,6-dihydro-5-thymyl radical.<sup>2a,14</sup> Pulse radiolysis of aqueous solutions of thymine at pH 7 indicate the thymine anion protonates at an oxygen.<sup>19-21</sup> Theard, *et al.*, suggest that a possible reason for this apparent discrepancy is that the pH affects the protonation mechanism.<sup>19</sup> The results found here in 12 M LiCl glasses do not support a pH dependence. The fact that there is evidence that "thymine" anions in irradiated wet DNA protonate upon warming also argues against this explanation.<sup>22</sup> Another possible explanation for this difference in results is that the ionic strength, not pH of the glasses, affects the mechanism of protonation. The results found in DNA would argue against this. In addition, Verma, *et al.*, report

that thymine anions protonate in mixtures of methanol and 0.5 M NaOH where the ionic strength is much lower.<sup>23</sup> A likely explanation for this difference is that the 6-protonation is a slow step not observed in the pulse radiolysis experiment.

The results found here and the results of a number of other workers leads to a mechanism of the direct effect of radiation on DNA. Gräslund, *et al.*, have shown that the initial effect of radiation is to produce ions which are stabilized on the DNA bases at low temperature.<sup>6</sup> The DNA strand can then be viewed as a semiconductor for excess charge and holes. At low temperatures the electrons and holes are immobile while as the temperature increases the charges can migrate through the  $\pi$ -orbital systems of the stacked DNA bases. In the migration process the bound electrons and holes can recombine, transfer out of the DNA strand if the DNA is in contact with another molecule,<sup>24</sup> or induce reactions at the most reactive DNA bases. Ion recombination would explain the loss of signal intensity observed when samples of DNA irradiated at low temperatures are warmed.<sup>5</sup> The results found for irradiated DNA clearly suggest that the electron would be expected to react at the thymine base to form the thymyl radical.<sup>22,25-28</sup> A number of workers have suggested this reaction to explain the appearance of the thymyl radical spectrum only when wet DNA initially irradiated at 77°K is warmed to temperatures above 200°K.<sup>2</sup> The fact that irradiated samples of dry DNA do not produce the thymyl spectrum is in accord with the anion protonation mechanism.<sup>5,22</sup> The results found here would suggest the deprotonation of the methyl group of thymine base in DNA as a possible reaction for the positive hole. Hartig and Dertinger's findings that irradiated *dry* DNA shows a predominant signal due to a deprotonated base thymine radical is good evidence that this reaction of the positive ion in DNA may be preferential over other possible reactions.<sup>5</sup> Thus it is likely that electrons and holes in wet DNA react predominantly with thymine base to produce radicals *via* mechanisms analogous to those in reactions 1 and 2.

(18) J. N. Herak and G. Schoffa, *Mol. Phys.*, **22**, 379 (1971).

(19) L. M. Theard, F. C. Peterson, and L. S. Myers, *J. Phys. Chem.*, **75**, 3815 (1971).

(20) G. Scholes and R. L. Willson, *Trans. Faraday Soc.*, **63**, 2983 (1967).

(21) E. Hayon, *J. Chem. Phys.*, **51**, 4881 (1969).

(22) A. Ehrenberg, A. Rupprecht, and G. Ström, *Science*, **157**, 1317 (1967).

(23) N. C. Verma, B. B. Singh, and A. R. Gopal-Ayengar, *Stud. Biophys. (Berlin)*, **13**, 231 (1969).

(24) Transfer of radiation induced free radicals from DNA to cysteamine has been reported [P. Milvy, *Radiat. Res.*, **47**, 83 (1971)].

(25) R. Salovey, R. G. Shulman, and W. M. Walsh, *J. Chem. Phys.*, **39**, 839 (1963).

(26) J. B. Cook and S. J. Wyard, *Nature (London)*, **219**, 526 (1966).

(27) J. B. Cook and S. J. Wyard, *Int. J. Radiat. Biol.*, **11**, 357 (1966).

(28) J. P. Elliott, *Proc. Roy. Soc., Ser. A*, **302**, 361 (1968).

*Acknowledgment.* We are indebted to Julien Gendell and John Fritz for their aid in the spectrum simulation.

We also would like to thank Anthony Ervin for his experimental aid.

## Studies of the Ester Bond. II.<sup>1</sup> Nuclear Magnetic Resonance

### Studies of *tert*-Butyl Formate

by Torbjörn Drakenberg\* and Sture Forsén

Division of Physical Chemistry, The Lund Institute of Technology, 220 07 Lund 7, Sweden (Received July 3, 1972)

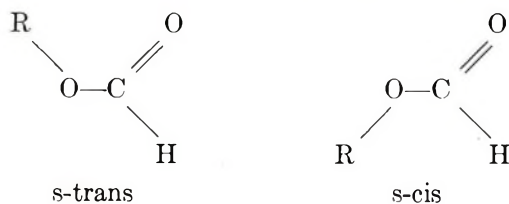
Publication costs assisted by The Lund Institute of Technology

The *s*-cis, *s*-trans interconversion barrier and *s*-cis, *s*-trans population ratio of *tert*-butyl formate in various solvents have been determined by means of nmr total line shape analysis. The free energy difference between the two conformers ( $\Delta G^\circ$ ) is found to vary linearly with the Onsager parameter  $(\epsilon - 1)/(2\epsilon + 1)$ . Extrapolation to  $\epsilon = 1$  (gas phase) results in  $\Delta G^\circ = 6$  kcal/mol. For a solution of *tert*-butyl formate in dimethylformamide-*d*<sub>7</sub>-dimethyl ether (1:1) the free energy of activation was found to be  $\Delta G^\ddagger_{183} = 8.75$  and 9.32 kcal/mol for the two isomeric forms. It has also been possible to estimate the population ratio at room temperature from the coupling constant  $^5J_{\text{H-H}}$ . These values show reasonable agreement with results derived from the total line shape data.

#### Introduction

It is now well known, from nmr studies, that there exist large barriers to internal rotation about the formal single bonds in amides,<sup>2</sup> nitrites,<sup>3</sup> and nitrosamines.<sup>4</sup> Due to the chemical similarity it is to be expected that the C-O bond of the ester group should possess a torsion barrier of a similar order of magnitude; this has, however, not been confirmed by nmr measurements. There do exist however, ir<sup>5</sup> and ultrasonic relaxation<sup>6</sup> data, showing that the barrier to hindered rotation in methyl formate is *ca.* 10 kcal/mol.

Chiefly on the basis of dipole moment measurements<sup>7</sup> and microwave spectroscopy<sup>8</sup> it has mostly been assumed that the conformation of formates is almost exclusively *s*-trans. In small ring lactons, however, the ester group is forced to be in the *s*-cis conformation, and it has by means of dipole moment measurements been found that in lactons with 8 or 9 atoms in the ring there is an equilibrium between the *s*-cis and *s*-trans conformers



and for larger rings the *s*-trans conformer dominates.<sup>9</sup> In a recent *ab initio* calculation<sup>1</sup> the energy difference

between the two conformers of methyl formate was calculated to be 9 kcal/mol with the *s*-cis conformer having the higher energy, in agreement with the microwave data.<sup>8</sup> These data show that the energy difference between the *s*-cis and *s*-trans conformers of the ester group is normally very high. This can probably explain the fact that the *cis*-*trans* isomerism of esters has, to date, not been observed by means of nmr spectroscopy.

Recently it has been shown that the formyl proton pmr signal from *tert*-butyl formate splits into an unequal doublet at low temperature (below  $-90^\circ$ ) in DMF solution,<sup>10</sup> showing that the population ratio in *tert*-butyl formate is not as far from unity as is that for methyl

(1) H. Wennerström, S. Forsén, and B. Roos, *J. Phys. Chem.*, **76**, 2430 (1972).

(2) W. E. Stewart and T. H. Siddall, III, *Chem. Rev.*, **70**, 517 (1970).

(3) P. T. Inglefield, E. Krakower, L. W. Reeves, and R. Stewart, *Mol. Phys.*, **15**, 65 (1968).

(4) R. K. Harris and R. A. Spragg, *Chem. Commun.*, 362 (1967).

(5) T. Miyazawa, *Bull. Chem. Soc. Jap.*, **34**, 691 (1961).

(6) (a) S. V. Subrahmanyam and J. E. Piercy, *J. Acoust. Soc. Amer.*, **37**, 340 (1965); (b) J. Bailey, S. Walker, and A. M. North, *Trans. Faraday Soc.*, **64**, 1499 (1968); (c) K. M. Burundukov and V. F. Jakovlev, *J. Fiz. Chim.*, **42**, 2149 (1968).

(7) R. J. B. Marsden and L. E. Sutton, *J. Chem. Soc.*, 1383 (1936).

(8) R. F. Curl, Jr., *J. Chem. Phys.*, **30**, 1529 (1959).

(9) R. Huisgen and H. Ott, *Tetrahedron*, **6**, 253 (1959).

(10) M. Oki and H. Nakanishi, *Bull. Chem. Soc. Jap.*, **43**, 2558 (1970).



formate. This is probably due to an increased steric repulsion in the *s*-trans conformer.

Since the dipole moments for the two conformers of methyl formate are unequal,<sup>1</sup> the *s*-cis/*s*-trans population ratio should change with the polarity of the solvent. The enthalpy difference between the *s*-cis and *s*-trans conformers of methyl formate was estimated to change from *ca.* 8 kcal/mol in gas phase to *ca.* 4 kcal/mol in a solvent with  $\epsilon = 30$ , with the *s*-trans conformer remaining lower in energy.

In the present work we have performed low-temperature pmr studies of *tert*-butyl formate in various solvents, in order to determine first the effect of the polarity of the solvent on *s*-cis/*s*-trans population ratio and second the torsional barrier, in *tert*-butyl formate.

### Experimental Section

**Material and Sample Preparation.** The *tert*-butyl formate was synthesized from a formic acid-acetic anhydride reaction mixture and *tert*-butyl alcohol according to the procedure of Stevens and van Es.<sup>11</sup> The boiling point was found to be 83°. The solvents, dimethylformamide-*d*<sub>7</sub>, dimethyl ether, and CF<sub>2</sub>Cl<sub>2</sub> were obtained from Merck A.G. (Darmstadt), Matheson, Inc. (Newark, N. J.), and Vorgania Chemicals, Inc. (Porthmouth, Va.), respectively, and used without further purifications.

The samples were prepared directly in 5-mm nmr tubes (Wilmad, Quality 505). All samples contained *ca.* 10% by volume of *tert*-butyl formate and a small amount of TMS and various amounts of the solvent components (see Table I). All solvents with the exception of DMF were condensed directly into the nmr tubes, which were cooled with liquid nitrogen. The tubes were sealed off and stored in a refrigerator.

**Table I:** Composition and Dielectric Constant of the Solvent Mixtures

Sample no.	DMF- <i>d</i> <sub>7</sub>	(CH <sub>3</sub> ) <sub>2</sub> O	CF <sub>2</sub> Cl <sub>2</sub>	CCl <sub>4</sub>	$\epsilon_{25^\circ}$	$\epsilon_{100^\circ}$ <sup>a</sup>
I	95	5			34.8	60
II	50	50			23.5	35
III		100			5.0	10.75
IV		50	50		3.5	6.5
V				100		

<sup>a</sup> Estimated from comparison with other compounds, for which the variation of  $\epsilon$  with temperature are given (Handbook of Chemistry and Physics, 46th ed, The Chemical Rubber Publishing Co., Cleveland, Ohio, 1965).

**Apparatus and Measurements.** The pmr spectra for line shape analysis were recorded on a Varian XL-100 spectrometer equipped with a V-6040 temperature controller and a V-4415 variable temperature probe. The signal from dimethyl ether or TMS was used as internal lock. The rf power of the observing field was always

kept sufficiently low to prevent saturation and a slow sweep rate (0.5 and 0.2 Hz/sec) was used to avoid distortion of the signals. The sweep expansion on the flatbed recorder varied from 1 to 5 Hz/cm.

The temperature was measured by means of a thermocouple, which was inserted into the probe and fixed just below the nmr tube. The readings of this thermocouple were in a separate experiment, calibrated against another thermocouple inside a spinning 5-mm sample tube, filled with dimethyl ether; the sensing point of this thermocouple was just in height with the receiver coil. The outer thermocouple was found to show 2.5° lower temperature than the inside thermocouple, at -100°. This difference was found to decrease with increasing temperature and at -30° there was no detectable difference between the two readings. No marked change in the difference temperature with small variations in the flow rate of the cooling gas was observed. The accuracy in the temperature measurements is estimated to be  $\pm 1^\circ$ .

For the determination of the *s*-cis/*s*-trans population ratio in samples not used for a total line shape analysis a Varian A-60A spectrometer was used. For the 60-MHz spectra the temperature was taken from the pre-calibrated dial on the temperature controller and is estimated to be accurate only to  $\pm 10^\circ$ .

**Line Shape Analysis and Determination of Population Ratios.** For samples III and IV the population ratios were determined directly from integration of low-temperature spectra, in which the signals from the two conformers were well resolved. For samples I and II, where total line shape analysis was performed, the population ratios were obtained from this analysis.

The line shape of the formyl proton pmr spectrum is determined by (i) the *s*-cis to *s*-trans population ratio; (ii) the chemical shift difference between the two signals,  $\Delta\nu$ ; (iii) the effective spin-spin relaxation time,  $T_2^{\text{eff}}$ ; (iv) the rate of exchange between the two conformers; and (v) the coupling constants between the formyl proton and the *tert*-butyl group protons,  $^5J_{\text{trans}}$  and  $^5J_{\text{cis}}$ . The McConnell<sup>12</sup> equation has been used to calculate theoretical spectra. In this equation, parameters i to iv are included; the spin couplings v were taken care of through the summation of 10 AX spectra; where the spacing between the A lines is given by  $J_{\text{trans}}$  and for the X lines by  $J_{\text{cis}}$ , and with intensities as 1:9:36:84:126:126:84:36:9:1.

$T_2^{\text{eff}}$  could be determined only at the fast exchange limit, normally at room temperature, where  $T_2^{\text{eff}}$  for TMS was additionally obtained. At all other temperatures, the following equation to extract  $T_2^{\text{eff}}$  was employed:  $1/T_2^{\text{tBF}} = 1/T_2^{\text{TMS}} + 1/T_2^+$ , where  $1/T_2^+$ , a correction term needed to determine  $T_2^{\text{tBF}}$  from  $T_2^{\text{TMS}}$ , was determined at room temperature.

(11) W. Stevens and A. van Es, *Recl. Trav. Chim. Pays-Bas*, **83**, 863 (1964).

(12) H. M. McConnell, *J. Chem. Phys.*, **28**, 430 (1958).

The population ratios and the chemical shift differences could only be determined in relatively narrow temperature interval at low temperatures, for sample I, 10° while for II, 20°. The *s*-cis/*s*-trans population ratios at higher temperatures were calculated under the assumption of constant  $\Delta G^\circ$ .<sup>13</sup> The shift difference between the two formyl proton signals attributed to the *s*-cis and *s*-trans conformers in sample II was found to decrease linearly with temperature from -112 to -91° and the same temperature dependence was assumed to be valid at higher temperatures for both samples I and II; this parameter was thus obtained from a linear extrapolation.

At all temperatures the rate of exchange was obtained from visual comparison of experimental and calculated spectra. In all, some 200 spectra were calculated.

### Results and Discussion

**Nmr Spectra.** The pmr spectrum of *tert*-butyl formate at room temperature consists of two sets of signals: a doublet at  $\delta$  1.46 (*tert*-butyl group) and a multiplet at  $\delta$  8.03 (formyl proton). The splittings, which vary with the solvent composition (Table II), are the same in both the doublet and the multiplet and are caused by a five-bond long-range coupling. Since *tert*-butyl formate consists of a mixture of *s*-cis and *s*-trans conformers, the observed splitting can be assumed to be a weighed mean of the coupling constants in the two conformers (eq 2). The variation in

$$\delta = J_{\text{trans}}p_{\text{trans}} + J_{\text{cis}}p_{\text{cis}} \quad (2)$$

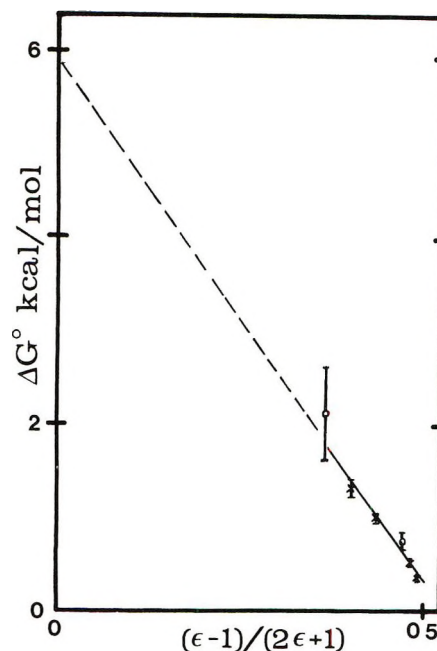
with the solvent composition indicates that the population ratio changes with solvent. The major cause for the variation of  $\delta$  with the solvent is assumed to be changes in the population ratio.

**Table II:** Chemical Shift Difference,  $\delta\nu$ , Molar Ratio of the *s*-Cis Conformer at -100 and 30°, and the Free Energy Difference between the *s*-Cis and *s*-Trans Conformers at -100 and 30°

Sample no.	$\delta\nu_{-100^\circ}$ , <sup>a</sup> ppm	( $p_{\text{cis}}$ ) <sub>-100°</sub>	$\Delta G^\circ_{-100^\circ}$	$\delta_{30^\circ}$	( $p_{\text{cis}}$ ) <sub>30°</sub>	$\Delta G^\circ_{30^\circ}$
I	0.815	27	0.34	0.31	36	0.34 <sup>b</sup>
II	0.823	17	0.55	0.35	23	0.73
III	0.67	5.5	0.98	0.41	3	2.1
IV	0.68	2.2	1.30			
V				0.42	0	

<sup>a</sup> Formyl proton signal. <sup>b</sup> Assumed to be the same as  $\Delta G^\circ_{-100^\circ}$ .

When the sample temperature is lowered, below -40°, the formyl proton signal begins to broaden and at *ca.* -90° the signal splits into an unequal doublet attributed to the *s*-cis and *s*-trans conformers. Due to the fact that the low-field signal intensity decreases



**Figure 1.**  $\Delta G^\circ$ , from the *s*-trans/*s*-cis population ratio in *tert*-butyl formate, vs.  $(\epsilon - 1)/(2\epsilon + 1)$  for the solvent:  $\times$ , low-temperature data from integration or line shape analysis;  $\circ$ , room temperature data from  $\delta = {}^5J_{\text{trans}}P_{\text{trans}} + {}^5J_{\text{cis}}P_{\text{cis}}$ .

with the decreasing polarity of the solvent, this signal is assigned to the more polar *s*-cis conformer. As shown below, this is also in agreement with a larger trans  ${}^5J$  than cis  ${}^5J$ , as is usually observed for amides.<sup>2</sup>

The *tert*-butyl signal has, however, not broadened more than the TMS signal, showing that the *s*-cis and *s*-trans chemical shift difference for the *tert*-butyl group are at least two orders of magnitude smaller than for the formyl proton signal. The low-temperature chemical shift difference for the formyl proton signal,  $\delta\nu$ ,  $p_{\text{cis}}$ , and the high-temperature splitting,  $\delta$ , are given in Table II.

**Solvent Dependence of the *s*-Cis to *s*-Trans Population Ratio.** From the low-temperature nmr spectra, it was possible to determine the population ratio either by integration or from the line shape analysis (Table II). These values have been used to calculate the free energy difference between the two conformers,  $\Delta G^\circ$ .

According to Onsager, eq 3,<sup>14</sup> where  $E_s$  is the sta-

$$E_s = \frac{\mu^2 (\epsilon - 1)}{a^3 (2\epsilon + 1)} \quad (3)$$

bilization energy,  $\mu$  is the dipole moment of the solute,  $a^3$  is the molar volume of the solute, and  $\epsilon$  is the dielectric constant of the solvent, the energy difference between the two conformers should be linearly related to

(13) From Figure 1 and reasonable values on the temperature variation in the dielectric constants it can be estimated that  $\Delta G^\circ$  should change *ca.* 0.05 kcal/mol over the whole temperature range used for sample II and much less for sample I.

(14) L. Onsager, *J. Amer. Chem. Soc.*, **58**, 1486 (1936).



**Table III:** Activation Parameters for the s-Cis-s-Trans Interconversion in *tert*-Butyl Formate

Sample no.	$\Delta H^\ddagger_1^a$	$\Delta S^\ddagger_1^b$	$\Delta G^\ddagger_{1, 188}^a$	$\Delta H^\ddagger_2^a$	$\Delta S^\ddagger_2^b$	$\Delta G^\ddagger_{2, 188}^a$
I	$9.16 \pm 0.5$	$1.93 \pm 3$	$8.81 \pm 0.1$	$9.50 \pm 0.5$	$1.79 \pm 3$	$9.17 \pm 0.1$
II	$9.18 \pm 0.5$	$2.39 \pm 3$	$8.75 \pm 0.1$	$9.40 \pm 0.5$	$0.45 \pm 3$	$9.32 \pm 0.1$

<sup>a</sup> In kcal/mol. <sup>b</sup> In cal/mol K.

$(\epsilon - 1)/(2\epsilon + 1)$ , which also has been found in the present work, see Figure 1. Upon extrapolation to  $\epsilon = 1$  an estimation on the value on  $\Delta G^\circ$  for *tert*-butyl formate in gas phase was obtained;  $\Delta G^\circ_{\epsilon=1} = 6 \pm 1$  kcal/mol. This is in reasonable agreement with the  $\Delta H^\circ$  values estimated for methyl formate, using the Onsager equation and theoretically estimated values for the constants  $a$  and  $\mu$ .<sup>1</sup>

Under certain assumption, it is possible to estimate the population ratio at room temperature from the variation in the effective coupling constant with solvent polarity. If we assume that (a) the last term in eq 2 can be neglected for the solvent  $\text{CCl}_4$ , (b)  $\Delta G^\circ$  is temperature independent for DMF solution, and (c)  ${}^5J_{\text{trans}}$  and  ${}^5J_{\text{cis}}$  are solvent independent, then  ${}^5J_{\text{trans}} = 0.42$  Hz and  ${}^5J_{\text{cis}} = 0.11$  Hz; the difference between the cis and trans coupling constants is similar to the difference between the cis and trans five-bond coupling constant in *N,N*-dimethylacetamide.<sup>15,16</sup> From this it is possible to calculate the population ratios for *tert*-butyl formate in samples II and III at 30° by means of eq 2; these results are given in Table II and in Figure 1. Owing to the temperature dependence of the solvent dielectric constants  $\Delta G^\circ$  will also be temperature dependent, which is in conflict with assumption b above; the value of  $(\epsilon - 1)/(2\epsilon + 1)$  does, however, change very little even for very large variations in  $\epsilon$  when  $\epsilon > 30$ , as for DMF. Assumption b is therefore probably not too crude. As can be seen from Figure 1, where the open circles refer to high-temperature and the crosses to low-temperature data, the agreement between the two data sets is satisfactory.

**Interconversion Barrier.** From the data presented here it is not possible to settle which one of the two possible internal motions, that can cause the s-cis to s-trans interconversion, have the lower activation energy. IBMOL calculations on methyl formate show, however, that the torsional barrier height should be much lower than that of inversion (7 and 31 kcal/mol, respectively).<sup>17</sup>

The rate constants for the hindered rotation process in *tert*-butyl formate, for samples I and II, have been evaluated by means of a total line shape analysis, in the temperature intervals from  $-96.6$  to  $-51.7^\circ$  for I and from  $-111.9$  to  $-43.9^\circ$  for II. The results are plotted as  $\log(\tau T)$  vs.  $1/T$  (Figure 2). Both series of measurements gave reasonably straight lines, and the activa-

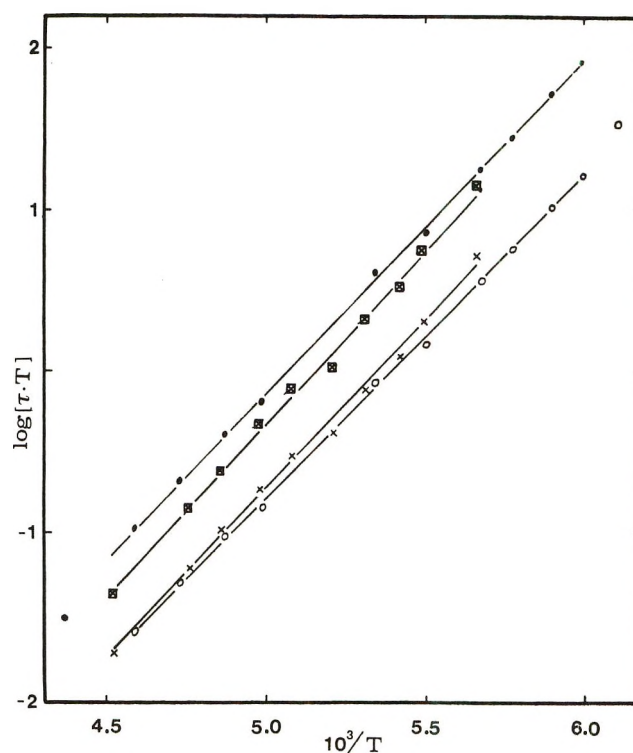


Figure 2.  $\log(\tau T)$  vs.  $1/T$  for *tert*-butyl formate:  $\times$ , sample I, cis barrier;  $\boxtimes$  sample I, trans barrier;  $\circ$ , sample II, cis barrier;  $\bullet$ , sample II, trans barrier.

tion parameters, calculated from the Eyring<sup>18</sup> equation, eq 4, are given in Table III.

$$\ln(\tau T) = \ln(kT/h) - \Delta G^\ddagger/RT =$$

$$\ln(kT/h) - \Delta H^\ddagger/RT + \Delta S^\ddagger/R \quad (4)$$

From Figure 2 it can be seen that the change in the torsional barrier height from solvent I to II is mostly caused by increase in the transition state energy and the s-cis conformer energy compared to the s-trans conformer energy. There is also a small decrease in the transition state energy compared to the s-cis conformer

(15) L. W. Reeves, R. C. Shaddick, and K. N. Shaw, *Can. J. Chem.*, **49**, 3683 (1971).

(16) T. Drakenberg, K.-I. Dahlqvist, and S. Forsén, *J. Phys. Chem.*, **76**, 2178 (1972).

(17) G. Karlström, personal communication.

(18) S. Glasstone, K. J. Laidler, and H. Eyring, "The Theory of Rate Processes," McGraw-Hill, New York, N. Y., 1941.

energy on going from I to II.<sup>19</sup> This is expected since the s-trans conformer should have the lowest dipole moment with the dipole moment of the transition state being intermediate.<sup>1</sup>

The steric interaction between the *tert*-butyl group and the carbonyl oxygen should tend to increase the s-trans conformer energy compared to the methyl formate in the same way as found for amides.<sup>20</sup> On the other hand, the inductive effect from the *tert*-butyl group should tend to increase the torsional barrier through an increased double bond character in the O-C(O) bond. It is thus not possible to predict how the barrier should change from methyl formate to *tert*-butyl formate; we believe, however, that the steric effect dominates (*cf.* amides<sup>21</sup>). The energy difference between the s-trans conformer and the transition state, as well as the energy difference between the s-trans and s-cis conformers, should thus be smaller for *tert*-butyl formate than for methyl formate, which is in good agreement with the present results and those of Subrahmanyan and Piercy.<sup>6a</sup>

From a comparison of the barriers to internal rotation in formates, nitrates,<sup>3</sup> amides,<sup>2</sup> and nitrosamines<sup>4</sup> it is obvious that the substitution of the carbonyl carbon in amides and formates with nitrogen increases the barrier by some 2 kcal/mol, possibly due to nitrogens greater electronegativity. In the same way it is seen

that the barrier height is reduced by more than 10 kcal/mol when an oxygen is substituted for the amino nitrogen in amides or nitrosamines. Both these effects are in agreement with the idea that it is the degree to which the resonance structure (2) contributes to the resonance hybrid that primarily determines the barrier height. The contribution from the resonance structure (2) will decrease with increasing electronegativity on X and decreasing electronegativity on Y.



activity on X and decreasing electronegativity on Y.

*Acknowledgments.* We wish to thank Dr. H. Wannerström for helpful discussions and Dr. W. Egan for valuable linguistic criticism. This work was supported by a grant from the Swedish Natural Science Research Council.

(19) This change is less than the error limits given in Table III, but as can be seen from Figure 2, the  $\tau$  values for the s-cis barrier of sample I are significantly higher than the  $\tau$  values for the s-cis barriers of sample II.

(20) L. A. LaPlanche and M. T. Rogers, *J. Amer. Chem. Soc.*, **86**, 337 (1964).

(21) R. M. Hammaker and B. A. Gugler, *J. Mol. Spectrosc.*, **17**, 356 (1965).

## Chemiluminescence Excited by Atomic Fluorine

by G. Schatz and M. Kaufman\*<sup>1</sup>

*Frick Chemical Laboratory, Princeton University, Princeton, New Jersey 08540 (Received July 11, 1972)*

*Publication costs assisted by the Office of Naval Research*

Visible or ultraviolet luminescence is observed in the reactions of atomic fluorine with many organic and inorganic molecules. In most cases, the radiation is produced by reaction with fluorine atoms generated by electric discharge through either CF<sub>4</sub> or F<sub>2</sub>-Ar mixtures, indicating that the luminescences are due neither to impurities nor to the very exothermic reactions of F<sub>2</sub>. Some emissions, such as OH(A → X) in the reaction with H<sub>2</sub>O, NH(A → X) with NH<sub>3</sub>, and Cl<sub>2</sub>(A → X) with Cl<sub>2</sub>, are best explained as due to atomic combination. In other cases, this mechanism can be precluded by thermochemical arguments. With hydrocarbons, CH, C<sub>2</sub>, CF, and CF<sub>2</sub> bands have been observed. The presence of oxygen is apparently not necessary to produce the CH emission. CO Cameron bands are one of the impurity-caused luminescences which have been observed in the hydrocarbon reactions. They are generated only when the atomic fluorine is produced from CF<sub>4</sub> and are possibly due to the reaction between atomic oxygen and CF.

### Introduction

The emission of light of variable intensity and color is certainly one of the most striking features of flames, and the measurement of the intensity and spectral distribution of this light has long been employed to fur-

ther our understanding of these combustion systems. Such investigations are most profitable when there exists prior knowledge of the mechanism producing the

(1) Correspondence should be addressed to Department of Chemistry, Emory University, Atlanta, Ga. 30322.



emission, since in most flames, explosions, etc., complicating factors, such as temperature gradients, diffusion, and wall effects, make it extremely difficult to unambiguously assign mechanisms. Much of the emission from flames is due to chemiluminescence, *i.e.*, specific reactions which produce products in radiating excited states. For flames employing oxygen or air as the oxidizer, the mechanism generating many of these emissions has been established by studying *atomic* flames, produced by adding reagents to flowing streams containing atomic oxygen or hydrogen. In the present work, luminescences generated in *atomic* fluorine flames have been investigated to acquire greater understanding of combustion systems in which F<sub>2</sub> or fluorine-containing compounds are employed as oxidizing agents.

Chemiluminescence has also played a key role in the study of the kinetics of some of the simplest chemical reactions, those involving atoms. By far the most popular method of measuring the concentration of gas phase N, O, and H has been by titration with a stable compound which reacts rapidly and specifically with the atom according to a known stoichiometry.<sup>2</sup> In chemiluminescent titrations, there is a change in the color or intensity of the luminescence at the equivalence point. To date, for atomic fluorine, no chemiluminescent titration has been devised which does not give erroneous results in the presence of F<sub>2</sub>.<sup>3</sup> Undoubtedly, the lack of availability of such a simple method for measuring fluorine atom concentrations has seriously inhibited work on atomic fluorine chemistry.

Luminescence from fluorine-containing flames<sup>4a</sup> and discharges<sup>4b</sup> has been previously investigated, and there has been extensive work on infrared radiation produced in reactions of atomic fluorine,<sup>5</sup> primarily directed toward laser development. The present paper, however, is the first to report on the visible and ultraviolet radiation produced in systems excited by *atomic* fluorine.

## Experimental Section

One of the most troublesome problems that arises in the study of chemiluminescence is emissions produced by impurities. In this work, spectral features assigned to CN, OH, CO, NO, and NF often appeared when the constituent elements of these molecules were not intentionally being introduced into the system. Contaminants are particularly difficult to avoid when handling atomic fluorine, since this corrosive atom reacts with Pyrex and quartz, liberating atomic oxygen, as well as a number of stable molecules. Fortunately, coating these materials with Teflon greatly reduces the rate at which they are attacked.

As an aid in identifying emissions that are caused by impurities, we have reacted each substrate with fluorine atoms produced by an electric discharge through both CF<sub>4</sub> and F<sub>2</sub>-Ar mixtures. These two sources of fluo-

rine atoms present somewhat different purification problems. Although discharging pure F<sub>2</sub> would not introduce unwanted elements into the system, commercially available F<sub>2</sub> (Matheson Co.) contains an appreciable air impurity. Due to the similarity of the boiling points of F<sub>2</sub>, O<sub>2</sub>, and N<sub>2</sub>, removal of this impurity in a continuous flow system is exceedingly difficult and was not attempted. Thus, unpurified F<sub>2</sub> was diluted five- to tenfold with Ar and discharged with 50–100 W of 2450-MHz power in an Evenson-type cavity<sup>6</sup> on an alumina section of a flow tube, as suggested by Rosner and Allendorf.<sup>3</sup> As anticipated, bands due to oxygen and nitrogen impurities were often excited by this fluorine atom source. The alternative source of atomic fluorine, discharged CF<sub>4</sub> (Matheson Co.), could be readily purified by outgassing at liquid N<sub>2</sub> temperature. It has been shown that a microwave discharge through CF<sub>4</sub> in an alumina discharge section of a Teflon-protected flow system produces primarily atomic fluorine and C<sub>2</sub>F<sub>6</sub>.<sup>7</sup> In addition to undissociated CF<sub>4</sub>, higher fluorocarbons, and a small amount of F<sub>2</sub>, there may also be some CF<sub>2</sub> present in this source of fluorine atoms.

Differences in the spectra excited by the two fluorine atom sources may result from their different concentrations of F and F<sub>2</sub>, as well as from their different impurity concentrations. Generally,  $[F]_{F_2-Ar}/[F]_{CF_4} = 2-5$  and  $[F_2]_{F_2-Ar}/[F_2]_{CF_4} = 3-30$ . At a total pressure of 1.0 Torr, a typical pressure of atomic fluorine is 100  $\mu$  for F<sub>2</sub>-Ar and 30  $\mu$  for CF<sub>4</sub>. In addition, some product of atomic fluorine reactions usually reacts with F<sub>2</sub>, regenerating the fluorine atom. This chain process results in a further increase of the *effective* atomic fluorine concentration in the F<sub>2</sub>-Ar source. It is noteworthy that many of these reactions of F<sub>2</sub> are more exothermic than the original atomic fluorine reaction and thus may be responsible for the observed luminescence. On the other hand, F<sub>2</sub> could eliminate emissions by effectively scavenging an active intermediate.

The experimental arrangement is shown in Figure 1. The alumina tube, in which F<sub>2</sub>-Ar or CF<sub>4</sub> is discharged,

(2) H. Melville and B. G. Gowenlock, "Experimental Methods in Gas Reactions," Macmillan, New York, N. Y., 1964, p 248; F. Kaufman, *J. Chem. Phys.*, **28**, 992 (1958); P. Hartek, R. Reeves, and G. Mannella, *ibid.*, **29**, 608 (1958).

(3) D. E. Rosner and H. D. Allendorf, *J. Phys. Chem.*, **75**, 308 (1971).

(4) (a) R. A. Durie, *Proc. Roy. Soc., Ser. A*, **211**, 110 (1952); G. Skirrow and H. G. Wolfhard, *ibid.*, **232**, 78 (1955); (b) for example, B. A. Thrush and J. J. Zwolenik, *Trans. Faraday Soc.*, **59**, 582 (1963).

(5) J. C. Polanyi and D. C. Tardy, *J. Chem. Phys.*, **51**, 5717 (1969); J. H. Parker and G. C. Pimentel, *ibid.*, **51**, 91 (1969); H. W. Chang, D. W. Setser, M. J. Perona, and R. L. Johnson, *Chem. Phys. Lett.*, **9**, 587 (1971); H. W. Chang, D. W. Setser, and M. J. Perona, *J. Phys. Chem.*, **75**, 2070 (1971); N. Jonathan, C. M. Melliar-Smith, and D. H. Slater, *J. Chem. Phys.*, **53**, 4396 (1970).

(6) F. C. Fehsenfeld, K. M. Evenson, and H. P. Broida, *Rev. Sci. Instrum.*, **36**, 294 (1965); commercially available from the Ophos Instrument Co.

(7) C. E. Kolb and M. Kaufman, *J. Phys. Chem.*, **76**, 947 (1972).

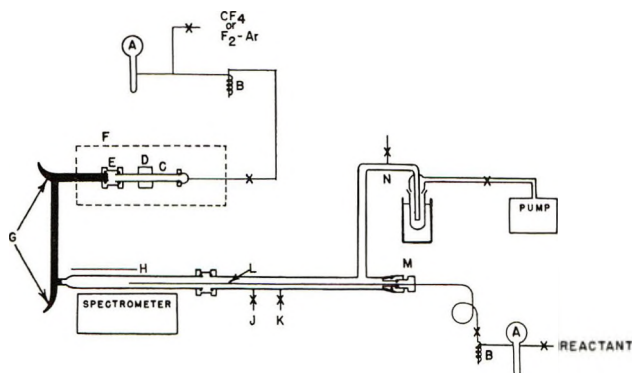


Figure 1. Flow system: A, bulbs for purifying reagents; B, helical traps; C, alumina tube; D, microwave cavity; E, Teflon connector; F, light-tight enclosure; G, light traps; H, Al foil reflector; J, McLeod gauge; K, thermocouple gauge; L, movable inlet tube; M, Teflon O-ring connector; N, trap.

is joined by a Teflon connector to a section of the flow system containing two light traps and the region where the luminescence is viewed. This section is easily removed for frequent cleaning and recoating with Teflon. Reactants are added through a movable inlet, which is positioned for maximum spectrometer response. Pressure is measured with either a McLeod or thermocouple gauge and generally falls in the range 0.5–2.0 Torr. The apparatus does not contain provisions for measuring flow rates. However, some of the more interesting reactions are currently being investigated with a more sophisticated flow system.

Spectra are recorded with a Jarrell-Ash, 0.25-m, Ebert monochromator ( $f/3.5$ ), having an ultimate resolution of *ca.* 3 Å and employing a photomultiplier detector sensitive from 1800 to 6200 Å. For the weaker spectra, an aluminum-foil reflector is employed, and the phototube is cooled with nitrogen chilled to Dry Ice temperature. A nitrogen purge of the monochromator and a Spectrosil viewing section of the flow tube are used when investigating the spectral region below 2000 Å. Wavelength calibration is from known lines in the spectrum and by comparison with a low-pressure mercury lamp. The entire apparatus is installed in a light-tight hood, and suitable shielding is employed so that light from the discharge does not enter the monochromator.

## Results

Table I summarizes the luminescences excited by reacting atomic fluorine with various substrates. Except for the few cases noted, the emissions are produced with both discharged  $\text{CF}_4$  and discharged  $\text{F}_2\text{-Ar}$  as the fluorine atom source. The intensity refers to the strongest line of each band system, with no allowance made for variation of the sensitivity of the spectrometer, which decreases rapidly below 2000 and above 6000 Å. Weak (w) emissions could usually be recorded only with resolution of *ca.* 50 Å. The intensity

of bands attributed to impurities varied considerably, undoubtedly owing to differences in the concentration of the impurity.

Table I: Summary of Luminescences Excited by Atomic Fluorine

Reactant	Emissions detected <sup>a</sup>
$\text{CO}, \text{CO}_2, \text{SO}_2$	None
$\text{H}_2, \text{H}_2\text{S}, \text{NO}_2$	None
$\text{N}_2\text{O}, \text{CCl}_4, \text{CF}_3\text{Cl}$	None
$\text{H}_2\text{O}$	$\text{OH}(\text{A} \rightarrow \text{X}, v' = 0,1)\text{m}$
$\text{NH}_3$	$\text{NH}(\text{A} \rightarrow \text{X}, v' = 0,1)\text{s}, \text{NF}(\text{b} \rightarrow \text{X}, v' = 0)\text{w}$
$\text{Cl}_2$	$\text{Cl}_2(\text{A} \rightarrow \text{X}, v' = 6-12,14)\text{m}$
$\text{Br}_2$	$\text{BrF}(0^+ \rightarrow \text{X}, v' = 1-9)\text{w}$
$\text{CF}_3\text{Br}$	$\text{BrF}(0^+ \rightarrow \text{X}, v' = 2-7)\text{w}$
$\text{CF}_3\text{I}$	$\text{IF}(0^+ \rightarrow \text{X}, v' = 0-6)\text{w}$
Hydrocarbons <sup>b</sup>	$\text{CF}(\text{A} \rightarrow \text{X}, v' = 0,1)\text{m}^c$ and $(\text{B} \rightarrow \text{X}, v' = 0)\text{m},^c$ $\text{CF}_2 \text{ m},^c$ $\text{CO}(\text{A} \rightarrow \text{X}, v' = 2-10)\text{m},^c$ and $(\text{a} \rightarrow \text{X}, v' = 0-5)\text{m},^d,^e$ $\text{C}_2(\text{d} \rightarrow \text{a}, v' = 0-5)\text{s}, \text{CH}(\text{A} \rightarrow \text{X}, v' = 0)\text{s}, \text{C}_3\text{w},^c$ $\text{OH}(\text{A} \rightarrow \text{X}, v' = 0-3)\text{v},^d$ $\text{CN}(\text{B} \rightarrow \text{X}, v' = 0-4)\text{v}^d$

<sup>a</sup> Intensities: s, strong; m, medium; w, weak; v, variable.

<sup>b</sup>  $\text{CH}_4, \text{C}_2\text{H}_2, \text{C}_2\text{H}_4, \text{C}_2\text{H}_6, \text{propylene}, 1,3\text{-butadiene}, \text{benzene}.$

<sup>c</sup>  $\text{F}_2\text{-Ar}$  fluorine atom source only. <sup>d</sup> Due to impurity. <sup>e</sup>  $\text{CF}_4$  fluorine atom source only.

## Discussion

Although we will speculate on mechanisms for some of the observed luminescences, such speculations are at this stage based primarily on thermochemical arguments and on analogy with other chemiluminescent systems. Reliable mechanisms can only be arrived at after detailed study of the dependence of emission intensities on total and partial pressures in the system.

Among the substrates for which no luminescence was observed,  $\text{CO}, \text{CO}_2, \text{N}_2\text{O}, \text{CCl}_4,$  and  $\text{CF}_3\text{Cl}$  react too slowly with atomic fluorine at 25° and pressures of a few Torr to generate appreciable amounts of light.<sup>8</sup> Fluorine does not have a great affinity for electronegative elements, such as oxygen or chlorine. The more electropositive elements in these reactants are protected, either by strong multiple bonds to nonreactive atoms or sterically, as in  $\text{CF}_3\text{Cl}$  and  $\text{CCl}_4$ . (Homann and MacLean, however, have suggested that, at flame temperatures, atomic fluorine is able to displace chlorine from such perhalomethanes.<sup>9</sup>) Not all of the "nonluminescent" reactions are slow, however. The

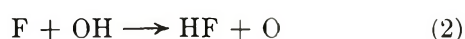
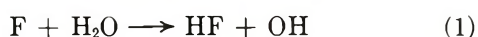
(8) These results have been established by brief studies of these reactions which employed molecular beam analysis, a new technique described in M. Kaufman and C. E. Kolb, *Chem. Instrum.*, **3**, 175 (1971). A more detailed investigation of the reaction with  $\text{CCl}_4$  has been reported in ref 7.

(9) K. H. Homann and D. I. MacLean, *Combust. Flame*, **14**, 409 (1970); *J. Phys. Chem.*, **75**, 3645 (1971).



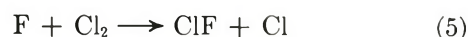
addition of atomic fluorine to  $\text{SO}_2$  to produce  $\text{F}_2\text{SO}_2$  is quite rapid,<sup>8</sup> as are the reactions  $\text{F} + \text{H}_2$  and  $\text{H} + \text{F}_2$ , which produce vibrationally excited HF and are the basis for HF lasers.<sup>5</sup> The combination of hydrogen and fluorine atoms does not provide sufficient energy to populate the first excited *electronic* state of HF.

It is interesting to compare the rapid reactions of atomic fluorine with the hydrides,  $\text{H}_2\text{O}$ ,  $\text{H}_2\text{S}$ , and  $\text{NH}_3$ . In the  $\text{H}_2\text{O}$  system, the A state of OH can energetically be populated by three-body combination of O and H atoms, these being generated by a sequence such as



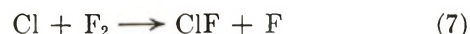
Reaction 3, which involves two intermediates, probably does proceed at an appreciable rate in this system, since its rate constant is *ca.*  $10^{13}$   $\text{cm}^3/\text{mol}\cdot\text{sec}$ ,<sup>10</sup> and oxygen atoms do not react with the major components of the system ( $\text{H}_2\text{O}$ ,  $\text{F}_2$ , and HF). Atomic combination has been proposed for  $\text{OH}(\text{A} \rightarrow \text{X})$  emission in combustion reactions employing  $\text{O}_2$ .<sup>11</sup> The mechanism is also in accord with the absence of  $\text{SH}(\text{A} \rightarrow \text{X})$  emission in the  $\text{H}_2\text{S}$  reaction, since combination of a sulfur atom with a hydrogen atom provides 5 kcal less energy than that necessary to populate the A state of SH. Durie has observed  $\text{SH}(\text{A} \rightarrow \text{X})$  emission from a  $\text{H}_2\text{-F}_2$  flame contaminated with sulfur-containing compounds. However, at flame temperatures, sufficient thermal energy is available to form the A state. Sulfur is deposited in the reaction of atomic fluorine with  $\text{H}_2\text{S}$ , and its formation could be initiated by a reaction analogous to (3). The reaction with  $\text{NH}_3$  completes the pattern, since here the observed  $\text{A}(^3\Pi) \rightarrow \text{X}(^3\Sigma^-)$  bands of NH can also be excited by combination of thermal atoms.

Both  $\text{Cl}_2$  and  $\text{Br}_2$  produce yellow luminescence when added to atomic fluorine. The glowing region in these reactions extends many centimeters downstream of the halogen inlet. In the  $\text{Cl}_2$  case the emission is due to the  $\text{A}(^3\Pi_0) \rightarrow \text{X}(^1\Sigma)$  transition of  $\text{Cl}_2$ , strongly suggesting that the mechanism producing the luminescence is<sup>12</sup>



Since recombination of atomic chlorine would be slow at our pressures, the large extent of the emitting zone is consistent with reaction 5 being very fast.<sup>13</sup> The intensity of the emission was measured with a photocell-filter combination sensitive in the range 4500–6200 Å and was found to maximize at a  $\text{Cl}_2$  flow very close to that which just removed all the atomic fluorine.<sup>14</sup> We have also noted that  $\text{F}_2$  concentrations, measured mass

spectrometrically, are hardly affected by addition of sufficient  $\text{Cl}_2$  to maximize the emission, indicating that the reaction



must be quite slow at 25°. These observations suggest that the reaction with  $\text{Cl}_2$  may be of some use as a chemiluminescent titration for atomic fluorine in the presence of molecular fluorine. In the  $\text{Br}_2$  reaction, the yellow color is due to the  $^3\Pi_0 \rightarrow \text{X}(^1\Sigma)$  transition of  $\text{BrF}$ , with bands originating from  $1 \leq v' \leq 9$ .  $\text{Br}_2$  emission from atomic bromine combination occurs at wavelengths longer than 6500 Å<sup>15</sup> and would not be detected by our photomultiplier.

The  $0^+ \rightarrow \text{X}$  transition of the corresponding interhalogen is also observed in the reaction of atomic fluorine with  $\text{CF}_3\text{Br}$  and  $\text{CF}_3\text{I}$ . There is considerable evidence that these reactions do not proceed by halogen displacement at room temperature.<sup>16</sup> Thus, either free Br and I atoms are formed by secondary reactions in these systems or the emission is produced by a mechanism other than atomic combination.

Characteristic luminescence is found for the reaction of atomic fluorine with hydrocarbons, as well as for molecules such as methyl bromide and ethylene oxide, which contain other elements in addition to carbon and hydrogen. The visible light from these systems is the brightest of all the reactions we have investigated, with the most intense bands being those of  $\text{CH}(\text{A} \rightarrow \text{X})$  and  $\text{C}_2$  (Swan system). The emissions are similar to those observed by Durie from flames of organic substances burning in  $\text{F}_2$ <sup>4a</sup> and also resemble the spectra of organics burning in  $\text{O}_2$  or air.<sup>11</sup> In the latter case, CH bands are generally ascribed to reactions of oxygen-containing species.<sup>17</sup> In our atomic fluorine reactions, however, CH emission was most prominent in runs with minimum oxygen contamination (as measured by the intensity of OH emission), and thus oxygen-containing

(10) D. D. Drysdale and A. C. Lloyd, *Oxid. Combust. Rev.*, **4**, 157 (1950).

(11) A. G. Gaydon, "The Spectroscopy of Flames," Wiley, New York, N. Y., 1957. The reaction may proceed by three-body recombination or by preassociation as suggested by S. Ticktin, G. Spindler, and H. I. Schiff, *Discuss. Faraday Soc.*, No. 44, 218 (1967).

(12) L. W. Bader and E. A. Ogryzlo, *J. Chem. Phys.*, **41**, 2926 (1964); M. A. A. Clyne and J. A. Coxon, *Proc. Roy. Soc., Ser. A*, **298**, 424 (1967); M. A. A. Clyne and D. H. Stedman, *Trans. Faraday Soc.*, **64**, 1816 (1968).

(13) J. Warnatz, H. Gg. Wagner, and C. Zetzsch, *Ber. Bunsenges. Phys. Chem.*, **75**, 119 (1971).

(14) The fluorine atoms were simultaneously monitored by molecular beam analysis; see ref 7 and 8.

(15) D. B. Gibbs and E. A. Ogryzlo, *Can. J. Chem.*, **43**, 1905 (1965).

(16) I. O. Leipunskii, I. I. Morozov, and V. L. Tal'roze, *Dokl. Akad. Nauk SSSR*, **198**, 1367 (1971); J. Bozzelli, C. Kolb, and M. Kaufman, to be published.

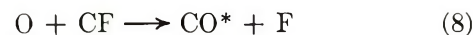
(17) P. H. Kydd and W. I. Foss, Eleventh Symposium on Combustion, The Combustion Institute, 1967, p 1179; J. Peeters, J. F. Lambert, P. Hertoghe, and A. Van Tiggelen, Thirteenth Symposium on Combustion, The Combustion Institute, 1971, p 321; see ref 11.

species are probably not necessary for its production. An oxygen-free reaction, that of two excited  $\text{CH}_2$  radicals, has recently been proposed by Quickert<sup>18</sup> to explain CH emission in the  $\text{O} + \text{C}_2\text{H}_2$  system.

Surprisingly, at wavelengths shorter than 3000 Å, the emission from hydrocarbon reactions is dramatically different depending on whether  $\text{F}_2\text{-Ar}$  or  $\text{CF}_4$  is used as the source of atomic fluorine. With  $\text{F}_2\text{-Ar}$ , the  $\text{A} \rightarrow \text{X}$  and  $\text{B} \rightarrow \text{X}$  transitions of CF, as well as bands of  $\text{CF}_2$ , are detected when fairly high concentrations of  $\text{F}_2$  are employed. Neither the A state (123 kcal/mol) nor the B state (141 kcal/mol) of CF ( $D_0 = 110$  kcal/mol<sup>4b</sup>) is accessible by combination of thermal, ground-state carbon and fluorine atoms. Thus, this mechanism can be ruled out, even though there is some heating of the flow tube at high  $\text{F}_2$  partial pressures. Although CF bands were not reported in Duric's study of  $\text{F}_2$  flames, they were observed by Skirrow and Wolfhard in the emission from  $\text{ClF}_3$ -supported flames.<sup>4a</sup> The reaction between discharged  $\text{F}_2\text{-Ar}$  and hydrocarbons also produces strong CO fourth positive impurity bands, extending to the short-wavelength limit of the spectrometer.

CF,  $\text{CF}_2$ , and CO fourth positive bands were never observed using discharged  $\text{CF}_4$ . Instead, in the region 1930–2760 Å, some 40 bands were generated by reaction with many hydrocarbons. Except for a few very weak features, all these bands can be assigned to the Cameron system,  $\text{a}(^3\Pi) \rightarrow \text{X}(^1\Sigma)$ , of CO. This is a surprising conclusion, since the  $\text{a}(^3\Pi)$  state of CO has a lifetime of approximately  $10^{-2}$  sec and is easily quenched by a variety of diamagnetic and paramagnetic collision partners.<sup>19</sup> However, the fit to the Cameron bands is quite good considering the quality of the spectra. Further confidence in this assignment is gained from the observation that no shifts or splittings of bands are observed when  $\text{CH}_2\text{D}_2$  is substituted for  $\text{CH}_4$  as the substrate. Since the intensity of the Cameron bands is not greatly affected by different methods of purifying the reagents, we must conclude that they are mainly due to the small amount of oxygen that is liberated by wall reactions. The bands are not produced by atomic fluorine formed by discharging  $\text{F}_2\text{-Ar}$  mixtures. Thus,

a reactant unique to the  $\text{CF}_4$  system must be necessary for their appearance. The reaction



provides an appealing mechanism for this luminescence because of its simplicity and the fact that it can populate the  $\text{a}(^3\Pi)$  state, but not the  $\text{A}(^1\Pi)$  state of CO. Some 15 kcal of vibrational excitation of the CF would be necessary, however, to excite levels up to  $v' = 5$ , from which emission is observed.

We have thus shown that visible and ultraviolet luminescence is quite a common occurrence in systems excited by atomic fluorine. In most cases these emissions can be produced with both discharged  $\text{CF}_4$  and discharged  $\text{F}_2\text{-Ar}$  mixtures as the source of fluorine atoms, indicating that they are due neither to reactions of impurities nor to the very exothermic reactions of  $\text{F}_2$ . One can also rule out a mechanism involving energy transfer from excited  $\text{F}_2$  molecules produced by fluorine atom recombination, analogous to the current explanation for many of the emissions excited by "active" nitrogen,<sup>20</sup> since in the fluorine case this would not supply sufficient energy to generate visible light. While in several instances, three-body combination of the constituent atoms of the emitting molecule seems to be a reasonable mechanism for the emission, in other cases this can be precluded by thermochemical or kinetics arguments. Further investigations directed toward understanding these interesting phenomena are currently underway.

*Acknowledgment.* The authors would like to thank J. Bozzelli, B. Hertzler, and Dr. C. E. Kolb for considerable aid with these experiments. This work was supported by the Office of Naval Research under Contract No. N0014-67-A-0151-0013.

(18) K. A. Quickert, *J. Phys. Chem.*, **76**, 825 (1972).

(19) G. M. Lawrence, *Chem. Phys. Lett.*, **9**, 575 (1971); T. S. Wanchop and H. P. Broida, *J. Chem. Phys.*, **56**, 330 (1972); T. G. Slanger and G. Black, *ibid.*, **55**, 2164 (1971); T. C. James, *J. Mol. Spectrosc.*, **40**, 545 (1971).

(20) A. H. Wright and C. A. Winkler, "Active Nitrogen," Academic Press, New York, N. Y., 1968.



# Vibrational Analyses and Barrier to Internal Rotation of 1,1-Dichloroethane and 1,1-Dichloroethane-*d*<sub>4</sub>

by J. R. Durig,\* A. E. Sloan, and J. D. Witt

Department of Chemistry, University of South Carolina, Columbia, South Carolina 29208 (Received June 15, 1972)

The infrared spectra of gaseous and solid 1,1-dichloroethane and 1,1-dichloroethane-*d*<sub>4</sub> have been recorded from 140 to 4000 cm<sup>-1</sup>. The corresponding Raman spectra of the gases and liquids have also been recorded and depolarization values have been measured. All spectra have been interpreted in detail and the 18 normal vibrations have been characterized on the basis of the band contours, isotopic shifts, depolarization values, and normal coordinate calculations. The internal torsional mode was observed at 196 cm<sup>-1</sup> in the infrared spectrum of solid CD<sub>3</sub>CDCl<sub>2</sub>. The threefold barrier to rotation was calculated to be 4.77 kcal/mol. This value is compared to those reported for other chloroethanes.

## Introduction

Since bromine and chlorine substitution appears to affect the barriers to internal rotation in ethane derivatives more than any of the other halogens, it would appear that a comparison of the theoretical and experimental barriers of several bromo- or chloro-substituted ethanes would provide a rather critical test of both empirical and theoretical barrier predictions. Most of the accurately determined barriers have been obtained by the microwave technique but this method does not readily lend itself to the study of multiple bromine or chlorine substitution because of the quadrupole splittings. Recently we reported the methyl torsional frequencies of 290 and 304 cm<sup>-1</sup> for methylchloroform<sup>1</sup> and methylbromoform,<sup>2</sup> respectively, which gave barriers of 5.5 and 6.08 kcal/mol. It has been postulated in the past that after the initial substitution of fluorine, chlorine, or bromine for a hydrogen atom on "one end" of an ethane molecule, that the barrier height to methyl rotation would not be drastically affected by substitution of the second and third halogen on the "same" end. Thus, the recent data for CH<sub>3</sub>CCl<sub>3</sub>, CH<sub>3</sub>CBr<sub>3</sub>, as well as that for CH<sub>3</sub>CF<sub>2</sub>Cl<sup>3</sup> indicate that this view may not be correct.

There is considerable conflict as to the effect of the addition of a second chlorine atom to the "same" end of ethane. A band assigned as the torsional frequency was reported at 239 cm<sup>-1</sup> in the Raman spectrum of the liquid by Daasch, *et al.*,<sup>4</sup> but in a more recent Raman study by Allen, *et al.*,<sup>5</sup> the 239-cm<sup>-1</sup> band could not be confirmed. Instead the latter authors report a weak band at 222 cm<sup>-1</sup>. The absence of other bands in this region of the Raman spectrum and the complete absence of bands below 274 cm<sup>-1</sup> in the infrared spectrum of 2-mm thick liquid films led Allen, *et al.*, to tentatively assign the torsional mode to the 222-cm<sup>-1</sup> Raman line. The heat capacity of 1,1-dichloroethane has been measured<sup>6</sup> and a comparison of the statistical and experimental entropy resulted in a barrier height

of 3550 ± 450 cal/mol. It is interesting to note that in the heat capacity report the authors state that an unpublished infrared spectrum of liquid 1,1-dichloroethane showed a weak band at 240 cm<sup>-1</sup> which was compatible with the thermodynamic barrier. Wulff<sup>7</sup> has calculated a barrier height of 3490 ± 200 cal/mol from thermal data on the solid phase.

We recently investigated<sup>1</sup> the far-infrared spectrum of 1,1-dichloroethane and reported the torsional mode at 231 and 232 cm<sup>-1</sup> for the vapor and solid, respectively. However, we could find no indication of the reported Raman bands. About the same time as our paper appeared, a neutron inelastic scattering study of 1,1-dichloroethane was reported by Brier, *et al.*<sup>8</sup> These authors reported bands at 290 and ~230 cm<sup>-1</sup> with the higher frequency one being more intense and tentatively assigned to the torsional mode for the gas. This value did not differ significantly from the 293 ± 10 cm<sup>-1</sup> torsional frequency which Brier<sup>9</sup> reported earlier for the liquid. Brier, *et al.*, suggested that the ~230 cm<sup>-1</sup> might be a hot band transition,  $\nu = 2 \leftarrow 1$ , of the anharmonic torsion but pointed out that it should only be about 12 cm<sup>-1</sup> lower than the fundamental. They concluded that further work on this molecule is required. Thus, we have investigated the infrared and Raman spectrum of the corresponding deuterium com-

(1) J. R. Durig, S. M. Craven, K. K. Lau, and J. Bragin, *J. Chem. Phys.* **54**, 479 (1971).

(2) J. R. Durig, S. M. Craven, C. W. Hawley, and J. Bragin, *ibid.*, **57**, 131 (1972).

(3) C. Graner and C. Thomas, *ibid.*, **49**, 4160 (1968).

(4) L. W. Daasch, C. Y. Liang, and J. R. Nielson, *ibid.*, **22**, 1293 (1954).

(5) G. Allen, P. N. Brier, and G. Lane, *Trans. Faraday Soc.*, **63**, 824 (1967).

(6) J. M. Li and K. S. Pitzer, *J. Amer. Chem. Soc.*, **78**, 1077 (1956).

(7) C. A. Wulff, *J. Chem. Phys.*, **39**, 1227 (1963).

(8) P. N. Brier, J. S. Higgins, and R. H. Bradley, *Mol. Phys.*, **21**, 721 (1971).

(9) P. N. Brier, *J. Mol. Struct.*, **6**, 23 (1970).

pound in order to try and remove the discrepancies which currently exist for the torsional mode. The Raman spectrum of the "light" compound in the gaseous state has not been previously reported nor has there been any data reported on the mid-infrared spectrum of the solid.

### Experimental Section

$\text{CH}_3\text{CHCl}_2$  was obtained from Columbia Organic Chemicals and purified by vapor-phase chromatography.  $\text{CD}_3\text{CDCl}_2$  was prepared by the addition of  $\text{PCl}_5$  to acetaldehyde- $d_4$  which was obtained from Merck & Co., Inc., of Canada. The resulting product was distilled and further purified by vapor-phase chromatography using a Carbowax column at  $60^\circ$ .

The far-infrared spectra were recorded from 33 to  $350\text{ cm}^{-1}$  with a Beckman Model IR-11 spectrophotometer. The atmospheric water vapor was removed from the instrument housing by flushing with dry air. The instrument was calibrated by using atmospheric water vapor.<sup>10</sup> Single beam energy checks were made periodically to ensure the energy transmission was at least 10–15% at all times. A low-temperature cell similar to one described earlier<sup>11</sup> was employed to record the spectra of solid samples. Modifications have been made to allow the circulation of cold nitrogen liquid through a hollow brass cold finger. A wedged silicon window was used for the solid film support plate. Conventional vacuum deposition techniques were used to obtain the solid film on the silicon substrate with the additional precaution that the samples were allowed to sublime slowly onto the silicon plate from the solid phase. The silicon substrate was held at  $-190^\circ$  during deposition. The solid films were then annealed until there was no change in the spectrum.

The Raman spectra were recorded on a Cary Model 82 Raman spectrophotometer<sup>12</sup> equipped with an argon ion laser source with a frequency of  $5145\text{ \AA}$  for excitation. The spectra of gas samples were recorded using a multipass gas cell, and the spectra of the liquids were obtained with the samples contained in sealed capillary tubes.

The mid-infrared spectra were recorded from 4000 to  $350\text{ cm}^{-1}$  with a Perkin-Elmer Model 620 spectrophotometer. A low-temperature cell equipped with a CsI window was employed to record the spectra of solid samples. Again, conventional vacuum techniques were used to obtain the solid film on the CsI substrate. A 20-cm gas cell with CsI windows was employed to record the spectra of the gaseous samples.

### Vibrational Assignment

Assuming  $C_s$  molecular symmetry, the 18 fundamental modes of 1,1-dichloroethane may be divided into  $11a'$  and  $7a''$  vibrations. The  $a'$  vibrations have polarized Raman bands, and may have B, C, or B/C hybrid contours in the infrared spectrum. The  $a''$

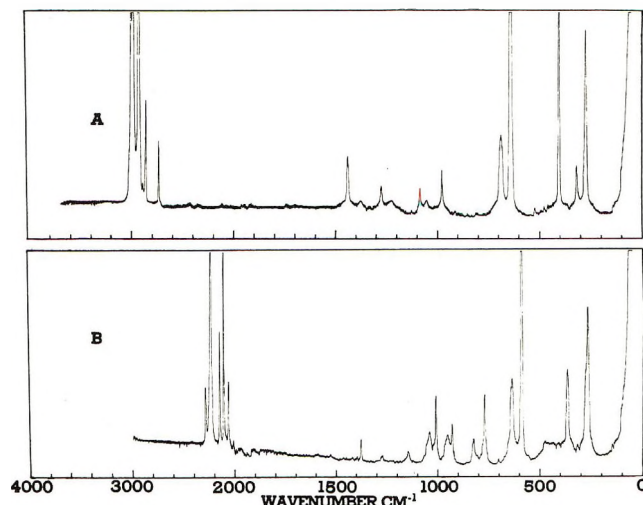


Figure 1. (A) Raman spectrum of  $\text{CH}_3\text{CHCl}_2$  in the gas phase. (B) Raman spectrum of  $\text{CD}_3\text{CDCl}_2$  in the gas phase.

vibrations have depolarized Raman lines and type A band contours in the infrared spectrum.

For the calculation of the infrared band contours, the moments of inertia for the "light" molecule were assumed to be 219.26, 154.17, and  $79.31\text{ amu \AA}^2$ ; the moments for the "heavy" molecule were 234.88, 159.80, and  $97.34\text{ amu \AA}^2$ . The resulting P-R separations for type A, B, and C contours were 15.8, 10.8, and  $18.0\text{ cm}^{-1}$ , respectively, in the "light" molecule, and 15.2, 8.7, and  $22.8\text{ cm}^{-1}$ , respectively, in the "heavy" compound.

The Raman spectra of the gases are shown in Figure 1. The polarized lines were characterized by strong Q branches whereas the depolarized lines were usually quite broad with considerably weaker Q branches. By using the Raman depolarization measurements along with the characteristic infrared band contours, a complete vibrational assignment is proposed. The frequencies for the observed bands along with the vibrational assignment are summarized in Tables I and II, for the light and heavy molecules, respectively.

The infrared spectrum of gaseous  $\text{CH}_3\text{CHCl}_2$  shows (see Figure 2) a type C band at  $3015\text{ cm}^{-1}$  which is partially overlapped, with a type A band centered at  $2995\text{ cm}^{-1}$ . The  $3015\text{-cm}^{-1}$  band has a polarized Raman counterpart, and it is assigned as the C-H stretch,  $\nu_1$ . With deuteration this band shifts to  $2168\text{ cm}^{-1}$ . A polarized Raman band appearing at  $2997\text{ cm}^{-1}$  in the gas phase might be considered to be the counterpart of the  $2995\text{-cm}^{-1}$  infrared band. However, the  $2995\text{-cm}^{-1}$  band has a type A contour, and, therefore, is unequivocally assigned as an  $a''$  vibration. Since the polarized band at  $2997\text{ cm}^{-1}$  is due to an  $a'$  motion, we assign the

(10) R. T. Hall and J. M. Dowling, *J. Chem. Phys.*, **47**, 2454 (1967); **52**, 1161 (1970).

(11) F. G. Baglin, S. F. Bush, and J. R. Durig, *ibid.*, **47**, 2104 (1967).

(12) This instrument was purchased with funds from the National Science Foundation through Grant No. GP-28068.



**Table I:** Observed Vibrational Frequencies for 1,1-Dichloroethane<sup>a</sup>

Raman $\Delta\nu$ , cm <sup>-1</sup>		Infrared $\nu$ , cm <sup>-1</sup>		Calculated values	Assignment and approximate descriptions
Gas	Liquid	Gas	Solid		
3017	3009 m, p	3015 m, C	2999	3025	$\nu_1(a')$ C-H stretch (97%)
2997	2991 m, p	3001 w	2990	3003	$\nu_2(a')$ CH <sub>3</sub> antisymmetric stretch (97%)
	2990 m, dp	2995 m, A	2980	3004	$\nu_{12}(a'')$ CH <sub>3</sub> antisymmetric stretch (99%)
2947	2936 s, p	2946 m, B	2931	2949	$\nu_3(a')$ CH <sub>3</sub> symmetric stretch (100%)
2879	2864 w, p	2876 w, B	2864		$2\nu_4 = 2896$
2749	2740 w		2738		$2\nu_5 = 2762$
1448	1442 m, dp	1446 m, C	1441	1450	$\nu_4(a')$ CH <sub>3</sub> antisymmetric deformation (92%)
			1435	1450	$\nu_{13}(a'')$ CH <sub>3</sub> antisymmetric deformation (92%)
1387	1380 vw, p	1381 m, B/C	1376	1367	$\nu_5(a')$ CH <sub>3</sub> deformation (100%)
1284	1278 w, p	1280 m, B	1283	1297	$\nu_6(a')$ CH symmetric bend (78%), C-C stretch (18%)
			1278		
1232	1227 vw, dp	1229 s, A	1208	1219	$\nu_{14}(a'')$ CH antisymmetric bend (87%)
1089	1087 w, p	1091 w, ?	1088	1056	$\nu_7(a')$ CH <sub>3</sub> in-plane rock (60%), C-C stretch (21%)
1067	1055 vw, dp	1058 s, A	1044	1051	$\nu_{15}(a'')$ CH <sub>3</sub> out-of-plane rock (66%), CH bend (13%)
984	979 m, p	982 B	978	970	$\nu_8(a')$ C-C stretch (50%), CH <sub>3</sub> in-plane rock (22%), CH symmetric bend (20%)
967					$\nu_{16} + \nu_{11}$
707	689 m, dp	704 s, A	680		$\nu_{16}(a'')$ CCl <sub>2</sub> antisymmetric stretch (55%), CCl <sub>2</sub> twist (27%), CH <sub>3</sub> rock (16%)
652	643 vs, p	650 m, B	641	654	$\nu_9(a')$ CCl <sub>2</sub> symmetric stretch (71%), CCl <sub>2</sub> scissor (14%)
636					?
405	406 s, p	405 w, B		399	$\nu_{10}(a')$ CCl <sub>2</sub> wag (60%), CCl <sub>2</sub> stretch (16%)
	319 m, dp		324	317	$\nu_{17}(a'')$ CCl <sub>2</sub> twist (60%), CCl <sub>2</sub> antisymmetric stretch (40%)
275	276 s, p		280	269	$\nu_{11}(a')$ CCl <sub>2</sub> scissor (70%), CCl <sub>2</sub> stretch (10%)
			274	277	$\nu_{18}(a'')$ CH <sub>3</sub> torsion (98%)

<sup>a</sup> Abbreviations used are as follows: vw = very weak, w = weak, m = medium, s = strong, vs = very strong, bd = broad, p = polarized, dp = depolarized; A, B, C refer to characteristic band contour types observed in the infrared spectrum of the gas phase.

2997, 2995 cm<sup>-1</sup> pair as the approximately degenerate antisymmetric CH<sub>3</sub> stretches,  $\nu_2$  and  $\nu_{12}$ . In the heavy compound, these vibrations shift to 2253 and 2248 cm<sup>-1</sup> with the higher frequency one being depolarized. The symmetric CH<sub>3</sub> stretch,  $\nu_3$ , is assigned to the strong, polarized Raman bands at 2947 and 2128 cm<sup>-1</sup> in the light and heavy molecules, respectively.

The a' component of the antisymmetric CH<sub>3</sub> deformation,  $\nu_4$ , is assigned to a sharp Q branch in the infrared spectrum at 1446 cm<sup>-1</sup> which shifts to 1047 cm<sup>-1</sup> for the heavy molecule. The a'' component,  $\nu_{13}$ , is not obvious in the spectrum of the gas, although two bands at 1441 and 1435 cm<sup>-1</sup> are clearly visible in the spectrum of the low-temperature solid. The symmetric CH<sub>3</sub> deformation,  $\nu_5$ , is assigned to a weak Q branch at 1381 cm<sup>-1</sup> (apparently, the center of a B/C hybrid contour) which shifts to 1013 cm<sup>-1</sup> in 1,1-dichloroethane-d<sub>4</sub>.

Between 1200 and 1300 cm<sup>-1</sup>, there are two infrared bands which are due to the CCH bending vibrations. A type B contour centered at 1280 cm<sup>-1</sup> on the infrared is assigned as  $\nu_6$ , the in-plane C-H bending motion. The out-of-plane bend,  $\nu_{14}$ , is assigned to a strong infrared band of type A contour centered at 1229 cm<sup>-1</sup>. Deuteration results in a shift to 964 cm<sup>-1</sup> for  $\nu_{14}$ . The assignment for the in-plane bend is less certain because

of the strong mixing with the symmetric CD<sub>3</sub> deformation. However,  $\nu_6$  is tentatively assigned to a polarized Raman band near 772 cm<sup>-1</sup> in the deuterated molecule.

The in-plane and out-of-plane CH<sub>3</sub> rocks,  $\nu_7$  and  $\nu_{15}$ , are assigned to bands at 1091 and 1058 cm<sup>-1</sup>, respectively. The 1091-cm<sup>-1</sup> band is featureless in the infrared, but has a weak polarized Raman counterpart. The 1058-cm<sup>-1</sup> band has a well-defined type A contour which is indicative of an a'' mode. The type B band centered at 982 cm<sup>-1</sup> with a polarized Raman counterpart is assigned as  $\nu_8$ , the C-C stretch. Normal coordinate calculations reveal a strong mixing of CH<sub>3</sub> rock/C-C stretch in both  $\nu_7$  and  $\nu_8$ .

In the heavy compound, a type A band in the infrared spectrum at 829 cm<sup>-1</sup> is assigned as the out-of-plane CH<sub>3</sub> rock,  $\nu_{15}$ . Location of the in-plane CH<sub>3</sub> rock is more difficult because of greater mixing of the normal modes in the deuterated molecule. However, for completeness, the band at 933 cm<sup>-1</sup> is assigned as  $\nu_7$ . A weak, polarized Raman band with a strong infrared counterpart of type B contour at 1150 cm<sup>-1</sup> is assigned as predominantly the C-C stretching motion for the deuterated molecule on the basis of the normal coordinate calculations.

The symmetric and antisymmetric CCl<sub>2</sub> stretches,  $\nu_9$  and  $\nu_{16}$ , are assigned to bands at 650 and 704 cm<sup>-1</sup>,

**Table II:** Observed Vibrational Frequencies for 1,1-Dichloroethane- $d_4^a$ 

Raman $\Delta\nu$ , $\text{cm}^{-1}$		Infrared $\nu$ , $\text{cm}^{-1}$		Calculated values	Assignment and approximate descriptions
Gas	Liquid	Gas	Solid		
2325	vw				?
2311	2298 w, p		2298		$2\nu_8$
2307					
2253	2248 s, dp	2256 m, C	2243	2248	$\nu_{12}(a'')$ CD <sub>3</sub> antisymmetric stretch (98%)
2248	2242 s, p	2248 m, A	2238	2245	$\nu_2(a')$ CD <sub>3</sub> antisymmetric stretch (67%), CD stretch (30%)
			2193		1045 + 1149 = 2194
2168	2158 s, p	2165 w, B	2156	2230	$\nu_1(a')$ CD stretch (68%), CD <sub>3</sub> antisymmetric stretch (31%)
2128	2118 vs, p	2125 w, B	2116	2124	$\nu_3(a')$ CD <sub>3</sub> symmetric stretch (98%)
2105	(shoulder)				?
2081	2072 m, p	2084 w, B	2078		$2\nu_{4,13} = 2094$
2073					
2025	2022 w, p		2020		$2\nu_5 = 2028$
	1380 w, p				$\nu_{10} + \nu_5 = 1387$
	1276 w, p				$2\nu_{16} = 1284$
1150	1150 w, p	1151 s, B	1149	1172	$\nu_8(a')$ C-C stretch (70%), CD <sub>3</sub> symmetric deformation (23%), CD bend (20%)
	1045 w, dp	1047 m, C	1045	1045, 1045	$\nu_{4,13}(a', a'')$ CD <sub>3</sub> antisymmetric deformation (92%), CD <sub>3</sub> antisymmetric deformations (95%)
1013	1015 m, p	1014 m, B	1016	1025	$\nu_5(a')$ CD <sub>3</sub> symmetric deformation (67%), CD bend (21%)
957 bd	957 w, dp	964 vs, A	943	1010	$\nu_{14}(a'')$ CD antisymmetric bend (43%), CD <sub>3</sub> rock (26%), CCl <sub>2</sub> stretch (21%)
			937		?
933	933 m, p		932	872	$\nu_7(a')$ CD <sub>3</sub> in-plane rock (45%), CD bend (21%)
818 bd	829 w, dp	829 m, A	819	797	$\nu_{15}(a'')$ CD <sub>3</sub> out-of-plane rock (32%), CD bend (56%)
772	774 m, p	775 m, B	776	749	$\nu_6(a')$ CD in-plane bend (45%), CD <sub>3</sub> rock (21%), C-C stretch (18%)
649 bd	649 m, dp	650 s?	637	602	$\nu_{16}(a'')$ CCl <sub>2</sub> antisymmetric stretch (47%), CD <sub>3</sub> rock (36%), CCl <sub>2</sub> twist (10%)
594	601 vs, p	600 m, B	597	595	$\nu_3(a')$ CCl <sub>2</sub> symmetric stretch (64%), CD <sub>3</sub> rock (22%), CCl <sub>2</sub> scissor (10%)
484 bd	483 vw, p				?
369	372 s, p	368	366	365	$\nu_{10}(a')$ CCl <sub>2</sub> wag (59%), CCl <sub>2</sub> stretch (12%)
358					"Hot band"
342					"Hot band"
272	275 m, dp (shoulder)		283	292	$\nu_{17}(a'')$ CCl <sub>2</sub> twist (62%), CCl <sub>2</sub> stretch (32%)
264	271 s, p		276	267	$\nu_{11}(a')$ CCl <sub>2</sub> scissor (71%)
			196	198	$\nu_{18}(a'')$ CD <sub>3</sub> torsion (98%)

<sup>a</sup> Abbreviations used in this table are identical with those in Table I.

respectively. The 704- $\text{cm}^{-1}$  band has a distorted type A contour, whereas the 650- $\text{cm}^{-1}$  band gives rise to a very strong polarized Raman line. These bands are shifted to 594 and 650  $\text{cm}^{-1}$  in the spectrum of the heavy molecule. There are three other low lying vibrational modes expected for the CCl<sub>2</sub> group; these are the CCl<sub>2</sub> wag ( $a'$ ), the CCl<sub>2</sub> twist ( $a''$ ), and the CCl<sub>2</sub> scissor ( $a'$ ). The two  $a'$  modes,  $\nu_{10}$  and  $\nu_{11}$ , are readily identified from the Raman spectrum as strong bands at 405 and 275  $\text{cm}^{-1}$ , respectively. The twisting motion,  $\nu_{17}$ , is assigned to a depolarized line of medium intensity at 319  $\text{cm}^{-1}$ . On deuteration,  $\nu_{10}$  shifts to 369  $\text{cm}^{-1}$ , while  $\nu_{11}$  shifts to 264  $\text{cm}^{-1}$ . The CCl<sub>2</sub> twist,  $\nu_{17}$ , is assigned to a band at 272  $\text{cm}^{-1}$  which appears as a high-frequency shoulder on  $\nu_{11}$  for the heavy compound.

With this vibrational assignment along with that given for the torsional mode in the next section, the Teller-Redlich product rule was found to be satisfied

within 3.5% for the  $a''$  symmetry species and 6% for the  $a'$  symmetry species. The difference between the experimental and calculated values for the  $a''$  modes is consistent with that expected due to anharmonicity. However, the difference for the  $a'$  modes is larger than expected from this effect and may be due to Fermi resonance for which no corrections have been made.

### Torsional Mode and Barrier

An inspection of Figure 3B shows a broad, well-defined peak at 196  $\text{cm}^{-1}$  in the spectrum of solid CD<sub>3</sub>-CDCl<sub>2</sub>. Since the spectrum was taken at such a low temperature, it is clear that it is not a difference band. Similarly it cannot be ascribed to a lattice mode or a two-phonon process because the band did not show the expected broadening or frequency shift with temperature that is observed for such modes. Thus, it is concluded that this band is the torsional mode since the



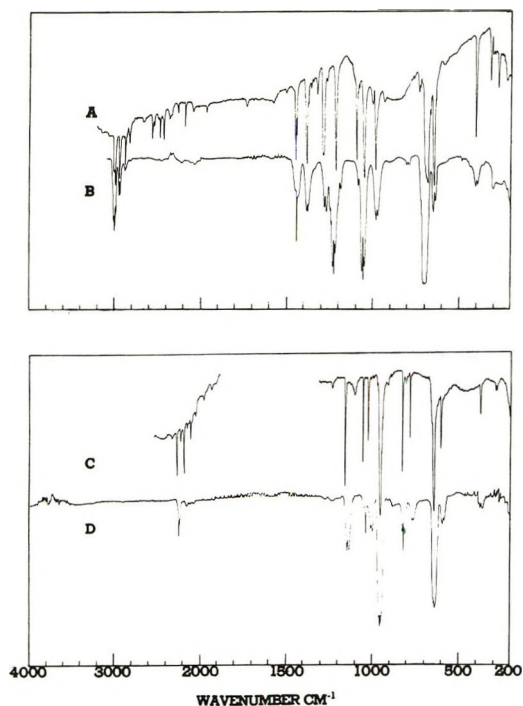


Figure 2. (A) Infrared spectrum of solid CH<sub>3</sub>CHCl<sub>2</sub>. (B) Infrared spectrum of gaseous CH<sub>3</sub>CHCl<sub>2</sub>. (C) Infrared spectrum of solid CD<sub>3</sub>CDCl<sub>2</sub>. (D) Infrared spectrum of gaseous CD<sub>3</sub>CDCl<sub>2</sub>.

three low-frequency bending modes are confidently assigned to other bands and no other intramolecular fundamental is expected in this frequency range.

From the expected shift factor of 1.414 with deuteration, one predicts the torsional frequency to fall at 277 cm<sup>-1</sup> in the light compound. Unfortunately, this is very nearly the frequency for the CCl<sub>2</sub> scissor which gives rise to a relatively strong infrared band (see Figure 3A). However, there is evidence for a shoulder on the low-frequency side of this CCl<sub>2</sub> scissoring mode which was measured to be approximately 274 cm<sup>-1</sup>. The obscurity of this shoulder would certainly account for the fact that the torsional mode has appeared very elusive in previous studies.<sup>4,5</sup> This assignment is then consistent with the recent inelastic neutron work<sup>8</sup> on both the liquid and solid in which the torsional mode was assigned to a band at 293 ± 15 cm<sup>-1</sup>. Since the neutron study is dependent on the density of states, the agreement is quite satisfactory.

This assignment of the torsion leaves unexplained the band at 232 cm<sup>-1</sup> previously reported in both the infrared<sup>3</sup> and neutron studies.<sup>8</sup> Since this band was reported in both the infrared spectrum of the gas and low-temperature solid, it cannot be ascribed to a difference tone. Also, it is doubtful that it could have arisen from water vapor leaking into the cell and condensing on the cold silicon plate. The most reasonable explanation seems to be that it arose from an impurity in the sample used in the previous investigations.

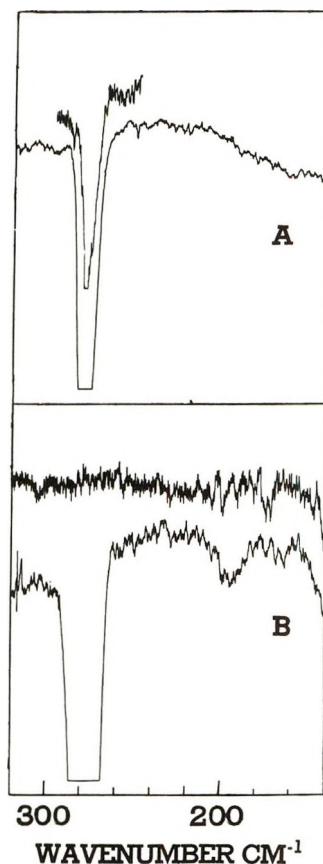


Figure 3. (A) Far-infrared spectrum of solid CH<sub>3</sub>CHCl<sub>2</sub>. (B) Far-infrared spectrum of solid CD<sub>3</sub>CDCl<sub>2</sub>.

To calculate the torsional barrier, we have assumed a cosine type potential of the form

$$V(\alpha) = \frac{1}{2}V_3(1 - \cos 3\alpha)$$

with all terms higher than threefold being considered negligible. The barrier was calculated according to the procedure outlined by Fateley and Miller.<sup>13</sup> The periodic barrier calculated for CD<sub>3</sub>CDCl<sub>2</sub> was 4.77 kcal/mol for the solid state.

With this new value of 4.77 kcal/mol for the barrier it is interesting to reconsider the effect of adding chlorine atoms to one "end" of ethane. The addition of one chlorine atom raises the barrier in the solid by 1.24 kcal/mol. The addition of a second chlorine atom further raises the barrier in the solid by 0.37 kcal/mol. The addition of a third chlorine atom again raises the barrier by about 0.64 kcal/mol. Although not following a linear relationship the barriers do seem to follow a trend of increasing restriction of the methyl rotation as the chlorine atoms are added. If one assumes nearly equal intermolecular effects for the three chlorine-containing compounds, then it appears that the second chlorine has the smallest effect. This trend is different from that found for the corresponding fluorides where

(13) W. G. Fateley and F. A. Miller, *Spectrochim. Acta*, **17**, 857 (1961).

the addition of the second and third fluorines to one end of ethane actually lowers the barrier. However, the trend is very similar to the one found for the substitution of a methyl group (see Table III) to one end of ethane. It is not possible to compare the bromide series since the barrier for the 1,1-dibromoethane molecule has not been reported.

**Table III:** Torsional Barriers (kcal/mol) for Some Chloro-, Fluoro-, and Methyl-Substituted Ethanes

Molecule	Gas	Solid	Reference
CH <sub>3</sub> CH <sub>3</sub>	2.928	3.24	a, b
CH <sub>3</sub> CH <sub>2</sub> Cl	3.71	4.48	c, d
CH <sub>3</sub> CHCl <sub>2</sub>		4.77	e
CD <sub>3</sub> CDCl <sub>2</sub>		4.84	e
CH <sub>3</sub> CCl <sub>3</sub>	5.10	5.49	f
CD <sub>3</sub> CCl <sub>3</sub>	5.05	5.41	f
CH <sub>3</sub> CH <sub>2</sub> F	3.33		g
CH <sub>3</sub> CHF <sub>2</sub>	3.18		h
CH <sub>3</sub> CF <sub>3</sub>	3.1	3.29	f
CH <sub>3</sub> CH <sub>2</sub> (CH <sub>3</sub> )	3.33	3.96	i, j, k
CH <sub>3</sub> CH(CH <sub>3</sub> ) <sub>2</sub>		3.94	l
CH <sub>3</sub> C(CH <sub>3</sub> ) <sub>3</sub>		4.3	m

<sup>a</sup> R. R. Getty and G. E. Leroi, 24th Symposium on Molecular Structure and Spectroscopy, Ohio State University, Columbus, Ohio, Sept 1969, Paper Q-7. <sup>b</sup> S. Weiss and G. E. Leroi, *J. Chem. Phys.*, **48**, 968 (1968). <sup>c</sup> C. M. Player, private communication. <sup>d</sup> R. H. Schwendeman and G. D. Jacobs, *J. Chem. Phys.*, **36**, 1245 (1962). <sup>e</sup> This work. <sup>f</sup> Reference 1; J. R. Durig, M. M. Chen, and Y. S. Li, *J. Mol. Struct.*, in press. <sup>g</sup> G. Sage and W. Klemperer, *J. Chem. Phys.*, **39**, 371 (1963). <sup>h</sup> O. R. Herschbach, *J. Chem. Phys.*, **25**, 358 (1966); W. G. Fateley and F. A. Miller, *Spectrochim. Acta*, **17**, 857 (1961). <sup>i</sup> L. H. Scharpen and V. W. Laurie, Symposium on Molecular Structure and Spectroscopy, Ohio State University, Columbus, Ohio, June 1965. <sup>j</sup> E. Hirota, C. Matsumura, and Y. Morino, *Bull. Chem. Soc. Jap.*, **40**, 1124 (1967). <sup>k</sup> P. M. Grant, R. J. Pugmire, R. C. Livingston, K. A. Strong, H. L. McMurry, and R. M. Brugger, *J. Chem. Phys.*, **52**, 4424 (1970). <sup>l</sup> J. R. Durig, S. M. Craver, and J. Bragin, *ibid.*, **53**, 3850 (1970). <sup>m</sup> J. R. Durig, S. M. Craven, and J. Bragin, *ibid.*, **52**, 2046 (1970).

Recently Abraham and Parry<sup>14</sup> calculated the internal rotational barriers for a series of halogenated ethane molecules by the summation of all steric and electrostatic interactions between nonbonded atoms plus a torsional term which was directly related to the intrinsic barrier to rotation in ethane. For example, they calculated barriers of 3.78, 4.56, and 5.89 kcal/mol for 1-chloro-, 1,1-dichloro-, and 1,1,1-trichloroethane, respectively. These results agree well with the latest experimental values of 3.71, 4.5, and 5.1 kcal/mol for these respective molecules (See Table III) for the vapor state. It would seem that a similar treatment for the bromo and methyl series would also provide barrier heights in agreement with the experimentally determined values.

## Normal Coordinate Analysis

As an aid in making the vibrational assignment, a normal coordinate analysis of CH<sub>3</sub>CHCl<sub>2</sub> and CD<sub>3</sub>-CDCl<sub>2</sub> was undertaken. The calculations were carried out by using the Wilson GF matrix method<sup>15</sup> with computer programs written by Schachtschneider.<sup>16</sup> The G matrix was calculated using assumed structural parameters.<sup>17</sup> Frequencies were given the weight (1/λ) in the least-squares procedure. Initial force constants for the CH<sub>3</sub>-C group were taken from the published values of Duncan<sup>18</sup> and force constants for the -CHCl<sub>2</sub> group were estimated from the work of Dempster and Zerbi.<sup>19</sup> Twelve force constants were adjusted to fit 34 observed frequencies, and the final force field of 18 constants is shown in Table IV. The calculated and observed frequencies for CH<sub>3</sub>CHCl<sub>2</sub> and CD<sub>3</sub>CDCl<sub>2</sub> are listed in Tables I and II, with an average error of 0.82 and 2.37%, respectively.

**Table IV:** Internal Force Constants for CH<sub>3</sub>CHCl<sub>2</sub><sup>a</sup>

Force constant	Group	This work	CH <sub>3</sub> -C group
$K_r$	C-H <sub>3</sub> stretch	4.86 ± 0.04	4.86
$K_r$	C-C stretch	4.28 ± 0.20	4.45
$F_r$	CH <sub>3</sub> str./CH <sub>3</sub> str.	0.07 ± 0.03	0.04
$K_d$	CH stretch	4.99 ± 0.04	
$H_\alpha$	∠HCH bend	0.53 ± 0.01	0.55
$H_\beta$	∠HCC bend	0.64 ± 0.03	0.64
$F_{R\beta}$	C-C str./∠HCC bend	0.25 <sup>b</sup>	0.30
$F_\beta$	∠HCC bend/∠HCC bend	-0.02 <sup>b</sup>	-0.02
$H_\gamma$	∠CCH bend	0.64 ± 0.04	
$H_\theta$	∠HCCl bend	0.61 ± 0.01	
$H$	∠CCCl bend	1.46 ± 0.13	
$H_\delta$	∠ClCCl bend	1.05 ± 0.17	
$H_\tau$	CH <sub>3</sub> torsion <sup>c</sup>	0.016 <sup>b</sup>	
$K_x$	C-Cl stretch	2.50 ± 0.13	
$F_x$	CCl/CCl stretch	0.67 ± 0.13	
$F_{X\delta}$	CCl str./∠CCl <sub>2</sub> bend	0.25 <sup>b</sup>	
$F_{RX}$	CC str./CCl str.	0.40 <sup>b</sup>	
$F_{X\theta}$	CCl str./∠HCCl bend	0.20 <sup>b</sup>	

<sup>a</sup> Stretching force constants in millidynes per ångström; bending constants in millidyne ångström per square radian; stretch-bend interaction constants in millidynes per radian. <sup>b</sup> Fixed during perturbation cycle. <sup>c</sup> Torsional coordinate is defined as the sum of three trans torsions about the C-C bond.

(14) R. J. Abraham and K. Parry, *J. Chem. Soc. B*, 539 (1970).

(15) E. B. Wilson, Jr., J. C. Decius, and P. C. Cross, "Molecular Vibrations," McGraw-Hill, New York, N. Y., 1958.

(16) J. H. Schachtschneider, "Vibrational Analysis of Polyatomic Molecules. V and VI," Tech. Rep. No. 231-64 and 57-65, respectively, Shell Development Co., Emeryville, Calif.

(17) Geometry used in CH<sub>3</sub>CHCl<sub>2</sub> calculations: C-H = 1.09 Å, C-Cl = 1.76 Å, ∠Cl-C-Cl = 112°, and ∠C-C-Cl = 110°. Tetrahedral values were assumed for the ∠H-C-H and ∠C-C-H angles.

(18) J. L. Duncan, *Spectrochim. Acta*, **20**, 1197 (1964).

(19) A. B. Dempster and G. Zerbi, *ibid.*, **39**, 1 (1971).



The PED (potential energy distribution) in Tables I and II reveals several cases of strong mixing between symmetry coordinates, although the exact nature of this mixing is somewhat dependent upon the assumed force field. In particular, the  $-CCl_2$  motions are strongly mixed. The resulting force constants show good agreement with the results of Duncan<sup>18</sup> for the  $CH_3-C$  group.

The C-Cl stretching constant of 2.5 mdyne/Å is somewhat smaller than the value of 3.2 mdyne/Å calculated by Dempster and Zerbi<sup>19</sup> for  $CH_3CH_2Cl$ .

*Acknowledgment.* The authors gratefully acknowledge the financial support given this research by the National Science Foundation by Grant No. GP-20723.

## The Crystal Structure of 2,4,6-Trinitroaniline

by James R. Holden,\* Charles Dickinson,

Naval Ordnance Laboratory, White Oak, Maryland 20910

and Charles M. Bock

Air Force Rocket Propulsion Laboratory, Edwards Air Force Base, California 93523 (Received March 22, 1972)

Publication costs assisted by the Naval Ordnance Laboratory

The crystal structure of 2,4,6-trinitroaniline,  $C_6H_3N_3O_6$ , has been determined by X-ray diffraction. The unit cell is monoclinic ( $a = 6.137$ ,  $b = 9.217$ ,  $c = 15.323$  Å,  $\beta = 99.67^\circ$ ), space group  $P2_1/c$  with four molecules per cell. The 2-, 4-, and 6-nitro groups are rotated 22.5, 4.0, and 8.5°, respectively, out of the plane of the benzene ring. This noncoplanarity and the type of intermolecular hydrogen bonding found in the structure of trinitroaniline are different than in the previously reported structures of diaminotrinitrobenzene and triaminotrinitrobenzene.

### Introduction

The crystal structure of 2,4,6-trinitroaniline (TNA) has been determined by single-crystal X-ray diffraction techniques as part of a study of the molecular conformations and hydrogen bond networks present in nitroaromatic amines. The structure completes the set of primary amines of *sym*-trinitrobenzene, because the structures of 1,3-diamino-2,4,6-trinitrobenzene (DATB)<sup>1</sup> and 1,3,5-triamino-2,4,6-trinitrobenzene (TATB)<sup>2</sup> have been reported. These two compounds crystallize as planar molecules joined by intermolecular hydrogen bonds in which an amine group bonds to both oxygen atoms of the same nitro group of an adjacent molecule.

In contrast, 4-nitroaniline<sup>3</sup> and 2,3,4,6-tetranitroaniline (TENNA)<sup>4</sup> form intermolecular hydrogen bonds in which the amine group is bound to oxygen atoms from two different molecules.

The cell dimensions and space group of 2,4,6-trinitroaniline have been reported as  $a = 6.02$ ,  $b = 9.30$ ,  $c = 15.3$  Å,  $\beta = 99.2^\circ$  (converted from kX units),  $P2_1/c$ <sup>5</sup> and the density as 1.762 g/cm<sup>3</sup>.<sup>6</sup> The values obtained in this study agree adequately with these early reports.

### Experimental Section

Suitable crystals of 2,4,6-trinitroaniline were grown from a commercial sample<sup>7</sup> by evaporation of an ethyl acetate solution. Cell dimensions and reflection intensities were determined from the same  $0.30 \times 0.40 \times 0.49$  mm crystal. After preliminary examination by Weissenberg and precession methods, this crystal was aligned on a Picker FACS-1 computer-controlled automatic diffractometer equipped with a lithium fluoride monochromator. The following monoclinic cell dimensions were obtained from a least-squares fit of the diffraction angles of 12 strong reflections using 0.70926 Å as the wavelength of Mo  $K\alpha$  radiation:  $a = 6.137 \pm 0.003$ ,  $b = 9.217 \pm 0.007$ ,  $c = 15.323 \pm 0.007$  Å,  $\beta = 99.67 \pm 0.02^\circ$ . These values give a calculated density

(1) J. R. Holden, *Acta Crystallogr.*, **22**, 545 (1967).

(2) H. H. Cady and A. C. Larson, *ibid.*, **18**, 485 (1965).

(3) K. N. Trueblood, E. Goldish, and J. Donohue, *ibid.*, **14**, 1009 (1961).

(4) C. Dickinson, J. M. Stewart, and J. R. Holden, *ibid.*, **21**, 663 (1966).

(5) E. Hertel and G. H. Romer, *Z. Phys. Chem. Abt. B*, **22**, 267 (1933).

(6) F. M. Jaeger, *Z. Kristallogr.*, **40**, 113 (1905).

(7) Eastman Organic Chemicals, Rochester, N. Y.

**Table I:** Atomic Parameters (Temperature Factors  $\times 100$ )

	<i>x</i>	<i>y</i>	<i>z</i>	<i>U</i> or <i>U</i> <sub>11</sub>	<i>U</i> <sub>22</sub>	<i>U</i> <sub>33</sub>	<i>U</i> <sub>12</sub>	<i>U</i> <sub>13</sub>	<i>U</i> <sub>23</sub>
C(1)	0.5334 (06)	0.3091 (05)	0.4597 (02)	3.67 (26)	3.13 (27)	2.80 (25)	0.25 (24)	0.08 (20)	-0.39 (23)
C(2)	0.3539 (07)	0.2111 (05)	0.4619 (03)	3.76 (27)	3.52 (30)	3.39 (27)	-0.08 (23)	0.28 (23)	0.83 (23)
C(3)	0.1776 (06)	0.1946 (05)	0.3946 (03)	3.03 (27)	4.19 (33)	4.02 (29)	0.33 (25)	0.28 (22)	-0.33 (27)
C(4)	0.1744 (07)	0.2772 (04)	0.3193 (03)	3.03 (25)	3.40 (29)	2.98 (27)	0.48 (22)	-0.63 (20)	-0.68 (22)
C(5)	0.3430 (07)	0.3699 (05)	0.3089 (03)	4.10 (26)	3.23 (30)	2.70 (25)	0.16 (24)	0.22 (22)	-0.16 (21)
C(6)	0.5172 (06)	0.3849 (05)	0.3776 (03)	2.94 (24)	3.49 (29)	3.21 (27)	-0.25 (22)	0.30 (21)	-0.63 (22)
N(1)	0.7015 (06)	0.3251 (04)	0.5271 (02)	4.67 (25)	5.97 (34)	3.36 (25)	-1.09 (23)	-1.00 (21)	0.60 (22)
N(2)	0.3515 (06)	0.1189 (05)	0.5404 (03)	3.42 (25)	6.59 (35)	4.92 (28)	0.05 (23)	0.86 (21)	0.96 (26)
N(4)	-0.0129 (06)	0.2614 (04)	0.2464 (03)	3.64 (23)	3.97 (28)	4.43 (24)	0.47 (20)	-0.75 (20)	-0.71 (21)
N(6)	0.6908 (06)	0.4847 (04)	0.3608 (03)	4.01 (24)	4.54 (28)	4.30 (23)	-0.30 (22)	-0.11 (21)	0.39 (21)
O(21)	0.4606 (05)	0.1561 (04)	0.6108 (02)	6.93 (25)	13.14 (39)	3.76 (21)	-3.08 (24)	-1.04 (18)	2.42 (23)
O(22)	0.2402 (05)	0.0093 (04)	0.5305 (02)	6.63 (25)	6.43 (27)	7.01 (25)	-1.63 (22)	1.06 (18)	2.41 (21)
O(41)	-0.1656 (05)	0.1825 (04)	0.2583 (02)	4.37 (20)	6.81 (26)	8.11 (26)	-2.26 (21)	-1.57 (19)	0.60 (22)
O(42)	-0.0057 (05)	0.3286 (04)	0.1782 (02)	5.58 (21)	7.79 (27)	3.77 (20)	-0.47 (20)	-1.58 (16)	0.79 (20)
O(61)	0.6834 (05)	0.5334 (04)	0.2876 (02)	8.34 (27)	7.91 (29)	4.76 (22)	-3.82 (22)	0.41 (19)	1.96 (21)
O(62)	0.8408 (05)	0.5148 (04)	0.4220 (02)	5.56 (22)	8.83 (30)	6.41 (22)	-3.47 (21)	-2.02 (19)	2.18 (22)
H(3)	0.0536 (67)	0.1266 (46)	0.4029 (26)	4.04					
H(5)	0.3452 (69)	0.4271 (48)	0.2548 (28)	4.04					
H(11)	0.8109 (70)	0.3862 (50)	0.5139 (30)	4.04					
H(12)	0.7047 (76)	0.2734 (49)	0.5759 (30)	4.04					

of 1.773 g/cm<sup>3</sup> with four molecules per cell. The measured density is 1.762 g/cm<sup>3</sup>.<sup>6</sup>

Reflection intensities were measured with the diffractometer operating in the  $\omega/2\theta$  scan mode. Reflections from one quadrant of reciprocal space ( $hkl$  and  $\bar{h}kl$ ) were measured out to a  $\sin \theta/\lambda$  value of 0.6. Three "standard" reflections were measured after each 50 measurements, and reflection intensities were corrected for instrument variations on the basis of the sum of the counts from the "standard" reflections. No general trend in the "standard" counts was evident indicating no detectable radiation damage to the crystal. Of the 1512 independent reflections measured, 948 had intensity counts more than two estimated standard deviations above measured background and were considered "observed" reflections.

The two sets of periodic absences observed ( $l = 2n + 1$  in  $h0l$  and  $k = 2n + 1$  in  $0k0$ ) indicate that the space group is  $P2_1/c$ .

The linear absorption coefficient of TNA for Mo  $K\alpha$  radiation is 1.74 cm<sup>-1</sup>. Therefore the transmission factors for all reflections from this crystal would fall between 0.93 and 0.96, and no absorption correction was applied.

### Determination of Structure

After initial data treatment with the application of the usual Lorentz and polarization factors, a set of quasinormalized structure factors (Karle-Hauptman  $E$ 's)<sup>8</sup> was obtained by means of the computer code FAME.<sup>9</sup> The structure was then solved by the symbolic addition procedure<sup>10,11</sup> using a modified version of the computer code MAGIC.<sup>9</sup> The correct rough structure was obtained from the "E map" calculated with the set of phases indicated by MAGIC to be most prob-

ably correct. The 15 strongest peaks in this "E map" were readily identified with 15 of the 16 nonhydrogen atoms of the molecule. The peak in a logical position for the remaining atom (O(21) in the listed structure) was weaker than several spurious peaks. It is perhaps significant that this atom has the largest anisotropic thermal parameter in the final structure.

The rough structure obtained from the "E map" gave an agreement index ( $R$ ) of 0.26. Subsequent refinement first by isotropic, then by anisotropic full-matrix least-squares lowered  $R$  to 0.11. The hydrogen atoms were then located from a difference Fourier synthesis and their positional parameters entered into the final cycles of least-squares refinement which lowered  $R$  to a final value of 0.084. The average shift/error ratio for all parameters in the last cycle was 0.01; the maximum was 0.08. Including the overall scale factor, the structure is based on 157 parameters; therefore, the overdetermination ratio is 6.0 (948/157). The maximum value in a final difference Fourier synthesis was 0.37 electrons/ $\text{\AA}^3$ .

In all least-squares refinements, the quantity minimized was  $w(F_o - F_c)^2$ , where  $w$  is the weight assigned to the reflection. For unobserved reflections,  $w(F_c - F_{\min})^2$  was included in the sum when the calculated structure factor,  $F_c$ , was greater than  $F_{\min}$ , the structure factor calculated from an intensity two standard deviations above measured background. No contri-

(8) H. Hauptman and J. Karle, "Solution to the Phase Problem I. The Centrosymmetric Crystal," ACA Monograph No. 3, Polycrystal Book Service, Pittsburgh, Pa., 1953.

(9) R. B. K. Dewar, "Use of Computers in the X-Ray Phase Problem," Ph.D. Thesis, University of Chicago, 1968.

(10) I. L. Karle and J. Karle, *Acta Crystallogr.*, **16**, 969 (1963).

(11) W. H. Zachariasen, *ibid.*, **5**, 68 (1952).



bution was included for unobserved reflections when  $F_o$  was smaller than  $F_{min}$ . The weight given each reflection was based on the standard deviation of  $F_o$ ,  $\sigma$ , estimated from counting statistics. The weight was  $(0.5/\sigma)^2$  for most reflections and  $(0.5/0.35)^2$  for a few reflections whose estimated  $\sigma$  values were less than 0.35.

The final atomic parameters are given in Table I. The numbers in parentheses are the errors in the last two digits as estimated from the inverse matrix from the last least-squares cycle. The anisotropic temperature factors are of the form

$$\exp[-2\pi^2(h^2a^{*2}U_{11} + k^2b^{*2}U_{22} + l^2c^{*2}U_{33} + 2hka^*b^* \cos \gamma^*U_{12} + 2hla^*c^* \cos \beta^*U_{13} + 2klb^*c^* \cos \alpha^*U_{23})]$$

These  $U_{ij}$  values are on the same scale as the isotropic  $U$  value assigned to the hydrogen atoms. This value, 0.0404, is the overall temperature factor estimated for the structure by the "E scaling" code, FAME.<sup>9</sup> A table of observed and calculated structure factors is included in the microfilm edition of this journal.<sup>12</sup>

### Discussion

Figure 1 is a diagram of the molecule projected onto the least-squares plane<sup>13</sup> of the six carbon atoms of the benzene ring. The equation of this plane is

$$-3.43x + 6.77y + 7.25z = 3.57$$

where  $x$ ,  $y$ , and  $z$  are fractional coordinates in the monoclinic cell. The root-mean-square distance of these atoms from the plane is 0.013 Å. The distances of the individual atoms of the molecule from the plane are given in parentheses in Figure 1.

The estimated standard deviations in the bond distances given in Figure 1 range from 0.004 to 0.006 Å for

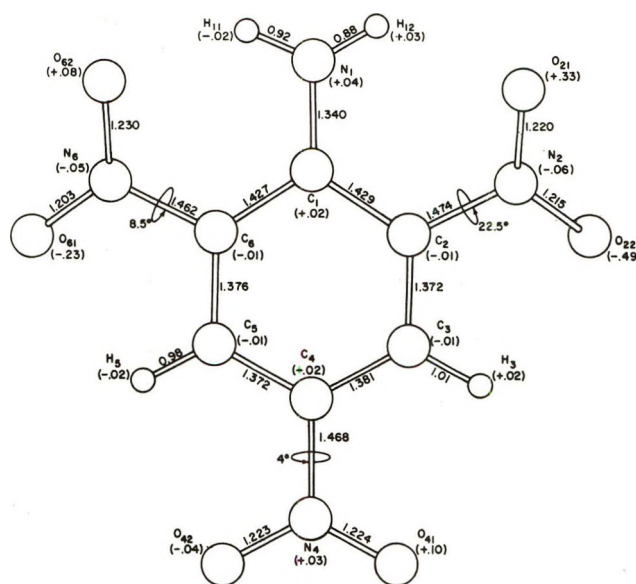


Figure 1. Projection of molecule onto plane of benzene ring.

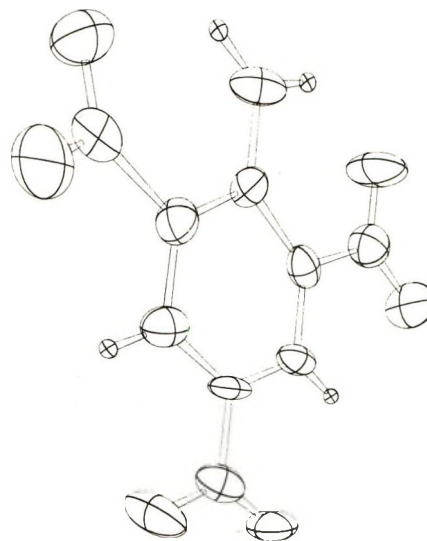


Figure 2. Thermal motion of the molecule.

Table II: Bond Angles (degrees)

C(6)-C(1)-C(2)	113.0	C(2)-N(2)-O(21)	118.7
C(1)-C(2)-C(3)	124.5	C(2)-N(2)-O(22)	117.4
C(2)-C(3)-C(4)	117.8	C(4)-N(4)-O(41)	117.9
C(3)-C(4)-C(5)	122.4	C(4)-N(4)-O(42)	117.6
C(4)-C(5)-C(6)	118.5	C(6)-N(6)-O(61)	119.0
C(5)-C(6)-C(1)	123.8	C(6)-N(6)-O(62)	118.8
C(6)-C(1)-N(1)	123.8	O(21)-N(2)-O(22)	123.9
C(2)-C(1)-N(1)	123.2	O(41)-N(4)-O(42)	124.5
C(1)-C(2)-N(2)	119.8	O(61)-N(6)-O(62)	122.2
C(3)-C(2)-N(2)	115.7		
C(3)-C(4)-N(4)	118.7		
C(5)-C(4)-N(4)	118.9		
C(5)-C(6)-N(6)	115.0		
C(1)-C(6)-N(6)	121.2		
C(2)-C(3)-H(3)	119.4		
C(4)-C(3)-H(3)	122.8		
C(4)-C(5)-H(5)	123.3		
C(6)-C(5)-H(5)	118.2		
C(1)-N(1)-H(11)	113.1		
C(1)-N(1)-H(12)	119.8		
H(11)-N(1)-H(12)	126.9		

bonds not involving hydrogen and from 0.043 to 0.046 Å for bonds to hydrogen. Those in the bond angles listed in Table II range from 0.32 to 0.42° for angles not involving hydrogen and from 2.2 to 2.9° for angles involving one hydrogen atom. That of angle H(11)-N(1)-H(12) is 3.9°. The rotation angles given in Figure 1 are the dihedral angles between the ring plane and the planes of the carbon and oxygen atoms attached to the nitrogen atom of each of the nitro groups.

(12) A structure factor table will appear immediately following this article in the microfilm edition of this volume of the journal. Single copies may be obtained from the Business Operations Office, Books and Journals Division, American Chemical Society, 1155 Sixteenth St., N.W., Washington, D. C. 20036, by referring to code number JPC-72-3597. Remit check or money order for \$4.00 for photocopy or \$2.00 for microfiche.

(13) V. Schomaker, J. Waser, R. E. Marsh, and G. Bergman, *Acta Crystallogr.*, 12, 600 (1959).

Within the accuracy of the determination, the amine group and the nitro groups are planar; that is, the nitrogen atom is in the plane of the atoms bonded to it.

Figure 2<sup>14</sup> shows the orientation of the thermal ellipsoids of the atoms, as indicated by the anisotropic refinement, and illustrates that they have no obvious correlation with the molecular conformation.

Perhaps the greatest significance of this crystal structure determination of 2,4,6-trinitroaniline (TNA) is the knowledge of conformation and hydrogen bonding of nitroaromatic amines which can be derived from comparison with the structures of 1,3-diamino-2,4,6-trinitrobenzene (DATB)<sup>1</sup> and 1,3,5-triamino-2,4,6-trinitrobenzene (TATB).<sup>2</sup> Both of these compounds crystallize as planar molecules in spite of the crowding inherent to adjacent amine and nitro groups coplanar with the benzene ring. The general tendency of nitro groups toward coplanarity has been established,<sup>15</sup> and resonance stabilization has been proposed as the reason for this tendency. Furthermore, intramolecular hydrogen bond formation has been proposed as the mechanism by which adjacent aromatic amine and nitro groups attain coplanarity with the ring.<sup>1</sup> The approximate coplanarity of the nitro groups of DATB<sup>1</sup> and TATB<sup>2</sup> and the 6-nitro group of 2,3,4,6-tetranitroaniline (TENA)<sup>4</sup> seem to indicate that this conformation is energetically favored. However, intermolecular forces also affect molecular conformation, because it is the total energy of the system which is minimized in crystal formation.

The most striking difference between the conformation found for the TNA molecule and those of DATB and TATB is the noncoplanarity of the 2-nitro group (see Figure 1). This is required by the crystallographic packing; that is, by the approach of H(3) and O(22) of the molecule located at  $(-x, -y, 1 - z)$ , (see Figure 3).

As has been reported for other nitroaromatic compounds,<sup>16,17</sup> the interior angles of the benzene ring are larger than  $120^\circ$  at the carbon atoms carrying nitro groups. The exterior bond angles indicate crowding between the amine group and the ortho nitro groups. Angle C(1)-C(2)-N(2) is  $4.1^\circ$  larger than C(3)-C(2)-N(2), and C(1)-C(6)-N(6) is  $6.1^\circ$  larger than C(5)-C(6)-N(6). These differences are well over ten times the estimated standard deviations in the angles. A similar in-plane deflection away from the amine group was found for the 6-nitro group in TENA.<sup>4</sup> In DATB,<sup>1</sup> both the 4- and 6-nitro groups are deflected away from their adjacent amine groups.

In TNA, the carbon-carbon bonds on either side of the amine group are significantly longer than the other bonds in the ring. That is, bonds C(1)-C(2) and C(1)-C(6) average  $1.428 \text{ \AA}$ , which is about ten standard deviations longer than the average length of the other four bonds,  $1.375 \text{ \AA}$ . This condition is also found in TENA,<sup>4</sup> 4-nitroaniline,<sup>3</sup> 2,6-dichloro-4-nitroaniline,<sup>18</sup>

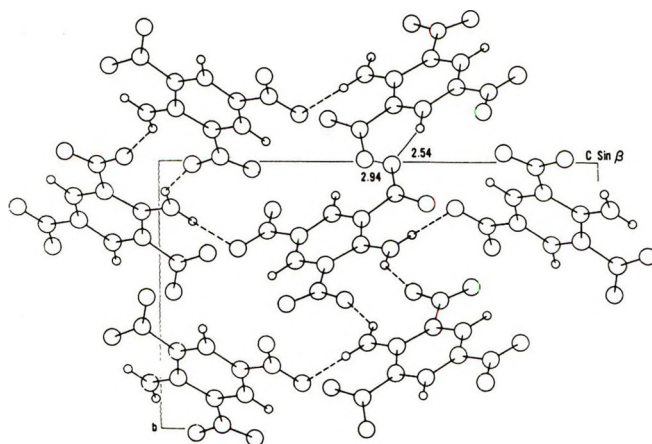


Figure 3. Projection of the structure down the  $a$  axis.

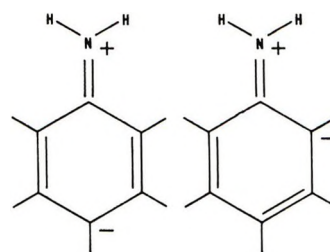


Figure 4. Resonance forms for aromatic amines.

and 2-amino-3-methylbenzoic acid.<sup>19</sup> In TATB,<sup>2</sup> where all of the ring bonds are adjacent to amine groups, they range in length from  $1.435$  to  $1.450 \text{ \AA}$ , about  $0.04 \text{ \AA}$  longer than the normal value for benzene,  $1.397 \text{ \AA}$ .<sup>20</sup> In DATB,<sup>1</sup> only C(1)-C(2) and C(2)-C(3) were found to be significantly long; however, this structure determination is less accurate than most of the others which have been cited.

In the report of the structure of DATB,<sup>1</sup> the long ring bonds were attributed to steric effects of the crowded substituents. However, in reports of the other structures cited above, they have been attributed to electronic effects associated with contributions of resonance structures of the type shown in Figure 4. If such structures make an important contribution, there should be an inverse correlation between the length of the ring bonds and the length of the C-N bond to the amine group.

Bond lengths from a number of primary aromatic

(14) C. K. Johnson, ORTEP Report No. ORNL-3794, Oak Ridge National Laboratory, Oak Ridge, Tenn., 1965.

(15) J. R. Holden and C. Dickinson, *J. Phys. Chem.*, **73**, 1199 (1969).

(16) A. S. Bailey and C. K. Prout, *J. Chem. Soc.*, 4867 (1965).

(17) O. L. Carter, A. T. McPhail, and G. A. Sim, *J. Chem. Soc. A*, 822 (1966).

(18) D. L. Hughes and J. Trotter, *ibid.*, 2181 (1971).

(19) G. M. Brown and R. E. Marsh, *Acta Crystallogr.*, **16**, 191 (1963).

(20) A. Langseth and B. P. Stoicheff, *Can. J. Phys.*, **34**, 350 (1956).



Table III: Bond Lengths in Primary Aromatic Amines

Compound	C <sub>j</sub> -N	<i>i</i>	<i>j</i>	<i>k</i>	C <sub>i</sub> -C <sub>j</sub>	C <sub>j</sub> -C <sub>k</sub>	A <sub>v</sub> C-C
2,4,6-Tribromoaniline <sup>a</sup>	1.426	6	1	2	1.365	1.386	1.376
2,5-Dichloroaniline <sup>b</sup>	1.407	6	1	2	1.398	1.423	1.411
4-Chloroaniline <sup>c</sup>	1.40	6	1	2	1.40	(1.40)	1.40
1,3,5-Triaminobenzene <sup>d</sup>	1.411	4	5	6	1.396	1.389	1.393
	1.392	6	1	2	1.407	1.386	1.397
	1.391	2	3	4	1.407	1.413	1.410
2-Chloro-4-nitroaniline <sup>e</sup>	1.382	6	1	2	1.420	1.394	1.407
2-Amino-3-methylbenzoic acid <sup>f</sup>	1.367	1	2	3	1.415	1.421	1.418
2,6-Dichloro-4-nitroaniline <sup>g</sup>	1.358	6	1	2	1.408	1.420	1.414
4-Nitroaniline <sup>h</sup>	1.353	6	1	2	1.405	1.412	1.409
2,4,6-Trinitroaniline	1.340	6	1	2	1.430	1.427	1.429
1,3-Diamino-2,4,6-trinitrobenzene <sup>i</sup>	1.32	6	1	2	1.39	1.47	1.43
	1.32	2	3	4	1.47	1.39	1.43
2,3,4,6-Tetranitroaniline <sup>j</sup>	1.312	6	1	2	1.428	1.434	1.431
1,3,5-Triamino-2,4,6-trinitrobenzene <sup>k</sup>	1.320	6	1	2	1.436	1.446	1.441
	1.311	2	3	4	1.435	1.450	1.443
	1.310	4	5	6	1.435	1.435	1.442

<sup>a</sup> Reference 21. <sup>b</sup> Reference 22. <sup>c</sup> Reference 23. <sup>d</sup> Reference 24. <sup>e</sup> Reference 25. <sup>f</sup> Reference 19. <sup>g</sup> Reference 18. <sup>h</sup> Reference 3. <sup>i</sup> Reference 1. <sup>j</sup> Reference 4. <sup>k</sup> Reference 2.

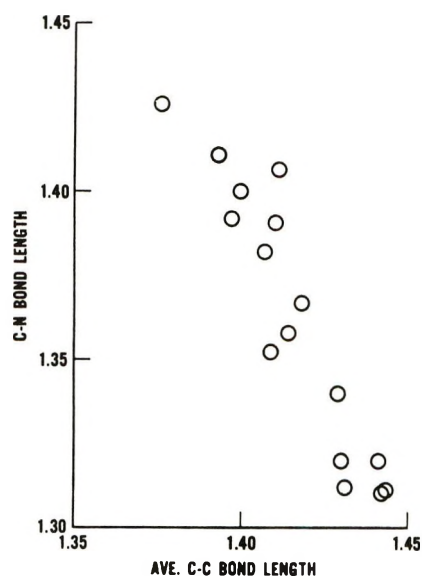


Figure 5. C-N bond lengths in primary aromatic amines vs. the average length of the adjacent C-C bonds in the ring; data from Table III (ångstrom units).

amine crystal structures are assembled in Table III.<sup>21-25</sup> The compounds are listed in order of decreasing C-N bond length. The ring positions (*i*, *j*, *k*) refer to the compound as named, not always as given in the reference. Note that the average length of the ortho C-C bonds tends to increase as the length of the C-N decreases as would be expected. The quality of this correlation is shown in Figure 5. Also note that aromatic amines containing no nitro groups fall at the top of the list in Table III (long C-N bonds), ones with para nitro groups fall in the middle, and ones with both ortho and para nitro groups fall at the bottom (short C-N bonds). It would appear that the resonance

structures illustrated in Figure 4 are important only when nitro groups are also present. This is probably due to the electron-withdrawing properties of the nitro group, and the position of 2-amino-3-methylbenzoic acid in Table III indicates that the acid group also serves this function.

The bond lengths reported for *N,N*-dimethyl-4-nitroaniline<sup>26</sup> and 2,6-dichloro-*N,N*-dimethyl-4-nitroaniline,<sup>27</sup> present further evidence for resonance interaction between amine groups and aromatic rings. In the former compound, the dimethylamino group is twisted only 7.3° about the C-N bond out of the aromatic plane. The C-N bond is 1.358 ± 0.016 Å in length and the adjacent C-C bonds average 1.435 Å (1.410, 1.460). In contrast, in the chlorinated compound where the dimethylamino group is twisted 60.5°, the C-N bond length is 1.41 ± 0.01 Å and the C-C bond lengths are both 1.39 Å (twofold axis). That is, rotation of the amine group to a point where it can no longer interact strongly with the aromatic system apparently results in a longer C-N bond accompanied by shorter adjacent C-C bonds. However, a more detailed discussion would require more accurate structure determinations.

(21) A. T. Christensen and K. O. Stromme, *Acta Cryst., Sect. B*, **25**, 657 (1969).

(22) T. Sakurai, M. Sundaralingam, and G. A. Jeffrey, *Acta Crystallogr.*, **16**, 354 (1963).

(23) J. H. Palm, *ibid.*, **21**, 473 (1966).

(24) F. Iwasaki and Y. Saito, *Acta Crystallogr., Sect. B*, **26**, 251 (1970).

(25) A. T. McPhail and G. A. Sim, *J. Chem. Soc.*, 227 (1965).

(26) T. C. W. Mak and J. Trotter, *Acta Crystallogr.*, **18**, 68 (1965).

(27) Ju. T. Struckov and T. L. Hocjanova, *Izv. Sib. Otd. Akad. Nauk SSSR, Ser. Khim. Nauk*, **11**, 1369 (1960); *Struct. Rept.*, **24**, 647 (1960).

The lengths of the C-C bonds adjacent to the amine groups of DATB differ much more from one another than those of any of the other compounds listed in Table III. This may be caused by steric factors, as suggested in the report of this structure,<sup>1</sup> or may be caused by the concerted electronic effects of the two amine groups. Further discussion of the conformation of the DATB molecule should be based on a more accurate structure determination.

Intermolecular hydrogen bonding seems to be an important factor in the crystallographic packing of both DATB and TATB. In the form I polymorph of DATB (stable below 217°),<sup>1</sup> each molecule forms one link in a hydrogen-bonded chain in which the N(1) amine group is attached to both oxygen atoms of the N(4) nitro group of the adjacent molecule. The nitrogen-oxygen distances in the bonds of this chain are 2.97 and 2.99 Å. The N(3) amine does not take part in strong hydrogen bonding, whereas in the TATB crystal, all three amines form double hydrogen bonds to nitro groups of neighboring molecules.<sup>2</sup> Here, the molecules are bonded into continuous sheets with the nitrogen-oxygen distances ranging from 2.93 to 3.00 Å (hydrogen-oxygen, 2.24-2.40 Å).

In trinitroaniline, the intermolecular hydrogen bonding is quite different, as shown by the broken lines in Figure 3. The amine group forms bonds to oxygen atoms of two different molecules; O(42) of the molecule at  $(1 + x, \frac{1}{2} - y, \frac{1}{2} + z)$  through H(12), and O(62) of the molecule at  $(2 - x, 1 - y, 1 - z)$  through H(11). The nitrogen-oxygen distances in these bonds are 3.03 and 3.15 Å; the hydrogen-oxygen distances are 2.36 and 2.38 Å. The first bond links the molecules into singly bonded chains; the second, with its symmetry-related mate from O(62) to the amine group of  $(2 - x, 1 - y, 1 - z)$ , doubly cross-links these chains. This type of intermolecular hydrogen bonding, in which the amine group is attached to two different molecules, is also observed in the crystal structures of TENA<sup>4</sup> and *p*-nitroaniline.<sup>3</sup>

A possible explanation for the different packing and hydrogen bond networks displayed by the mono-, di-, and triaminotrinitrobenzenes lies in the overall van der Waals interaction between the molecules as indicated by their densities. The last number in each column in Table IV is the density of the compound at the left as calculated from the unit cell dimensions of its stable form at room temperature. Since a hydrogen atom is smaller than an amine group, DATB or TNA could replace TATB in its crystal structure. Likewise, TNA

could replace DATB in its structure. The other numbers in Table IV are the densities which these compounds would have if they crystallized in the other possible structures. The actual density of each compound is greater than that calculated for any alternate structural arrangement as would be expected. However, the difference in density between DATB in its observed structure and DATB in the TATB structure is very small, implying that the energy difference for DATB in these two crystal structures is quite small. This is in agreement with the known polymorphism of DATB.

Table IV: Calculated Density (g/cm<sup>3</sup>)

Compound	Crystal lattice		
	Aniline	Di-amine	Tri-amine
2,4,6-Trinitroaniline (TNA)	1.773	1.724	1.712
1,3-Diamino-2,4,6-trinitrobenzene (DATB)		1.838	1.824
1,3,5-Triamino-2,4,6-trinitrobenzene (TATB)			1.937

On heating, the room temperature stable polymorph of DATB, form I, undergoes a solid-solid transformation at 217° to a high temperature form II which is stable to the melting point. When supercooled to room temperature, form II gives an X-ray powder pattern which is nearly superimposable upon that of TATB. Form II DATB is apparently isostructural with TATB which would mean that DATB can indeed exist in the TATB structure.

Following this reasoning, the fact that TNA crystallizes as found, and not in the DATB structure, implies that the reduction in the total energy of the system associated with an increase in density of 0.049 g/cm<sup>3</sup> (1.773 - 1.724) more than compensates for the energy increase associated with the observed rotation of the nitro groups of TNA from the plane of the benzene ring.

*Acknowledgment.* The authors gratefully acknowledge the Independent Research Fund, Task IR-44, of the Naval Ordnance Laboratory, White Oak, Maryland, for financial support of this work, and the Air Force Rocket Propulsion Laboratory, Edwards, California, for use of their X-ray diffractometer and computing facilities.



# Non-Poisson Distributions Observed during Counting of Certain Carbon-14-Labeled Organic (Sub)Monolayers<sup>1</sup>

by John Lynde Anderson<sup>2</sup>

Chattanooga, Tennessee 37409 (Received July 12, 1971)

As shown by the index of dispersion statistic  $s^2/m$ , anomalous narrow statistical distributions have been consistently obtained from counts of  $\beta$  radiation emitted by adsorbed, high specific activity carbon-14-labeled organic (sub)monolayers (1) when first-order desorptions from metal oxide surfaces occur, (2) when adsorbed stearic acid-1-<sup>14</sup>C on certain nongrounded surfaces is counted, and (3) when aluminum foil containing such stearic acid-1-<sup>14</sup>C is charged at a positive potential (*e.g.*, 90 V positive with respect to an adjacent, grounded aluminum "window") for sequential periods of up to 450 min. The markedly low variances, observed with external detectors, were in contrast to "normal" or Poisson-expected values which were invariably obtained using the same equipment when the surfaces had either nonadsorbed radiochemicals or nonevaporating radiochemicals under grounded or negative polarity conditions. Based on a number of individual experiments involving several different counting systems and detectors and representing several thousands of degrees of freedom, *the radioactive decay process observed under these certain conditions is not properly described by the Poisson distribution.* The inconsistency of this phenomenon with known and generally accepted theories of radioactive decay raises serious questions relative to the generality of the independence of radioactive decay events and/or the randomness of emissions.

## Introduction

A cornerstone of modern nuclear physics and fundamental to many uses of radioisotopes, the assumption that radioactive decay events within a given species are independent of each other was first phrased in 1905 when von Schweidler projected the thesis that radioactive decay processes are exponential.<sup>3</sup> The experimental testing of this assumption has invariably involved derivation of statistics of detected radioactive emissions and/or of times between detected emissions followed by comparison of such statistics with those expected for random events. The "proof" of the assumption has thus also involved the often tacit hypothesis that the statistical properties of emissions are directly and necessarily related to the decay process itself, a hypothesis which has proved difficult to verify experimentally but which is reasonable and is generally accepted.<sup>4</sup> [(1s)<sup>4</sup> A discussion of some of the factors relative to the use of external window detectors apropos of the hypothesis.]

If detected radioactive emissions are random and if there are sufficient events for statistical significance, then the statistical distribution of the counts (or of the recorded times-between-emissions) will be closely approximated by the Poisson distribution provided also that the events are rare (a low probability that any single event will occur) and that a single species of isotope is involved (all events have the same probability of occurrence).<sup>5</sup> [(2s)<sup>4</sup> A discussion of an exception (non-Poisson) which is not applicable in the present case. (3s)<sup>4</sup> A short discussion of mother-daughter deviations from the Poisson.]

The converse is also true. If, barring artifactuality, the distribution of detected emissions is statistically *not* of the same population as the Poisson, one or more of the cited conditions must be false.

Detection and counting of the single species carbon-14  $\beta$  particles involving  $1-6 \times 10^3$  counts/min arising from approximately  $3 \times 10^{14}$  carbon-14 atoms per specimen appear to limit the hereinafter detailed cases of low variance to questions involving only independence and randomness, particularly since the several types of equipment employed have invariably exhibited expected variances during reference and/or standard source counting (index of dispersion  $s^2/m = \sim 1.000$ ). [(4s)<sup>4</sup> The remote possibility that carbon-14 might not always be a single species isotope is discussed.]

## Background

Following the projections by von Schweidler that

(1) Presented in part at the 161st National Meeting of the American Chemical Society, Los Angeles, Calif., Mar 29, 1971.

(2) Correspondence should be addressed to the author at Wideview Route 4, Chattanooga, Tennessee 37409.

(3) E. von Schweidler, *Congres Internationale de Radiologie*, Liege, 1905.

(4) Listings of supplemental notes and material appearing in the microfilm edition of this volume of the journal are designated throughout the article with "s" notation, together with a brief comment on the nature of the supplemental material in brackets. Single copies may be obtained from the Business Operations Office, Books and Journals Division, American Chemical Society, 1155 Sixteenth St. N.W., Washington, D. C. 20036, by referring to the code number JPC-72-3603. Remit check or money order for \$4.00 for photocopy or \$2.00 for microfiche.

(5) R. D. Evans, "The Atomic Nucleus," McGraw-Hill, New York, N. Y., 1962, Chapters 26-28. The text includes references to a number of the prior studies which "verified" the generality of the Poisson.

natural radioactive decay processes are exponential, Rutherford and Geiger tested the distributions of observed  $\alpha$  particles and found them in good agreement with the expectation for random emissions. They therefore concluded that the evidence was in accord with the projection that the events were independent.<sup>6</sup> Many other workers, *e.g.*, Curtiss, subsequently confirmed these observations primarily using  $\alpha$  emitters.<sup>7</sup> Kovarik similarly reported that  $\beta$  emissions also appeared to exhibit random behavior.<sup>8</sup> As recently as 1966, Berkson reported a critical statistical study of times between detected  $\alpha$  emissions and observed no exception to the presumed universality of independent events. He carefully refrained, however, from concluding that his work *proved* the randomness concept pointing out that the particular statistical tests employed might have missed certain deviations from randomness.<sup>9</sup>

In 1924, Kutzner, while studying  $\alpha$  emissions from polonium, consistently observed low values of a variance index (Lexis divergence coefficient) and suggested his results were possibly due to nuclear-nuclear interactions.<sup>10</sup> Even though his findings were subsequently duplicated by Curtiss, the thesis was advanced by others—and apparently it has become firmly held—that the cause of the low values of the index was due to the phenomenon of aggregate recoil rather than to a lack of independence of the events.<sup>11,12</sup> At this time in view of the present work, the possibility that Kutzner did observe a manifestation of non-independence cannot be disregarded.

Despite the Kutzner reports, the independence of radioactive decay events and the resultant applicability of the Poisson distribution appear to be accepted almost universally, and determinations of probabilities in a variety of fields involving radioactive decay depends on the generality of this assumption. Evans<sup>6</sup> states unequivocally "Nuclear processes ... are random in ultimate character."

With the exception of the Kovarik reference,<sup>8</sup> a major portion of the earlier literature references involved studies of  $\alpha$  particle decay. Thus, historically, the development of the concept of the *general* validity of radioactive decay independence and randomness depended in large part on the additional hypothesis that all types of decay processes are alike with respect to the independence-of-events characteristic. This largely unphrased hypothesis does not appear to have been seriously tested in the literature at least with respect to solid experimental evidence.

### Statistical Method

To evaluate experimental data (such as counts resulting from radioactive emissions) for conformance with the Poisson expectation, a number of statistical tests may be used, each one of which tends to examine only particular characteristics of the observed dis-

tributions and none of which, if conformal with the expectation, guarantees that other tests will also be conformal. [(5s)<sup>4</sup> The close approximation of exponential behavior during determinations of exponential constants does not preclude nuclear interactions. (6s)<sup>4</sup> A discussion of the significance of single statistical tests.] The ones used in most of the work reported earlier were the  $\chi^2$  goodness-of-fit test which is a comparison of an observed frequency distribution to a theoretic one and the Lexis divergence coefficient cited earlier. The  $\chi^2$  test is primarily an overall or global test of the distribution, but, as Berkson has shown, the index of dispersion ( $s^2/m$ ) is oftentimes more sensitive.<sup>13</sup>

The index of dispersion statistic ( $s^2/m$ ) is the ratio of the observed variance ( $s^2$ ) to the expectation ( $m$ ) where  $m$  is the best estimate of  $\sigma^2$  for the Poisson; it has been employed in this paper to test the observed distributions of counts obtained from radioactive emissions. The index is calculated as

$$s^2/m = \sum_{n=1}^n (a_i - m)^2 / (DF \times m) \quad (1)$$

$$m = \sum_{n=1}^n a_i / n \quad (2)$$

where  $s^2$  is the variance,  $m$  the mean,  $n$  the number of observations,  $a_i$  the counts per unit time, and DF the degrees of freedom. When the mean does not sensibly change with time,  $DF = n - 1$ . When the "mean" is calculated for each point, as for example in a rapid exponential change,  $DF = n - 2$ .

Within a statistical set, several values of the index may be combined so as to determine an overall value of the index and thereby to determine an overall probability that the observed variance for a series of runs is due to chance alone, as

$$\overline{s^2/m} = [(s^2/m \times DF)_i + (s^2/m \times DF)_j + \dots] / (DF_i + DF_j + \dots) \quad (3)$$

The index is itself variable, a variability about 1.000 which is predictable theoretically as a function of the number of degrees of freedom. Standard tables showing the distribution are readily available.<sup>14</sup>

(6) E. Rutherford and H. Geiger, *Phil. Mag.*, **20**, 698 (1910).

(7) L. F. Curtiss, *J. Res. Nat. Bur. Stand., Sect. A*, **8**, 339 (1932).

(8) A. F. Kovarik, *Phys. Rev.*, **13**, 272 (1919).

(9) J. Berkson in "Research Papers in Statistics," F. N. David, Ed., Wiley, New York, N. Y., 1966, pp 37-54.

(10) W. Kutzner, *Z. Phys.*, **21**, 281 (1924); *ibid.*, **44**, 655 (1927).

(11) L. F. Curtiss, *J. Res. Nat. Bur. Stand., Sect. A*, **4**, 595 (1930).

(12) Cf. R. W. Lawson, *Nature (London)*, **114**, 121 (1924).

(13) J. Berkson, *J. Amer. Statist. Assoc.*, **33**, 526 (1938); *ibid.*, **35**, 362 (1940).

(14) Cf. "Handbook of Tables for Probability and Statistics," 2nd ed, Chemical Rubber Publishing Co., Cleveland, Ohio, pp 295-298.



## Monolayers

In this work carbon-14-labeled organic (sub)monolayers adsorbed on activated metal (oxide) surfaces have been prepared by the evaporative deposition of suitably labeled organic compounds using the technique known as Evaporative Rate Analysis (ERA).<sup>15</sup> In this method chemisorption through functional group-surface site interaction is believed to take place at or near the retreating interface of an evaporating liquid cyclopentane solution containing approximately one monolayer equivalent of radiolabeled solute. [(7s)<sup>4</sup> A discussion of the number of molecules adsorbed per unit surface area.] The radiation emitted by the monolayers was then analyzed simply by observing the emissions using an adjacent "window" detector.

In particular, low variances of the detected radiation have been observed involving two types of monolayers, namely (1) desorbing monolayers in which the adsorbed species tends to desorb and to be swept out from under the detector by means of flowing gaseous nitrogen; thus the detected emissions arise almost exclusively from the adsorbed species; and (2) nondesorbing monolayers of stearic acid-1-<sup>14</sup>C under conditions that a positive or adventitious charge is permitted to build on the surface on which the radiochemical is adsorbed.

In each case of the restricted or narrow statistical distributions, the carbon-14 radioisotope was incorporated either within the adsorbed functional group or immediately adjacent to it.

In the case of the desorbing monolayers, the adsorbed material is essentially volatile under the conditions of test (ambient) and in the absence of adsorption evaporates virtually instantaneously. Thus, *e.g.*, 2-ethylbutyric acid-1-<sup>14</sup>C completely evaporates from non-adsorbent surfaces within a period of *ca.* 30 sec. Even when adsorbed on aluminum, it tends to desorb spontaneously. The observed radiation thus decreases with time as the molecules evaporate and as they are swept out from under the detector by the metered stream of nitrogen gas always employed. [(8s)<sup>4</sup> A discussion of the effect of the changing "mean" encountered in desorptions.]

Monolayer desorption phenomena are normally best described by simple first-order kinetics—that is,  $\log y$  vs.  $t$  plots are straight lines over extended periods. In the desorptions so far observed, no other method of data analysis—*e.g.*, linear-linear, log-log, Elovich, etc.—permits such general and extended straight line analysis from run to run or within runs. As a result, the changing values of  $y$  are derived from the equations

$$y = y_0 e^{-kt} \quad (4a)$$

or in  $\ln$  form

$$\ln y = \ln y_0 - kt \quad (4b)$$

by least-squares fitting of the  $\ln a_i$  values, and eq 1

therefore involves a series of  $y_i$  values rather than  $m$  calculated as a constant mean.

In a sense this type of desorption is thus somewhat similar, insofar as activity reaching the detector is concerned, to the decay process of a much shorter half-life radioisotope. For the desorptions described, the apparent half-lives vary downward from approximately 18 hr.

The calculation of the statistical distribution about each linear regression may be made on the basis of the real numbers (as in eq 1) or on the basis of  $\ln$  or  $\log$  values or in combination. In converting from real numbers into  $\log$  values for  $\log y$  vs.  $t$  plots and least-squares fitting, weighting is recommended primarily when orders of magnitude differences of  $y$  are encountered. With relatively small changes (10–20%) as are encountered herein, the differences are of no appreciable significance with respect to the derived "best" line and weighting has not been used herein. [(9s)<sup>4</sup> If any derived line is not the best possible line to describe the actual process, the derived variance statistic must be higher than would otherwise obtain.]

## Experimental Section

*Counting Systems.* Three counting systems based on completely independent design were employed in this work also involving four differing detector models.

System I (used primarily in the desorption experiments) is a commercially available solid state counting and control system marketed under the trade name MESERAN Model 720.<sup>16</sup> The total system comprises an electronic and control section with provision for accurately regulating the flow of gaseous nitrogen over the test surface and between the surface and the detector face, a thin end-window GM detector assembly which also provides for control of the evaporative environment and for reproducible positioning and maintenance of the test surfaces during counting, and a precision dispenser for depositing preformulated test solution (radiochemical and low-boiling cyclopentane solvent) onto the test surface. [(10s)<sup>4</sup> A description of the counting mechanism.]

The primary thin end-window GM tubes (diameter 2.9 cm, 1.4–2.0 mg/cm<sup>2</sup> grounded mica window, halogen quench) were those of Amperex Model 18526. An additional 0.0038 mm (0.15 mil) Mylar shield was provided to reduce system background arising from adsorption of vapor phase labeled molecules; the Mylar protected window was positioned 0.5 to 0.8 cm above the test surface in each case—in the "standard source" counting *and* in the low variance examples. No anticoincidence circuit was used. The shape of the

(15) *Cf.* J. L. Anderson, R. A. Baker, and J. F. Forbes, *J. Colloid Interface Sci.*, **31**, 372 (1969).

(16) The MESERAN Model 720 systems are produced and sold by AMETEK/Technical Products, a Division of AMETEK, Inc. *Cf.* J. L. Anderson, D. E. Root, Jr., and G. Greene, *J. Paint Technol.*, **40**, 320 (1968).

GM pulse appeared identical for both "normal" and narrow distributions. Overall counting efficiencies of 4–7% (including backscatter) of the emitted radiation obtained.

Several different units of this system were employed, and the four referees who carried out desorptions independently also used these systems.

The timing circuit utilizes a Cramer cyclic cam timer equipped with micro switches which were mechanically adjusted to provide the necessary on-off gates for the count totals. Each timer is based on a 60-Hz synchronous motor.

Not available commercially, System II is an integrated circuit advanced prototype of the MESERAN systems equipped with automatic data printout. It employs a timing circuit based on 60 Hz in which all switching is carried out electronically. It expressed all detected counts observed with an Amperex 18536 thin end-window GM tube whose experimentally determined resolution time was less than 100  $\mu$ sec. The detector-surface mechanical equipment was identical with that of System I.

System III is a Nuclear Data Model 1100 1024 multichannel analyzer which was used in the multiscale mode and was equipped with automatic data printout.<sup>17</sup> Count rates were maintained at a level low enough so that no observable loss was apparent. The timing circuit consisted of an external clock based on a crystal oscillator. The mechanical detector-surface setup approximated that used in the earlier experiments but was not identical due to a lack of the same equipment at time of confirmation. Two detectors were employed: a Tracerlab thin end-window organic quench GM tube of less than 100- $\mu$ sec resolution time (experimentally determined) and an anthracene crystal-photomultiplier tube assembly which was operated in the dark and which in one experiment had the Mylar shield removed. These detectors are designated in Table III as ND/GM and ND/A, respectively.

*Substrates.* The aluminum foil employed in this study was kindly supplied by Kaiser Aluminum and Chemical Corp., and consisted of two rolls of "smooth" 3003 aluminum foil of approximately 0.076 mm (3 mil) thickness which reportedly had triglyceride rolling oil residues left on the surfaces and which was in a "hard" or nonannealed condition. Approximately 10  $\times$  10 cm sections of the foil were removed and heated over thermostatically controlled, horizontally positioned cylindrical heaters (10 cm diameter) at 320° for at least 20 min to remove the rolling oil residues and to "activate" the surfaces. The sections were draped over the heater with their parallel, horizontal edges weighted to ensure intimate contact of the central portion with the heater surface. Only the top side (exposed to the laboratory atmosphere) was used for monolayer adsorptions. Following heating each specimen was removed, permitted to cool for a few seconds

to ambient, and then positioned on a vacuum-activated (from below) hold-down stage so that the now dead-soft foil formed a slight concavity into which the test solution was deposited. For the desorptions measurements, the specimens were then used in the hold-down stage following deposition and evaporation of low-boiling solvent cyclopentane by positioning the GM detector and initiating the counting sequence (which also started the gaseous nitrogen flow—ca. 600 ml/min). For the nondesorbing stearic acid-1-<sup>14</sup>C, each specimen was copiously rinsed with cyclopentane and/or trifluorotrichloroethane following evaporation of the deposition solvent. Then the portion of the specimen containing the monolayer (ca. 1.5  $\times$  1.5 cm) was cut out and positioned for counting.

The glass substrates (Table V) were prepared by sectioning the roughened portion of glass microscope slides, cleaning in hot sulfuric acid-dichromate (sample 2) or in hot sulfuric acid-nitric acid (sample 3) followed by copious rinsing with deionized water and drying in the atmosphere for 30 min.

The boehmite surface (Table IV) was prepared by immersing a specimen of the 3003 aluminum in boiling distilled water for 3 min followed by momentary drying at 168°. Then the surface was positioned and examined on the hold-down stage as above.

The nickel surface was prepared by heating a 0.125-mm section of nickel foil (kindly supplied by the General Electric Co.) in the same manner as was used for the aluminum surface (*cf.* Table IV).

The chromous oxide on steel surface (Table IV), kindly supplied by Kaiser Steel Co., was heated over a Bunsen burner for ca. 30 sec and cooled, and the surface away from the flame was employed for the desorption experiment.

*Radiochemical Test Solutions.* The 2-ethylbutyric acid-1-<sup>14</sup>C, the *N,N*-dimethyl-*N-n*-decylamine-1-<sup>14</sup>C, and the 2-cyclohexylethanol-1-<sup>14</sup>C were custom synthesized by Mallinckrodt/Nuclear and had, at time of receipt, no detected impurities, either radio or chemical. Each was dissolved upon receipt in a large volume of cyclopentane, having been dissolved in a smaller volume of the same solvent immediately following synthesis. At least double-distilled from an all-glass column (no greased joints), the cyclopentane had less than 0.5% volatile impurity by gc and nonvolatile residue of less than 1 part in 30 million by ERA.

The specific activities of the three above-mentioned radiochemicals were 60 mCi/mM (1 position essentially carrier-free <sup>14</sup>C) since they were synthesized without dilution from barium carbonate of similar activity. The overall rationale for using such high specific radiochemicals was based on the overall counting efficiencies involving thin end-window GM detectors.

(17) Located at the Special Training Division of Oak Ridge Associated Universities, Oak Ridge, Tenn.



Thus with approximately 5% efficiencies, ethylbutyric acid monolayers of  $6 \times 10^{14}$  molecules/cm<sup>2</sup> (roughness factor of ca. 2) emit sufficient  $\beta$  particles to give 8,000–10,000 cpm. Thus with coverages of 0.6 to 0.7 cm<sup>2</sup>, 5000–6000 cpm are customary.

The lower specific activity ethylbutyric acid-1-<sup>14</sup>C was obtained by diluting the previously prepared test solutions with appropriate concentrations of cold ethylbutyric acid (Aldrich) in similarly purified cyclopentane.

The stearic acid-1-<sup>14</sup>C was obtained in benzene solution from Chicago-Nuclear Corp. and had a specific activity of 48+ mCi/mM; following evaporation of the benzene, it was diluted in cyclopentane for the initial experiments but in cyclohexane for those confirmatory ones carried out at ORAU. (Note: The wettability of the stearic acid-1-<sup>14</sup>C–cyclopentane solution was considerably less than that of the corresponding cyclohexane one. Thus no assurance that a similarly deposited monolayer at time of confirmation is available.)

*Monolayer Preparation.* The monolayers of radioactive organic compounds were prepared simply by permitting the radioactive test solutions (e.g., 20  $\mu$ l of ethylbutyric acid-1-<sup>14</sup>C–cyclopentane solution of ca. 1 part of radiochemical to 10<sup>5</sup> parts of solvent) to evaporate into the atmosphere following deposition of the liquid onto the suitably positioned heat-activated foil (or other) surfaces.

When less than 60 mCi/mM specific activity radio-material was employed, increased area coverages involving greater volumes of test solutions were used so that the number of retained molecules having carbon-14 incorporated in them would approximate those of high specific activity, the total number of retained molecules on a particular surface being a function of the area occupied by each molecule.

*Counting and Statistical Procedures.* The summaries as listed in the several tables include all the desorptions and nondesorbing experiments known to the author and in which statistical distributions have been calculated and in which the particular characteristics (such as the 42+ data point log  $y$  vs.  $t$  straight line condition in the desorptions) apply. In all the work so far carried out and reported herein, no data point (counts per unit time) has ever been eliminated from a statistical set regardless of the extent of the anomaly of any particular point.

In the cases of the desorptions, counting was invariably initiated by positioning the detector as soon as the solvent visibly disappeared by evaporation. In the cases of the nondesorbing stearic acid monolayers, an initial period of 50 min was routinely used to permit equilibration of conditions prior to the start of the counting sequences.

In the desorptions, end points of the log  $y$  vs.  $t$  straight lines were routinely first estimated by plotting

log  $y$  vs.  $t$  values on a greatly expanded scale (e.g., 0.01000/5 cm on the log  $y$  axis) followed by sighting and placing of transparent straight edges to approximate the end points and intercepts. Such sightings were then routinely re-analyzed by at least one other person to reduce the possibility of adverse judgmental selectivity in such allocations. Secondly, the points within each line grouping were least-squares fitted by standard computer programs and the overall index by eq 3 computed so as to include the adjacent lines as well. In cases where the intercepts and/or end points were not completely obvious, one or two points at each end of the major line were then added to and subtracted from the adjacent lines and the statistics recalculated so that a minimal overall index was obtained. Then the first line of at least 42+ data points based on the minimum index criterion was used in the analysis. In general, reduced distributions in the lengthy lines (42+) were quite obvious as were the lines; intercepts were normally apparent to within one data point. [(11s)<sup>4</sup> The observed desorptions varied considerably in log  $y$  vs.  $t$  patterns from run to run. Illustrations are shown.]

In many cases the desorptions were continued beyond the limits cited in Table III. However the statistical summary includes only the first 42+ period lines so that the percentage of the monolayer involved would be relatively consistent.

While every effort was made to arrive at the proper and best line in each desorption by consensus of opinion as well as by computer-based analysis, ultimately the author takes the final responsibility in each case. Such decisions thus represent, to a degree, a judgment factor.

In the nondesorbing experiments, most of the incidental charge and deliberate charge runs were halted after approximately 8 hr although in two much longer times were observed. However to ensure that the summary included only relatively homogeneous conditions, an arbitrary limit ca. the first 500 data points in each case has been used. In those shorter runs listed, the runs were interrupted at the end points listed.

## Results

*"Standard Source" Counting.* As a criterion of "normal" equipment performance and using the very same experimental setup in each case as was used later to observe the statistical abnormalities, the three equipment systems were each qualified with respect to the statistical index of dispersion ( $s^2/m$ ) using so-called "standard sources" and/or adsorbed stearic acid-1-<sup>14</sup>C on grounded aluminum surfaces. [(12s)<sup>4</sup> A description of the New England Nuclear Corp. "standard sources." ] As shown in Table I not only did the overall statistical index approximate 1.000 with each system but also the variance of the statistic itself was that expected. It is apparent from even a casual inspection of the derived statistics that the values vary above and below 1.000.

Table II (whose values were taken from ref 14 cited above) illustrates the theoretically expected probabilities for these two degrees of freedom (49 and 53) and also the marked tendency to approach a very limited variance as the number of degrees of freedom increases.

Table I

System	Degrees of freedom (DF)	Index ( $s^2/m$ )	Sources				
A. "Standard Source" Counting							
I	1063	1.030	Stearic acid, NENC				
II	2546	0.990	Stearic acid, NENC				
III <sup>a</sup>	741	0.985	Stearic acid				
B. "Standard Source" Distributions of $s^2/m$							
1. System I: NENC Source; DF = 53 <sup>b</sup>							
1.243	1.434	1.056	0.727	1.208	1.415	1.154	1.422
1.022	0.831	1.126	0.893	1.129	1.010	0.890	1.216
0.730	1.024	0.965	1.137	1.122	0.781	0.854	1.210
Mean = 3733		$s^2/m = 1.067$					
2. System II: Stearic Acid on Aluminum (Grounded) DF = 49 <sup>c</sup>							
1.411	0.969	0.916	1.136	0.944	1.052	0.843	
1.049	1.030	0.984	1.306	0.685	0.998	0.835	
Mean = 5399		$s^2/m = 1.011$					

<sup>a</sup> Including both GM and anthracene-PMT detectors. <sup>b</sup> Based on eight 54-period groups of each of three 200-data period sets and involving three different units of System I. <sup>c</sup> Based on 14 sequential groups of 50-data periods each during 700 min of counting employing System II.

Table II: Expected Variability of the Index of Dispersion<sup>a</sup>

Degrees of freedom	Probability (P), %					
	0.1	1.0	2.5	97.5	99.0	99.9
49	0.4894	0.5906	0.6440	1.4331	1.5290	1.7418
53	0.5050	0.6041	0.6562	1.4151	1.5065	1.7089
100	0.6192	0.7007	0.7422	1.2956	1.3581	1.4945
1000	0.8675	0.8989	0.9143	1.0895	1.1070	1.1440
3000	0.9221	0.9409	0.9500	1.0513	1.0611	1.0817

<sup>a</sup> Data taken from ref 14, pp 297, 298.

*Desorptions.* Table III lists the values of the variance index obtained from the desorptions involving (sub)monolayers of 2-ethylbutyric acid-1-<sup>14</sup>C and encompassing all the desorptions so far examined having at least a 42+ data point log  $y$  vs.  $t$  straight line. Only the statistics of the first such line in each desorption are listed although only in a very few such cases was a second such lengthy line observed within the first 150 data points. The statistics are listed with increasing values of the slope,  $k$ , of the log  $y$  vs.  $t$  line. There appears to be no general relationship of statistical index with slope except for the possibility that at the higher

values ( $k$  greater than 0.00200) the index may approach a more normal index.

In none of the 22 desorptions was an index as high as 1.000 observed. (Note: Of a total of 33 desorptions so far observed and analyzed, 11 did not have a line of at least 42+ data points in length.)

As noted, the referee-run desorptions are listed by the names of the referees. The desorptions employing less than 60 mCi/mM specific activity radiomaterial are noted and do not appear to have as low a statistical index as the others; more work needs to be carried out before definitive conclusions can be drawn in this regard.

Table IV lists the results obtained from three other "desorptions" involving other substrates and/or radiochemicals. These data seem to indicate that the phenomenon of narrow statistical distributions is general for a variety of surfaces and monolayers. No data are available to the author involving these or other materials than those listed. [(13s)<sup>4</sup> Table I (S) includes all the data points obtained for four of the desorptions which are illustrative of the patterns of desorption.]

*Nondesorbing Monolayers.* Adsorbed monolayers of stearic acid-1-<sup>14</sup>C on heat-activated aluminum foil (grounded) have been shown to emit radiation which follows very closely to Poisson expectations (*cf.* Table I). On the other hand, nongrounded substrates having adsorbed monolayers of stearic acid-1-<sup>14</sup>C exhibit restricted or narrow distributions as are shown in Table V. The *identical* sample that was described in Table IB and also listed as sample 1a in Table V was further counted using System II after placing the sample on a piece of polyethylene film and thereby effectively isolating it electrically from ground, as listed in sample 1b. The generation of charge was presumably due both to the continuous flow of extremely dry nitrogen gas over the surface during counting as well as the net emission of  $\beta$  particles. The ground on the adjacent end-window of the GM tube was that provided by the metallic flash with which all such tubes are constructed. The observed mean was essentially that observed in the grounded configuration recognizing that differences in geometry presumably occurred as a result of a small change in positioning of the sample relative to the detector.

The same sample was then recounted a second time for 500 min except in this case an additional electrically grounded aluminum foil absorber (*ca.* 0.0125 mm thick) was placed between the monolayer emitter and the detector window; the mean detected count decreased approximately 60% which is that expected for the absorber. In both cases of nongrounding, the  $s^2/m$  statistic was considerably low over the first 500 min of counting, and in each case during a 300-min sequence (of the 500) the statistic was markedly lower. The similarities are striking.

Samples 2 and 3 of Table V consisted of stearic acid-



**Table III:** Values of Variance Index for Desorptions

Sample	Limits	Length, min	Av $\Delta C/\text{min}$	Means $y_a, y_w$	$k$ in $\log y =$ $\log y_0 - kt$	Index $s^2/m$
Sok	58-147	90	4.5	6797, 6389	0.00030	0.444
1421	34-97	64	3.7	5282, 5047	0.00031	0.695
0814	1-74	74	4.5	5427, 5095	0.00037	0.796
5119	37-89	53	5.1	5850, 5580	0.00039	0.766
0750 <sup>a</sup>	19-64	46	1.8	1656, 1574	0.00048	0.860
0999 <sup>a</sup>	20-97	78	4.9	4442, 4068	0.00049	0.817
0997 <sup>a</sup>	15-58	44	5.6	4960, 4715	0.00050	0.701
0617	46-107	62	5.9	4511, 4146	0.00059	0.732
ND/A1	61-122	62	7.5	4690, 4225	0.00064	0.786
0861 <sup>a</sup>	24-65	42	9.1	6035, 5652	0.00068	0.642
Miranda	7-64	58	8.1	3848, 3381	0.00097	0.915
0734	23-96	74	10.4	4667, 3895	0.00106	0.870
0732	51-118	68	10.5	4730, 4019	0.00108	0.659
0454	1-65	65	11.7	5096, 4335	0.00108	0.638
ND/GM1	1-52	52	14.4	4910, 4163	0.00137	0.457
0299	23-74	52	14.6	4863, 4102	0.00142	0.466
ND/A2 <sup>b</sup>	9-102	94	9.2	3240, 2380	0.00151	0.722
Jennings	34-83	50	10.1	2451, 1947	0.00200	0.624
Pietras	26-70	45	5.0	1042, 817	0.00234	0.658
1429 <sup>a</sup>	40-96	57	14.1	3026, 2222	0.00236	0.972
ND/GM2	55-108	54	11.6	2165, 1533	0.00278	0.766
0453 <sup>c</sup>	9-60	52	34.6	3248-1451	0.00673	0.819

For 1292 degrees of freedom, overall  $\overline{s^2/m} = 0.717$

<sup>a</sup> Low specific activity runs (ca. 6.7-7.5 mCi/mM). <sup>b</sup> 30-sec accumulations; when 9,10; 11,12; etc., were summed and the index recalculated on the basis of 47-min periods,  $s^2/m = 0.709$ . <sup>c</sup> Nitrogen gas saturated with respect to water vapor.

**Table IV:** Other Substrate Desorptions

Surface	Adsorbate	$s^2/m$	Remarks
(1) Boehmite on 3003 Al (AlOOH)	$\beta$ -Cyclohexylethanol-1- <sup>14</sup> C	0.644 ( $N = 47$ )	200 30-sec accumulations (data points); six slopes: three more-or-less horizontal ones—separated by much more rapid ones—had low index values; the lowest is shown
(2) Nickel (oxide)	<i>N,N</i> -Dimethyl- <i>N-n</i> -decylamine-1- <sup>14</sup> C	0.666 ( $N = 48$ )	The cited low index was for a slope positioned between two others of 1.000 ( $N = 39$ ) and 1.049 ( $N = 43$ ); total $N = 149$
(3) Chromous oxide on mild steel ("tin-free steel")	2-Ethylbutyric acid-1- <sup>14</sup> C	0.515 ( $N = 32$ )	First "lengthy" $\log y$ vs. $t$ straight line

1-<sup>14</sup>C as monolayers on freshly cleaned glass surfaces which had been placed on polyethylene film (2) and on cast sulfur (3) to electrically isolate from the environment. In keeping with the observations of Perkins and MacDonald, 170 min was required before the "mean" settled down to a constant value in (2) and 30 min in (3).<sup>18</sup> [(14s)<sup>4</sup> A short description of the observations.] In both cases the variance about the initial regressions (varying means) *appeared* low but was not calculated.

Figure 1 is a scatter diagram of counts obtained using System II in the same configuration (with the aluminum absorber in place) as described above in which the identical monolayer on aluminum (Table V, samples

1a-1c) was positioned on polyethylene film and was attached by a thin silver wire (crimped along one side of the specimen) to an external battery pair (two 45-V dry cells in series) and held for 436 min at 90 V + (the first 20 min of which were used for equilibration and counts for which have not been included in the figure or in the statistical summary), then at 90 V - for 580 min and then at 90 V + for a final 60 min. The changes in polarity were accomplished externally without altering the surface-detector relationship. The marked change in the statistical index as a function of the applied potential from 0.846 (90 V +) to 1.088

(18) H. J. Perkins and M. D. MacDonald, *Science*, **138**, 1259 (1962).

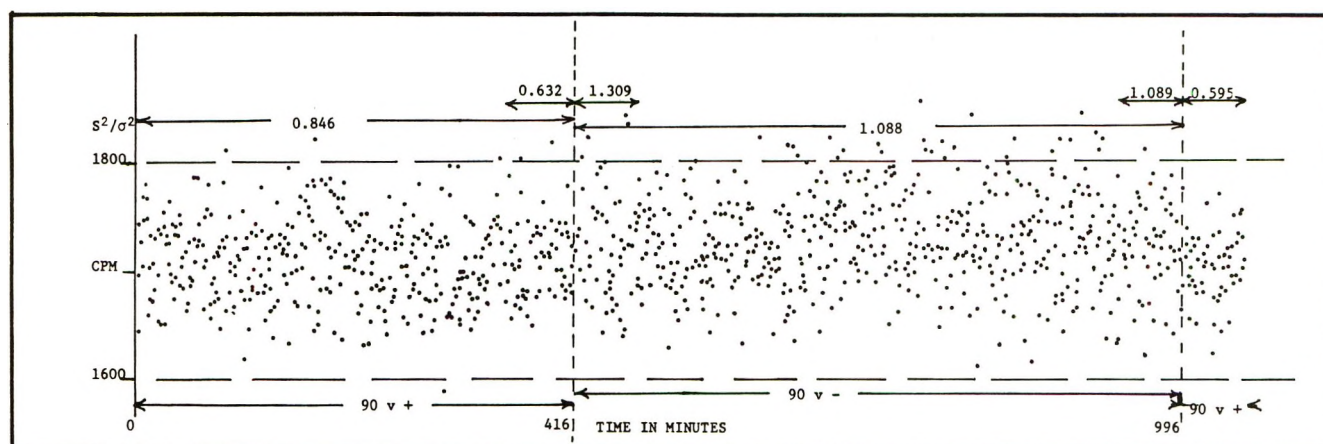


Figure 1. Scatter diagram.

**Table V:** Effect of Adventitious Surface Charge Involving Stearic Acid-<sup>14</sup>C Monolayers

Sam- ple	Mean	Number of data points	$s^2/m$	Remarks
1a	5399	700	1.011	Aluminum surface, grounded
1b	5164	500	0.893	Sample 1a on polyethylene
		300	0.793	A 300 data point sequence of sample 1b
1c	1865	500	0.871	Same as sample 1b; Al absorber
		300	0.818	A 300 data point sequence of sample 1c
2	4080	530	0.862	Glass surface, on polyethylene
3	2326	230	0.854	Glass surface, on cast sulfur

(90 V -) and to 0.595 (90 V +) are indicated on the diagram together with the 60-min statistics just prior to and just following each change in polarity.

The initial mean at 90 V + was 1713 over 416 periods, followed by 1728 at 90 V -, and then by 1707 at 90 V +. In the absence of an artifact, the change in mean from 1713 to 1728 and back to 1707 is statistically extremely unlikely. The standard deviation of the mean for Poisson distributions is defined as

$$\sigma_v = \frac{\sigma}{(n)^{1/2}} \quad (5)$$

Thus, assuming the mean during the negative charge (90 V -) is "normal,"  $\sigma_v = (1728)^{1/2}/(580)^{1/2} = 1.73$ . The mean during the 90 V + conditions is therefore more than *nine* standard deviations lower than was observed at 90 V -. The extent of this shift is, statistically, even more remarkable than that of the shift of the index of dispersion, but since the detected emissions are  $\beta$  particles, the mean shift is more difficultly separated from the artifactual possibility. No data were observed at zero voltage.

A similar experiment was carried out using the ND/A System III (ORAU) in which the initial 90 V + index

was 0.929 (400 min) and the second 90 V + index was 0.911 (350 min). The change from 90 V + to 90 V - was not as dramatic as is shown in Figure 1 since the "normal" index at 90 V - (450 min) was somewhat less than 1.000, *i.e.*, 0.962. The means changed just as dramatically—from 12,885 to 12,994 and back to 12,828 ( $\sigma = 5.4$ ). The similarity of the initial increase and then larger decrease is, percentagewise, striking. [(15s)<sup>4</sup> Figures 2 (S) and 3 (S) are histograms of the ( $a_i - m$ ) distributions for the two cases. A marked skewness at + voltage is apparent.]

Table VI lists the statistics ( $s^2/m$ ) showing the effect of positive charge and of incidental charge buildup (believed to be positive in each case) and the total or overall variance index for the group as a whole. To keep the conditions of counting as uniform as possible, only the first series for each run is included. An overall index for a number of runs at 90 V - is also listed for comparison purposes.

**Table VI:** Effect of Adventitious or Positive Charge

Number of of periods	Charge	$s^2/m$	Remarks
1-416	90 V +	0.846	See Figure 2 (scatter diagram)
1-450	90 V +	0.912	
1-350	160 V +	0.877	
1-400	90 V +	0.929	ND/A system
1-500	+ !	0.893	See Table V, sample 1b
1-500	+ !	0.871	See Table V, sample 1c
1-530	+ !	0.862	See Table V, sample 2
1-230	+ !	0.854	See Table V, sample 3
	Overall $\frac{s^2}{m}$	0.881	DF = 3339 (+)
	$\frac{s^2}{m}$	0.989	DF = 2914 (-)

Assuming the absence of all artifactuality, the overall probabilities that the two examples (desorptions and positive charge buildup) are of the same population as that of the Poisson expectation are less than  $10^{-12}$  and  $10^{-8}$ , respectively.



## Discussion

*"Standard Source" Counting.* As listed in Table I, the "standard sources" always appear to exhibit the expected Poisson distributions when counted in bulk (the NENC benzoic acid-7-<sup>14</sup>C reference sources) or when held grounded or at negative potential. Not only are the overall values of the index those which are expected, but the variability of the statistical index of dispersion is also quite similar to that shown in the theoretic probability tables (Table II).

The "normal" or expected statistical behavior of the several "standard sources" is believed to be an excellent test of the proper operation of the equipment used for counting at least with respect to the particular statistical test employed; such a criterion has been adopted.

*Monolayer Desorptions.* The ultimate validity of the log  $y$  vs.  $t$  straight lines with respect to the assumption of first-order behavior—and to the end points of the straight lines in each case—obviously determines the variance statistics from such lines. As mentioned above, many other models were examined including log-log, Elovich, and even linear-linear ones. With the variety of desorptive patterns (*cf.* 11s),<sup>4</sup> only the log  $y$  vs.  $t$  consistently yielded lengthy (*e.g.*, 42+ data point) straight line constructions in a substantial majority of the cases (two-thirds). When the limit is reduced to 35+ data points, more than 90% of the desorptions possess such lines. The assumption of first-order behavior in each case is certainly strengthened by the lengths of the lines and even by the "too good" fit of the data points. The straight line patterns illustrated cannot be improved by the other types of constructions; to use one and only one method for data analysis, the overall generality of the first-order process was thus assumed.

With an average length of straight line of 60 data points, the assumption of the first-order model certainly is not unreasonable. Adding or subtracting a point or two from the ends of any lines does not materially alter the value of the overall index. While the values given in Table III comprise 70% of the total data points, in no case does the major line comprise fewer than 50% of the points listed. [(16s)<sup>4</sup> A discussion of some of the other factors influencing desorptive behavior.]

Since it early became apparent that the restricted statistical distributions (low values of  $s^2/m$ ) constituted an unexplained phenomenon at considerable variance with accepted theories of radioactive decay, four scientists (see acknowledgments) in other parts of the United States were asked to perform similar desorptive measurements using the same type of equipment (System I) and using similar radiochemical and foil as those employed earlier by the author. These referees observed desorptions which were just as restricted and low as those seen earlier. Since the referees did not have the benefit of the cylindrical, thermostatically controlled heaters, flame or oven heating was substituted

to drive off the prior adsorbents and to prepare the surfaces.

*Nondesorbing Monolayers.* The several studies involving monolayers of stearic acid-1-<sup>14</sup>C on surfaces held at electrical potentials above ground (positive charge) illustrate a marked alteration of the statistical behavior caused by a single environmental parameter although in no single case did the anomalous statistical variance approach the extremely low level found in the desorptions.

In many respects the use of the nondesorbing species has significant advantages over the necessarily dynamic conditions of the desorbing monolayers. The identical sample was used time and again in observing the condition of low variance whereas no single specimen was used more than once in the desorption experiments.

Though insufficient statistical evidence is available for definitive assessment, the characteristic low variance did not appear to exist at 1.4 V +, at 30 V +, or even at 800 V +. Whether the phenomenon of non-Poisson character is a function of certain more or less specific voltages—and perhaps of the precise geometry employed, a factor which might affect the electrical force field—is as yet unknown.

In only two cases was the experimental setup of such a nature to permit direct comparison of the means during the 90 V +/90 V - conditions and, in both cases, the means and the statistical index changed significantly. While the change in the means might have been due to simply pushing the  $\beta$  particles into or out of the subtended cone, the possibility that the variance ratio was also affected by the same more or less trivial effect appears most improbable. Obviously if such an effect can be observed employing other than  $\beta$  emitters, the question of the triviality of the mean shift can be largely resolved at the same time.

There is no obvious or even known reason why the mean and the index of dispersion should vary simply as a result of the applied potential.

*Potential Errors.* A number of potential errors such as equipment related errors, possible double pulsing of the GM tubes, resolution time errors, potential back scatter errors, and even a possible correlation between decay and desorption have been considered and analyzed; they are discussed in detail in the appended or supplemental notes. None appears to be causal in any degree with respect to the anomalous values of the index of dispersion. [(17s) A discussion of possible errors and a discussion of the effect of possible judgmental selectivity.]

*General.* The necessary and sufficient assumption on which the applicability of the Poisson distribution depends—that radioactive decay events are independent of each other—does not require that the events are necessarily independent of the environment. As has been pointed out by Kandel, a body of evidence now exists that, at least for so-called  $k$ -capture radio-

activity or radioactivity which involves internal conversion processes, significant differences in half-lives of  $^{99}\text{Tc}$  and  $^7\text{Be}$  have been observed as a function of chemical composition.<sup>19</sup> No hint of an exception to the generality of the Poisson distribution was made in the cited references although conceivably such a phenomenon might exist unrecognized.

One may well postulate that the effect of environment could be of at least two quite different types: (1) an effect in which the rate of decay changes but which does not involve cooperation or mutuality of the decaying nuclei, and (2) an effect which does involve, or at least permits, such cooperation or mutuality.

The cited references in footnote 19 are presumably examples of type 1 while the abnormal statistics cited herein—in the absence of artifactuality—appear to be manifestations of type 2.

Throughout this work, opinions of a large number of independent scientists encompassing many and diverse disciplines have been sought to criticize the work and to comment on it. Listed in the acknowledgments, these men have generously given of their time and have suggested many of the avenues of verification employed. Where suggested experiments have been performed, the results have invariably confirmed and extended the phenomenon of non-Poisson character. At this writing, the author is unaware of any substantive arguments, other than disbelief, which are germane to the experiments, the statistics, or even the more-or-less obvious implications.

*Conclusions. Assuming the absence of artifactuality, at least under the two cited conditions of measurement—the desorbing monolayers and the (positively) charged monolayer-surface systems, the  $\beta$  emissions detected by external counters positioned adjacent to the adsorbed carbon-14-labeled monolayers are not properly described by the Poisson distribution. The further pronounced change in the means, as a result of change in the polarity of the applied surface potential alone, probably independently substantiates the inapplicability of the Poisson.*

*Unanswered Questions.* (1) What possible mechanisms are operating to cause the restricted statistical distributions and the changes in means? (1a) Are there unsuspected nuclear-nuclear interactions? (1b) Does the surface charge couple, or permit coupling of, such interactions? (2) Is it possible that radiation following emission is so altered in random behavior that the distribution is altered? (2a) If so, are the decay events themselves independent of the emissions at least insofar as the statistics of emissions are concerned? (3)

In some manner is the backscatter effect responsible for the anomaly? (4) Are the factors causing narrow or low distributions different in the case of desorbing monolayers and the case of nongrounded surfaces? (5) Does the orientation of the molecules at the interface relate to the effect? (5a) If so, are the nuclei also oriented? (5b) If the nuclei are oriented with respect to the surface, are they also oriented with respect to each other? (5c) If nuclei are oriented with respect to each other, can they cooperate in the decay process? (6) Does the rate of decay change more than incidentally from mutuality in the decay process?

*Acknowledgments.* I thank and wish to acknowledge the interest and aid of the following friends and acquaintances: R. J. Adams, L. K. Akers, R. D. Anderson, T. R. Anderson, J. Arnold, J. C. Bailar, R. H. Biehn, W. H. Bradley, Miss E. Christman, L. A. Currie, H. W. Dickson, J. L. Duggan, K. N. Edwards, P. H. Emmett, R. D. Evans, B. R. Fish, T. Fort, Jr., N. Gardner, R. V. Gentry, G. I. Gleason, I. D. Glover, J. R. Grover, E. L. Haines, R. S. Hansen, J. P. Hummel, J. M. R. Hutchinson, R. J. Kandel, H. H. Ku, W. F. Libby, J. H. Lux, W. S. Lyons, M. Manes, M. S. McCay, H. McCloud, R. M. McIntyre, J. B. Minter, R. R. Myers, A. O. C. Nier, J. E. Noakes, E. P. O'Connell, J. H. Olivier, S. A. Reynolds, C. W. Roberts, J. Robinson, and A. Schaff, Jr. Needless to say, many of these find the observations and the implications difficult to accept. C. W. Jennings of Sandia Laboratories, T. J. Miranda of Whirlpool Research, C. S. Pietras of Lord Corporation, and B. A. Sok of Inland Steel Research volunteered to carry out the referee desorptions and I greatly appreciate their help. I particularly wish to thank J. F. Forbes without whom this study could not have been completed, J. M. Carter for his early recognition of the anomaly and his continuing encouragement and support, and G. W. Spangler for his willingness to counsel during the latter stages. Much of the earlier experimental work was performed in the Laboratories of AMETEK/Technical Products, Los Angeles, Calif. The help and aid of AMETEK, Inc. is appreciated.

The help of the U. S. Atomic Energy Commission in providing the use of the facilities at the Special Training Division of Oak Ridge Associated Universities for the confirmatory studies is gratefully acknowledged.

(19) R. J. Kandel, U. S. Atomic Energy Commission, personal communication; *cf. Phys. Rev.*, **90**, 430 (1953); *Phys. Rev. C*, **2**, 1616 (1970).



## Model Calculations of Secondary $\alpha$ -Deuterium Isotope Effects in

### Addition Reactions to Olefinic Double Bonds

by I. Safarik and O. P. Strausz\*

Department of Chemistry, University of Alberta, Edmonton, Alberta, Canada (Received April 17, 1972)

Publication costs assisted by the National Research Council of Canada

In detailed calculations within the framework of transition state theory it is shown that in the addition of methyl or trifluoromethyl radicals to ethylene, as in the previously reported  $S(^3P) + \text{ethylene}$  system, the main single contributing factor to secondary  $\alpha$ -H/D isotope effects is, contrary to earlier notions, not the rehybridization of the carbon atoms but the creation of new normal modes during the reaction. Although calculations thus far have been carried out only for three systems, the effect is clearly independent of the nature of the reagents and in general it may be stated that at least one of the newly created vibrations will be isotopically sensitive and generate a secondary  $\alpha$ -H/D kinetic isotope effect larger in magnitude than that generated by the rehybridization of the carbon atoms.

The secondary  $\alpha$ -deuterium isotope effect in addition reactions involving olefins has been attributed<sup>1-5</sup> to changes in vibrational frequencies accompanying the partial rehybridization of the reactant carbon atom during passage from the reactant to the transition state. The earlier attempts by Seltzer<sup>1</sup> and by Szwarc, *et al.*,<sup>3</sup> to reproduce theoretically the experimental values of this isotope effect were based on the intuitive extension and generalization of Streitwieser's original postulate<sup>6</sup> in which the main cause of secondary  $\alpha$ -isotope effect is the frequency increase in one of the out of plane C-H vibrations on the central carbon atom during transition from the  $sp^2$  to the  $sp^3$  configuration.

The experimentally obtained values of  $k_D/k_H$  for the secondary  $\alpha$ -deuterium isotope effect in addition reactions to olefinic double bonds lie between 1.07-1.14 indicating an inverse isotope effect.

In an earlier theoretical study from this laboratory<sup>7</sup> on the secondary  $\alpha$ -deuterium isotope effect in the addition reaction of  $S(^3P)$  atoms with ethylene an important factor contributing to isotope effect was uncovered, the significance of which has been completely overlooked before. It was found that, contrary to currently accepted notions, the main single source of isotope effect in this reaction is not the relatively small change in the force constants of the reactant accompanying the rehybridization of the central carbon atom but the creation of new, isotopically sensitive vibrations in the activated complex by the formation of the new bond, corresponding to a relatively large change in the force field by introducing additional force constants.

Furthermore, relying on a model for the transition state that was derived on the basis of molecular orbital theory it was possible from a comparison of the computed and measured values of the isotope effect to

conclude that the transition state lies about half way between reactant and product in terms of geometrical changes.

On the other hand Szwarc, *et al.*,<sup>3</sup> on the generally accepted premises that the cause of the secondary  $\alpha$ -isotope effect is the rehybridization of the olefinic carbon atom concluded from the small value of the measured isotope effect in the addition of  $\text{CH}_3$  and  $\text{CF}_3$  radicals to olefinic double bonds that the bond between the radical and the carbon atom is relatively long, consequently the extent of the rehybridization is small and the reaction center retains its planar structure in the transition state. Similar considerations led Van Sickle, *et al.*,<sup>4</sup> to analogous conclusions regarding the Diels-Alder reaction between cyclopentadiene and maleic anhydride.

In order to assess the generality of the isotope effect caused by the creation of new vibrations in addition reactions and to examine the structure of the activated complex we have performed model calculations for the reactions  $\text{CH}_2\text{CH}_2 + \text{X} \rightarrow \cdot\text{CH}_2\text{CH}_2\text{X}$  and  $\text{CD}_2\text{CD}_2 + \text{X} \rightarrow \cdot\text{CD}_2\text{CD}_2\text{X}$ , where X is a group or atom with mass of 15( $\text{CH}_3$ ), 32(S), and 69( $\text{CF}_3$ ).

#### Results

The isotopic rate ratio  $k_H/k_D$  was calculated by the

- (1) S. Seltzer, *J. Amer. Chem. Soc.*, **83**, 1861 (1961).
- (2) M. Takahashi and R. J. Cvetanović, *Can. J. Chem.*, **40**, 1037 (1962).
- (3) M. Feld, A. P. Stefani, and M. Szwarc, *J. Amer. Chem. Soc.*, **84**, 4451 (1962).
- (4) D. E. Van Sickle and J. O. Rodin, *ibid.*, **86**, 3091 (1964).
- (5) W. A. Pryor, R. W. Henderson, R. A. Patsiga, and N. Carroll, *ibid.*, **88**, 1199 (1966).
- (6) A. Streitwieser, Jr., R. H. Jagow, R. C. Fahey, and S. J. Suzuki, *ibid.*, **80**, 2326 (1958).
- (7) O. P. Strausz, I. Safarik, W. B. O'Callaghan, and H. E. Gunning, *ibid.*, **94**, 1828 (1972).

equation derived from transition state theory<sup>8,9</sup>

$$\frac{k_H}{k_D} = \left( \frac{\left( \frac{I_{A_2} I_{B_2} I_{C_2}}{I_{A_1} I_{B_1} I_{C_1}} \right)^{1/2} \left( \frac{M_2}{M_1} \right)^{3/2}}{\left( \frac{I_{A_2}^* I_{B_2}^* I_{C_2}^*}{I_{A_1}^* I_{B_1}^* I_{C_1}^*} \right)^{1/2} \left( \frac{M_2^*}{M_1^*} \right)^{3/2}} \right) \left( \frac{\prod_i^{3N-6} \left[ \frac{1 - \exp(-u_{1i})}{1 - \exp(-u_{2i})} \right]}{\prod_i^{3N^*-7} \left[ \frac{1 - \exp(-u_{1i}^*)}{1 - \exp(-u_{2i}^*)} \right]} \right) \left( \frac{\exp \left[ \sum_i^{3N-6} (u_{1i} - u_{2i})/2 \right]}{\exp \left[ \sum_i^{3N^*-7} (u_{1i}^* - u_{2i}^*)/2 \right]} \right) \quad (1)$$

where the dagger signifies the transition state, and the numbers 1 and 2 refer to the light and heavy molecules, respectively.  $I$ 's are the principal moments of inertia,  $M$ 's the molecular masses,  $\mu_i = hc\omega_i/kT$  and  $\omega_i$  is a normal vibrational frequency.

Equation 1 has usually been abbreviated as a product of three factors

$$k_H/k_D = (\text{MMI})(\text{EXC})(\text{ZPE})$$

where MMI, EXC, and ZPE represent the contributions from the translational and rotational energies, vibrational energies, and the zero point energies, respectively.

The configurations of the models used for the activated complex are shown in Figure 1. In model A, the planar ethylene structure is completely preserved; the C-C-X angle is 100° and the C-C-X plane is perpendicular to the plane of the ethylene. This model represents a situation where formation of the C-X bond in the activated complex causes only negligible deviation from the ethylene structure and approximates that suggested by Szwarc, Van Sickle, and coworkers. In model B the progress of the formation of the C-X bond causes a partial rehybridization of the C atom, accompanied by structural changes in the activated complex; the distance of the C-C double bond is increased compared to that of model A, and the two C-H bonds on the C atom are bent by 10° from the C<sub>2</sub>H<sub>4</sub> plane. In this model we assumed that the formation of the new bond is accompanied by a gradual progression of the geometry from initial to final state.

Values of the three factors in equation 1 were computed individually for the two models and three masses 15, 32, and 69 of the attacking radicals.

The data for the MMI factor are given in Table I. It is seen that the values are larger than unity and they are affected but little by the model chosen or the mass of the attacking radical.

For the calculation of the values of the EXC and ZPE factors the normal vibrational frequencies of the activated complex are needed, therefore we have per-

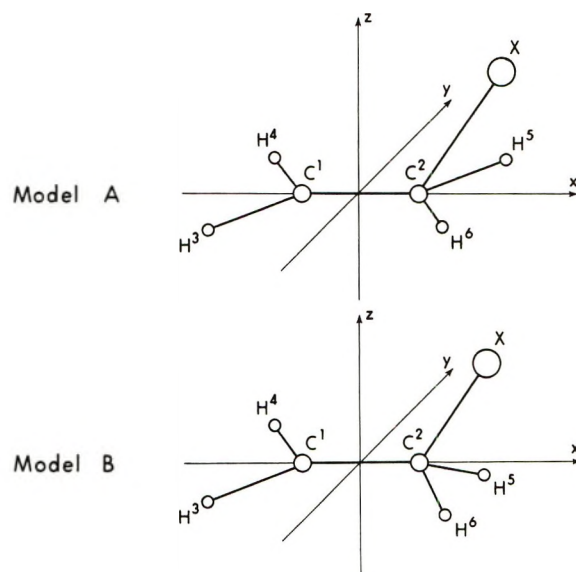


Figure 1. Illustration of geometries for the two models of the activated complex.

Table I: Values of the MMI Factor Calculated for the Two Models of the Activated Complex

	$M_X = 15$	$M_X = 32$	$M_X = 69$
Model A	1.434 <sup>a</sup>	1.466 <sup>c</sup>	1.426 <sup>a</sup>
Model B	1.423 <sup>b</sup>	1.455 <sup>d</sup>	1.417 <sup>b</sup>

<sup>a</sup> C-X = 2.0 Å. <sup>b</sup> C-X = 1.7 Å. <sup>c</sup> C-X = 2.1 Å. <sup>d</sup> C-X = 1.8 Å.

formed normal coordinate analyses on our models. The computer program used for the numerical calculations has been described elsewhere.<sup>7,9</sup> The C-X stretching mode was taken as the reaction coordinate by setting the C-X stretching force constant equal to zero, as is usual in model calculations when the potential surface for the reaction is not known.<sup>9</sup> Assumption of some negative value for this force constant would have no bearing on the result since the imaginary frequencies would be insensitive to deuterium substitution.

In model A, we used the force constants reported in the literature for the ethylene molecule,<sup>10</sup> and for the H-C-X and C-C-X bending force constant 0.1 and 0.2 mdyn Å, respectively. In stable molecules, the bending force constants for H-C-C and H-C-S are about 0.6 mdyn Å, and those for C-C-C and C-C-S about 0.9-1.1 mdyn Å; therefore, the H-C-X and C-C-X force constants in model A were assumed to be small in order to indicate a very weak bond be-

(8) J. Bigeleisen and M. Wolfsberg, *Advan. Chem. Phys.*, **1**, 15 (1958).

(9) M. Wolfsberg and M. J. Stern, *Pure Appl. Chem.*, **8**, 225, 325 (1964).

(10) B. N. Cyvin and S. J. Cyvin, *Acta Chem. Scand.*, **17**, 1831 (1963).



tween C and X and consequently a negligible perturbation of the configuration of the C atom.

In model B some of the force constants were altered in accordance with the structural changes. For the longer C-C bond the force constant was lowered from 10.8 to 8.0 mdyn/Å, and because of the stronger C-X bond, the force constants for the C-C-X and H-C-X bending motions were increased from 0.2 to 0.4 mdyn Å and from 0.1 to 0.2 mdyn Å, respectively. Recent quantum chemical calculations<sup>11</sup> have indicated a decrease in the rotational barrier for the terminal methylene group in the activated complex and we accordingly lowered the torsional force constant in model B from 0.54 to 0.34 mdyn Å.

The mass of X was taken to be 15 in both models, thus representing a structureless methyl group. Variation of the mass of X from 15 to 32 and 69 resulted in negligible small changes of the frequencies used in the calculation of the isotope effect.

The normal vibrational frequencies obtained from these calculations, with the corresponding values of the EXC and ZPE factors at 400°K, are collected in Table II for model A and in Table III for model B, respectively. For comparison, related frequencies of the ethylene molecule are also listed.

**Table II:** Values of the EXC and ZPE Factors Calculated for Model A of the Activated Complex

		Vibration, cm <sup>-1</sup>		EXC	ZPE	(EXC) × (ZPE)
C-C stretch	1623	1625	1.000	0.999	0.999	
CH <sub>2</sub> deform	1342	1349	1.000	0.997	0.997	
	1443	1444	1.000	1.000	1.000	
CH <sub>2</sub> rock	1236	1236	1.000	1.000	1.000	
	810	811	1.000	1.000	1.000	
CH <sub>2</sub> wag	943	956	1.002	0.986	0.988	
	949	974	1.003	0.972	0.974	
CH <sub>2</sub> twist	1027	1046	1.004	0.993	0.996	
		267	0.836	0.858	0.717	
Π(EXC)(ZPE) = 0.685						

<sup>a</sup> From ref 9.

The four normal modes assigned to the C-H stretching frequencies were assumed to remain unchanged in the activated complex and are not included in Tables II-IV. Similarly, the normal mode assigned to the C-C-X bend, because of its negligible sensitivity to the deuterium substitution, is left out.

Table IV gives the potential energy distribution of the normal modes among the internal coordinates in

**Table III:** Values of the EXC and ZPE Factors Calculated for Model B of the Activated Complex

		Vibration, cm <sup>-1</sup>		EXC	ZPE	(EXC) × (ZPE)
C-C stretch	1623	1544	0.999	1.010	1.010	
CH <sub>2</sub> deform	1342	1375	1.001	0.981	0.982	
	1443	1448	1.000	0.995	0.995	
CH <sub>2</sub> rock	1236	1240	1.000	1.002	1.002	
	810	810	1.000	1.000	1.000	
CH <sub>2</sub> wag	943	980	1.001	0.969	0.970	
	949	1036	1.005	0.949	0.954	
CH <sub>2</sub> twist	1027	944	0.995	1.080	1.074	
		380	0.874	0.788	0.689	
Π(EXC)(ZPE) = 0.677						

<sup>a</sup> From ref 9.

the ethylene molecule and in model A of the activated complex. It was calculated by the expression<sup>12</sup>

$$\frac{L_{ji}^2 F_{jj}}{\lambda_i} 100$$

where  $L$  is the eigenvector matrix,  $F$  is the force field matrix, and  $\lambda_i$  is the eigenvalue for normal mode  $i$ . Table IV illustrates the fractional contributions of the diagonal terms of the force field to the normal modes and clearly shows the extent of the participation of the H-C-X bending coordinates in the different normal modes.

## Discussion

In eq 1 the magnitude of the isotope effect is determined by the product of the three individual factors, MMI, EXC, and ZPE.

It is evident from Table I that the values of the MMI factor are always greater than one and contribute toward a direct isotope effect regardless of the C-X bond distance or the mass of X. This follows from the fact that addition reactions in general are accompanied by an increase in the moments of inertia and this increase is always smaller for the deuterated than protiated molecule.

Inspection of Table II reveals that when no changes of the ethylene force constants are assumed in the transition from reagent to activated complex, that is when the reaction center preserves its original planar

(11) O. P. Strausz, H. E. Gunning, A. S. Denes, and I. G. Csizmadia, *J. Amer. Chem. Soc.*, in press; O. P. Strausz, R. K. Gosavi, A. S. Denes, and I. G. Csizmadia, *Theor. Chim. Acta*, **26**, 376 (1972).

(12) E. B. Wilson, J. C. Decius, and P. C. Cross, "Molecular Vibrations," McGraw Hill, New York, N. Y., 1955.

**Table IV:** Potential Energy Distribution of the Diagonal Elements of the  $F$  Matrix in the Ethylene Molecule and in the Activated Complex (Model A)<sup>a</sup>

Normal modes	C <sup>1</sup> -C <sup>2</sup> stretch	H <sup>3</sup> -C <sup>1</sup> -C <sup>2</sup> bend	H <sup>4</sup> -C <sup>1</sup> -C <sup>2</sup> bend	H <sup>5</sup> -C <sup>2</sup> -C <sup>1</sup> bend	H <sup>6</sup> -C <sup>2</sup> -C <sup>1</sup> bend	H <sup>6</sup> -C <sup>2</sup> -X bend	H <sup>5</sup> -C <sup>2</sup> -X bend	H <sup>3</sup> -C <sup>1</sup> -H <sup>4</sup> torsion	H <sup>5</sup> -C <sup>1</sup> -H <sup>6</sup> torsion	H <sup>3</sup> -C <sup>1</sup> -H <sup>4</sup> out of plane bend	H <sup>5</sup> -C <sup>2</sup> -H <sup>6</sup> out of plane bend
C-C stretch	94 (94)	1.5 (1.5)	1.5 (1.5)	1.5 (1.5)	1.5 (1.5)						
CH <sub>2</sub> deform	5.2 (6)	23.7 (24.2)	23.7 (24.2)	23.7 (23.2)	23.7 (23.2)						
CH <sub>2</sub> deform		25 (24)	25 (24)	25 (26)	25 (26)						
CH <sub>2</sub> rock		25 (27)	25 (27)	25 (23)	25 (23)						
CH <sub>2</sub> rock		25 (25)	25 (25)	25 (24.5)	25 (24.5)	(0.5)	(0.5)				
CH <sub>2</sub> wag						(2)	(2)			50 (59)	50 (37)
CH <sub>2</sub> wag						(2)	(2)	(6)	(6)	44 (35)	44 (49)
CH <sub>2</sub> twist						(15)	(15)	50 (35)	50 (35)		
CH <sub>2</sub> twist						(30)	(30)	(20)	(20)		

<sup>a</sup> Values are given in per cent. Bracketed figures refer to the activated complex (model A).

structure, the frequencies related to the frequencies of the reactant ethylene molecule are hardly changed. However, the mere presence of X in the activated complex with only a very weak bond to the carbon atom creates a new, highly isotope-sensitive vibrational degree of freedom, the frequency of which determines the value of the product of the EXC and ZPE factors. Furthermore, it is apparent from Table IV, that the new normal mode contains a significant contribution from the CH<sub>2</sub> torsion coordinates in addition to that of the H-C-X bending coordinates, therefore its frequency must be significantly high even in the case of only a very weak C-X bond and correspondingly low H-C-X force constant.

It should also be noted that a change in the mass of the reagent radical (X) between 15 and 69 has no discernible effect on the computed values of the isotopic rate ratio.

Model A with the described force field provides an inverse isotope effect  $k_D/k_H = 1.02$ . In view of the large difference from the experimental values, 1.07-1.14, it is unlikely that, as was proposed in the literature,<sup>3</sup> only a negligible deviation of the transition state configuration from that of the reactant could generate an inverse isotope effect with the experimentally obtained magnitude.

Wolfsberg and Stern<sup>9</sup> attributed the secondary isotope effect to force constant changes in the reactant

when going over to the transition state. Our results illustrate that the creation of new vibrational degrees of freedom or the introduction of new force constants in the force field of the activated complex in the process of addition can generate an isotope effect even in the case when the force constants of the reactant are kept unchanged.

Table III illustrates the effect of altering the structure and the force field of the activated complex. As X approaches the C atom, the higher H-C-X bending force constant will increase some of the normal frequencies to different extents.

It is seen from Table III that the frequencies of the activated complex related to the out of plane wagging vibrations of the ethylene molecule somewhat increased, but contrary to Streitwieser's explanation,<sup>6</sup> this change alone cannot account for the observed inverse isotope effect. The magnitude of the isotope effect is principally determined again by the newly created twisting vibration in the activated complex.

Model B with the described force field provides an inverse isotope effect,  $k_D/k_H = 1.04$ . If the effect of lowering the torsional force constant in the ethylene molecule is neglected, then  $k_D/k_H = 1.12$ . This gives an indication of the importance of the effect caused by the reduction of the rotational barrier of the terminal methylene group in the activated complex.

The value  $k_D/k_H = 1.12$  calculated with model B



without considering the reduction of the rotational barrier reproduces the experimentally obtained isotope effect. However, lowering of the torsional force constant in the ethylene molecule generates a direct isotope effect and decreases the calculated value for  $k_D/k_H$ . In this case the experimental isotope effect can only be approached by further increase of the H-C-X and C-C-X bending force constants.

The results obtained with model B show that the reproduction of the experimental value of  $k_D/k_H$  requires H-C-X bending force constant in the activated complex, about half as large as those in stable molecules. Although no physical theory exists at present which would relate the formation of a new bond to the accompanying changes in geometry and force constants of the reacting system, a gradual, probably linear, progression from initial to final state can be assumed. Therefore the relatively large values for the H-C-X bending force constant in the activated state implies a stronger link between C and X and consequently a significant deviation from the planar ethylene structure.

It should be noted that the related normal modes of the ethylene molecule and the activated complex, as it is apparent from Table IV, are not always identical. However, the formal resolution of the isotope effect according to individual frequencies shows clearly the profound influence of the change in the vibrational degrees of freedom on the isotope effect.

It can be concluded from our calculations that the isotope effect in addition reactions involving olefinic bonds is the result of several factors acting in opposite directions: the moment of inertia increases, therefore the factor MMI is always larger than unity, and the ZPE, owing to the increase in the force field by the creation of the new twisting vibration, always decreases. The values of the factor representing vibrational excitation are affected little by isotopic substitution. Consequently the product of the three factors giving  $k_D/k_H$ , eq 1, will always lie close to unity by coincidence,

but it would be conceptually incorrect to relate this fact to the structure of the transition state without a detailed analysis.

Furthermore the present calculations clearly reveal that, contrary to the currently generally accepted notion, the main single source of secondary  $\alpha$ -isotope effects in addition reactions involving olefinic bonds is the large increase in the force field caused by the creation of new, isotopically sensitive normal mode in the course of the reaction and not the relatively small force constant change which accompanies the rehybridization of the central carbon atom. This rule applies for all reactive systems irrespective of the mass or nature of the attacking reagent and whether the reaction is a simple addition or a true cycloaddition. Naturally it follows that all previous interpretations of secondary  $\alpha$ -deuterium isotope effects in addition reactions must be reassessed.

In the previous study on the  $S(^3P) + C_2H_4$  system the appropriate calculations could be carried out because of the availability of a satisfactory model for the transition state from the combination of accumulated experimental data and detailed *ab initio* molecular orbital calculations.

At present there is no satisfactory physical model for interrelating force constant changes, and as their variations can be combined in many different ways to yield the same final results, agreement between calculated and experimental values generally cannot be considered as proof of a particular activated complex. Therefore, in lieu of additional information about the structure of the activated complex it would be pointless to calculate the numerical values of force constants of the activated complexes. Nonetheless, our results illuminate the problem of the origin of secondary isotope effect within the framework of transition state theory.

*Acknowledgment.* The authors thank the National Research Council of Canada for continuing financial support.

## Theoretical Models for Acid-Base Equilibrium Data in Nonaqueous Solvents

by Neal G. Sellers, Peter M. P. Eller, and Joseph A. Caruso\*

*Department of Chemistry, University of Cincinnati, Cincinnati, Ohio 45221 (Received April 10, 1972)*

Interpretations of conductance, potentiometric, and spectrophotometric behavior of weak acids and bases in nonaqueous solvents have been made in terms of complex equilibria. A theoretical model was used which assumed possible existence of some or all of the following species: HA, H<sup>+</sup>, A<sup>-</sup>, AHA<sup>-</sup>, HAH<sup>+</sup>, (HA)<sub>2</sub>, A(HA)<sub>2</sub><sup>-</sup>, H(HA)<sub>2</sub><sup>+</sup>, (HA)<sub>3</sub>, A(HA)<sub>3</sub><sup>-</sup>, and H(HA)<sub>3</sub><sup>+</sup>. The effects of the various equilibrium combinations on the shape of  $-\log \Lambda$  vs.  $-\log C$ ,  $E$  vs.  $-\log C$ , and  $-\log [A^-]$  vs.  $-\log C$  plots are illustrated. Explanations in terms of appropriate equilibrium systems are given for slopes obtained from theoretical conductance, potentiometric, and photometric plots. Theoretical data from these models are compared with experimental conductance, potentiometric, and photometric data from the literature.

### Introduction

Within the past 20 years many studies of acid-base equilibria in nonaqueous solvents have been undertaken.<sup>1-12</sup> These studies have involved both amphiprotic and aprotic solvents and generally have utilized conductance,<sup>3,8</sup> potentiometric,<sup>10,12</sup> or spectrophotometric<sup>2,11</sup> methods of measurement and have been done in both buffered and unbuffered solutions. Kolthoff has demonstrated that trace acidic or basic impurities can have a marked effect on acid-base equilibria in dipolar aprotic solvents.<sup>12</sup> Hence, acid-base equilibrium studies at low concentrations ( $<10^{-3}$  M) in dipolar aprotic solvents may necessitate the use of an appropriate buffer system.<sup>11,12</sup> However, some successful acid-base equilibrium studies in these solvents have been accomplished without the aid of a buffer system. For example, Kolthoff, Bruckenstein, and Chantooni reported that picric acid exists in the form of (HPi)<sub>2</sub>Pi<sup>-</sup> at concentrations above 0.10 M in acetonitrile. At these concentrations the effect of an acidic or basic impurity in the solvent would probably be small. Also, Muney and Coetzee successfully studied the conductance behavior of bases in unbuffered acetonitrile, AN, solutions.<sup>3</sup> They gave special attention to purifying their solvent in such a manner as to minimize any acidic impurities.

The effect of trace acidic or basic impurities are not as pronounced in amphiprotic solvents such as glacial acetic acid,<sup>1</sup> ethylenediamine,<sup>10</sup> or tetramethylguanidine,<sup>13</sup> and measurements in an unbuffered system of highly purified solvent are usually possible. In amphiprotic solvents of moderate or low dielectric constant the phenomena of ion pairing has been well established.<sup>1,10</sup> In dipolar aprotic solvents instances of association beyond ion pairing have been observed.<sup>2-5,12</sup> Evidence of this behavior also has been found by potentiometric and conductometric titrations.<sup>6,7,14</sup> In cases where the degree of dissociation is small, the theoretical treatments of Fuoss, Onsager, and Kraus play only a minor role in describing the equilibrium behavior.<sup>15-17</sup>

The purpose of this study was to develop models based on a generalized multiple equilibrium scheme which would yield qualitative and semiquantitative information as to the types and extent of the equilibria occurring. Thus, the bounds are defined within which experimental data for acids and bases in nonaqueous media must lie for a particular equilibrium scheme to be valid. It must be emphasized that the following models are intended for pure solvents only. A study presently is being conducted in order to determine the effect of various impurities on the equilibrium processes. The need for several experimental techniques to provide unique explanations for some of the observed behavior will become apparent. Also illustrated is the possibility of error in postulating a set of equilibria involving two or more parameters and then varying these to fit the data. Good agreement between data and

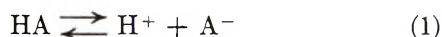
- (1) I. M. Kolthoff and S. Bruckenstein, *J. Amer. Chem. Soc.*, **78**, 1 (1956).
- (2) I. M. Kolthoff, S. Bruckenstein, and M. K. Chantooni, *ibid.*, **83**, 3927 (1961).
- (3) W. S. Muney and J. F. Coetzee, *J. Phys. Chem.*, **66**, 89 (1962).
- (4) J. A. Rutgers and M. DeSmet, *Trans. Faraday Soc.*, **48**, 639 (1952).
- (5) J. F. Coetzee and R. J. Bertozzi, *Anal. Chem.*, **43**, 961 (1971).
- (6) I. M. Kolthoff and M. K. Chantooni, *J. Amer. Chem. Soc.*, **85**, 426 (1963).
- (7) I. M. Kolthoff and M. K. Chantooni, *J. Phys. Chem.*, **70**, 856 (1966).
- (8) C. M. French and I. G. Roe, *Trans. Faraday Soc.*, **49**, 314 (1953).
- (9) J. F. Coetzee and R. J. Bertozzi, *Anal. Chem.*, **41**, 860 (1969).
- (10) S. Bruckenstein and L. M. Mukherjee, *J. Phys. Chem.*, **66**, 2228 (1962).
- (11) I. M. Kolthoff, M. K. Chantooni, and S. Bhowmik, *Anal. Chem.*, **39**, 315 (1967).
- (12) I. M. Kolthoff and M. K. Chantooni, *J. Amer. Chem. Soc.*, **87**, 4428 (1965).
- (13) J. A. Caruso and A. I. Popov, *J. Phys. Chem.*, **72**, 918 (1968).
- (14) S. L. Culp and J. A. Caruso, *Anal. Chem.*, **41**, 1329 (1969).
- (15) R. M. Fuoss and C. A. Kraus, *J. Amer. Chem. Soc.*, **55**, 476 (1933).
- (16) R. M. Fuoss and L. Onsager, *Proc. Nat. Acad. Sci. U. S. A.*, **41**, 274, 1010 (1955).
- (17) R. M. Fuoss and L. Onsager, *J. Phys. Chem.*, **61**, 668 (1957).



theoretical explanations is possible while the theory may be inherently incorrect.

### Theory and Discussion

It may be shown that a simple dissociation of  $\text{HA} \rightleftharpoons \text{H}^+ + \text{A}^-$  will give a constant slope of  $-0.5$  when  $-\log \Lambda$  is plotted *vs.*  $-\log C$  if the degree of ionic dissociation is not large. If ion-molecule conjugation is involved in the dissociation,  $2\text{HA} \rightleftharpoons \text{H}^+ + \text{AHA}^-$ , the predicted slope is 0 or there is no dependence of conductance on concentration. Of special interest are conductance data which give slopes considerably more negative than  $-0.50$ . French and Roe attempted to explain these slopes on the basis of eq 1 and 2 where ion solvation is assumed but not indicated.<sup>8</sup>



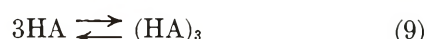
Both paths of dissociation were assumed to make a substantial contribution to the overall dissociation. However, the application of this model to explain slopes appreciably more negative than  $-0.50$  requires that the conductance of  $\text{H}^+$  plus  $\text{AHA}^-$  be negligible with respect to the conductance of  $\text{H}^+$  plus  $\text{A}^-$ .

Slopes more negative than  $-0.50$  also have been attributed to impurities in the solvent.<sup>18</sup> Muney and Coetzee<sup>3</sup> showed that dimer formation before dissociation would give a  $-\log \Lambda$  *vs.*  $-\log C$  plot with a slope of  $-0.75$ . Since most conductance data are taken over ranges of 3 to 4 orders of magnitude in concentration, the manner of dissociation dominant at one concentration may be relatively unimportant at a different concentration. Therefore, in many cases the interpretation of conductance data cannot be made in terms of a single mode of dissociation.

In order to derive conductance data from the concentrations of the various charged species predicted by the equilibrium model, some physical properties of the solvent such as the dielectric constant must be known. Kohlrausch's law is assumed to apply and the limiting ionic conductance of higher order species is assumed to be a fraction of the limiting ionic conductance of the simple ions as given by Harned and Owen.<sup>19</sup> The activity coefficients of neutral species are assumed to be unity while those of charged species are calculated by the Debye-Hückel limiting law.<sup>20</sup> With the model presented, the extended Debye-Hückel equation could be used if a constant ionic radius is assumed. However, this refinement is unnecessary since all of the activity coefficients as calculated in this investigation are greater than 0.90. For illustrative purposes these calculations are based on a "typical" solvent with a dielectric constant of 40 although other values could be used. The limiting ionic equivalent conductances of both the simple anion and cation arbitrarily are assigned values of 80. These solution properties are not unlike those of many electrolytes in acetonitrile. The

shape of the  $-\log \Lambda$  *vs.*  $-\log C$  plot is primarily a function of the equilibria present and is relatively independent of the physical properties of the system.

The equilibria given in eq 3-11 are used to represent the major reactions possible in the "typical" solvent having the properties given above. The various equilibrium constants are represented in eq 12-20.



$$K_1 = [\text{H}^+][\text{A}^-]f^2/[\text{HA}] \quad (12)$$

$$K_2 = [\text{AHA}^-]/([\text{A}^-][\text{HA}]) \quad (13)$$

$$K_3 = [\text{HAH}^+]/([\text{H}^+][\text{HA}]) \quad (14)$$

$$K_4 = [(\text{HA})_2]/[\text{HA}]^2 \quad (15)$$

$$K_5 = [\text{A}(\text{HA})_2^-]/([\text{A}^-][(\text{HA})_2]) \quad (16)$$

$$K_6 = [\text{H}(\text{HA})_2^+]/([\text{H}^+][(\text{HA})_2]) \quad (17)$$

$$K_7 = [(\text{HA})_3]/[\text{HA}]^3 \quad (18)$$

$$K_8 = [\text{A}(\text{HA})_3^-]/([\text{A}^-][(\text{HA})_3]) \quad (19)$$

$$K_9 = [\text{H}(\text{HA})_3^+]/([\text{H}^+][(\text{HA})_3]) \quad (20)$$

The equilibrium constant expressions as well as the electroneutrality and mass balance equations are treated appropriately and solved for the concentration of each of the particular species.<sup>21</sup> This information is then used to calculate a theoretical conductance ultimately leading to a  $\log \Lambda$  *vs.*  $\log C$  curve.

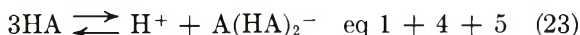
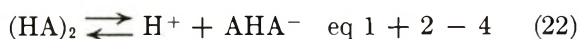
This set of proposed equilibria includes all dissociation mechanisms involving species up to the order of the most complex species assumed to exist ( $\text{A}(\text{HA})_3^-$  and  $\text{H}(\text{HA})_3^+$ ). Any other dissociation mechanism can be expressed in terms of the equilibria given in eq 3-11. Some typical examples are given in eq 21-23.

(18) A. D'Aprano and R. M. Fuoss, *J. Phys. Chem.*, **73**, 223 (1969).

(19) H. S. Harned and B. B. Owen, "The Physical Chemistry of Electrolytic Solutions," 2nd ed, Reinhold, New York, N. Y., 1950, p 195.

(20) H. A. Laitinen, "Chemical Analysis," McGraw-Hill, New York, N. Y., 1960, p 11.

(21) The mathematical derivations as well as additional conductance, potentiometric, and photometric plots with appropriate discussion will appear following these pages in the microfilm edition of this volume of the journal. Single copies may be obtained from the Business Operations Office, Books and Journals Division, American Chemical Society, 1155 Sixteenth St., N.W., Washington, D. C. 20036. Remit check or money order for \$4.00 for photocopy or \$2.00 for microfiche, referring to code number JPC-72-3618.



An analogous set of eq 3-11 exists for bases. Any manner of dissociation can be emphasized by a suitable choice of the magnitude of the equilibrium constants, *i.e.*, if an equilibrium constant is set to zero then this particular equilibrium is eliminated from the scheme.

The effect of ion pairing to form complex polymeric ions such as are shown in eq 24 can be included without major alteration of the above treatment.<sup>21</sup>



The simplest type of dissociation is given by assigning  $K_1$  a finite value and  $K_2$  through  $K_9$  values of 0. This manner of dissociation is given by eq 3. Figure 1 shows a family of curves obtained by varying the value of  $K_1$  from  $10^{-12}$  to  $10^{-6}$ . These curves are nearly linear and have slopes of approximately  $-0.50$ . This case is approached by all theoretical equilibria as the concentration approaches 0. Deviations from linearity are due to the lower activity coefficients at high concentrations and the changing degree of dissociation,  $\alpha$ , at low concentrations. This is most evident for the curve in which  $K_1$  has a value of  $10^{-6}$ . The approximate slopes by calculation are  $-0.48$  and  $-0.32$  at concentrations of  $0.316$  and  $3.16 \times 10^{-6}$ , respectively. It should be noted that the slope approaches a limit of 0 as the concentration approaches 0, since  $\alpha$  does not remain small with respect to unity as infinite dilution is approached.

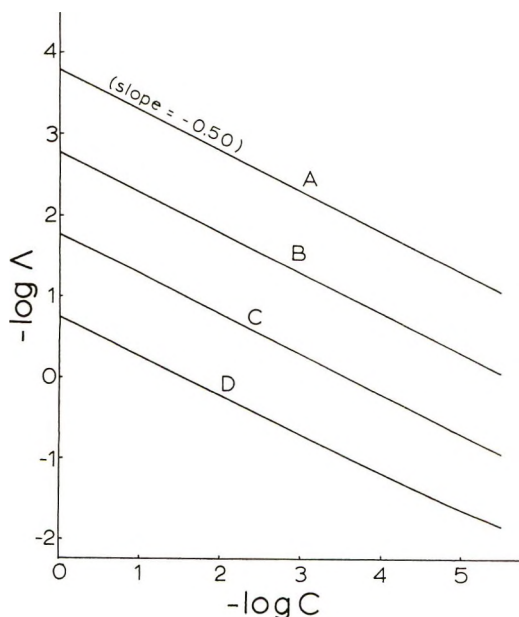


Figure 1. Conductance for ionization of HA. The equilibrium is  $\text{HA} \rightleftharpoons \text{H}^+ + \text{A}^-$ : A,  $K_1 = 10^{-12}$ ; B,  $K_1 = 10^{-8}$ ; C,  $K_1 = 10^{-6}$ ; D,  $K_1 = 10^{-6}$ .

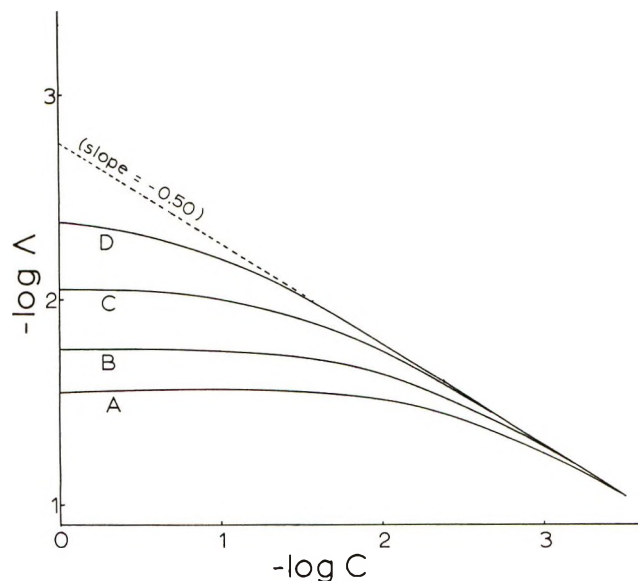


Figure 2. Conductance for ionization of HA involving autoassociation. The equilibria are  $\text{HA} \rightleftharpoons \text{H}^+ + \text{A}^-$  and  $\text{A}^- + \text{HA} \rightleftharpoons \text{AHA}^-$ : A,  $K_1 = 10^{-10}$ ,  $K_2 = 500$ ; B,  $K_1 = 10^{-10}$ ,  $K_2 = 200$ ; C,  $K_1 = 10^{-10}$ ,  $K_2 = 50$ ; D,  $K_1 = 10^{-10}$ ,  $K_2 = 10$ .

For a singly charged species to associate with a neutral molecule as in eq 4,  $K_2$  must be greater than 0. Figure 2 illustrates the variation in the shape of the curve with  $K_2$  for a constant value of  $K_1$ . At low concentrations only the simple dissociation, eq 3, occurs. The slope varies from approximately 0 to  $-0.50$  as shown in Figure 2. This type of behavior is typical of a singly charged species associating with an uncharged ion-pair or molecule. It makes no difference whether the charged species are anionic or cationic. For this model there is little effect on the conductance curves shown in Figure 2 by extensively changing the relationship between the limiting ionic conductivities.<sup>21</sup> If both the anion and the cation conjugate with a neutral species, a maximum occurs. This behavior is obtained by making  $K_1$ ,  $K_2$ , and  $K_3$  greater than 0.<sup>21</sup> The qualitative effect of conjugation of ionic and neutral species on the shape of the curve is to continuously make the slope more positive as  $K_2$  and  $K_3$  are increased until it reaches a value of  $+0.50$  at higher concentrations.<sup>21</sup>

Dimerization, in addition to simple ionization, can account for slopes more negative than  $-0.50$ . The theoretical slope of  $-0.75$  is approached at higher concentrations. At lower concentrations dimer formation becomes less important depending upon the magnitudes of  $K_1$  and  $K_4$ . A family of curves is presented in Figure 3 with  $K_1$  set equal to  $10^{-10}$  and  $K_4$  given values from 0 to  $10^8$ . These curves show that the stronger the tendency to form dimers (higher  $K_4$ ) the lower is the equivalent conductance at any given concentration. The formation of trimer species and simple dissociation gives a slope of  $-0.833$  at high concentrations. By allowing the formation of higher order polymers,  $(\text{HA})_n$ , in addition to simple ionization, the slope ap-



Table I

Major equilibrium	Slope	Intercept
$\text{HA} \rightleftharpoons \text{H}^+ + \text{A}^-$	$-1/2$	$-1/2 \log K_1 \Lambda_0^2 \text{HA}$
$2\text{HA} \rightleftharpoons \text{H}^+ + \text{AHA}^-$	0	$-1/2 \log 4K_1 K_2 \Lambda_0^2 \text{H}^+ \text{AHA}^-$
$3\text{HA} \rightleftharpoons \text{HAH}^+ + \text{AHA}^-$	$+1/2$	$-1/2 \log 7K_1 K_2 K_3 \Lambda_0^2 \text{HAH}^+ \text{AHA}^-$
$(\text{HA})_2 \rightleftharpoons 2\text{H}^+ + 2\text{A}^-$	$-3/4$	$-1/4 \log [(K_1^2/2K_4) \Lambda_0^4 \text{HA}]$
$(\text{HA})_2 \rightleftharpoons \text{H}^+ + \text{AHA}^-$	$-1/2$	$-1/2 \log [(2K_1 K_2/K_4) \Lambda_0^2 \text{H}^+ \text{A} \text{EA}^-]$
$3(\text{HA})_2 \rightleftharpoons 2\text{H}^+ + 2\text{A}(\text{HA})_2^-$	$-1/4$	$-1/4 \log \left[ \left( \frac{81}{8} K_1^2 K_5 / K_4 \right) \Lambda_0^4 \text{H}^+ \text{A}(\text{HA})_2^- \right]$
$5(\text{HA})_2 \rightleftharpoons 2\text{H}(\text{HA})_2^+ + 2\text{A}(\text{HA})_2^-$	$+1/4$	$-1/4 \log \left[ \left( \frac{625}{32} \frac{625}{32} K_1^2 K_5 K_6^3 / K_4 \right) \Lambda_0 \text{H}(\text{HA})_2^+ \text{A}(\text{HA})_2^- \right]$

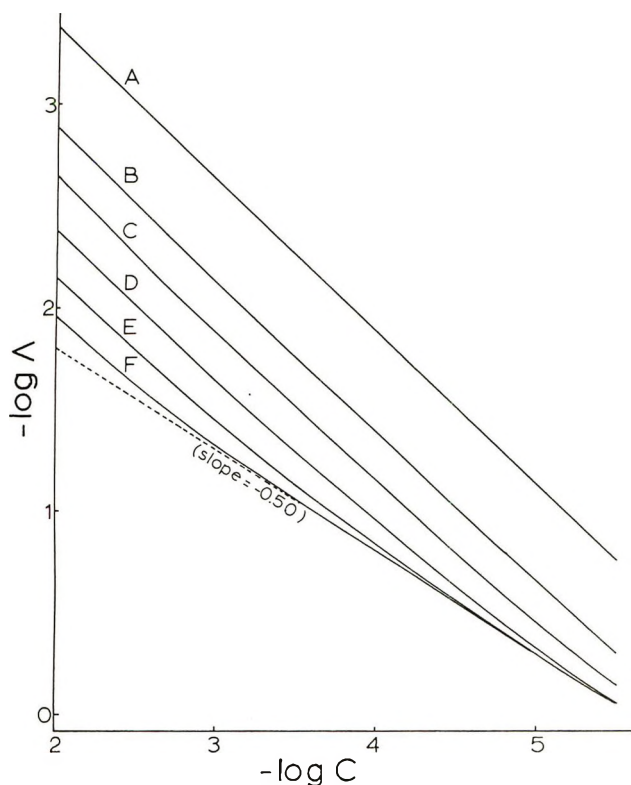


Figure 3. Conductance for ionization of HA and dimerization of neutral species. The equilibria are  $\text{HA} \rightleftharpoons \text{H}^+ + \text{A}^-$  and  $2\text{HA} \rightleftharpoons (\text{HA})_2$ : A,  $K_1 = 10^{-10}$ ,  $K_4 = 10^8$ ; B,  $K_1 = 10^{-10}$ ,  $K_4 = 10^6$ ; C,  $K_1 = 10^{10}$ ,  $K_4 = 10^3$ ; D,  $K_1 = 10^{-10}$ ,  $K_4 = 10^4$ ; E,  $K_1 = 10^{-10}$ ,  $K_4 = 10^3$ ; F,  $K_1 = 10^{-10}$ ,  $K_4 = 10^2$ .

proaches a limiting value of  $-1.00$ . However, the transition to the simple ion pair may occur at moderate concentrations ( $10^{-3}$  to  $10^{-4}$  M), and unless the formation constant,  $K_n$ , is greater than  $10^4$ , the effect of these species on the shape of the curve is insignificant.

The formation of charged conjugates involving dimers parallels the effects exhibited by the conductance curves cited above for simple conjugation. Singular conjugation tends to increase the slope to  $-0.25$  as a limit at high concentrations and conjugation with both charged species gives a limiting slope of  $+0.25$ .<sup>21</sup> These types of conjugation are important at concentrations above  $10^{-2}$  M.

Application of these types of results to a particular solvent can be used to make a qualitative and semi-quantitative analysis of experimental conductance data. It is advantageous to plot data in the form of  $-\log C$  vs.  $-\log \Lambda$  first and then speculate as to which equilibria are involved from the shape of the curves. This technique is more flexible than assuming two or at most three specific equilibria and then forcing the theoretical model to fit the data by the proper choice of the magnitude of the required equilibrium constants. The information sought from the curve is the presence or absence of a maximum and inflection point and linear regions of one or more slopes. The slopes of the linear portions of the curve indicate the possible equilibria which are occurring in that region. The intercept of a linear portion of the curve or its extrapolation is used to estimate the overall equilibrium constants for the particular equilibria predominant in this region. A few typical cases are shown in Table I. An independent value of the limiting equivalent conductance for the species of interest is necessary for calculating the appropriate  $K$  from the intercept.

Select literature data for the conductance of acids and bases were evaluated in terms of the proposed model. When necessary, experimental data were taken from graphs instead of tables. Figure 4 shows plotted data for two bases studied by Muney and Coetzee.<sup>3</sup> The solid curve is that predicted by the theoretical model using the appropriate values for the equilibrium constants. It is not necessary to use only a portion of the curve for the evaluation as was done originally for dimethylguanidine. Good agreement is evident for the entire range of experimental data by using the equilibrium models proposed by Coetzee. It is of interest to note the change in slope toward a more positive value in the  $-\log \Lambda$  vs.  $-\log C$  plot for dimethylguanidine at higher concentrations. This change could possibly be explained by allowing formation of cationic or anionic conjugate species such as  $\text{B}_2\text{BH}^+$  at high concentrations. Data for hydrochloric and sulfuric acid taken from Kolthoff and coworkers<sup>2</sup> also were evaluated in terms of the proposed model.<sup>21</sup>

Potentiometric measurements in solutions of acids

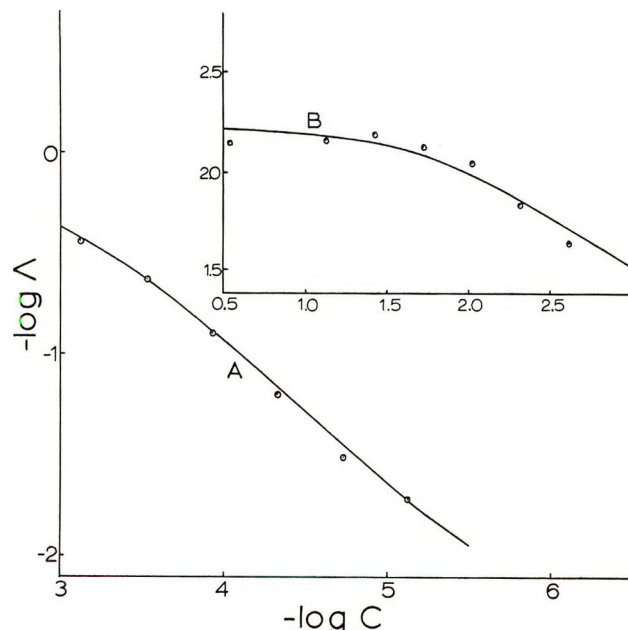


Figure 4. Conductance of bases in acetonitrile taken from the literature. Points are experimental and lines are theoretical: A, 1,1-dimethylguanidine  $B + SH \rightleftharpoons BH^+ + S^-$ ,  $2B \rightleftharpoons (B)_2$ ,  $(B)_2 + BH^+ \rightleftharpoons (B)_2BH^+$ ; 1,3-diphenylguanidine  $B + SH \rightleftharpoons BH^+ + S^-$ ,  $BH^+ + B \rightleftharpoons BHB^+$ .

and bases depend on the application of the Nernst equation to the potential of an electrode reversible to hydrogen-containing ions. The dependence of such an indicator electrode upon solute concentration is given by  $E = E_k^0 + (RT/F) \ln a_H$ , where the symbols have their usual meanings ( $E_k^0$  contains all standard potentials, junction potentials, and reference electrode potentials). The factors of interest in potentiometric studies are the ionic equilibria involved and the degree of selectivity of the indicator electrode toward solvated hydrogen ion. While it is believed that the hydrogen electrode measures the "escaping tendency" of a proton or responds to the solvated proton, included here are theoretical responses to solvated polymeric hydrogen ion containing species including  $HAH^+$ ,  $H(HA)_2^+$ ,  $H(HA)_3^+$ , . . .  $H(HA)_n^+$ .<sup>21a</sup>

It can be shown that the slopes of the potentiometric plots ( $E$  vs.  $-\log C$ ) depend on the equilibria involved.<sup>21</sup> Some evidence of large potentiometric slopes has been reported<sup>9</sup> in nonaqueous solvents and two intersecting slopes also have been seen.<sup>10,13</sup> As will be seen below, theoretical consideration of complex cations such as  $H(HA)_n^+$  where  $n = 1, 2, \dots$ , can alter potentiometric plots considerably compared to those in which only solvated protons are assumed to influence the indicator electrode.

The same equilibria as discussed above also apply here. It should be noted that the following Figures were plotted using  $(RT/F) \ln a_{H^+}$  as the ordinate,  $E$ . This means that  $E_k^0$  arbitrarily has been assigned a

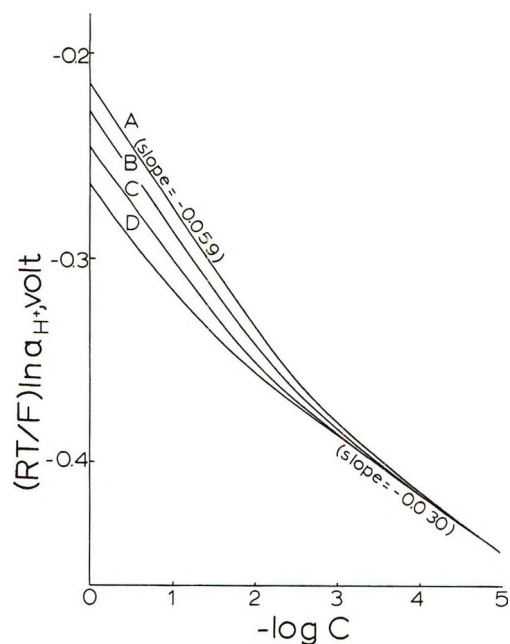


Figure 5. Potentiometry for ionization of HA involving autoassociation. The equilibria are  $HA \rightleftharpoons H^+ + A^-$  and  $A^- + HA \rightleftharpoons AHA^-$ : A,  $K_1 = 10^{-10}$ ,  $K_2 = 500$ ,  $K_3$  through  $K_9 = 0$ ; B,  $K_1 = 10^{-10}$ ,  $K_2 = 200$ ,  $K_3$  through  $K_9 = 0$ ; C,  $K_1 = 10^{-10}$ ,  $K_2 = 50$ ,  $K_3$  through  $K_9 = 0$ ; D,  $K_1 = 10^{-10}$ ,  $K_2 = 10$ ,  $K_3$  through  $K_9 = 0$ .

value of 0.00. The only effect this value has on the curves is to shift their vertical position. It does not alter the slopes which are diagnostic as to the type of equilibria. The potentiometric behavior of an acid, HA, dissociating according to eq 1 yields linear plots with slopes of  $-0.30$  for values of the dissociation constant,  $K_1$ , ranging from  $10^{-6}$  to  $10^{-12}$ .

Simple dissociation in combination with conjugation of the anion with the undissociated acid, as given by eq 1 and 2, causes the slopes of the potentiometric curves to change from  $-0.030$  at low concentrations to  $-0.059$  at high concentrations. These curves are shown in Figure 5. This behavior was observed by Bruckenstein and Mukherjee while studying the equilibrium behavior of phenols in ethylenediamine.<sup>10</sup>

The family of curves shown in Figure 5 also can be used to represent simple dissociation and conjugation with the proton, ( $HA \rightleftharpoons H^+ + A^-$  and  $H^+ + HA \rightleftharpoons HAH^+$ ) if the indicator electrode responds to  $HAH^+$  as well as  $H^+$ . This similar behavior can be predicted by considering the electroneutrality equations,  $[H^+] = [A^-] + [AHA^-]$  and  $[A^-] = [H^+] + [HAH^+]$  for each case in combination with eq 12, 13, and 14.

If both anion and cation conjugate with the neutral species and the electrode responds to both  $H^+$  and

(21a) NOTE ADDED IN PROOF. It is not suggested that these species are either highly likely or unlikely in nonaqueous solvents, only that they should be considered possibilities as part of a general equilibrium scheme. It will be shown that the formation of  $HAH^+$  may provide an alternate explanation for certain literature data.



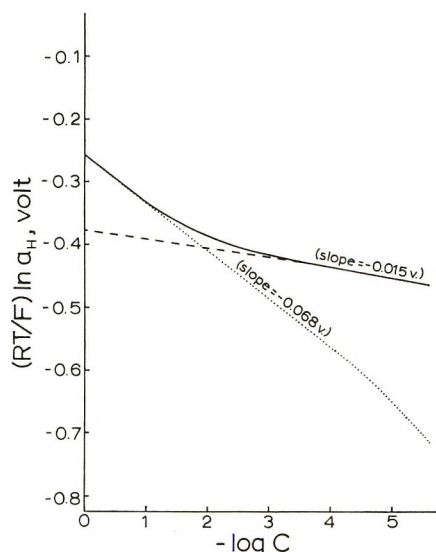


Figure 6. Potentiometry of hydrogen ion containing species.  $K_1 = 10^{-10}$ ,  $K_2 = K_3 = 0$ ,  $K_4 = 10^8$ ,  $K_5 = K_6 = 200$ ,  $K_7 = K_8 = K_9 = 0$ .  $a_H$  refers to the activity of (—) the sum of  $H^+$  and  $H(HA)_2^+$ , (---)  $H^+$  only, and (.....)  $H(HA)_2^+$  only.

$HAH^+$ , the slopes of the potentiometric plots approach  $-0.089$  at high concentrations.<sup>21</sup> Bruckenstein and Mukherjee noted this behavior for 3-methyl-4-phenylazophenol in ethylenediamine. They postulated the formation of  $HA_2^-$  and  $(HA)_2A^-$  at high concentrations. Slopes of  $-0.089$  are obtained only if  $(HA)_2A^-$  is formed in the manner shown by eq 25.



For the concentration range investigated,  $10^{-1}$ – $10^{-3}$   $M$ , the assumptions of both cationic and anionic conjugation mechanisms with response to both  $H^+$  and  $HAH^+$  may be a plausible alternate explanation of the observed slopes. For an acid,  $HA$ , of the type represented by 3-methyl-4-phenylazophenol, the formation of a species of the  $HAH^+$  type seems reasonable.

An analogous case, involving the  $H(HA)_2^+$  species (instead of  $HAH^+$ ), is shown in Figure 6. A potentiometric slope of  $-0.068$  is seen in concentrated solutions, with a decrease to  $-0.015$  V in dilute solutions. If  $H(HA)_3^+$  is formed, potentiometric slopes as large as  $-0.104$  V are seen in concentrated solution.<sup>21</sup> The conductance curves for these equilibria show minima in  $\Lambda$  at high concentrations and limiting slopes,  $d \log \Lambda / d \log C$ , of  $-0.75$  at low concentrations similar in shape to the curves shown in Figure 3 of the microfilm edition of this paper.<sup>21</sup>

The pairing of neutral species to form dimers in addition to simple dissociation as well as conjugation of an anion, cation, or both with the ion pair (or molecule) also have been studied.<sup>21</sup>

In suitable solute-solvent systems, photometric methods can be used to determine the concentrations of the various species present. Beer's law,  $A_t =$

$b \sum_{i=1}^n \epsilon_i C_i$ , relates the concentration of these species to the measured absorbance<sup>22</sup> where  $A_t$  is the absorbance,  $b$  the light path,  $C$  the concentration of the absorbing species, and  $\epsilon$  the molar absorptivity.

This relationship allows for the absorbance, at a particular wavelength, of all species present. If conjugation occurs, species such as  $AHA^-$ ,  $A(HA)_2^-$ , or  $A(HA)_3^-$  may exist in addition to the simple anion,  $A^-$ . Photometric data have been analyzed on the basis of identical spectral properties of  $A^-$  and higher order conjugates such as  $AHA^-$  or  $A(HA)_2^-$ . It also may be possible that these species have different molar absorptivities and spectral properties. In either case the sum of the anionic species  $\sum_{j=0}^n [A(HA)_j^-]$  may be determined spectrophotometrically.

Photometric data can be displayed conveniently by plotting  $-\log \sum_{j=0}^n [A(HA)_j^-]$  vs.  $-\log C$ . The manner of dissociation of the solute then can be determined from the shape of these curves. It may be shown that data from an acid which undergoes simple dissociation as given by eq 1 will plot as a straight line with a slope of 0.5. In this case,  $[H^+] = [A^-]$ . From eq 12,  $[A^-]$  can be expressed in terms of the equilibrium constant,  $K_1$ , and the undissociated acid  $HA$  as shown in eq 26.

$$[A^-] = (1/f)(K_1[HA])^{1/2} \quad (26)$$

For small degrees of dissociation,  $[HA]$  may be approximated by  $C$  and the activity coefficient by unity. Taking logarithms of eq 26 and substituting the above approximation gives eq 27.

$$\log [A^-] = 1/2 \log C + 1/2 \log K_1 \quad (27)$$

This relationship shows that a lot of  $-\log [A^-]$  vs.  $-\log C$  for an acid which undergoes simple dissociation will be linear with a slope of 0.5. If anion conjugation with the uncharged acid occurs, it can be shown that the predicted slope is 1. This slope also is obtained if the acid dissociates completely.

The simple dissociation according to eq 1 produces only the unconjugated anionic species,  $A^-$ . For values of the dissociation constant,  $K_1$ , ranging from  $10^{-6}$  to  $10^{-12}$ , the relationship between  $-\log [A^-]$  and  $-\log C$  is linear with a slope of 0.5.<sup>21</sup> At low concentrations and increased values of  $K_1$ , however, the slope increases and is approaching  $+1.0$ . This curvature is due to the degree of dissociation becoming appreciable as infinite dilution is approached.

Slopes of 1.0 are exhibited if the anion conjugates with the neutral species. This behavior is the same as that predicted for acids which dissociate completely. However, as the concentration decreases, conjugation becomes less and the slopes approach 0.50 which indicates simple dissociation of a weak acid. This change of slope with concentration is shown in Figure 7. It

(22) H. A. Strobel, "Chemical Instrumentation," Addison-Wesley, New York, N. Y., 1962, pp 152, 154.

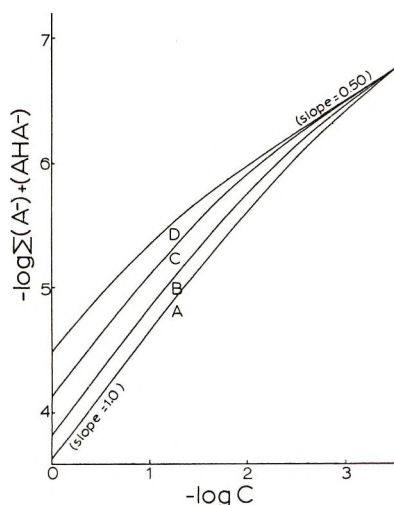


Figure 7. Photometry for ionization of HA involving autoassociation. The equilibria are  $\text{HA} \rightleftharpoons \text{H}^+ + \text{A}^-$  and  $\text{A}^- + \text{HA} \rightleftharpoons \text{AHA}^-$ : A,  $K_1 = 10^{-10}$ ,  $K_2 = 500$ ,  $K_3$  through  $K_9 = 0$ ; B,  $K_1 = 10^{-10}$ ,  $K_2 = 200$ ,  $K_3$  through  $K_9 = 0$ ; C,  $K_1 = 10^{-10}$ ,  $K_2 = 50$ ,  $K_3$  through  $K_9 = 0$ ; D,  $K_1 = 10^{-10}$ ,  $K_2 = 10$ ,  $K_3$  through  $K_9 = 0$ .

should be noted that the shapes of the curves in Figure 7 are the same if only hydrogen ion conjugation occurs instead of anion conjugation. It is necessary to know the concentrations of the individual species of anion,  $\text{A}^-$  and  $\text{AHA}^-$ , in order to determine which type of conjugation is occurring. It can be shown that if strong anion conjugation occurs (large  $K_2$ ), the concentration of the simple anion,  $\text{A}^-$ , remains constant with respect to  $C$ .

Equal conjugation of anion and cation to the neutral acid, HA, causes an initial slope of 1.50. As the concentration decreases, the degree of conjugation decreases and simple dissociation becomes the major reaction. If conjugation forms one complex species over the other, the slopes at high concentrations will lie between 1.0 and 1.50.<sup>21</sup>

Dimerization and simple dissociation produce slopes of 0.25. As the concentration decreases, the contribution of the dimeric species becomes less and simple dissociation is predominant. Conjugation of either cation, anion, or both with the dimer increases the slope at higher concentrations. A maximum slope of 1.25 occurs for an equivalent amount of cation and anion conjugation. This effect is shown in Figure 8.

The graphs plotted as  $-\log \sum_{j=0}^n [\text{A}(\text{HA})_j^-]$  vs.  $-\log C$  are directly related to the potentiometric plots of  $(RT/F) \ln \sum_{j=0}^n a_{\text{H}(\text{HA})_j^+}$  vs.  $-\log C$ . These curves are related through the Nernst equation and the condition of electroneutrality. Thus, the potentiometric slopes are negative multiples of 0.0591 times the photometric slopes.<sup>21</sup> Therefore, additional information can be obtained from photometry only with respect to providing a means for evaluation of an  $E_k^0$  for a selected system unless the various anionic

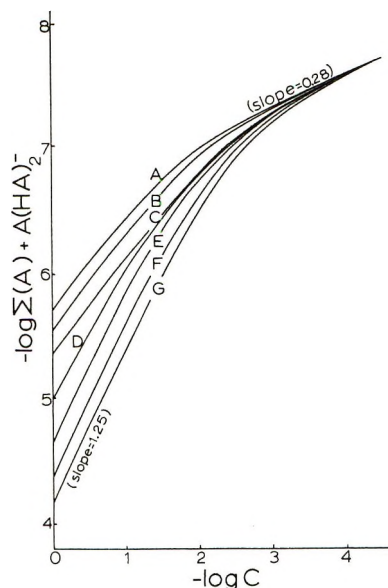


Figure 8. Photometry for ionization of HA, dimerization of neutral species, and autoassociation of charged species with dimer. The equilibria are  $\text{HA} \rightleftharpoons \text{H}^+ + \text{A}^-$ ,  $2\text{HA} \rightleftharpoons (\text{HA})_2$ ,  $\text{A}^- + (\text{HA})_2 \rightleftharpoons \text{A}(\text{HA})_2^-$ , and  $\text{H}^+ + (\text{HA})_2 \rightleftharpoons \text{H}(\text{HA})_2^+$ : A,  $K_1 = 10^{-10}$ ,  $K_4 = 10^6$ ,  $K_5 = 100$ ,  $K_6 = 0$ ; B,  $K_1 = 10^{-10}$ ,  $K_4 = 10^6$ ,  $K_5 = 200$ ,  $K_6 = 0$ ; C,  $K_1 = 10^{-10}$ ,  $K_4 = 10^6$ ,  $K_5 = 500$ ,  $K_6 = 0$ ; D,  $K_1 = 10^{-10}$ ,  $K_4 = 10^6$ ,  $K_5 = 500$ ,  $K_6 = 10$ ; E,  $K_1 = 10^{-10}$ ,  $K_4 = 10^6$ ,  $K_5 = 500$ ,  $K_6 = 50$ ; F,  $K_1 = 10^{-10}$ ,  $K_4 = 10^6$ ,  $K_5 = 500$ ,  $K_6 = 200$ ; G,  $K_1 = 10^{-10}$ ,  $K_4 = 10^6$ ,  $K_5 = 500$ ,  $K_6 = 500$ .

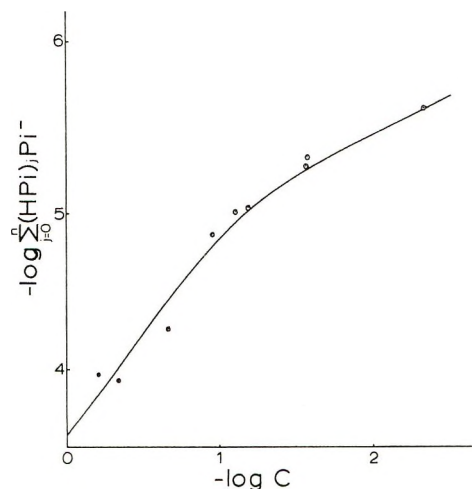


Figure 9. Photometric data from literature of picric acid in acetonitrile. Points are experimental and lines are theoretical: reactions,  $\text{HA} \rightleftharpoons \text{H}^+ + \text{A}^-$ ,  $2\text{HA} \rightleftharpoons (\text{HA})_2$ ,  $\text{A}^- + (\text{HA})_2 \rightleftharpoons \text{A}(\text{HA})_2^-$ .

species can be distinguished. If the various anionic species have identical absorbing characteristics, it is impossible to differentiate between cationic or anionic conjugation. Experimental photometric data were taken from Kolthoff, *et al.*,<sup>2</sup> and are presented in Figure 9. In this case the  $x$  and  $y$  axes are  $-\log C$  and  $-\log \sum_{j=0}^n [(\text{HPI})_j \text{Pi}^-]$ , respectively. An excellent fit



is obtained by assigning  $K_1 = 10^{-9}$ ,  $K_4 = 10^{-2}$ , and  $K_5 = 10^4$ . This model agrees with their postulation that the species  $\text{Pi}(\text{HPi})_2^-$  exists at concentrations higher than 0.1  $M$ . Also, the slopes of their curves

agree with those of the theoretical model presented in Figure 8. It was not possible to obtain an adequate fit of the data by ignoring the formation of  $\text{Pi}(\text{HPi})_2^-$  and by assuming the formation of  $\text{Pi}(\text{HPi})^-$ .

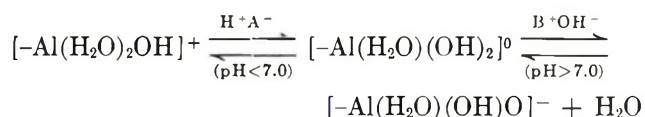
## Kinetics of Adsorption of Mineral Acids on Alumina

Lj. Jaćimović,\* J. Stevović, and S. Veljković

*Institute Boris Kidrič, Beograd, Yugoslavia (Received May 8, 1972)*

Rates of adsorption of  $\text{H}_6\text{TeO}_6$  and  $\text{H}_3\text{PO}_4$  on alumina were examined in varying pH conditions at 25° with the purpose of estimating the nature and the extent of reactions of anions with  $-\text{Al}(\text{OH})_2(\text{H}_2\text{O})_3$  sites. The experimental data were interpreted in terms of a multistage reaction, dominated by dissociative processes on the alumina. Two dissociation constants were introduced in a reaction model, based on the reaction of surface ions with anions in solutions. The reaction was found to be of one-third order in relation to acids, suggesting loose surface complexes having free orientation of anions.

The adsorption of mineral acids on alumina is generally described in terms of the equivalent exchange of aqueous electrolytes with  $\text{OH}^-$  and  $\text{H}^+$  ions at the surface.<sup>1,2</sup> Recently, it was shown that the equilibrium distribution of these ions, at the solid-solution interface, is dependent on the concentration of  $\text{H}^+$  ions in the solution.<sup>3</sup> The occurrence of a charged ( $\pm$ ) or neutral surface has been attributed to the formation of metal-aquo complexes of the type



The accompanying ions,  $\text{A}^-$  and  $\text{B}^+$ , may stay as counterions outside the primary hydration shell of the surface. In some cases,  $\text{A}^-$  can replace  $\text{OH}^-$  inside the complex, while  $\text{B}^+$  can react with the negatively charged complex. The final result is analogous to the ion exchange of these ions.

Existing data on the adsorption of acids do not take into consideration above double-layer characteristics of alumina. Kinetics of adsorption of electrolytes were not studied in details at low pHs, while some thermodynamic studies at high pHs support the above scheme.<sup>3</sup> It is, therefore, necessary to evaluate general kinetics of adsorption of acids in varying pH and concentration conditions.

In the present study, we have investigated these phenomena by using  $\text{H}_6\text{TeO}_6$  and  $\text{H}_3\text{PO}_4$ . Their dissociation constants allow for a systematic study of the adsorption in a wide region of pH values. Available data show that their kinetics of adsorption were poorly

defined, being inconsistent with standard ion exchange kinetics.<sup>4,5</sup> Our studies are aimed at the evaluation of an adequate kinetic expression which should describe the influence of surface equilibria (at the alumina) on the rate of adsorption. Our results fit a kinetic scheme which confirms that influence.

### Experimental Section

**Materials.** The adsorbent used was aluminium oxide, Merck, Code No. 1078, particle size 100–200 mesh. After washing with double distilled water, the oxide was dried for 24 hr at 140°. When necessary, the oxide was treated with  $2.7 \times 10^{-1} M$  HCl for 20 hr at 25°. After removal of acid, samples were washed with distilled water until the reaction was neutral and were dried as above.

In some experiments, oxide Code No. 1097, Brockmann type, was used.

X-Ray analysis showed that the oxide was mainly amorphous. According to data given by the manufacturer, oxides No. 1078 and 1097 belong to the group "for column chromatography," which contains  $\chi$  and  $\gamma$  aluminas, produced mainly from Hydrargillite. Many geometric irregularities of oxide particles were

(1) F. Umland, *Z. Elektrochem. Ber. Bunsenges. Phys. Chem.*, **60**, 711 (1956).

(2) K. C. Williams, J. L. Daniel, W. J. Thomson, and R. I. Kaplan, *J. Phys. Chem.*, **69**, 250 (1965).

(3) S. M. Ahmed, *ibid.*, **73**, 3546 (1969).

(4) S. Takahashi, E. Shikata and H. Amano, *J. Nucl. Sci. Technol.*, **7** (3), 130 (1970).

(5) P. R. Sinha and A. K. Choudhury, *J. Indian Chem. Soc.*, **31**, 311 (1954).

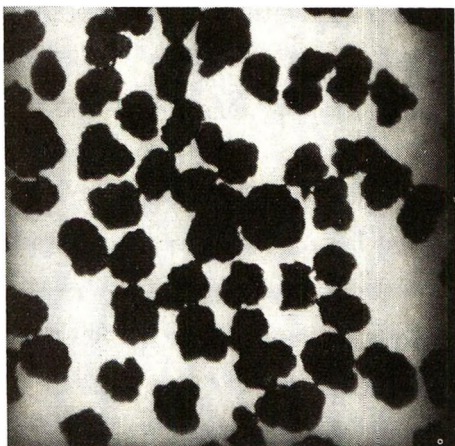


Figure 1. Particles of  $\text{Al}_2\text{O}_3$  No. 1078  $\times 40$  (Reichert binocular microscope).

revealed by microscopic examinations, as shown in Figure 1. The bulk material could be easily ground to very fine powder, indicating that the microstructure of the original gel is preserved inside the particles. It is probable that many channels between smaller agglomerates facilitate the penetration of liquids into the particles. Then most kinetics studies could be based on a homogeneous reaction model (used in case of reactions occurring in ion exchange resins).<sup>6</sup> Singular actions of some specific surface sites are thus masked by the behavior of bulk material.

Both types of alumina, No. 1078 and 1097, had surface areas, as measured by  $\text{N}_2$  adsorption (BET, sorptometer, Perkin-Elmer-Shell), in the range 95–115  $\text{m}^2/\text{g}$ .

pHs of 10% suspensions in  $\text{H}_2\text{O}$  were found to be 4.1 (No. 1078) and 9.2 (No. 1097). According to data supplied by the manufacturer there are 0.2%  $\text{Cl}^-$  and 0.1%  $\text{SO}_4^{2-}$  in No. 1078, and 0.1%  $\text{Cl}^-$  and 0.1%  $\text{SO}_4^{2-}$  in No. 1097. The sodium content was determined; samples No. 1078 and 1097 were first analyzed at the end of the standardization by  $\text{H}_2\text{O}$ , the determination of sodium being done by radioactivation analysis. Sample No. 1078 has 0.07% Na, while No. 1097 has 0.4% Na. The treatment of the samples by  $2.7 \times 10^{-1} M$  HCl decreases the content of sodium in No. 1097 to 0.15%; sample No. 1078 is practically unaffected (0.06% Na). Other impurities were determined spectroscopically: Fe (<20 ppm); Si (<20 ppm); Cu, Ca, Ni, Mn, Mg, Zn, Ge, Be, and K (<10 ppm).

The dissolution of  $\text{Al}_2\text{O}_3$  by mineral acids at low pHs was estimated by the complexometric titration of  $\text{Al}^{3+}$  ions with EDTA at pH 4.1 (the buffer was 1  $M$  acetic acid plus 1  $M$  ammonium acetate).<sup>7</sup> All reagents were of the pure analytical grade.

In most experiments acids marked by radioactive indicators were used.

<sup>32</sup>P tracer (Institute Boris Kidrič) as  $\text{H}_3\text{PO}_4$  was used, diluted by carrier  $\text{H}_3\text{PO}_4$ .

Radioactive  $\text{H}_6\text{TeO}_6$  was obtained by the oxidation

of  $\text{TeO}_2$  (BDH), previously irradiated in the RA reactor in Vinča. After 9 months of cooling,  $\text{TeO}_2$  was dissolved in 3.5  $M$   $\text{HNO}_3$  at a temperature close to the boiling point.  $\text{KMnO}_4$  (1  $M$ ) addition, followed by  $\text{H}_2\text{O}_2$ , completed the oxidation.  $\text{H}_6\text{TeO}_6$  crystals were further purified by recrystallization from  $\text{HNO}_3$  solutions.<sup>8</sup>

**Adsorption Procedure.** Adsorption measurements were carried out in aqueous solutions of acids, 1 g of  $\text{Al}_2\text{O}_3$  plus 10 ml of solution. Concentrations of acids and pHs of solutions were varied according to requirements of experiments, but the temperature was kept at 25° in all experiments. Dry alumina was added to acids. The suspension was constantly agitated during the equilibration. The equilibration time was 2 hr, except in some tests aimed at the control of the solubility of  $\text{Al}_2\text{O}_3$ . Adsorption yields were determined by the difference in radioactivity of the solutions before and after the equilibration with  $\text{Al}_2\text{O}_3$ .<sup>9</sup> Use of radioactive isotopes enables direct estimates of acid distribution. Moreover, the appropriate dosage of the radioactivity assures an easy control of both, small and large adsorption yields of acids.

Measurements of the radioactivity of Te isotopes was done by the use of a single channel  $\gamma$  scintillation spectrometer, while a  $\beta$  scintillation counter was employed for <sup>32</sup>P. The standard error in all measurements was 1%.

A controlling series of spectrophotometric measurements was performed, based on absorption of phosphomolybdate complexes, as well as dilute ammoniacal solutions of  $\text{H}_6\text{TeO}_6$ .<sup>10</sup> These results were in satisfactory agreement with the radioactivity measurements.

Investigations of pH effects on the adsorption were performed in presence of either NaOH (1  $M$ ) or  $\text{HNO}_3$  (1  $M$ ), avoiding standard buffer solutions because of possible secondary adsorption of these ions. pH values at the end of the equilibration were used.

## Results and Discussion

**Rates of Adsorption.** Rates of adsorption were studied in solutions ranging from  $1.2 \times 10^{-3}$  to  $1.2 \times 10^{-1} M$ . The equilibration times for  $\text{H}_6\text{TeO}_6$  were below 2 hr, while they could not be precisely defined for  $\text{H}_3\text{PO}_4$ , because of its chemical attack on alumina. Data on the dissolution of alumina in  $\text{H}_3\text{PO}_4$  are given in Table I. Therefore, all calculations which were based upon equilibrium values were related to  $\text{H}_6\text{TeO}_6$ . Two-hour values for  $\text{H}_3\text{PO}_4$  were used as a rough approximation in calculations of adsorption isotherms,

(6) M. Ishida and C. Y. Wen, *AIChE J.*, **14**, 311 (1968).

(7) E. Wänninen and A. Ringbom, *Anal. Chim. Acta*, **12**, 308 (1955).

(8) L. F. Andrieth, *Inorg. Syn.*, **3**, 143 (1950).

(9) Lj. Jačimović, S. Veljković, and N. Ajdačić, *Radiochim. Acta*, **12**, 49 (1969).

(10) F. Snell and C. Snell, "Colorimetric Methods of Analysis," Vol. II, Van Nostrand, New York, N. Y., 1955, p 683.



Table I: Kinetic Data for Adsorption of  $H_6TeO_6$  and  $H_3PO_4$  on  $Al_2O_3$  (No. 1078 and 1097) at  $25^\circ$

Reacting system	$Y_m, 10^{-1}$ mmol/ g of $Al_2O_3$	$Y_\infty,^a 10^{-1}$ mmol/ g of $Al_2O_3$	$t(50\%),$ sec	$k', \text{sec}^{-1} =$ $[k(\text{sec}^{-1}/s)]^2$	% $Al_2O_3$ dissolved
$H_6TeO_6$ (1078) <sup>b</sup>					
$1.2 \times 10^{-3}$ – $3.5 \times 10^{-2}$ M	1.61		35	$1.0 \times 10^{-2}$	
$1.04 \times 10^{-1}$ M		2.02	38	$0.92 \times 10^{-2}$	
$1.04 \times 10^{-1}$ M + $Al_2O_3$ pre-treated by HCl		1.66	110	$2.6 \times 10^{-3}$	
$1.04 \times 10^{-1}$ M + $Al_2O_3$ saturated by $1.1 \times 10^{-1}$ M $H_3PO_4$		0.41			
(1097)					
$1.2 \times 10^{-3}$ – $3.5 \times 10^{-2}$ M	2.20		32	$1.05 \times 10^{-2}$	
$H_3PO_4$ (1078) <sup>c</sup>					
$11 \times 10^{-3}$ – $4.0 \times 10^{-2}$ M	3.86		~100		<0.35
$1.1 \times 10^{-1}$ M		3.33 <sup>d</sup>	160		0.90
(1097)					
$1.2 \times 10^{-3}$ – $3.8 \times 10^{-2}$ M	4.25		~100		<0.42
HCl (1078)					
$2.8 \times 10^{-1}$ M					1.35

<sup>a</sup> Two hours. <sup>b</sup> pH  $\approx$  4.0. <sup>c</sup> pH  $\approx$  2.20. <sup>d</sup>  $Y_\infty = 5.8$  after 20 hr equilibration.

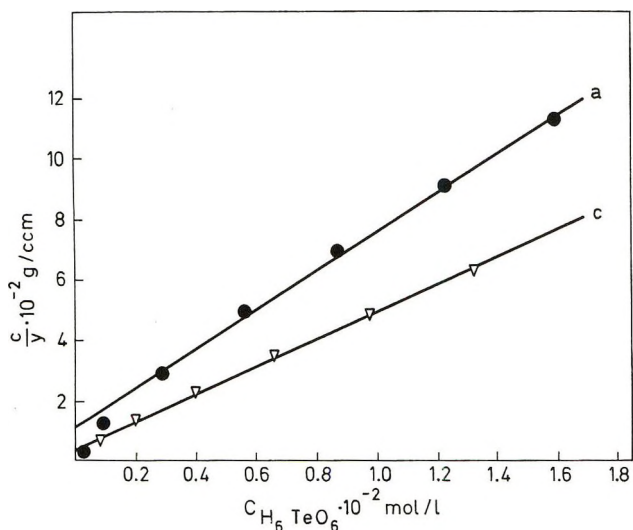


Figure 2. Linear Langmuir plots,  $H_6TeO_6 + Al_2O_3, T = 25^\circ$ : O, (1078); and  $\nabla$ , (1097).

limited to lower concentrations of acids. Then, the error in data for  $H_3PO_4$  was between 5–10%, while above  $1.0 \times 10^{-1}$  M it was 15%, the adsorption being found to continue even after 20 hr.

Linear Langmuir plots were constructed for both acids whose concentration was below  $5 \times 10^{-2}$  M. The slope of the relation  $C/Y$  vs.  $C$  gives  $1/Y_m$ , where  $Y_m$  is the monomolecular layer of adsorbed acid,  $Y$  is equilibrium value of adsorbed acid,  $C$  is equilibrium concentration of residual acid in solution. Plots are given in Figures 2 and 3. Adsorption of  $H_6TeO_6$  on alumina No. 1097 is included in Figure 2 for comparison purposes.  $Y_m$  for  $H_3PO_4$  is twice the value

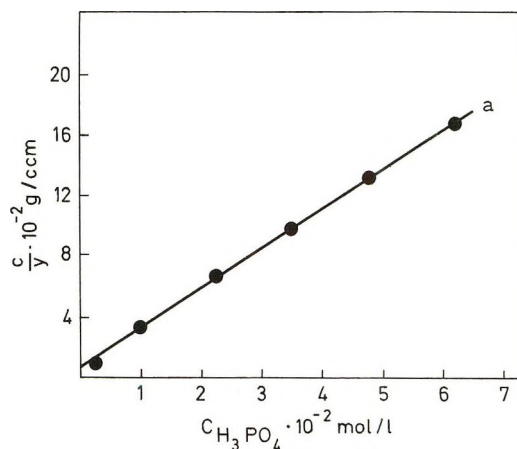


Figure 3. Linear Langmuir plot,  $H_3PO_4 + Al_2O_3$  (1078),  $T = 25^\circ$ .

for  $H_6TeO_6$ , but it was found later that this is due to different pHs of solutions.

Although the applicability of the Langmuir equation is limited to lower concentrations, the above data serve as an indication of the reversibility and the statistical distribution of processes on fixed sites on alumina.<sup>1,2</sup>

At concentrations above  $5 \times 10^{-2}$  M, the adsorption is sufficiently complex to impose deviations from linearity in above plots. Most data were found to obey a Freundlich isotherm of the type  $Y = kC^{1/n}$ , with  $n = 3$  for  $H_6TeO_6$  and  $n \approx 2.76$  for  $H_3PO_4$ . Because of these complexities, we have limited our kinetic studies to systems whose concentration was between  $3 \times 10^{-2}$  and  $1.1 \times 10^{-1}$  M.

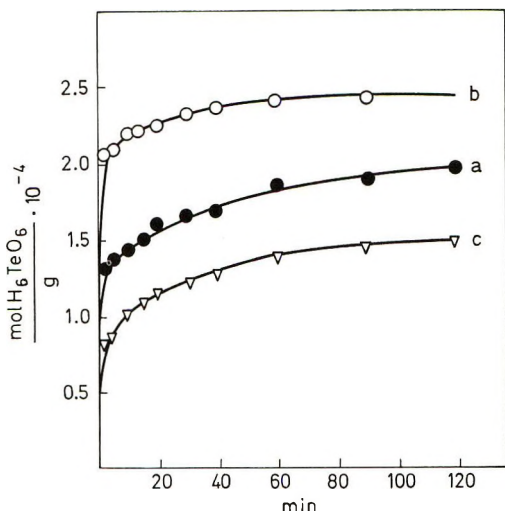


Figure 4. Adsorption rate of  $\text{H}_6\text{TeO}_6$  ( $3.5 \times 10^{-2} M$ ) on  $\text{Al}_2\text{O}_3$ ,  $T = 25^\circ$ : ●, (1078); ○, (1097); ▽, (1078) pretreated by HCl.

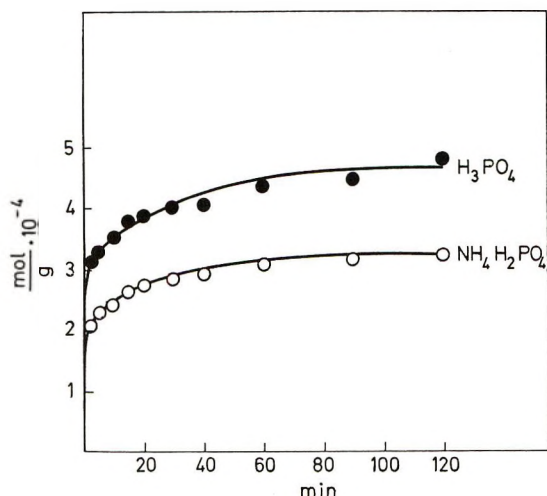


Figure 5. Adsorption rate of  $\text{H}_3\text{PO}_4$  ( $4.0 \times 10^{-2} M$ ) and  $\text{NH}_4\text{H}_2\text{PO}_4$  ( $4.0 \times 10^{-2} M$ ) on  $\text{Al}_2\text{O}_3$  (1097).

Regarding rates of adsorption, our data show no clear trend. Fast initial reactions were observed with both acids. Some typical plots are shown in Figures 4 and 5. For  $\text{H}_6\text{TeO}_6$  on  $\text{Al}_2\text{O}_3$  No. 1078 and on  $\text{Al}_2\text{O}_3$  No. 1097, amounts adsorbed within first 5 min were found to be 76 and 85% of the corresponding equilibrium values. With  $\text{H}_3\text{PO}_4$  and both aluminas 65–70% of an estimated adsorption plateau were obtained. Because of errors mentioned above, all data on initial rates should be given in mmoles of adsorbed acid, without references to  $t_\infty$ . Such a presentation will be done in further sections, while a general kinetic analysis will be based on data for  $\text{H}_6\text{TeO}_6$ .

The above data could not be fitted to ion exchange kinetics, neither grain nor solution diffusion controlled.<sup>11</sup> Most data for  $\text{H}_6\text{TeO}_6$  were fitted with a fair accuracy to an exponential law which has already been applied

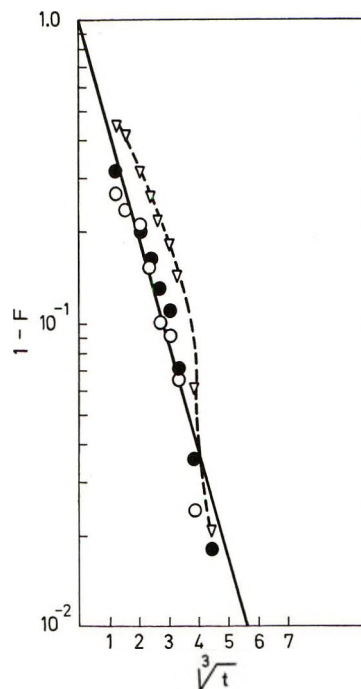


Figure 6. Application of eq 1 to the adsorption of  $\text{H}_6\text{TeO}_6$  on  $\text{Al}_2\text{O}_3$ : ●,  $3.5 \times 10^{-2}$  and  $1.04 \times 10^{-1} M$  (1078); ○,  $3.5 \times 10^{-2} M$  (1097); ▽,  $1.04 \times 10^{-1} M$  (1078) pretreated by HCl.

to the adsorption of  $\text{H}_2\text{O}$  vapor on  $\text{Al}_2\text{O}_3$ .<sup>12</sup> This expression was generally used to describe the diffusion-controlled precipitation of a new phase in heterogeneous systems<sup>13</sup>

$$1 - F = \exp(-kt^{1/n}) \quad (1)$$

$F = Y/Y_\infty$  ( $Y_\infty$  = the adsorption yield after 2 hr). The best fit was found for  $1/n = 1/3$ , as shown in Figure 6. Here, the new phase may be considered as an ensemble of small particles (or domains) having the shapes of spheres, rods, or plates. The kinetic law exponent  $n$  was found to vary with the growth habit of particles.<sup>14</sup>  $1/n = 3/2, 4/2,$  and  $5/2$  for above mentioned shapes.  $1/n \approx 1/2$  if complete edgewise impingement of thin plates takes place at an early stage of their precipitation.<sup>13</sup> In many instances the kinetics of impurity precipitation on dislocations was found to be well represented by eq 1, where  $1/n = 1/2, 2/3,$  etc.<sup>15,16</sup> The same applies to the annealing of vacancies on dislocations.<sup>16</sup> A general equation of the same form was used to describe kinetics of adsorption of  $\text{CO}_2$  and  $\text{NH}_3$  on glass<sup>17</sup> and of  $\text{H}_2$  and  $\text{O}_2$  on plat-

(11) C. B. Amphlett, "Inorganic Ion Exchangers," Elsevier, Amsterdam, 1964.

(12) T. Papyjczak, *Zesz. Nauk Politech. Lodz., Chem.*, **19**, 58 (1969).

(13) D. Turnbull, "Solid State Physics," Vol. 3, Academic Press, New York, N. Y., 1956, p 256.

(14) C. Wert and C. Zener, *J. Appl. Phys.*, **21**, 5 (1950).

(15) S. Harper, *Phys. Rev.*, **83**, 709 (1951).

(16) R. Balluffi and D. Seidman, *Phil. Mag.*, **17**, 843 (1968).

(17) E. B. Maxted and C. H. Moon, *J. Chem. Soc.*, 1542 (1936).



inum.<sup>18</sup> However, these data could be better represented by the Elovich equation;  $Y = (2.3/\alpha) \log(1 + \alpha at)$ , where  $a$  and  $\alpha$  are constants. Since this equation is best understood in the light of a constant site generation and decay in the course of adsorption,<sup>19</sup> the validity of both equations is justified. In fact, data for  $H_6TeO_6$  in this work could also fit the Elovich equation. We prefer the use of eq 1 in order to demonstrate the extensive rearrangement of surface layers in presence of aqueous solutions.

Kinetic parameters for the adsorption of  $H_6TeO_6$  on samples No. 1078 and 1097 are given in Table I.

*Hydrated Alumina.* Data in Figures 4 and 6 and in Table I illustrate the fast adsorption of  $H_6TeO_6$  on alumina. A decrease in the rate of adsorption of  $H_6TeO_6$  was found on samples with preadsorbed  $H_3PO_4$  ( $\approx 2 \times 10^{-4}$  mol/g of  $Al_2O_3$ ) and HCl (traces).  $H_3PO_4$  may block a great part of the surface being readily adsorbed on alumina. HCl is less reactive. Data in Table I demonstrate the corresponding reduction of adsorption yields. Beside these competitive effects, these acids impose further alterations of surface layers by dissolving more than 1%  $Al_2O_3$  (equivalent to  $2 \times 10^{-4}$  g-ions of  $Al^{3+}$ /g of  $Al_2O_3$ ). In case of a reversed procedure, they may desorb completely preadsorbed  $H_6TeO_6$  ( $\approx 2 \times 10^{-4}$  mol/g of  $Al_2O_3$ ). Similar effects were noticed in earlier works.<sup>1,4</sup> The site density remains the same in all above processes, suggesting that an equilibrium distribution of reacting Al-hydroxy (or aquo) complexes is established prior to any surface reaction. Kinetics of adsorption of acids should, therefore, reflect some basic traits of that equilibration.

The comparison of rates of equilibration of alumina in  $H_2O$  (as shown by pH changes of 10% suspensions in water) and rates of adsorption of  $H_6TeO_6$  is presented in Figure 7. At least, the initial rates appear to be determined by similar kinetics.

The hydration of alumina by excess water is a complex process, which is influenced by the initial state of dry oxide.<sup>20,21</sup> A great deal of the rearrangements of surface hydroxyls and molecular water may take place. The transition of  $\gamma-Al_2O_3$  to Boehmite was suggested by de Boer,<sup>22</sup> while Kipling and Peakall<sup>23</sup> postulate the formation of a Gibbsite-like surface. Peri<sup>20</sup> takes care of the extensive mobility of surface ions, the transfer of protons, the formation of hydrogen bonds, the crowding of water molecules on some crystal faces, and of processes on surface defects. Obviously, most of these processes belong to mentioned groups of reactions, whose kinetics were found to obey eq 1.

The hydration of our samples was done partly in the course of their standardization (*cf.* Experimental Section). The amount of residual water was determined by drying samples for 20 hr at 400°. (Although great errors might be induced by drying in air,<sup>20</sup> this procedure gives rather useful informations). Weight losses of

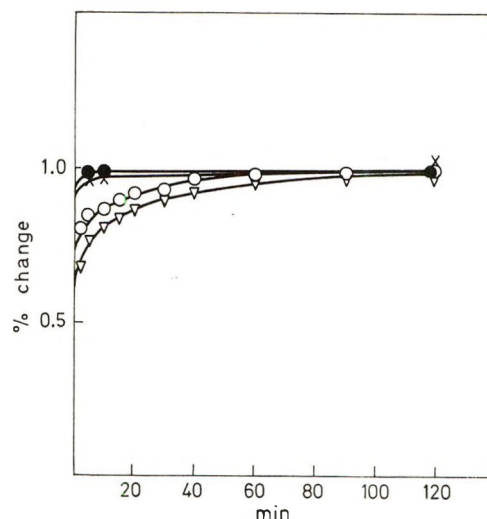


Figure 7. Rates of equilibration of  $Al_2O_3$  in  $H_2O$  ( $\bullet$ ,  $\times$ ) and of adsorption of  $H_6TeO_6$  ( $3.5 \times 10^{-2} M$ ) on  $Al_2O_3$ ;  $\bullet$ , (1097);  $\circ$ , (1097);  $\times$ , (1078);  $\nabla$ , (1078).

samples No. 1078 and 1097 were 3.4 and 3.7%, respectively. The surface coverage, based on the surface area equal to  $100 m^2/g$ , should correspond to 12 molecules of  $H_2O/100 \text{ \AA}^2$ . Part of that is bound in the form of hydroxyls, while other part is held as molecular water. In the presence of aqueous solutions, these layers may be rearranged easily.<sup>20</sup> The final structure, in form of aquo complexes, described in ref 3, is highly probable. It is in fact, similar to a Gibbsite-like surface.

In view of above changes, the validity of eq 1 is justified. The exponent  $1/n \approx 1/3$  should reflect present fast processes, as well as an easy coalescence of hydrated regions. That may be due to multilayer deposits of  $H_2O$  (slow penetration through solids being less probable).<sup>20,23</sup> Internal hydrogen bonding and specific packings (ice-like and liquid water-like structures) in these deposits might impose some limits to the site density for adsorption of acids; 1–2 sites/ $100 \text{ \AA}^2$  (based on data from Table I and a surface area,  $S = 100 m^2/g$  of  $Al_2O_3$ ). The reaction stoichiometry should therefore take care of geometric factors rather than chemical equivalencies. Equation 1 has served well to that purpose. However, its general nature, analogous to Elovich equation, requires further investigations in order to get details on the mechanism of adsorption of acids on alumina.

(18) E. B. Maxted and N. J. Hassid, *Trans. Faraday Soc.*, **29**, 698 (1933).

(19) H. A. Taylor and N. Thon, *J. Amer. Chem. Soc.*, **74**, 4169 (1952).

(20) J. B. Peri, *J. Phys. Chem.*, **69**, 211, 220 (1965).

(21) R. L. Venable, W. H. Wade, and N. Hackerman, *ibid.*, **69**, 317 (1965).

(22) J. H. de Boer, *Angew. Chem.*, **64**, 563 (1952).

(23) J. J. Kipling and D. B. Peakall, *J. Chem. Soc.*, 834 (1957).

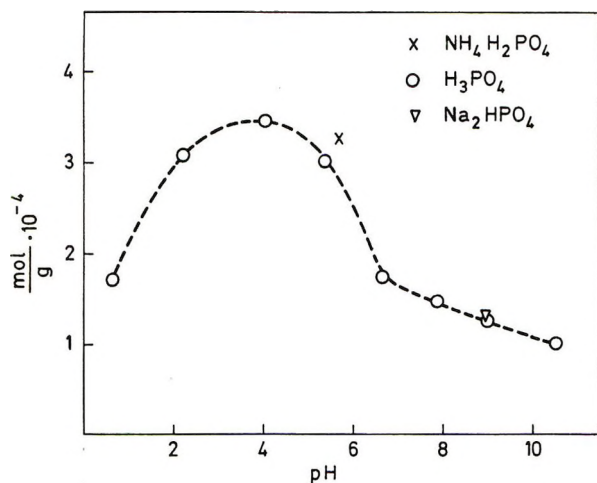


Figure 8. Adsorption yield (2 hr) of  $1.1 \times 10^{-1} M$   $H_3PO_4$  on  $Al_2O_3$  (1078) vs. pH of final suspensions.

### Interpretation of Rate Processes

The available evidence suggests that the distribution of aquo complexes on alumina should depend on the concentration of protons.<sup>3</sup> In view of that most surface reactions including the adsorption of electrolytes should depend on pH.

We did a series of measurements of reaction rates in the pH range from 1.0 to 11.0. Care was taken to avoid large pH and concentration oscillations in the course of the work. Therefore,  $1.1 \times 10^{-1} M$   $H_3PO_4$  was used, while the concentration of less reactive  $H_6TeO_6$  solutions was kept at  $3.5 \times 10^{-2} M$  (comparative solutions of  $1.04 \times 10^{-1} M$  were also used). pHs of these solutions were 1.6 and 4.1 (and 3.9). Adjustment of pH to higher or lower values was made by adding small quantities (0.2–1 ml) of 1 M NaOH and 1 M  $HNO_3$  to initial solutions. pHs of mixtures of adjusted solutions and  $Al_2O_3$  were determined at the end of adsorption with the aim of correlating all rate data to a single representative pH value. The variations of pHs in the course of adsorption were in general less than 15–20%, the greatest changes occurring in solutions of acids alone, especially in  $H_3PO_4$ . However, the use of a more concentrated acid was avoided because of possible acceleration of chemical reaction with alumina. A detailed study of these phenomena in the system  $Al_2O_3$ – $H_3PO_4$  will be presented elsewhere.<sup>24</sup>

Illustrations of pH influence on the adsorption rate of acids, based upon 2-hr yields and representative pHs, are given in Figures 8 and 9. Adsorption yields are given in mmole per gram  $Al_2O_3$  in order to avoid errors in relative yields (notably in  $H_3PO_4$  solutions). Analogous curves were found for 5-min yields and same pHs.

It is evident that both acids behave in the same way, their maximum adsorption being practically the same,  $\approx 4 \times 10^{-1}$  mmole/gram of alumina ( $1 \times 10^{-1} M$  initial solutions of acids). Furthermore, both acids

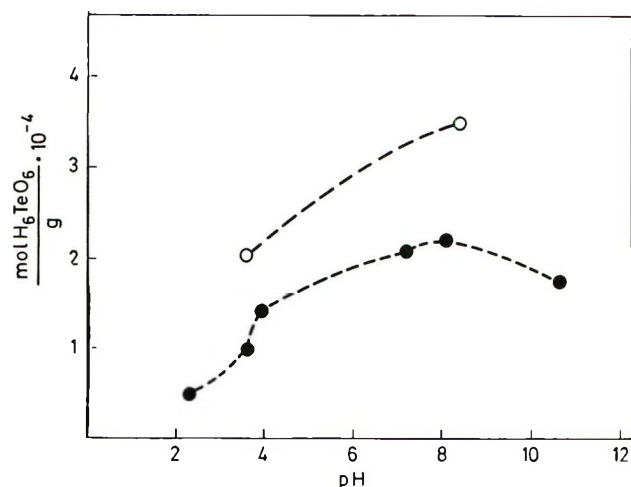


Figure 9. Adsorption yield (2 hr) of  $1.1 \times 10^{-1} M$   $H_6TeO_6$  on  $Al_2O_3$  (1078) vs. pH of final suspensions: ●,  $3.5 \times 10^{-2} M$ ; ○,  $1.04 \times 10^{-1} M$ .

are fully dissociated to monovalent ions at pHs of maxima; 4.2 for  $H_3PO_4$  and 8.5 for  $H_6TeO_6$ . This may be checked by calculating the concentration of each ion according to the relation

$$[A^-] = [K_{AH}/(H^+) + K_{AH}](AH) \quad (2)$$

$K_{(H_3PO_4)} = 7.52 \times 10^{-3} M$  and  $K_{(H_6TeO_6)} = 6.82 \times 10^{-7} M$  at  $25^\circ$ .<sup>25</sup> Such a behavior is consistent with the anion exchange of weak acids.<sup>11</sup>

It is therefore easy to explain enhanced adsorption of both acids on Na-rich Brockmann alumina (sample No. 1097) shown in Figures 2–5. Its alkalinity suffices to shift the pH of suspensions toward higher values, where higher adsorption yields could be measured.

Nevertheless, most data fit eq 1 better than standard equations of ion exchange kinetics. We may therefore suspect the final products of adsorption to be rather complex. In fact, an  $(A^-)^{1/3}$  dependence of reaction rates was determined. That is easily checked by comparison of data for  $3.5 \times 10^{-2}$  and  $1.04 \times 10^{-1} M$   $H_6TeO_6$  in Figure 9. Calculations on that basis were simplified by taking maximum adsorption yields at pH 4.2 and 8.5 to be equal to 100%, all other yields being expressed as per cent values. However, some deviations were found below pH  $\sim 4.0$  for  $H_6TeO_6$ .

According to ref 3 an alumina surface should be neutral at higher pHs, while positively charged aquo complexes are formed at pH  $\sim 4.0$ . Our results may be due to this difference. Since our surfaces bear great similarities to  $Al(OH)_3$ , they may be analyzed in the light of dissociation processes of this hydroxide.  $Al(OH)_3$  begins to dissociate at pH 8.0 to  $Al(OH)_2^+$  and  $OH^-$ , the dissociation constant being  $K_I = 1.29 \times$

(24) Z. Todorović, to be submitted for publication.

(25) "Gmelins Handbuch der Anorganischen Chemie," System No. 11, Verlag Chemie, Berlin, 1940, p 299.



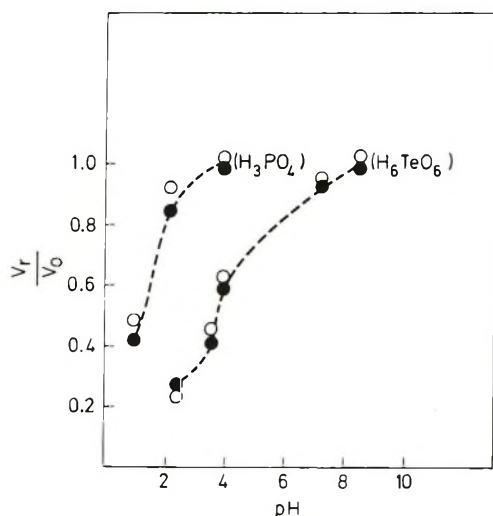


Figure 10. Application of eq 3 to the adsorption of  $1.1 \times 10^{-1} M$   $H_3PO_4$ , and  $3.5 \times 10^{-2} M$   $H_6TeO_6$  on  $Al_2O_3$  (1078).  $V_r$  and  $V_0 = \Delta Y/5$  min,  $V_0$  at pH maximum. ●, calculated values; ○, experimental values.

$10^{-5} M$ .<sup>26</sup> The second dissociation step, to  $Al(OH)_2^{2+}$  and  $OH^-$ , takes place at pH 5.5 (with  $K_{II} = 3.68 \times 10^{-6} M$ .<sup>26</sup> Hydrated forms correspond to conjugate acids of these ions,  $Al(H_2O)(OH)_2^+$  and  $Al(H_2O)_2(OH)^{2+}$ , their dissociation constants being  $K' = 10^{-14}/K_I$  and  $K'' = 10^{-14}/K_{II}$ , respectively.

At the surface of alumina one OH group of  $Al(OH)_3$  is substituted by a lattice bond to the Al atom. However, the remaining two OH groups could undergo the same changes as those described above. Then, reactions at high and low pHs should be influenced by the dissociation constants of hydrated ions  $K'$  and  $K''$ . According to our data and to the above discussion, the transition should take place in the pH range 4.0–5.5.

A final rate expression may be suggested

$$V_r = k_r S_{eff} K' \text{ (or } K'') (A^-)^{1/3} \quad (3)$$

where  $V_r$  represents the reaction rate (in mmole per gram oxide, per 5 min or per 2 hr), and  $S_{eff}$  the concentration of reacting Al-OH complex in a hydrated form whose dissociation is specified by  $K'$  and  $K''$ .

The applicability of eq 3 was demonstrated by using 5-min values. A plot of  $V_r/V_0$  vs. pH for both acids was constructed,  $V_0$  being the reaction rate at the maximum, as seen in Figure 10.

The agreement of calculated and experimental values is satisfactory, even for  $H_6TeO_6$ , below pH 4.0. The use of  $K'$  and  $K''$  is justified. We may therefore assume that surface reactions of Al-OH complexes and aqueous electrolytes depend primarily upon surface equilibria between aquo complexes, and also upon the protonization of hydrated oxide.

To specify more closely the conditions under which the adsorption of acids takes place, we recall that the steady-state concentration of active sites could be

given by the relation<sup>27</sup>  $N_s = N_0 b(A^-)/(j + b(A^-))$ , where  $N_0$  is the maximum possible number of sites, and  $b$  and  $j$  are constants, that is, numerically equivalent to a fractional order  $(A^-)^{1/m}$  ( $m > 1$ ). If the rate of spontaneous interaction with adsorbed  $A^-$  is  $k_d N_s$  ( $k_d$  is included above in  $j$ ), the initial rate of reaction is of the same fractional order, as is the case of eq 3, where  $1/m = 1/3$ .  $N_0$  is proportional to  $S_{eff} K'$  (or  $K''$ ). If we assume  $S_{eff}$  to correspond to the amount of  $H_2O$  necessary to form a monomolecular layer, then we take the coverage of 7 molecules of  $H_2O/100 \text{ \AA}^2$ ,<sup>20</sup> or  $1.1 \times 10^{-3}$  mol of  $H_2O/\text{gram}$  of oxide ( $1 H_2O/14 \text{ \AA}^2$ ), whose surface is  $100 \text{ m}^2/\text{g}$ . This value is somewhat less than those based on dimensions of surface  $O^-$  ions ( $O^-/6.74 \text{ \AA}^2$ ).<sup>26</sup> For a two-dimensional hexagonal configuration of closely packed layer, suggested by Emmett and Brunauer,<sup>28</sup> the above coverage gives 1 mol of  $H_2O$  per  $9 \times 10^8 \text{ cm}^2$ . In view of variations of surface packings, the conversion of a number of  $\text{cm}^2$  to number of moles which cover them should be based on a conversion factor  $\sim 10^8$ . All constant values in eq 3 could be represented by a new constant  $k^+ = k_r 10^8 K' (K'')$ . In aqueous suspensions, multilayer deposits of water are formed on  $Al_2O_3$  and they impose a geometric concept of the reaction order. Simple geometric considerations of the surface-to-volume distribution of active water allows for the relationship  $S_{eff} \approx (C_{eff})^{2/3}$ .<sup>28</sup> Since 10% suspensions of alumina were used in this work, true molar density of surface aquo complexes should be  $1.1 \times 10^{-1} M$ .

By introducing measured changes of  $(A^-)$  in eq 3,  $V_0 = 1.77 \times 10^{-2} M$  per 5 min and  $(A_0^-) = 3.5 \times 10^{-2} M$   $H_6TeO_6$ , the following result is obtained:  $k^+ \approx 10^{-3} \text{ sec}^{-1}$ ,  $k_r \approx 10^{-2} \text{ sec}^{-1}$ . Calculations of  $k'$  ( $k$  from eq 1),<sup>3</sup> based on Figure 6, give the same order of magnitude,  $k \approx 10^{-2} \text{ sec}^{-1}$ , as seen in Table I.

### Chemical Effects

Data in Table I illustrate the solubility of  $Al_2O_3$  in acids. The choice of working conditions in the study of reaction rates was carefully made in order to avoid great solubility errors; for instance, the mixture of 1  $M$   $HNO_3$  plus  $1 \times 10^{-1} M$   $H_6TeO_6$  (pH 1.0) dissolved 0.5%  $Al_2O_3$  within 2 hr. Solutions whose pH was above 2.5 were inactive. Combinations of  $HNO_3$  and  $H_3PO_4$  were more reactive; at pH 1.0, 1.12%  $Al_2O_3$  was dissolved, and at pH 1.60 in pure  $1.1 \times 10^{-1} M$   $H_3PO_4$  0.9% was dissolved. Above pH 2.8 the dissolution was less than 0.4%. After 5 min, only one-third or less of above values was detected.

The validity of eq 3 was therefore demonstrated by using 5-min data, as shown in Figure 10.

(26) V. A. Nazarenko and E. M. Nevskaja, *Zh. Neorg. Khim.*, **14**, 3215 (1969).

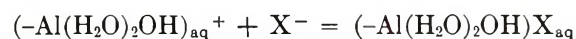
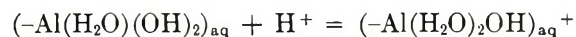
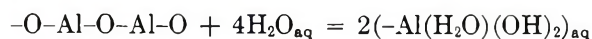
(27) K. H. Lin, *Ind. Eng. Chem.*, **60**, No. 5, 61; No. 7, 56 (1968).

(28) P. H. Emmett and S. Brunauer, *J. Amer. Chem. Soc.*, **59**, 1533 (1937).

Although the choice of working conditions secures reliable kinetic conclusions, any work at low pHs should be avoided, and under extreme conditions the kinetic data were unusable. For instance, washing of  $\text{Al}_2\text{O}_3$  five times with  $2.8 \times 10^{-1} M$  HCl (2 hr each) reduced  $\text{H}_6\text{TeO}_6$  adsorption at pH 8.5 to such an extent that the rate curve could not be constructed. Five-minutes values were higher than the rest of the curve, while the error in measurements surpassed 20%. The adsorption yield was less than 25% of the original values. The same reduction of adsorption yields was found when alumina was previously equilibrated with  $1 \times 10^{-1} M$   $\text{H}_3\text{PO}_4$ .

### Conclusion

Equations 1 and 3 describe reaction kinetics of adsorption of electrolytes on alumina. They are equally applicable to all the compounds studied:  $\text{H}_3\text{PO}_4$ ,  $\text{H}_6\text{TeO}_6$ , and their monovalent sodium salts. Reaction rates are influenced by ionic equilibria in the solution and at the surface of alumina, and hence on dissociation constants of acids and on dissociation constants of aquo complexes on the alumina surface:  $K_{(\text{H}_3\text{PO}_4)}$ ,  $K_{(\text{H}_6\text{TeO}_6)}$ ,  $K'$ , and  $K''$ . It is therefore possible that ion exchange takes place in the course of adsorption. Measured rates suggest a different reaction mechanism, which is dominated by the solvation of the oxide surface. The alumina trihydrate surface reacts readily with protons giving two types of charged species, the transition point being in the pH range 4.0–5.5. These species could react with monovalent anions according to a 1:1 stoichiometry. The establishment of the steady-state conditions should impose a fractional reaction order with respect to concentration of anions, while additional modifications are due to geometric parameters of the surface layers. This model is consistent with basic principles of the homogeneous model of reactions (gas–solid, liquid–solid) in a spherical particle.<sup>6</sup> A schematic presentation of reaction steps should be as follows.



The polarization of hydrated alumina, suggested earlier to take place in acid media,<sup>3</sup> was shown to be an important reaction step in the kinetics of acid adsorption.

The distribution of anions in between surface hydroxyls is described by  $(A^-)^{1/2}$ . Data in Table I give  $Y_\infty \approx 2-4 \times 10^{-4}$  mol of acid/gram of  $\text{Al}_2\text{O}_3$ . In fully hydrated monolayer,  $C_{\text{eff}(\text{H}_2\text{O})} = 1.1 \times 10^{-3}$  mol/gram of  $\text{Al}_2\text{O}_3$ . Obviously, a 1:3 relation is the best approximate. Since polyhydroxy complexes with Al atoms could be formed, the stoichiometry related to Al should be different. A similar relation to surface hydroxyls was found for phosphate anions adsorbed on other metal oxides (zirconium, thorium, cerium).<sup>29</sup> On account of this an effective area of  $40 \text{ \AA}^2$  per phosphate molecule was suggested.<sup>29</sup> The radius of the phosphate molecule is  $2.74 \text{ \AA}$ , while the radius of crystalline Al hydrates is near to  $3.2 \text{ \AA}$ .<sup>30</sup> The adsorption of  $\text{H}_3\text{PO}_4$  (and  $\text{H}_6\text{TeO}_6$ ) on alumina should be therefore described in terms of a heterogeneous reaction, instead of exchange of anions and surface OH groups. The incompatibility of dimensions is even greater when related to OH groups, their surface being less than  $10 \text{ \AA}^2$ .<sup>30</sup> According to ref 29 the mentioned distribution of anions in surface layers is the indication of a relatively free rotation of sorbed species. If the chemical interaction is small in relation to the adsorption (*e.g.*, with  $\text{H}_6\text{TeO}_6$ ) adsorbed anions participate in the formation of double layers on the surface of alumina.<sup>3</sup> Our kinetic calculations support these suggestions.

*Acknowledgment.* Authors are thankful to Mrs. B. Pavlovska for her participation in the experimental work, and to Miss Z. Todorović for the help in work.

(29) D. R. Vissers, *J. Phys. Chem.*, **72**, 3236 (1968).

(30) R. W. G. Wicknoff, "Crystal Structure," Vol. III, Interscience, New York, N. Y., 1960.



## Brønsted Acid Sites on Porous Glass from Membrane Potentials

by L. S. Hersh\* and M. P. Teter

Research and Development Laboratories, Corning Glass Works, Corning, New York 14830 (Received May 3, 1971)

Publication costs assisted by Corning Glass Works

The surface of a porous glass is characterized by KCl concentration cell membrane potentials interpreted by a Donnan-Planck model that includes the dissociation constant of fixed-ionic sites. The best fit is obtained with a two-site model with fixed-on concentration of  $\bar{T}_1 = 0.017$  and  $\bar{T}_2 = 0.177 m$  with dissociation constants  $K_1 = 3.9 \times 10^{-3}$  and  $K_2 = 5.0 \times 10^{-7}$ . These surface concentrations of acidic sites correspond quite closely to the bulk concentration of  $Al_2O_3$  and  $B_2O_3$ , respectively.

### Introduction

The study of glass surfaces is complicated by the instability and heterogeneous nature of an amorphous solid which can be contaminated by trace species. Because of its extremely high surface area, the use of a porous borosilicate glass minimizes some of the problems due to trace contamination and may offer a reasonable model surface for the borosilicate glass in general laboratory use.

This report describes the determination of the dissociation constants for Brønsted acid groups on a borosilicate porous glass surface from membrane potentials of a KCl concentration cell with varying pH. The theoretical model is based on a Donnan-Planck ion distribution concept applied to an ion exchanger considered as a quasihomogeneous phase in which one ionic species (the fixed ionic groups) is immobile. This model was first successfully applied to membranes by Teorell<sup>1,2</sup> and Meyer.<sup>3</sup> It has been critically discussed by Teorell,<sup>4</sup> Helfferich,<sup>5</sup> and Spiegler.<sup>6</sup> The basic concept of the Teorell-Meyer theory has been confirmed by many experimental results.<sup>5,6</sup>

Previous approaches to the study of the acid groups found on porous glass have involved aqueous titration,<sup>7</sup> infrared techniques,<sup>8-17</sup> and emf measurements.<sup>18,19</sup>

The aqueous titration method used by Altug and Hair<sup>7</sup> suffers from the fact that silica is attacked by alkali, and, therefore, the nature of the surface may be modified during the titration.<sup>20</sup> In addition, this approach may not have sufficient sensitivity to detect small concentrations of polybasic surface sites.

Hair and Hertl<sup>17</sup> used an infrared method to calculate the dissociation constants of well-defined surface hydroxyl groups on porous mixed-oxide systems. Their method would not apply to Brønsted acid sites produced by tetrahedrally coordinated aluminum or boron.<sup>21,22</sup>

Other infrared studies have examined the nature of active sites on porous glass.<sup>8-16</sup> There is general agreement that in addition to silanol groups there are sur-

face B-OH groups<sup>12-14</sup> and surface sites demonstrating Lewis acidity which have been assigned to trigonally coordinated boron.<sup>9,11-14</sup>

The previous emf studies of porous glass membranes have shown the applicability of the Teorell-Meyer model but have ignored the weak electrolyte character of the surface acid sites.<sup>18,19</sup> The present study includes the dissociation constant and the hydrogen ion activity in the bulk and interfacial region to gain additional information about the nature of these acid sites. In addition, it is demonstrated that the Teorell model may be extended to include the more general case of fixed ionic groups having finite dissociation constants.<sup>23</sup>

- (1) T. Teorell, *Proc. Soc. Exptl. Biol. Med.*, **33**, 282 (1935).
- (2) T. Teorell, *Z. Elektrochem.*, **55**, 460 (1951).
- (3) K. H. Meyer and J. F. Sievers, *Helv. Chim. Acta*, **19**, 649 (1936).
- (4) T. Teorell, *Progr. Biophys. Mol. Biol.*, **3**, 305 (1953).
- (5) F. Helfferich, "Ion Exchange," McGraw-Hill, New York, N. Y., 1962.
- (6) K. S. Spiegler and M. R. Wyllie in "Physical Techniques in Biological Research," Vol. 2, G. Oster and A. W. Pollister, Ed., Academic Press, New York, N. Y., 1956, p 301.
- (7) I. Altug and M. L. Hair, *J. Phys. Chem.*, **71**, 4260 (1967).
- (8) A. N. Sidorov, *Zh. Fiz. Khim.*, **30**, 995 (1956).
- (9) M. Folman and D. J. C. Yates, *Proc. Roy. Soc., Ser. A*, **246**, 32 (1958).
- (10) L. H. Little, H. E. Klauser, and C. H. Amberg, *Can. J. Chem.*, **39**, 42 (1961).
- (11) N. W. Cant and L. H. Little, *Can. J. Chem.*, **42**, 802 (1964).
- (12) I. D. Chapman and M. L. Hair, *Trans. Faraday Soc.*, **61**, 1507 (1965).
- (13) M. L. Hair and I. D. Chapman, *J. Amer. Ceram. Soc.*, **49**, 651 (1966).
- (14) M. J. D. Low, N. Ramasubramanian, and V. V. Subba Rao, *J. Phys. Chem.*, **71**, 1726 (1967).
- (15) M. J. D. Low and N. Ramasubramanian, *J. Phys. Chem.*, **71**, 3077 (1967).
- (16) N. W. Cant and L. H. Little, *Can. J. Chem.*, **46**, 1573 (1968).
- (17) M. L. Hair and W. Hertl, *J. Phys. Chem.*, **74**, 91 (1970).
- (18) I. Altug and M. L. Hair, *ibid.*, **72**, 599 (1968).
- (19) L. S. Hersh, *ibid.*, **72**, 2195 (1968).
- (20) K. C. Bryant, *J. Chem. Soc.*, 3017 (1952).
- (21) J. J. Fripiat, A. Leonard, and J. B. Uytterhoeven, *J. Phys. Chem.*, **69**, 3274 (1965).
- (22) K. H. Bourne, F. R. Cannings, and R. C. Pitkethly, *ibid.*, **74**, 2197 (1970).

### Experimental Section

**Porous Glass Disks.** Alkali borosilicate glass was made into 39 mm diameter, 0.65 mm thick disks for phase separation and acid-leaching treatment. The glass was heated for 3 hr at 580° and then cooled at 80°/hr. After being soaked for 15 min in a 10%  $\text{NH}_4\text{HF}_2$  solution and rinsed with distilled water, the disks were leached and washed at 95° for 24 hr each in 1.0 *N* and 0.1 *N*  $\text{HNO}_3$  and 48 hr in 0.05 *M*  $\text{KCl}$ , respectively. The disks were then heated in air at 800° for 2.6 hr. A final wash was given in 6 *N*  $\text{HCl}$  at 95° for 5.5 hr. The disks were then washed in doubly distilled water until brought to a steady pH of 5.7.

A BET  $\text{N}_2$  adsorption analysis of the porous glass gave the surface area as 175  $\text{m}^2/\text{g}$  with a pore volume of 0.35  $\text{cm}^3/\text{g}$ . The pore volume distribution, as determined by the Kelvin equation, had a very sharp peak at a radius of 27 Å. The same glass had a measured composition of (% by wt) 95.5  $\text{SiO}_2$ , 3.6  $\text{B}_2\text{O}_3$ , 0.46  $\text{Al}_2\text{O}_3$ , 0.28  $\text{K}_2\text{O}$ , and 0.23%  $\text{ZrO}_2$  (Table III).

**Membrane Potentials.** The cell used is shown in Figure 1. Three electrodes were inserted into the solution on each side. These were (1) Corning monovalent cation electrode (Cat. No. 476220), (2) Corning pH electrode (Cat. No. 476022), and (3) Fisher calomel reference electrode, saturated  $\text{KCl}$  (Cat. No. 13-639-57). The reference electrodes were carefully chosen for extremely low  $\text{KCl}$  leak and low noise in dilute solutions. They were left in the measuring mode at all times. The cation and pH electrodes were used to check the level of  $\text{K}^+$  and  $\text{H}^+$  before and after the emf difference between the two calomel electrodes was determined. The membrane potential was taken as the difference between the readings of the calomel electrodes observed for the case when identical  $\text{KCl}$  solutions were in both cells 1 and 2 and when the concentrations  $K_2^+/K_1^+ = 2$ . Differences in the liquid junction potential at the calomel electrodes were neglected. Temperature was maintained at  $23.5 \pm 0.3^\circ$ . The voltages of the cation and pH electrodes were measured with a Corning Model 12 research pH meter and a Leeds & Northrup 11-in. recorder. The calomel electrode's voltage difference was measured with a Keithley 150B microvoltmeter and Keithley 370 recorder.

The porous glass membranes were equilibrated overnight in the more concentrated  $\text{KCl}$  solution at pH values of 3.0, 4.0, and  $5.7 \pm 0.05$ . This was repeated if a change in pH was observed. All the solutions were allowed to equilibrate with  $\text{CO}_2$  in the atmosphere. Doubly distilled water was used to make up all solutions and washes.

The measurement of  $E_m$  as a function of  $\text{KCl}$  concentration and pH was performed using two different methods. In one, the pH was held constant, and the  $\text{KCl}$  concentration was both increased and decreased. In the other approach, the  $\text{KCl}$  concentration was constant, and pH values of 3.0, 4.0, and 5.7 were em-

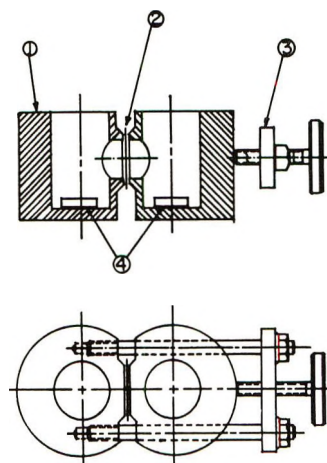


Figure 1. Side and top view of emf cell: 1, Lucite; 2, porous glass membrane; C, tightening nut; 4, Teflon-covered magnetic stirrers.

ployed. There was negligible hysteresis in either case of varying  $\text{KCl}$  concentration or pH. Each voltage measurement reported at a particular pH and  $\text{KCl}$  ratio is an average of measurements made with six different glass membranes. The standard deviation for each membrane and the pooled standard deviation was about  $\pm 0.3$  mV.

### Theory

A porous glass membrane is an open skeletal silicate framework containing the ions dissolved in water as the internal electrolyte. We are assuming that aside from tortuosity factors, the pores are large enough that the internal electrolyte can be considered similar to the bulk solution. From this we imply that the activity coefficients and the mobility ratios are the same in the bulk and membrane phases.

The derivation and basic assumptions have been presented by Teorell.<sup>2,4</sup> His model consists of the application of the Nernst-Planck equation together with Planck's concept of a constrained diffusion layer. We have further introduced the more general condition of finite dissociation constants for the fixed-ionic sites.<sup>23</sup>

For  $\text{KCl}$  concentration cell membrane potentials at varying pH we have the electroneutrality conditions in the solution and membrane phase

$$K^+ + H^+ = Cl^- \quad (1)$$

and

$$\bar{H}^+ + \bar{K}^+ = \sum \bar{X}_i + \bar{Cl}^- \quad (2)$$

respectively, where  $\bar{X}_i$  represents the concentration of fixed dissociated sites of species *i*. The  $\text{OH}^-$  has been omitted since the ratio  $\text{Cl}^-/\text{OH}^-$  is at all times  $\geq 10^2$ . The requirement of Donnan equilibrium implies

(23) H. P. Gregor, J. Belle, and R. A. Marcus, *J. Amer. Chem. Soc.*, **77**, 2713 (1955).



$$\frac{\bar{H}^+}{H^+} = \frac{\bar{K}^+}{K^+} = \frac{Cl^-}{Cl^-} \quad (3)$$

As previously stated, the various activity coefficients are assumed to be the same in the bulk and membrane phases. The bar indicates the membrane phase.

The fundamental difference between this model and the Teorell model is that finite dissociation constants for the charged sites are assumed, therefore

$$K_i = \frac{\bar{H}^+ \cdot \bar{X}_i}{\bar{H} \bar{X}_i} \quad (4)$$

where the ratio of activity coefficients is assumed constant.

Each different species of site has its own  $K$ . We furthermore have the condition that the sum of the dissociated sites and the associated sites must be equal to the total number of sites of that type

$$\bar{T}_i = \bar{X}_i + \bar{H} \bar{X}_i \quad (5)$$

The meaning of  $\bar{T}$ , the fixed-ion concentration, has been discussed by Helfferich<sup>5</sup> and Spiegler.<sup>6</sup> In this case, the quasihomogeneous membrane phase consists of the surface concentration of acid sites considered as homogeneously distributed throughout the aqueous solution contained in the membrane pores.

With a knowledge of  $K^+$ ,  $Cl^-$ , and  $H^+$ , the  $\bar{T}_i$ 's and the  $K_i$ 's eq 1-5 are sufficient to determine all the unknowns at the boundary. Unfortunately the equations are nonlinear. Combining eq 4 and 5 we obtain

$$\bar{X}_i = \frac{K_i \bar{T}_i}{\bar{H}^+ + K_i} \quad (6)$$

Inserting (3) and (6) into (2) results in the following equation

$$\bar{H}^+ + \frac{K^+ \bar{H}^+}{H^+} = \sum \frac{K_i \bar{T}_i}{\bar{H}^+ + K_i} + Cl^- \frac{H^+}{\bar{H}^+} \quad (7)$$

Using Newton-Rapheson techniques this may be solved for  $\bar{H}^+$ , and all other concentrations at the boundary follow immediately. For a single species of site, eq 7 becomes an ordinary cubic which may be solved analytically. In the limit of large  $K_i$ , this reduces to the result of Teorell.<sup>4</sup>

These results establish the concentration at the interfaces, and a knowledge of these concentrations and the ion mobility ratios enables the calculation of the diffusion potential through the Planck diffusion theory. Following Teorell's notation,<sup>4</sup> the diffusion potential  $E_D$  is

$$E_D = \frac{RT}{F} \ln \xi$$

where  $\xi$  may be determined by the equation

$$\ln \xi = q \ln \bar{k}$$

and  $q$  and  $\bar{k}$  are related by the equation

$$\bar{k} = \frac{2C_2^+ + (1+q)\bar{X}_2}{2C_1^+ + (1+q)\bar{X}_1}$$

The third equation needed to complete the solution relates  $\xi$  and  $\bar{k}$

$$\frac{\bar{U}_2 \xi - U_1}{\bar{V}_2 - \bar{V}_1 \xi} = \frac{C_2^+ \xi - C_1^+ \ln \bar{k} - \ln \xi}{C_2^- - C_1^- \xi \ln k + \ln \xi}$$

where

$$\bar{U} = C_1^+ U_1 + C_2^+ U_2 + \dots$$

and

$$\bar{V} = C_1^- V_1 + C_2^- V_2 + \dots$$

Here  $C_1$  is the concentration of anions or cations at the  $i$ th interface.  $U_k$  and  $V_k$  are the bulk solution mobilities of the  $k$ th cation and anion, respectively.  $\bar{X}_i$  is the concentration of dissociated fixed ionic sites at the  $i$ th interface. The solution of these three equations in three unknowns must again be done numerically.

The Donnan potential is, of course, known when the concentrations at the interfaces are known. If

$$r = \frac{\bar{K}^+}{K^+}$$

then the Donnan or boundary potential is

$$E_B = \frac{RT}{F} \ln \frac{r_2}{r_1}$$

and the total membrane potential is

$$E_m = E_B + E_D$$

With a given set of solutions, pH's and membrane potentials the  $\bar{T}_i$ 's and  $K_i$ 's can be determined by assuming a set of  $\bar{T}$ 's and  $K_i$ 's, calculating the membrane potentials at the given solutions and pH's and comparing the results with the measured potentials. The residual sum of squares

$$S = \sum (E_{\text{meas}} - E_{\text{calcd}})^2$$

is then minimized.

## Results

The experimental values of the average  $E_m$  are plotted in Figure 2 vs.  $\log 1/K_2^+$  at pH values of 3.0, 4.0, and 5.7. The solid lines are theoretical values of  $E_m$  calculated from a two-site model with fixed-ion concentrations of  $\bar{T}_1 = 0.017 m$  and  $\bar{T}_2 = 0.177 m$  and with dissociation constants  $K_1 = 3.9 \times 10^{-3}$  and  $K_2 = 5.0 \times 10^{-7}$ . The data were also fitted to two additional models: a single site, completely dissociated, and a single site, finite dissociation constant.

The two simpler models gave distinctly poorer fits to the data. This is summarized in Table I. The inclusion of finite dissociation constant in the single site

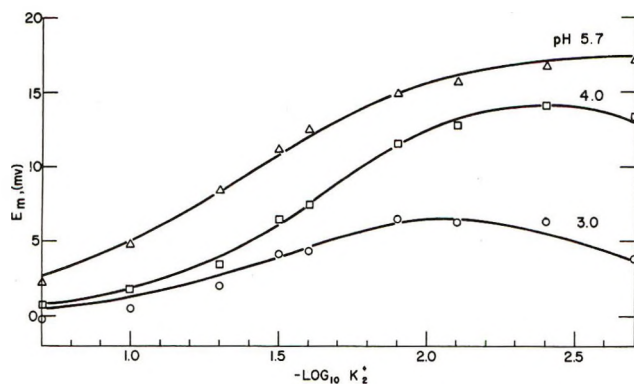


Figure 2. Two acid site model;  $\bar{T}_1 = 1.7 \times 10^{-2} m$ ,  $K_1 = 3.9 \times 10^{-3}$ ,  $\bar{T}_2 = 1.77 \times 10^{-1} m$ ,  $K_2 = 5 \times 10^{-7}$ .

model did, however, greatly improve the fit over the customary Teorell model. Statistically the probability is greater than 0.9999 that the two-site model is a better representation of the actual phenomena than the single-site model.

Table I: Analysis of Variance of the Three Models

Model	Total sum of squares	Residual sum of squares
One site, completely dissociated	760.4	248.9
One site, finite dissociation constant	760.4	32.7
Two site, finite dissociation constants	760.4	4.4

This is borne out in a predictive test of the model as shown in Figure 3. Here we have plotted experimental values of  $E_m$  obtained with NaCl at pH 5.7 and 23.5°. The three curves represent calculated values of  $E_m$  obtained from the various models using constants derived from the KCl data only. The only change made was to convert the mobility of potassium in the equation for the diffusion potential into that of sodium. The value  $5.19 \times 10^{-4} \text{ cm}^2/\text{sec V}$  was used for the mobility of  $\text{Na}^+$ . The best fit is obviously that of the two-site model, and the agreement over three orders of magnitude of concentration is good support for both the model and the values of  $K$  and  $\bar{T}$  determined from KCl solutions.

Due to the nonlinearity of the model, it is difficult to place confidence bands on the estimates of  $K$  and  $\bar{T}$ ; however, the variables were not highly correlated and the results could be considered well defined to approximately 10%.

In Table II we present calculated values of the pH in the membrane phase at various bulk KCl concentrations and pH at 25°. These calculated interfacial pH's may be used to approximate the hydrogen ion

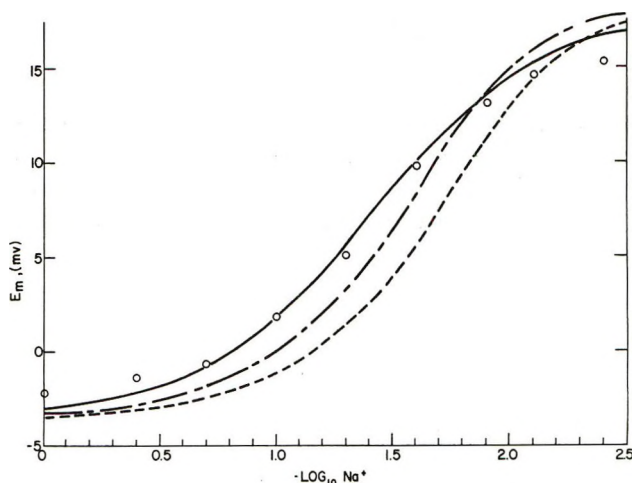


Figure 3. Calculated vs. experimental values of membrane potentials for NaCl concentration cell at pH 5.7 and 23.5°: ---, one site, complete dissociation; - · -, one site, finite dissociation; —, two sites, finite dissociation.

concentration at a glass-aqueous solution interface (e.g., Corning Code 7740 borosilicate glass) under conditions of similar ionic strength. The Donnan equilibrium conditions at the interface that determine the pH depend on ionic activity and do not depend on ionic mobilities.

Table II: Calculated pH in the Membrane Phase as a Function of Bulk KCl Concentration and pH at 23.5°

$K_2^+$ , M	Solution pH		
	3.0	4.0	5.7
0.002	2.47	3.14	4.67
0.004	2.60	3.38	4.91
0.008	2.73	3.61	5.12
0.0125	2.81	3.73	5.24
0.025	2.89	3.85	5.40
0.032	2.91	3.88	5.45
0.050	2.94	3.92	5.52
0.10	2.97	3.96	5.60
0.20	2.99	3.98	5.65

## Discussion

Altug and Hair<sup>18</sup> have performed a similar study using a porous glass of slightly different composition. Their results may be directly compared with ours. They applied Teorell's extended fixed-charge theory, but they neglected two aspects of our approach: (1) the effect of  $\text{H}^+$  on both the boundary and internal potential and (2) a dissociation constant for the fixed-charge groups.

By omitting these factors, Altug and Hair<sup>18</sup> could not explicitly rationalize some of the data, e.g., a dependence of  $\bar{T}$  on the pH of the bulk solution. For the case of KCl solutions at pH 5.0 and 5.7, they obtained "best-fit" values of  $\bar{T}$  of 0.04 and 0.06 M, respectively.



Using our two-site model we calculate values of dissociated fixed sites of 0.025 and 0.052 *M* for our porous glass at the corresponding pH's. A large discrepancy between observed and calculated values was also observed by Altug and Hair for HCl concentration cells. This difference—the observed values were always lower than the calculated—increased with increasing H<sup>+</sup>. This lowering of *E<sub>m</sub>* which results largely from the effect of H<sup>+</sup> on the dissociated fixed site is predicted by our model.

In an earlier study, Altug and Hair<sup>7</sup> examined the alkali cation uptake of the same glass used in their emf work. Their titration data indicated that the K<sup>+</sup> uptake from KCl solutions at pH 5.0 and 8.5 is about  $4 \times 10^{-3}$  and  $1 \times 10^{-1}$  mequiv/g, respectively. At pH 5, their uptake value converts into 0.045 *m* for exchanged fixed sites, which is in fair agreement with our calculated value of 0.025 *m* for  $\Sigma X_i$  using the two-site model. However, their value at pH 8.5 is equivalent to 1.1 *m* of dissociated sites. Our two-site model predicts a maximum concentration of about 0.2 *m*.

Altug and Hair<sup>7</sup> also used the cation uptake values to calculate a dissociation constant for the fixed site. Using a method derived by Helfferich,<sup>5</sup> they obtained a value of 1.6 *m* of fixed sites with a *K* of  $1.6 \times 10^{-6}$  at 25°. Their *K* is about 30 times the value we calculated for *K*<sub>2</sub> ( $5 \times 10^{-7}$ , 0.177 *m*). It is easy to explain why Altug and Hair missed the more acidic site (type 1). The cation uptake of  $1.7 \times 10^{-2}$  *m* of fixed sites amounts to about  $6 \times 10^{-3}$  mequiv/g which is below the range of their data.<sup>7</sup>

A greater discrepancy results from the combined effect of Altug and Hair's cation uptake value of 1.6 *m* and a *K* of  $1.6 \times 10^{-6}$ . Using the latter values, we calculate 0.22 *m* of dissociated sites at pH 5. Our model yields a value of 0.025 *m*, an order of magnitude less. In addition, their predicted value of 0.22 *m* at pH 5 is inconsistent with their own cation uptake at this same pH. A conversion of 0.22 *m* yields a calculated cation uptake value of  $1.94 \times 10^{-2}$  mequiv/g which is at odds with their observed values of  $4 \times 10^{-3}$  mequiv/g at pH 5.<sup>18</sup>

This internal inconsistency of Altug and Hair's titration data could be rationalized by the effect that alkaline solutions have on the structure of silica materials. The anomalously high values of fixed-site concentration and *K* may have been caused by the breakdown of the silica network caused by the lengthy contact of their porous glass with solutions whose pH ranged about 7–9.

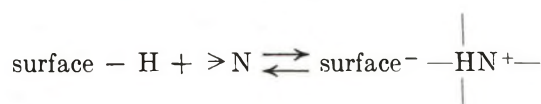
We now turn our attention to the chemical nature of the fixed-acid sites on porous glass. If the effective area of a surface silica site<sup>24</sup> is 12.5 Å<sup>2</sup>, the fraction of sites corresponding to our two-site model is about 0.3 and 2% for the concentrations  $1.7 \times 10^{-2}$  and 0.177 *m*, respectively (Table III). Of course, the emf data are not sufficient to identify the chemical nature of the

acid sites. The similarity between the emf-derived acid site concentrations and the bulk concentrations of any oxide may be fortuitous.<sup>13</sup> However, assuming no extremely large concentration gradients, such that the surface concentration of either Al<sub>2</sub>O<sub>3</sub> or ZrO<sub>2</sub> is an order of magnitude greater than their bulk concentration, the weaker acid site (type 2) should correspond to boron.

**Table III:** Chemical Composition of the Porous Glass Membrane and Surface Site Concentrations

Oxide	Mol %	% of surface sites
SiO <sub>2</sub>	96.3	
B <sub>2</sub> O <sub>3</sub>	3.13	2.1 type 2
Al <sub>2</sub> O <sub>3</sub>	0.27	0.26 type 1
K <sub>2</sub> O	0.179	
ZrO <sub>2</sub>	0.113	

There are other experimental data that imply that the stronger acid sites on porous glass (type 1) are primarily a result of the presence of alumina. Recent spectroscopic studies with boric oxide–silica systems have shown that surface boron atoms are not catalytically active sites for olefin reactions<sup>16</sup> reported previously with porous glass.<sup>10</sup> Earlier work indicated that a surface leached porous glass which affected the Al<sub>2</sub>O<sub>3</sub> and ZrO<sub>2</sub> contents, but not the B<sub>2</sub>O<sub>3</sub>, showed less ability to polymerize and isomerize hydrocarbons.<sup>10</sup> Furthermore, there is no evidence of the presence of adsorbed NH<sub>4</sub><sup>+</sup><sup>11,13,14,16</sup> or pyridinium ion<sup>25</sup> resulting from the gas phase adsorption of ammonia and pyridine on porous glass, as is the case for similar adsorption on silica–alumina.<sup>16,22,26</sup> The reaction on silica–alumina is presumably between Brønsted acid sites and the above bases, and is shown by



### Summary

The surface of borosilicate porous glass is believed to be polybasic in the Brønsted acid sense. In addition to the weakly acidic silanol and boronol sites there are low concentrations of at least two additional Brønsted acid sites whose *K*'s have been estimated by the present report to be about  $3.9 \times 10^{-3}$  and  $5 \times 10^{-7}$ . These more strongly acidic sites are believed to result from the presence of aluminum and boron on the surface of porous glass.

(24) R. K. Iler, "Colloid Chemistry of Silica and Silicates," Cornell University Press, Ithaca, N. Y., 1955, pp 242–248.

(25) M. L. Hair, "Infrared Spectroscopy in Surface Chemistry," Marcel Dekker, New York, N. Y., 1967, p 118.

(26) J. E. Mapes and R. P. Eischens, *J. Phys. Chem.*, **58**, 1059 (1954).

*Acknowledgments.* Much appreciation to M. Burke for measuring the emf, to J. M. Mandzak for the sur-

face area analysis, and to K. Sugawara for the elemental analysis.

## Hyperfiltration in Charged Membranes. Prediction of Salt Rejection from Equilibrium Measurements

by E. Hoffer\* and O. Kedem

*Department of Plastics Research, Weizmann Institute of Science, Rehovot, Israel (Received May 1, 1972)*

*Publication costs assisted by the Office of Saline Water*

Ion distribution between polybase-collodion membranes and aqueous salt solutions was measured and could be described by an effective charge density, following the association model for polyelectrolyte solutions. The osmotic factor,  $\varphi_p$ , derived from these measurements is close, but not equal, to that measured in the corresponding polybase solutions. The effective charge density resulting from the equilibrium measurements was introduced into the equation for salt rejection, derived previously for the TMS model. Satisfactory agreement with measured rejections was found.

### Introduction

In a previous publication,<sup>1</sup> salt rejection was calculated for membranes described by the simple Teorell, Meyer, and Sievers (TMS) model. These model calculations predicted the influence of flow rate, membrane, and electrolyte parameters on salt rejection. Some of the conclusions of the model calculations were tested in polybase-collodion membranes and qualitative agreement between experiments and model calculations was obtained.<sup>2</sup>

The aim of the present work is the establishment of a quantitative correlation between coion uptake and salt rejection. For this purpose, the simple TMS model had to be modified to take into account the electrostatic interaction between the charged matrix and the counterions.

### Models

The basic assumption of the TMS model is the homogeneous distribution of fixed charges and of ions throughout the membrane volume. The model assumes also the ideality of the interstitial solution and, consequently, ideal Donnan distribution of salt between membrane and external solutions.

In fact, it was shown long ago that the distribution of ions around polyionic chains in solutions is not homogeneous, but may be represented by a diffuse double layer. Correspondingly, in charged membranes, the ion distribution in pores is far from being homogeneous; counterion concentration is larger along

the pore walls and solution passing in a region removed from the wall will find itself in a weaker electrical field than that caused by the original charge density.

The association model developed in the course of the study of polyelectrolyte solutions<sup>3,4</sup> offers a simple and convenient way to describe the thermodynamic behavior of polyelectrolyte solutions. Instead of representing the ion distribution around the polyions by a continuous function of distance, the association model assumes a step function; up to a certain distance from the polyion all the counterions are "bound" or "immobilized;" from that distance all are "free." In other words, only a certain fraction of counterions is available to participate in the Donnan equilibrium.

In the original association model proposed by Wall, *et al.*,<sup>3</sup> it was assumed that the fraction of free counterions is identical, whether determined by equilibrium or by transport measurements. It was found, however,<sup>4</sup> that although transport phenomena may be interpreted by the association model, the fraction of free counterions is not identical with that determined by equilibrium measurements. In the following, we will use the original association model for an estimate of

(1) E. Hoffer and O. Kedem, *Desalination*, **2**, 25 (1967).

(2) E. Hoffer and O. Kedem, *ibid.*, **5**, 167 (1968).

(3) J. R. Huizenga, P. F. Gregor, and F. T. Wall, *J. Amer. Chem. Soc.*, **72**, 2636, 4228 (1950).

(4) A. Katchalsky, Z. Alexandrowicz, and O. Kedem in "Chemical Physics of Ionic Solutions," B. E. Conway and R. G. Barradas, Ed., Wiley, New York, N. Y., 1966.



the polyelectrolyte effect, although the process of hyperfiltration is a typical transport process. We will assume, as in the TMS model, that the interstitial solution is an ideal one, but the counterion concentration is given by the "free" counterions.

The Donnan equilibrium between solution and membrane, at the interface is then given by

$$\frac{\bar{c}_1}{\phi_w} \cdot \frac{\bar{c}_2}{\phi_w} = \frac{X + \bar{c}_s}{\phi_w} \cdot \frac{\bar{c}_s}{\phi_w} = c_s^2 \quad (1)$$

where  $\bar{c}_2$  is the coion concentration per cubic centimeter of membrane phase, identified with the salt concentration  $\bar{c}_s$ ,  $\bar{c}_1$  is the concentration of free counterion per cubic centimeter,  $X$  is the effective charge density, and  $c_s$  is the salt concentration in the external solution. Here, as in the treatment of polyelectrolyte solutions, it was assumed that the activity coefficient of the coions is unity.

Equation 1 may be written in terms of the coion distribution coefficient between external and interstitial solutions,  $K$ , defined by

$$K = \frac{\bar{c}_s}{c_s \phi_w}$$

$$(X/(c_s \phi_w) + K)K = 1 \quad (2)$$

Hence, the experimental determination of the coion distribution coefficient gives also the effective charge density or free counterion concentration.

### Experimental Section

Polyamine-collodion membranes have been prepared by cross-linking polylysine in a collodion membrane. The collodion membrane was cast from a 3% collodion solution in 50% ether, 48% ethanol, and 2% water. This solution was spread on a glass plate with a casting knife of 1.2-mm thickness, and the collodion membrane was formed after immersion of the glass plate in water. Adsorption of polylysine (PL-HBr, mol wt 6900, purchased from Miles Yeda Chemicals) in the collodion membrane is achieved by keeping the membrane for 5 days in a 5% polylysine solution. The polymer solution contained 1 *M* sodium chloride buffered to pH 8.6. The polymer was mechanically fixed in the collodion support by air drying the membrane for 30 min. Then, the cross-linking of the polymer in the membrane was carried out by immersing the membrane in a pH 8.6 buffer solution which contained 0.5 ml of a 25% glutaraldehyde solution. After 30 min, the membrane was rinsed and hyperfiltration experiments were started. If the flow rate was larger than 0.04 cm/min at 200 psi, additional air-drying of the membrane was allowed (15–30 min).

For the determination of sodium or chloride concentration in the membrane, the membranes were equilibrated with solutions of sodium chloride containing trace amounts of  $^{22}\text{Na}$ . After equilibration, the membrane

was blotted with filter paper and washed under shaking with 3 vol of another, more concentrated electrolyte solution. These volumes are combined and samples of  $^{22}\text{Na}$  are counted, together with samples of the original solution, in a Packard Auto Gamma Counter. In the same samples, chloride was analyzed with the Aminco Cotlove Automatic Titrator. The amount of liquid in the membrane was determined from the difference in weight between the blotted membrane and the dried one.

Hyperfiltration experiments were performed in a stainless steel cell with a nitrogen cylinder as pressure sources. Stirring of the feed was provided by a magnetic stirrer placed at a small distance above the mem-

**Table I:** Electrolyte Distribution Coefficients and Rejection in a Polylysine-Collodion Membrane (PL-174)<sup>a</sup>

Concn of equilibrating solution	Coion concn, equiv/l. $\times 10^3$	$K'$	$R_\infty^b$	$R$ (exptl)
0.005	1.08	0.22	66	77.8
0.0098	2.36	0.24	61.5	63.2
0.023	9.3	0.40	39.3	42.9
0.048	27.7	0.57	21.2	22.9
0.095	77.5	0.81	11	13.4

<sup>a</sup> Water content of the membrane 45%; rejection measured at 0.02 cm/min at 200 psi. <sup>b</sup> See eq 6.

**Table II:** Electrolyte Distribution Coefficients and Rejection in a Polylysine-Collodion Membrane (PL 175)<sup>a</sup>

Concn of equilibrating solution	Coion concn, equiv/l. $\times 10^3$	$K'$	$R_\infty^b$	$R$ (exptl)
0.0048	0.85	0.18	71.3	71.5
0.0098	2.36	0.24	61.3	59
0.023	10.2	0.43	35.6	39.3
0.048	29.8	0.62	18.4	21.3
0.095	70.7	0.74	10.3	10.3

<sup>a</sup> Water content of the membrane 44.4%; rejection measured at 0.02 cm/min at 200 psi. <sup>b</sup> See eq 6.

**Table III:** Electrolyte Distribution Coefficients and Rejection in a Polylysine-Collodion Membrane (PL 72)<sup>a</sup>

Concn of equilibrating solution	Coion concn, equiv/l. $\times 10^3$	$K'$	$R_\infty^b$	$R$ (exptl)
0.005	1.02	0.20	67	69
0.0074	1.89	0.25	60	63
0.0096	2.47	0.26	59	59.2
0.024	11.4	0.46	33	37.7
0.049	34.7	0.70	12	19

<sup>a</sup> Water content of the membrane 48%; rejection measured at 0.03 cm/min at 200 psi. <sup>b</sup> See eq 6.

**Table IV:** The "osmotic coefficient"  $\phi_p$  in Membranes 174 and 175 at Various External Concentrations

Concentration of equilibrating solution	Membrane PL-collodion 174			Membrane PL-collodion 175		
	Counterions concn, equiv./l. $\times 10^3$	Free counterion concn from (2) and coion measurements, equiv./l. $\times 10^3$	$\phi_p$	Counterion concn, equiv./l. $\times 10^3$	Free counterion concn from (2) and coion measurements, equiv./l. $\times 10^3$	$\phi_p$
0.005	372	22.1	0.059	366	25.7	0.07
0.01	372	38.6	0.108	375	37.8	0.1
0.0225	392	5.13	0.13	395	42.5	0.107
0.048	405	60.1	0.146	391	45	0.115
0.1	448	38.5	0.086	449	57	0.127

brane. Samples of feed and produce were taken simultaneously and were analyzed for chloride ions.

### Results and Discussion

The effectiveness of hyperfiltration is described by the salt rejection,  $R$ , defined as<sup>5</sup>

$$R = 1 - \frac{c_s''}{c_s'} \quad (3)$$

where  $c_s'$  and  $c_s''$  are the salt concentrations in feed and product solutions, respectively. At stationary hyperfiltration the concentration of the product is given by the ratio between salt flow and volume flow

$$c_s'' = \frac{J_s}{J_v} \quad (4)$$

The calculation of salt rejection for membranes represented by the TMS model, showed that at high flow rates the concentration profile of the salt in the membrane flattens in the vicinity of the feed boundary. Then, the whole process is governed by the salt exclusion at feed boundary, and the rejection may be expressed as a function of the membrane charge density and the relative mobilities of the ions. A consideration of the Donnan equilibrium at the feed interface and the maintenance of electroneutrality during hyperfiltration led to a simple expression for the salt rejection at high flow rates  $R_\infty$ <sup>1</sup>

$$R_\infty = 1 - \frac{c_s' \phi_w}{\bar{c}_s' + t_1 X} \quad (5)$$

where  $t_1 = u_1/(u_1 + u_2)$ ,  $u_1$  and  $u_2$  are the mobilities of the counterion and coion, respectively, and thus  $t_1$  is the transport number in free solution.

Regarding  $X$  as the effective charge density, eq 2 and 5 give the relation between salt rejection and the measured equilibrium distribution of the coion, at the external concentration  $c_s'$

$$R_\infty = 1 - K' \frac{1}{t_2 K'^2 + t_1} \quad (6)$$

where  $t_2 = 1 - t_1$ .

As is clear from the derivation, the validity of eq 6 is limited to the simple association model, in which a

single effective charge density is used to describe both equilibrium and transport properties.

Three polylysine membranes were equilibrated with a number of sodium chloride solutions and coion concentration was determined in each membrane, at each external concentration. The measured values of the coion concentration, as well as the distribution coefficient and  $R$  computed from (6) are given in Tables I, II, and III. Salt rejection was determined in hyperfiltration experiments with feeds of the same concentration as the equilibrating solutions. Since there is no flow rate dependence of salt rejection in these experiments, one may identify the measured rejection with  $R_\infty$ . The results given in the last column of Tables I, II, and III show fair agreement with the rejections computed from equilibrium data. Thus, from relatively simple models one may predict the hyperfiltration behavior of charged membranes.

In the association model, the osmotic coefficient  $\phi_p$  is regarded as the ratio between the free counterions and the total concentration of counterions.  $\phi_p$  was determined experimentally in polylysine-salt solutions by Daniel and Alexandrowicz and was found to vary between 0.16 and 0.19 for a large range of salt and polyelectrolyte concentrations.<sup>6</sup> Inbar and Miller<sup>7</sup> found the value  $\phi_p = 0.14$  for polylysine solutions.

The concentration of counterions was determined in the two polylysine membranes represented in Tables I and II. The ratio between these values and those computed from the coion concentrations and the Donnan equation is equivalent to an osmotic coefficient  $\phi_p$  for the cross-linked polyelectrolyte in the membrane. The  $\phi_p$  values of the two membranes are given in Table IV for each external concentration. One sees that the values are close but not equal to those found for the polyelectrolyte solutions.<sup>6,7</sup> Also, the  $\phi_p$  values determined in the membranes are concentration dependent. A possible explanation for this behavior is the clustering of the polylysine chains adsorbed on the collodion strands.

(5) J. S. Johnson, L. Dresner, and K. A. Kraus in "Principles of Desalination," K. S. Spiegler, Ed., Academic Press, New York, N. Y., 1966.

(6) E. Daniel and Z. Alexandrowicz, *Biopolymers*, **1**, 473 (1963).

(7) I. R. Miller and L. Inbar, *ibid.*, **7**, 619 (1969).



Clustering could affect both ion distribution and ion transport. Model calculations were recently carried out by Simons and Kedem<sup>8</sup> for an array of rectangular pores in an ion-exchange medium, not assuming homogeneous ion distribution. From these calculations it appears that the distribution coefficient is quite sensitive to pore size, at given average charge density, but the relation between salt rejection and salt distribution is only slightly influenced. It is thus possible

that in practice the correlation given in eq 6 is valid in systems for which not all the assumptions of the TMS model are justified.

*Acknowledgments.* The authors thank the Office of Saline Water for a grant to support work on hyperfiltration membranes (OSW Contract No. 14-01-0001-961).

(8) R. Simons and O. Kedem, to be published.

## Oxidation Kinetics of 2-Dimethylaminoethanethiol Hydrochloride by Ferricyanide Ion in Acid Medium

by R. K. Chohan, B. P. Sinha, and R. C. Kapoor\*

*Department of Chemistry, University of Jodhpur, Jodhpur, Rajasthan, India (Received April 24, 1972)*

The oxidation kinetics of 2-dimethylaminoethanethiol hydrochloride in aqueous hydrochloric acid medium have been described. The stoichiometry is found to be 1:1 and the substrate is shown to be oxidized to the corresponding disulfide. The order is unity both in ferricyanide and thiol hydrochloride. The rate decreases on increasing the initial concentration of ferricyanide and hydrogen ion concentration. Addition of ferrocyanide, disulfide, and neutral salt produces no change in rate. A tentative reaction scheme is suggested.

### Introduction

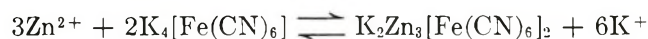
In a recent publication<sup>1</sup> the oxidation kinetics of 2-mercaptoethylamine hydrochloride by the ferricyanide ion in aqueous hydrochloric acid medium were described. Besides, this oxidant has also been used earlier for oxidation of a number of other thiols.<sup>2-6</sup> The present investigations stems from an extension of the work being carried out in this laboratory on ferricyanide oxidation of compounds containing a sulfhydryl group. There is a marked divergence in the oxidation scheme of the two thiol hydrochlorides largely due to the role of ferrocyanide.

### Experimental Section

The sample of 2-dimethylaminoethanethiol hydrochloride (assay 98%) was from Evans Chemetics Inc., U.S.A. An approximate solution of this compound was first prepared in air-free double-distilled water. This was subsequently standardized with a standard solution of iodine in presence of hydrochloric acid.<sup>7</sup> A standard solution of potassium ferricyanide (E. Merck reagent grade) was prepared by direct weighing. A fresh solution was prepared for each run. 2,2'-Dimethylaminodiethyl disulfide dihydrochloride (*i.e.*, the disulfide of the present thiol hydrochloride) was obtained

by oxidizing the latter with dimethyl sulfoxide.<sup>8</sup> The indicator solution of 3,3'-dimethylnaphthidinedisulfonic acid (B.D.H., L.R.) was prepared in dilute ammonia solution. All other chemicals used were of analytical grade.

The kinetics of the reaction were followed by estimating the product ferrocyanide volumetrically with the aid of a standard solution of zinc sulfate as done earlier.<sup>9</sup> The overall reaction is



- (1) R. C. Kapoor, R. K. Chohan, and B. P. Sinha, *J. Phys. Chem.*, **75**, 2036 (1971).
- (2) O. P. Kachhwaha, B. P. Sinha, and R. C. Kapoor, *Indian J. Chem.*, **8**, 806 (1970).
- (3) R. C. Kapoor, O. P. Kachhwaha, and B. P. Sinha, *J. Phys. Chem.*, **73**, 1627 (1969).
- (4) I. M. Kolthoff, P. J. Meehan, M. S. Tsao, and Q. W. Choi, *ibid.*, **66**, 1233 (1962).
- (5) E. J. Meehan, I. M. Kolthoff, and H. Kakinchi, *ibid.*, **66**, 1238 (1962).
- (6) J. J. Bohning and K. Weiss, *J. Amer. Chem. Soc.*, **82**, 4724 (1960).
- (7) H. Kramer, *J. Ass. Offic. Agr. Chem.*, **35**, 285 (1952).
- (8) W. W. Epstein and F. W. Sweat, *Chem. Rev.*, **67**, 247 (1967).
- (9) A. I. Vogel, "Quantitative Inorganic Analysis," Longmans, Green and Co., New York, N. Y., 1962, p 402.

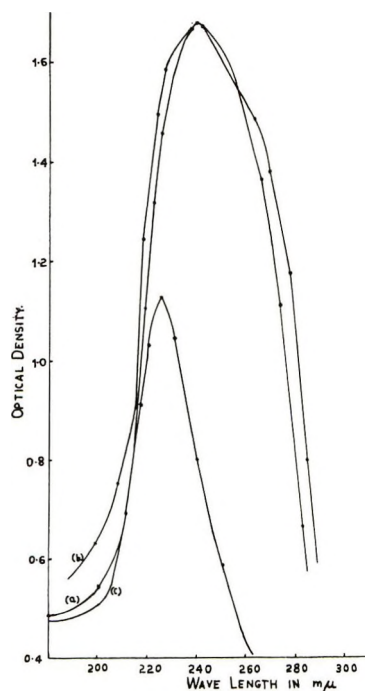
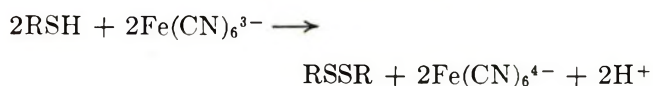


Figure 1. Absorption spectra of (a) 2-dimethylaminoethanethiol hydrochloride ( $1 \times 10^{-2} M$ ), (b) 2,2'-dimethylaminodiethyl disulfide dihydrochloride ( $1.0 \times 10^{-2} M$ ), and (c) the disulfide produced in the reaction mixture.

The absorption spectra of 2-dimethylaminoethanethiol hydrochloride and its disulfide were recorded using a Hilger Uvispeck spectrophotometer Model H 700-8 fitted with a thermostatic arrangement.

**Polymerization Test.** Vincyl cyanide and the acidified thiol were kept in a conical flask and the vessel was flushed with nitrogen for about 15 min. Potassium ferricyanide solution which had been previously flushed with nitrogen was then added and the nitrogen was again bubbled through the mixture. Each experiment was accompanied by a blank control. The reaction greatly catalyzed the polymerization of vinyl cyanide and a thick polymer was obtained in each case.

**Stoichiometry.** Here again, both analytical and polarographic methods<sup>10</sup> were employed to determine the stoichiometry. The latter method helped not only in the estimation but also the characterization of one of the final products of oxidation, *viz.*, the disulfide. The spectrophotometric studies also led to a similar conclusion, *i.e.*, the reaction leads to the formation of disulfide as the sole oxidation product of thiol hydrochloride. This is demonstrated by Figure 1, where absorption spectra of thiol hydrochloride, the disulfide, and that of a reaction mixture, which had been allowed sufficient time, are recorded. All these methods led to one and the same finding regarding the stoichiometry being 1:1. The overall reaction is therefore



## Results

**Order of Reaction.** A number of runs having equimolar concentration of ferricyanide and thiol hydrochloride were made in hydrochloric acid and sodium chloride buffer. A plot of  $[1/(a-x)]$  vs. time (where  $a$  denotes the initial concentration of the two reactants and  $x$  is the decrease in their concentration at time  $t$ ) gave a straight line for nearly 70% of the reaction. The second-order velocity coefficients in all these runs were calculated by using the modified equation

$$k_2 = \frac{1}{(t_2 - t_1)} \left[ \frac{1}{(a - x_2)} - \frac{1}{(a - x_1)} \right]$$

obtained on solving the differential equation  $dx/dt = k_2(a-x)^2$  between limits  $t_1, t_2$  and  $x_1, x_2$ . The results of a typical run are presented in Table I. A good agreement was found between the bimolecular rate coefficients calculated from the above formula and the ones obtained graphically. It may be mentioned here that the above equation was used because of the difficulty in exact experimental estimation of ferrocyanide formed at the commencement of the reaction. A standard rate constant is

$$k_s = 6.98 \times 10^{-3} \left( \frac{5}{2 \times 10^{-2}} \right)$$

where numerator in parentheses denotes the volume of reaction mixture withdrawn for estimation and denominator signifies the concentration as required by factor  $v/s$  for conversion of an arbitrary second-order rate constant ( $k_{\text{obsd}}$ ) into the standard second-order rate constant ( $k_s$ ). Hence  $k_s = 1.74 \pm 0.04 M^{-1} \text{ min}^{-1}$  and  $k_s$  (graphically) =  $1.73 \pm 0.04 M^{-1} \text{ min}^{-1}$ . All rate constant recorded hereafter are standard rate constant unless otherwise mentioned. Runs were also made at constant ionic strength by changing the initial concentration of ferricyanide in one series of experiments and thiol hydrochloride in the other. In all such variations, plots of  $\log [(b-x)/(a-x)]$  against time gave a straight line (where  $a$  is initial concentration of thiol hydrochloride and  $b$  that of ferricyanide). For variations in the initial concentration of ferricyanide, these plots are shown in Figure 2. The second-order rate coefficients for all such variations as calculated from the slopes ( $k_s = (2 \times 303)/(b-a) \times \text{slope} \times v/s$ ) are recorded in Table II.

The variations in the magnitude of second-order rate coefficients is due to the effect of initial concentration of ferricyanide as the other substrates concentration yields no such influence. The ionic strength was kept constant throughout with the help of sodium chloride.

The order in ferricyanide ion was also confirmed by isolating it in a number of runs by keeping the concentration of thiol hydrochloride in 10–20-fold excess over

(10) O. P. Kachhwaha, B. P. Sinha, and R. C. Kapoor, *Proc. Symp. Electrode Processes*, 1966, 84 (1969).



Table I<sup>a</sup>

Time, min	Volume of 0.005 M ZnSO <sub>4</sub> required, ml	Volume of 0.02 M ferrocyanide produced (x), ml	Volume of 0.02 M ferricyanide left, ml	$k_{\text{obsd}} \times 10^3$
5	4.7	0.783	4.21	
10	7.95	1.32	3.67	7.00
15	10.45	1.74	3.25	6.97
20	12.4	2.06	2.93	6.91
25	14.1	2.35	2.65	7.01
30	15.4	2.56	2.43	6.94
35	16.6	2.76	2.23	7.01
40	17.55	5.92	2.07	7.00

$$Av = 6.98 \times 10^{-3}$$

<sup>a</sup>  $[K_3Fe(CN)_6] = 2.0 \times 10^{-2} M$ ,  $[HS(CH_2)_2N(CH_3)_2 \cdot HCl] = 2.0 \times 10^{-2} M$ ,  $[HCl] = 5.0 \times 10^{-2} M$ ,  $[KCl] = 11.0 \times 10^{-2} M$ ,  $I = 0.3 M$ , temperature  $35^\circ$ .

Table II<sup>a</sup>

$[K_3Fe(CN)_6] \times 10^2 M$	$[RSH] \times 10^2 M$	$k_2, M^{-1} \text{min}^{-1}$
2.0	2.0	2.18
1.0	1.0	2.03
3.0	3.0	2.55
2.0	2.5	2.21
2.0	3.0	2.19
2.0	3.5	2.39
2.5	2.0	1.72
3.0	2.0	1.31
3.5	2.0	1.14
4.0	2.0	0.98

<sup>a</sup>  $[HCl] = 5.0 \times 10^{-2} M$ ,  $I = 0.3 M$ , temperature  $35^\circ$ .

the former. The reactions showed a pseudo-first-order kinetics in ferricyanide. These constants are recorded in Table III. When the pseudo-first-order rate coefficients are divided by the concentration of thiol hydrochloride the quotients are found to be practically constant which incidentally confirms the first-order kinetics in the substrate. The total order of the reaction was further verified by an application of Vant Hoff's differential method. Initial rates were measured corresponding to the different initial concentrations  $C$

Table III<sup>a</sup>

$[HS(CH_2)_2N(CH_3)_2 \cdot HCl] \times 10^2 M$	Pseudo-first-order constant, $k_1 \times 10^2 \text{min}^{-1}$	$k_1/c$
10.0	1.40	14.0
15.0	2.07	13.8
20.0	2.84	14.2
25.0	3.56	14.1
30.0	4.31	14.3

<sup>a</sup>  $[K_3Fe(CN)_6] = 1.0 \times 10^{-2} M$ ,  $[HCl] = 2.0 M$ ,  $I = 2.4 M$ , temperature  $35^\circ$ .

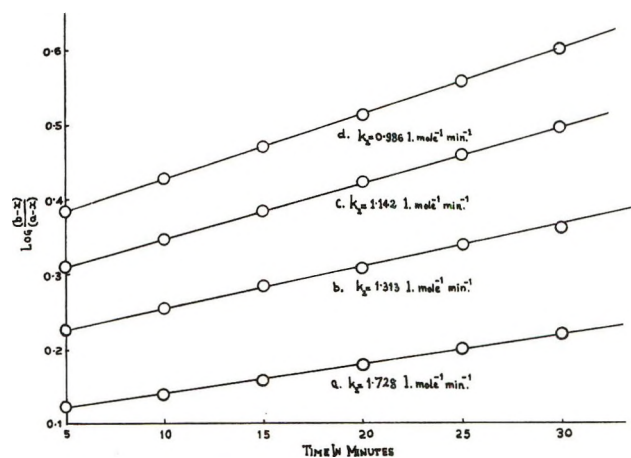


Figure 2. Second-order plot of four different runs (temperature  $35^\circ$ , [thiol hydrochloride] =  $2.0 \times 10^{-2} M$ ,  $[HCl] = 5.0 \times 10^{-2} M$ ,  $[K_3Fe(CN)_6] =$  (a)  $2.5 \times 10^{-2} M$ ; (b)  $3.0 \times 10^{-2} M$ , (c)  $3.5 \times 10^{-2} M$ , (d)  $4.0 \times 10^{-2} M$ ,  $I = 0.3 M$ ).

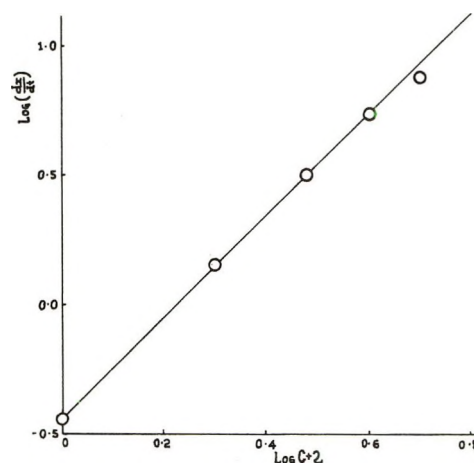


Figure 3. Relationship between initial rate and corresponding different initial concentrations of reactants (temperature  $35^\circ$ ,  $[HCl] = 5.0 \times 10^{-2} M$ ,  $I = 0.3 M$ ).

of the two reactants. A plot of  $\log (dx/dt)$  against  $\log C$  (where  $C$  denotes the concentration of both ferricyanide and thiol hydrochloride) gave a straight line with a slope equal to 1.8–2 (Figure 3).

As remarked earlier, the rate of oxidation is also dependent on the initial concentration of ferricyanide. The increase in the initial concentration produced retardation in rate. This is further demonstrated by the results shown in Table IV, but no simple relationship could be observed between the two. On the contrary, the variation of initial concentration of thiol hydrochloride produced no effect when all other parameters were kept constant (Table II and also on the basis of practically constant values of pseudo-first-order rate coefficient when variation of thiol hydrochloride in isolation is followed). The rate was found to be highly dependent on hydrogen ion concentration. The effect was studied in the presence of different concentration

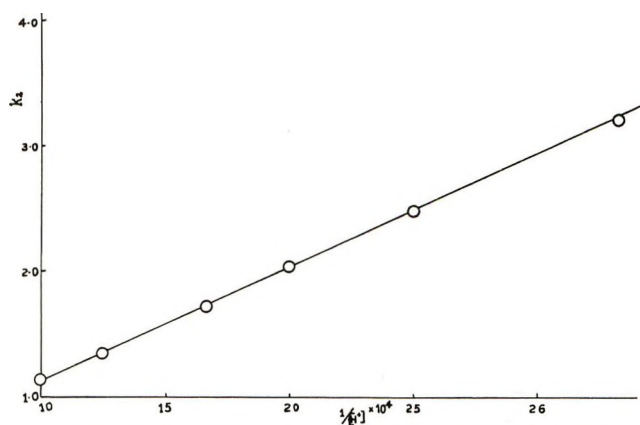


Figure 4. Dependence of the rate on hydrogen ion concentration (temperature  $35^\circ$ ,  $[\text{K}_3\text{Fe}(\text{CN})_6] = 2.0 \times 10^{-2} M$ , [thiol hydrochloride] =  $2.0 \times 10^{-2} M$ ,  $I = 0.3 M$ ).

of hydrochloric acid. The ionic strength was maintained constant in the usual manner. An inverse linear relationship between the rate and  $[\text{H}^+]$  was found to exist as shown in Figure 4.

Table IV<sup>a</sup>

$[\text{K}_3\text{Fe}(\text{CN})_6] \times 10^3 M$	Pseudo-first-order rate constant, $k_1 \times 10^2 \text{ min}^{-1}$
20.0	2.34
15.0	2.45
10.0	2.64
8.0	2.95

<sup>a</sup>  $[\text{HS}(\text{CH}_2)_2\text{N}(\text{CH}_3)_2 \cdot \text{HCl}] = 2.0 \times 10^{-3} M$ ,  $[\text{HCl}] = 2.0 M$ ,  $I = 2.4 M$ , temperature  $35^\circ$ .

The rate of reaction remained uninfluenced by ionic strength, though some specific ion effect appeared likely. The values of second-order rate coefficients were found to be  $2.17 \pm 0.07$  for NaCl and  $1.61 \pm 0.20$  for KCl at reactant concentrations  $2.0 \times 10^{-2} M$ ,  $[\text{HCl}] = 5.0 \times 10^{-2} M$  at  $35^\circ$  while the ionic strength was varied from 0.2 to 0.6  $M$ . Likewise addition of the disulfide and ferrocyanide produced no effect which shows that the reaction products are not involved in any reversible step of the likely reaction scheme. The latter observation is unlike that in 2-mercaptoethylamine hydrochloride where an autocatalysis due to ferrocyanide (*loc. cit.*) was observed.

Runs were also made in the presence of potassium cyanide. The addition showed no effect up to a concentration of  $10.0 \times 10^{-3} M$  beyond which an increase in the rate was observed as shown in Table V. The effect of dielectric constant ( $D$ ) variation was also investigated. Twice distilled ethanol was used for the purpose. A plot of  $\log k_2$  against  $1/D$  gave a straight line (Figure 5).

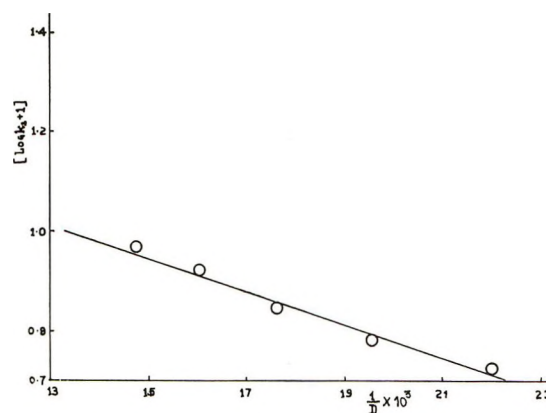


Figure 5. Dependence of the rate on dielectric constant (temperature  $35^\circ$ ,  $[\text{K}_3\text{Fe}(\text{CN})_6] = 2.0 \times 10^{-2} M$ , [thiol hydrochloride] =  $2.0 \times 10^{-2} M$ ,  $[\text{HCl}] = 5.0 \times 10^{-2} M$ ,  $I = 0.3 M$ ).

Table V<sup>a</sup>

$[\text{KCN}] \times 10^3 M$	Second-order rate constant, $k_2, M^{-1} \text{ min}^{-1}$	$[\text{KCN}] \times 10^3 M$	Second-order rate constant, $k_2, M^{-1} \text{ min}^{-1}$
0.0	2.19	10.0	2.03
4.0	2.04	20.0	2.52
7.0	2.04	30.0	3.14

<sup>a</sup>  $[\text{K}_3\text{Fe}(\text{CN})_6] = 2.0 \times 10^{-2} M$ ,  $[\text{HS}(\text{CH}_2)_2\text{N}(\text{CH}_3)_2 \cdot \text{HCl}] = 2.0 \times 10^{-2} M$ ,  $[\text{HCl}] = 5.0 \times 10^{-2} M$ ,  $I = 0.3 M$ , temperature  $35^\circ$ .

Runs were also made at different temperatures ranging between  $30$  and  $50^\circ$  and at intervals of  $5^\circ$ . Obedience to the Arrhenius equation was observed both in aqueous and water-ethanol media. Various thermodynamic parameters determined with the aid of usual expressions are recorded in Table VI.

Table VI

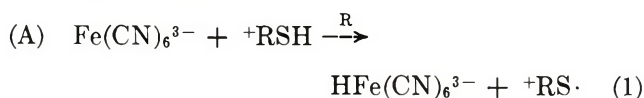
$D$	$\Delta H^\ddagger$ , kcal mol <sup>-1</sup>	$\Delta S^\ddagger$ , eu	$\Delta G^\ddagger$ , kcal mol <sup>-1</sup>
73.1	$23.9 \pm 0.5$	$11.2 \pm 1.1$	$20.6 \pm 0.6$
62.4	$21.1 \pm 0.5$	$8.5 \pm 1.1$	$20.8 \pm 0.6$

## Discussion

As remarked earlier, the reaction under consideration is different from the oxidation of a somewhat similar thiol hydrochloride, namely, 2-mercaptoethylamine hydrochloride, by the same oxidant, as this shows no autocatalytic effect due to ferrocyanide. It is, therefore, natural to assume that the mechanisms in the two cases are not identical. However, it can be assumed that the present thiol hydrochloride will also exist mostly in the ionized form in aqueous medium with its cationic part as  $\text{HS}-(\text{CH}_2)_2\text{N}(\text{CH}_3)_2\text{H}^+$ , *i.e.*,  $^+\text{RSH}$ ,



and not  $-\text{S}(\text{CH}_2)_2\text{N}(\text{CH}_3)_2\text{H}^+$ , *i.e.*,  $+\text{RS}^-$ , due to the strongly acidic medium employed in the present study which precluded the ionization of the weak  $-\text{SH}$  group. Since disulfide is the sole final product of oxidation, undoubtedly the sulfhydryl group ( $-\text{SH}$ ) provides the site of attack. For the sake of convenience, the above species is referred later as  $+\text{RSH}$  (where  $+\text{R}$  represents the remaining part of the cation). A simple reaction scheme of type A may explain the simple second-order kinetics but, admittedly, would fail to account for some observations such as the effect of initial concentration of ferricyanide, cyanide ion effect, etc.

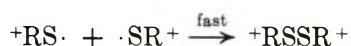
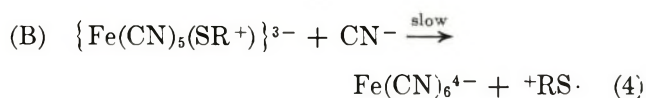


which gives

$$-d[\text{Fe}(\text{CN})_6^{3-}]/dt = k[\text{Fe}(\text{CN})_6^{3-}][\text{RSH}] \quad (3)$$

where  $k$  is the experimentally determined second-order rate constant.

In order to explain the decrease in rate observed on increasing the initial concentration of ferricyanide it may be assumed that this behavior may be due to formation of a relatively less reactive 1:1 complexes  $\{\text{Fe}(\text{CN})_5\text{SR}^+\}^{3-}$  (reduction in the effective concentration of ferricyanide due to formation of this complex). The complex of the type shown will have transient existence. It would combine with the cyanide ion to give rise to the products. The rate of this reaction would be very slow as it is governed by two factors: first very low concentration of this complex and second slow electron transfer from sulfur to iron. It has been shown that an electron-withdrawing group adjacent to the sulfur atom ( $\text{R}^+$  in the present case) decreases the rate of oxidation.<sup>11</sup>



This reaction mechanism is similar to one described by Kolthoff<sup>4</sup> and Stewart.<sup>12</sup> Such a step, if existent, would be able to explain the observed acceleration in rate at a large concentration of potassium cyanide. The formation of a complex of the type assumed above also finds some support from the observed values of  $\Delta S^\ddagger$  which are found to be moderately large and positive. The value of  $\Delta S^\ddagger$  equal to  $+11.2 \pm 1.1$  can be possibly interpreted as a consequence of greater internal freedom in the transition state compared with the relatively inflexible reactants. This is due to solvent participation, electrostatic interactions, molecular structure, and the nature of the reaction. Simple electron transfer reactions for the formation of free

radicals and subsequent dimerization of free radicals to give rise to product generally exhibit moderately large negative values of entropy of activation.<sup>13,14</sup> A reaction involving the electron transfer for the formation of free radicals *via* intermediate complex formation will include terms both for electron transfer and for the lengthening of the bond between the metal and the ligand for the calculation of activation parameters.<sup>15</sup> The system involving stronger metal-sulfur bond may give an overall positive value of  $\Delta S^\ddagger$ . This suggests that both the reaction mechanisms A and B are equally responsible for the observations. However entropy criterion has to be exercised with caution and preferably in conjugation with other factors.

In the reaction under consideration an inverse linear relationship between the rate and  $[\text{H}^+]$  has been observed, whereas by and large, this relationship has been found to be complex<sup>16</sup> in such oxidations. In Scheme A such a relationship can be explained if the dissociation step of the sulfhydryl group in the thiol hydrochloride molecule is also included. This, however, appears unlikely in the acidic medium under consideration. In fact, it is difficult to state with any amount of certainty the extent of involvement of proton *vis-a-vis* ferricyanide and ferrocyanide ion, and a simple relationship is probably more of an accidental nature.

Ferricyanic acid is a strong acid, but ferrocyanic acid is strong only for the first two protons. According to Nekrasov and Zotov,<sup>17</sup> below pH 4 only a negligible fraction of iron(II) is present as  $\text{Fe}(\text{CN})_6^{4-}$  and mainly  $\text{HFe}(\text{CN})_6^{3-}$  or  $\text{H}_2\text{Fe}(\text{CN})_6^{2-}$  will exist.

The plot of  $\ln k$  against the reciprocal of the dielectric constant is a straight line with a negative slope. This is in agreement with Brønsted-Christiansen-Scatchard equation and indicates the presence of similarly charged reactants.<sup>18</sup> This indicates that the rate of decomposition of the complex (eq 4) is due to the reaction between anionic complex and cyanide anion. Variation of the thermodynamic parameters, like energy of activation with dielectric constant, is in agreement with the equation relating dielectric constant and activation energy.<sup>18</sup>

The participation of free radicals in the reaction is demonstrated by the initiation of polymerization of vinyl cyanide by such a system. Kolthoff and Mee-

(11) D. A. House, *Chem. Rev.*, **62**, 185 (1962).

(12) R. Stewart, "Oxidation Mechanism," W. A. Benjamin, New York, N. Y., 1961, p 85-86.

(13) Y. D. Gomwalk and A. McAuley, *J. Chem. Soc. A*, **3**, 2948 (1968).

(14) C. Walling, "Free Radicals in Solution," Wiley, New York, N. Y., 1957, p 38.

(15) J. Hill and A. McAuley, *J. Chem. Soc. A*, **3**, 2405 (1968).

(16) M. Kharasch, "Organic Sulfur Compounds," Vol. I, Pergamon Press, London, 1961, p 99.

(17) B. A. Nekrasov and G. V. Zotov, *Zh. Prikl. Khim. (Leningrad)*, **14**, 264 (1941).

(18) E. S. Amis, "Kinetics of Chemical Change in Solution," Macmillan, New York, N. Y., 1949, p 180.

han<sup>19</sup> have stated that polymerization of olefins occur during ferricyanide-thiol reactions. Similarly Turney<sup>20</sup> has also shown that radicals are produced during oxidation of mercaptans.

*Acknowledgment.* One of us (R. K. C.) is grateful to the Council of Scientific and Industrial Research, New

Delhi, for the award of a fellowship. Thanks are due to Evans Chemetics Inc. for the gift sample of 2-dimethylaminoethanethiol hydrochloride.

(19) I. M. Kolthoff and E. J. Meehan, *J. Polym. Sci.*, **11**, 71 (1953).

(20) T. A. Turney, "Oxidation Mechanism," Butterworths, London, 1965.

## Kinetics of Oxygen Reduction on Graphite|Cobalt-Iron Oxide Electrodes with Coupled Heterogeneous Chemical Decomposition of H<sub>2</sub>O<sub>2</sub>

by J. R. Goldstein and A. C. C. Tseung\*

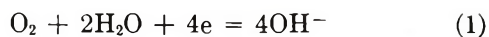
*Department of Chemistry, The City University, London, E.C.1, England (Received March 20, 1972)*

*Publication costs assisted by The American Chemical Society*

The oxygen reduction reaction can be treated as a catalytic regenerative process; in alkaline solution, oxygen is initially reduced to give hydrogen peroxide,  $O_2 + H_2O + 2e = HO_2^- + OH^-$ , which is then catalytically decomposed,  $2HO_2^- = O_2 + 2OH^-$ , yielding oxygen for recycling. In the present analysis of this system, expressions have been derived predicting a higher open circuit voltage and exchange current density for an oxygen electrode incorporating the regeneration step, over that with no regeneration; both increases are mathematically related to the rate constant for hydrogen peroxide decomposition in the regeneration step. These effects have been studied using graphite|cobalt-iron oxide electrodes as model systems for oxygen reduction by catalytic regeneration. On graphite, the  $O_2$ - $HO_2^-$  reaction proceeds reversibly, while cobalt-iron oxides are good hydrogen peroxide catalysts possessing negligible oxygen reduction activity. Porous hydrophobic graphite|oxide electrodes were characterized in terms of diffusion-free pseudoexchange current density parameters. Incorporation of cobalt-iron oxides of known hydrogen peroxide decomposition activity into graphite electrodes produced increases in both open circuit voltage and pseudoexchange current density ( $i_0^*$ ) in agreement with theoretical predictions. Furthermore, the theory also indicated that only limited performance improvements are possible with oxygen electrodes operating solely according to the regenerative route. The maximum possible enhancement for graphite|cobalt-iron oxide electrodes is a doubling of  $i_0^*$ , and the improvement in performance from an oxide of given hydrogen peroxide decomposition activity falls off with increasing  $i_0^*$ .

### 1. Introduction

The electrochemical reduction of oxygen in alkaline solution should ideally proceed according to the equation



at a standard reduction potential of 0.401 V.<sup>1</sup> On most materials, however, reaction 1 is slow and irreversible at room temperature. This causes performance limitations in power sources such as fuel cells and metal-air batteries, in which oxygen reduction is the cathodic reaction.<sup>2</sup>

A considerable research effort has been directed at developing an oxygen electrode at which reaction 1 might occur more efficiently, thereby yielding acceptably high-current densities at potentials close to the

theoretical. A suitable electrode must be structure optimized, so that the three-phase reaction 1 can proceed with minimal mass-transport restrictions; the electrode must also incorporate electrocatalysts to increase the rate of the electrochemical reaction. Hitherto, the most promising results have been obtained for electrocatalysts such as platinum black and silver, but even with these costly materials, the electrode potential at practical current densities falls well below the reversible value for reaction 1.

One approach to the oxygen electrode problem is based on the fact that, for many electrocatalysts, oxygen reduction occurs initially by a two-electron pro-

(1) W. H. Latimer, "Oxidation Potentials," 2nd ed, Prentice-Hall, Englewood Cliffs, N. J., 1952.

(2) W. Vielstich, "Fuel Cells," Wiley, 1970, pp 119, 327, 468.



cess.<sup>3</sup> This produces hydrogen peroxide (H<sub>2</sub>O<sub>2</sub>), present in alkaline solution as the perhydroxyl ion, HO<sub>2</sub><sup>-</sup>.



Reaction 2 occurs rapidly, but its standard reduction potential,  $-0.076 \text{ V}$ ,<sup>1</sup> lies very much below the corresponding potential for reaction 1. However, the HO<sub>2</sub><sup>-</sup> may be chemically decomposed at the electrocatalyst surface

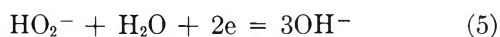


If the product oxygen is completely recycled *via* reaction 2, then the overall stoichiometry of (2) and (3) approaches that of the four-electron process (1). Moreover, the Nernst equation for reaction 2 at 25°, requires

$$E = -0.076 + 0.0296 \log \frac{[\text{O}_2][\text{H}_2\text{O}]}{[\text{HO}_2^-][\text{OH}^-]} \quad (4)$$

where  $E$  is the electrode potential *vs.* a standard hydrogen electrode (SHE), and the square brackets represent activities. Assuming unit activities for O<sub>2</sub>, H<sub>2</sub>O, and OH<sup>-</sup>, then if [HO<sub>2</sub><sup>-</sup>] < 1,  $E$  rises above  $-0.076 \text{ V vs. SHE}$ . A low value for [HO<sub>2</sub><sup>-</sup>] would result if the electrocatalyst were markedly active in H<sub>2</sub>O<sub>2</sub> decomposition. In particular, if HO<sub>2</sub><sup>-</sup> could be maintained at concentrations as low as 10<sup>-16</sup>  $M$ ,  $E$  would then be equal to 0.4 V, the standard reduction potential for reaction 1.<sup>4</sup>

Hence, by setting up an oxygen electrode system based primarily on fast reactions 2 and 3, it might in principle be possible to approximate to the overall stoichiometry and high potential of (1), without its intrinsic sluggishness.<sup>5</sup> An important restriction would be the exclusion of any further chemical or electrochemical reactions. Thus, on platinum black and silver electrocatalysts, both reactions 2 and 3 proceed rapidly, yet reversible potentials are not attained. On such materials, however, many other reactions can simultaneously occur during oxygen reduction. These may either be largely irreversible, as in the case of further electrochemical reduction of HO<sub>2</sub><sup>-</sup><sup>6</sup>



or involve species with low standard reduction potentials,<sup>7</sup> for instance, the Pt(OH)<sub>2</sub>|Pt couple (0.15 V).<sup>1</sup> In both cases the working electrode potential will be below 0.401 V *vs.* SHE.

From the viewpoint of electrode kinetics, an oxygen electrode operating solely according to reactions 2 and 3 could be described in terms of an electrochemical reaction with a coupled heterogeneous regenerative (catalytic) reaction.<sup>8</sup> In the literature, however, there is little quantitative work available on such an oxygen electrode system. Conventional oxygen electrodes are empirically optimized, with a complex and ill-defined electrocatalyst composition on which many reac-

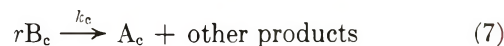
tions can occur simultaneously. Although the importance of an electrocatalyst also being a good H<sub>2</sub>O<sub>2</sub> decomposition catalyst is frequently stressed,<sup>9,10</sup> there has been no quantitative approach to correlate the catalyst activity toward H<sub>2</sub>O<sub>2</sub> with the overall electrode performance.

In the present paper, the properties of a composite electrocatalyst system, operating essentially *via* reactions 2 and 3 alone, are described. A mathematical correlation is developed relating electrochemical performance to H<sub>2</sub>O<sub>2</sub> decomposition activity, and is verified experimentally. The correlation is finally used to evaluate the H<sub>2</sub>O<sub>2</sub> decomposition route as a means of achieving reversible oxygen electrode behavior.

## 2. Theory

McIntyre,<sup>8</sup> following earlier work by Delahay and co-workers<sup>11,12</sup> and Koutecky,<sup>13</sup> has considered the kinetics of an electrochemical reaction such as (2), coupled with a regenerative heterogeneous catalytic process such as (3), occurring on or close to an electrode surface. An extended form of his analysis, applicable to the case in which reaction 3 is first order with respect to HO<sub>2</sub><sup>-</sup>, is presented here.

In schematic form the overall electrode process may be represented as follows.



Thus, equation 6 represents the electrochemical slow step, in which the oxidant A is electroreduced to the reductant B with the passage of  $n$  electrons. Subscripts E refer to an electrochemical process, with  $k_E$  and  $k_{-E}$  the formal heterogeneous electrochemical rate constants for the forward and backward reactions, respectively. Equation 7 represents the coupled heterogeneous chemical regeneration reaction, in which the product B from the electrochemical reaction is decomposed, regenerating A, which is recycled in eq 6. In

(3) W. G. Berl, *Trans. Electrochem. Soc.*, **83**, 253 (1943).

(4) A. B. Hart and G. J. Womack, "Fuel Cells: Theory and Application," Chapman and Hall, London, 1967, p 73.

(5) J. R. Goldstein and A. C. C. Tseung, *Nature (London)*, **222**, 869 (1969).

(6) K. J. Vetter, "Electrochemical Kinetics," Academic Press, New York, N. Y., 1967, p 639.

(7) T. P. Hoar, *Proc. Roy. Soc., Ser. A*, **142**, 628 (1933).

(8) J. D. E. McIntyre, *J. Phys. Chem.*, **71**, 1196 (1967).

(9) H. M. Cota, J. Katan, M. Chin, and F. J. Schoenweis, *Nature (London)*, **203**, 1281 (1964).

(10) K. V. Kordesch in "Handbook of Fuel Cell Technology," C. Berger, Ed., Prentice-Hall, Englewood Cliffs, N. J., 1958, p 361.

(11) P. Delahay and G. L. Stiehl, *J. Amer. Chem. Soc.*, **74**, 3500 (1952).

(12) P. Delahay, C. C. Mattax, and T. B. Berzins, *ibid.*, **76**, 5319 (1954).

(13) J. Koutecky, *Collect. Czech. Chem. Commun.*, **18**, 311, 611 (1953).

eq 7, subscripts c are used to refer to a chemical step, and the heterogeneous rate constant  $k_c$  is defined according to the formation rate of  $A_c$

$$\frac{d[A_c]}{dt} = \frac{-1}{r} \frac{d[B_c]}{dt} = k_c[B_c]^s \quad (8)$$

where  $t$  is time,  $r$  is the stoichiometric ratio, moles of  $B_c$ /moles of  $A_c$ , of reaction 7, and  $s$  is the reaction order with respect to  $B_c$ . The flux of A,  $J_A$ , is the net gain of A from both electrochemical and chemical sources

$$J_A = \frac{d[A]}{dt} = -k_E[A] + k_{-E}[B] + k_c[B]^s \quad (9)$$

[A] and [B] are the solution concentrations of A and B, respectively, close to the electrode surface; the E and c subscripts in these terms need no longer be specified. Similarly,  $J_B$ , the flux of B, is the net gain of B.

$$J_B = \frac{d[B]}{dt} = k_E[A] - k_{-E}[B] - rk_c[B]^s \quad (10)$$

Equations 9 and 10 give, on summing the fluxes of A and B, the equation

$$J_A + J_B + (r - 1)k_c[B]^s = 0 \quad (11)$$

The cathodic current density  $i$  is given by

$$i/nF = k_E[A] - k_{-E}[B] \quad (12)$$

Using eq 9 and 10 to eliminate A from eq 12

$$i/nF = -J_A + k_c[B]^s = J_B + rk_c[B]^s \quad (13)$$

Equations 11 and 13 constitute the general boundary conditions for this system.

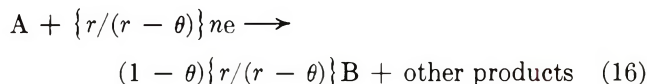
McIntyre defined  $\theta$ , the regeneration rate fraction, as that fraction of the electrolysis product  $B_E$  which is consumed in the regenerative cycle after each occurrence of the electrolysis reaction.  $\theta$  is accordingly a measure of the regenerative efficiency of the coupled catalytic process, and may be defined by the fraction

$$\theta = \frac{\text{flux of B from chemical decomposition}}{\text{flux of B produced electrochemically}} \quad (14)$$

Whereupon

$$\theta = \frac{rk_c[B]^s}{i/nF} \quad (15)$$

and  $(1 - \theta)$  is the fraction of the electrolysis product which escapes into the solution by mass transport, thereby avoiding the regeneration process. By considering each mole of A supplied to the electrode surface by either mass transport or regeneration, and summing all products over the course of the reaction as a geometric series, McIntyre showed the overall electrode reaction to be



Hence, for a diffusional flux  $J_A$ , the cathodic current density is given by

$$i/nF = -\left\{ \frac{r}{r - \theta} \right\} J_A \quad (17)$$

From eq 9

$$i/nF = \left\{ \frac{r}{r - \theta} \right\} \{ k_E[A] - k_{-E}[B] - k_c[B]^s \} \quad (18)$$

or, neglecting the back electrochemical reaction

$$i/nF = \left\{ \frac{r}{r - \theta} \right\} \{ k_E[A] - k_c[B]^s \} \quad (19)$$

In McIntyre's analysis, predictions were made as to the limiting current densities associated with infinitely fast regeneration rates. The present analysis, however, considers the contribution of the regeneration step to the overall electrode current density  $i$ . An electrode system represented by eq 6 and 7, should, in the absence of diffusion control, obey a Tafel relationship

$$\eta_a = \frac{2.3RT}{\alpha nF} \{ \log i - \log j_0 \} \quad (20)$$

with  $\eta_a$ , the activation polarization;  $R$ , the gas constant;  $T$ , the absolute temperature;  $\alpha$ , the transfer coefficient;  $F$ , the Faraday; and  $j_0$ , the exchange current density for the system. In the case of a negligibly slow regeneration reaction ( $k_c = 0$  in eq 7),  $j_0$  falls to a lower value  $i_0$ , the exchange current density for the slow electron transfer reaction 6 alone.

Now, substituting eq 20 into eq 15 with the condition  $\eta_a = 0$ , gives

$$\theta = \frac{rk_c[B]^s}{j_0/nF} \quad (21)$$

But, from the stoichiometry of 16

$$[B] = [A](1 - \theta) \left\{ \frac{r}{r - \theta} \right\} \quad (22)$$

$$\theta = \frac{rk_c[A]^s(1 - \theta)^s \left\{ \frac{r}{r - \theta} \right\}^s}{j_0/nF} \quad (23)$$

or, on rearranging

$$k_c = \frac{\{ \theta/(1 - \theta)^s \} \{ (r - \theta)/r \}^s j_0}{rnF[A]^s} \quad (24)$$

Expression 24 gives  $k_c$ , the rate constant for the regeneration step, in terms of  $j_0$ , the exchange current density for the system,  $\theta$ , the regeneration rate fraction, and [A], the oxidant concentration in the electrode vicinity. This expression may be greatly simplified, particularly in its application to experimental results, by employing an independent expression for  $\theta$ . Thus, the increase in exchange current density from  $i_0$ , when there is no regeneration, to  $j_0$ , when the regeneration step is effective, must arise entirely from the product A recycled *via* eq 7. Inspection of eq 14 and 15, defining  $\theta$ , should yield an expression for  $\theta$  in terms of  $i_0$



and  $j_0$ . The difference term ( $j_0 - i_0$ ) represents the flux of A arising from the regeneration step; since each mole of A arises from  $r$  moles of B, the numerator in eq 14 may be written  $r(j_0 - i_0)$ . Proportionally, the denominator is given by  $j_0$ , whereupon

$$\theta = \frac{r\{j_0 - i_0\}}{j_0} \quad (25)$$

The two expressions, (24) and (25), relate mathematically the three parameters  $i_0$ ,  $j_0$ , and  $k_c$  governing the electrode kinetics of the regenerative system. Furthermore, the boundary conditions for the regenerative effect are satisfied. For example, with no or ineffective catalysis,  $i_0 = j_0$  and  $\theta = 0$  (eq 25). Substitution of  $\theta = 0$  in eq 24 gives  $k_c = 0$  as required. The case of ideal catalysis,  $\theta = 1$ , may be demonstrated for a regeneration reaction which is first order with respect to B ( $s = 1$ ), and in which the stoichiometric ratio,  $r$  in eq 8, is 2. Substitution of  $\theta = 1$  and  $r = 2$  in eq 25 gives  $j_0 = 2i_0$ , while, with the added condition  $s = 1$ , eq 24 gives  $k_c = \infty$ . Both these results are conditions for ideal catalysis.<sup>8</sup>

### 3. Oxygen Electrode System

In order to subject the theory of Section 2 to experimental analysis, it was necessary to set up a model oxygen electrode system functioning essentially *via* reactions 2 and 3 above. A two-component electrocatalyst system, with reaction 2 alone occurring on one component and reaction 3 alone occurring on the other, seemed most convenient for study, since kinetic effects corresponding to either process could easily be separated, and the relative contribution of the regeneration step to the overall process directly controlled.

Fundamental oxygen electrode investigations are normally carried out with the test material in solid form, since this permits a simple kinetic treatment. The dual electrocatalyst system, however, implied an intimate mixture of components, thereby closely resembling a supported catalyst system. In addition a basic prerequisite for the model system, that reactions 2 and 3 be rapid (Section 1), could only be achieved using high surface area materials. The solid electrode approach, involving low surface area test specimens of homogeneous composition, was thus precluded from these studies, and a method of evaluating high surface electrocatalysts as fine powder mixtures was adopted.

Electrocatalyst powders may be fabricated as porous electrodes and their performance assessed from current-voltage curves under controlled conditions. These curves may be expressed as  $\eta$ - $i$  plots, where  $\eta$  is the polarization from the observed electrode open circuit voltage (ocv), and  $i$  is the electrode current density (current per unit geometric surface area). Generally,  $\eta$  is subdivided into activation ( $\eta_a$ ), mass transfer ( $\eta_m$ ), and ohmic ( $\eta_R$ ) components. While  $\eta_m$  and  $\eta_R$  are

largely structure and electrolyte dependent, the  $\eta_a$  component is a measure of the intrinsic activity of the electrocatalyst for accelerating the electrode reaction. Consequently, to assess this intrinsic activity, mass transfer and ohmic effects must be corrected for in an electrode polarization curve. This ideally leaves a purely activation-controlled  $\eta_a$ - $i$  plot, from which fundamental electrochemical parameters (such as the exchange current density for the reaction) may be obtained.

With solid planar electrodes, it is relatively easy to establish pure activation dependence; a notable example is the use of such electrodes in a rotating disk configuration, where the mass transfer effects are accurately known. With porous systems, however, the electrode processes are regulated by a number of variables, such as the electrochemically active surface area, the electrode pore structure, and the aggregate size of the electrocatalyst. The equations governing the diffusion of electroactive species in such systems are most complex, and the elimination, particularly of  $\eta_m$ , from the  $\eta$ - $i$  plots is at best empirical.

However, Tantram and Tseung,<sup>14</sup> in a study of oxygen reduction on high surface area graphite in alkaline solution, showed that diffusion effects in porous electrodes could be greatly minimized by close control of the electrode structure. In their investigation, porous hydrophobic graphite electrodes were shown to exhibit reproducible performance characteristics, and mass transfer effects only became significant at very high current densities. The graphite employed was reversible with respect to the HO<sub>2</sub><sup>-</sup> formation reaction,<sup>3</sup> yet was rather inert as an H<sub>2</sub>O<sub>2</sub> decomposition catalyst.<sup>15</sup> Neither was any participation from other electrochemical processes, such as reaction 5, envisaged. By incorporating H<sub>2</sub>O<sub>2</sub> catalysts in such graphite-based porous electrodes, it might be possible to obtain relatively diffusion-free oxygen reduction characteristics.

The selection of a suitable H<sub>2</sub>O<sub>2</sub> decomposition catalyst posed a considerable problem, since the most active catalysts for reaction 3, silver, platinum black, and palladium,<sup>15</sup> also catalyze other electrochemical processes such as reaction 2, thereby excluding them from this study (Section 1). A catalyst for reaction 3 of similar high activity, but otherwise electrochemically inert, was required. However, Cota, Katan, Chin, and Schoenweis<sup>9</sup> had reported that cobalt-iron spinel oxides were among the most active H<sub>2</sub>O<sub>2</sub> decomposition catalysts in alkaline solution. These oxides bear the general formula Co<sub>x</sub>Fe<sub>3-x</sub>O<sub>4</sub>, where  $x$ , the composition variable, can take values between 0 and 3. By using the hydroxide coprecipitation technique of Saito, Sugihara, and Sato,<sup>16</sup> cobalt-iron oxides could

(14) A. D. S. Tantram and A. C. C. Tseung, *Nature (London)*, **221**, 167 (1969).

(15) W. C. Schumb, C. N. Satterfield, and R. N. Wentworth, "Hydrogen Peroxide," Reinhold, New York, N. Y., 1955.



be prepared in high surface area form over the entire composition range of the system. The resulting powders, particularly within the composition range  $1 < x < 3$ , exhibited activities for reaction 3 comparable to platinum black, when tested under controlled conditions.<sup>17</sup>

The cobalt-iron oxides exhibited properties well suited to the present study. The activity toward  $H_2O_2$  was high and readily adjusted by variation in  $x$ . There was no apparent catalyst degradation even on prolonged exposure to  $H_2O_2$ , and the oxides were highly insoluble in alkaline solution by virtue of their preparation technique. Corrosion resistance at oxygen reduction potentials might well prove favorable. The oxides, in addition, possessed poor electrical conductivity, several orders of magnitude below that of the graphite, as shown by powder compression measurements under controlled conditions. The likelihood of the oxides supporting any electrochemical processes comparable to reaction 2 on the graphite was thus small. Finally, the microstructural characteristics of the oxide powders were suitably different from those of the graphite, the graphite powder being considerably finer than the oxides. The electrode structure from graphite-oxide mechanical mixtures would hence be overwhelmingly determined by the fine graphite, at least in the presence of small additions of oxide.

#### 4. Experimental Section

**4.1. Preparation and Pretreatment of the Oxygen Electrode Components.** A series of cobalt-iron oxides was prepared by the hydroxide coprecipitation technique, with  $x$  values of 0, 0.6, 1.0, 1.5, 2.0, 2.4, and 3.0 so as to cover the complete composition range of the spinel system. The preparation and characterization of these oxides are described elsewhere.<sup>17</sup> The graphite employed<sup>14</sup> was B. P. Acheson graphite, Type L.4. This was pretreated ( $800^\circ$ , 3 hr,  $O_2$ -free  $N_2$ ) so as to remove surface impurities, and stored in a  $CO_2$ -free atmosphere.

**4.2 Activity of Materials Toward  $H_2O_2$ .** The activity of the graphite and oxides for  $H_2O_2$  decomposition was evaluated gasometrically using the technique of Cota, *et al.*<sup>9,17</sup> Since the kinetic results on decomposition activity were to be applied to the electrochemical situation of oxygen reduction, the catalysts were pretreated ( $300^\circ$ , 1 hr,  $O_2$ -free  $N_2$ ) so as to approximate to the electrode fabrication conditions, and in addition, stabilizer-free  $H_2O_2$  was employed for the kinetic runs.

Catalyst samples (50 mg) were injected into a reaction mixture consisting of 5 *N* KOH (50 ml, made up from Analar grade pellets, Hopkin and Williams, Ltd.) and 5 ml of 1.0 ( $\pm 0.01$ ) *M*  $H_2O_2$  (Laporte stabilizer-free 85%  $H_2O_2$  diluted appropriately, and standardized before runs).<sup>17</sup> The reaction was conducted at  $25 \pm 0.1^\circ$  and atmospheric pressure, and the rate of oxygen evolution monitored over the complete reaction period.

The rate constant and reaction order were evaluated, and the dependence of the rate constant on the catalyst mass investigated. All runs were corrected for self-decomposition of  $H_2O_2$ .

**4.3 Electrode Fabrication.** The electrode fabrication technique was a modification of that employed by Tantram and Tseung.<sup>14</sup> Weighed quantities of electrocatalyst powder(s) and aqueous Teflon dispersion (Fluon GP1, I.C.I., Ltd.) were slurried in methanol and ultrasonically dispersed for a 5-min period. The dispersion was transferred by painting onto a nickel gauze and after drying at  $70^\circ$  the electrodes were cured ( $300^\circ$ , 1 hr,  $O_2$ -free  $N_2$ ). Electrocatalyst loadings were calculated from the gauze weight before and after fabrication, assuming that the components of the electrocatalyst-Teflon dispersion were transferred to the gauze in the same ratio as in the original mix.

Electrodes were fabricated from graphite alone, for each oxide, and for graphite-oxide mixtures corresponding to each oxide composition, thereby covering the complete composition range of the spinel system. The electrodes were fabricated so as to exhibit the following compositions: graphite electrodes, 10 ( $\pm 0.3$ )  $mg\ cm^{-2}$  graphite, graphite to Teflon ratio = 3:1; oxide electrodes, 10 ( $\pm 0.3$ )  $mg\ cm^{-2}$  oxide, oxide to Teflon ratio = 3:1; graphite|oxide electrodes, 10 ( $\pm 0.3$ )  $mg\ cm^{-2}$  graphite, 10 ( $\pm 0.3$ )  $mg\ cm^{-2}$  oxide, graphite to Teflon ratio = 3:1.

The loadings and Teflon content were chosen to provide optimum hydrophobic properties and performance reproducibility, and to minimize in-series electrode variations. Electrodes were also fabricated from graphite-inert filler oxide mixtures, in order to establish that the electrode performance was overwhelmingly graphite dependent. The oxide filler was ferric oxide prepared by hydroxide coprecipitation; this was as inert toward  $H_2O_2$  as the graphite, yet possessed similar microstructural characteristics to the oxides.

**4.4 Electrode Testing.** The electrodes, mounted at the end of nickel foil, and of known geometrical surface area (*ca.* 1  $cm^2$ ) were tested for oxygen reduction in 5 *N* KOH at  $25^\circ$  using the floating cell technique.<sup>14</sup> In the cell, a gold foil counter electrode was used, and the reference electrode was a dynamic hydrogen electrode (DHE),<sup>18</sup> calibrated against a standard mercury|mercuric oxide electrode. The electrolyte was freshly prepared from KOH pellets and deionized, distilled water, and the working electrode compartment was swept with oxygen gas at about 1 atm, supplied from a cylinder without further purification.

Electrode ocv's *vs.* DHE under oxygen were measured using a high-impedance (20 Mohm) digital voltmeter

(16) T. Sato, M. Sugihara, and M. Saito, *Rev. Elec. Commun. Lab.*, **11**, 26 (1963).

(17) J. R. Goldstein and A. C. C. Tseung, submitted for publication.

(18) J. Giner, *J. Electrochem. Soc.*, **111**, 376 (1964).



**Table I:** Observed and Calculated Open Circuit Potentials for Graphite and Graphite|Cobalt-Iron Oxide Oxygen Reduction Electrodes<sup>a</sup>

Electrode system	Value of $x$ in $\text{Co}_x\text{Fe}_{3-x}\text{O}_4$ for added oxide	Observed ocv vs. SHE (25°), mV ( $\pm 5$ )	First-order rate constant for $\text{H}_2\text{O}_2$ decomposition per unit mass catalyst $k_{f,m}$ at 25° ( $\pm 5\%$ ), $\text{sec}^{-1} \text{g}^{-1}$	Calculated steady-state $\text{HO}_2^-$ concn, mol	Calculated ocv vs. SHE (25°), mV ( $\pm 10$ )
Graphite alone		100	$6.7 \times 10^{-5}$	$3.7 \times 10^{-7}$	80
Graphite cobalt-iron oxides	0	160	0.0087	$3.1 \times 10^{-9}$	140
	0.6	165	0.0308	$8.1 \times 10^{-10}$	160
	1.0	175	0.117	$2.1 \times 10^{-10}$	180
	1.5	190	0.0927	$2.7 \times 10^{-10}$	175
	2.0	190	0.175	$1.4 \times 10^{-10}$	180
	2.4	200	0.243	$1.0 \times 10^{-10}$	185
	3.0	170	0.0899	$2.8 \times 10^{-10}$	175

<sup>a</sup> For data on electrode fabrication and test conditions see Section 4.

**Table II:** Tabulation of  $i_0^*$ ,  $j_0^*$ ,  $\theta$ ,  $k_{f,m}$ , and Tafel Slope Parameters (25°)

Electrode system	Value of $x$ in $\text{Co}_x\text{Fe}_{3-x}\text{O}_4$ for added oxide	Tafel slope ( $\pm 5\%$ ), mV per current density decade	Mean pseudo-exchange current density $j_0^*$ ( $\pm 5\%$ ), $\text{mA cm}^{-2}$	Regeneration rate fraction $\theta = \frac{2(j_0^* - i_0^*)}{j_0^*}$	Electrochemical parameter $\left\{ \frac{\theta}{(1-\theta)} \right\} \left\{ \frac{2-\theta}{\theta} \right\} j_0^*$ , $\text{mA cm}^{-2}$	First-order rate constant for $\text{H}_2\text{O}_2$ decomposition per unit mass catalyst $k_{f,m}$ ( $\pm 5\%$ ), $\text{sec}^{-1} \text{g}^{-1}$
Graphite alone		220	1.08 ( $i_0^*$ )	0	0	Negligible
Graphite cobalt-iron oxides	0	220	as $i_0^*$	0	0	0.0087
	0.6	225	1.42	0.479	0.995	0.0308
	1.0	240	1.70	0.729	2.91	0.117
	1.5	225	1.60	0.650	1.25	0.0927
	2.0	240	1.87	0.845	5.89	0.175
	2.4	240	1.84	0.826	5.13	0.243
	3.0	235	1.72	0.744	1.83	0.0899

(DVM, Solartron LM 1620). Steady-state polarization curves for oxygen reduction were then obtained using a potentiostat (Wenking 68TS10), and the curves were corrected for ohmic drop using the interrupter technique.<sup>19</sup> Corrosion scans were also carried out, with the working electrode and electrolyte equilibrated with O<sub>2</sub>-free N<sub>2</sub>.

## 5. Results

**5.1. Activity of Catalysts Toward H<sub>2</sub>O<sub>2</sub>.** The H<sub>2</sub>O<sub>2</sub> decomposition reaction on Acheson graphite, and on cobalt-iron oxides prepared by hydroxide coprecipitation, was found to be first order with respect to H<sub>2</sub>O<sub>2</sub> in alkaline solution.<sup>17</sup> First-order kinetics were also reported by Parravano for H<sub>2</sub>O<sub>2</sub> decomposition by sintered cobalt-iron oxides,<sup>20</sup> and were explained in terms of a rate-determining surface reaction (topochemical control) involving reactant-substrate orientations. The first-order kinetics plot for H<sub>2</sub>O<sub>2</sub> decomposition by CoFe<sub>2</sub>O<sub>4</sub> at 25° is shown in Figure 1, while the rate constant per unit mass catalyst  $k_{f,m}$  at 25° for each of the materials tested is included in Tables I and

II.  $k_{f,m}$  was found to be directly proportional to the catalyst mass, at least in the range 5–100 mg, and, as expected for first-order kinetics, was independent of the initial H<sub>2</sub>O<sub>2</sub> concentration. The  $k_{f,m}$  values were subject to experimental error amounting to  $\pm 5\%$ .

**5.2. Electrode Testing.** **5.2.1. Oxygen Reduction on Graphite and Graphite|Cobalt-Iron Oxide Electrodes.** After preliminary cathodic-anodic cycling to remove surface-adsorbed impurities and to achieve optimum wetting characteristics for the hydrophobic structures, reproducible performance levels were achieved for oxygen reduction on graphite and graphite|cobalt-iron oxide electrodes. Electrodes were least susceptible to irreversible effects, such as flooding by the electrolyte or hysteresis on cathodic-anodic cycling, when subjected to low-current density drains ( $< 200 \text{ mA cm}^{-2}$ ). The dynamic hydrogen reference electrode (DHE), in 5 N KOH at 25°, maintained a steady potential of

(19) K. R. Williams, "An Introduction to Fuel Cells," Elsevier, Amsterdam, 1966, pp 39 and 57.

(20) G. Parravano, *Proc. Int. Congr. Catal.*, 4th, 1968, 1, 157 (1970).

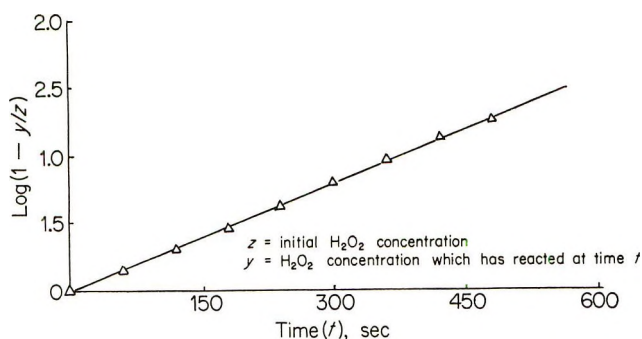


Figure 1. First-order kinetics plot for  $\text{H}_2\text{O}_2$  decomposition by  $\text{CoFe}_2\text{O}_4$  at  $25^\circ$ .

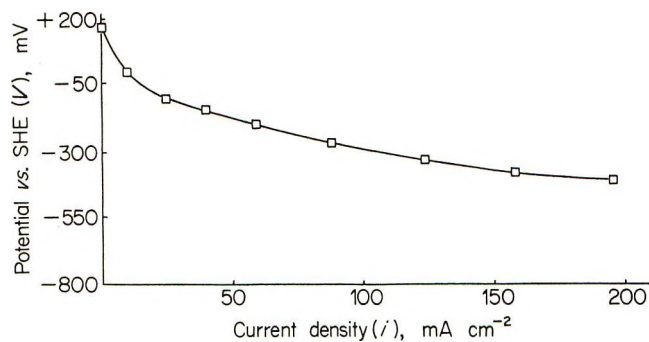


Figure 2. Resistance-free  $V-i$  plot for oxygen reduction at a graphite| $\text{CoFe}_2\text{O}_4$  electrode in  $5\text{ N KOH}$  at  $25^\circ$ .

$-960 (\pm 2)$  mV with respect to a standard  $\text{Hg}|\text{HgO}$  electrode. Since the  $\text{Hg}|\text{HgO}$  electrode is itself  $98\text{ mV}$  positive to SHE at  $25^\circ$ , all potential measurements *vs.* DHE were decreased by  $862\text{ mV}$  for expression *vs.* SHE.

The observed oxygen reduction ocv's for the various systems, expressed on the SHE scale, are included in Table I. Each ocv listed is derived from the mean of several separate ocv determinations *vs.* DHE; the general irreproducibility at this purification level yielded an error margin of  $\pm 5\text{ mV}$ . Polarization characteristics were initially expressed as resistance-corrected  $V-i$  curves, with  $V$ , the electrode potential *vs.* SHE, and  $i$  the electrode current density (normalized to unit geometric surface area). Figure 2 shows the resistance-free  $V-i$  curve for a graphite| $\text{CoFe}_2\text{O}_4$  electrode at low-current density drain, while Figure 3, also resistance-free, indicates the high-current density capabilities of a standard graphite electrode. These results are typical of the graphite and graphite|cobalt-iron oxide systems investigated; Figure 3 is especially significant in that there is no evidence of a diffusion-limited plateau for current densities approaching  $2\text{ A cm}^{-2}$ .

The oxygen reduction characteristics of the electrodes were quantitatively assessed from resistance-free  $\eta-\log i$  plots, with  $\eta$  the overpotential from the observed ocv. These plots were linear for graphite and graphite|oxide electrodes in the range  $\eta > 50\text{ mV}$  and  $5 < i < 100\text{ mA cm}^{-2}$ . A representative plot for the graphite| $\text{CoFe}_2\text{O}_4$

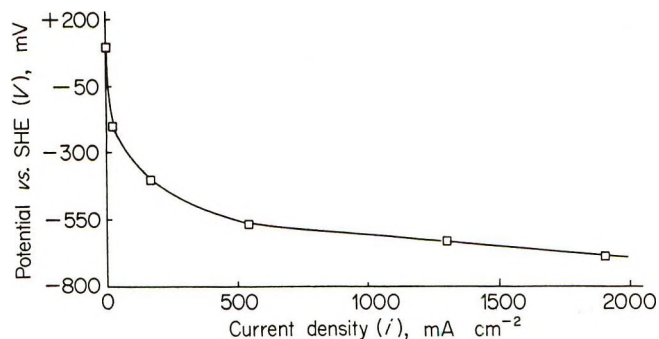


Figure 3. Resistance-free  $V-i$  plot for oxygen reduction at an Acheson graphite electrode in  $5\text{ N KOH}$  at  $25^\circ$ .

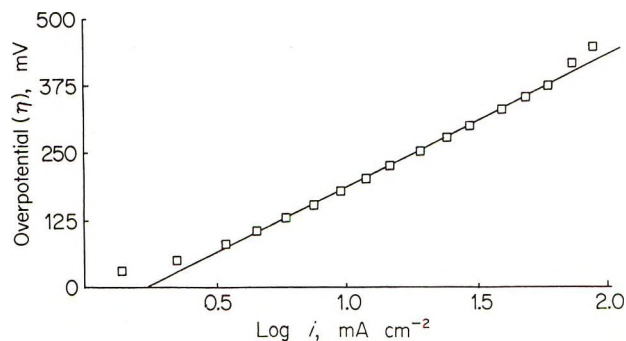


Figure 4. Tafel plot for graphite| $\text{CoFe}_2\text{O}_4$  electrode for oxygen reduction in  $5\text{ N KOH}$  at  $25^\circ$ .

system is shown in Figure 4. The electrodes thus obeyed a Tafel relationship (Section 2), but the slope and exchange current density (pseudoexchange current density) derived from  $\eta-\log i$  plots would be characteristic of porous electrodes. In Table II the Tafel slopes and pseudoexchange current densities for the various electrode systems are presented, the experimental error for each parameter being  $\pm 5\%$ . Each value in the table is the mean of several determinations with successively fabricated electrodes.

**5.2.2. Oxygen Reduction on Cobalt-Iron Oxide Electrodes.** Cobalt-iron oxides tested alone exhibited considerable inertness for oxygen reduction. Thus at  $-400\text{ mV vs. SHE}$ , the cathode current densities observed for the various compositions were in the range  $0.1\text{--}0.5\text{ mA cm}^{-2}$ , nearly three orders of magnitude below the corresponding values in the presence of graphite. The oxide ocv's under oxygen were unstable and irreproducible,  $150 (\pm 25)\text{ mV vs. SHE}$ , in sharp contrast to the behavior of the oxides in the presence of graphite, when ocv fluctuations decreased to  $\pm 5\text{ mV}$ .

**5.2.3. Corrosion Scans.** The cobalt-iron oxide electrodes, when scanned under  $\text{O}_2$ -free  $\text{N}_2$ , gave negligible corrosion currents, and similar ocv's to those under oxygen. Graphite electrodes, after preliminary cathodic-anodic cycling to remove adsorbed oxygen, performed similarly.



## 6. Analysis of Results

The experimental work had established the suitability of the graphite|cobalt-iron oxide system for the present study in terms of (i) relative inertness of graphite for reaction 3; (ii) high activity of cobalt-iron oxides for reaction 3; (iii) corrosion resistance and electrochemical inertness of cobalt-iron oxides alone during oxygen reduction; and (iv) fabrication of electrodes with controlled quantities of graphite and oxides, showing reproducible performance for oxygen reduction. It was now possible to show that reaction 2 proceeds reversibly on the graphite, and to assess quantitatively the response of the graphite-oxide system to the regeneration step, in terms of the theory of Section 2.

*6.1. Observed Ocvs.* In Table I, the ocvs *vs.* SHE developed by the various systems are listed, together with the first-order rate constant per unit mass catalyst,  $k_{f,m}$ , for H<sub>2</sub>O<sub>2</sub> decomposition at 25°. There is a broad correlation between the ocv value for a given electrode and the activity for H<sub>2</sub>O<sub>2</sub> decomposition of the oxide it contains. Thus the higher the value of  $k_{f,m}$  the higher is the ocv *vs.* SHE. This suggested that the ocvs were governed according to eq 2 by the steady-state concentration of HO<sub>2</sub><sup>-</sup> maintained by the catalyst at the electrode surface.

Accordingly, the HO<sub>2</sub><sup>-</sup> steady-state concentration maintained by each catalyst was calculated, and used to predict the ocv from the Nernst eq 4. Consider the case of a typical graphite|CoFe<sub>2</sub>O<sub>4</sub> electrode. The DVM has an impedance of 20 Mohm in the 2-V range used for measurements *vs.* DHE. During an ocv measurement of about 1 V, the electrode current density is hence  $5 \times 10^{-8}$  A cm<sup>-2</sup>, corresponding to an HO<sub>2</sub><sup>-</sup> production rate (eq 2) of  $2.5 \times 10^{-13}$  mol HO<sub>2</sub><sup>-</sup> sec<sup>-1</sup> cm<sup>-2</sup> for the two-electron process. At the steady state the rate of formation of HO<sub>2</sub><sup>-</sup> from this source may be equated with the rate of destruction of HO<sub>2</sub><sup>-</sup> from the CoFe<sub>2</sub>O<sub>4</sub> contained in the electrode (the decomposition from the graphite is negligible compared with this). For 10 mg of CoFe<sub>2</sub>O<sub>4</sub> in the electrode, and with  $k_{f,m} = 0.117$  sec<sup>-1</sup> g<sup>-1</sup>, the steady-state HO<sub>2</sub><sup>-</sup> concentration is  $2.15 \times 10^{-10}$  M. In the Nernst eq 4, [O<sub>2</sub>] = 1, and [OH<sup>-</sup>] = 8 for 5 N KOH at 25°. <sup>21</sup> Moreover

$$H_2O = \frac{\text{partial vapor pressure } 5 \text{ N KOH at } 25^\circ}{\text{partial vapor pressure water at } 25^\circ}$$

which is 0.58.<sup>22</sup> Using [HO<sub>2</sub><sup>-</sup>] =  $2.15 \times 10^{-10}$  M gives  $E = 180$  mV *vs.* SHE in eq 4. This is in reasonable agreement with the observed value of 175 mV *vs.* SHE.

Errors in predicted ocvs are likely to be large, due to uncertainty in the Nernst equation parameters, particularly [HO<sub>2</sub><sup>-</sup>]. Thus, a variation of  $\pm 10\%$  in [HO<sub>2</sub><sup>-</sup>] produces a shift of  $\pm 20$  mV in the ocv. The HO<sub>2</sub><sup>-</sup> value is largely dependant on  $k_{f,m}$ , itself subject

to experimental error of  $\pm 5\%$ . Moreover, there is some doubt concerning the application of the full  $k_{f,m}$  values to the electrochemical situation, due to Teflon screening of catalyst particles and escape of HO<sub>2</sub><sup>-</sup>. However, these factors should not affect the relative order of ocv values in similarly fabricated electrodes. Table II lists the predicted ocvs *vs.* SHE for the several electrode systems. There is fair agreement with observed ocvs within the stated error limits, providing confirmation of the reversibility of reaction 2 on Acheson graphite, and justifying the Nernst equation reasoning of Section 1.

The quantitative treatment implies that the observed ocv is a function of the DVM impedance, and the amount of H<sub>2</sub>O<sub>2</sub> decomposition catalyst present in the electrode. With a higher impedance value, slightly higher ocvs are to be expected; however, the contribution of impurity depolarizing processes might then become more significant. Similarly, the use of a greater mass of H<sub>2</sub>O<sub>2</sub> decomposition catalyst should yield lower [HO<sub>2</sub><sup>-</sup>] values, giving higher ocvs. In addition, for a typical graphite|oxide electrode, it is possible to calculate the necessary  $k_{f,m}$  value of the oxide component, such that the reversible potential for reaction 1 (0.4 V *vs.* SHE) might be achieved by depression of [HO<sub>2</sub><sup>-</sup>] in reaction 2.

Considering such an electrode, fabricated and tested as for the electrodes in Table II, a value for [HO<sub>2</sub><sup>-</sup>] of  $6 \times 10^{-18}$  M gives  $E = 0.4$  in eq 4; this would require  $k_{f,m} = 4 \times 10^6$  sec<sup>-1</sup> g<sup>-1</sup> for the oxide at 25°. However, the most active cobalt-iron oxide tested, Co<sub>2.4</sub>Fe<sub>0.6</sub>O<sub>4</sub>, has only  $k_{f,m} = 0.243$  sec<sup>-1</sup> g<sup>-1</sup>. Consequently, several orders of magnitude increase in catalyst activities are required to achieve ocvs close to the reversible potential for reaction 1, if the only reaction path is *via* eq 2 and 3.

*6.2 Electrode Performance Characteristics.* As discussed in Section 3, the elimination of ohmic and mass transfer effects from electrode polarization curves is an important step toward obtaining fundamental electrochemical parameters for an electrode system. However, a reliable estimation of mass transfer effects is often impossible for porous electrodes. The present studies with hydrophobic graphite-based systems were rather exceptional, in that no evidence of diffusion-limited plateaux was observed for current densities up to 2 A cm<sup>-2</sup> (Figure 3). Since mass transfer effects may be neglected provided  $i < 0.1i_L$ , where  $i_L$  is the limiting current density of an electrode system,<sup>19</sup> it could be assumed that the resistance free  $V-i$  curves were largely diffusion free, at least for current densities below 200 mA cm<sup>-2</sup>.

Throughout this range the electrode behavior was

(21) R. A. Robinson and H. A. Stokes, *Trans. Faraday Soc.*, **45**, 612 (1949).

(22) "International Critical Tables," Vol. 3, E. W. Washburn, Ed., McGraw-Hill, New York, N. Y., 1928, p 373.

most reproducible and ohmic corrections small and most reliable. Moreover, the corresponding  $\eta$ - $\log i$  plots had their region of best linearity within this range. Consequently, Tafel slope and pseudoexchange current density parameters (Table II) derived from such plots would be representative of pure activation control in the porous systems.

Austin<sup>23</sup> has considered the equations governing Tafel behavior in porous electrodes. In the absence of ohmic effects, for a system in which concentration gradients outside the electrode may be neglected, a Tafel relationship may be developed for a simple pore, thin-film model. The model assumes that linear diffusion occurs along pores whose diameter is negligible compared with their length, and that the electrochemical reaction is confined to a thin film. At low current densities, the  $\eta_a$ - $i$  relationship is given by

$$\eta_a = \frac{4.6RT}{\alpha nF} \{\log i - \log j_0^*\} \quad (26)$$

This differs from the usual Tafel form (eq 20), in that a pseudoexchange current density term  $j_0^*$ , characteristic of the porous electrode system, replaces the usual exchange current density term  $j_0$ , characteristic of solid electrodes. In addition, the Tafel slope (coefficient of the  $\log i$  term) for porous systems has twice its normal value. The doubled Tafel slope is caused by depletion of reactant in the electrode interior, by ohmic effects within the electrode pores, or by a combination of both effects.<sup>23</sup>

The observed Tafel slopes in Table II fall in the range 220–240 mV per current density decade. If the doubled Tafel slope relationship (26) holds for the Teflon-bonded electrodes, the true Tafel slope on Acheson graphite is 110–120 mV. This is in good agreement with the Tafel slope result (110 mV) found by Yeager, Krouse, and Rao<sup>24</sup> for oxygen reduction on smooth graphite in alkaline solution. In eq 26 a Tafel slope of 240 mV results by setting  $\alpha = 0.5$  (its usual value) and  $n = 1$ . This implies that in all graphite-based electrodes, there is one rate-determining step involving a single electron transfer,<sup>23,25</sup> irrespective of  $\text{H}_2\text{O}_2$  decomposition catalyst additions.

Table II also lists the  $k_{f,m}$  values for  $\text{H}_2\text{O}_2$  decomposition by the electrode components, together with the pseudoexchange current densities for the various systems. A key feature of the results is that the lowest pseudoexchange current densities are shown for electrodes containing graphite alone. As cobalt-iron oxides with successively greater activity for  $\text{H}_2\text{O}_2$  decomposition are incorporated into the graphite electrodes, the pseudoexchange current density steadily increases.

It is now possible to employ the theoretical analysis of Section 2. The porous electrodes obey the modified Tafel eq 26, so real exchange current densities in Section 2 may be replaced by the corresponding pseudoexchange current densities. The pseudoexchange cur-

rent density on graphite alone is hence referred to as  $i_0^*$ ; in the presence of appreciable regeneration this increases to a higher value,  $j_0^*$ . For cobalt-iron oxides involved in  $\text{H}_2\text{O}_2$  decomposition, the reaction order with respect to  $\text{HO}_2^-$  (s) is unity (Section 4.2), while the stoichiometric ratio ( $r$ ) for the regeneration step is 2 (eq 3). In addition, the rate constant for  $\text{H}_2\text{O}_2$  decomposition,  $k_e$ , can be replaced by measured first-order  $k_{f,m}$  values, and  $n$ , defined by eq 6, is unity for eq 2.<sup>23,25</sup> Equation 24 may be rewritten as

$$k_{f,m} = \frac{\{\theta/(1-\theta)\}\{(2-\theta)/2\}j_0^*}{2F[A]} \quad (27)$$

where  $\theta$ , the regeneration rate fraction, from eq 25 is given by

$$\theta = \frac{2\{j_0^* - i_0^*\}}{j_0^*} \quad (28)$$

In Table II the  $i_0^*$  and  $j_0^*$  values are used to calculate values for  $\theta$  corresponding to each electrode system. The  $\theta$  values are employed to evaluate the electrochemical parameter

$$\frac{\theta}{1-\theta} \left\{ \frac{2-\theta}{2} \right\} j_0^* \quad (29)$$

for each system, and in Figure 5, the calculated values for expression (29) are plotted vs.  $k_{f,m}$ , thereby testing the validity of eq 27.

Figure 5 is subject to an error margin dependent on the individual variation in the  $k_{f,m}$ ,  $i_0^*$ , and  $j_0^*$  parameters. Although kinetic measurements determined  $k_{f,m}$  to within  $\pm 5\%$ , a maximum accuracy of  $\pm 10\%$

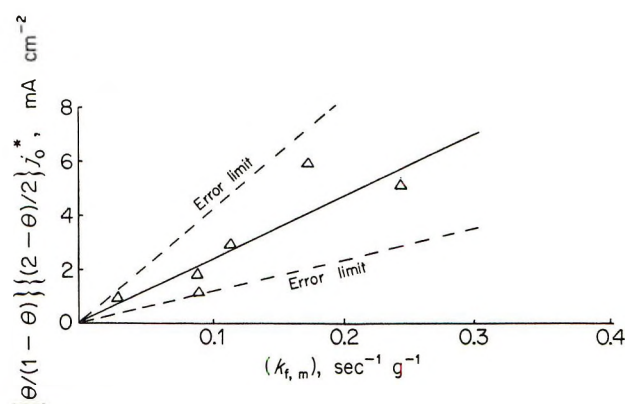


Figure 5. Plot of the electrochemical parameter  $\{\theta/(1-\theta)\}\{(2-\theta)/2\}j_0^*$  for oxygen reduction at Acheson graphite|cobalt-iron oxide electrodes vs.  $k_{f,m}$ , the first-order rate constant per unit mass catalyst for  $\text{H}_2\text{O}_2$  decomposition by the oxide, at 25°.

(23) L. G. Austin, ref 10, pp 63, 184.

(24) E. Yeager, P. Krouse, and K. V. Rao, *Electrochim. Acta*, **9**, 1057 (1964).

(25) R. Cornelissen and L. Gierst, *J. Electroanal. Chem.*, **3**, 219 (1962).



was adopted for the electrochemical situation. This would allow for Teflon screening of catalyst surfaces in the various electrode compositions, and compensate for departures from the required catalyst loading levels. A  $\pm 5\%$  error in pseudoexchange current densities arises mainly from extrapolation errors on  $\eta \log i$  plots, from variations in properties of successively fabricated electrodes (particularly the ocv value), and from inaccuracy in measuring the electrode geometric surface area. The error margin of  $\pm 5\%$  is remarkably small for exchange current measurements, and partly reflects the high reversibility of reaction 2 on the high surface area graphite. Thus, observed pseudoexchange current densities are several orders of magnitude above real exchange current densities measured for oxygen reduction at solid electrodes.

Figure 5 is accordingly constructed allowing  $\pm 10\%$  variation in  $k_{f,m}$  and  $\pm 5\%$  in  $i_0^*$  and  $j_0^*$ . The error limits resulting are large because  $\theta$  is proportional to a small difference between two large quantities, and expression 29 contains a  $\theta^2$  term. However, the experimental points fall within the stated error limits, providing strong evidence for the validity of eq 27. The graphite|cobalt-iron oxide system thus obeys the predictions of Section 2. Support is also given to the viewpoint that the Tafel regions for the graphite-based electrodes are effectively under pure activation control, and that the electrochemical parameters in Table II are uniformly affected by the Teflon loading and electrode structure.

The slope in Figure 5, by analogy to eq 27, is related to  $[A]$ , the oxygen concentration at the electrode surface, and possesses the value  $1.2 \times 10^{-5} \text{ g mol cm}^{-2}$ . This quantity cannot be given an absolute physical significance, since it is dependent on other unknown factors, such as the fraction of catalyst mass actually involved in H<sub>2</sub>O<sub>2</sub> decomposition or the electrochemically active specific surface area of the graphite. The slope is presumably a characteristic of the Acheson graphite-based electrodes.

The present analysis allows predictions to be made as to the feasibility of achieving high efficiency oxygen electrode performance by the use of the regenerative path. The oxide additions to Acheson graphite produced changes in  $i_0^*$  ranging from a negligible increase (composition  $x = 0$ , the least active H<sub>2</sub>O<sub>2</sub> catalyst in the series) to a 70% increase (composition  $x = 2.4$ , the most active catalyst). Thus, the practical limit for the system (100% increase in  $i_0^*$ , from Section 2) has almost been achieved with present catalysts, and high efficiency has not been achieved for oxygen reduction.

If a different carbon base were employed for the electrodes, possessing a much higher  $i_0^*$  value than Acheson graphite, the intrinsic performance level in the absence of H<sub>2</sub>O<sub>2</sub> decomposition catalysts would be greatly improved. In principle it would then be possible to improve this new  $i_0^*$  still further by incorpo-

rating cobalt-iron oxides. Consider a carbon base with  $i_0^* = 10 \text{ mA cm}^{-2}$  showing an order of magnitude increase over  $i_0^*$  for Acheson graphite. If it is further assumed that the electrochemically active specific surface area of the carbon is similar to that of Acheson graphite, such that the  $[A]$  term remains unchanged at its value of  $1.2 \times 10^{-5} \text{ g mol cm}^{-2}$ , then the addition of 10 mg of oxide of composition  $x = 2.4$  ( $k_{f,m} = 0.243 \text{ sec}^{-1} \text{ g}^{-1}$ ) would now only produce an increase in  $i_0^*$  of 20% (from eq 27 and 28 by successive approximation). This is considerably below the 70% increase obtained for the Acheson graphite system with  $i_0^* = 1 \text{ mA cm}^{-2}$ , yet this oxide possesses the highest activity for H<sub>2</sub>O<sub>2</sub> decomposition.

The analysis implies that high-performance oxygen electrodes cannot be achieved using the regenerative route alone. Thus, with a graphite or carbon base possessing an acceptably high-pseudo-exchange current density  $i_0^*$  for oxygen reduction, any added catalyst would require a rate constant for H<sub>2</sub>O<sub>2</sub> decomposition appreciably greater than can be obtained with presently available materials, in order to significantly increase  $i_0^*$ .

## 7. Conclusions

The Acheson graphite|cobalt-iron oxide system has been shown to be a suitable model for the investigation of oxygen reduction solely by the HO<sub>2</sub><sup>-</sup> formation reaction 2, and the regeneration reaction 3. Teflon-bonded hydrophobic electrodes, fabricated from graphite-oxide mechanical mixtures, may be characterized reproducibly in terms of a pseudoexchange current density parameter obtained from Tafel plots. These plots are essentially activation controlled and possess a doubled Tafel slope from that observed with solid graphite electrodes. The oxide additions to the graphite electrodes produce an increase in both ocv and the pseudoexchange current density ( $i_0^*$ ) of the graphite electrode alone; these effects may be correlated with  $k_{f,m}$ , the rate constant per unit mass for H<sub>2</sub>O<sub>2</sub> decomposition by the oxide.

However, only limited improvements in oxygen electrode efficiency are possible with presently available catalysts using the regenerative route alone. The maximum possible effect in graphite|oxide electrodes is a doubling of  $i_0^*$ , and the effect for an oxide of given  $k_{f,m}$  falls off with increasing  $i_0^*$ . Conventional carbon or graphite-based oxygen electrodes, catalyzed with platinum or silver, and exhibiting much higher performance levels than the uncatalyzed systems, presumably rely on nonregenerative oxygen reduction routes for their high efficiency.

Further work is required to test the applicability of the mathematical analysis to other systems. Of particular interest are carbon-based regenerative systems in which the carbon has an appreciably different  $i_0^*$  from Acheson graphite. It is possible to use a similar

approach to investigate oxygen reduction in acid solution. A suitable system for study is the carbon-iron phthalocyanine system, which closely resembles the graphite-cobalt-iron oxide system in its mode of oxygen reduction.<sup>26</sup>

*Acknowledgment.* This work was supported by the Science Research Council on Grant No. B/SR 4334.

(26) H. Jahnke and M. Schönberg, *Proc. J. Int. Etudes Piles Combust., Brussels, 1969*, 60 (1969).

## Dissolution of Copper in Weakly Acidic Solutions

by A. J. Read

*Chemistry Division, Department of Scientific and Industrial Research, Gracefield, New Zealand (Received February 7, 1972)*

The dissolution of copper in weakly acidic perchlorate solutions was measured over a range of pH (4.0–5.5),  $P_{O_2}$  (0.05–1.0 bar), and cupric ion concentrations ( $1 \times 10^{-4}$ – $16 \times 10^{-4}$  M) at constant ionic strength (0.05 M). The method used allowed several measurements to be made under pseudo-zero-order conditions on a single piece of copper *in situ*. The order dependence on  $(H^+)$  and  $P_{O_2}$  was found to be 1.0 and 0.25, respectively. Increasing the temperature from 16.9 to 45.0° increased the rate by a factor of 6.2. Addition of  $Cl^-$  and  $Br^-$  ions enhanced the dissolution rate while added  $F^-$ ,  $NO_3^-$ ,  $SO_4^{2-}$ , and  $Zn^{2+}$  had a negligible effect. These results are discussed in terms of a solid-state mechanism involving the formation, transport, and destruction of cation vacancies and positive holes.

### Introduction

Numerous publications have appeared dealing with the corrosion of copper under a wide variety of conditions.<sup>1–16</sup> However, few authors studied dissolution under conditions allied to natural water systems.<sup>6, 16, 17</sup> The reaction mechanism was not fully elucidated under acidic conditions<sup>1, 17</sup> and is even less well understood in solutions containing low concentrations of complexing ions. The present work seeks to improve the understanding of the dissolution reaction in weakly acidic media (pH range 4.0–5.5).

The oxide films, formed initially on copper single crystals in water, were shown to consist of cuprous oxide<sup>18–20</sup> even though thermodynamic considerations indicated cupric oxide was the stable phase.<sup>21</sup> At room temperature, these films grew more rapidly in water than in air.<sup>18</sup> It seemed likely, therefore, that cuprous oxide would be an intermediate in the dissolution of copper in the present study.

It is often difficult to control all the variables for a heterogeneous reaction, to a suitable level of precision. In the present work a technique was used which allowed the precise control of reaction variables (*e.g.*,  $P_{O_2}$ , pH,  $(Cu^{2+})$ , and ionic strength) and minimized the problem of reproducing characteristic metal surfaces. Further, as relative rate measurements are sufficient for a mechanistic study, no great importance was attached to the variation of rate with surface preparation.

### Experimental Section

The samples of copper used in the present investigation were of Analar copper foil for which an emission spectrographic analysis is given.

- (1) B. C. Y. Lu and W. F. Graydon, *Can. J. Chem.*, **32**, 153 (1954).
- (2) J. R. Weeks and G. R. Hill, *J. Electrochem. Soc.*, **103**, 203 (1956).
- (3) R. P. Russel and A. White, *Ind. Eng. Chem.*, **19**, 116 (1927).
- (4) G. H. Damon and R. C. Cross, *ibid.*, **28**, 231 (1936).
- (5) I. Cornet, E. A. Barrington, and G. U. Behring, *J. Electrochem. Soc.*, **108**, 947 (1961).
- (6) A. I. Kinevski, *J. Appl. Chem. USSR*, **28**, 1088 (1955).
- (7) W. D. Robertson, V. F. Nole, W. H. Davenport, and F. P. Talboom, Jr., *J. Electrochem. Soc.*, **105**, 569 (1958).
- (8) Z. Zembura and W. Glodzinska, *Rocz. Chem.*, **42**, 1525 (1968).
- (9) R. Glauner, *Z. Phys. Chem., Abt. A*, **142**, 67 (1929).
- (10) T. Hurlen, *Acta Chem. Scand.*, **15**, 1239 (1961).
- (11) G. R. Hill, *J. Electrochem. Soc.*, **100**, 345 (1953).
- (12) J. Halpern, *ibid.*, **100**, 421 (1953).
- (13) Z. Szabo, *J. Amer. Chem. Soc.*, **71**, 1511 (1949).
- (14) W. Katz, *Werkst. Korros. (Weinheim)*, **1**, 393 (1950).
- (15) T. Hurlen, *Acta Chem. Scand.*, **15**, 1246 (1961).
- (16) D. J. G. Ives and A. E. Rawson, *J. Electrochem. Soc.*, **109**, 452 (1962).
- (17) Z. Zembura and W. Glodzinska, *Rocz. Chem.*, **40**, 911 (1966).
- (18) J. Kruger, *J. Electrochem. Soc.*, **106**, 847 (1959).
- (19) J. Kruger, *ibid.*, **108**, 503 (1961).
- (20) A. Goswami, *Indian J. Pure Appl. Phys.*, **7**, 211 (1969).
- (21) M. Pourbaix, "Atlas of Electrochemical Equilibria," Pergamon Press, London, 1966.



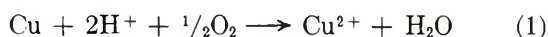
Copper	99.99+%		
Lead	<1 ppm	Cadmium	<5 ppm
Bismuth	<5 ppm	Beryllium	<1 ppm
Antimony	<5 ppm	Tellurium	<10 ppm
Arsenic	<20 ppm	Cobalt	<2 ppm
Manganese	<0.2 ppm	Iron	10 ppm
Tin	<1 ppm	Nickel	1 ppm
Zinc	<5 ppm	Silver	5 ppm
		Aluminum	5 ppm

Strips of copper foil (usually 15 cm × 3 cm) were corroded by a magnetically stirred solution in a cylindrical water-jacketed vessel. One such vessel was fitted with a Teflon lid with holes for introducing the ancillary apparatus and for sample withdrawal. The copper samples were shaped to fit the vessel, and the metal in close contact with the glass was coated with paraffin wax. Another vessel (and lid) was of all glass construction with the copper supported on a glass stand to allow free access of the solution to both surfaces of the sample.

The water bath temperature was maintained to ±0.02° at 25° and to about ±0.04° at 45°. The thermometers were calibrated against NPL certified mercury-in-glass standards. The stirred thermostated cell solution attained a temperature within 0.01° of that of the water bath in about 20 min at 25°. The O<sub>2</sub>-N<sub>2</sub> mixtures, used to vary P<sub>O<sub>2</sub></sub>, were analyzed to about ±1% of their oxygen content with a commercial oxygen meter by comparison with laboratory standards of similar composition.

Because of the difficulty of reproducing surface conditions several measurements were made using the same surface. A series of rate measurements was often made and finally the rate was remeasured under the initial (or similar) conditions without handling the surface. A comparison of the rates measured under the initial (or similar) conditions indicated whether the nature of the substrate changed during the measurement series.

For a reaction proceeding according to the overall equation



the dissolution may be followed by a number of methods. Here the rate of removal of H<sup>+</sup> was measured. Experimental conditions were chosen to keep P<sub>O<sub>2</sub></sub>, (Cu<sup>2+</sup>), and (H<sup>+</sup>) constant in any given run. The P<sub>O<sub>2</sub></sub> was maintained by bubbling O<sub>2</sub> or O<sub>2</sub>-N<sub>2</sub> mixtures through the solution. To maintain the other two variables invariant the solution containing cupric ions was titrated to constant pH with an acid solution of the same equivalent concentration as that of the cupric ions (see eq 1) using an automatic pH titrator (Radiometer TT1C). Rate measurements were therefore made under pseudo-zero-order conditions. In addition, the ionic strength was kept constant (usually 0.05 M) using sodium perchlorate.

The dissolution rate is defined by the equation

$$\frac{d(\text{Cu}^{2+})}{dt} = R = \frac{m}{2A} \frac{dv}{dt}$$

where *m* = the concentration of acid added, *A* = the area of copper exposed, and *dv/dt* = the rate of acid addition.

To investigate any extraneous effects of paraffin wax, the dissolution rate was measured (at controlled pH, (Cu<sup>2+</sup>), and P<sub>O<sub>2</sub></sub>) before and after coating half of each plane surface with paraffin wax. These results (Table I) show that the presence of paraffin wax was without significant effect.

Table I: Effect of Paraffin Wax on the Dissolution Rate<sup>a</sup>

$10^{10}R$ , mol min <sup>-1</sup> cm <sup>-2</sup>	Comment
1.22	No paraffin wax
1.18	Half total surface coated with wax

$$^a (\text{Cu}^{2+}) = 2.27 \times 10^{-4} M; \text{pH} = 5.5; \text{air.}$$

Immediately before a series of measurements the copper surface was cleaned in an organic solvent (*e.g.*, diethyl ether or ethanol) and then usually etched in 1:1 *N* hydrochloric acid solution. At the end of a run, the copper was washed in distilled water, dried with tissue, and stored. This sample was then used subsequently without removing the oxide layer (see Table II).

Table II: Series of Dissolution Rates with the Same Copper Sample<sup>a</sup>

$10^{11}R$ , mol min <sup>-1</sup> cm <sup>-2</sup>	Comment
8.85	Same copper sample used
8.56	for successive measure-
9.16	ments over a period of
8.68	days
9.24	

$$^a (\text{Cu}^{2+}) = 7.5 \times 10^{-6} M; \text{pH} = 5.5; \text{air.}$$

The linear response of the glass electrode was established using four standard buffers.<sup>22</sup> Stability checks before and after each run usually agreed to within 0.01 pH. The identification of pH values with pH(S)<sup>22</sup> should be reliable to about ±0.05 pH and the relative accuracy of the pH measurements would be much better than this (±0.02 pH).

(22) R. G. Bates, "Determination of pH," Wiley, New York, N. Y., 1964.

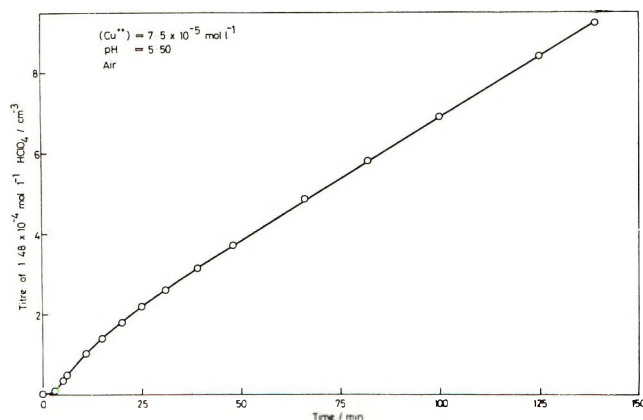


Figure 1. Rate of dissolution of copper.

A number of factors determined the time over which a particular run was followed in order to achieve a suitable level of precision. These included the pH, the concentration of titrating acid, the precision with which the volume of added acid was known, and errors due to instability of the glass electrode assembly. With the  $\text{HClO}_4$  solutions used, the correction for the proportion of the titer required to maintain the pH constant due to the volume increase was minor. (Generally less than 1% and never more than 10%.) It was shown that it was necessary to bubble and stir the solution for 20–30 min to remove the small amount of carbon dioxide introduced simultaneously with the copper sample. The initial portions of the titer–time plots were rejected for this reason, the linear portions being generally followed for about 1 hr (Figure 1). During the runs periodic checks by atomic absorption spectrophotometry (to an accuracy of about  $\pm 2\%$ ) showed that the cupric ion concentration remained constant.

The cupric perchlorate solution prepared from Analar cupric oxide and Analar perchloric acid was analyzed both gravimetrically<sup>23a</sup> and by atomic absorption spectrophotometry. The perchloric acid stock solution prepared from Analar material was standardized against Borax.<sup>23b</sup> Other chemicals used were of analytical reagent grade.

Experiments using hydrochloric acid solutions (0.01–0.0001  $M$ ) confirmed the equivalence of cupric ion formation (measured by atomic absorption) and acid consumption indicated by eq 1.

The marked acceleration of the dissolution reaction<sup>7,10,24</sup> by chloride ions prevented the use of either a “combination glass electrode” or an agar-saturated potassium chloride<sup>23c</sup> salt bridge. (If used under the present solution conditions ( $\text{Cl}^- \approx 10^{-3} M$ ) after about 60 min.) Therefore, a salt bridge of sodium perchlorate supported on agar was used. The effect of agar on the dissolution rate was investigated. Successive rates obtained under similar conditions with a single piece of copper are summarized in Table II while in Table III experiments showing the effect of deliberately

adding agar to the solution at two pH values are recorded. No effect was apparent. The results in Table II also indicate the reproducibility attained with this system.

Table III: Dissolution Rate in the Presence of Agar<sup>a</sup>

pH	$10^{10}R$ , $\text{mol min}^{-1}$ $\text{cm}^{-2}$	Comment
5.24	1.17	Agar junction only
5.24	1.16	Agar added
4.53	2.69	Agar junction only
4.53	2.63	Agar added

<sup>a</sup> ( $\text{Cu}^{2+}$ ) =  $2.27 \times 10^{-4} M$ ; air.

## Results

*Effect of Stirring.* The magnitude of the change in dissolution rate on altering the stirring speed may provide information on the nature of the reaction.<sup>1,25</sup> In this work most measurements were made with the highest stirring speed conducive to long-term stability of the system. When this stirring rate was doubled, the dissolution rate was increased by about 10%.

*Effect of Light.* In one experiment (pH = 5.5, ( $\text{Cu}^{2+}$ ) =  $7.5 \times 10^{-5} M$ ) the dissolution rate was measured both with normal lighting and with light excluded using blackened aluminum foil. No measurable change in rate was detected, and this effect was not investigated further.

*Effect of Cupric Ion Concentration.* The effect of cupric ion concentration was investigated at the pH values 4.52, 5.31, and 5.50. After determining the initial rate, successive rates were measured after additions of ( $\text{Cu}^{2+}$ ) ( $I = 0.05 M$  at correct pH). Figure 2 shows these results in terms of an equation of the type  $R = k(\text{Cu}^{2+})^n$ . The values of  $n$  show no trend with pH.

Some attempts were made to measure equilibrium cupric ion concentrations in the system. When the copper sample was allowed to corrode with the titrator disconnected, there was an initial increase in the pH which passed through a maximum (e.g., pH 5.87, ( $\text{Cu}^{2+}$ ) =  $4.3 \times 10^{-4} M$ ) and finally decreased. Simultaneous with this decrease, loosely adhering material was deposited on the “copper” surface. This pH oscillation would not be expected for reactions approaching “equilibrium” in homogeneous media. At the maximum pH the product ( $\text{Cu}^{2+}$ )( $\text{OH}^-$ )<sup>2</sup> exceeds that for cupric oxide<sup>21</sup> (but not for  $\text{Cu}(\text{OH})_2$ ) indicating

(23) A. I. Vogel, “Quantitative Inorganic Analysis,” 3rd ed, Longmans, Green and Co., London, 1961: (a) p 498; (b) p 238; (c) p 912.

(24) T. Hurlen, *Acta Chem. Scand.*, **15**, 1231 (1961).

(25) C. V. King, *Trans. N. Y. Acad. Sci.*, **10**, 262 (1948).



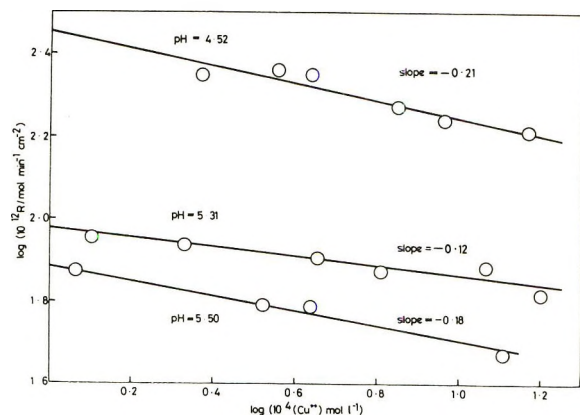
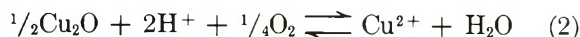


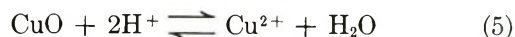
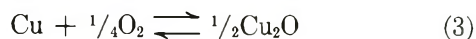
Figure 2. Effect of cupric ion concentration on the rate of dissolution of copper at different pH values.

the deposited material to be  $\text{CuO}$ . The "stationary state" conditions (pH 5.55,  $(\text{Cu}^{2+}) = 4.3 \times 10^{-3} M$ ) are consistent with this suggestion. This conclusion was further supported by some work of Kruger<sup>19</sup> who corroded copper samples in distilled water and noticed that the cuprous oxide finally became covered with cupric oxide. Hence we are concerned with the system  $\text{Cu-Cu}_2\text{O-CuO-Cu}^{2+}$  which is in an oxygenated environment and, therefore, not in true equilibrium.

The standard free energy change for the reaction<sup>26</sup>



is  $-23.7 \text{ kcal mol}^{-1}$  giving an equilibrium constant of  $10^{17.4} M^{-1} \text{ bar}^{-1/4}$  at  $25^\circ$ . Calculations utilizing the experimental pH and  $(\text{Cu}^{2+})$  indicated  $P_{\text{O}_2}$  values for the solution phase as low as  $10^{-40} \text{ bar}$  which was clearly not so. The significance of this low  $P_{\text{O}_2}$  value is seen by considering the equilibria between the phases



The sum of (4) and (5), *i.e.*, (2) describes the equilibrium between cuprous oxide and an aqueous solution containing cupric ions where  $P_{\text{O}_2}$  is that existing at the  $\text{Cu}_2\text{O-CuO}$  interface. The  $P_{\text{O}_2}$  value for the  $\text{Cu}_2\text{O-CuO}$  stability boundary is about  $10^{-37.6} \text{ bar}$ .<sup>27</sup> Values calculated from stationary state experiments deviate from this probably as a result of the nonstoichiometric nature of the cuprous oxide, an incomplete coverage of the  $\text{Cu}_2\text{O}$  by a  $\text{CuO}$  film, and the system not being at equilibrium.

At the stationary state there would be a slow growth of the cuprous and cupric oxide layers with a corresponding utilization of oxygen. Once the cuprous oxide was covered with a layer of cupric oxide no change in pH would be expected.

In view of the interest in the corrosion of copper in natural waters it is useful to consider the possible role

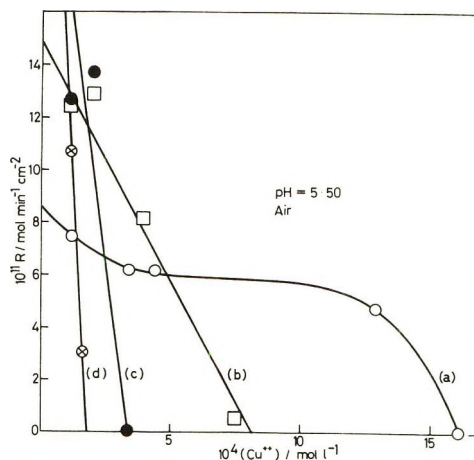


Figure 3. Effect of cupric ion concentration on the rate of dissolution of copper at pH 5.50 with different amounts of cupric oxide deposited on the surface (see text).

of cupric oxide in this process. Copper is usually passivated when coated with an impervious layer of corrosion product.<sup>28</sup> There are instances when this does not happen<sup>21</sup> and the presence of cupric oxide may be relevant. Some related data are now given. After determining the curve in Figure 2 for pH 5.50 (curve a in Figure 3) the sample was allowed to corrode with the pH titrator disconnected, until a stationary state was attained. As indicated above, material is deposited on the sample surface. Curves b, c, and d of Figure 3 show the rate dependence on  $(\text{Cu}^{2+})$  after successive increments of material had been deposited from solution. The increase in rate at zero  $(\text{Cu}^{2+})$  for curves a-d might be the result of increased surface area, the deposited material being rather loosely adherent.<sup>19</sup> The increased sensitivity of the rate to increasing  $(\text{Cu}^{2+})$  for a-d may indicate how corrosion is rapidly stifled when growth of mixed oxide film has occurred under certain conditions.

*Effect of Oxygen.* The rate dependence on  $P_{\text{O}_2}$  was determined at different  $(\text{Cu}^{2+})$  and pH values and in the presence of chloride (Table IV).  $P_{\text{O}_2}$  was varied using  $\text{O}_2\text{-N}_2$  mixtures and without removing the copper sample a series of measurements at constant pH,  $(\text{Cu}^{2+})$ ,  $I$ , and stirring conditions but at different  $P_{\text{O}_2}$  values was made. To ascertain whether the copper surface had changed during the series a redetermination of the dissolution rate under the initial conditions of  $P_{\text{O}_2}$  was made. A typical plot of  $\log R$  ( $\text{mol min}^{-1} \text{ cm}^{-2}$ ) vs.  $\log P_{\text{O}_2}$  (bar) is shown in Figure 4 while Table IV records the range of conditions for which the oxygen dependence was measured. The slopes of these plots are approximately 0.25.

(26) *Nat. Bur. Stand. (U. S.), Circ. 500* (1952).

(27) R. M. Garrels and C. L. Christ, "Solutions, Minerals, and Equilibria," Harper and Row, New York, N. Y., 1965, p 155.

(28) L. Giuliani, A. Tamba, and C. Modena, *Corros. Sci.*, **11**, 485 (1971).

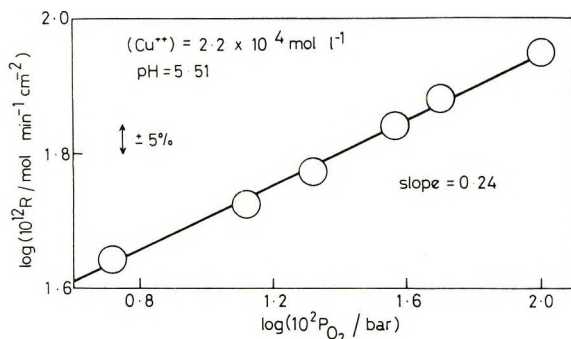


Figure 4. Effect of oxygen on the dissolution of copper.

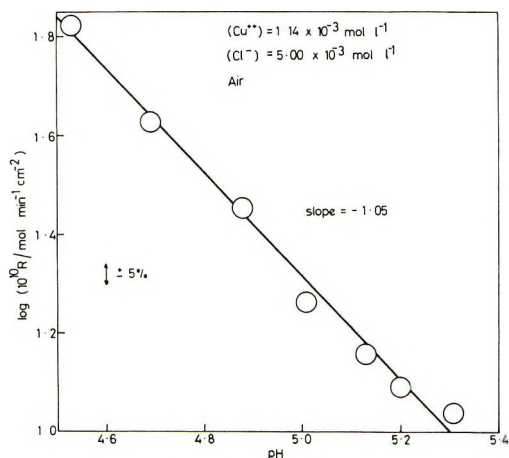


Figure 5. Effect of pH on the dissolution of copper.

**Table IV.** Range of Conditions for Which the Rate Dependence on Oxygen Concentration Was Determined

$10^4(\text{Cu}^{2+})$ , $M$	$10^4(\text{Cl}^-)$ , $M$	pH	Slope of order plot
2.22		5.51	0.24
4.93		5.32	0.26
17.1	100	5.58	0.27
17.1		4.33	0.25

**Effect of pH.** The effect of pH on the dissolution reaction was studied over the range 4.0–5.5 at varying  $(\text{Cu}^{2+})$  and in the presence of chloride (Table V). Following additions of  $\text{HClO}_4$  solution a series of rate measurements was made at constant  $P_{\text{O}_2}$ ,  $(\text{Cu}^{2+})$ , and  $I$  but at varying pH. To check whether the surface had altered during the series, the rate was occasionally re-measured after the pH had been increased by the addition of carbonate-free  $\text{Ba}(\text{OH})_2$  solution. A sample plot of  $\log R$  ( $\text{mol min}^{-1} \text{cm}^{-2}$ ) vs. pH is shown in Figure 5. The dependence on pH (Table V) appears to vary with cupric ion concentration and only at the higher concentrations<sup>29</sup> used was the dependence typical of a simple linear relationship of the type  $R = k(\text{H}^+)$  giving

$$\log R = \log k - \text{pH}$$

**Effect of Added Ions.** The effects produced by the addition of fluoride, chloride, bromide, sulfate, nitrate, or zinc ions on the dissolution rate are plotted in Figure 6 as  $R/R_s$  where  $R_s$  was the rate without added ions present. After measuring  $R_s$  (usually at pH 5.5,  $(\text{Cu}^{2+}) = 2.3 \times 10^{-4} M$ ) successive rate measurements were made with additions of  $\text{CO}_2$ -free solutions (at correct

**Table V:** Range of Conditions for Which the Rate Dependence on pH Was Determined<sup>a</sup>

$10^4(\text{Cu}^{2+})$ , $M$	$10^4(\text{Cl}^-)$ , $M$	Slope of order plot	pH range
17.0		-1.07	4.0–4.9
17.0		-1.07	4.4–4.8
17.0		-1.07	4.5–5.2
11.4	10.0	-1.02	4.1–5.3
11.4	50.0	-1.05	4.5–5.3
2.22		-0.77	4.5–5.5
2.27		-0.66	4.4–5.5
1.48		-0.54	4.5–5.5
0.75		-0.68	4.6–5.5

<sup>a</sup> Air was the aerating gas.

pH,  $(\text{Cu}^{2+})$ , and ionic strength) of the various ions. The anions were added as their sodium or potassium salts and the zinc ions as zinc sulfate. Chloride and bromide ions which complex strongly with cuprous ions,<sup>30a</sup> greatly enhanced the dissolution rate, while the ions  $\text{Zn}^{2+}$ ,  $\text{F}^-$ ,  $\text{SO}_4^{2-}$ , and  $\text{NO}_3^-$  had no appreciable effect. Robertson, *et al.*,<sup>7</sup> similarly observed a positive catalytic effect for chloride additions and a minor effect for sulfate additions at pH 6.

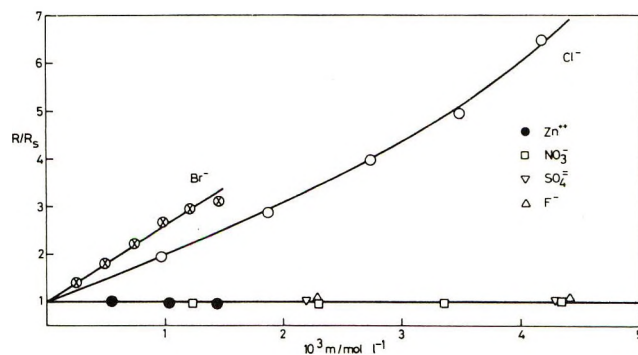


Figure 6. Catalytic effect of added ions on the rate of dissolution of copper.

(29) Although the results in Table V appear self-consistent it is apparent from Figure 2 that under certain conditions one may obtain a much lower dependence on pH at relatively high cupric ion concentrations.

(30) (a) L. G. Sillen, *Chem. Soc., Spec. Publ.*, No. 17, (1964); (b) "International Critical Tables," Vol. III, McGraw-Hill, New York, N. Y., 1928, p 257.



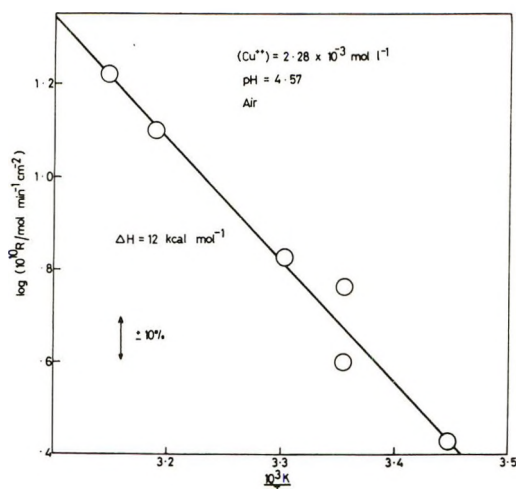
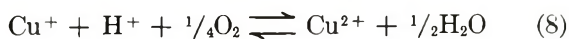
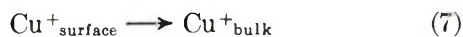
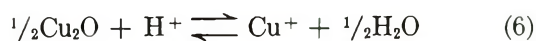


Figure 7. Dissolution rate of copper as a function of reciprocal temperature.

**Effect of Temperature.** The data showing the effect of temperature (16.9–45.0°) on the dissolution rate (Figure 7) were obtained as follows. After the rate was measured at 25° the temperature was raised to 45° and the rate remeasured. The other points were obtained after cooling the bath by various amounts. The glass electrode assembly was calibrated before and after the run at each temperature and a minor correction has been made for the change in oxygen solubility with temperature<sup>30b</sup> in terms of the dependence given in Table IV. As the measurements at 25° indicated that the sample surface may have altered during the temperature cycling, the activation energy cannot be accurate. The value obtained was in the range  $12 \pm 3$  kcal mol<sup>-1</sup>.

## Discussion

The rate of dissolution of metals and compounds in aqueous reagents has been discussed in terms of a diffusion layer theory.<sup>25</sup> The elementary model describes the formation of an extremely thin layer of saturated solution at the solid surface, the rate being determined by diffusion from this layer. The corresponding model for the dissolution of copper covered with cuprous oxide would be



Equation 6 describes the reaction occurring at the Cu<sub>2</sub>O–H<sub>2</sub>O interface while (8) describes the overall reaction in the bulk solution. If (7) is the slow step, reactions 6 and 8 must be rapid. Yet if (8) is rapid, the cuprous ions will be oxidized before they move from the surface. The rate dependence on  $P_{\text{O}_2}$  eliminates (6) as the rate-determining step, suggesting that the oxidation of Cu<sup>+</sup> may be slow. This is considered later.

On the other hand, control by solution diffusion of O<sub>2</sub>, H<sup>+</sup>, or Cu<sup>2+</sup> was untenable in view of the observed

rate dependence on  $P_{\text{O}_2}$ , (H<sup>+</sup>), (Cu<sup>2+</sup>), (Cl<sup>-</sup>), and (Br<sup>-</sup>). This conclusion was supported by the relatively minor effect of increased stirring, although such evidence must be treated with caution. While the dependence of a diffusion-controlled reaction generally weakens with more violent agitation, this is not necessarily synonymous with a transition into a region of kinetic control. In fact, lack of a stirring effect was shown to occur in the diffusional range,<sup>31</sup> due to a slipping effect with the stirrer failing to carry the liquid along with it at the higher rotational rates. Therefore, additional information must be available to enable a distinction between a chemical reaction and a solution diffusion process to be made unequivocally. We conclude that the dissolution is not controlled by a simple diffusion process in solution. A solid-state mechanism is now proposed.

The oxidation of a metal in a gaseous environment has been described in terms of reactions at the metal–oxide and oxide–gas interfaces and the transport of material through the oxide film.<sup>32</sup> The slowest of these steps will control film growth. In an aqueous environment film growth is opposed by dissolution and for films of constant thickness we expect the rate of oxide growth to equal the rate of dissolution. In the present investigation, when steady-state rates were observed (pseudo-zero-order conditions) we consider the film thickness to be constant. The oxidation and dissolution of copper will now be considered in terms of the production of cation vacancies and positive holes at the Cu<sub>2</sub>O–H<sub>2</sub>O interface, their migration across the oxide film with their consequent destruction at the Cu–Cu<sub>2</sub>O interface.

The following reactions may take place at the Cu<sub>2</sub>O–H<sub>2</sub>O interface.

(i) The transfer of a cuprous ion to the aqueous phase<sup>33</sup>



(ii) The oxidation of cuprous ions in oxygenated aqueous solution at the surface for which the overall reaction is described by (8).

(iii) The formation of a “positive hole” in the Cu<sub>2</sub>O structure by a cupric ion occupying a cation vacancy.

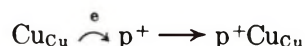


In these equations Cu<sub>Cu</sub> represents a cuprous ion on a normal site of Cu<sub>2</sub>O with an apparent charge of zero; V<sup>-</sup><sub>Cu</sub> is a cuprous ion vacancy with an apparent charge of -1; p<sup>+</sup> is a cupric ion (a cuprous ion with an electron removed, a “positive hole”) with an apparent charge of +1. Whereas a positive hole may migrate by electron transfer<sup>34a</sup>

(31) D. A. Frank-Kamenetskii, “Diffusion and Heat Exchange in Chemical Kinetics,” translated by N. Thon, Princeton University Press, Princeton, N. J., 1955, p 66.

(32) T. B. Grimley, “Chemistry of the Solid State,” W. E. Garner, Ed., Butterworths, London, 1955, Chapter 14.

(33) R. F. North and M. J. Pryor, *Corros. Sci.*, **10**, 297 (1970).

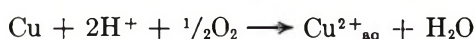


the movement of vacancies is by migration of cuprous ions into a vacant structural site.<sup>34a</sup>

At the Cu-Cu<sub>2</sub>O interface the defects are removed by an overall reaction of the type

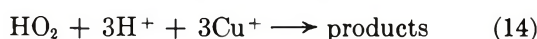
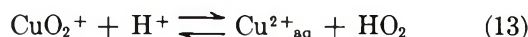


The sum of  $2 \times (8)$ ,  $2 \times (9)$ , (10), and (11) gives the familiar eq 1, describing the overall process, *viz.*



(a) It does not appear possible to explain the rate dependence on  $(\text{H}^+)$ ,  $(\text{Cu}^{2+}_{\text{aq}})$ , and  $P_{\text{O}_2}$  in terms of (9) being rate determining and this suggestion is not considered further.

(b) The mechanism for the oxidation of the cuprous ion in aqueous solution (8) has not been resolved. Following Nord<sup>35</sup> we consider the following steps



Nord regarded (13) to be rate determining giving

$$R = k_{13}(\text{CuO}_2^+)(\text{H}^+) = k_{13}K_{12}(\text{Cu}^+)(\text{H}^+)(\text{O}_2)$$

This fails to account for the rate dependence on  $P_{\text{O}_2}$ . Similarly (12) is rejected as the slow step. The simple steps of (14) are unknown and will not be considered. Henceforth the oxidation of cuprous ion in aqueous solution is considered to be rapid compared with the dissolution process.

(c) If (10) is rate determining then

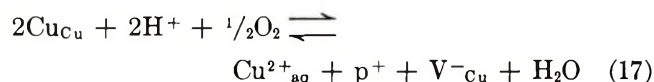
$$R = k_{10}(\text{Cu}^{2+}_{\text{aq}})(\text{V}^-_{\text{Cu}}) \quad (15)$$

which upon substitution using (8) and (9) gives

$$R = k_{10}K_8K_9(\text{O}_2)^{0.25}(\text{H}^+) \quad (16)$$

This equation correctly describes the observed dependence on  $P_{\text{O}_2}$  and  $(\text{H}^+)$  (Tables IV and V) and predicts a zero-order dependence on  $(\text{Cu}^{2+}_{\text{aq}})$  (*cf.* Figure 2).

(d) For control by a slow diffusion process across the oxide layer the reactions at the two interfaces may be regarded as rapid. At the stationary state the distribution of cation vacancies and positive holes within the bulk oxide will be equal.<sup>32</sup> Hence the rates of production of cation vacancies and positive holes will also be equal and their formation<sup>36</sup> is derived from (9), (10), and (11) as



Thus

$$K_{17} = (\text{p}^+)(\text{V}^-_{\text{Cu}})(\text{Cu}^{2+}_{\text{aq}})/(\text{O}_2)^{0.5}(\text{H}^+)^2 \quad (18)$$

An essential requirement is the maintenance of elec-

trical neutrality in both the solid and aqueous phases so that  $(\text{p}^+) = (\text{V}^-_{\text{Cu}})$ . This is strictly true only in the bulk phases and not in the space charge regions in the vicinity of each interface.<sup>32</sup> Hence

$$(\text{V}^-_{\text{Cu}}) = K_{17}^{0.5}(\text{O}_2)^{0.25}(\text{H}^+)/(\text{Cu}^{2+}_{\text{aq}})^{0.5} \quad (19)$$

To maintain electrical neutrality, cation vacancies and positive holes migrate at equal rates across the bulk oxide and, for a process governed by the diffusion of these, vacancy migration is considered to be the slow step.<sup>34b</sup> This will take place under an electrochemical potential gradient due to the concentration gradient of  $\text{V}^-_{\text{Cu}}$  across the film and to the electric field in the film. In simple terms

$$R = k_m(\text{V}^-_{\text{Cu}})$$

where  $k_m$  is a function describing charged particle migration in an electric field.<sup>34c</sup> Utilizing (19)

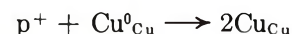
$$R = k_m K_{17}^{0.5}(\text{O}_2)^{0.25}(\text{H}^+)/(\text{Cu}^{2+}_{\text{aq}})^{0.5} \quad (20)$$

This rate equation also correctly describes the observed dependence on  $P_{\text{O}_2}$  and  $(\text{H}^+)$  (Tables IV and V) and predicts an order of  $-0.5$  with respect to  $(\text{Cu}^{2+}_{\text{aq}})$ .

(e) Suppose a reaction at the Cu-Cu<sub>2</sub>O interface is rate controlling. The slow step might be the diffusion of copper atoms on to a vacant structural site<sup>39</sup>



followed by a rapid transfer of electrons



where  $\text{Cu}^0_{\text{Cu}}$  is a copper atom on a normal site with an apparent charge of  $-1$ . In this case

$$R = k_{21}(\text{V}^-_{\text{Cu}})$$

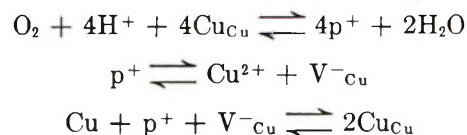
where  $(\text{V}^-_{\text{Cu}})$  will be described by eq 19, the production and transport of cation vacancies being rapid. Thus

$$R = k_{21}K_{17}^{0.5}(\text{O}_2)^{0.25}(\text{H}^+)/(\text{Cu}^{2+}_{\text{aq}})^{0.5} \quad (22)$$

(34) O. Kubaschewski and B. E. Hopkins, "Oxidation of Metals and Alloys," Butterworths, London, 1962: (a) p 22; (b) p 82; (c) Chapter 2.

(35) H. Nord, *Acta Chem. Scand.*, **9**, 430 (1955).

(36) An alternative set of rapid interfacial equilibria<sup>37</sup> for the formation of positive holes and vacancies may be written as follows



From these, the equations describing the overall rapid equilibrium at the Cu-H<sub>2</sub>O interface and the overall reaction may be found identical with (17) and (1), respectively. These reactions suggest an alternative path for the formation of positive holes and vacancies, though the dissolution of cuprous oxide in aqueous media is known to be rapid.<sup>38</sup>

(37) P. C. A. Bailey and G. A. Wright, private communication.

(38) W. Feitknecht and P. Schindler, *Pure Appl. Chem.*, **6**, 130 (1963).

(39) T. B. Grimley and B. M. W. Trapnell, *Proc. Roy. Soc., Ser. A*, **234**, 405 (1956).



This formulation satisfies the  $P_{O_2}$  and  $(H^+)$  dependence found experimentally (Tables IV and V) and predicts an order of  $-0.5$  with respect to  $(Cu^{2+}_{aq})$ .

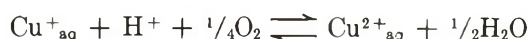
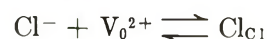
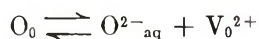
A distinction between (10), (21), and cation vacancy migration (all of which predict the observed rate dependence on  $P_{O_2}$  and  $(H^+)$ ) as the rate-determining step cannot be made in terms of the measured rate dependence on  $(Cu^{2+})$  (see Figure 2). The significance of the order dependence ( $-0.2$ ) as compared with  $-0.5$  ((21) or vacancy migration rate determining) and zero ((10) rate determining) is not clear. However, the energy of activation provides additional information. In the present work this was  $12 \text{ kcal mol}^{-1}$ . From high-temperature oxidation experiments using radioactive copper, Moore and Selikson<sup>40</sup> calculated the activation energy for the self-diffusion of Cu in  $Cu_2O$  to be  $36.1 \text{ kcal mol}^{-1}$ . The activation energy for the self-diffusion process represents the sum of the activation energies for the formation and diffusion of cation vacancies.<sup>41</sup> Thus, using the enthalpy of formation derived by O'Keeffe and Moore<sup>42</sup> ( $21.7 \text{ kcal mol}^{-1}$ ), the enthalpy of migration is calculated as  $14.4 \text{ kcal mol}^{-1}$ . This compares well with that obtained in the present work ( $12 \text{ kcal mol}^{-1}$ ). However, in a recent publication,<sup>43</sup> the enthalpy for the self-diffusion has been found to be  $24.0 \text{ kcal mol}^{-1}$ . Further, some of the earlier data<sup>40</sup> was indicated to be of inferior quality. In view of the large discrepancy between the enthalpies reported for self-diffusion, it cannot be concluded without reservation that the slow step in the current study is a cation vacancy migration.

As noted earlier, added  $Cl^-$  and  $Br^-$  ions enhance the rate with  $Br^-$  having the greater effect (Figure 6). In contrast, added  $F^-$ ,  $SO_4^{2-}$ , and  $NO_3^-$  ions have a negligible effect. This behavior parallels the ability of these ions to complex with cuprous ions in aqueous solution.<sup>29</sup> However, let us consider complexing reactions of the type



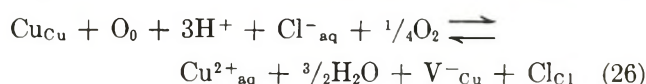
Incorporating this type of complexing in equations corresponding to (9) and (8), we find that the sum of these with (10) is identical with (12), demonstrating that the dependence of the rates on  $P_{O_2}$  and  $H^+$  would be unchanged (Table IV and V) but also that there would be no catalysis by chloride.

On the other hand, the effect of chloride has been described in terms of the substitution of Cl for O in the crystal lattice.<sup>33</sup> This substitution would create a charge imbalance leading to the formation of cation vacancies to maintain electrical neutrality, *i.e.*



where  $O_0$  represents an oxygen ion on a normal lattice site with an apparent charge of zero;  $Cl_{Cl}$  is a chloride ion occupying a normal lattice site with an apparent charge of  $+1$ ,  $V_0^{2+}$  is an anion vacancy with an apparent charge of  $+2$ .

The overall equation satisfying electroneutrality requirements in both the aqueous and solid phases is



giving

$$(V^-_{Cu}) = K_{26}(H^+)^3(Cl^-_{aq})(O_2)^{0.25}/(Cu^{2+}_{aq})$$

On this basis, the observed rate dependence on  $(H^+)$  is not satisfactorily explained. Furthermore, increased substitution of oxygen ions of the lattice by bromide ions to account for the increased effect of the latter would not be expected from simple ion size considerations. Thus while some substitution may take place, it does not appear to be the dominant mechanism. In addition, the negligible effect of added fluoride ions (Figure 6) would indicate only minor substitution in the structure. Neither suggestion for the catalytic effect of chloride fits the data well.

It is worth noting that the substitution model describing the effect of  $(H^+)$  on the corrosion of aluminium<sup>44</sup> also does not appear to apply in the present case.

To summarize, each solid-state model predicts the same dependence on  $P_{O_2}$  and  $(H^+)$  and the data showing the rate dependence on  $(Cu^{2+})$  does not clarify the situation. Hence the conclusion that the slow step is a slow cation vacancy migration rests on the available evidence concerning the enthalpy of migration.

*Acknowledgments.* The author is most grateful to Professor G. A. Wright and to Drs. A. J. Ellis, K. J. D. MacKenzie, W. H. Robinson, and T. M. Seward for their useful comments on this work. The oxygen analyses were performed by W. J. Harrison, and Miss J. Beanland helped with some of the measurements.

(40) W. J. Moore and B. Selikson, *J. Chem. Phys.*, **19**, 1539 (1951).

(41) P. G. Shewmon, "Diffusion in Solids," McGraw-Hill, New York, N. Y., 1963.

(42) M. O'Keeffe and W. J. Moore, *J. Chem. Phys.*, **36**, 3009 (1962).

(43) S. Mrowec and A. Stoklosa, *Bull. Acad. Pol. Sci., Ser. Sci. Chim.*, **18**, 523 (1970).

(44) M. A. Heine and M. J. Prior, *J. Electrochem. Soc.*, **110**, 1205 (1963).

## Sodium and Magnesium Sulfate Ion Pairing:

### Evidence from Raman Spectroscopy

by Francis P. Daly, Chris W. Brown,\* and Dana R. Kester

Department of Chemistry and Graduate School of Oceanography, University of Rhode Island, Kingston, Rhode Island 02881 (Received April 20, 1972)

Publication costs assisted by the Office of Naval Research

Raman spectra of aqueous solutions of sodium and magnesium sulfates were measured but failed to reveal any evidence of ion pairing. However, sulfate solutions with HCl added did exhibit relatively strong bands due to  $\text{HSO}_4^-$ . Evidence for  $\text{MgSO}_4$  and  $\text{NaSO}_4^-$  ion pairs has been obtained by the addition of sodium and magnesium salts to the latter solution; both cations compete with hydrogen ions for the  $\text{SO}_4^{2-}$ . This is clearly demonstrated in the Raman spectra by a decrease in intensity of the band assigned to  $\text{HSO}_4^-$  at  $1053\text{ cm}^{-1}$  and an increase in intensity of the band assigned to  $\text{SO}_4^{2-}$  at  $982\text{ cm}^{-1}$  in the solutions with sodium or magnesium added.

#### Introduction

Considerable attention has been given to the use of ion association models to interpret the physical-chemical characteristics of electrolytic solutions.<sup>1-3</sup> This work considers the ion pairing of sulfate ions with sodium and magnesium ions. The tendency of magnesium and sulfate ions to form ion pairs has been examined extensively using conductometric,<sup>4</sup> potentiometric,<sup>4-7</sup> solubility,<sup>8</sup> and ultrasonic relaxation<sup>9-10</sup> techniques. The consistency of these studies supports the ion association model for magnesium and sulfate. The case for sodium ion pairing with sulfate is not as clearly established as that for magnesium. In some studies  $\text{Na}_2\text{SO}_4$  has been assumed to be a completely dissociated electrolyte,<sup>6,11,12</sup> whereas others have considered the formation of  $\text{NaSO}_4^-$  ion pairs.<sup>13-15</sup> It has been subsequently shown that Harned's rule behavior of activity coefficients in multicomponent solutions does not preclude an ion association model for the ionic interactions.<sup>15-17</sup>

The effects of various cations on the Raman spectra of nitrates, sulfates, and perchlorates have been investigated by Hester and Plane.<sup>18</sup> Only  $\text{In}^{3+}$  produced new bands in the spectrum of the  $\text{SO}_4^{2-}$  ion; all other cations studied, including  $\text{Na}^+$  and  $\text{Mg}^{2+}$ , gave approximately the same spectra. In this work we extend the observations of Hester and Plane to lower ionic strengths and to multicomponent sulfate solutions.

Recently, Irish and Chen examined the Raman spectra of various solutions containing  $\text{HSO}_4^-$  and  $\text{SO}_4^{2-}$ .<sup>19-21</sup> They found that the integrated intensity of the  $\text{SO}_4^{2-}$  band at  $981\text{ cm}^{-1}$  is proportional to the  $\text{SO}_4^{2-}$  molarity and that the integrated intensity of the  $\text{HSO}_4^-$  band at  $1053\text{ cm}^{-1}$  is proportional to the  $\text{HSO}_4^-$  molarity. They further showed that the ratio of these bands is a

qualitative measure of the extent of dissociation of  $\text{HSO}_4^-$ .

In the present investigation Raman spectra of multicomponent aqueous solutions of HCl, NaCl,  $\text{Na}_2\text{SO}_4$ , and  $\text{MgCl}_2$  in the range 0.3-1.3 ionic strength have been examined in terms of an ion-pairing model. We have assumed that the chlorides of  $\text{H}^+$ ,  $\text{Na}^+$ , and  $\text{Mg}^{2+}$  are completely dissociated. Even though this assumption is contrary to some interpretations,<sup>22-24</sup> it is consistent

- (1) C. W. Davies, "Ion Association," Butterworths, Washington, D. C., 1962.
- (2) G. H. Nancollas, "Interactions in Electrolyte Solutions," Elsevier, Amsterdam, 1966.
- (3) R. A. Robinson and R. H. Stokes, "Electrolyte Solutions," Butterworths, London, 2nd revised ed, 1965.
- (4) H. W. Jones and C. B. Monk, *Trans. Faraday Soc.*, **48**, 929 (1952).
- (5) V. S. K. Nair and G. H. Nancollas, *J. Chem. Soc.*, 3706 (1958).
- (6) J. M. T. M. Gieskes, *Z. Phys. Chem. (Frankfurt am Main)*, **50**, 78 (1966).
- (7) D. R. Kester and R. M. Pytkowicz, *Limnol. Oceanogr.*, **13**, 670 (1968).
- (8) W. L. Marshall, *J. Phys. Chem.*, **73**, 3584 (1967).
- (9) M. Eigen and K. Tamm, *Z. Elektrochem.*, **66**, 107 (1962).
- (10) G. Atkinson and S. Petrucci, *J. Phys. Chem.*, **70**, 3122 (1966).
- (11) R. D. Lanier, *ibid.*, **69**, 3992 (1965).
- (12) J. N. Butler, P. T. Hsu, and J. C. Synnott, *ibid.*, **71**, 910 (1967).
- (13) E. C. Righellato and C. W. Davies, *Trans. Faraday Soc.*, **26**, 592 (1930).
- (14) J. M. Austin and A. D. Mair, *J. Phys. Chem.*, **66**, 519 (1962).
- (15) R. M. Pytkowicz and D. R. Kester, *Amer. J. Sci.*, **267**, 217 (1969).
- (16) J. N. Butler and R. Huston, *J. Phys. Chem.*, **74**, 2976 (1970).
- (17) J. N. Butler and R. Huston, *Anal. Chem.*, **42**, 1308 (1970).
- (18) R. E. Hester, R. A. Plane, and G. E. Walrafen, *J. Chem. Phys.*, **38**, 249 (1963); R. E. Hester and R. A. Plane, *Inorg. Chem.*, **3**, 769 (1964).
- (19) D. E. Irish and H. Chen, *J. Phys. Chem.*, **74**, 3796 (1970).
- (20) H. Chen and D. E. Irish, *ibid.*, **75**, 2672 (1971).
- (21) H. Chen and D. E. Irish, *ibid.*, **75**, 2681 (1971).



**Table I:** Observed Frequencies ( $\text{cm}^{-1}$ ) and Assignments of the Bands in the Raman Spectra of the Sulfate Solutions

Assignments	0.1 M $\text{Na}_2\text{SO}_4$	0.1 M $\text{Na}_2\text{SO}_4$ - 1.0 M NaCl	0.1 M $\text{Na}_2\text{SO}_4$ - 0.1 M $\text{MgCl}_2$	0.1 M $\text{Na}_2\text{SO}_4$ - 0.1 M HCl
$\text{SO}_4^{2-}$ , $\nu_3$	$\sim 1110$ w, b	$\sim 1110$ w, b	$\sim 1110$ w, b	
$\text{HSO}_4^-$ , $\text{SO}_3$ sym stretch				1053 m
$\text{SO}_4^{2-}$ , $\nu_1$	982 vs	982 vs	982 vs	982 vs
$\text{HSO}_4^-$ , S-OH stretch				$\sim 895$ w, b
$\text{SO}_4^{2-}$ , $\nu_4$	$\sim 620$ w, b	$\sim 615$ w, b	$\sim 610$ w, b	
$\text{HSO}_4^-$ , $\text{SO}_3$ sym bend				$\sim 595$ w, b
$\text{SO}_4^{2-}$ , $\nu_2$	448 w	448 w	446 w	445 w
$\text{HSO}_4^-$ , S-OH wag				410 w

with many of the present concepts of electrolytic solutions.<sup>13,15,25-28</sup> The success of the following analysis supports the adequacy of this assumption.

### Experimental Section

All solutions were prepared from J. T. Baker reagent grade chemicals. The NaCl and  $\text{Na}_2\text{SO}_4$  were dried at  $125^\circ$  and 0.5 atm pressure for 2 hr prior to weighing. The HCl was added by weight from a 37.5% aqueous solution. Magnesium was added as  $\text{MgCl}_2 \cdot 6\text{H}_2\text{O}$ .

Raman spectra were recorded at  $24 \pm 1^\circ$  using a Spex Industries Model 1401 double monochromator with photon counting detection and a C.R.L. Model 52A argon ion laser emitting at  $4880 \text{ \AA}$  as the excitation source. Spectra were measured of samples contained in Pyrex capillary tubes with an inner diameter of 1.2 mm, and duplicate spectra were measured of samples contained in a vertically mounted, quartz liquid cell with an inner diameter of 8 mm. During the experiments in which relative integrated intensities of bands of different samples were measured, the integrated intensity of the  $1625\text{-cm}^{-1}$  band of water ( $\nu_2$ ) was measured for each sample. It was found that the intensity of this band remained the same from one sample to the next, if care was taken in exchanging samples. The spectra of the samples to be compared were measured consecutively, and the spectrum of each sample was measured a minimum of five times.

### Results and Discussion

The Raman spectrum of a 0.1 M  $\text{Na}_2\text{SO}_4$  solution in the  $800\text{--}1200\text{-cm}^{-1}$  region is shown in Figure 1. There is a very strong band at  $982 \text{ cm}^{-1}$  assigned as  $\nu_1$ , the symmetric  $\text{SO}_4$  stretching mode, and a weak, broad band at  $\sim 1110 \text{ cm}^{-1}$  assigned as  $\nu_3$ , the antisymmetric  $\text{SO}_4$  stretching mode.<sup>29</sup> Two other very weak, broad bands are observed at lower frequencies. All of the observed frequencies and assignments are listed in Table I.

To test the feasibility of using Raman spectroscopy to detect sodium and magnesium ion pairs with sulfate, spectra of three additional solutions were recorded. In the first solution excess sodium was added to the 0.1 M  $\text{Na}_2\text{SO}_4$  solution by the addition of NaCl (making the solution 1.0 M in NaCl). It was assumed that the

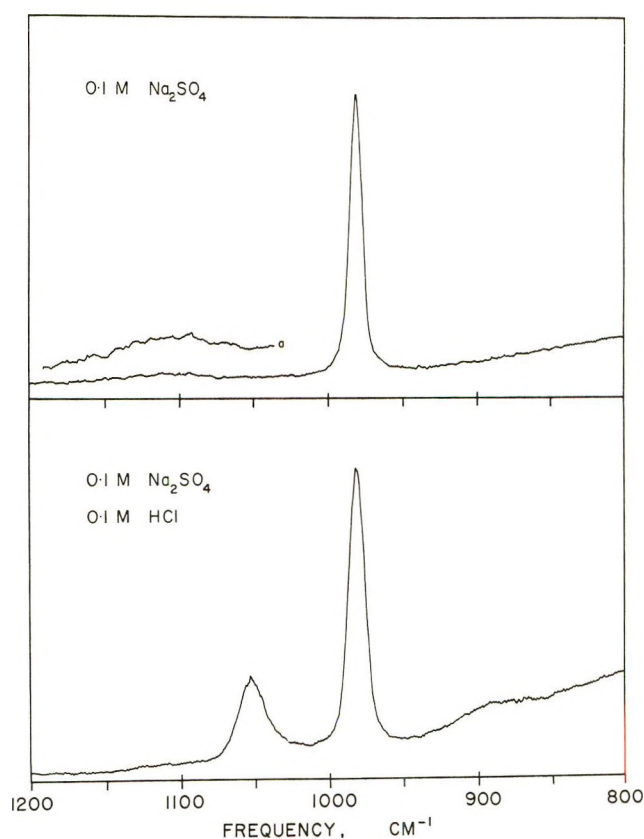


Figure 1. Top, Raman spectrum of 0.1 M  $\text{Na}_2\text{SO}_4$  solution between  $800$  and  $1200 \text{ cm}^{-1}$  (a, sensitivity increased by  $3\times$ ). Bottom, Raman spectrum of 0.1 M  $\text{Na}_2\text{SO}_4$ -0.1 M HCl solution. Spectral slit widths  $<10 \text{ cm}^{-1}$ .

NaCl completely dissociated and that any changes in the spectrum were due to the formation of  $\text{NaSO}_4^-$  ion

- (22) R. M. Fuoss and K. L. Hsia, *Proc. Nat. Acad. Sci. U. S.*, **57**, 1550 (1967).  
 (23) A. B. Gancy and S. B. Brummer, *J. Phys. Chem.*, **73**, 2429 (1969).  
 (24) F. J. Millero, *ibid.*, **74**, 356 (1970).  
 (25) L. G. Sillen and A. E. Martell, *Chem. Soc., Spec. Publ.*, No. 17, 272 (1964).  
 (26) H. C. Helgeson, *Amer. J. Sci.*, **267**, 729 (1969).  
 (27) R. E. Creekmore and C. N. Reilley, *J. Phys. Chem.*, **73**, 1563 (1969).  
 (28) R. H. Stokes, *Trans. Faraday Soc.*, **41**, 642 (1945).  
 (29) K. Nakamoto, "Infrared Spectra of Inorganic and Coordination Compounds," Wiley, New York, N. Y., 1963.

**Table II:** Composition of the Sulfate Solutions at 25°

Solution	Composition	Molarity of sulfate species				Ionic strength
		SO <sub>4</sub> <sup>2-</sup>	NaSO <sub>4</sub> <sup>-</sup>	MgSO <sub>4</sub>	HSO <sub>4</sub> <sup>-</sup>	
a	0.1 M Na <sub>2</sub> SO <sub>4</sub> , 0.1 M HCl	0.0340	0.0139	...	0.0521	0.268
b	0.1 M Na <sub>2</sub> SO <sub>4</sub> , 0.1 M HCl, 0.7 M NaCl	0.0194	0.0388	...	0.0417	0.939
c	0.1 M Na <sub>2</sub> SO <sub>4</sub> , 0.1 M HCl, 0.2 M MgCl <sub>2</sub>	0.0198	0.0080	0.0324	0.0398	0.775

pairs. The spectrum was exactly the same as the one obtained for 0.1 M NaSO<sub>4</sub>. Magnesium was added in the second solution by adding MgCl<sub>2</sub>·6H<sub>2</sub>O (0.1 M) to the 0.1 M Na<sub>2</sub>SO<sub>4</sub>. Again it was assumed that MgCl<sub>2</sub> completely dissociated and that any changes were due to the formation of MgSO<sub>4</sub> ion pairs. As before there were no changes in the spectrum. The third solution contained 0.1 M Na<sub>2</sub>SO<sub>4</sub> and 0.1 M HCl. In this case it was assumed that HCl completely dissociated and that changes in the spectrum were due to the formation of HSO<sub>4</sub><sup>-</sup>. There were definite changes in the spectrum.

The Raman spectrum of the 0.1 M Na<sub>2</sub>SO<sub>4</sub>-0.1 M HCl solution is also shown in Figure 1. Two new bands appear in the spectrum at ~895 and 1053 cm<sup>-1</sup>. Previously, these two bands have been assigned to HSO<sub>4</sub><sup>-</sup>;<sup>30</sup> the former band is assigned as the S-OH stretching mode and the latter as the SO<sub>3</sub> symmetric stretching mode. In addition, two other very weak bands are observed at lower frequencies; these are listed in Table I along with the observed frequencies and assignments for all of the solutions.

Within experimental limits Raman spectra of the solutions with excess Na<sup>+</sup> and Mg<sup>2+</sup> were the same as those obtained by Hester and Plane.<sup>18</sup> Hester and Plane interpreted their data as indicating that metal sulfate complexes are solvent separated, except in the case of indium. Since it is well established that MgSO<sub>4</sub> ion pairs exist in solution,<sup>4-10</sup> we believe that an outer-sphere or solvent-separated interpretation is correct and that this type of ion pairing does not affect the Raman spectrum of SO<sub>4</sub><sup>2-</sup>. In the case of the NaSO<sub>4</sub><sup>-</sup> ion pair there is no direct evidence for its existence; therefore, either it does not exist or it is solvent separated in the same way as the MgSO<sub>4</sub> ion pair, and hence it is not detected in the Raman spectrum.

To determine if the formation of NaSO<sub>4</sub><sup>-</sup> and MgSO<sub>4</sub> ion pairs can be detected indirectly by competing with HSO<sub>4</sub><sup>-</sup>, we have recorded the Raman spectrum of three additional solutions. The compositions and predicted molarities of the sulfate species in these solutions are listed in Table II. The calculated molarities of sulfate species in Table II are based on values for the concentration equilibrium constants  $K^*_{M\text{SO}_4} = [M\text{SO}_4]/([M][\text{SO}_4])$ , where M is Na<sup>+</sup>, Mg<sup>2+</sup>, or H<sup>+</sup> and the brackets represent concentrations of the en-

closed species. The  $K^*_{M\text{SO}_4}$  varies with ionic strength, and it was necessary to calculate the ionic strength by iteration to account for the effect of the ion pairs on it.

Potentiometric techniques were used to determine  $K^*_{\text{NaSO}_4}$ <sup>15</sup> and  $K^*_{\text{MgSO}_4}$ <sup>31</sup> at various ionic strengths. The results were

$$K^*_{\text{NaSO}_4} = 2.73 - 2.58\mu + 2.28\mu^2$$

and

$$\log K^*_{\text{MgSO}_4} = 2.32 - 2.84[\sqrt{\mu}/(1 + \sqrt{\mu})]$$

These empirical expressions are valid only over the range  $0.2 \leq \mu < 1.0$ . The ionic strength dependence of  $K^*_{\text{HSO}_4}$  at 25° was determined in conjunction with this study. The emf response of a combination glass pH electrode with a ceramic frit junction reference electrode (Corning No. 476051) was determined in a 0.100 M HCl solution which was titrated to  $\mu = 1.0$  with NaCl. These results provided a calibration of emf relative to [H<sup>+</sup>] which accounted for the effects of ionic strength on the activity coefficient of H<sup>+</sup> and on the liquid junction potential of the reference electrode in HCl-NaCl solutions. A second titration was performed in which NaCl was added to a 0.100 M HCl-0.100 M Na<sub>2</sub>SO<sub>4</sub> to cover the range  $0.26 \leq \mu \leq 1.12$ . The values of [H<sup>+</sup>] and [HSO<sub>4</sub><sup>-</sup>] = 0.100 - [H<sup>+</sup>] were obtained from the electrode response in the second titration, and the relationship was derived from the calibration measurements. The previously determined  $K^*_{\text{NaSO}_4}$  was used with these results to calculate [SO<sub>4</sub><sup>2-</sup>]. A least-squares polynomial regression of seven values of  $K^*_{\text{HSO}_4}$  provided the following relationship for  $0.26 \leq \mu \leq 1.12$

$$K^*_{\text{HSO}_4} = 34.8 - 13.1\mu + 9.2\mu^2 + 4.2\mu^3 + 3.5\mu^4$$

Since we have already shown that neither Mg nor Na affect the Raman spectrum of SO<sub>4</sub><sup>2-</sup>, we can assume that SO<sub>4</sub><sup>2-</sup>, MgSO<sub>4</sub>, and NaSO<sub>4</sub><sup>-</sup> (if it does exist) all contribute to the 982-cm<sup>-1</sup> band of SO<sub>4</sub><sup>2-</sup>. Therefore, it is possible to predict the changes in intensities of the 982-cm<sup>-1</sup> band and the HSO<sub>4</sub><sup>-</sup> band at 1053 cm<sup>-1</sup>. The SO<sub>4</sub><sup>2-</sup> band in the spectrum of solution c should

(30) R. J. Gillespie and E. A. Robinson, *Can. J. Chem.*, **40**, 644 (1962).

(31) D. R. Kester, Ph.D. Thesis, Oregon State University, Corvallis (1969).



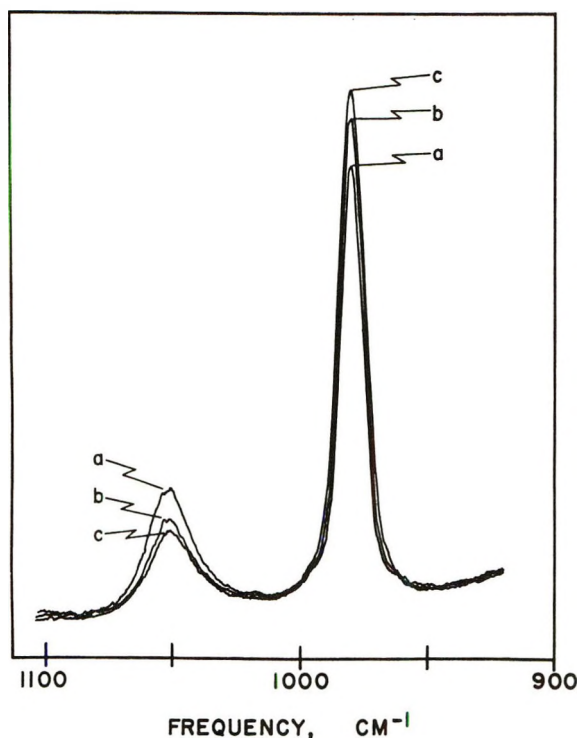


Figure 2. Raman spectra of sulfate solutions: a, 0.1 *M* Na<sub>2</sub>SO<sub>4</sub>-0.1 *M* HCl; b, 0.1 *M* Na<sub>2</sub>SO<sub>4</sub>-0.1 *M* HCl-0.7 *M* NaCl; c, 0.1 *M* Na<sub>2</sub>SO<sub>4</sub>-0.1 *M* HCl-0.2 *M* MgCl<sub>2</sub>. The band at 1053 cm<sup>-1</sup> is due to HSO<sub>4</sub><sup>-</sup> and the band at 982 cm<sup>-1</sup> is due to SO<sub>4</sub><sup>2-</sup>, NaSO<sub>4</sub><sup>-</sup>, and MgSO<sub>4</sub>. Spectral slit width <10 cm<sup>-1</sup>.

be 1.26 times as intense as the same band in solution a, whereas the HSO<sub>4</sub><sup>-</sup> band should be 0.76 as intense. For solution b the SO<sub>4</sub><sup>2-</sup> band should be 1.22 times as intense as the band in the solution a, whereas the HSO<sub>4</sub><sup>-</sup> band should be 0.80 as intense.

The Raman spectra of the three solutions are shown in Figure 2. It is seen that both Na and Mg decrease the intensity of the HSO<sub>4</sub><sup>-</sup> band (1053 cm<sup>-1</sup>) and increase the intensity of the SO<sub>4</sub><sup>2-</sup> band (982 cm<sup>-1</sup>). The observed ratios of the HSO<sub>4</sub><sup>-</sup> and SO<sub>4</sub><sup>2-</sup> bands are compared with the predicted values in Table III. The plus and minus values for the predicted ratios represent the effects on the calculation of varying  $K^*_{\text{NaSO}_4}$

Table III: Predicted<sup>a</sup> and Observed<sup>b</sup> Ratios for the SO<sub>4</sub><sup>2-</sup> Band and the HSO<sub>4</sub><sup>-</sup> Band

Solution	Predicted ratio for SO <sub>4</sub> <sup>2-</sup>	Observed ratio for SO <sub>4</sub> <sup>2-</sup> (982-cm <sup>-1</sup> band)	Predicted ratio for HSO <sub>4</sub> <sup>-</sup>	Observed ratio for HSO <sub>4</sub> <sup>-</sup> (1053-cm <sup>-1</sup> band)
b/a	1.22 ± 0.01	1.15 ± 0.03	0.80 ± 0.01	0.73 ± 0.05
c/a	1.26 ± 0.01	1.26 ± 0.01	0.76 ± 0.01	0.60 ± 0.05

<sup>a</sup> Predicted from the molarities in Table II assuming that SO<sub>4</sub><sup>2-</sup>, NaSO<sub>4</sub><sup>-</sup>, and MgSO<sub>4</sub> all contribute to the 982-cm<sup>-1</sup> band of SO<sub>4</sub><sup>2-</sup>. <sup>b</sup> Integrated intensities of the bands.

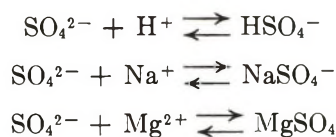
by ±2%,  $K^*_{\text{MgSO}_4}$  by ±5%, and  $K^*_{\text{HSO}_4}$  by ±2%; these percentages reflect the precision within which each constant has been determined. The uncertainties listed for the observed ratios represent the variability in repetitive Raman spectra. The ratios for c/a are close to the predicted values, *i.e.*, 1.26 for SO<sub>4</sub><sup>2-</sup> compared to the predicted value of 1.26 and 0.60 for HSO<sub>4</sub><sup>-</sup> as compared to the predicted value of 0.76. These observations confirm the fact that MgSO<sub>4</sub> ion pairs exist in solution and that they can compete with HSO<sub>4</sub><sup>-</sup>. The fact that the intensities of the bands in the spectrum of solution b also change in accord with the predicted values is a strong indication that NaSO<sub>4</sub><sup>-</sup> ion pairs also exist in solution and that they too can compete with HSO<sub>4</sub><sup>-</sup>.

Our interpretation of the effects of sodium and magnesium ions on the Raman spectra of the HSO<sub>4</sub><sup>-</sup>-SO<sub>4</sub><sup>2-</sup> system provides a possible explanation for the "salt effects" discussed by Chen and Irish.<sup>21</sup> At salt (*e.g.*, NaCl) concentrations ≥ 1 *M* they found that the formation of sulfate from bisulfate is depressed by the salt. They further state that in dilute salt solutions there is an indication that the concentration of sulfate is enhanced by the salt. This is exactly what we observed at salt concentrations < 1 *M*. Chen and Irish note that for dilute solutions the degree of dissociation of HSO<sub>4</sub><sup>-</sup> is directly proportional to the ionic strength but that the magnitude varies with the type of cation present in the solution. Our results are analogous, *i.e.*, the ratios of the 982-cm<sup>-1</sup> band to the 1053-cm<sup>-1</sup> band as well as the ionic strengths are greater for both solutions b and c in comparison to solution a. However, for solution c the ratio is greater than that of b, whereas the ionic strength is less than that of b. This is in agreement with the predicted order of the ratios using the ion-pair model.

## Conclusion

Raman spectra of sulfate ions in aqueous solutions of sodium and magnesium salts do not reveal the presence of NaSO<sub>4</sub><sup>-</sup> or MgSO<sub>4</sub> ion pairs directly. These species are most likely solvent separated which, in the case of MgSO<sub>4</sub> ion pairs, is suggested by the interpretations of ultrasonic relaxation measurements.<sup>9</sup>

In aqueous solutions containing HSO<sub>4</sub><sup>-</sup> as well as SO<sub>4</sub><sup>2-</sup>, the Raman spectra indicate that the following competing equilibria occur



The presence of Na<sup>+</sup> or Mg<sup>2+</sup> competes with H<sup>+</sup> for SO<sub>4</sub><sup>2-</sup> diminishing the intensity of the HSO<sub>4</sub><sup>-</sup> band and increasing the intensity of the (SO<sub>4</sub><sup>2-</sup> + NaSO<sub>4</sub><sup>-</sup> + MgSO<sub>4</sub>) band.

*Acknowledgment.* This work was supported by the Office of Water Resources Research, Department of Interior, and by the Office of Naval Research. The

Raman instrumentation was purchased with matching funds from the National Science Foundation and the University of Rhode Island.

## Quenching of the Excited States of Benzene and Substituted Benzenes by Olefins

by G. Das Gupta and D. Phillips\*

*Department of Chemistry, The University, Southampton SO9 5NH, England (Received March 16, 1972)*

The quenching of the excited singlet state of benzene and substituted benzenes in the vapor phase by various olefins has been investigated, and rate constant data have been tabulated. The possible role of a charge-transfer quenching mechanism is discussed. Quenching of  $^3B_{1u}$  benzene by the olefins, probably through an energy transfer mechanism, was also investigated, and rate parameters were determined.

### Introduction

The quenching of the excited singlet state of benzene ( $^1B_{2u}$ ) by various mono- and conjugated and non-conjugated olefins<sup>1</sup> and other  $\pi$ -bonded molecules<sup>2</sup> has been studied recently by monitoring fluorescence yields. The interaction between the excited state of the aromatic and the olefin can lead to adduct formation,<sup>3</sup> and selection rules,<sup>4</sup> based on orbital symmetry considerations, have been proposed for such interactions. The quenching of the excited triplet state of the aromatic ( $^3B_{1u}$ ) by but-2-ene has been studied directly<sup>5</sup> and results in excellent agreement with those from competitive quenching experiments in which either biacetyl<sup>6</sup> or but-2-ene<sup>7,8</sup> was used as a reference compound were obtained. The triplet quenching almost certainly arises in all cases from triplet energy transfer from the aromatic to the additive. The mechanism of singlet quenching can be, however, different in the case of different additives. In the case of ketones,<sup>2</sup>  $CS_2$ ,<sup>2</sup> etc., the singlet state of the additive lies lower than that of the aromatic and thus an electronic energy transfer mechanism is probably responsible for quenching. For monoolefins however, electronic energy transfer is an endothermic process, and thus would have to occur to a twisted "nonvertical" state of the olefin. In the case of conjugated diolefins singlet energy levels are more nearly degenerate, and thus the energy transfer process would be expected to be more efficient than in the case of monoolefins and nonconjugated diolefins. Although measured quenching rate constants for singlet quenching by the various molecules studied to date fit the above pattern, the role of chemical interactions

must also be considered. Thus it has been proposed that the "allowedness" of the cycloaddition reaction of ground state buta-1,3-diene and ethylene to  $^1B_{2u}$  benzene can also explain the relative quenching efficiencies for these two molecules.<sup>4</sup> It is of interest to note that if charge-transfer interaction between the benzene-olefin collision complex can occur, the cycloaddition reactions become much more allowed.<sup>4</sup> It seemed of interest therefore to study the quenching interactions between the excited singlet state of benzenes and olefins containing substituent groups which might enhance such charge-transfer interactions.

### Experimental Section

The experimental system was similar to that described in earlier reports,<sup>9,10</sup> and details will not be given here.

- (1) A. Morikawa and R. J. Cvetanovic, *J. Chem. Phys.*, **49**, 1214 (1968).
- (2) E. K. C. Lee, M. W. Schmidt, R. G. Shortridge, Jr., and G. A. Haninger, Jr., *J. Phys. Chem.*, **73**, 1805 (1969).
- (3) A. Morikawa, S. Brownstein, and T. J. Cvetanovic, *J. Amer. Chem. Soc.*, **92**, 1471 (1970).
- (4) D. Bryce-Smith, *Chem. Commun.*, 806 (1969).
- (5) H. E. Hunziker and H. R. Wendt, *Chem. Phys. Lett.*, **12**, 180 (1971).
- (6) G. A. Haninger, Jr., and E. K. C. Lee, *J. Phys. Chem.*, **73**, 1815 (1969).
- (7) A. Morikawa and R. J. Cvetanovic, *Can. J. Chem.*, **46**, 1813 (1967).
- (8) M. W. Schmidt and E. K. C. Lee, *J. Amer. Chem. Soc.*, **92**, 3579 (1970).
- (9) K. Al-Ani and D. Phillips, *J. Phys. Chem.*, **74**, 4046 (1970).
- (10) D. Gray, K. Al-Ani, and D. Phillips, *J. Chem. Soc. A*, 905 (1971).



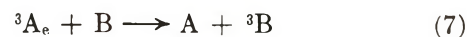
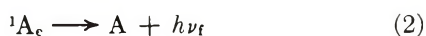
*Materials. Allene.* We wish to thank Dr. M. C. Flowers of this department for his gift of a sample of highly purified allene.

Details of the other materials have been given in earlier reports.<sup>9,11</sup> Care was taken to ensure that diolefins were not present in any of the quenching gases which might lead to spurious results. In all cases the level of impurity was such that the observed quenching could be attributed only to the additive itself and not impurity levels.

## Results and Discussion

It has been found that at a pressure of 15 Torr of benzene vibrational relaxation is incomplete, and the addition of saturated hydrocarbon molecules causes reduction in the fluorescence quantum yield of this pressure of benzene excited at 235.7 nm.<sup>1</sup> In the liquid phase, the fluorescence quantum yield is only 0.06,<sup>12</sup> and this reduction compared to the gas phase value is attributable to some nonradiative decay process which is effected by collisions with the environment of the excited molecule, possibly *via* vibrational effects. In the present experiment, therefore, it is possible that vibrational relaxation-redistribution plays a part in the singlet quenching by some of the olefins used. However, it must be stated that addition of up to 100 Torr of CF<sub>4</sub> caused no discernible decrease in the fluorescence quantum yield of 20 Torr of benzene excited at 254 nm. This result is unexpected if vibrational relaxation were playing a significant role in the present case. Morikawa and Cvetanovic have shown that the rate constant for apparent quenching of 15 Torr of benzene excited at 254 nm is of the order of 10<sup>8</sup> l. mol<sup>-1</sup> sec<sup>-1</sup>,<sup>1</sup> and thus mechanisms other than vibrational relaxation can only be considered where quenching rate constants significantly in excess of this value are obtained. It has been demonstrated<sup>13-15</sup> that thermal equilibration produces a wide distribution of emitting levels of the excited state. There is no apparent reason to suppose that different vibrational levels, which have different fluorescence decay times,<sup>16</sup> will be quenched with equal efficiency by added molecules. The quenching parameters quoted here thus represent average values for the vibrational distribution produced by Boltzmann relaxation at 25°, but as such are directly comparable to those obtained by other workers under similar circumstances.<sup>1,2</sup> The average fluorescence decay time and fluorescence quantum yield of this distribution of vibrational levels have been given as 77 ± 3 nsec<sup>17</sup> and 0.18,<sup>18</sup> respectively, leading to an average value for the radiative lifetime (τ<sub>R</sub>) of 428 ± 17 nsec.

The quenching of the excited singlet (<sup>1</sup>B<sub>2u</sub>) and triplet (<sup>3</sup>B<sub>1u</sub>) can be represented by the simple kinetic scheme



where A = benzene, B = biacetyl, O = olefin, super-

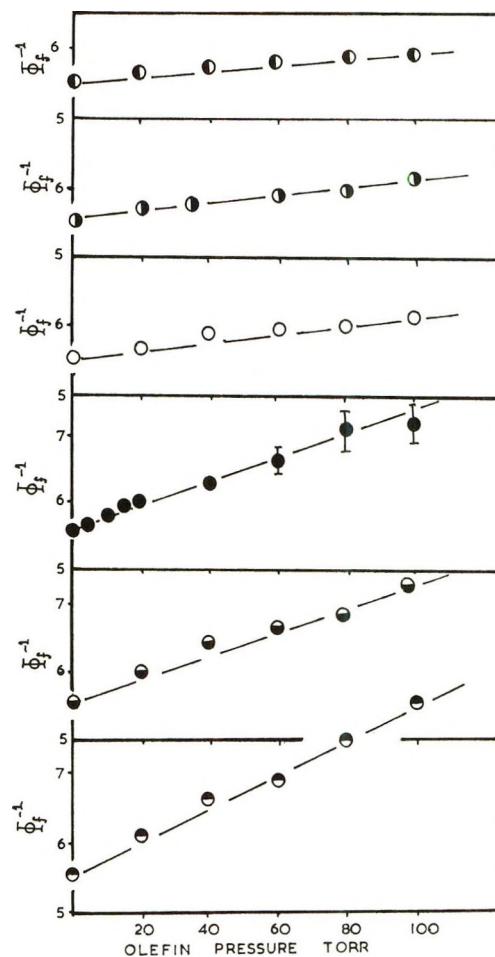


Figure 1. Plots of the reciprocal of the quantum yield of fluorescence ( $\Phi_f^{-1}$ ) against pressure of added olefin; benzene pressure 20 Torr, temp 23°, exciting wavelength 253.7 nm: ●, CH<sub>2</sub>=C=CH<sub>2</sub>; ○, CH<sub>2</sub>=CHF; ○, ClHC=CClH; ○, CF<sub>3</sub>CF=CF<sub>3</sub>; ○, CH<sub>2</sub>=CF<sub>2</sub>; ○, ClHC=CClH.

(11) P. A. Hackett and D. Phillips, *J. Chem. Soc., Faraday Trans. 1*, **68**, 335 (1972).

(12) J. B. Birks, "Photophysics of Aromatic Molecules," Wiley-Interscience, New York, N. Y., 1970.

(13) H. F. Kemper and M. Stockburger, *J. Chem. Phys.*, **53**, 268 (1970).

(14) C. S. Parameter and M. W. Schuyler, *ibid.*, **52**, 5366 (1970).

(15) J. M. Blondeau and M. Stockburger, *Ber. Bunsenges. Phys. Chem.*, **75**, 450 (1971).

(16) K. G. Spears and S. A. Rice, *J. Chem. Phys.*, **55**, 5561 (1971).

(17) M. Nishikawa and P. K. Ludwig, *ibid.*, **52**, 107 (1970).

(18) W. A. Noyes, Jr., W. A. Mulac, and D. A. Harter, *ibid.*, **44**, 2100 (1966).

Table I: Quenching of  $^1B_{2u}$  Benzene Vapor by Olefins; Exciting Wavelength 253.7 nm

Additive	$k_5 \times 10^{-3},^a$ l. mol $^{-1}$ sec $^{-1}$	$\sigma^2 \times 10^{18},^b$ cm $^2$	Ionization potential, $^c$ eV	Refer- ence
CH $_2$ =CHF	1.75 $\pm$ 0.1	1.9 $\pm$ 0.1	10.41	d
CH $_2$ =CHCH $_3$	2.35 (0) $^e$	2.6 (0) $^e$	9.77	f
CF $_3$ CF=CFCF $_3$	2.35 $\pm$ 0.1	3.7 $\pm$ 0.15	11.24	d
CH $_2$ =CF $_2$	2.5 $\pm$ 0.2	3.9 $\pm$ 0.4	10.31	d
CH $_3$ CH=CHCH $_3$	3.45 (0.75) $^e$	4.0 (0.9) $^e$	9.30	f
Trimethylethylene	4.3 (1.5) $^e$	5.2 (1.9) $^e$	8.81	f
1,4-Pentadiene	4.7 (1.86) $^e$	5.7 (2.3) $^e$	...	f
Tetramethylethylene	5.2	6.9	8.41	f
1,5-Hexadiene	5.5	7.3	...	f
1,2-Butadiene	6.1	6.9	9.32	f
CH $_2$ =C=CH $_2$	7.7 $\pm$ 0.7	8.3 $\pm$ 0.8	10.32	d
<i>trans</i> -ClHC=CHCl	7.6 $\pm$ 0.7	10.5 $\pm$ 1	9.86	d
<i>cis</i> -ClHC=CHCl	10.4 $\pm$ 0.9	14 $\pm$ 1.5	9.65	d
CH $_2$ =CHCH=CH $_2$	55.8 (52.0) $^e$	63 (58) $^e$	8.99	f
CH $_2$ =CHCH=CH $_2$	57	66	8.99	g
Isoprene	95 (92) $^e$	116	8.97	f
<i>trans</i> -1,3-Pentadiene	137	167	...	g
<i>cis</i> -1,3-Pentadiene	140 (136) $^e$	173 (168) $^e$	8.64	f
<i>cis</i> -1,3-Pentadiene	149	184	8.64	g

$^a$  Results based upon a radiative lifetime for benzene vapor of 428 nsec.  $^b$  Cross section  $\sigma^2$  obtained from equation  $\sigma^2 = k_5(8\pi kT/\mu)^{-1/2}$ .  $^c$  Averaged data from R. P. Blaunstein and L. O. Christophorou, *Radiat. Res. Rev.*, **3**, 69 (1971).  $^d$  This work.  $^e$  Figure in parentheses is that estimated to be due to electronic quenching alone. First figure includes effects of vibrational relaxation. / Reference 1.  $^g$  Reference 2.

scripts refer to multiplicity, subscript e refers to the equilibrium vibrational distribution assumed to be reached prior to another process occurring. The nature of the quenching steps 5 and 8 will be discussed later.

The mechanism predicts the usual Stern-Volmer relationship that

$$\Phi_f^{-1} = 1 + k_3\tau_0 + k_4\tau_0 + k_5\tau_0[\text{O}] \quad (\text{I})$$

where  $\tau_0 = k_2^{-1} = 428 \pm 17$  nsec. Thus plots of  $\Phi_f^{-1}$  against olefin concentration are expected to yield straight lines of slope  $k_5\tau_0$ . Actual plots are shown in Figure 1, and rate constants  $k_5$  and corresponding quenching cross sections for the various olefins studied here are given in Table I together with comparable data for other olefins obtained previously.

If the fate of the triplet biacetyl is accounted for by reactions 9 and 10, the complete expression for the quantum yield of sensitized phosphorescence from biacetyl is given by eq II. Under the conditions of the



$$\Phi_s = \frac{k_3}{(k_2 + k_3 + k_4 + k_e[\text{O}])} \times \frac{k_7[\text{B}]}{(k_6 + k_7[\text{B}] + k_8[\text{O}])} \times \frac{k_9}{(k_9 + k_{10})} \quad (\text{II})$$

experiments carried out here  $k_7[\text{B}] \gg k_6$ . For olefins which do not significantly quench the singlet state of

benzene at the pressures used in the biacetyl-sensitized emission experiments the expression for the reciprocal of  $\Phi_s$  reduces to

$$\Phi_s^{-1} = \Phi_{isc}^{-1} \left( \frac{k_9 + k_{10}}{k_9} \right) \left[ 1 + \frac{k_8[\text{O}]}{k_7[\text{B}]} \right] \quad (\text{III})$$

where  $\Phi_{isc} = k_3/(k_2 + k_3 + k_4)$ .

Thus from the ratio of slope to intercept of plots in

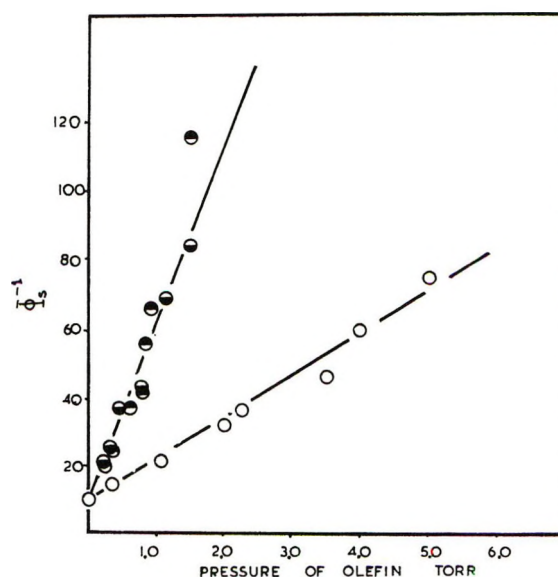


Figure 2. Plots of the reciprocal of the quantum yield of phosphorescence from 0.375 Torr of biacetyl sensitized by 20 Torr of benzene ( $\Phi_s^{-1}$ ) at 253.7 nm and 23° as a function of added olefin pressure. Symbols as for Figure 1.



**Table II:** Quenching Parameters for  $^3B_{1u}$  Benzene by Olefins in Competition with Biacetyl; Benzene Pressure 20 Torr, Biacetyl Pressure 0.375 Torr, Exciting Wavelength 253.7 nm, Temp 25°

Quencher	$k_8 \times 10^{-9},^a$ l. mol $^{-1}$ sec $^{-1}$	$\sigma \times 10^{16},^b$ cm $^2$	Reference
CH $_2$ =CH $_2$	2.0	0.2	c
CH $_2$ =CHF	1.3 $\pm$ 0.1	0.15 $\pm$ 0.01	d
CH $_2$ =CF $_2$	0.07 $\pm$ 0.005	0.01 $\pm$ 0.001	d
<i>cis</i> -ClHC=CHCl	65 $\pm$ 5	9 $\pm$ 0.7	d
<i>trans</i> -ClHC=CHCl	65 $\pm$ 5	9 $\pm$ 0.7	d
CH $_3$ CH=CHCH $_3$	8.91	1.01	c
CH $_3$ CH=CHCH $_3$	8.95 $\pm$ 0.33	1.02	e
CF $_2$ CF=CFCF $_3$	17 $\pm$ 1	2.7 $\pm$ 0.15	d
CH $_2$ =C=CH $_2$	1.8	0.18	d
CH $_2$ =C=CH $_2$	2.5	0.25	f
CH $_2$ =CHCH=CH $_2$	187.2	21.7	c

<sup>a</sup> Computed from best straight lines of plots in Figures 2 and 3, and using rate constant  $k_7 = 3.43 \times 10^{10}$  l. mol $^{-1}$  sec $^{-1}$  [C. S. Parmenter and B. L. Ring, *J. Chem. Phys.*, **46**, 1998 (1967)].

<sup>b</sup> Derived from the equation  $\sigma^2 = k_8(8\pi kT/\mu)^{-1/2}$ . <sup>c</sup> Reference 6. <sup>d</sup> This work. <sup>e</sup> Direct measurement of Hunziker and Wendt.<sup>5</sup> <sup>f</sup> Reference 8.

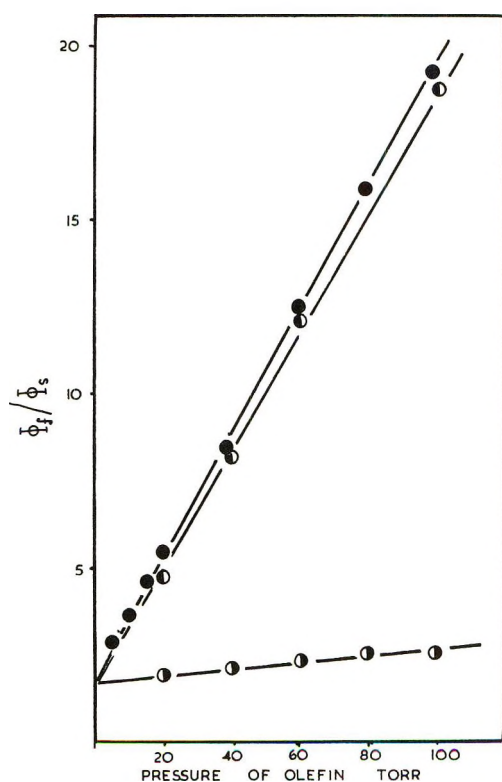


Figure 3. Plots of  $\Phi_f/\Phi_s$  against pressure of added olefin. Conditions as for Figure 2, symbols as in Figure 1.

Figure 2 of  $\Phi_s^{-1}$  against  $[O]$ , the ratio  $k_8/k_7[B]$  can be obtained.  $k_7$  is known to be  $3.43 \times 10^{10}$  l. mol $^{-1}$  sec $^{-1}$ ,<sup>15</sup>  $[B]$  is known, and thus  $k_8$  can be evaluated. Table II gives values of  $k_8$  with corresponding quenching cross sections.

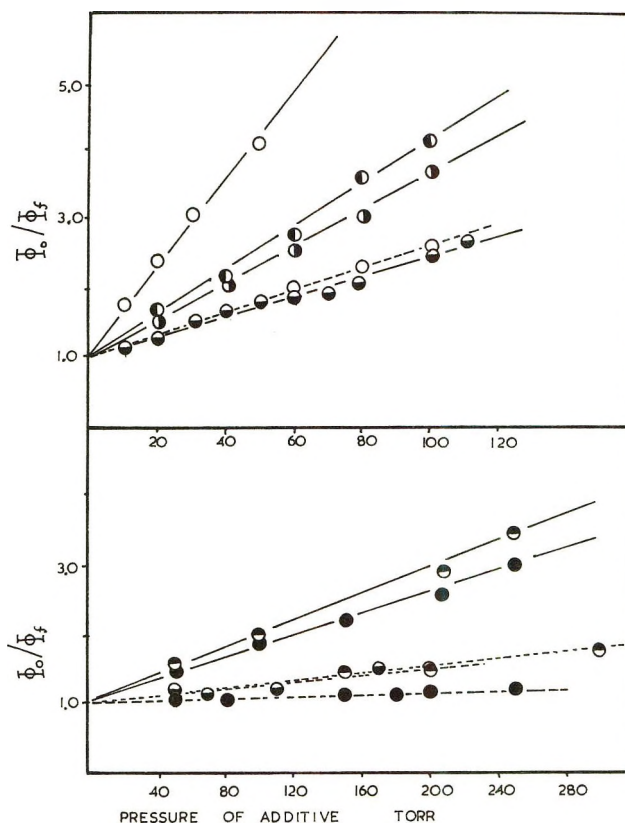


Figure 4. Stern-Volmer plots of the ratio of the fluorescence quantum yield of substituted benzenes in the absence of additive ( $\Phi_s$ ) to the fluorescence quantum yield at any pressure of additive ( $\Phi_f$ ) as a function of added buta-1,3-diene and but-2-ene: ●, 1,2-difluorobenzene; ○, 1,3-difluorobenzene; ◐, 1,4-difluorobenzene; ○, 1,4-bis(trifluoromethyl)benzene; ◑, 1-fluoro-2-(trifluoromethyl)benzene; ◒, 1-fluoro-3-(trifluoromethyl)benzene; —, buta-1,3-diene additive; ---, *cis*-but-2-ene additive. Aromatic pressure = 2 Torr, exciting wavelength 266 nm.

Where the olefin also quenches the singlet state efficiently, plots of  $\Phi_f/\Phi_s$  against  $[O]$  allow estimation of the rate constant for the triplet quenching. Thus


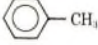
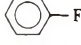
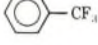
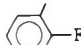



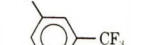
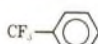
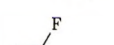
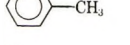
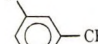
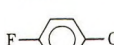
$$\Phi_f/\Phi_s = \frac{k_2}{k_3} \times \frac{(k_9 + k_{10})}{k_9} \left[ 1 + \frac{k_8[O]}{k_7[B]} \right] \quad (\text{IV})$$

These plots are shown in Figure 3, and values of  $k_8$  given as before in Table II.

*Nature of Reaction 5.* Excluding vibrational relaxation the possible mechanisms by which the singlet state of benzene may be quenched include (a) electronic energy transfer, (b) charge-transfer complex formation, (c) chemical reaction, and (d) enhancement of  $S_1 \rightarrow T_1$  intersystem crossing. In the case of the olefins used here, energy transfer to the olefin from  $^1B_{2u}$  benzene would be an endothermic process and can thus be ruled out. Studies with high pressures of methyl halides and more heavily fluoro- and chloro-substituted alkanes have not revealed any evidence of enhancement of

(19) C. S. Parmenter and B. L. Ring, *J. Chem. Phys.*, **46**, 1998 (1967).

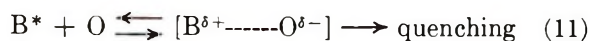
**Table III:** Quenching of the Excited Singlet States of Substituted Benzenes by *cis*-But-2-ene and Buta-1,3-diene, Vapor Phase

Aromatic molecule	Quencher <sup>a</sup>	Exciting wavelength, nm	Quenching rate constant $\times 10^{10}$ , l. mol <sup>-1</sup> sec <sup>-1</sup>	Quenching cross section $\times 10^{-16}$ , cm <sup>2</sup>	Reference
	BD	254	0.57	0.66	<i>b</i>
	B	254	0.035 (0.008)	0.04 (0.009)	<i>c</i>
	BD	254	1.54	1.87	<i>b</i>
	BD	266	2.23	3.2	<i>d</i>
	B	266	0.066	0.085	<i>d</i>
	BD	266	5.57	7.4	<i>e</i>
	B	266	0.93	1.22	<i>e</i>
	BD	266	2.68 $\pm$ 0.15	3.4 $\pm$ 0.17	<i>f</i>
	B	266	0.28 $\pm$ 0.02	0.35 $\pm$ 0.03	<i>f</i>
	BD	266	2.97 $\pm$ 0.15	3.75 $\pm$ 0.19	<i>f</i>
	B	266	0.77 $\pm$ 0.3	0.97 $\pm$ 0.4	<i>f</i>
	BD	266	3.6 $\pm$ 0.3	4.6 $\pm$ 0.5	<i>f</i>
	B	266	0.58 $\pm$ 0.03	0.73 $\pm$ 0.04	<i>f</i>
	BD	266	10.67	14.7	<i>g</i>
	B	266	2.45	3.4 $\pm$ 0.3	<i>g</i>
	BD	266	10.8	14.9	<i>f</i>
	B	266	2.8 $\pm$ 0.2	3.7 $\pm$ 0.3	<i>f</i>
	BD	266	0.9	1.3	<i>h</i>
	BD	266	1.16	1.15	<i>h</i>
	BD	266	2.98	3.83	<i>h</i>
	BD	266	6.9 $\pm$ 0.3	9.4 $\pm$ 0.5	<i>f</i>
	B	266	0.7 $\pm$ 0.1	0.9 $\pm$ 0.1	<i>f</i>
	BD	266	5.6 $\pm$ 0.3	8.3 $\pm$ 0.5	<i>f</i>
	B	266	1.25 $\pm$ 0.1	1.6 $\pm$ 0.1	<i>f</i>

<sup>a</sup> BD = buta-1,3-diene, B = *cis*-but-2-ene. <sup>b</sup> Reference 20. <sup>c</sup> Reference 1; values in parentheses are those corrected for vibrational relaxation effects; value quoted here was recalculated using fluorescence decay time of 77 nsec. <sup>d</sup> K. Al-Ani and D. Phillips, *J. Phys. Chem.*, **75**, 3662 (1971). <sup>e</sup> D. Gray and D. Phillips, *J. Chem. Phys.*, **55**, 5753 (1971). Values have been normalized to measured fluorescence decay time. <sup>f</sup> This work. Quoted values are those derived from the slopes of Figure 4, using the relationship  $\Phi_0/\Phi = 1 + k_{QT}Q$ . Fluorescence decay times for the difluorobenzenes were taken from G. M. Breuer and E. K. C. Lee, *Chem. Phys. Lett.*, **14**, 404 (1972), and for the CF<sub>3</sub> compounds from G. M. Breuer, P. A. Hackett, D. Phillips, and M. G. Rockley, *J. Chem. Soc., Faraday Trans. 2*, **68**, 1995 (1972). <sup>g</sup> D. Gray and D. Phillips, *J. Chem. Phys.*, in press. Values normalized to measured fluorescence decay time. <sup>h</sup> K. Al-Ani and D. Phillips, *J. Phys., Chem.* in press.

S<sub>1</sub>→T<sub>1</sub> intersystem crossing,<sup>20</sup> and thus (d) may also be discounted as a possibility.

Cvetanovic and Morikawa have considered the possibility of the quenching of <sup>1</sup>B<sub>2u</sub> benzene by conjugated olefins as being initially due to the reversible formation of a charge-transfer complex in which the excited singlet state of the aromatic molecule acts as an electron acceptor<sup>1</sup>



If this mechanism were operative, the quenching efficiencies of various olefins should correlate approximately with the ionization potential of the olefin. Data in Table I show that such a correlation may exist although only for efficient quenchers. Again assuming such a mechanism, the quenching efficiency for a single donor and a series of acceptors should correlate with

(20) G. Das Gupta and D. Phillips, *J. Chem. Soc., Faraday Trans. 2*, **68**, 2003 (1972).



the electron affinity of the acceptor. Such data are of course not available for excited electronic states, but it has been shown<sup>21</sup> that for ground state fluorobenzenes, the electron affinity increases by approximately 0.4 eV per fluorine substituent. Assuming the same to hold true for excited states of these compounds, increase in fluorine substitution should lead to enhanced quenching. The effect would be expected to be even more pronounced for substitution of CF<sub>3</sub> groups into the benzene ring for which the estimated increase in electron affinity per substituent group is approximately 1 eV.<sup>22</sup> Figure 4 shows the Stern–Volmer plots for the quenching of the excited singlet states of a series of mono- and disubstituted benzenes by but-2-ene and buta-1,3-diene, and quenching parameters are given in Table III. It is evident that monofluoro substitution in benzene, toluene, and (trifluoromethyl)benzene does apparently enhance the efficiency of quenching of the aromatic molecule by the olefins, and it is also evident that CF<sub>3</sub> substitution has a similar but much more dramatic effect, lending support to the proposed mechanism.

*Reaction 8.* As far as can be ascertained electronic energy transfer from <sup>3</sup>B<sub>1u</sub> benzene to all olefins studied here (with the exception of 1,1-difluoroethylene) is an exothermic process, and it thus seems likely that this mechanism is predominantly responsible for the observed quenching of triplet benzene in these experiments. In no case was the phosphorescence of biacetyl excited directly at 404.7 nm quenched by the addition of the olefins, and thus in the case of benzene–biacetyl

mixtures quenching is a directly attributable to quenching of an excited state of benzene.

Perfluorobut-2-ene and *cis*- and *trans*-dichloroethylene are seen to be efficient quenchers of triplet benzene, indicating low-lying triplet olefin energy levels. The fact that *cis*- and *trans*-dichloroethylene quench with the same rate, whereas slightly different rates are observed for singlet quenching, is indicative that different mechanisms pertain for singlet and triplet quenching. Vinyl fluoride and allene are less efficient triplet quenchers and 1,1-difluoroethylene is very inefficient, indicating perhaps that in this case electronic energy transfer would be an endothermic process. The results for allene support the contention that in the benzene-sensitized photolysis of this type of olefin,<sup>23</sup> triplet energy transfer rather than singlet sensitization is the mechanism, although it has recently been reported that in solution allene may undergo photoaddition to the excited singlet state of benzene by a nonconcerted process.<sup>24</sup>

*Acknowledgments.* The authors gratefully acknowledge partial financial support from NATO European Office of Scientific Affairs and payment of fees by the British Council during the tenure of a research studentship by Miss Das Gupta. Helpful discussions with Dr. M. Godfrey are gratefully acknowledged.

(21) W. T. Naff and C. P. Cooper, *J. Chem. Phys.*, **49**, 2787 (1968).

(22) M. Godfrey, private communication.

(23) H. R. Ward and E. Karafiath, *J. Amer. Chem. Soc.*, **91**, 7475 (1969).

(24) D. Bryce-Smith, B. E. Foulger, and A. Gilbert, *J. Chem. Soc., Chem. Commun.*, 664 (1972).

## COMMUNICATIONS TO THE EDITOR

---

### Ultraviolet Absorption Spectra of Polyphosphate Solutions

*Sir:* Although the uv absorption spectra of pyrophosphate and orthophosphate have been given<sup>1</sup> no detail is given of polyphosphate absorption bands. The shoulder on the  $\pi$ - $\pi^*$  peak reported here for trimethyl phosphate and pyrophosphate has not previously been demonstrated. The effect of solvents on the  $n$ - $\pi^*$  absorption bands in the uv is to give the well-known "blue shift." The effect is well documented for organic molecules,<sup>2,3</sup> nitrates, and nitrites<sup>4</sup> but no  $n$ - $\pi^*$  transition is given in the literature for ortho and polyphosphate anions. Although the peak in the region of

45,000 cm<sup>-1</sup> reported here is a suspected  $n$ - $\pi^*$  transition no definite blue shift with change of solvent has been established.

The trimethyl phosphate was British Drug House technical reagent grade soluble in three solvents, distilled water, spectroscopically pure ethanol, and *n*-hexane. Sodium metaphosphate was prepared by heating AR quality NaH<sub>2</sub>PO<sub>4</sub> in a clean platinum dish in

(1) R. P. Buck, S. Singadya, and L. B. Rogus, *Anal. Chem.*, **26**, 1240 (1954).

(2) J. N. Murrell, "The Theory of the Electronic Spectra of Organic Molecules," Methuen, London, 1963.

(3) J. W. Sidman, *Chem. Rev.*, **58**, 689 (1958).

(4) S. J. Strickler and M. Kasha, "Molecular Orbitals in Chemistry, Physics, and Biology," P. O. Lowdin and B. Pullman, Ed., Academic Press, New York, N. Y., 1964.

a muffle furnace at 950° for 8 hr. Five sodium phosphates with varying composition were prepared by heating the metaphosphate with calculated weights of AR Na<sub>2</sub>CO<sub>3</sub> to give glasses with Na<sub>2</sub>O:P<sub>2</sub>O<sub>5</sub> ratios of 1.1:1; 1.2:1; 1.3:1; 1.4:1; 1.5:1. The chain lengths of these glasses were determined by pH titration<sup>5</sup> and the chain lengths are recorded in Table I, together with the  $\pi$ - $\pi$  uv absorption peak. Potassium metaphosphate and related phosphates were prepared in a similar manner by using AR KH<sub>2</sub>PO<sub>4</sub> and AR K<sub>2</sub>CO<sub>3</sub> as above.

**Table I:** Variation of Absorption Peak Wavenumber, Wavelength, and Molar Absorptivity with Composition and Chain Length for a Series of Sodium Phosphates

Molar ratio Na <sub>2</sub> O:P <sub>2</sub> O <sub>5</sub>	Chain length, $\bar{n}$	Wave-numbers, cm <sup>-1</sup>	Wave-length, nm	Molar absorptivity
1:1	57.1	49,380	202.5	1.400 × 10 <sup>3</sup>
1.1:1	17.70	49,660	201.4	1.278 × 10 <sup>3</sup>
1.2:1	9.79	49,800	201.0	1.204 × 10 <sup>3</sup>
1.3:1	7.23	49,960	200.2	3.742 × 10 <sup>2</sup>
1.4:1	5.20	50,900	196.5	1.516 × 10 <sup>2</sup>
1.5:1	2.01	51,680	193.5	6.304 × 10 <sup>1</sup>

All spectra were recorded on an Optica CF<sub>4</sub> and SP800 spectrophotometers at room temperature in matched 1-cm quartz absorption cells. The effect of solvents on the suspected n- $\pi$ \* peak near 45,000 cm<sup>-1</sup> is shown in Table II and Figure 1 for trimethyl phosphate. The intensity of the band near 45,500 cm<sup>-1</sup> is much less than that near 50,000 cm<sup>-1</sup> and the 45,500 cm<sup>-1</sup> band may be due to an n- $\pi$ \* transition. The peak is found in all spectra we have measured.

The variation in the  $\pi$ - $\pi$ \* peak near 50,000 cm<sup>-1</sup> with decreasing chain length for 5 × 10<sup>-4</sup> polyphosphate solution is shown in Table I and Figure 2. A similar trend in the absorption spectrum of solutions of potassium phosphates is shown in Table III. As the number of phosphorus atoms in the chain decreases, so the  $\pi$ - $\pi$ \* peak decreases in wavelength. The decrease of phosphate chain length of potassium phosphates with increasing metal oxide content is a well-established effect being shown by Westman and coworkers<sup>6a</sup> by paper chromatographic studies of K<sub>2</sub>O P<sub>2</sub>O<sub>5</sub> solutions and by Williams, *et al.*,<sup>6b</sup> from both infrared studies of

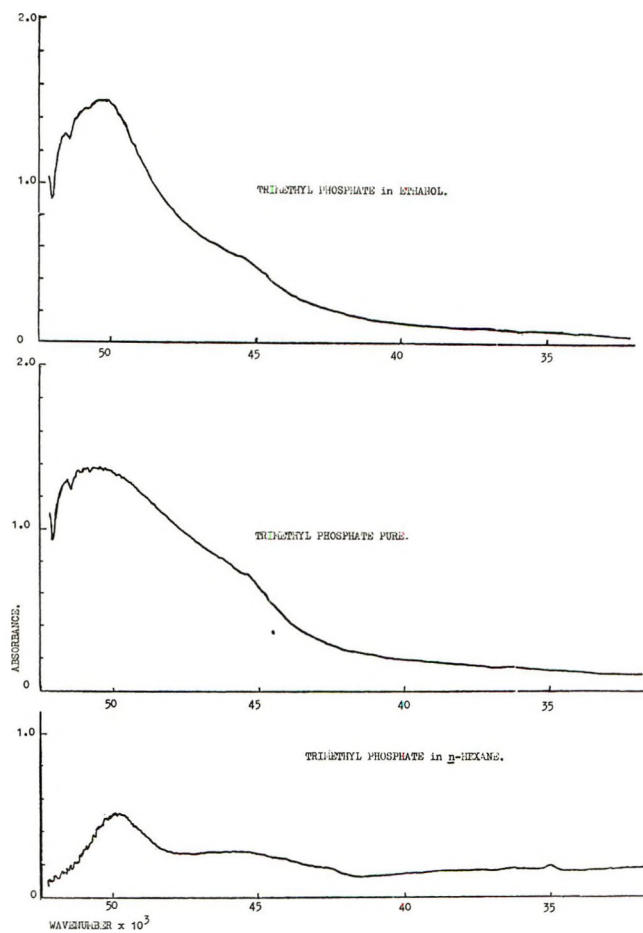


Figure 1. Spectrum of (a) trimethyl phosphate in ethanol, (b) pure trimethyl phosphate, and (c) trimethyl phosphate in *n*-hexane.

solids and glasses and by surface tension studies<sup>6c</sup> of molten potassium phosphates. Similar trends in the position of a  $\pi$ - $\pi$ \* transition have been shown by Murel (see ref 2, chapter 5) for conjugated phenyl and carboxyl groups, for polyene acids, and for  $\alpha$ - $\omega$  dimethyl polyenes. For conjugated organic molecules both free electron theory and simple MO theory predict that the numerical value of the wavelength of the first absorption

(5) (a) J. R. Van Wazer, "Phosphorus and its Compounds," Vol. 1, Interscience, New York, N. Y., 1958, p 419 ff.; (b) *ibid.*, p 717 ff  
(6) (a) A. E. R. Westman and P. A. Gartaganis, *J. Amer. Ceram. Soc.*, **40**, 293 (1957); (b) D. J. Williams, B. T. Bradbury, and W. R. Maddocks, *J. Soc. Glass Tech.*, **43**, 337 (1959); (c) B. T. Bradbury and W. R. Maddocks, *ibid.*, **43**, 325 (1959).

**Table II:** Variation of Absorption Peak Wavenumber, Wavelength, and Molar Absorptivity with Solvent for Trimethyl Phosphate

Solvent	Wavenumbers, cm <sup>-1</sup>	Wavelength, nm	Molar absorptivity	Wavenumbers, cm <sup>-1</sup>	Wavelength, nm	Molar absorptivity
Distilled H <sub>2</sub> O	51,000	196.1	2.56 × 10 <sup>-1</sup>	45,500	219.8	7.5 × 10 <sup>-2</sup>
Spectroscopically pure ethanol	50,500	198.0	3.04 × 10 <sup>-1</sup>	45,500	219.8	8.0 × 10 <sup>-2</sup>
<i>n</i> -Hexane	50,000	200	1.25 × 10 <sup>-1</sup>	45,500	219.8	7.5 × 10 <sup>-2</sup>
Nonsolvated (CH <sub>3</sub> ) <sub>3</sub> PO <sub>4</sub>	50,500	198.0		45,500	219.8	



peak is proportional to the number of carbon atoms in the chain of the molecule. With increasing chain length of the molecule the first absorption peak tends to a limited value and theoretically this limit can be calcu-

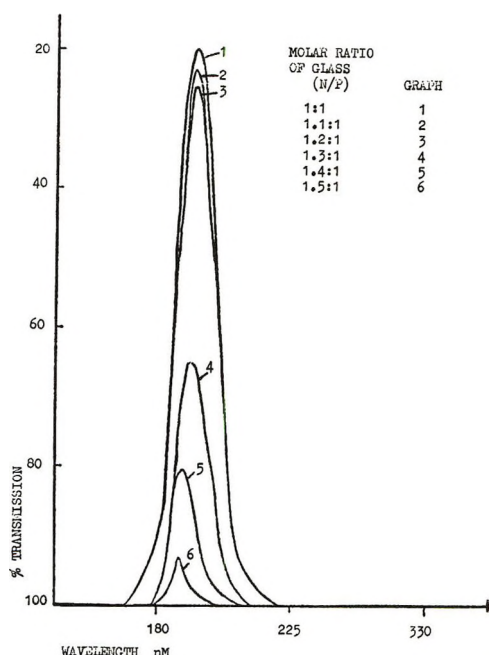


Figure 2. Uv absorption spectra of polyphosphate solutions.

Table III: Variation of Absorption Peak, Wavenumber, and Wavelength for a Series of Potassium Phosphates

Mole ratio of potassium phosphate $K_2O:P_2O_5$	Wavenumbers, $cm^{-1}$	Wavelength, nm
1:1	51,300	195
1.1:1	51,679	193.5
1.2:1	51,800	193
1.3:1	51,813	193
1.4:1	52,100	192
1.5:1	52,219	191.5

lated by allowing for an alteration in bond length along the conjugated chain of the molecule. It is likely that similar theoretical interpretations can be used to explain the shift in  $\pi-\pi^*$  absorption peak with chain length in polyphosphates. Detailed calculations are being performed in these laboratories.<sup>7</sup>

(7) L. J. Stanley, personal communication.

CHEMISTRY DEPARTMENT  
UNIVERSITY OF BRADFORD  
BRADFORD 7, ENGLAND

M. BENNOSON  
D. J. WILLIAMS\*

RECEIVED MARCH 20, 1972

## On the Alleged Resolution of an Infrared Band of HDO

Publication costs assisted by Université Laval

*Sir:* In a recent communication, Bonner<sup>1</sup> reports measurements of the near-infrared spectrum of dilute (5%) solutions of  $H_2O$  in  $D_2O$  in which he has observed two adjacent bands with opposite temperature behavior. He interprets them as resolved components of the same combination band due to hydrogen-bonded and non-bonded HDO molecules. He claims this to be the first instance of a single band resolved into such components. However, his results and interpretation are at variance with those of a recent study,<sup>2</sup> which he does not quote.

The two bands in question, at 2030 nm ( $4935\text{ cm}^{-1}$ ) and 1905 nm ( $5250\text{ cm}^{-1}$ ), have already been described by Luck and Ditter (their Figure 10) who found their intensity to be rather insensitive to temperature over the range from 0 to  $80^\circ$ . In contrast, Bonner observes a large temperature effect over a narrower range. Thus, his weak band at  $5250\text{ cm}^{-1}$  increases nearly tenfold from 25 to  $70^\circ$  while that at  $4935\text{ cm}^{-1}$  decreases by roughly 40%. Since Bonner's conclusions are based mainly on this temperature effect, the discrepancy with the previous authors raises serious doubt about his interpretation.

Following Bayly, *et al.*,<sup>3</sup> he assigns the main band at  $4935\text{ cm}^{-1}$  to the combination of O-H stretching (at  $3410\text{ cm}^{-1}$ ) and bending modes (at  $1460\text{ cm}^{-1}$ ) of the hybrid molecule HOD. Now, this assignment had first been suggested on the assumption that the assignment of the corresponding (?) vapor band (at  $5089\text{ cm}^{-1}$ )<sup>4</sup> was correct. However, assignment to the overtone of the O-D stretching (at  $5363.6\text{ cm}^{-1}$  in the vapor) gives a more realistic frequency shift on condensation, and likewise, a more reasonable anharmonicity ( $2 \times 2500\text{ cm}^{-1}$ ) for the liquid bands. As for the weaker band at  $5250\text{ cm}^{-1}$ , Bonner simply mentions that the corresponding combination ( $\nu_2 + \nu_3$ ) =  $5332\text{ cm}^{-1}$  in the vapor state<sup>5</sup> shows the right frequency shift upon condensation. That conclusion is unfounded because the vapor band belongs in fact to the  $H_2O$  molecule, not to HDO.<sup>6</sup>

(1) O. D. Bonner, *J. Phys. Chem.*, **76**, 1228 (1972).

(2) W. A. P. Luck and W. Ditter, *Z. Naturforsch.*, **24b**, 482 (1969).

(3) J. G. Bayly, V. B. Kartha, and W. H. Stevens, *Infrared Phys.*, **3**, 311 (1963).

(4) W. S. Benedict, N. Gaylar, and K. Plyler, *J. Chem. Phys.*, **24**, 1139 (1956).

(5) G. Herzberg, "Infrared and Raman Spectra of Polyatomic Molecules." Van Nostrand, Princeton, N. J., 1959.

(6) The confusion here arises from the erroneous nomenclature adopted by infrared spectroscopists for the fundamental modes of the hybrid HDO molecule: namely,  $\nu_1$  for the O-D stretching,  $\nu_2$  for the bending, and  $\nu_3$  for the O-H stretching. Since the fundamentals of HDO are all of the same species, they should normally be numbered in the order of their decreasing frequency, but this also would be confusing in relation to the fundamentals of  $H_2O$  and  $D_2O$ . It is preferable to identify them simply as  $\nu_{O-H}$ ,  $\nu_{O-D}$ , and  $\partial_{HOD}$ .

The combination ( $\nu_{O-D} + \partial_{HOD}$ ) for the free hybrid molecule should have a frequency near  $5050 \text{ cm}^{-1}$ , judging from the sum of the fundamentals ( $3680 + 1402 \text{ cm}^{-1}$ ).<sup>5</sup>

In conclusion, it must be stressed that the said pair of HDO bands coincides precisely with a fairly strong combination band of the major component,  $D_2O$  (at about  $5080 \text{ cm}^{-1}$ ). The extinction thickness of that band has been estimated<sup>3</sup> at 1 mm. Under such conditions accurate measurements become almost impossible.

DEPARTMENT OF CHEMISTRY  
UNIVERSITÉ LAVAL  
QUÉBEC, CANADA

PAUL A. GIGUÈRE

RECEIVED JULY 26, 1972

### Concerning the Direct Effect in the Radiolysis of 0.4 M Sulfuric Acid

Publication costs assisted by the French Atomic Energy Commission

*Sir:* Matthews, Mahlman, and Sworski<sup>1</sup> have recently studied the  $^{60}\text{Co}$   $\gamma$  radiolysis of  $\text{Ce}^{\text{IV}}$  in aqueous solutions containing  $\text{Ce}^{\text{IV}}$ ,  $\text{Ce}^{\text{III}}$ ,  $\text{HCOOH}$ , and various concentrations of sulfuric acid. Kinetic analysis of their results led the authors to conclude that the radical  $\text{SO}_4^-$  was formed by direct action upon sulfuric acid. The yield of  $\text{SO}_4^-$  radicals formed in this way, though small, was significant even for 0.4 M solutions:  $G_{\text{SO}_4^-} = 0.20$ .

In the course of work on the pulse radiolysis of vanadium(IV) and (V)<sup>2</sup> in aqueous solutions containing sulfuric acid, we have studied the absorption spectra of deaerated 0.4 M solutions of sulfuric acid, free from other solutes, subjected to a 12-nsec pulse of 1.8-MeV electrons produced by a modified Febetron 707.<sup>3</sup> Under these conditions, we observed a transient species which was present less than 10 nsec after the end of the pulse and which had the absorption spectrum shown in Figure 1. The spectrum corresponds to that attributed<sup>4-7</sup> to the radical-ion  $\text{SO}_4^-$  formed under other experimental conditions, and we believe the transient species we observe to be  $\text{SO}_4^-$  (or  $\text{HSO}_4$ ). Under our conditions, this cannot be formed by the reaction  $\text{OH} + \text{HSO}_4^- \rightarrow \text{H}_2\text{O} + \text{SO}_4^-$  since the rate constant of this reaction ( $3.4 \times 10^5 \text{ M}^{-1} \text{ sec}^{-1}$ ),<sup>8</sup> is too low for it to contribute significantly, and we believe the radical

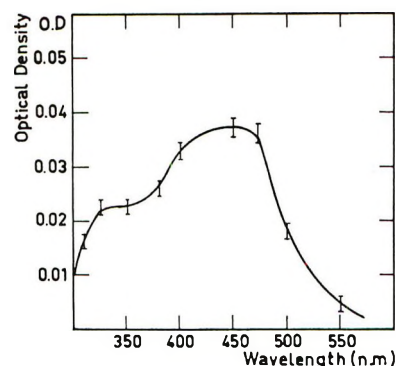


Figure 1. Spectrum of transient in 0.4 M  $\text{H}_2\text{SO}_4$  5 nsec after a 12-nsec 96-krad electron pulse ( $l = 2.5 \text{ cm}$ ).

$\text{SO}_4^-$  to be produced by direct action upon sulfuric acid, as suggested by Matthews, Mahlman, and Sworski.

The absorbed dose was determined from the amount of ferricyanide formed 100 nsec after the pulse in a neutral 0.1 M ferrocyanide solution containing nitrous oxide ( $\epsilon_{440 \text{ nm}} = 600 \text{ M}^{-1} \text{ cm}^{-1}$ ,<sup>9</sup>  $G_{\text{OH}} + G_e = 5.5^{10}$ ) and gave  $G_e = 182 \pm 30$  at 450 nm for the ion-radical  $\text{SO}_4^-$ . If  $\epsilon_{450} = 1000 \text{ M}^{-1} \text{ cm}^{-1}$ , as determined by the radiolysis of sulfuric acid,<sup>5,6</sup> we find  $G_{\text{SO}_4^-}$  to be  $0.18 \pm 0.03$  in good agreement with the value already cited.<sup>1</sup>

The effect of sulfuric acid concentration upon the yield of transient and the decay kinetics of the transient will be the subject of a subsequent article.

(1) R. W. Matthews, H. A. Mahlman, and T. J. Sworski, *J. Phys. Chem.*, **76**, 1265 (1972).

(2) L. Gilles, B. Lesigne, C. Ferradini, and J. Pucheault, to be published.

(3) B. Lesigne and R. Sauneuf, to be published.

(4) L. Dogliotti and E. Hayon, *J. Phys. Chem.*, **71**, 2511 (1967).

(5) E. Heckel, A. Henglein, and G. Beck, *Ber. Bunsenges. Phys. Chem.*, **70**, 149 (1966).

(6) A. K. Pikaev and C. I. Zolotarevskii, *Izv. Akad. Nauk SSSR*, 188 (1967).

(7) D. M. Brown and F. R. Dainton, *Trans. Faraday. Soc.*, **62**, 1139 (1966).

(8) C. Ferradini, "Actions Chimiques et Biologiques des radiations," M. Haissinsky Editeur, Xe série, Masson, Paris, 1966.

(9) S. R. Cohen and R. A. Plane, *J. Phys. Chem.*, **61**, 1096 (1957).

(10) E. D. Black and E. Hayon, *ibid.*, **74**, 3199 (1970).

DRA/SRIRMA, CEN. SACLAY  
91190 GIF S/YVETTE, FRANCE

B. LESIGNE\*

C. N. R. S.  
94200 IVRY, FRANCE

C. FERRADINI  
J. PUCHEAULT

RECEIVED AUGUST 8, 1972



# Directory of Graduate Research 1971



*Biennial publication of the  
ACS Committee on  
Professional Training*

The guide to graduate schools, research, and personnel in the universities and colleges in the United States and Canada known to offer an organized curriculum leading to the doctoral degree in chemistry, biochemistry, chemical engineering, and pharmaceutical or medicinal chemistry.

#### Covers

- 212 Departments of Chemistry
- 171 Departments offering Biochemistry
- 109 Departments of Chemical Engineering
- 30 Departments of Pharmaceutical or Medicinal Chemistry

Lists 3018 full- and part-time staff members, each with outline of career, teaching and research specialties, and list of publications for the past two or five years. Other listings include interdisciplinary programs and doctoral theses accepted during the past two years. Statistical data on departments include graduate enrollment, number of Ph.D. degrees conferred during the past two years, number of staff members, and number of postdoctoral appointments.

*796 + xx pages, with index of names. Cloth. (1971) \$15.00 post-paid in U.S., plus 50¢ in Canada and PUAS, 75¢ foreign.*

#### **Order from:**

Special Issues Sales  
American Chemical Society  
1155 Sixteenth St., N.W.  
Washington, D. C. 20036

